TB & The Sphinx

An investigation into the ways host sphingolipids affect *Mycobacterium tuberculosis* infection.

A dissertation prepared

in partial fulfillment of the requirements for the degree of

Doctor of Philosophy

2024-02-16

Gaelen Guzman

ORCID: 0000-0002-7696-6034

Department of Molecular Microbiology and Immunology

Oregon Health & Science University School of Medicine

Certificate of Approval

This is to certify that the PhD dissertation of

Gaelen Donnelly Guzman

has been approved.

Dissertation Advisory Committee

Fikadu G. Tafesse, PhD (mentor)

Scott Landfear, PhD (chair)

Carsten Schultz, PhD

David Lewinsohn, PhD

Larry David, PhD

Isabella Rauch, PhD

Table of contents

Certificate of Approval **1**
Foreword . . . 1
Introduction . . . 1
Main Results . . . 1
Additional chapters . . . 1
Discussion & Conclusion . . . 1

Acknowledgements **3**
The Tafesse Lab (current and former) . . . 3
Collaborations and facilities . . . 5
Other . . . 5
Co-authors . . . 6

Glossary **9**
Immunology and bacteriology terms . . . 9
Sphingolipid terms . . . 9
Non-sphingolipid Lipids . . . 10
Lipid nomenclature . . . 10
Methods, techniques, & miscellaneous . . . 11

I. Introduction: TB and the Sphinx **13**
Section overview . . . 15
Introduction Part 1 . . . 15
Introduction Part 2 . . . 15

1. Introduction Part 1 **17**
1.1. Abstract . . . 17
1.2. Introduction . . . 18
1.3. *Mycobacterium tuberculosis*: an ancient pathogen . . . 18
1.4. Galenic humors to Koch's postulate: A long history of TB therapy . . . 20
1.5. TB, racism, & inequity: an intertwined history . . . 24
1.6. *Mycobacterium tuberculosis* today: questions, challenges, and goals . . . 26
1.7. The lipid connection . . . 28
1.8. Sphingolipids: enigmatic like the sphinx . . . 32
1.9. Conclusion . . . 34
1.10. Contributions . . . 36

2. Introduction Part 2 **37**
2.1. Abstract . . . 37
2.2. Introduction . . . 38

2.3. *Mtb* and the innate immune system: a tug of war in the lung . . . 38
2.3.1. Infection start & the granuloma . . . 38
2.3.2. A Trojan Horse in the belly of the beast . . . 39
2.3.3. Arresting development: the blockade of lysosomal maturation. . . . 41
2.3.4. Breaking free: damaging the phagosomal membrane . . . 42
2.3.5. Lipid droplet formation in late-stage infection . . . 44
2.3.6. Cytokine production in the granuloma . . . 44
2.4. *Mtb* and Lipids: A recipe for pathogenicity . . . 45
2.5. Sphingolipids overview . . . 46
2.5.1. Sphingolipid synthesis and trafficking . . . 46
2.5.2. Sphingolipid breakdown: signaling through salvage . . . 48
2.5.3. Sphingolipids and disease . . . 49
2.6. Open questions regarding sphingolipids in *Mtb* infection . . . 50
2.7. Challenges and breakthroughs in studying lipids . . . 52
2.8. Conclusion . . . 53
2.9. Contributions . . . 53

II. Main Results **55**
Chapter summaries . . . 57
Breaking and entering . . . 57
Sealing the Gaps . . . 57
Living off the Fat of the cell . . . 57
An Affinity for Sphingolipids . . . 57

3. Breaking and Entering **59**
3.1. Abstract . . . 59
3.2. Importance . . . 60
3.3. Introduction . . . 60
3.4. Results . . . 61
3.4.1. Manipulation of sphingolipid levels in mammalian phagocytes . . . 61
3.4.2. Sphingolipid-deficient cells display a reduced capacity to phagocytose *Mtb* . 63
3.4.3. Sptlc2$^{-/-}$ cells are permissive to herpes simplex virus entry and clathrin-mediated endocytosis. . . . 63
3.4.4. Sptlc2$^{-/-}$ cells display defects in filamentous actin dynamics during phagocytic uptake. . . . 65
3.4.5. Sptlc2$^{-/-}$ cells fail to exclude CD45 from the pathogen contact site. . . . 67
3.4.6. Activation of Rho GTPases Rac1 and Cdc42 is impaired in Sptlc2$^{-/-}$ cells. . . . 67
3.4.7. Phosphoinositide turnover is impaired in Sptlc2$^{-/-}$ cells. . . . 69
3.4.8. Production of sphingomyelin, not glycosphingolipids, is critical for efficient *Mtb* uptake. . . . 71
3.5. Discussion . . . 71
3.6. Materials and Methods . . . 74
3.6.1. Reagents . . . 74
3.6.2. Plasmids . . . 74
3.6.3. Cell culture and small-molecule-inhibitor treatment . . . 75
3.6.4. Metabolic labeling and thin-layer chromatography . . . 75
3.6.5. Lipodome analysis . . . 75

3.6.6. Generation of lentiviruses . . . 76
3.6.7. Generation of CRISPR/Cas9-mediated knockout cell lines . . . 76
3.6.8. Culturing of *Mtb* and *M. marinum* . . . 77
3.6.9. *Mtb* and *M. marinum* infection . . . 77
3.6.10. Zymosan A uptake assay . . . 78
3.6.11. Phagocytosis assay . . . 78
3.6.12. Herpes simplex virus 1 infection . . . 78
3.6.13. Binding assay zymosan A particles . . . 78
3.6.14. Real time imaging of phagocytosis . . . 79
3.6.15. Live imaging of dectin-1–GFP . . . 79
3.6.16. Live image analysis (quantification) . . . 79
3.6.17. Dectin-1 and CD45 displacement assay . . . 80
3.6.18. Immunoblot analysis . . . 80
3.6.19. Flow cytometry . . . 80
3.6.20. Transferrin uptake analysis . . . 81
3.7. Acknowledgements . . . 81
3.8. Supplementary materials . . . 81
3.8.1. Supplementary videos . . . 82

4. Sealing the Gaps **87**
4.1. Abstract . . . 87
4.2. Introduction . . . 88
4.3. Results . . . 89
4.3.1. Manipulating the sphingolipid metabolic pathway . . . 89
4.3.2. Host sphingolipids protect against *Mtb*-induced endosomal membrane damage. 90
4.3.3. Sphingolipids protect cells from endo/lysosomal damage before the ESCRT repair pathway activation. . . . 92
4.3.4. Sphingomyelin accumulates at the sites of *Mtb*-induced membrane damage. . 94
4.3.5. Sphingolipids restrict intracellular *Mtb* replication. . . . 94
4.4. Discussion . . . 96
4.4.1. Lipids in early membrane repair . . . 98
4.4.2. Sphingolipid production restricts *Mtb* replication . . . 98
4.4.3. Conclusions . . . 99
4.5. Methods . . . 100
4.5.1. Cell culturing and cell lines used . . . 100
4.5.2. Plasmids and small molecule inhibitors . . . 100
4.5.3. Cytotoxicity screening . . . 101
4.5.4. Thin-layer chromatography . . . 101
4.5.5. Microscopy staining . . . 101
4.5.6. *Mtb* culturing and THP-1 infection . . . 102
4.5.7. *Mtb* membrane damage assay and quantification . . . 102
4.5.8. LLOME Membrane damage repair assay . . . 103
4.5.9. ESCRT recruitment assay . . . 103
4.5.10. Lysenin-GFP colocalization assays . . . 104
4.5.11. Live/Dead reporter-based mycobacterium growth assay . . . 104
4.5.12. Luminescence-based mycobacterium growth assay . . . 104
4.5.13. CFU-based *mycobacterium* growth assay . . . 105
4.6. Contributions and Acknowledgements . . . 105

4.7. Supplemental data . . . 106

5. Living Off the Fat of the Cell **111**
5.1. Abstract . . . 111
5.2. Introduction . . . 112
5.3. Results . . . 113
5.3.1. Global lipidomics reveals acute changes in the host lipidome during pathogenic Mycobacterium tuberculosis infection. . . . 113
5.3.2. Comparing lipidomes during H37Rv and H37Rv-ΔRD1 reveals signatures of pathogenic *Mtb* infection . . . 116
5.3.3. *Mtb* cell wall components map to selective *Mtb*-infection-induced lipidomic effects . . . 118
5.3.4. Treatments with *Mtb* cell wall components recapitulate some, but not all, effects of *Mtb* infection . . . 120
5.4. Discussion . . . 122
5.5. Methods . . . 124
5.5.1. Cell lines, *Mycobacterium tuberculosis* strains, and *Mycobacterium tuberculosis* cell wall components . . . 124
5.5.2. *Mycobacterium tuberculosis* infection . . . 124
5.5.3. *Mycobacterium tuberculosis* cell wall treatments . . . 124
5.5.4. Resazurin Viability Assay . . . 125
5.5.5. Lipid extraction & sample preparation . . . 125
5.5.6. Mass spectrometric analysis . . . 126
5.5.7. Data analysis and presentation . . . 126
5.6. Acknowledgements, & Contributions . . . 127
5.6.1. Acknowledgements . . . 127
5.6.2. Contributions . . . 127
5.7. Supplementary figures . . . 128

6. An Affinity for Sphingolipids **133**
6.1. Abstract . . . 133
6.2. Introduction . . . 134
6.3. Results . . . 135
6.3.1. Trifunctional lipid probes offer unique utility in assessing functions, localization, and interaction partners of a given lipid species . . . 135
6.3.2. Trifunctional probes reveal protein-lipid interactions of the THP-1 macrophage 138
6.3.3. Proteomics of trifunctional probes reveals protein-sphingolipid interactions during pathogenic *Mtb* infection . . . 141
6.4. Pathogenic versus attenuated *Mtb* infections induce highly similar changes to the tf-Sph interactome . . . 144
6.5. *Mtb* protein Rv3466 is enriched by tf-Sphingosine during infection . . . 146
6.6. Discussion . . . 148
6.7. Materials and Methods . . . 149
6.7.1. THP-1 cell culturing and plating . . . 149
6.7.2. Mycobacterium tuberculosis culturing and infection . . . 149
6.7.3. Trifunctionalized lipid treatments, uncaging, crosslinking . . . 150
6.7.4. Cell lysis and protein collection . . . 150
6.7.5. Fluorescence click reaction & In-gel/on-blot fluorescence . . . 151

6.7.6. Affinity purification of probe-bound proteins . . . 151
6.7.7. Liquid chromatography and tandem mass spectrometry analysis (LC-MS/MS) 152
6.7.8. Data analysis . . . 153
6.8. Contributions . . . 154
6.9. Supplemental Data . . . 155

III. Additional work **165**
Section overview . . . 167
Genetic tools to study sphingolipids in disease . . . 167
The Squeaky Yeast Gets Greased . . . 167
Rapid visualization and quantification of phagocytosis in neutrophils . . . 167
Systematic analysis of the sphingomyelin synthase family in *C. elegans* . . . 167

7. Genetic tools to study sphingolipids in disease **169**
7.1. Abstract . . . 169
7.2. Introduction . . . 170
7.3. Considerations When Ablating Lipid-Metabolizing Enzymes . . . 170
7.4. The Early Sphingolipid Synthesis Cascade . . . 172
7.5. Terminal Branches of the Sphingolipid Synthesis Pathway . . . 174
7.6. SL Degradation and Salvage . . . 175
7.7. Discussion/Conclusion . . . 177
7.8. Contributions . . . 179

8. The Squeaky Yeast Gets Greased **181**
8.1. Abstract . . . 181
8.2. Introduction . . . 182
8.3. The Offense . . . 182
8.4. The Defense . . . 182
8.5. Phagocytosis: The Weapon of Choice . . . 184
8.6. The Phagolysosome: The Final Stage for Eliminating Fungal Pathogens . . . 186
8.7. Conclusions and Perspectives . . . 187
8.8. Funding, Contributions, Acknowledgments, and Conflicts of Interest . . . 189
8.8.1. Funding . . . 189
8.8.2. Contributions . . . 189
8.8.3. Acknowledgements . . . 189
8.8.4. Conflicts of Interest . . . 189

9. Rapid visualization and quantification of phagocytosis in neutrophils **191**
9.1. Abstract . . . 191
9.2. Key words . . . 191
9.3. Introduction . . . 192
9.4. Materials . . . 193
9.5. Methods . . . 193
9.5.1. Differentiation of HL-60 Cells into Granulocytic Neutrophils . . . 193
9.5.2. Immobilization of dHL-60 Cells to Glass-Bottom Plate or Coverslip . . . 194
9.5.3. Phagocytosis of Phagocytic Particles by dHL-60 . . . 194
9.5.4. Fluorescent Cell Staining . . . 194

9.5.5. Image Acquisition . . . 195
9.5.6. Image Analysis (Quantification) . . . 195
9.6. Footnotes . . . 197
9.7. Contributions . . . 199

10. Systematic analysis of the sphingomyelin synthase family in *C. elegans* 201
10.1. Abstract . . . 201
10.2. Introduction . . . 202
10.3. Results . . . 203
10.3.1. Phylogenetic analysis and expression of SMS family members in *C. elegans* . . . 203
10.3.2. *C. elegans* SMS family members display distinct sub-cellular distributions . . . 203
10.3.3. The *C. elegans* SMS family harbors both SM and CPE synthases . . . 205
10.3.4. Lipid profiling of ceSMS-expressing HeLa SMS1/2$^{-/-}$ mutant cells . . . 208
10.3.5. Characterization of *C. elegans* sms mutants . . . 208
10.3.6. *C. elegans* contains at least three distinct SM synthases . . . 211
10.4. Discussion . . . 214
10.5. Materials and Methods . . . 215
10.5.1. Chemicals and antibodies . . . 215
10.5.2. Phylogenetic analysis of SM synthase family . . . 216
10.5.3. DNA constructs . . . 216
10.5.4. Yeast culture . . . 216
10.5.5. Cell culture and transfection . . . 216
10.5.6. Nematode culture . . . 217
10.5.7. Creation of double mutant (ΔceSMSα ΔceSMSβ) . . . 217
10.5.8. RT-PCR . . . 217
10.5.9. Immunofluorescence microscopy . . . 218
10.5.10. Western blotting . . . 218
10.5.11. In vitro enzyme assays . . . 218
10.5.12. Metabolic labeling . . . 219
10.5.13. Lipidomic analysis – sample preparation . . . 219
10.5.14. Lipidomic analysis – LC-MS/MS analysis and lipid identification . . . 219
10.6. Acknowledgements . . . 220
10.7. Contributions . . . 220
10.8. Supplemental materials . . . 221

IV. Final thoughts & future directions 223
Section overview . . . 225

11. Discussion 227
11.1. Are sphingolipids a double-edged sword during *Mtb* infection? . . . 227
11.2. A lipid map of the tug-of-war between *Mtb* and the macrophage . . . 228
11.3. Interacting with the Sphinx: does *Mtb* infection alter the sphingosine interactome? . . . 229
11.4. Thinking forward: . . . 230
11.4.1. Chapter 1 – Does particle size affect the requirement for sphingolipids during phagocytosis? . . . 231
11.4.2. Chapter 2 – Autophagy & a/nSMase: what happens to a chronically-damaged lysosome? . . . 232

11.4.3. Chapter 3 – DG & TG? Lysolipids, Plasmalogens, & Lysoplasmalogens? . . . 234
11.4.4. Chapter 4 – Biological impact of interactions? *Mtb* sphingolipid interactome? 234
11.5. Concluding remarks 239

References **241**

About **295**
Philosophy 295

Certificate of Approval

Foreword

Introduction

This dissertation project lies at the intersection between two understudied fields: host-pathogen interactions and sphingolipids during *Mycobacterium tuberculosis* infection. I have prepared two chapters to introduce the topics and concepts underlying my work.

The first introduction chapter is a historical overview of tuberculosis treatment and sphingolipid research. The second chapter reviews some mechanisms underlying *Mtb* immune subversion and the known connections between sphingolipid biology and TB pathology.

Main Results

In the primary four chapters of this dissertation, I present four independent research projects that sought to answer a specific question about how sphingolipids (or lipids in general) influence the course of an *Mtb* infection. In order, each chapter serves to address the following questions:

1. Do sphingolipids affect *Mtb* entry to a host cell?
2. Do sphingolipids affect the intracellular stage of an _Mtb infection?
3. What changes does an *Mtb*-infection induce in the lipid composition of the cell?
4. What proteins interact with sphingolipids during an *Mtb* infection?

Additional chapters

In addition to these four main chapters, I present four additional chapters that do not fit neatly within the central scope of this work. This includes two reviews and a methods chapter which have already been published. The fourth additional chapter is a research article that we have uploaded to BioRxiv pending review.

Discussion & Conclusion

Finally, I have collated the main findings of this work to consider how they contribute to the search for novel antitubercular therapy. I discuss the open questions remaining in each chapter and the next steps for each avenue of research.

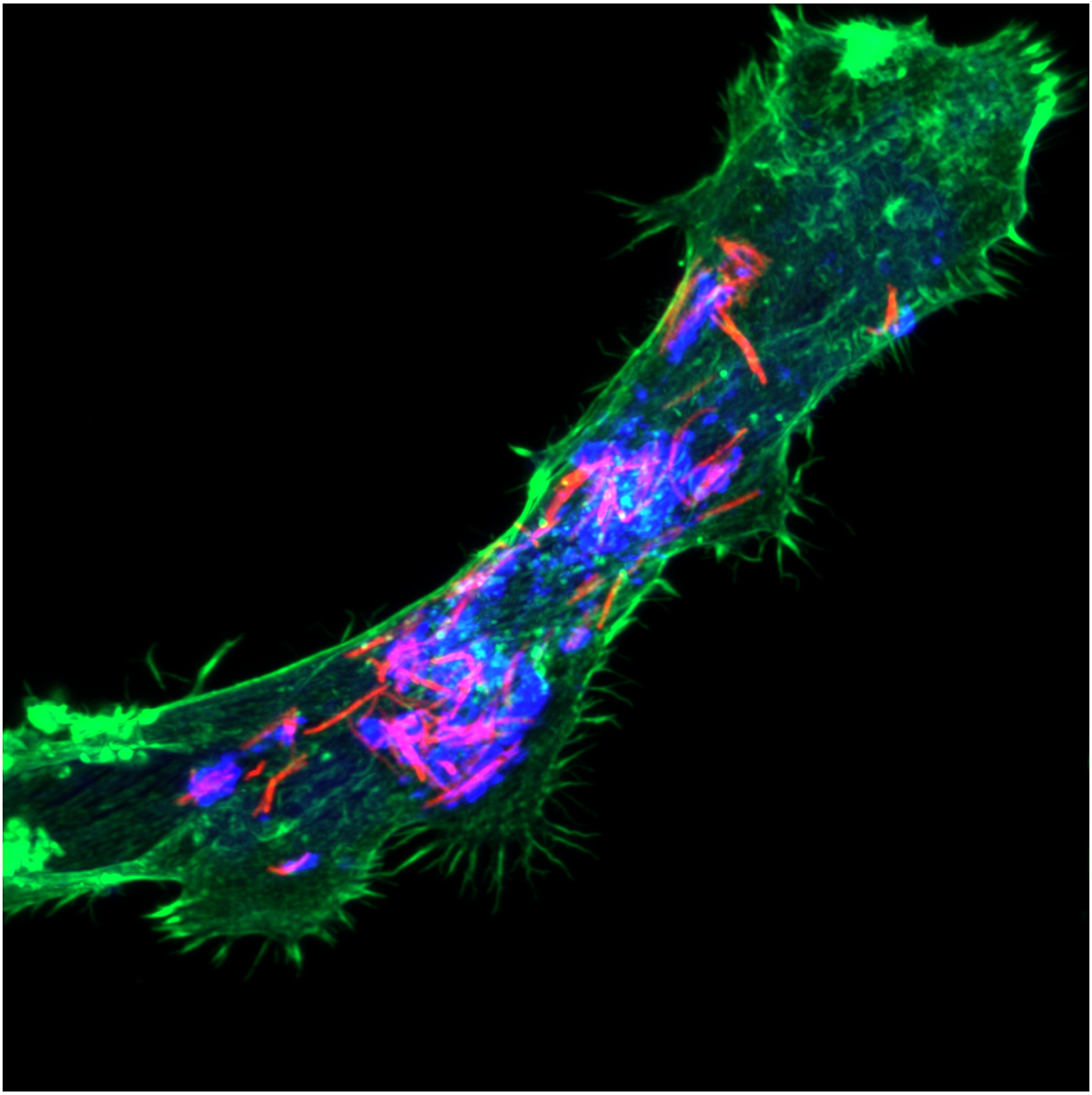


Figure 1. – **A cell heavily infected with *Mycobacterium tuberculosis*.** A THP-1 monocyte-derived macrophage expressing BFP-galectin 3 (Blue) infected with *Mtb* strain H37Rv-dsRed (Red) and stained for its actin cytoskeleton with phalloidin (Green).

Acknowledgements

Thank you, Madeleine, for always believing in me, even when I do not make any sense.

Rich, I cannot begin to thank you for being so willing to drop anything to help me fix my messes when I break things. Someday, I'll learn how to back things up correctly. Lindsey, thank you for discovering your aggressive hate/love for puzzles at the same time as me.

John. Raymond. Kemper. Mootz. One. Brain. One. Brain.

Alexis, your creativity and skills are inspiring. Britt, your creativity and skills are terrifying.

Casey & Ryan, you two bring such light and joy wherever you go. 11/10 marriage officiant. 11/10 cottagecore.

Jossef, you're up next!

Scott & Colleen, I remembered to put my name on this one!

Mom & Dad, I wouldn't be where I am today without the encouragement to learn and ask questions you've always given me. I love you very much.

The Tafesse Lab (current and former)

Fikadu's greatest strength is his capacity to find remarkable people. The Tafesse Lab has been a consistent joy over these years, though many faces have changed around me.

Jules, Tim, Scotty, it's been a wild experience being your labmate for the last six and a half years. I've learned from each of you an inordinate about science and life. Each of you is an astounding scientist and a wonderful friend. Mila and Helene, I will forever need to apologize to you both for being the way I am. Alec, you're a wonderful protégé, it's been fantastic to work with you. Michelle, thanks for the BSL3 jam sessions.



Figure 2. – **Tafesse Lab Logo.** Design by Tephra Bates.

Aidan Anastas
Alec Griffith
Audrey Hinchliff
Helene Jahn, PhD
Judah Evangelista, PhD
Jules Weinstein
Mila Trank Greene
Scotland E. Farley, PhD
Sentayhu Gurmessa, PhD
Teketay Anley, PhD
Timothy Bates, PhD
Xammy Nguyenla

Hans Leier
Ilaria Merutka
Michelle Garcia
Sascha Kuhn
Savannah McBride

Collaborations and facilities

I must also thank several OHSU facilities for their patience and incredible instruction. I utilized the OHSU Flow Core *just* frequently enough that I was only trained three separate times on properly using the flow cytometers in six years (about two years between each visit to the core). I much appreciate the expertise with which the flow core staff helped me rectify my wrongs.

The Advanced Light Microscopy Core felt like my second home, though. I want to thank Dr. Stefanie Kaech Petrie, Dr. Felice Kelly, Dr. Brian Jenkins, and Dr. Hannah Bronstein – each of you has been immeasurably helpful when I had exceedingly dumb questions about microscopy; this dissertation is rife with beautiful images (some of which even support my hypotheses!), and I wouldn't have acquired half as many images of half the quality without your help.

In addition to OHSU-internal facilities, this project has allowed me to work with several groups inside and outside of OHSU – exposure to the collaborative and exciting science I hope to pursue throughout my career. I want to thank Dr. Jennifer Kyle, who heads the Multi-Omics Core at the Pacific Northwest National Laboratory and has always been incredibly generous with her time and expertise – thank you for helping me learn so much about lipidomics these last few years. I would also like to thank Dr. Per Haberkant and Dr. Frank Stein of the European Molecular Biology Laboratory for your expertise in planning, executing, and analyzing our proteomics data – I should say that the experiments that we performed together (see Chapter 6) were the reason that I joined Dr. Tafesse's lab, so thank you for helping me execute on our experiments. Finally, I thank Dr. Schultz for the opportunity to work with you and your group, utilizing your tools and expertise. As stated above, the chance to use the trifunctional lipid probes most sparked my interest in this work.

Other

There are many commercial entities to whom I owe much sanity. Among these are: New Taste of India, purveyor of naan wraps; Adams Peanut Butter, my caloric staple; Trek Bicycle Company, for raffling away bicycles; The Circuit, shredder of tips; Ironman, for parting me from my time and money; and most of all Rancillio for producing a true workhorse of an espresso machine.

Co-authors

Beyond and coinciding with the personal help I've received in completing this dissertation, these projects were remarkably collaborative experiences, and this document encompasses so much work from so many people. I've listed here the people who directly contributed to these works and in which chapters their work can be found.

Table 2. – **Co-authors.** Mostly organized by order of appearance in each chapter.

Author	Affiliation	Chapters of contribution
Fikadu G. Tafesse, PhD	Department of Molecular Microbiology and Immunology, Oregon Health & Science University	Chapter 1, Chapter 2, Chapter 3, Chapter 4, Chapter 5, Chapter 6, Chapter 7, Chapter 8, Chapter 9, Chapter 10
Patrick Niekamp, PhD	Molecular Cell Biology Division, Department of Biology and Chemistry, University of Osnabrück	Chapter 3, Chapter 8
Hans Leier, MD	Department of Molecular Microbiology and Immunology, Oregon Health & Science University	Chapter 3 Chapter 4
Ali Rashidfarrokhi, PhD	Department of Molecular Microbiology and Immunology, Oregon Health & Science University (previously)	Chapter 3
Veronica Richina, PhD	Department of Molecular Microbiology and Immunology, Oregon Health & Science University (previously)	Chapter 3
Joost C.M. Holthuis, PhD	Molecular Cell Biology Division, Department of Biology and Chemistry, University of Osnabrück	Chapter 3, Chapter 8, Chapter 10
Alec Griffith	Department of Molecular Microbiology and Immunology, Oregon Health & Science University	Chapter 4
Mila Trank-Greene	Department of Molecular Microbiology and Immunology, Oregon Health & Science University	Chapter 4
Lisa Bramer, PhD	Integrative Omics Core, Pacific Northwest National Laboratories	Chapter 5, Chapter 10
Jennifer Kyle, PhD	Integrative Omics Core, Pacific Northwest National Laboratories	Chapter 5, Chapter 10
Scotland E. Farley, PhD	Department of Molecular Microbiology and Immunology, Oregon Health & Science University	Chapter 6, Chapter 7
Carsten Schultz, PhD	Department of Chemical Physiology and Biochemistry, Oregon Health & Science University	Chapter 6

Author	Affiliation	Chapters of contribution
Frank Stein, PhD	Proteomics Core Facility, European Molecular Biology Laboratory, Heidelberg, Germany	Chapter 6
Per Haberkant, PhD	Proteomics Core Facility, European Molecular Biology Laboratory, Heidelberg, Germany	Chapter 6
Cameron Creek	Department of Molecular Microbiology and Immunology, Oregon Health & Science University (previously)	Chapter 7

Glossary

Immunology and bacteriology terms

- TB – tuberculosis disease, a deadly lung infection caused by the bacterium *Mycobacterium tuberculosis*.
- *Mtb – Mycobacterium tuberculosis*.
- HDT – Host-directed therapy, a form of potential antitubercular treatment that seeks to reduce the permissivity of a patient as a host for *Mtb* Infection.
- WHO – The World Health Organization.
- DAMP/PAMP – Damage- or Pathogen-Associated Molecular Patterns, signatures of cell distress that trigger immune response.
- PRR – Pathogen Recognition Receptors, proteins that recognize PAMPs and DAMPs. Some are expressed in every cell type, others are solely expressed on immune cells.
- IFN-γ – Interferon-γ or Type II interferon, an inflammatory cytokine that stimulates/modulates a wide array of immune responses.
- BCG – Bacillus Calmette-Guerin, the strain of *M. bovis* widely used as a vaccine against TB.
- H37Rv – A clinical strain of pathogenic *Mtb* originally isolated in 1905, the most common laboratory strain in TB research.
- H37Rv-ΔRD1 – An attenuated mutant strain of H37Rv that lacks several crucial pathogenicity factors.

Sphingolipid terms

- SPT – Serine palmitoyltransferase, the first step in sphingolipid synthesis
- Spa/KDS – Sphinganine or 3-ketodihydrosphingosine, the sphingolipid precursor
- Cer – Ceramide
- CerS – Ceramide synthase
- CERT – Ceramide transfer protein
- SM – Sphingomyelin
- SMS – Sphingomyelin synthase
- a/nSMase – acid/neutral Sphingomyelinase

- GlcCer – Glucosylceramide
- GSL – Glycosphingolipid (a broad term encompassing many hundreds of distinct lipids)
- Sph – Sphingosine
- S1P – Sphingosine 1-phosphate
- LSD – Lysosomal storage disorder
- ERT – Enzyme replacement therapy

Non-sphingolipid Lipids

- PI – Phosphatidylinositol
- PE – Phosphatidylethanolamine
- PS – Phosphatidylserine
- PG – Phosphatidylglycerol
- PC – Phosphatidylcholine
- DG – Diacylglycerol (also diglyceride)
- TG – Triacylglycerol (also triglyceride)
- Chol/CE – Cholesterol/Cholesteryl esters
- CL – Cardiolipin

Lipid nomenclature

“Molecular lipid species” are annotated with the following formula: AA(BB:CC/DD:EE)

- AA = the lipid headgroup/core structure (e.g., phosphatidylcholine (PC), diacylglyceride (DG))
- BB = the number of carbons in the first fatty acyl chain.
- CC = the number of unsaturations in the first fatty acyl chain.
- DD = the number of carbons in the second fatty acyl chains.
- EE = the number of unsaturations in the second fatty acyl chains.

Note: “Lipid species” annotation encompasses less detail, summarizing the total number of carbons in the acyl chains and the total number of unsaturations (e.g., TG(56:5))

Methods, techniques, & miscellaneous

Compounds & methods

- Myr – Myriocin, an inhibitor of the serine palmitoyltransferase complex (SPT, see above). Thereby blocks the production of all sphingolipids.
- FB1 – Fumonisin B1, an inhibitor of all ceramide synthases (CerS, see above). Thereby blocks the production of ceramide and all higher sphingolipids.
- PMA – Phorbol 21-myristate 13-acetate, a synthetic diacylglycerol that stimulates monocytes to differentiate into macrophages.
- LLOME – Leucine-leucine dimethyl ester, a compound that selectively causes membrane damage within the lysosome.
- MOI – Multiplicity of infection, the ratio between the desired number of bacteria to infect a given number of target host cells.
- CFU – Colony-forming units, a measure of the number of viable bacteria in a solution.

Techniques

- TLC – Thin-layer chromatography, a technique for visualizing lipids
- LC-MS/MS – Liquid chromatography with tandem mass spectrometry, an analytical technique for determining the molecular composition of a sample.
- PUFA – **P**oly**u**nsaturated **f**atty **a**cid, a term used in lipidomics analysis to denote identified lipids with multiple unsaturated carbon bonds.
- TMT – Tandem Mass Tags, a technique for quantitative proteomics by which mass tags are added to peptides to trace their relative abundance between samples.
- CRISPR – "Clustered regularly interspaced short palindromic repeats," a technique for introducing double-strand breaks into a selected gene site; enables mutagenesis and knockout of a target gene.

Cellular anatomy & Microscopy

- PM – Plasma membrane
- ER – Endoplasmic reticulum
- EE - Early endosomes
- LE – Late endosome
- EEA1 – Early endosome antigen 1
- LAMP1 – Lysosome-associated membrane protein 1

- DAPI – 4□,6-diamidino-2-phenylindole, a fluorescent DNA stain that enables visualization of the nucleus.
- GFP/BFP/RFP – Green/Blue/Red fluorescent protein, small fluorescent protein domains which can (among other things) be genetically fused to target proteins to visualize localization of the target protein.

Part I.

Introduction: TB and the Sphinx

Section overview

In the following two chapters, I will give the reader the necessary context and background to understand the topics discussed in the main results chapters.

Introduction Part 1

Because the main body of this dissertation will be technical descriptions of my contributions to science, I have strived to make the first introductory chapter as accessible as possible. We will first talk about the bacteria *Mycobacterium tuberculosis* and why we care about it still. We will then give a 10,000-foot view of lipids and why sphingolipids are the most exciting category.

Introduction Part 2

The second introductory chapter partially starts over but is more technical. We will discuss some of the ways that *Mycobacterium tuberculosis* overcomes the human immune defenses to establish infection and how host lipids are known to influence infection. We will then discuss in greater detail the synthesis and biological roles of sphingolipids in mammalian cells. We will finally discuss some of the unique challenges of studying lipids and the tools that allowed us to overcome these challenges.

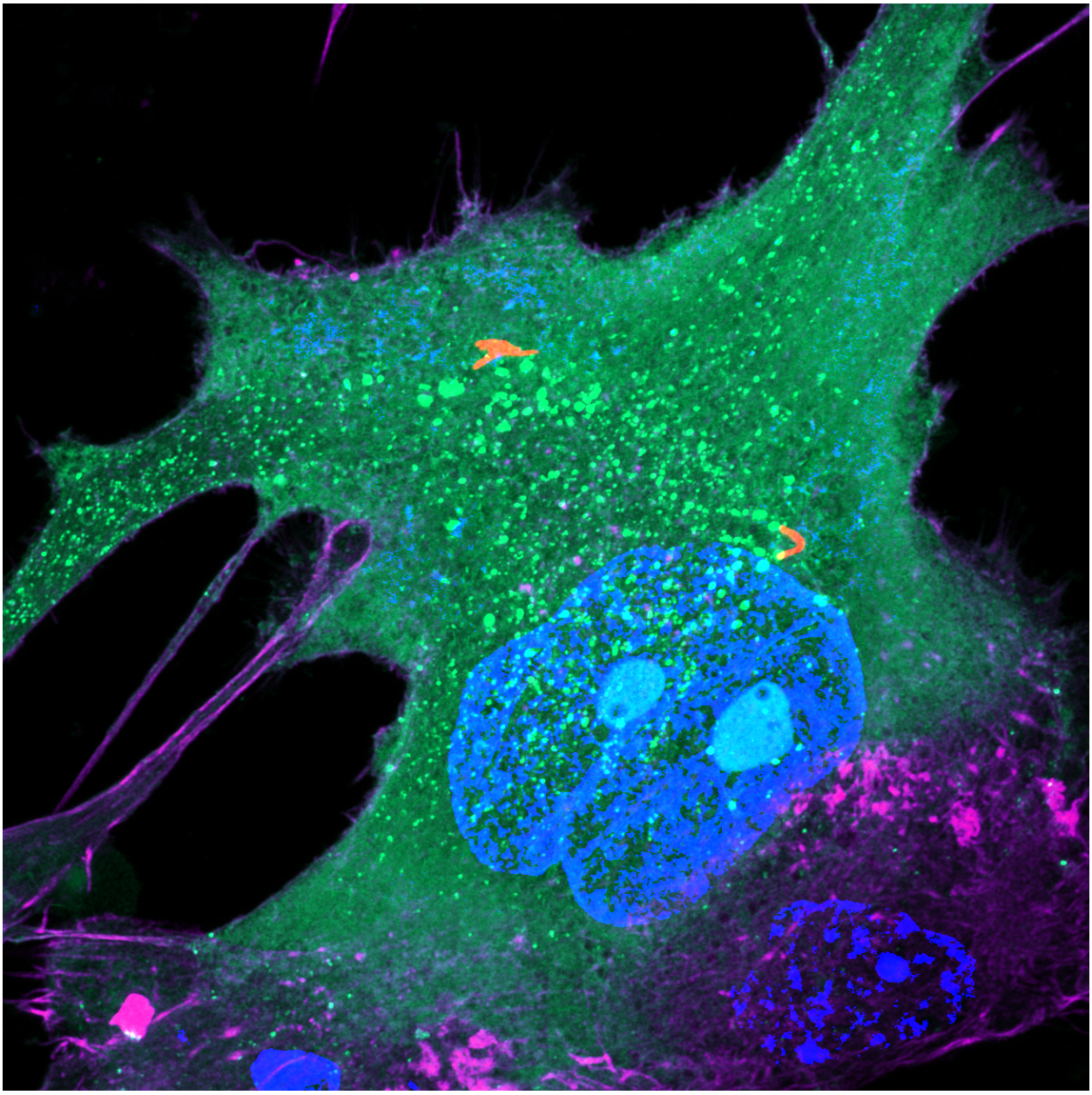


Figure 3. – ***Mycobacterium tuberculosis* infecting a human macrophage.** A THP-1 monocyte-derived macrophage expressing mAG-galectin 3 (Green) infected with *Mtb* strain H37Rv-dsRed (Red) and stained for its plasma membrane with CellMask (Magenta) and its nucleus with DAPI (Blue).

Chapter 1.

Introduction Part 1

Authors: Gaelen Guzman[1], Fikadu G. Tafesse[1,*]

[1] = Department of Molecular Microbiology and Immunology, Oregon Health & Science University, Portland, Oregon, USA. [*] = corresponding author: tafesse@ohsu.edu

1.1. Abstract

This chapter explores the devastating illness of tuberculosis (TB) and the growing interest in host-directed therapy (HDT) as a potential avenue for novel anti-TB therapies. We aim to convey how one niche class of human lipids, sphingolipids, may affect the course of a *Mycobacterium tuberculosis* (*Mtb*) infection. We introduce TB, its historical context, and the evolution of mycobacteria alongside humans. We also introduce the crucial and enigmatic roles of sphingolipids throughout human biology and how they may present novel ways of treating TB infections. These historical contexts are essential for a deeper discussion on the interplay between *Mtb* infection and the lipids in the host cell. Further, it is necessary for individuals attempting to discover potential tuberculosis treatments to consider the disease's historical background. A low-cost, effective therapy is a crucial first step in rectifying the long-standing systemic injustices of tuberculosis treatment.

1.2. Introduction

Tuberculosis (TB) is a devastating illness. The annual WHO Global TB Report estimates that 2 billion people currently host a latent TB infection and that there were 9 million new cases of active TB disease in 2022[1]. In 2022 alone, 1.3 million people died from TB disease – it ranks 14th among overall causes of death worldwide. It is the 2nd leading cause of infectious death worldwide (trailing just behind COVID for the third year running)[1]. Historical estimates suggest that TB has killed more humans than any other infectious disease[2].

In the search for novel anti-TB therapies, there is growing interest in host-directed therapy (HDT), which seeks to synergize with frontline antibiotics by altering the host conditions – making us a less hospitable host – and re-sensitizing the bacteria to antibiotic therapy. Before modern medicine can accomplish this, basic research is needed to understand how *Mtb* interacts with us as a host organism. As discussed below (and in nearly every chapter of this work), Mtb's reliance on host lipids may be an ideal avenue for HDT.

The overarching goal of this dissertation is to understand how one niche class of human lipids affects the course of a *Mtb* infection. These enigmatic lipids are the sphingolipids, which play essential roles throughout human biology: they are crucial in enabling neuronal activity, maintaining membrane integrity, and regulating cellular decisions between life and death, among many other roles throughout the cell.

We have prepared this introduction to the introduction to bridge a gap between the scientific and non-scientific audiences who may read this dissertation. Historical context often needs to be improved in the academic discourse. It provides an excellent point to jump into a more detailed molecular description of sphingolipids during *Mycobacterium tuberculosis* infection.

1.3. *Mycobacterium tuberculosis*: an ancient pathogen

Sometimes called the "White Plague" (in contrast to the Black Death), TB is estimated to have killed one billion humans over the last two centuries[1]. Pulmonary tuberculosis (TB) is a lung infection caused by a family of bacteria called *Mycobacterium*. While *Mycobacterium tuberculosis* (*Mtb*) causes the vast majority of TB in humans today, other *Mycobacterium* species such as *M. bovis*, *M. canettii*, and *M. africanum* can cause similar illnesses in immunocompromised humans and non-human animals.

Mycobacteria have evolved alongside humans for tens of thousands of years – paleopathology studies have shown that TB disease in humans has existed since at least the Neolithic age 70,000 years ago[3]. *Mycobacterial* molecular signatures (chiefly DNA) have been found in the lungs of ancient Egyptian mummies[4]. Ancient Greek medical literature written by Hippocrates and Soranus of Ephesus vividly describe clinical cases of TB in language still applicable to modern TB infections[5,6].

> "There is a latent fever which generally begins towards the end of the day and is relieved with the coming of the new day; this is accompanied by much coughing at the beginning and the end of the night, with the discharge of sanious sputa. The sputa are at first bright red, then muddy, then bluish or greenish and finally white and purulent, and either sweet or salt. The voice is either hoarse or high pitched, breathing difficult, cheeks flushed and the rest of the body, ashen colored. The patient is emaciated. In some cases there is a

hissing sound or wheezing in the chest; and, as the disease spreads, there is sweating in the upper parts down to the end of the chest. There is a loss of appetite for food. Sometimes there is a feeling of heaviness in the ravaged lung and the patient spits up fiber of it; sometimes there is a stabbing pain due to the ulceration within the chest. The pulse is weak and thick; the tops of the fingers become thick and there is a hooking of the nails. The feet swell up."

Soranus of Ephesus, ~200 B.C.



Figure 1.1. – **Death points an arrow at a female dancer.** Aquatint by J. Gleadah, 1822. Wellcome Collection. Public Domain Mark. Source: Wellcome Collection.

The disease has been so pervasive throughout history that it influenced art and beauty standards(Figure 1.1)[7,8]. "Consumptives" in the early stages of TB disease are marked by a pale pallor and flushed cheeks, weight loss, and chronic cough – dovetailing neatly with the Victorian feminine ideal: corseted waist, domestic, and frail[7]. In her 2017 book, -Consumptive Chic: A History of Beauty, Fashion, and Disease-, Carolyn A. Day writes: "Tuberculosis and its accompanying symptoms were construed as the physical manifestation of an inner passion and drive. It was the outward sign of genius and fervour that literally lit the individual, providing the pallid cheek with a glow"[9].

"Consumption, I am aware, is a flattering malady."

Charlotte Brontë, 1849

Despite these aesthetic "boons" and long co-evolution, tuberculosis is a devastating disease that was a nearly guaranteed death sentence for much of human history[10]. Some estimates suggest that over

1 billion humans have died from this bacterial infection. Over the millennia, TB treatment has taken many forms, as will be discussed below.

1.4. Galenic humors to Koch's postulate: A long history of TB therapy

The Greek doctor Galen of Pergamon theorized that the human body contained four "humors": phlegm, blood, yellow bile, and black bile[11]. In addition to his advances in anatomical research, patient care, and sanitation, his humoral theory hypothesized that it was the balance of these four essential liquids that defined health – and in disease, a physician must remove the excess humor via bloodletting or purgative (a concoction that induces vomiting)[12]. Alongside this model of disease was that of the "miasma," which postulated rank and odorous "bad air" conferred that illness. It was in this context that the Romans prescribed a combined therapy of rich foods (milk, cheese, wine, and the like) and a change of air (long sea voyages and high-altitude escapes)[13]. However, through the 19th century, it was broadly accepted that there was no actual cure for the consumption. There was merely the temporary relief of symptoms. In many ways, the length of a consumptive's life following diagnosis aligned to the size of their bank account and social stature: Was the disease discovered early? Could they afford to travel to exotic locales? Could they maintain this lavish, fatty diet[10]?

The essential components of Greek and Roman TB therapy were maintained as the standard of care through the early 20th century. However, the advent of the sanatorium (a specialized hospital for TB patients) significantly improved the TB therapy paradigm. The first sanatorium facility was formally opened in 1854 by Hermann Brehmer at his sister-in-law's hydropathic spa in Görbersdorf in Silesia (then part of Prussia, now Sokołowsko, Poland)[14–16]. Using Brehmer's example, many notable sanatoria were established over the subsequent century, including the Sanatorium Turban in Davos, Switzerland, the Adirondack Cottage Sanatarium in Sanarac, New York, and the Oregon University Tuberculosis Hospital on Marquam Hill in Portland, Oregon. The University State Tuberculosis Hospital is now the Campus Services Building on the Oregon Health & Science University campus[17].

According to contemporary wisdom, these sanatoria provided three primary benefits:

1. Rarefaction of the air – which stimulated deep breathing.
2. Purification of the air – which rid the patient of miasmas.
3. Infrigidation of the air – which was believed to have an antiseptic effect[14].

The typical treatment regimen consisted of exercise (some practitioners believed in leisurely exercise to stimulate blood flow to the lungs, while others believed in militaristic exercise to build character) and long "air rests" in reclined chairs and solariums. We can thank the sanatorium for the popularity of the Adirondack chair: these "cure chairs" were believed to be an essential component of the sanatorium panacea[18,19]. The patients typically received abundant, rich diets consisting of milk, cheese, butter, fatty meats, and wine[10,14,20]. However, sanatoria regimens were rarely thoroughly relaxing experiences. Sanatoria often employed patients in manual labor to strengthen their character and bodies and prepare them to reintegrate into society[21].

The medical establishment of the late 19th and early 20th centuries embraced the sanatorium. Murray describes that the first American sanatorium was founded in 1875[22]. By 1904, there were 115



Figure 1.2. – **University State Tuberculosis Hospital** Black and white photograph of the University State Tuberculosis Hospital on Marquam Hill, Portland, Oregon. Date: 1953. By the University of Oregon Medical School. CC: OHSU Digital Collections[17].



Figure 1.3. – TB patients receive "open air" therapy in the Harlow Wood Orthopaedic Hospital in Nottinghamshire, England Photo by Harry Shepherd/Fox Photos/Getty Images Source: TRVL Channel

across America, and by 1952, there were 839 sanatoria in the US[22]. The true impact of the sanatorium on a patient's outcome is somewhat unclear, though certainly better than no treatment at all. For certain forms of TB pathology (namely laryngeal tuberculosis), the success of sanatorium treatment was relatively high, and researchers at the time lauded the effectiveness of the sanatorium regimen[23]:

> To be able to change certain disaster to relative or complete recovery by a little skilful (sic.) interference is such a satisfaction that the treatment of laryngeal tuberculosis in sanatoria deserves every consideration.
>
> Parfit, The Treatment of Laryngeal Tuberculosis in Sanatoria, 1926[23]

Other reports also support that the sanatorium regimen did excellently combat the primary symptoms of TB – the cough and sputum, color and wasting, night sweats and fever – all faded within weeks[10]. However, we must note that many sanatoria only accepted patients of upper-class society – and only those with fair prognoses at that. The "hopeless cases" were excluded from treatment[10]. Even given these idealized conditions, one survey found that of 1707 admitted to the King Edward VII Sanatorium in Sussex between 1907 and 1914, 751 had died by 1916 – a 44% mortality rate[10,24].

Contemporary media held some suspicion toward the sanatorium. In the 1906 George Bernard Shaw stage play, *The Doctor's Dilemma*, a character altercates with a doctor about medicine at the time:

> "RIDGEON. I know nothing about smallpox. My line is tuberculosis and typhoid and plague. But of course the principle of all vaccines is the same.
>
> SIR PATRICK. Tuberculosis? M-m-m-m! You've found out how to cure consumption, eh?
>
> RIDGEON. I believe so.
>
> SIR PATRICK. Ah yes. It's very interesting. What is it the old cardinal says in Browning's play? "I have known four and twenty leaders of revolt." Well, I've known over thirty men that found out how to cure consumption. Why do people go on dying of it, Colly? Devilment, I suppose. There was my father's old friend George Boddington of Sutton Coldfield. He discovered the open-air cure in eighteen-forty. He was ruined and driven out of his practice for only opening the windows; and now we won't let a consumptive patient have as much as a roof over his head. Oh, it's very, VERY interesting to an old man."
>
> George Bernard Shaw, The Doctor's Dilemma, 1906

Despite these misgivings, groundbreaking TB research was performed at sanatoria, driving infectious disease medicine toward one historically crucial understanding: that diseases such as tuberculosis spread as a contagion – not the product of breathing miasmas or having too-lively a spirit. In 1720, Benjamin Martin published the first clue that TB may disperse via a specific, mysterious "animalcule" infecting the lung[25,26]. This hypothesis was largely ignored until 168 years later when Robert Koch experimentally verified this in his seminal 1888 work *The Etiology of Tuberculosis*[27]. Shortly after this publication, he would propose the now-famous Koch postulates. These are the gold-standard experimental criteria for establishing that certain microbes cause specific diseases. It was at this point that campaigns for public knowledge about TB and its cause began, greatly aiding in limiting the spread of TB in North America and Europe (Figure 1.4)[2].



Figure 1.4. – **Christmas Seals poster, 1919.** Photo: Library of Congress[28]

The sanatorium would only begin to decline once the mass production of antibiotics in the 1930s. The history of anti-tubercular therapies was summarized by Iseman in 2002[29] with the following timeline:

Table 1.1. – Advances in TB antibiotic therapy.

1928	Discovery of penicillin (not effective on *Mtb* but induced a paradigm shift in treating bacterial infections).
1944	Discovery of first anti-tubercular antibiotics: streptomycin and para-aminosalicylic acid.
1952	Roll-out of first therapeutic cocktail: 18-month "triple therapy," consisting of streptomycin, para-aminosalicylic acid, and isoniazid.
1970s	9-month course of isoniazid and rifampicin.
1980s	6-month course of isoniazid, rifampicin, and pyrazinamide.
2020s	6-9 month course of isoniazid, rifampicin, pyrazinamide, and ethambutol (RIPE) or 4-month course of rifapentine-moxifloxacin, depending on the drug susceptibility of the *Mtb* strain and toxicity of drugs in the individual patient[30,31].

Currently, the success rate of standard anti-tubercular treatment is impressively high, with total bacterial clearance in about 88% of drug-susceptible cases[1]. However, recent years have seen a rise in antibiotic-resistant strains of *Mtb*, threatening the future of these highly effective therapies. The WHO reports that an estimated 410,000 cases of rifampicin-resistant or multi-drug-resistant TB arose in 2022[1]. Numerous reports have shown that prisons in Post-Soviet states (e.g., Russia, Latvia, Azerbaijan) have rates of multi-drug resistant *Mtb* approaching 16 times those of other countries, warranting a coordinated, multi-national response to limit the spread of these strains[32–34].

Given these multi-drug resistant strains, many fundamental biological questions remain about *Mycobacterium tuberculosis* before improved therapies may be developed. We will discuss these below, but first, we must address a critical feature of the history of tuberculosis treatment: structural discrimination and racism.

1.5. TB, racism, & inequity: an intertwined history

It is impossible to discuss TB epidemiology without addressing systemic inequity in the medical establishment. Tuberculosis has long been and remains to this day a disease of poverty and discrimination. Even in the most literal sense, colonialism drove the spread of tuberculosis: Brynildsrud et al. used genetic lineage mapping to show that colonialist expansion repeatedly expanded the global spread of pathogenic *Mtb* strains[35]. Beyond this literal sense, the history of TB treatment is rife with systemic discrimination.

Sanatoria were indisputably tools of segregation, discrimination, and colonialism. Many reports on systematic discrimination have been published in recent years. In one such report, Smith et al. extensively review discrimination in Canadian sanatoria in their 2021 book *Tuberculosis Stigma and Racism, Colonialism, and Migration: A Rapid Qualitative Review*[36]. They write that TB was merely one facet of colonialist violence employed against the native populations of Canada. Even while medical institutions would dismiss symptoms and delay TB diagnosis, medical institutions would strictly enforce the separation of TB-infected indigenous people from their communities in manners strikingly similar to the practice of residential schooling. Bennett of the Canadian Broadcasting Company writes about the shipping of hundreds of Inuit TB patients to the Sanatorium on the Mountain in Hamilton, Ontario[37]:

> "The evacuation split families, left parents and children wondering about their loved one's fate, sometimes for years. Some died and were buried without their families knowledge; others were sent from hospital to hospital without being tracked."
>
> Shawn Selway, quoted by Bennett in 2016, Source: CBC News

As Bennett notes in their 2016 article, the mass transfer of Inuit to the Hamilton Sanatorium occurred primarily between the 1940s and the 1960s, following the roll-out of antibiotic therapy. These new therapies rapidly emptied the Hamilton Sanatorium's 700 beds of white patronage. This general departure provided a unique opportunity for enforced migration and assimilation. In 2016, the CBC also reported the story of a family's 50-year search for a lost daughter's grave[38]. Marieyvonne Alaka died of tuberculosis meningitis (one example of an extra-pulmonary TB infection). Officials buried Alaka's remains without record after transferring her between multiple medical facilities. She was just one child forcibly removed from her family among hundreds of indigenous children lost within the Canadian medical system in the mid-1900s.

The inequity seeded by Canadian tuberculosis policy for the Inuit people is deeply rooted and continues into the current era. In 2017, LaFreniere et al. found that the incidence rate of TB disease in Inuit communities was 205.8 cases per 100,000[39]. In contrast, the national rate was 4.9 cases per 100,000[39]. A 2021 financial analysis by Uppal et al. examined data reported by the Quebec Ministry for Health and Social Services – they found that the 2019 TB incidence rate was 495 cases per 100,000 in the Nunavik community in Northern Quebec[40]. Uppal et al. further examined the cost-effectiveness of TB screening. They showed that one-off rounds of community screening for TB disease can reduce incidence rates in a community by 13%, and biennial screening could reduce incidence by up to 59%[40]. These relatively low screening frequencies were substantially more cost-effective than having no screening programs at all[40].

Of course, framing these numbers as financially cost-effective dehumanizes the members of these communities as they seek medical attention. However, such reports are crucial first steps toward equitable models of TB treatment and undoing historical injustice. In this, the Canadian government has pledged to take action. In 2019, Canadian Prime Minister Justin Trudeau formally apologized to the Inuit people for the 20th-century tuberculosis policies and promised to rectify the harm done. The Inuit Tuberculosis Elimination Framework, established in 2018, seeks to abolish TB in the Inuit populace by 2030[41,42].

> "For too long, the government's relationship with Inuit was one of double standards, and of unfair, unequal treatment … While the government was hard at work creating universal healthcare, it was forcing Inuit into settlements where disease and infection ran rampant. … Today, I'm here to offer an official apology for the federal government's management of tuberculosis in the Arctic from the 1940s to the 1960s."
>
> Speech by Justin Trudeau, 2019. Full text[41].

Of course, Canada is not alone in historically discriminatory tuberculosis policies. Connolly and Gibson reviewed in 2011 the role that race had in TB disparity in the US between 1900 and 1935[43]. They cite the 1915 US Census Bureau's national tuberculosis incidence data, which reported that 23 white children per 100,000 died of TB, while the rate among non-white children was 155 per 100,000 – nearly a seven-fold increase[43]. They write of a 1918 tax passed in Virginia to fund a whites-only Sanatarium in the Blue Ridge Mountains to add to the already-existing "whites-only" Roanoke Catawba Sanatarium. The "colored" Piedmont Sanatorium in Burkeville, VA, was only one

of four facilities in the south that would offer beds to black TB patients and charged a two-dollar-a-night fee[43]. Connolly and Gibson write that the main sentiment for offering a sanatorium to black TB patients was to limit the potential to infect whites[43].

These disparities still exist in the US today, even as the rate of TB incidence has substantially reduced. As reported by Schildknect et al., there were fewer than 2500 cases of TB among US-born citizens in 2022 – 30% of these patients were identified as Black, 26% as Hispanic, and 25% as White[44]. The incidence rates for Black US-born citizens is 1.9 (cases per 100,000), for Hispanic US-born citizens is 1.4, and for White US-born citizens is 0.3[45]. The TB incidence among American Indian or Alaskan Native people is 4.4 cases per 100,000 – over 14-times higher than that of White US-born citizens[45]. Among Native Hawaiian and other Pacific Islander US-born citizens, the TB incidence rate is 6.6 per 100,000[45]. As in Canada, much work remains to rectify the inequitable health disparities among minority populations in the US.

Countless examples of systematic racism and colonialist violence in TB treatment exist, and we cannot adequately summarize the scope of this injustice here. However, we must note that modern-day epidemiology continues to follow global trends in poverty and post-colonialism. The 2023 Global Tuberculosis Report by the WHO reports that[1]. They find that the top eight countries with the highest numbers of total TB cases are all previously colonized nations, amassing over two-thirds of the total cases globally: India (27% of global cases), Indonesia (10%), China (7.1%), the Philippines (7.0%), Pakistan (5.7%), Nigeria (4.5%), Bangladesh (3.6%) and the Democratic Republic of the Congo (3.0%)[1]. In the same report, the WHO cites that, globally, 50% of all TB patients will incur catastrophic costs for their treatment[1] – demonstrating that there is a massive need for reduced cost of treatment for individuals. As will be discussed further below, the most significant risk factors for TB incidence all increase with poverty.

1.6. *Mycobacterium tuberculosis* today: questions, challenges, and goals

With the increasing prevalence of antibiotic-resistant *Mtb* strains, many essential open questions about TB disease exist. Chief among these includes: Why do some people with latent TB infections go on to get sick and others do not? How does TB so effectively elude treatment? Are there mechanisms we can use to prevent the onset of infection? We will address some of these questions below. Still, these questions have stood for years, decades, and centuries – the existence of these questions drove much of the research in this dissertation project.

A profound distinction lies between a latent TB infection and an active TB infection. The WHO reports that less than 5% of incipient *Mtb* infections will go on to produce active disease within two years[1]. The WHO identified five major risk factors for developing active TB disease (Table 1.2).

Table 1.2. – **Major risk factors for active TB disease onset**

Risk Factor	# of directly attributable cases (% of total incident cases)	Source
Undernourishment	~2.2 million (21%)	[46,47]
HIV Infection	~0.8 million (7.5%)	[48]
Alcohol use disorder	~0.6 million (5.6%)	[49]

Risk Factor	# of directly attributable cases (% of total incident cases)	Source
Smoking	~0.5 million (4.7%)	[1]
Diabetes mellitus	~0.4 million (3.8%)	[50]

In addition, ongoing conflicts, poverty, food and energy insecurity, and the long-term effects of the COVID-19 pandemic indirectly contribute to many more cases.

In observing the list of primary TB risk factors, one may note that many of these factors are known to impose harmful effects on the human immune system. We must emphasize that "hosting a latent TB infection" is no passive state: every *Mtb*-infected person is waging a war kept at a stalemate for months or years. The human immune system has adapted to fight off most bacterial pathogens we experience daily. It is usually sufficient to destroy and repel would-be invaders. However, *Mtb* has selectively utilized humans as hosts for millennia, thereby developing a bristling arsenal of molecular tools that block or subvert our typical immune control measures. The above risk factors appear to tip the balance towards -Mtb-. However, it is essential to note that in parallel to -Mtb- acquiring these pathogenic tools, the millennia have allowed humans to develop immune mechanisms to restrict tuberculosis disease progression.

The tug-of-war between bacteria and the immune system allows a latent tuberculosis infection to go unnoticed for months or years in an immunocompetent host: structures called granulomas sequester the bacteria and prevent their dissemination throughout the lung. These structures are composed of immune cells recruited to the site of infection and prevent the bacteria from disseminating throughout the lung. In this encapsulated space, immune cells release anti-microbial factors and inflammatory molecules restricting the bacteria's growth. Researchers have shown that in some – perhaps many – immunocompetent patients will spontaneously clear an *Mtb* infection[51,52].

Ironically, though, many of the cells recruited to the granuloma are also ideal hosts for *Mtb*. These cells can become infected and sustain the bacterial population within the granuloma[53]. Confusingly, individual granulomas within a single host can lie along a spectrum of *Mtb* burden. Gideon et al. investigated the range of *Mtb* burdens within individual granulomas in individual macaques. They found that, within one animal, some granulomas may have no living bacteria and will soon heal; in contrast, other granulomas can host thousands of bacteria and show signs of immune failure[52]. Thus, each granuloma is a disputed battleground in a precarious balance. Any risk factor listed in Table 1.2 above can tip the balance toward active TB disease. Additionally, immunocompromising events such as HIV, chemotherapy, or organ transplant can significantly reduce an individual's ability to fight a latent TB infection and have high co-mortality with TB.

Because the immune system is essential for restricting active TB disease, many studies have sought to prepare an effective vaccine against *Mtb* to improve the host response. Robert Koch, the discoverer of the *Mycobacterium tuberculosis* bacillus, produced the first anti-TB vaccine. He found that a glycerol extraction of cultured *Mycobacterium tuberculosis* produced a substance, tuberculin, that had a meager ability to immunize against infection. However, tuberculin's ineffectiveness (a rate of protection less than 5%) and irreproducibility (he kept the formulation of this extract secret for a suspiciously long time) would lead to the end of Koch's career[54,55]. The current *Mtb* vaccine, Bacillus Calmette-Guerin (BCG), is a live attenuated form of *Mycobacterium bovis*, and has been in use since 1921 and has been widely administered to approximately 5 billion people[29,56]. The BCG vaccine is estimated to have saved tens of millions of lives[55]. However, its effectiveness leaves much room

for improvement: it is somewhat effective in lessening TB disease in children (~50%), though it has nearly no effect in adults[29]. There are many ongoing efforts to improve this vaccine to prevent disease onset. However, these efforts face many nuanced challenges, discussed at length by Zhang et al. and others[57].

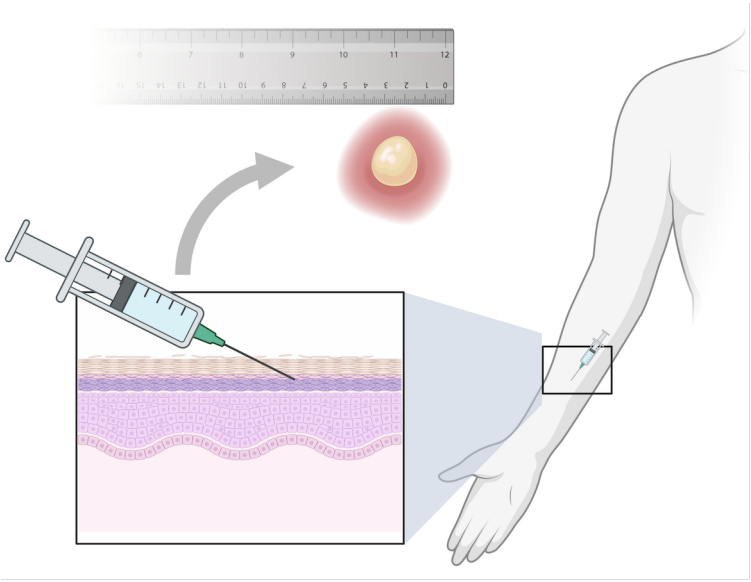


Figure 1.5. – **The tuberculin skin test** Despite its failure as a TB vaccine, Koch's tuberculin was used extensively as a front-line tuberculosis screening tool until the late 1960s. Today the antigen mixture has been refined for greater reliability – relying more on purified protein derivatives now than a total glycerin extraction – but the procedure is fundamentally similar. A small quantity of *Mtb* antigen is injected between the epidermis and dermis, and the resulting recruitment of immune cells causes a red welt to appear over the course of several days. The size of the welt correlates with potential disease – in general, a test is considered positive if the welt is > 15 mm in diameter (if the patient has no other risk factors for tuberculosis).

A growing interest in the TB field is in applying so-called host-directed therapies (HDT). The goal of HDT is to indirectly affect *Mtb*'s survival within an infected patient by altering the patient's biochemistry to make them a less hospitable host. Many authors have described in detail various possible avenues of HDT in *Mtb*[58–60]. In one recent example, Dutta et al. show that in *Mtb*-infected mice, cholesterol-reducing statins synergized with antibiotic therapy and cleared the *Mtb* at a significantly enhanced rate. Clinical trials are ongoing to assess the effect of statins on human *Mtb* infections.

1.7. The lipid connection

Mycobacterium tuberculosis is an intracellular pathogen. Within the lung space, it infects host cells in a Trojan Horse-style infection, allowing itself to be ingested by immune cells called alveolar macrophages (macrophage translates to "big eater" in Greek). These cells are typically the first line of defense against a would-be pathogen. However, *Mtb* reprograms the macrophage and turns it into a suitable host for replication. Accordingly, many have described *Mtb* as a "master manipulator" of host biology[61,62].

As a pathogen living within host cells, *Mtb* must acquire all its nutrients and implement all its machinations through lipid membranes. *Mtb* appears to be highly attuned to host lipid biology, leading to new potential routes of antitubercular therapy.

In this chapter and the next, we will extensively discuss the intricate ties between host lipid biology and an infecting *Mtb* bacillus. First, though, we have to step back to look at what lipids are.

1.7.0.1. So what is a lipid?

Lipids are one of the main four macromolecules in biology. We will describe these macromolecules in the order of the central dogma – the direction that information flows in life on Earth. The first biological macromolecule is nucleic acid, which comes in the form of DNA and RNA in the human body. DNA encodes all the heritable genetic information within every cell within the human body (as well as all other plants, animals, fungi, bacteria, and many viruses on Earth) and serves as the permanent record of all information in the cell. RNA is transcribed from DNA as needed to serve as a short-term blueprint for immediate use in the cell – a quick printout of the instructions for the cell to follow, quickly destroyed but easily remade. The third macromolecule is protein, which is a sequence of amino acids translated from the RNA blueprint – these long chains of amino acids are carefully folded into precise three-dimensional structures with catalytic clefts, binding sites, and hydrophobic domains that combine to allow each protein to perform a specific chemical reaction or interaction in the cell. Proteins mediate the production of the third and fourth macromolecules: carbohydrates and lipids. Carbohydrates encompass the sugars that serve as rapid energy sources and the cellulose made by plants for structural rigidity and chitin in the shells of crabs and other arthropods. Finally, lipids are the (relatively) small, greasy molecules commonly known as fats – they serve as long-term energy storage, are the root structure of many hormones, and, most importantly, self-assemble into membranes.

At its most fundamental, a membrane defines "inside" and "outside" – these are the crucial barriers that allow a cell to perform chemistry. We can simplify every cell on Earth down to a tiny compartment enclosing a concert of chemical reactions. The walls delineated by these compartments are lipid membranes. Without these membranes, it would be impossible to amass chemical inputs and outputs, store energy, and build ion gradients – the fundamental processes underlying all life on Earth.

All biological membranes are primarily composed of lipids, which all have a broad similarity: a hydrophilic structure that preferentially interacts with water (the "head" or "headgroup"), a hydrophobic structure (the "tail") that preferentially avoids interaction with water by aggregating with other hydrophobic molecules, and a backbone structure, which links the headgroup with the tail (Figure 1.6A). In this manner, lipid membranes self-assemble in an aqueous solution into bilayers with headgroups facing out into the water and tails shielding each other from the water (Figure 1.6C)[63].

A human cell has thousands of molecularly distinct lipids ("species"). There are five major lipid headgroups: glycerol, sterol, inositol, ethanolamine, and serine (and many modifications of these core structures, such as phosphorylation and glycosylation); there are also many possible lengths of the hydrophobic tail and many sites of possible desaturation (Figure 1.6B). Lipid-metabolizing enzymes mediate the combinatorial addition of these components in the cell to produce a vast mosaic for membrane composition(Figure 1.6C).

For much of the history of biological research, lipids were considered the inert backdrop upon which the cell performed its chemical act – just the walls and roof that proteins (the real stars of the show) used as a stage. However, researchers are increasingly recognizing lipids for the nuanced and dynamic cadre they are. These molecules are synthesized in precise proportions, distributed in

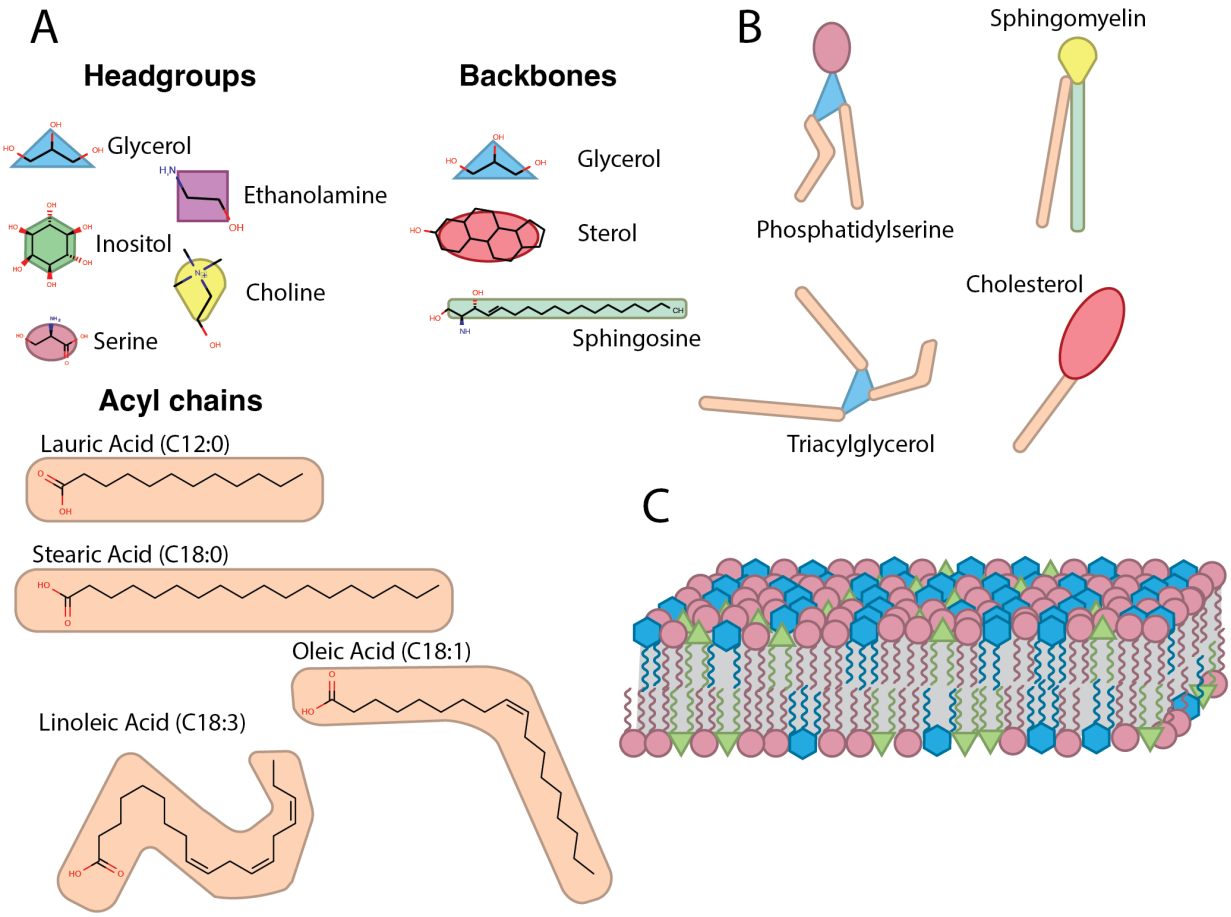


Figure 1.6. – **Lipid combinatorics and the lipid mosaic model** (A) Simplified cartoons depicting the three basic ingredients for a lipid: headgroups, backbones, and acyl chains. These lists are far from exhaustive and are intended to highlight the heterogeneity of lipid composition. (B) Many thousands of molecularly distinct lipids can be produced and interchanged in all combinations of headgroups, backbones, and acyl chains. Simplified example lipid structures highlight the myriad possibilities of the lipid repertoire. (C) A cartoon depicting the heterogeneity of a lipid membrane according to the lipid mosaic model. (These cartoons are not to scale and are purely for illustration.)

careful patterns throughout membranes, and induce potent effects in the cell – how could anyone have thought these were random and inert molecules?

Careful studies have shown that each compartment in the cell is defined by a membrane with distinct properties[64]. For example, a highly fluid membrane encloses the endoplasmic reticulum, which must flow dynamically to traffic freshly synthesized proteins throughout the cell; accordingly, the ER membrane is primarily composed of phospholipids and contains virtually no sterols, cardiolipins, or complex sphingolipids which confer rigidity.[63]. In contrast, the outer membrane of the cell (the plasma membrane) needs more structural rigidity to withstand shear forces and protect the cell; this membrane is composed of less-fluid lipids that aggregate in structurally rigid microdomains such as cholesterol and sphingomyelin[63]. Mitochondria need even more structural stability and insulation because their role as the cellular powerplant requires the production of steep electrochemical gradients and reactive molecules such as peroxides; these organelles are encased in a rigid double membrane composed of cardiolipins[65,66]. The containment of the mitochondrial contents is so crucial to cell survival that the mitochondria serve as a self-destruct button for the cell: controlled cell death (i.e., apoptosis) relies on permeabilizing the mitochondrial membrane to trigger a reactor meltdown[66].

Even within a single membrane, there can be tight, localized regulation of lipid composition: the plasma membrane lipid bilayer is asymmetrically composed of negatively charged lipids on the inner leaflet (mainly phosphatidylserine, PS) and neutral lipids on the outer leaflet of the bilayer. This asymmetry encourages the transfer of select ions into the cell and can serve as an instant reporter of cell damage for surveilling immune cells. When a cell dies, it actively flops PS from the inner leaflet of the plasma membrane to the outer leaflet, transferring negative charges to the outside of the cell; nearby macrophages (cells that we will discuss in much more detail in the following chapter) have receptors that recognize this outside-facing PS and immediately clear the dead cell away so a neighbor can take its place.

1.7.0.2. What do lipids have to do with TB?

In many ways, *Mycobacterium tuberculosis* is a bacterium distinguished by its unique lipid composition and sensitivity to environmental lipids.

Garcia-Vilanova et al. discuss how *Mtb*'s lipid composition appears to change between the intracellular stages of the Mtb lifecycle versus the airborne, transmissible stage[62]: it enriches itself of diacyl trehalose, triacyl trehalose, phthiocerol dimycocerosate and other waxy lipids appears to confer strong hydrophobicity. These waxy and greasy cell wall lipids confer *Mtb*'s astounding ability to stay in aerosols (the essential transmission mechanism for TB)[67]. Within the lung space, *Mtb* alters its lipid coating toward a cohort of lipids known to induce pathology: it up-regulates the production of phosphatidyl-*myo*-inositol mannosides (PIMs) and mannose-capped lipoarabinomannan (ManLAM)[62]. These waxy coats are an essential source of difficulty in the search for rapid anti-TB antibiotics. This greasy coating physically excludes many molecules and protects *Mtb* from many antimicrobial toxins[62].

In another example, *Mtb* is known to induce massive changes to the host lipid landscape during infection. So-called "foamy" macrophages in the lung are a clinical sign of an active TB infection. These infected macrophages are replete with structures called lipid droplets (visually appearing as a foam inside the cell) and typically serve as energy storage deposits for lipids such as triacylglycerol. Much work has shown that *Mtb* infection drives the production of these lipid droplets[68] and the

selective delivery of these structures to the *Mtb*-containing compartment[69]. These dramatic changes to the host lipid composition are part of why *Mtb* is called a master manipulator of host biology[61].

Host lipids also play a critical role in driving the bacteria along the drug-resistant versus drug-susceptible axis. As referenced above, Dutta et al. showed that *Mtb*-infected mice treated with cholesterol-reducing statins are highly responsive to antibiotic treatment and resolve their *Mtb* infections much more quickly than control mice[70]. This possible avenue for host-directed therapy has drawn significant attention, and ongoing clinical trials seek to discover its effect in humans. What other lipids may influence a TB infection?

1.8. Sphingolipids: enigmatic like the sphinx

Sphingolipids are a family of lipids with a central chemical structure, the sphingoid base. These lipids were named by Johann Ludwig Wilhelm Thudichum in 1884 because they are "as enigmatic as the sphinx." Of course, this has been the source of more than a lifetime's worth of embarrassing paper titles, including: *Taming the Sphinx: Mechanisms of cellular homeostasis*[71]; *HDL Dysfunction: Is the Answer in the Sphinx's Riddle?*[72]; *Sphingosine-1-Phosphate and Macrophage Biology—How the Sphinx Tames the Big Eater*[73]; *The Squeaky Yeast Gets Greased: The Roles of Host Lipids in the Clearance of Pathogenic Fungi* (See Chapter 8)[74].

Until quite recently, biologists knew very little about what sphingolipids do. We now know that sphingolipids play critical roles in immune signaling, nervous system function, brain development, and apoptosis. The dysregulation of sphingolipid production and metabolism is associated with various cancers[79–81], immune disorders[82,83], and bone disease[84], among many, many other diseases[81].

Sphingolipids play an intricate role in a cell deciding between life and death. The so-called "sphingolipid rheostat" is a well-described program in which the proportion of ceramide versus sphingosine tips the cell toward death versus life (respectively). At first glance, this seems counterintuitive: why should a cell actively initiate its own death? However, programmed cell death (apoptosis) is critical in multicellular organisms: when a cell senses that it is irreparably damaged or infected by a pathogen, it must be destroyed and replaced for the good of the whole organism[85]. For this reason, deficiencies in sphingolipid regulation are tightly associated with neurological disease, autoimmune disorders, and cancer[80,86,87]. Recent work even suggests that sphingolipids may play crucial roles in aging and aging-related diseases[88].

We have also previously written on the ways that sphingolipids have been shown as critical determinants of microbial pathogenesis (see Chapter 7 and Chapter 8). These lipids play crucial roles in nearly every context in which they've been investigated. Despite this, much research remains to uncover how sphingolipids influence a *Mycobacterium tuberculosis* infection. The ties that sphingolipids have to cell death, membrane repair, membrane structure, and immune signaling are all highly intriguing connections between sphingolipids and *Mtb*. Throughout this document, we will discuss these connections in great detail.

Some researchers have ventured beyond entirely scientific avenues to philosophize that the tight regulation apparent in the sphingolipid pathway serves as evidence of "fine-tuning" – the notion of inexplicable sensitivity to perturbation which belies a grand universal architecture and hints toward directed evolution[89]. These authors point to this pathway, which decides the life and death of the cell by the interconversion of a few mol% of one molecule into another, and dismay that it



Figure 1.7. – **Johann Ludwig Wilhelm Thudichum (1809 - 1901)** Named the "father of neurochemistry," Thudichum is a highly influential, though also sometimes controversial, figure in the study of neurology. Over the course of his career he independently characterized and purified over 140 individual chemicals from the brain[75,76]. Thudichum faced wide criticism for his isolationistic research practices, disinterest in training successors, and propensity for re-naming previously-identified molecules[75,77]. He wasn't fully acknowledged as a groundbreaking figure in neurology until after his death[75]. We must assume Thudichum an enjoyer of Greek legend, as his thoughts immediately turned to the mysterious Sphinx upon identifying sphingomyelin[78]. Photo: National Library of Medicine

could not arise spontaneously. That is not to say there is no awe to feel when thinking about the vast complexity of biological systems. Imagine thousands of unique sphingolipid species dancing in swirling membranous majesty within every cell of your body, triggering cell death or disease with any stumble. But now, consider that this pathway predates the separation of eukaryotes from prokaryotes[90]. The tight regulation of sphingolipids is the product of *2.5 billion* years of evolution. 2.5 billion years ago, the Moon had active volcanos and was visibly closer to the Earth[91,92]. A day was 17 hours long (because the Moon has been gently slowing the rotation of the Earth)[92]. Saturn did not yet have rings[93]. The rise of photosynthesis would soon cause the Great Oxygenation Event and kill the majority of all life on Earth[94]. This span of these aeons should inspire at least as much awe as the complexity of a membrane. The fact that sphingolipids are so intricately tied to cell life and death merely highlights the strength of the evolutionary pressures that produced this self-regulating network. In short, fine-tunedness is as controversial in biology as in cosmology.

1.9. Conclusion

Tuberculosis is a complex, sometimes self-contradictory disease. Sphingolipids are a complex, sometimes self-contradictory family of lipids. Accordingly, this introduction has rambled and sprawled over many topics and only scraped the surface of many detailed processes.

We hope this chapter has provided some historical context and introduced vital concepts we will expand upon as the following chapters increase in technical detail.

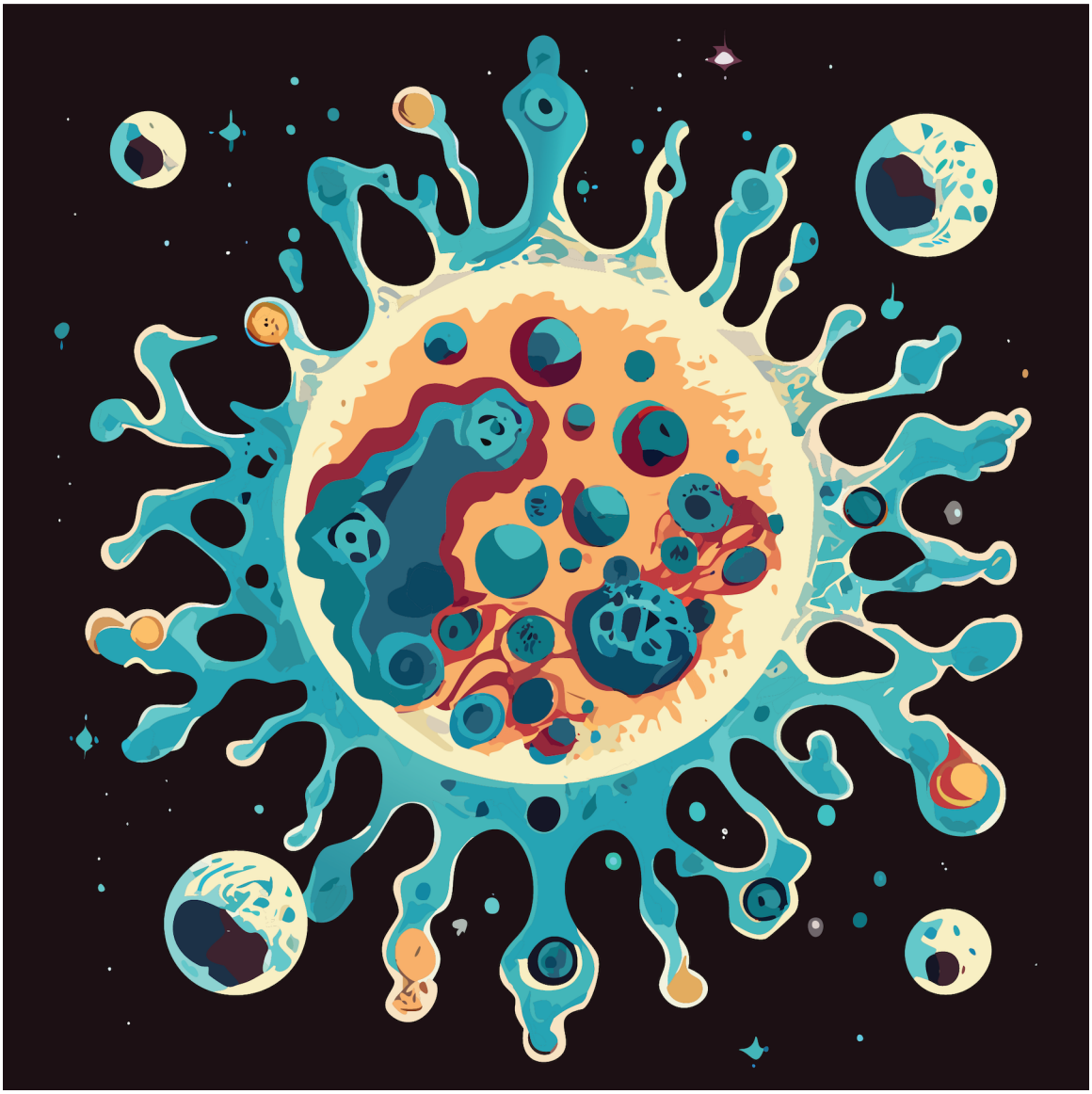


Figure 1.8. – **"A galaxy of lipids floating in space"** We asked an AI image generator to use this prompt to make a picture. Source: Adobe Illustrator, Text To Vector Graphic (Beta).

1.10. Contributions

GG compiled the concepts discussed in this article and wrote the entirety of the text. FGT oversaw the preparation of this article.

Chapter 2.

Introduction Part 2

Authors: Gaelen Guzman[1], Fikadu G. Tafesse[1,*]

[1] = Department of Molecular Microbiology and Immunology, Oregon Health & Science University, Portland, Oregon, USA. [*] = corresponding author: tafesse@ohsu.edu

2.1. Abstract

Mycobacterium tuberculosis (*Mtb*) is a significant cause of infectious death worldwide. This intracellular pathogen uses many mechanisms to subvert the host immune system and lie undetected before causing active disease. This subtle pathogen is uniquely dependent on host lipids for energy, production of host-damaging materiel, and immune subversion. In the face of antibiotic-resistant *Mtb* strains, researchers have turned toward lipid biology for potential avenues of novel antitubercular therapy. The sphingolipid family has gained attention for its profound roles in determining cell fate, immune signaling, and antimicrobial activity. We review the state of the field regarding sphingolipids as candidate targets of host-directed antitubercular intervention.

2.2. Introduction

Mtb has co-evolved with humans for millennia and thus possesses an astounding capacity to subvert the host antimicrobial defenses, establishing a latent TB infection that can persist for years before progressing to active TB disease[53]. Among its adaptations is a profound reliance on host lipids. This intracellular pathogen utilizes host lipids as a source of energy and carbon source and is highly sensitive to subtle changes in its host lipidome[70,95]. Thus, in recent years, researchers have turned toward lipid biology as a potential route of host-directed therapy. A particular lipid family of interest is the sphingolipids. Sphingolipids are dual cell death and inflammation regulators, and they play a crucial role in host defense against pathogenic infections. Thus, studying the host-pathogen interactions and sphingolipid biology may provide new insights into developing effective TB therapies.

In addition to its direct impact on human health, studying Mtb provides unique opportunities to explore and unravel typical human immune function. As a highly adapted pathogen, Mtb has evolved redundant pathways to subvert host immune defenses, making it an excellent teacher and model for understanding human immune function. This chapter will discuss how host sphingolipid biology intersects with *Mtb* biology and how this niche class of lipids may provide promising routes for new antitubercular drugs.

2.3. *Mtb* and the innate immune system: a tug of war in the lung

2.3.1. Infection start & the granuloma

The primary TB infection route is inhaling cough aerosols an active TB patient produces. In daily life, humans constantly experience airborne microbes and particulates – every breath will contain fungal, bacterial, and viral particles that reach the lungs[96]. Many of these particles are filtered out and destroyed in the sinus cavity[97], but many will make their way down to the alveolar sacs, the deepest regions of the deepest regions of the lung. The alveoli are surveilled by resident immune cells called alveolar macrophages[98]. These resident macrophages use damage recognition receptors and pathogen recognition receptors to probe for cells, objects (like silica dust), or invaders decorated with damage-associated molecular patterns (DAMPs) or pathogen-associated molecular patterns (PAMPs)[99].

In most cases, a macrophage will uptake these foreign or effete particles through phagocytosis and destroy them in a specialized cellular organelle called the lysosome. The destruction of would-be pathogens in the lysosome is directly beneficial for clearing an infection. However, the macrophage will also present peptides from the destroyed pathogen to the adaptive immune system, enabling the host to mount a concerted and long-lived immune response. These processes protect most immunocompetent (non-immunocompromised) individuals from infection by environmental pathogens. However, *Mtb* is adept at avoiding and subverting these processes.

Mycobacterium tuberculosis has spent millennia adapting to the human immune response. Few microbes are as well-suited for aerosol transmission as mycobacteria: recent work has shown that the waxy, hydrophobic composition of the *Mtb* cell wall confers a high capacity to remain airborne for long periods[67,100]. Others have shown repeatedly that many, if not most, TB infections are initiated

by an individual *Mtb* bacillus (first shown in guinea pigs housed in TB wards and recently verified by infecting macaques with aerosolized, barcoded *Mtb* bacilli)[101–104].

Within the lung space, *Mtb* infects alveolar macrophages in a Trojan Horse-style infection: *Mtb* bacilli allow themselves to be internalized via phagocytosis, initiating a program of immune subversion that, in a successful infection, culminates in the recruitment of more alveolar macrophages as well as other immune cells including monocyte-derived (hematopoietic) macrophages, neutrophils, natural killer cells, T cells, and dendritic cells, and non-immune fibroblasts. As reviewed by Ehlers and Schaible in 2013, the cyclic recruitment of immune cells to the site of *Mtb* infection has two simultaneous, opposing effects: (1) encapsulating the infection in a fibrous net of fibroblasts and antimicrobial immune cells, which prevents the spread of *Mtb* bacilli throughout the lung and (2) serving the bacteria fresh macrophages, which serve as host cells and propagate the ongoing infection[105,106].

These self-contradictory roles for the granuloma result in restricted bacterial spread *and* sustained infection – it is thus how a latent TB infection is maintained for potentially years before activation to active TB disease. In 2009, Cardona proposed a model in which the same individual is "reinfected" repeatedly as infected macrophages spontaneously escape from the granuloma and seed infection in a new site[107]. In support of this, Lin et al. (2014) used longitudinal scanning to show that macaque granulomas are often sterilized and cleared[104]. However, this is counteracted by the formation of new granulomas in new sites[104]. In this now-widely accepted model of granuloma containment of *Mtb*, a patient with a latent TB infection can control infection for long periods but will proceed to active TB disease if the immune regulation within the granuloma fails.

The dissolution of the granuloma structure is marked by widespread necrotic cell death, caseation (tissue degradation with a "cheese-like" appearance[108]), and eventual cavitation (total collapse, leaving a hole in the lung space) of the granuloma releases the contained bacteria from its restriction and allows them to replicate uncontrolled. At this point, bacteria and necrotic cellular detritus spill into the airway, and the patient's coughing spreads the released bacteria.

Shortly, we will discuss how lipids influence the interactions between an infecting *Mtb* bacillus and an individual host cell. First, though, we must note that lipid dysregulation is a hallmark trait of uncontrolled TB disease, even at the organismal level. Histological studies by Hunter et al. in 2007 showed that activation of latent TB disease occurs in tandem with a spillage of lipidated material from ruptured granulomas into the airway[109] – a form of lipidated pneumonia in which cholesterols and cholesteryl esters, triacylglycerols, and lactocylceramides accumulate in the caseum[108]. In many ways, the moment-to-moment stability/integrity of the granuloma reflects the immunocompetence of the host: immunocompromising events such as HIV, chemotherapy, or malnutrition tip the balance in favor of the invading *Mycobacterium tuberculosis*. The granuloma's structure is the product of many host-pathogen interactions, the sum of many individual battles between host and microbe. In the unique *Mtb* infection, many host-pathogen interactions occur via a lipid or membrane interface. We will now discuss the *Mtb* lifecycle within a host cell: how *Mtb* subverts the typical immunological processes of the macrophage.

2.3.2. A Trojan Horse in the belly of the beast

Alveolar macrophages surveil the lung space for would-be pathogens, foreign material, or dying cells. To accomplish this, they express an array of receptors that recognize pathogen-associated or damage-associated molecular patterns (PAMPs and DAMPs, respectively). These receptors, or

pathogen-recognition receptors (PRRs), bind to a cognate antigen and initiate a signaling cascade that can trigger phagocytosis, cytokine secretion, and adaptive immune system activation.

As is the case with most bacterial pathogens, a variety of *Mtb* surface structures are recognized by phagocytic receptors such as Dectin-1, the Mannose Receptor, and DC-SIGN, as well as non-phagocytic receptors such as TLR2. Upon recognizing the *Mtb* pathogen-particle, the alveolar macrophage internalizes the bacterial cell via phagocytosis. However, unlike other pathogens, *Mtb* appears to selectively engage receptors that fail to initiate immune signaling. Van Kooyk and others have reported that *Mtb* selectively binds receptors that fail to initiate inflammatory signaling[110,111].

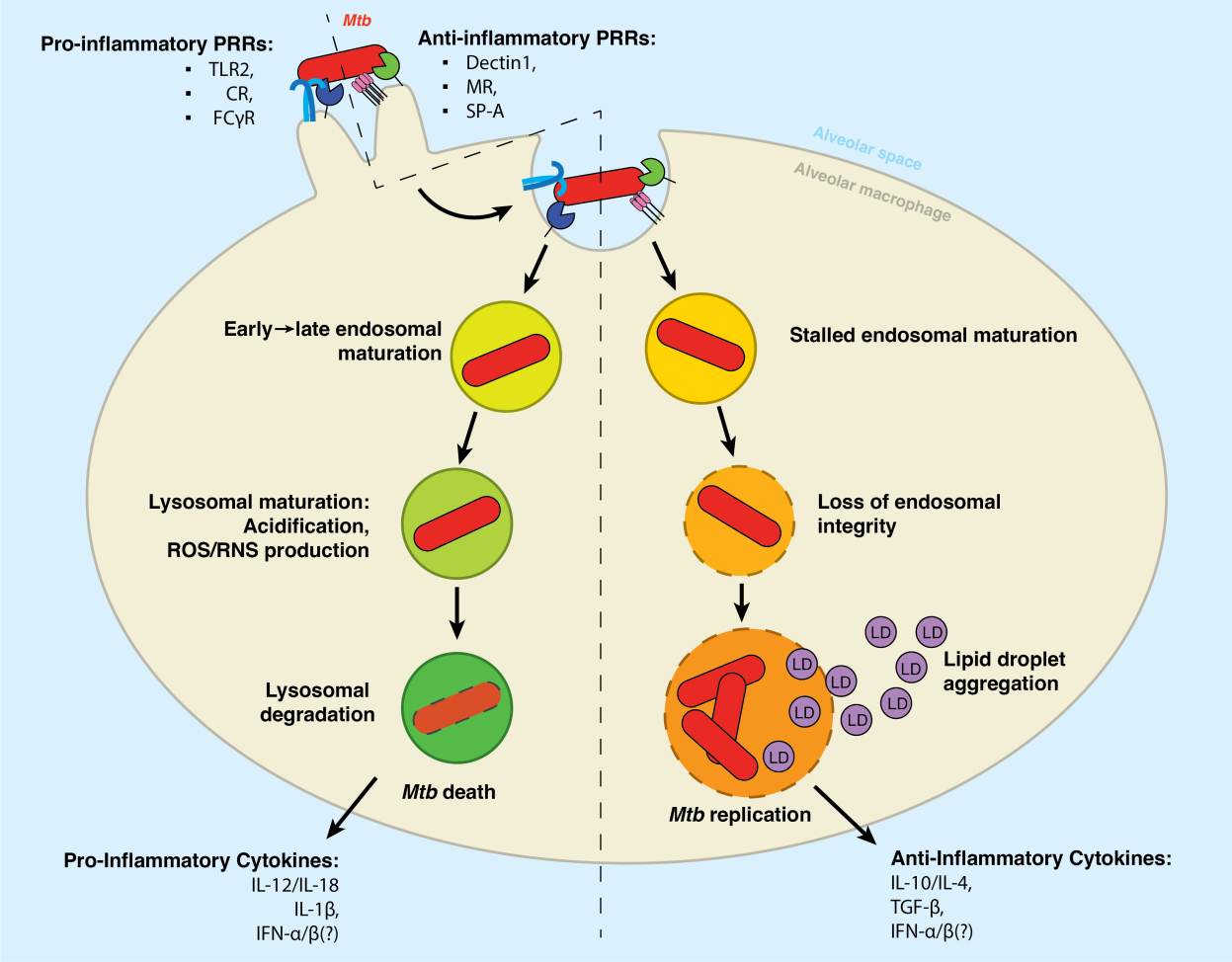


Figure 2.1. – **The balancing act of *Mtb* control.** A highly simplified cartoon depicting the anti-/pro-*Mtb* features of infected macrophages. The terminal fate of internalized *Mtb* appears related to programming initiated with the sensing and internalization of the bacteria by PRRs. Inflammatory PRRs direct the bacteria toward a maturing endosome, resulting in ROS/RNS production, bacterial death, and secretion of inflammatory cytokines involved in overall infection control. Uptake by anti-inflammatory PRRs results in the bacteria residing in a non-maturing endosome, gaining cytosolic access via membrane disruption, the accumulation of lipid droplets, and finally, anti-inflammatory cytokine production — resulting in tuberculosis disease progression. (Abbreviations: PRR = pathogen recognition receptor; TLR2 = toll-like receptor 2; CR = complement receptor; FCγR = Fc-gamma receptor; MR = mannose receptor; SP-A = surfactant protein A; ROS/RNS = reactive oxygen/nitrogen species; IL-12/18/1β/10/4 = interleukins 12/18/1β/10/4; TGF-β = transformative growth factor-β; IFN-α/β = interferon-α/β).

Therein lies the Trojan Horse infection: the macrophage internalizes the *Mtb* bacillus as a part of its typical antimicrobial program – but *Mtb* subverts this programming to hijack the cell and enable its survival therein. Much evidence has shown that the polarization of the infected macrophage has an immense impact on whether it will destroy the bacteria or succumb to its machinations[112]. In 2022, Arish and Naz described that the plasticity of the macrophage might be a therapeutic target for TB therapy: inducing a so-called M1 inflammatory polarization enhances the cell's capacity to mount an antimicrobial defense against *Mtb*, among which is the upregulated expression of inflammatory pathogen recognition receptors such as TLR2[113].

2.3.3. Arresting development: the blockade of lysosomal maturation.

For most phagocytosed particles, the lysosome is the end of the line. This organelle is responsible for destroying unwanted material in the cell. It thus contains hydrolases (which can cleave proteins, lipids, sugars, and nucleic acids), vATPases (which produce a highly acidic pH), and antimicrobial peptides (which are directly bactericidal)[99,114].

The contents of the phagosome are delivered to the lysosomal compartment through a series of fusion/fission events with the endosomal compartment. As depicted in the left hand of Figure 2.1, the phagosome will fuse with the early endosome, the late endosome, and then the lysosome. We and others have written extensively on the maturation of the phagosome, and we recommend further reading for an in-depth discussion on standard endosomal trafficking (Chapter 8)[74,115–117].

However, *Mtb* initiates a cascade of immune subversion once inside the host cell[53]. Environmental cues such as reduced pH and increased sodium concentration trigger these pathogenic programs, which block the typical maturation of the phagosome and allow the bacteria to survive within an atypical endosomal compartment commonly called the mycobacteria-containing vacuole[118]. We recommend the 2019 review by Carranza et al. for an in-depth description of the mechanisms that *Mtb* utilizes to halt phagosomal maturation[119].

Following phago/lysosomal blockade, the *Mtb*-containing vacuole retains many canonical features of the early phagosome[120,121]. This compartment has a nearly neutral pH, is decorated with early endosomal markers such as Rab5[120]. Additionally, the *Mtb*-containing phagosome retains Rab14 and Rab22a. Unlike the early endosome, however, the *Mtb*-contaiing vacuole is largely devoid of Vps34, a class III phosphotidylinositol-3 kinase which produces phosphatidylinositol-3-phosphate (PI(3)P)[121]. PI(3)P is an essential inducer of autophagy and lysosomal trafficking, and, accordingly, several crucial PI(3)P-binding proteins are not recruited to the *Mtb*-containing vacuole – including the hepatocyte growth factor-regulated tyrosine kinase substrate (HGS/HRS), which responsible for recruiting the ESCRT complex to initiate lysosomal degradation[121,122]. Intriguingly, in 2017, Schnettger et al. found that *Mtb* subverts the Rab20-dependent membrane trafficking pathway to reside in so-called "tight" phagosomes (as opposed to "spacious" phagosomes, which are associated with IFN-γ-induced immunoproteolysis)[123].

There are several *Mtb* pathogenicity factors critical for the subversion of lysosomal maturation. Perhaps the most significant is the *Mtb* ESX Type VII secretion system[124]. This secretion system mediates the transfer of many *Mtb* factors into the lumen of the lysosome, including proteins, lipids, and small molecules[125–127]. Several of these factors appear to independently serve as membrane-damaging agents – these include the highly characterized ESAT-6/CFP-10 protein heterodimer and the glycolipid phthiocerol dimycocerosate[128,129]. Other factors directly remodel the phagosomal environment; for example, the terpene nucleoside 1-tuberculosinyladenosine is reported to act as

an "antacid" that neutralizes the acid pH in the nascent phagosome[130] and eventually induces the formation of lipid droplets[131]. We will discuss lipid droplets further below.

As will be discussed below, however, this vacuole is dynamic and undergoes dramatic changes as the *Mtb* continues to overcome the macrophage's defenses and wrests control over the cell. Prior to phagosomal escape, however, Russell proposed in 2016 a model in which intracellular *Mtb* will spend an outsize proportion of its time within the endosomal compartment, surreptitiously avoiding immune recognition by existing in a semi-quiescent state[132]. Among many pieces of supporting evidence, the long-observed paucibacillary quality of the TB lung aligns well with Russell's model – there are simply very few individual *Mtb* bacilli in a latent TB infection. Expanding on this model, Russell suggests that it is upon progression to active disease via immune suppression, malnutrition, or some other trigger that the *Mtb* bacillus will begin a program of phago/endosomal damage[132] – a topic discussed further below.

2.3.4. Breaking free: damaging the phagosomal membrane

2.3.4.1. *Mtb* and other intracellular bacterial pathogens benefit from endo/lysosomal membrane damage

Many intracellular bacterial pathogens utilize phago/lysosomal membrane damage as a mechanism of immune escape; these include *Mtb*, *Salmonella enterica* serovar Typhimurium, *Lysteria monocytogenes* and many others[133,134].

The reason for this convergent mechanism of pathogenicity is apparent: by permeabilizing the phagosomal membrane as it matures through the endosomal pathway, the pathogen can inhibit the acquisition of antimicrobial factors[135]. Chief among these factors is the intraluminal pH of the maturing phagosome: the membrane-bound proton pump vATPase is delivered via fusion with the early endosome shortly after bacterial lumen, which accumulates on the maturing phagosome and acidifies the phagosomal interior[114]. A variety of pH-regulated antimicrobial factors are simultaneously delivered to the maturing phagosome via fusion with the early endosome, then the late endosome, and finally the lysosome; these include hydrolases which cleave proteins, lipids, and glycans (proteases, lipases, and glycosidases, respectively), as well as pore-forming antimicrobial peptides, and reactive oxygen and nitrogen species[136]. By perforating the phagosomal membrane, intracellular pathogens such as *Mtb* prevent the accumulation of these factors within the pathogen-containing vacuole, enabling escape from lysosomal degradation and the presentation of antigens to the adaptive immune system[136,137].

To achieve phagosomal perforation, *Mtb* utilizes a cohort of Type VII secretion systems to transfer soluble pathogenicity factors into the phagosomal lumen – chiefly ESX-1 and ESX-5[138]. Among the most well-characterized of these soluble effectors are EsxA and EsxB – more commonly referred to as early secreted antigenic target-6 (ESAT-6) and culture filtrate protein-10 (CFP-10)[138]. These proteins are the immunodominant antigens of an *Mtb* infection and are major determinants of *Mtb* virulence[134,139]. Many reports have shown that the loss of either ESAT-6 or CFP-10 results in the significant attenuation of pathogenic *Mtb* strains[139–141]. Though not the first to show this, Smith et al. elegantly demonstrated in 2007 that ESAT-6 directly induces the formation of pores in the phago/lysosomal membrane[140]. Consequently, the permeabilization of the phago/lysosome is a significant driver of *Mtb*-induced cell death and pathogenicity[142].

However, as with other stages of an *Mtb* infection, membrane damage represents a fulcrum of control for the host cell: the cell has several layers of redundant membrane repair mechanisms which seek to counteract the membranolytic activities of *Mtb* and regain control over the infection.

2.3.4.2. An arms race for control: Host response to membrane damage *Mtb*'s inhibition of membrane repair

As described above, the lysosome encloses a toxic milieu of acidic pH, antimicrobial peptides, proteases, lipases, glycosidases, and nucleases[143]. Independent of pathogenic action, unmitigated lysosomal damage is a potent inducer of cell death[144] – thus, the cell utilizes independent and redundant mechanisms of membrane repair. These repair mechanisms operate at different levels of damage and timespan: from the minor and acute to the major and chronic.

In the case of minor membrane damage resulting from an acute membranolytic injury, a suite of proteins called the Sequestosome-like receptors (SLRs), which includes Sequestosome, NDP52, and the galectins[145]. These SLRs are also used to mark defunct organelles, depolarized mitochondria, protein aggregates, and cytosolic bacteria. These membrane sensors initiate membrane repair by directing the polymerization of components of the ESCRT-III complex. ESCRT-III is composed of a cohort of charged multivesicular body proteins: CHMP1, CHMP2A, -2B, -3, -4A, -4B, -4C and -6[146]. These monomers insert into damaged membranes and polymerize into a spiral which induces membrane curvature around the site of membrane damage. ATP hydrolysis by VPS4 provides the requisite energy to constrict the polymerized ESCRT-III complex and pinch off the targeted membrane region[146]. This membrane-repairing behavior of the ESCRT-III complex is somewhat ancillary to its primary role of producing multivesicular bodies (MVB) during secretory trafficking: the same complex assembles at the surface of these complex organelles and mediates the scission of microvesicles into the lumen of the MVB[146].

In circumstances of major or chronic damage – instances where, despite the efforts of the ESCRT-III complex, an organelle is beyond repair – the deposition of ubiquitin and Sequestosome-like receptors over time induces the recruitment of autophagy machinery[146,147]. Autophagy results in the destruction of damaged endosome; this is a process used by the cell to degrade defunct or unneeded organelles[148]. Autophagy involves the construction of a double membrane around a targeted organelle and fusion with to pre-formed lysosomes in order to degrade targeted organelle[148]. This process is highly dependent on the recruitment of the acyl-CoA synthetase Faa1[149]. This enzyme enables the on-site assembly of phospholipids in the double membrane of the autophagosome, and is critical for the encapsulation of the targeted organelle[149].

Autophagy is a central mechanism for restricting *Mtb* infection[150–152]. This process that enables the destruction of chronically damaged membranes further enables the proteasomal degradation of the bacterial contents within: the resulting microbe-derived peptides can thus be loaded onto the MHC-II complex and presented to the adaptive immune system via the cross-presentation pathway[148]. Accordingly, as seen at many other points of the host-pathogen interface, *Mtb* proactively interferes with the autophagic membrane damage repair response of the host[153]. In one notable example, Divangazi et al. showed in 2009 that *Mtb* infection induces membrane damage both at the plasma membrane and the in lysosome, and that the bacteria produces a molecule called lipoxin A_4 (LXA_4), which blocks prostaglandin E_2 (PGE_2) synthesis[154]. These authors show that PGE_2 is essential for the recruitment/activation of synaptotagmin, a cytosolic Ca^{2+} sensor[154]. Similarly, Mittal et al. showed in 2018 that the secreted *Mtb* effectors EsxG and EsxH[155] directly interfere with the ESCRT response

pathway. And as a final example (though this is not to say that these examples are exhaustive), authors such as Saini et al. (and many others) have shown that *Mtb* suppresses the autophagy response of the cell and directly benefits from the subsequent escape from the adaptive immune response[153,156,157].

These examples of the membrane damage response highlight the tit-for-tat manner of an *Mtb* infection – an arms race over the millennia. As alluded above and as will be discussed further below, the cell's capacity to respond to and limit the damage caused by *Mtb* is highly influenced by the immunological priming of the cell prior to infection: a cell primed for antimicrobial effect via IFN-γ stimulation has a higher propensity for maintaining phago/lysosomal integrity and directing the bacterial to lysosomal degradation. It is in an inadequate immune environment that the bacteria is able to inflict major damage to the maturing phagosome and gain cytosolic access.

2.3.5. Lipid droplet formation in late-stage infection

Lipid droplets (LDs) are organelles consisting of a phospholipid monolayer encapsulating a hydrophobic core composed mainly of triacylglycerol species (TG) and sterol esters[158]. Research suggests that LDs are a central feature of mycobacterial infection, where mature granulomas are replete with "foamy" macrophages[68]. It is not unique to mycobacteria as many bacteria, viruses, eukaryotic parasites, and fungi are known to induce LDs in infected hosts. Prior reports suggest that LDs are trafficked toward the mycobacteria-containing vacuole in a cytoskeleton-dependent manner[159]. Further, Barisch et al. showed that *Mtb* hydrolyzes TG from LDs to fuel its metabolism as a primary source of energy[68]. Thus, LDs are believed to play a crucial role in the host-pathogen interaction during *Mtb* infection. Recent work by Bedard et al. showed that individual *Mtb* pathogenicity factors, such as 1-tuberculosinyladenosine, are sufficient to induce the accumulation of lipid droplets[131].

Further research is required to fully understand the mechanisms involved in the formation and utilization of LDs by Mtb, which could lead to developing new therapeutic interventions for TB. Many points in this pathway may serve as targets of antitubercular therapy, including blocking the formation of these organelles, halting the trafficking of LDs to the *Mtb*-containing vacuole, inhibiting the *Mtb* phospholipases that hydrolyze TG, or disrupting the *Mtb* fatty acid β-oxidation pathway. Much research is needed to determine which, if any, of these lipid droplet-targeted therapies may have the most significant effect.

2.3.6. Cytokine production in the granuloma

The cytokines within the granuloma microenvironment hold immense sway in the direction a TB infection can go. Inflammatory cytokines such as Type II interferon (IFN-γ) can potently stimulate the antimicrobial capacity of macrophages, stimulating lysosomal activity, antigen cross-presentation, and heightened production of other inflammatory cytokines such as IL-1β, which further initiate a broad antimicrobial response[98]. This immune cross-talk allows a fully immunocompetent host to limit the spread of *Mtb* within the lung and limit bacterial growth[98]. However, *Mtb* is also adept at subverting these immune processes – reports by Fortes et al. and others demonstrate that *Mtb* can prevent the production of inflammatory cytokines and instead induce the secretion of anti-inflammatory cytokines such as TGF-β and suppress the secretion of IFN-γ[160,161]. Consequently, the overarching immunocompetence of the host can result in feedback loops of either *Mtb* restriction or *Mtb* success.

With these feedback loops in mind, cytokine therapy is under study as a potential form of host-directed therapy. Berns et al. reviewed the clinical efficiency of exogenous IFN-γ therapy and found repeated benefits to aerosolized or subcutaneous IFN-γ adjunctive treatment in clinical trials[162]. Berns et al. write that IFN-γ strongly stimulates antigen presentation and can overcome *Mtb*'s inhibition of immune processing, resulting in a coordinated and multifaceted attack on the infecting *Mtb*[162]. In addition, IFN-γ robustly activates macrophages and stimulates chemotactic migration toward the site of infection. Highly activated macrophages release nitric oxide into the granuloma microenvironment, placing extreme oxidative stress on infected cells and bacteria.

However, some studies have suggested that cytokine therapy can inadvertently cause increased pathology by increasing damage to surrounding lung tissue and exacerbating lung infection[163,164]. Thus, cytokine therapies, including IFN-γ, are still controversial and subjects of clinical trials. Nonetheless, IFN-γ is a highly cost-effective adjunctive therapeutic in the Russian Federation[162]. It reduces treatment time and antibiotics, thereby reducing costs and increasing supplies.

2.4. *Mtb* and Lipids: A recipe for pathogenicity

Many papers describe the dependence of *Mtb* on host lipid biology. As Ghazaei beautifully wrote in their 2018 review on lipid metabolism in *Mtb* infection: "If the metabolism of the pathogen is studied, the use of lipid metabolism has been documented"[165]. In summary, *Mtb* is an intracellular pathogen with unique lipid dependency, and the full description of this statement would encompass too many topics for this review. However, we will briefly discuss a few examples of *Mtb*'s unique lipid biology.

A critical phenomenon preceding the progression to active TB disease is the accumulation of "foamy" macrophages in the granuloma[166]. The accumulation of lipids within these cells gives them their name: these cells have undergone significant dyslipidemia, driving the formation of many lipid droplets within them[166]. When these cells undergo necroptosis, they release this lipidated material into the granuloma/alveolar space – foamy macrophages are the source of the lipid pneumonia associated with active TB disease. DAG and TAG species have been previously observed to increase upon infection with *Mtb*[167] and are a significant component of TB-associated lipid droplets[166]. More than a visual cue of metabolic dysfunction in the cell, lipid droplets are a significant energy and carbon source for *Mtb*[68]. In some agreement with this, *Mtb* enzyme Rv2252 is a verified diacylglycerol kinase involved in the production of phosphatidyl-*myo*-inositol mannosides, *Mtb*-specific lipids[168].

In fact, *Mtb* depends on host lipids as a primary carbon source during infection. Jain et al. show that *Mtb* prefers β-oxidation of fatty acids over glycolysis during infection, shifting its metabolism upon entry into the host cell[169]. These authors found an increase in membrane content of odd-chain lipids in *Mtb* isolated from infected cells, suggesting that the bacteria selectively shifts to β-oxidation during infection[169]. Along the same lines, Chandra et al. used inhibitors of fatty acid β-oxidation and found that they severely restrict the intracellular growth of *Mtb* in tissue culture[170], and Yang et al. showed that inhibiting β-oxidation enhances *Mtb* clearance in a mouse infection model[171]. Beyond β-oxidation, many reports have found links between *Mtb* and host cholesterol. Mendum et al. used a transposon mutant library to identify genes that enable *Mtb* fitness during infection[124]. Among their findings, they identify a preponderance of cholesterol-catabolizing enzymes that are required for bacterial persistence/growth[124]. These findings are supported by many similar reports dating back decades[172–177].

These are only a few of the many examples of the manners in which lipids are essential for *Mycobacterium tuberculosis* during infection. We must now shift course briefly to introduce sphingolipids, as this enigmatic class of lipids appears to play decisive roles in *Mtb*'s struggle for control of the macrophage.

2.5. Sphingolipids overview

2.5.1. Sphingolipid synthesis and trafficking

Sphingolipids are a diverse class of membrane lipids distinguished by a shared sphingoid base. Through much concerted effort, these enigmatic lipids are slowly being recognized for their many roles in neuronal health, development, apoptosis, membrane stability, and signaling capacity. We and others have extensively described the mechanisms of sphingolipid synthesis and trafficking. We recommend the following references for more in-depth reviews of these topics: Chapter 7[178], Chapter 3[179], Chapter 4, Hannun, 2018[180], Wattenberg, 2018[181], Quinville et al., 2021[81], and Gault et al., 2010[182]. For this review, we, too, must dive into the sphingolipid synthesis and salvage pathways to begin discussing how sphingolipid biology may influence a *Mycobacterium tuberculosis* infection.

As depicted in Figure 2.2, sphingolipid production begins in the endoplasmic reticulum. The first and rate-limiting step of sphingolipid synthesis is the condensation of the amino acid L-serine with palmitoyl-CoA via the serine palmitoyltransferase complex (SPT) to produce the transient product 3-ketodihydrosphingosine (KDS). SPT is composed of two primary subunits (SPTLC1 and SPTLC2, though SPTLC3 appears partially redundant with SPTLC2) and acts in tight conjunction with two downstream enzymes: 3-ketodihydrosphingosine reductase reduces KDS to dihydrosphingosine and a cohort of [dihydro]ceramide synthases (CerS1-6) append a secondary acyl chain of varying length. Dihydroceramide Δ4-desaturase (DES) reduces dihydroceramide to produce ceramide (Cer), the nexus of sphingolipid metabolism. After all these initial steps of sphingolipid synthesis, it is from Cer that all complex sphingolipids will be made.

Why maintain the redundancy of six individual ceramide synthases? Recent work has shown that CerS enzymes prefer appending fatty acyl chains of distinct lengths (with some overlap), and different tissues express different proportions of each enzyme. CerS selectivity for chain length was excellently reviewed by Ho et al. in 2022[183] – here, briefly: CerS1 is most expressed in the brain and skeletal tissues and appends a C18 acyl-CoA; CerS2 appends a C22-24 acyl-CoA and is ubiquitously expressed, though enriched in the liver and kidney; CerS3 appends C26-34 acyl-CoA and is expressed in skin and testes; CerS4 is expressed in skin, leukocytes, heart, and liver and adds a C18-20 acyl-coA; CerS5 and CerS6 both append a C14-16 acyl-CoA chain, but CerS5 is minimally expressed save for the skin, testes, and kidneys while CerS6 is expressed primarily in the intestine and kidneys[183]. The many chain length variants of Cer will be differentially modified into many variants of "higher" sphingolipids within the *trans*-Golgi apparatus, a process which occurs in tight coordination with Cer synthesis. Crucially, the total Cer content in the ER membrane is kept at trace levels by ORMDL proteins, which sense excessive Cer buildup and inhibit the SPT complex if excess Cer accumulates in the ER[71]. Many have previously shown that ER Cer accumulation triggers an apoptotic cascade, resulting in cell death[184].

The Cer transport protein (CERT) mediates the transfer of Cer to the *trans*-Golgi. Here, a relatively small portion of Cer is modified with glucose, galactose, or lactose to produce a cohort of glyco-

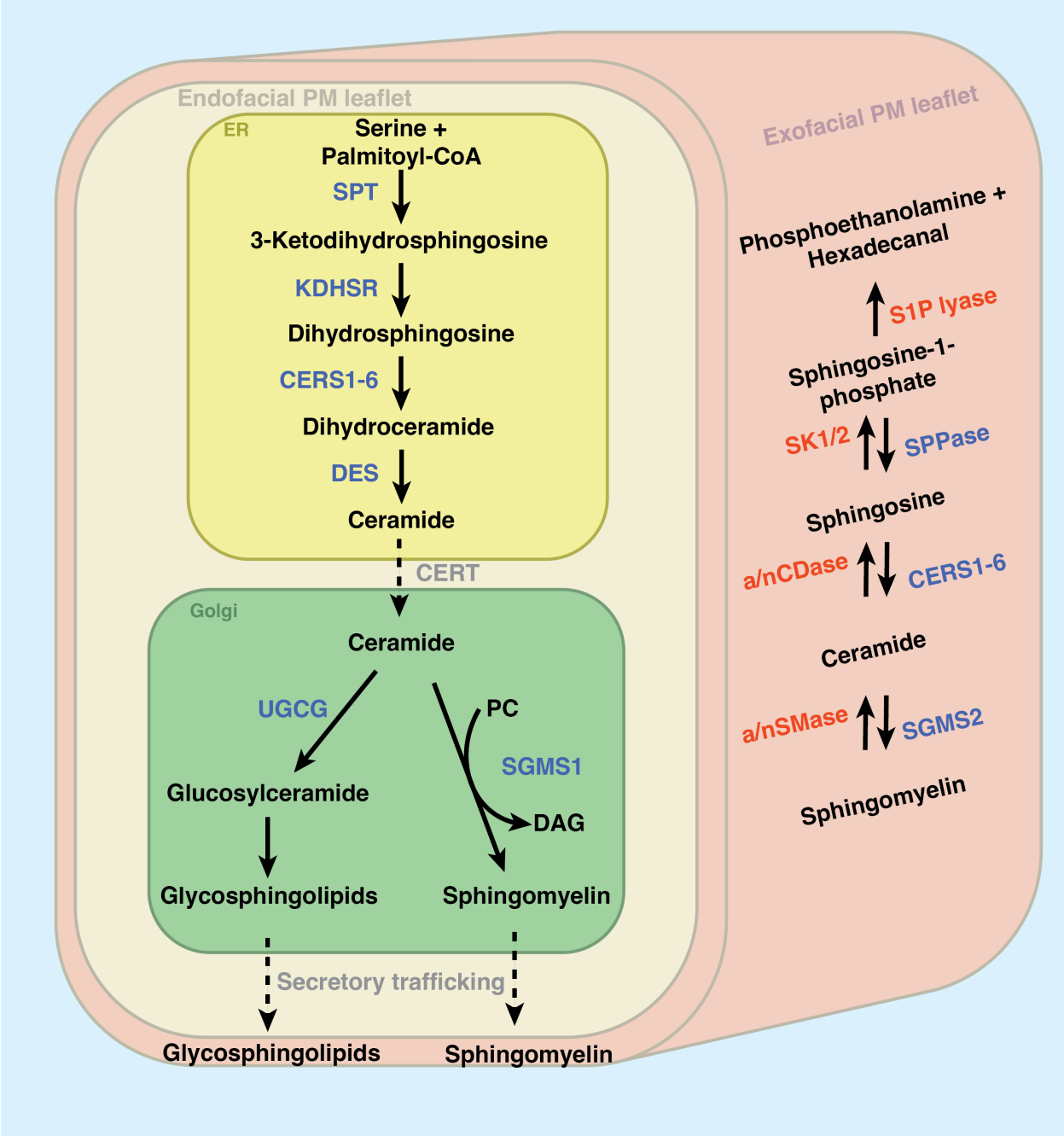


Figure 2.2. – **Sphingolipid synthetic and metabolic pathway** Abbreviations: SPT = Serine palmitoyltransferase; KDHSR: 3-Ketodihydrosphingosine reductase; CerS1-6 = Ceramide synthase 1-6; DES = dihydroceramide Δ4-saturase; CK = Ceramide kinase; C1PP = Ceramide-1-phosphate phosphatase; UGCG = UDP-glucose ceramide glucosyltransferase; PC = phosphatidylcholine; SGMS1/2 = Sphingomyelin synthase 1/2; DAG = Diacylglycerol; a/nCDase = Acid/neutral ceramidase; a/nSMase = Acid/neutral sphingomyelinase; S1PL = Sphingosine-1-lyase; SK1/2 = Sphingosine kinase 1/2; SPPase = Sphingosine-1-phosphate phosphatase.

ceramides, further modified into products such as globosides, gangliosides, sulfatides, and many so-called glycosphingolipids (GSLs)[87,182]. However, the bulk of total Golgi Cer is converted into sphingomyelin (SM) by sphingomyelin synthase 1 (SMS1) by transferring a phosphocholine headgroup from phosphatidylcholine, producing diacylglycerol (DAG) as a side-product[182]. Intriguingly, this secondary role for SMS1 (producing DAG) is a primary mechanism of regulating DAG synthesis in the Golgi[185]. Among others, Cerbon et al. report that DAG produced by SMS1 regulates PKC activity and cell proliferation[186].

Once synthesized, the vast majority of SM and glycosphingolipids are exported to the plasma membrane via secretory vesicular trafficking. These trafficking patterns are mediated by highly selective proteins that direct the newly synthesized lipids to the appropriate compartments in the cell. In 2007, Koivusalo et al. showed that the chain length of the secondary acyl chain of SM impacts its trafficking throughout the cell[187]. In support of this, in 2012, Contreras et al. identified an SM binding domain in the COPI sorting protein p24. This domain selectively binds one particular SM species, SM(d18:0/18:0), and mediates its transport to the plasma membrane[188]. Genetically transferring this binding domain to p23 confers SM binding capacity. Similarly, the protein FAPP2 transports glucosylceramide within the Golgi for further modifications[189] and, as its name would suggest, the ceramide 1-phosphate transport protein mediates the transport of ceramide 1-phosphate between the Golgi and the plasma membrane[190].

Most sphingolipids in the cell accumulate as SM or GSLs at the plasma membrane[191]. The glut of the remaining intracellular pool of sphingolipids is located in the endosomal compartment of the cell[191]. The endosomal SM primarily comprises lipids re-internalized from the plasma membrane during events such as phagocytosis[187]. The role of these endosomal SM and GSLs will be discussed extensively in Chapter 4. These intracellular sphingolipids are the primary source of the so-called "bioactive sphingolipids," which are short-lived and induce potent cellular effects.

2.5.2. Sphingolipid breakdown: signaling through salvage

Freysz and Mandel showed in 1980 that the half-life of SM can be measured in weeks or years, depending on the tissue[192,193] – in contrast, sphingosine 1-phosphate (S1P) has a half-life as low as fifteen minutes in the blood[194]. The shorter half-lives of sphingolipids such as S1P reflect the potency of their effect as signaling molecules. Perhaps the most well-characterized example of sphingolipid signaling, S1P is a potent chemotactic signal for lymphocytes: T cells express S1PR1 (one of five S1P receptors) and rapidly extravasate from the circulatory system to sites of tissue damage or infection up a gradient of S1P concentration[195]. Because lymphocytes must travel up an S1P gradient during chemotaxis, S1P in the plasma and healthy tissue must be kept at exceedingly low concentrations and produced in rapid excess in damaged or infected tissue. Given these potent effects and these short half-lives, one may ask: "Where do signaling sphingolipids come from?"

Of course, the cell can synthesize bioactive signaling lipids such as Cer and S1P via *de novo* synthesis, trafficking these products through the Golgi, and exporting them through secretory vesicular trafficking. Indeed, Menuz et al. and others have shown that *de novo* ceramide synthesis is upregulated in response to hypoxia and anoxia[196,197]. However, recent work has shown that the primary source of bioactive sphingolipids is the degradation of SM and GSLs at the plasmas membrane and within the endosomal compartment[81,194]. As depicted in the right side of Figure 2.2, SM can be sent back through the sphingolipid synthesis cascade to result in localized accumulation of Cer, Sph, and S1P[182]. Several sphingomyelinases (SMases) are known. Neutral SMase is most active at neutral

pH and mainly resides in the outer leaflet of the plasma membrane (mainly cleaving extracellular SM). The highly related acid sphingomyelinase (aSMase) is regulated by acidic pH – this enzyme is primarily active within the lysosome. The degradation of lysosomal SM (and the subsequent production of sphingosine) induces targeted autophagy of the lysosome (lysophagy) and, subsequently, programmed cell death[198]. Additionally, cytosolic SMase activity has been shown to play a role in coordinating membrane repair mechanisms[199,200]. Similar glycosphingolipid-degrading enzymes can send glycosphingolipids back through the synthesis cascade to produce ceramide[182].

Enzymes such as sphingomyelinase also allow cells to acquire extracellular sphingolipids and incorporate them as membrane constituents via salvage[182]. We have previously reported that ablating all forward sphingolipid synthesis (via genetic knockout or inhibition of the SPT complex) does not fully deplete a cell of all sphingolipids[179] – and in fact, we anecdotally note that cells inhibited in sphingolipid production rapidly die when cultured in serum-free media.

Having described the sphingolipid metabolic network, we can discuss how sphingolipids are involved in disease before returning to their potential roles during *Mycobacterium tuberculosis* infection.

2.5.3. Sphingolipids and disease

Dysregulation of sphingolipid biology is intricately tied to many diseases. We and others have written extensively on this topic (Chapter 7)[82,180,201], and this review will only briefly touch on some of the most well-characterized examples of diseases of sphingolipid dysregulation, as the scope of sphingolipid metabolism disorders encompasses every step of the sphingolipid pathway and could easily fill many volumes.

Several of the most studied sphingolipid disorders cause lysosomal storage disorder (LSD). A spectrum of more than 70 individual diseases, LSD is generally a progressive disorder that results in the accumulation of lysosomal contents[202]. The most common LSD is Gaucher disease, a genetic deficiency in the glucocerebrosidase (GBA) enzyme. GBA mediates the cleavage of glucosylceramide into glucose and ceramide, and the severity of the disease aligns with the activity of a patient's GBA alleles[202]. Gaucher disease is characterized by developmental neurological delays, progressive loss of bone density, and cachexia[202]. Beyond Gaucher disease, GBA mutations are strongly associated with the neurodegenerative Parkinson's disease[203].

Similarly, Fabry disease is the product of mutations in the alpha-galactosidase (GLA) enzyme, which results in the accumulation of another glycosphingolipid, globotriasylceramide (GL3)[202]. Enzyme replacement therapy (ERT) is an effective treatment for many Gaucher and Fabry patients. In ERT, patients receive infusions of exogenous enzyme to complement the deficient endogenous activity[202,204]. During the production of these therapies, the recombinant enzyme is mannosylated – this encourages endocytic uptake and, conveniently, the trafficking of the enzyme directly to the site in which it is needed[204]. Ongoing efforts are underway to find delivery methods to treat the neurological manifestations of these diseases, as in ERT, the recombinant enzyme does not efficiently cross the blood-brain barrier[203].

Beyond lysosomal storage disorders, sphingolipids are known to play intricate roles throughout development, aging, osteoporosis, and many cancers. The interface between host and pathogen is an intriguing and developing research arena. We have previously written on this topic (including several of the works presented in this dissertation: Chapter 8[74], Chapter 7[178]), as have others.

Utermolen et al. discussed in 2008 the role of aSMase as a target for several bugs, including *Neisseria gonorrhoeae* and *Listeria monocytogenes*[133]. These authors find that aSMase appears essential for enabling the many membrane fission/fusion events that must occur as the lysosome matures. We have published similar reports on the necessity of sphingolipid production for efficient phagocytosis of environmental pathogens (Chapter 3)[179,205].

Notably, sphingolipids are largely absent from the prokaryotic lipidome - with the exception of a handful of bacterial phyla, including *Bacteroides*, *Sphingomonas*, and *Sphingobacterium*[206–209]. The many roles that these bacterial sphingolipids play in human health are discussed at length by Bai et al, 2023[209] – these roles span from pro- to anti-inflammatory among commensal bacterial strains[207,210]. Here it must be noted that *Mtb* is not among the bacterial families which are capable of *de novo* sphingolipid synthesis – an *in vitro*, cultured *Mtb* bacillus is devoid of all sphingolipids; however, numerous reports have shown that *Mtb* does express a gene, Rv0888, which has demonstrable sphingomyelinase activity[211], and which allows *Mtb* to utilize carbon from SM during replication[212].

With this context, we can return to the roles of sphingolipids during *Mtb* infection.

2.6. Open questions regarding sphingolipids in *Mtb* infection

There are many open questions regarding how sphingolipids may influence the progression of a tuberculosis infection. We can categorize these questions into groups: (1) Does *Mtb* utilize host sphingolipids as a carbon source? (2) Does sphingolipid dysfunction in host cells impact *Mtb* survival/growth or TB disease progression? And, finally, (3) Can sphingolipid biology be modulated to serve as host-directed therapy? We will briefly summarize the current literature surrounding each of these questions below.

It is known that *Mtb* utilizes host lipids as a source of carbon and energy: this includes stimulating cells to produce triacylglycerides and sterols in high abundance and storing them in lipid droplets, and subsequently utilizing fatty acids released from these triacylglycerol and sterols by lipases; these fatty acids appear to be used in both fatty acid β-oxidation (energy production) and directly utilized in the synthesis of *Mtb* lipids[68,176,213–216] Many fewer studies have investigated the utilization of host sphingolipids – however, as noted above, in 2015, Speer et al. identified the sole enzyme with SMase activity in the *Mtb* genome, Rv0888, and that the expression of this enzyme is dependent on the presence of SM and enables *Mtb* growth on SM-supplemented minimal growth media[212]. Further, Dang et al. showed that this enzyme is both membrane-bound and secreted and contributes to lung pathology by exacerbating neutrophil-induced inflammation[217]. Much work remains to fully understand whether other sphingolipids may similarly serve as energy sources for *Mtb* during infection. For instance, the above studies by Speer et al. and Dang et al. do not investigate GSLs or Cer as potential catabolites of Rv0888.

More work has sought to characterize the roles of sphingolipids in the host antimicrobial response to *Mtb*. In one example, Nadella et al. and others have reported that the potently bioactive sphingolipid sphingosine 1-phosphate (S-1P) is a crucial factor in stimulating the recruitment of T cells and macrophages to the site of *Mtb* infection and that high localized levels of this sphingolipid product stimulate potent M1 differentiation in macrophages – activating the production of inducible nitric oxide synthase (iNOS)[218–220]. Nadella et al. also showed that S-1P treatment enhanced control of *Mtb* infection in both *in vivo* and *in vitro* mouse models[218]. However, other studies have shown that

direct S-1P treatment via aerosolization can induce hyperresponsiveness to bronchoconstriction – perhaps precluding its utility as an antitubercular therapeutic[221]. An alternative to direct S-1P would be to increase the activity of sphingosine kinase (SphK), which produces S-1P, or increase the abundance of sphingosine substrate for SphK, as discussed below.

In another example of sphingolipids modulating the severity/progression of infections, McGovern et al. showed that aSMase deficiency confers high susceptibility to infectious pneumonia[222] and that active TB patients display lower aSMase activity[220]. Wu et al. found in 2020 that aSMase deficient mice are highly susceptible to infection by the attenuated Bacillus Calmette-Guerin (BCG) strain of *M. bovis*. Adoptive transfer of wildtype (aSMase+) macrophages into knockout mice (aSMase-) restores the ability to control BCG infection[223]. Vasquez et al. observe that Functional inhibitors of acid sphingomyelinase (FIASMAs), a common category antidepressant including amitriptyline and desipramine, have been shown to result in enhanced mycobacterial growth[224]. These reports on aSMase regulating the antimicrobial response to *Mtb* are intriguing because several mechanisms appear simultaneously enabled by aSMase activity.

Ceramide produced by aSMase has direct biological effects within the lysosome. In one example, Cer directly regulates proteases such as Cathepsin D (CTSD). While CTSD has been long known to be inhibited via membrane association[225], Heinrich et al. showed in 2000 that CTSD activity is directly coupled to aSMase activity, and it has since been shown that direct binding of Cer stimulates autoproteolysis to release a 32 kD catalytically active CTSD protein from the lysosomal membrane fraction[226,227]. Others have similarly found that Cer binds to Cathepsin B[228], phospholipase A2[229], and the kinase suppressor of Ras-1[230]. Cer's activation of these and many other proteins is at least partially related to this lipid's self-association into Cer-enriched platforms[231,232]. As described above, Cer produced by aSMase induces direct cellular effects and also serves as the primary cellular source for other signaling sphingolipids, such as sphingosine 1-phosphate.

As a product of the above mechanisms, aSMase activity has been tightly linked to the regulation of cell death pathways – namely, the decision between inflammatory necrotic cell death and non-inflammatory apoptotic cell death. Lysosomal SM-derived Cer serves as a second messenger that induces translocation of BAX from the cytosol to the mitochondria, inducing loss of mitochondrial integrity and cytochrome *c* release[233]. In parallel, it has been long known that mycobacterial infection appears to manipulate this pathway to induce non-inflammatory necrotic cell death[234]. The subtlety between routes of cell death that promote *Mtb* control versus those that enable unrestricted *Mtb* growth is yet to be fully characterized – though this has been the subject of many studies: Butler et al. review contradicting evidence by several studies, and they report that mycobacterial virulence is not a factor on necrotic versus apoptotic cell death[235–238]. Bringing a long point home: there are many open questions regarding how aSMase activity may be a critical inflection point in the success or failure of an *Mtb* infection, and much work remains to explore the possibility of modulating this enzyme in a host-directed therapy.

As noted by Mohammed et al. in their 2022 review, the sphingolipid pathway is ripe with HDT possibilities[220]. However, the nuances of infection mean that different patients may require dramatically different paradigms of sphingolipid modulation, depending on their latent-vs-active TB state, lipid profile, and immunocompetence. Much work remains to uncover how sphingolipids influence the progression of an *Mtb* infection. Questions such as these have compelled the work in this dissertation. In Chapter 3, we will explore our findings that sphingolipids are essential for the initial stage of *Mtb* infection: entry into the host cell via phagocytosis. In Chapter 4, we will discuss the apparent role of sphingolipid synthesis in repairing endosomal/lysosomal damage induced by *Mtb* pathogenicity factors.

2.7. Challenges and breakthroughs in studying lipids

With all the evidence described above establishing sphingolipids as strong candidates for host-directed therapy, one must ask: why are there so many open questions about how SM, Cer, and S-1P affect *Mtb* infection? With the clear ties with cell survival and immune signaling, one would expect a concerted effort to address whether this pathway is amenable to HDT. However, studying lipids can be challenging, with logical pitfalls and technical challenges.

I describe many such challenges in studying sphingolipids during viral infections in detail in Chapter 7[178]. In brief, however, lipids lie at the terminus of the central dogma – they are the product of a long series of chemical reactions mediated by proteins. One cannot use simple genetic tools (knockout or point mutations) to alter a lipid's structure or trafficking subtly. Each lipid species is a part of a complex metabolic network with astounding potential to be modified and subsumed into other lipid classes or degraded into base components. The comparatively small size of most lipid species precludes changing their structure dramatically, and their hydrophobicity/biochemistry often precludes ectopic treatment. Similarly, their small size means there are few interfaces with which a lipid-binding protein can strongly interact; for example, few lipids can participate in hydrogen bonding. Finally, the biophysics and effects of specific lipids prevent simple complementation via add-back experiments.

Sphingomyelin is an excellent example of a challenging lipid to study directly. Add-back experiments with SM are nearly impossible because this conical lipid strongly prefers planar, rigid, impermeable membrane structures, and treating cells with SM-enriched micelles can only provide a low percentage of SM content. Some studies have even proposed SM/Cholesterol liposomes as slow-release encapsulations for drug/vaccine delivery[239,240]. The utility of encapsulating drugs in liposomes of this composition lies in the fact that SM-enriched membranes are notably recalcitrant to fuse with other membranes, allowing these encapsulations to stay in the plasma longer[239,240]. In contrast, ceramide can be fed to cells as an ectopic source of sphingolipids[241]. However, it is well-documented that excess Cer is a potent inducer of apoptosis[86]. The apoptosis-inducing effects of Cer have driven substantial research into using Cer-loaded liposomes as a chemotherapeutic against cancer[241].

And, though this list is not comprehensive, a final challenge in studying lipids is that their metabolic network is a sprawling and complex architecture in which lipids are rapidly interconverted, modified, and catabolized. Blocking the synthesis of a particular lipid will result in accumulating its source inputs and losing any secondary products. For example, inhibiting sphingomyelin production results in ceramide accumulation, phosphatidylcholine accumulation, *and* a reduction in diacylglycerol production; the cell will partially respond to ceramide accumulation by reducing SPT activity, but it will also result in increased glycosphingolipid production[242,243]. In addition to these direct effects resulting from inhibiting the pathway, there can be secondary effects: blocking SMS activity also induces a significant loss of cellular cholesterol content[242]. Inhibiting or knocking out one enzyme is much like removing a node in a spider's web – the whole network must adjust to the node's absence.

These examples demonstrate that the reductionist approach has suited many aspects of biological study (observe the effects of gene knockout, then determine if reconstituting restores the *status quo*). With these challenges in mind, a question arises: "How *does* one study sphingolipids?" We have previously written extensively on genetic knockout to study the roles of sphingolipids (Chapter 7)[178]. Here, we will briefly touch on techniques that allow for measuring and visualizing native lipids and

techniques that employ synthetic lipid analogs to track the metabolism and interactions of the target lipids.

As with the field of genomics and the advent of next-generation sequencing, the fields of proteomics and lipidomics have seen an explosive maturation in the sensitivity, throughput, and depth of coverage that a mass spectrometer can achieve. The major hurdle has rapidly become: "How do we glean information from these tens/hundreds of thousands of mass spectra?" Tools like LIQUID[244] allow for rapidly identifying many lipid species from mass spectrometry data. Databases such as MycoMass also annotate many lipid species unique to mycobacteria. These improvements in computational tools allow for deeper exploration into the broad changes that occur during a complex event such as an *Mtb* infection.

However, even highly sensitive mass spectrometers have difficulty identifying and quantifying the presence of highly transient lipid species such as plasma membrane Cer or serum S1P. The speed and quality of sample preparation can have an immense impact on the concentrations measured for these lipids. Greene et al. recently reported a new technique for measuring plasma membrane Cer[245].

Similarly, a panel of sphingolipid-binding proteins serves as valuable tools in visualizing the localization and density of a sphingolipid. For example, the fluorescent fusion proteins lysenin-GFP and Equinatoxin-GFP enable the visualization of sphingomyelin via fluorescence microscopy. Lysenin and Equinatoxin were produced from pore-forming toxins isolated from *Eisenia fetida*[246] and *Actinia equina*[247]. Similarly, an anti-ceramide antibody allows one to visualize ceramide in fixed cells and tissue[248,249].

In parallel to these techniques, which enable the detection and visualization of native sphingolipids, a variety of synthetic sphingolipid analogs allow for in-depth analysis of the trafficking, protein-lipid interactions, and metabolism of select lipid species. Chief among these are the trifunctionalized lipid analogs reported by Höglinger, Haberkant, Farley, and Schultz[198,250–255]. These lipid analogs will be discussed in great detail in Chapter 6.

2.8. Conclusion

After years of research, it is clear that lipids play a crucial role in the interaction between *Mycobacterium tuberculosis* and host cells. Recent studies have further highlighted the importance of sphingolipids in directing the course of Mtb infection, and there is much interest in exploring the potential of sphingolipids as targets for host-directed therapy. This area of research has implications for developing new antitubercular therapies and broader implications for understanding how sphingolipids enable mammalian immune activity. As we unravel the complexities of Mtb infection, it is clear that a multidisciplinary approach to understanding the role of lipids in infection will be essential for developing new treatments and improving human health.

2.9. Contributions

GG compiled the concepts discussed in this review and wrote the entirety of the text. FGT oversaw the preparation of this review.

Part II.

Main Results

Chapter summaries

The four chapters presented here are the main body of this dissertation. In each chapter, we offer our findings regarding the roles of sphingolipids (or all lipids) during *Mtb* infection.

Breaking and entering

In this chapter, we explore sphingolipids' roles during the phagocytosis of *Mtb*. We find that sphingolipid synthesis, particularly that of sphingomyelin, is required to efficiently uptake bacterial particles. In characterizing the activation of the phagocytic signaling pathway, we find that sphingolipid depletion significantly alters the dynamics of the phagocytic receptor upon binding an *Mtb* bacillus. This co-authored chapter was published in mBio in 2021.

Sealing the Gaps

Here, we assess how sphingolipids influence the lifecycle of *Mtb* after entry into the host cell. We find that sphingolipid-deficient cells are sensitized to *Mtb*-induced endosomal damage and are deficient in membrane repair. We find that the loss of sphingolipid production in the host cell enables the bacteria to replicate more readily. These results are expected to be submitted imminently for review.

Living off the Fat of the cell

In this chapter, we investigate the effects of *Mtb* infection on the lipid composition of the host. We compare pathogenic and attenuated *Mtb* strains in search of signatures of *Mtb* machinations. Among many findings, we report that diacylglycerides are upregulated during all mycobacterial infections but that triacylglycerol production is only upregulated during pathogenic infection. Further, we find that antimicrobial lipids such as lysophospholipids and plasmalogens are significantly depleted during pathogenic infection. In contrast, these lipids are enriched during attenuated infection – suggesting that pathogenic *Mtb* directly subverts these antimicrobial efforts in the cell.

An Affinity for Sphingolipids

Finally, we use synthetic analogs of sphingolipid precursors to identify sphingolipid-interacting proteins during *Mtb* infection. We find significant differential interaction between infected and uninfected cells – including among several previously reported sphingolipid interactors. *Mtb* infection drives the *loss* of interaction with many endosomal and lysosomal proteins, suggesting dysregulation of these compartments. We also observe significantly differential enrichment of ribosomal, proteasomal, and chromatin-remodeling proteins – suggesting a dramatic reorganization of the protein content of the cell.

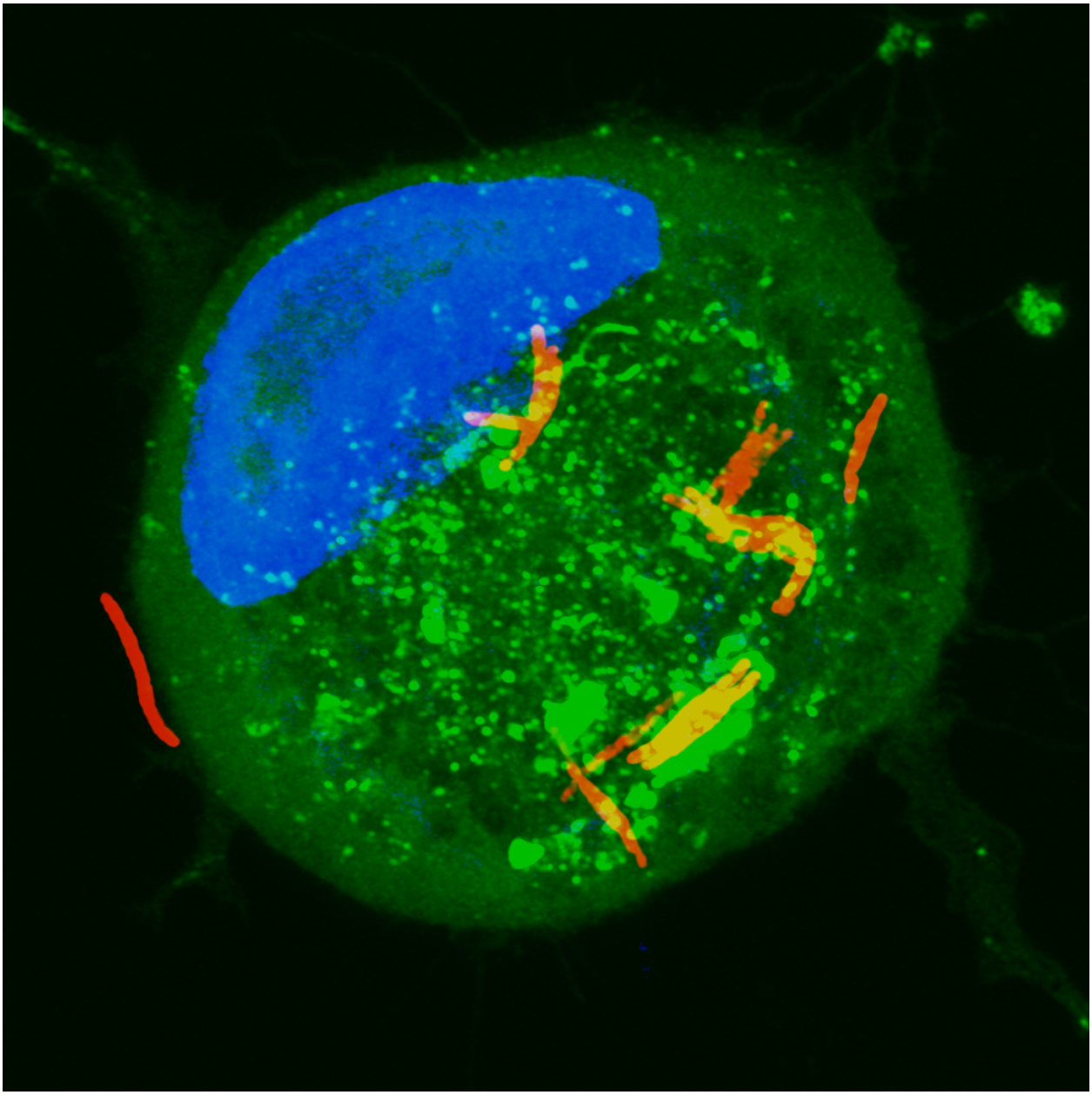


Figure 2.3. – ***Mtb* induces widespread intracellular damage throughout its host cell** A THP-1 macrophage expressing the fluorescent intracellular damage reporter mAG-Gal3 (Green) is infected with *Mtb* strain H37Rv-dsRed (Red). The nucleus is stained with DAPI (Blue).

Chapter 3.

Breaking and Entering

Sphingomyelin Biosynthesis Is Essential for Phagocytic Signaling during *Mycobacterium tuberculosis* Host Cell Entry

Authors: Patrick Niekamp[*,1], Gaelen Guzman[*,2], Hans C. Leier[2], Ali Rashidforokhi[2], Veronica Richina[2], Fabian Pott[2], Caroline Barisch[1], Joost C.M. Holthuis[1], Fikadu G. Tafesse[2]

[*] Patrick Niekamp and Gaelen Guzman contributed equally to the study. Since Patrick Niekamp started working on the project before Gaelen Guzman, his name is listed first. [1] Molecular Cell Biology Division, Department of Biology and Chemistry, University of Osnabrück, Osnabrück, Germany. [2] Department of Molecular Microbiology and Immunology, Oregon Health & Science University, Portland, Oregon, USA.

This chapter has been published in mBio at the following: https://doi.org/10.1128/mbio.03141-20

3.1. Abstract

Phagocytosis by alveolar macrophages is the obligate first step in *Mycobacterium tuberculosis* (*Mtb*) infection, yet the mechanism underlying this process is incompletely understood. Here we show that *Mtb* invasion relies on an intact sphingolipid biosynthetic pathway. Inhibition or knockout of early sphingolipid biosynthetic enzymes greatly reduces *Mtb* uptake across multiple phagocytic cell types without affecting other forms of endocytosis. While the phagocytic receptor Dectin-1 undergoes normal clustering at the pathogen contact sites, sphingolipid biosynthetic mutant cells fail to segregate the regulatory phosphatase CD45 from the clustered receptors. Blocking sphingolipid production also impairs downstream activation of Rho GTPases, actin dynamics, and phosphoinositide turnover at the nascent phagocytic cup. Moreover, we find that production of sphingomyelin, not glycosphingolipids, is essential for *Mtb* uptake. Collectively, our data support a critical role of sphingomyelin biosynthesis in an early stage of *Mtb* infection and provide novel insights into the mechanism underlying phagocytic entry of this pathogen.

3.2. Importance

Mycobacterium tuberculosis (*Mtb*) invades alveolar macrophages through phagocytosis to establish infection and cause disease. The molecular mechanisms underlying *Mtb* entry are still poorly understood. Here, we report that an intact sphingolipid biosynthetic pathway is essential for the uptake of *Mtb* by phagocytes. Disrupting sphingolipid production affects the segregation of the regulatory phosphatase CD45 from the nascent phagosome, a critical step in the progression of phagocytosis. We also show that blocking sphingolipid biosynthesis impairs activation of small GTPases and phosphoinositide turnover at the host-pathogen contact sites. Moreover, production of sphingomyelin, not glycosphingolipids, is critical for the phagocytic uptake of *Mtb*. These data demonstrate a vital role for sphingomyelin biosynthesis in an early step of *Mtb* infection, defining a potential target for anti-mycobacterial therapeutics.

3.3. Introduction

Mycobacterium tuberculosis (*Mtb*), the etiologic agent of tuberculosis (TB), remains a significant global health threat. It is estimated that more than two billion people around the world are infected with the latent form of *Mtb* and about 1.5 million die every year[256]. The success of *Mtb* as a pathogen relies on its ability to effectively enter the immune cells and establish its niche by subverting the defense mechanisms of the host[53,61]. Phagocytosis of *Mtb* by lung resident alveolar macrophages represents the obligate first step in the *Mtb* infection cycle. *Mtb* can proliferate in these cells, escape from the phagosome, and migrate to local lymph nodes to disseminate and spread the infection. Precise knowledge of the mechanism exploited by *Mtb* to invade immune cells is desirable, as this may yield novel targets and treatment options to combat TB.

Macrophages, along with dendritic cells and neutrophils, serve as professional phagocytic cells of the immune system that are specialized in the recognition, engulfment and elimination of microbial pathogens, thereby contributing to the first line of defense against infection. Phagocytosis is a receptor-initiated process involving a massive reorganization and deformation of the cell membrane coordinated by the underlying actin cytoskeleton to enable the internalization of microbial pathogens[257]. To this end, phagocytes are equipped with pattern-recognition receptors (PRRs) that bind ligands on the surface of the pathogen[115,258]. Prototypical PRRs include Toll-like receptors, scavenger receptors and C-type lectin receptors of the Dectin family. Activation of PPRs results from the clustering of several receptors upon binding to multiple adjacent ligands on the pathogen surface, which brings their cytosolic domains in close apposition. This initiates signaling by non-receptor tyrosine kinases of the Src family and the recruitment of phosphoinositide-modifying enzymes[115,259]. Local alterations in phosphoinositide levels and concomitant activation of Rho family GTPases orchestrate a remodeling of the actin cytoskeleton, which drives an extension of the plasma membrane along the particle to form a phagocytic cup. Further actin polymerization and contractile activity lead to membrane apposition and eventual sealing of the nascent phagosome, which then evolves into a degradative phagolysosome[115,259]. While the precise mechanism by which *Mtb* invades immune cells remains to be established, a wide variety of PPRs has been implicated in the recognition and phagocytic uptake of mycobacteria[260–262]. This apparent redundancy in the entry process hampers the development of an effective strategy to target a critical step in the infection cycle of *Mtb*.

Sphingolipids are essential lipids enriched in the plasma membrane of mammalian cells, where they interact with cholesterol to control vital membrane properties, serve as adhesion sites for extracel-

lular proteins, and play important roles in signal transmission and cell recognition[180,263,264]. Sphingolipids have also emerged as active participants in various infectious diseases. Various pathogens, including bacteria, fungi and viruses, modulate host membrane sphingolipids and their metabolites to manipulate host defense, thereby promoting their survival and pathogenicity[265]. For instance, *Neisseria gonorrhoeae* and *Pseudomonas aeriginosa* exploit the hydrolysis of cell surface sphingomyelin (SM) to generate ceramide-rich microdomains that serve as portals for their entry into macrophages[266,267]. Sphingolipids also play a critical role in the in vivo clearance of the pathogenic fungi *Candida albicans* through phagocytosis[205]. Moreover, mycobacteria utilize host sphingolipids and cholesterol as nutrient source for their growth and survival[268]. Although the role of host membrane cholesterol in the entry of different *Mycobacterium* species have previously been addressed[269], the function of sphingolipids in *Mtb* invasion has not been explored.

Here, we show that blocking sphingolipid biosynthesis causes a substantial reduction in the uptake of both *Mtb* and *Mycobacterium marinum* by a panel of macrophages and dendritic cells without affecting clathrin-mediated endocytosis or micropinocytosis. Time-lapse microscopy revealed that sphingolipid-deficient macrophages are capable of pathogen recognition and actin assembly at the contact site, but impaired in the subsequent remodeling of the actin cytoskeleton necessary to complete internalization of the pathogen. We also show that sphingolipid-deficient macrophages fail to exclude the regulatory tyrosine phosphatase CD45 from the receptor-pathogen contact site, a crucial step in the development of a functional phagocytic synapse. This defect was accompanied by an impaired activation of Rho GTPases and significant reduction in phosphoinositide turnover. Finally, we show that the production of SM, not glycosphingolipids, is essential for efficient *Mtb* uptake. Our findings offer fresh mechanistic insights into how *Mtb* invades immune cells and establish a critical role for SM in this process.

3.4. Results

3.4.1. Manipulation of sphingolipid levels in mammalian phagocytes

As depicted in Figure 3.1A, the initial and rate limiting step of sphingolipid biosynthesis is the production of a sphingoid base through the condensation of serine and palmitoyl-CoA, a reaction performed by the serine palmitoyltransferase (SPT) enzyme complex[270]. Genetic ablation of the SPT subunit Sptlc2 blocks the de novo synthesis of all sphingolipids, as does treatment with the atypical amino acid myriocin (Myr), a potent inhibitor of SPT activity[205]. The fungal toxin fumonisin B1 (FB1) acts several steps downstream in the sphingolipid biosynthetic pathway by blocking the activity of ceramide synthases (CerS)[205,271]. As the central nexus of sphingolipid biosynthesis, ceramide is converted into a variety of complex sphingolipids, including sphingomyelin (SM) and glycosphingolipids[182,272]. To define the role of sphingolipid biosynthesis in the phagocytic uptake of *Mtb*, we employed four different phagocytic cell lines: murine RAW246.7 macrophages, murine DC2.4 dendritic cells, human THP-1 and U937 monocytes (Figure 3.1B).

To verify the reported effects of Myr and FB1 on de novo sphingolipid biosynthesis, we monitored the incorporation of 3-L-[14C]-serine into sphingolipid species in RAW246.7, THP-1, DC2.4 and U937 cells after 3 days of drug treatment using thin layer chromatography (TLC) analysis. Across all four cell lines examined, treatment with Myr or FB1 in each case reduced incorporation of the serine isotope into SM by more than 90%; in contrast, incorporation of the isotope into phosphatidylserine (PS) was largely unaffected, (Figure 3.1D-F and Figure S3.1A and B). Genetic ablation of Sptlc2 in

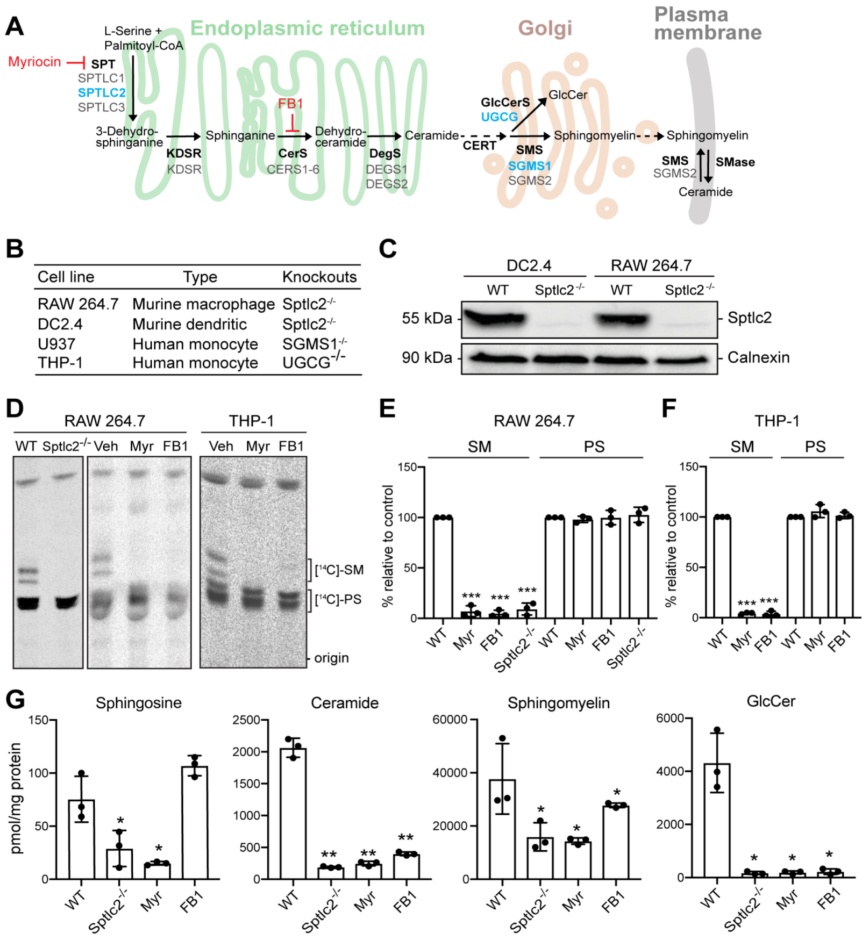


Figure 3.1. – Manipulation of cellular sphingolipid levels using genetics and chemical tools. (A) Schematic outline of the sphingolipid biosynthetic pathway. Inhibitors of sphingolipid biosynthetic enzymes used in this study are in red. Genes deleted using CRISPR/Cas9 are in blue. SPT, serine palmitoyltransferase; KDSR, 3-ketodihydrosphingosine reductase; CerS, ceramide synthase; DegS, δ4-desaturase; GlcCerS, glucosylceramide synthase; SMS, sphingomyelin synthase; FB1, fumonisin B1. (B) Phagocytic cell lines used in this study. (C) DC2.4 and RAW264.7 wild-type (WT) and Sptlc2$^{-/-}$ cells were processed for immunoblotting with antibodies against Sptlc2 and calnexin. (D) Sptlc2$^{-/-}$ and wild-type RAW264.7 or THP-1 cells were treated with myriocin or fumonisin B1 for 3 days and then metabolically labeled with 3-l-[14C]serine for 4 h. Total lipids were extracted and analyzed by thin-layer chromatography (TLC) and autoradiography. Veh, vehicle treated. (E and F) Quantification of [14C]SM and [14C]PS signals from TLCs shown in panel D. (G) Wild-type, Sptlc2$^{-/-}$, and inhibitor-treated RAW264.7 cells were subjected to total lipid extraction. Sphingosine, ceramide, sphingomyelin, and glucosylceramide (GlucCer) levels were quantified by LC-MS/MS. Data are means ± standard deviations (SD) (n = 3). *, P < 0.05; **, P < 0.01; ***, P < 0.001 (two-tailed unpaired t test).

RAW246.7 and DC2.4 cells also virtually abolished de novo SM production without affecting PS biosynthesis (Figure 3.1C-E and Figure S3.1A), in line with our previous findings[205].

We next examined the impact of drug treatment and Sptlc2 removal on the steady state sphingolipid levels. Both Myr-treated and Sptlc2$^{-/-}$ cells contained significantly (>=3-fold) reduced levels of sphingosine, ceramides, SM and glucosylceramide (GlcCer) in comparison to control cells (Figure 3.1G). In FB1-treated cells, we observed a reduction in the levels of ceramide, SM and GlcCer concomitant with an increase in sphingosine levels, as expected, (Figure 3.1G)[273]. The residual sphingolipid levels detected in Sptlc2$^{-/-}$, Myr- and FB1-treated cells are likely due to the activity of sphingolipid salvage pathways, through which cells may acquire sphingolipids from additives in the culture medium – primarily serum. This enables them to bypass the growth defect that is generally observed when sphingolipid biosynthetic mutants are cultured in serum-depleted medium. Indeed, we observed that RAW264.7 and DC2.4 cells lacking Sptlc2 grew equally well in serum-containing medium as their wild type counterparts (Figure S3.1C and D)[205].

3.4.2. Sphingolipid-deficient cells display a reduced capacity to phagocytose *Mtb*

To address whether sphingolipids participate in the phagocytic uptake of *Mtb*, RAW264.7, THP-1, DC2.4 and U937 cells were treated with Myr and FB1 for 3 days and then infected with a mCherry-expressing strain of *Mtb*. In brief, cells were infected at a multiplicity of infection (MOI) of 10 for 2 h, fixed and then stained with DyLight 488-conjugated phalloidin and DAPI to visualize filamentous actin (F-actin) and cell nuclei, respectively. Fluorescence microscopy was used to quantify uptake efficiency by automated counting of cell number (blue nuclei) and internalized bacteria (red fluorescent particles within green cell boundary; Figure 3.2A). Uptake efficiency was defined as the ratio of the total number of internalized *Mtb* particles against the total number of identified nuclei. The ratio is reported as a percentage of phagocytosis relative to the control cells. In all four cell models analyzed, we observed that Myr and FB1 treatment caused a significant (40-60%) reduction in *Mtb* uptake (Figure 3.2B and C; Figure S3.2A-D). Similarly, genetic ablation of Sptlc2 in RAW264.7 and DC2.4 cells results in a ~50% reduction in uptake relative to their wild type controls (Figure 3.2D and E). Collectively, these results indicate that an intact sphingolipid biosynthetic pathway is essential for an efficient uptake of *Mtb* by professional phagocytes. To test whether the same holds true for other mycobacteria, we used *Mycobacterium marinum*, a natural pathogen of poikilotherms that is closely related to *Mtb* and serves as a widely accepted model for TB[274,275]. Similar to infections with *Mtb*, Sptlc2$^{-/-}$ RAW264.7 and DC2.4 cells showed a ~50% reduction in phagocytic uptake of *M. marinum* relative to wild type cells (Figure 3.2F and G).

3.4.3. Sptlc2$^{-/-}$ cells are permissive to herpes simplex virus entry and clathrin-mediated endocytosis.

To determine whether an intact sphingolipid biosynthetic pathway is a general prerequisite for the entry of pathogens in professional phagocytes, we performed parallel infections of wild-type and Sptlc2$^{-/-}$ RAW264.7 cells with a fluorescent reporter strain of herpes simplex virus 1 (HSV-1) encoding a fusion of the viral protein VP26 and mCherry (28). HSV-1 is an enveloped virus that gains entry to host cells through the phagocytosis-like process of micropinocytosis; the viral receptor involved is nectin-1, also known as herpesviruses entry mediator[276,277]. At 12 h post-infection, we quantified the rates of HSV-1 infection using high-content imaging as described above. Because the

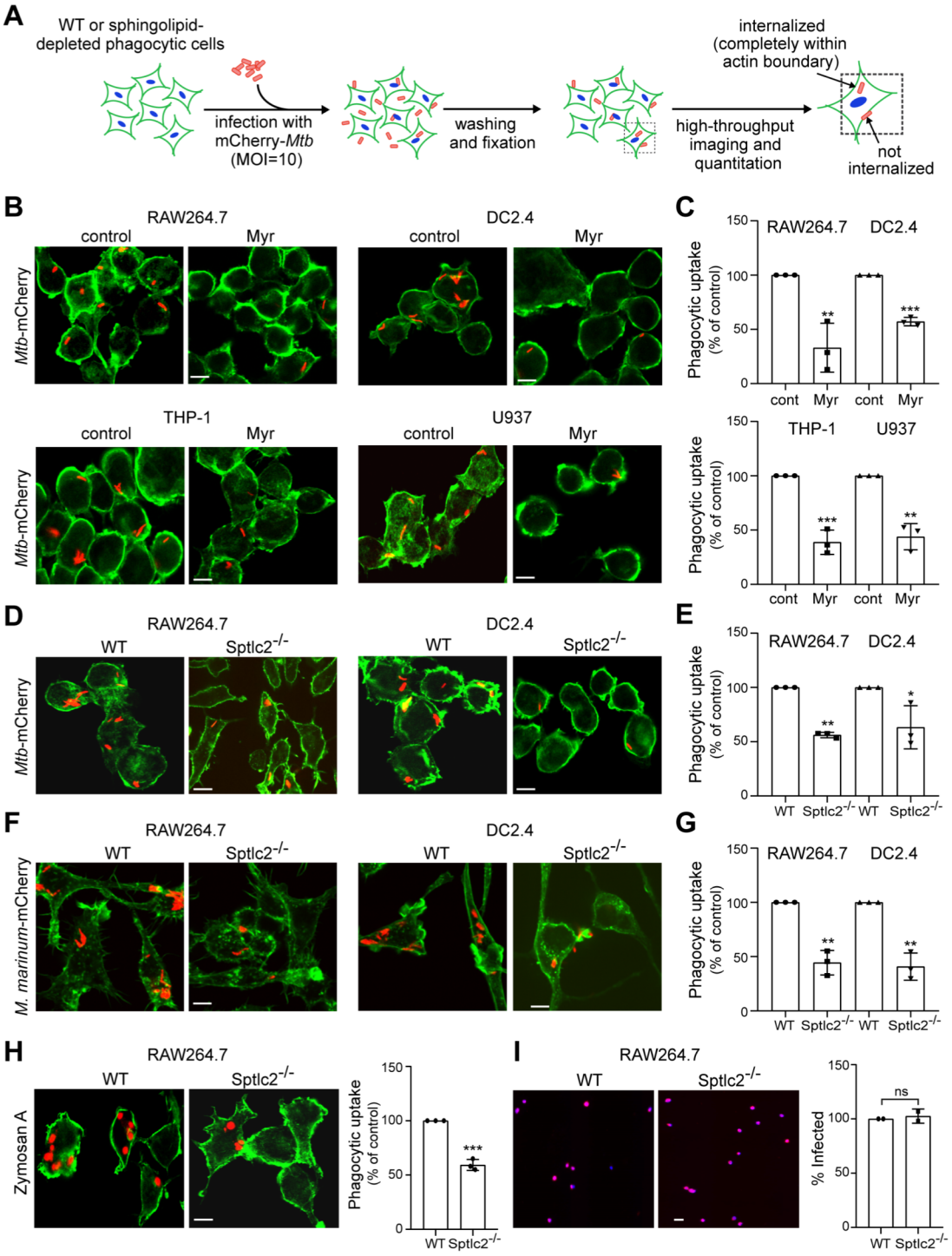


Figure 3.2. – **Sphingolipid biosynthesis is required for efficient phagocytosis of *Mtb*.** (A) Control and sphingolipid-depleted phagocytic cells were infected with mCherry-expressing *Mtb* at an MOI of 10 for 2 h, washed, fixed, stained with phalloidin Alexa Fluor 488 and DAPI, and then analyzed by high-throughput fluorescence imaging. The efficiency of phagocytic uptake was determined by dividing the total number of internalized bacteria by the total number of cells. (B) RAW264.7, DC2.4, THP-1, and U937 cells were grown in the presence or absence of myriocin for 3 days, infected with mCherry-expressing *Mtb*, and then processed as for panel A. (C) Quantification of *Mtb* uptake by cells treated as for panel B. (D) Wild-type and Sptlc2$^{-/-}$ RAW264.7 and DC2.4 cells were infected with mCherry-expressing *Mtb* and then processed as for panel A. (E) Quantification of *Mtb* uptake by cells treated as for panel D. (F) Wild-type and Sptlc2$^{-/-}$ RAW264.7 and DC2.4 cells were infected with mCherry-expressing *M. marinum* at an MOI of 10 for 2 h and then processed as for panel A. (G) Quantification of *M. marinum* uptake by cells treated as for panel F. (H) Wild-type and Sptlc2$^{-/-}$ RAW264.7 cells were incubated with zymosan A particles at an MOI of 1 for 1 h and then processed as for panel A. (I) Representative images of wild-type and Sptlc2$^{-/-}$ RAW264.7 cells infected with mCherry-tagged herpes simplex virus (HSV) at an MOI of 1. At 12 h post-infection, cells were fixed, stained with DAPI, and analyzed by high-throughput fluorescence

VP26-mCherry reporter construct localizes to the nucleus, we did not stain cells using phalloidin and instead used the co-localization of DAPI with mCherry to determine infection efficiency. However, we observed no significant difference in the HSV-1 infection rates between wild-type and Sptlc2$^{-/-}$ cells (Figure 3.2I). We also analyzed Myr-treated and control THP-1 cells for their ability to take up transferrin (Tf), which binds Tf receptors on the cell surface to enter cells via clathrin-mediated endocytosis[278]. As shown in Figure S3.2G and H, Myr treatment did not affect the endocytic uptake of transferrin. Collectively, these data indicate that sphingolipid biosynthesis is dispensable for HSV-1 entry and clathrin-mediated endocytosis, thus supporting a more specific role of sphingolipids in the phagocytic uptake of *Mtb*.

3.4.4. Sptlc2$^{-/-}$ cells display defects in filamentous actin dynamics during phagocytic uptake.

Particle ingestion by phagocytosis results from sequential rearrangements of F-actin and the overlying membrane. F-actin polymerization is the force driving membrane extension and phagosome formation. Nucleation of filaments at the site of particle recognition initiates F-actin polymerization and promotes formation of pseudopodia or lamellae. Then, actin filaments depolymerize at the base of the phagocytic cup, while polymerization proceeds in the tips of the lamellae to promote phagosomal membrane extension and closure[279] (Figure 3.3A). To determine at which step in this process sphingolipids exert their critical role, we monitored F-actin dynamics in wild-type and Sptlc2$^{-/-}$ RAW264.7 cells expressing LifeAct-mKate during infection with a monomeric GFP (mGFP)-expressing strain of *M. marinum*. Time-lapse fluorescence microscopy revealed that in wild-type RAW264.7 cells, F-actin readily assembled at sites of pathogen binding (Figure 3.3B; Supplemental Movie 1 3.8.1). In nearly all cases (89%; n = 46), this led to a successful internalization of the pathogen and clearance of F-actin polymers (Figure 3.3C). In contrast, while RAW264.7 Sptlc2$^{-/-}$ cells readily assembled F-actin at the site of pathogen recognition, in about half of the cases (47%; n = 30) the pathogen failed to enter and F-actin remained assembled at the contact site (Figure 3.3B and C; Supplemental Movie 1 3.8.1).

An in-depth microscopic analysis of the role of sphingolipids in the phagocytic uptake of *Mtb* and *M. marinum* is hampered by the fact that these pathogens are often internalized as heterologous clusters that comprise multiple bacteria. To overcome this limitation, we also analyzed wild-type and Sptlc2$^{-/-}$ RAW264.7 cells for their ability to take up zymosan A beads. These pathogen-mimicking particles engage the C-type lectin receptor dectin-1[205,280,281], which is one of several pathogen recognition receptors on professional phagocytes that recognize *Mtb* and initiate phagocytic signaling to facilitate host cell entry[282,283]. Sptlc2$^{-/-}$ RAW264.7 cells displayed an 40% reduction in the phagocytic uptake of zymosan A particles relative to wild-type cells (Figure 3.2H), similar to the defect in *Mtb* and *M. marinum* uptake observed in these cells (Figure 3.2D to G). Time-lapse microscopy revealed that in wild-type RAW264.7 cells, zymosan A particles initiating F-actin assembly at the recognition site were efficiently internalized, whereby depolymerization of F-actin at the base of the phagocytic cup and subsequent F-actin polymerization in the leading edges of the lamellae could be readily visualized in real time (90%; n = 30) (Figure 3.3D and E; Supplemental Movie 2 3.8.1). Again, while RAW264.7 Sptlc2$^{-/-}$ cells readily assembled F-actin at the site of particle recognition, in a significant number of cases the particles failed to enter (40%; n = 30) and F-actin polymers remained assembled at the contact site (Figure 3.3D and E; Supplemental Movie 2 3.8.1). In a complementary approach, wild-type and Sptlc2$^{-/-}$ RAW264.7 cells were incubated with IgG-opsonized zymosan A particles for 10 min and cell surface-bound particles were discriminated from

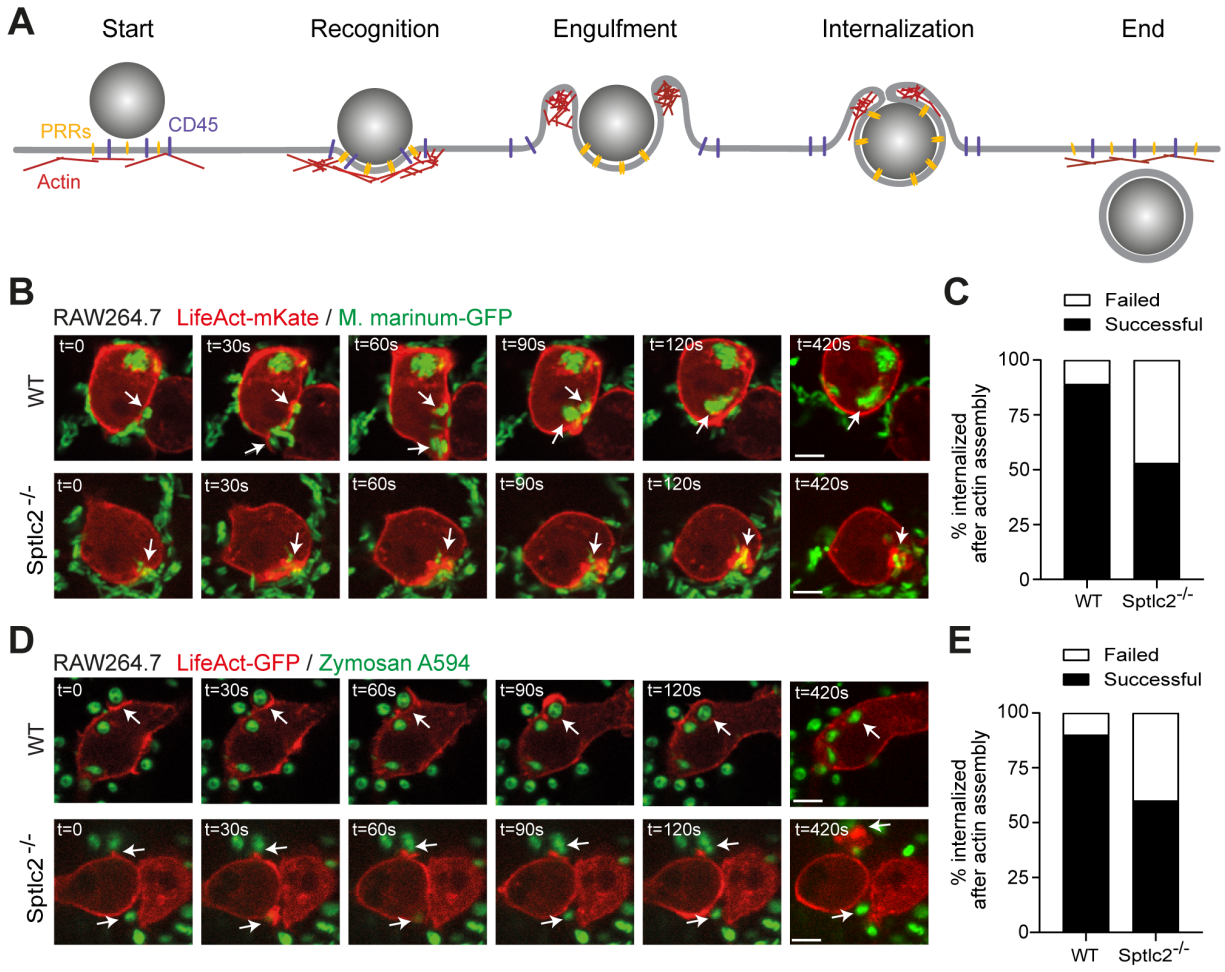


Figure 3.3. – **Sptlc2$^{-/-}$ cells display a defect in actin dynamics during phagocytic cup formation.** (A) Schematic outline of F-actin remodeling during phagocytosis. Clustering of pattern recognition receptors (PRRs) at the pathogen interaction site generates second messengers that promote local actin polymerization. Actin continues to be actively polymerized to extend the phagosomal membrane while being remodeled at the base of the phagocytic cup. Further actin polymerization and contractile activity lead to membrane apposition and eventually fusion to complete phagosome formation. (B) Time-lapse confocal images of wild-type and Sptlc2$^{-/-}$ RAW264.7 cells stably transduced with LifeAct-mKate (red) and infected with GFP-expressing *M. marinum* (green). Arrows indicate sites where mycobacteria trigger actin assembly, initiating formation of a phagocytic cup. Unlike wild-type cells, Sptlc2$^{-/-}$ RAW264.7 cells often failed to disassemble actin at the base of phagocytic cups, thus blocking entry of the mycobacteria. (C) Quantification of the percentage of successful versus failed phagocytic uptake events of *M. marinum* in wild-type and Sptlc2$^{-/-}$ RAW264.7 cells. (D) Time-lapse confocal images of wild-type and Sptlc2$^{-/-}$ RAW264.7 cells stably transduced with LifeAct-GFP (red) and incubated with zymosan A particles (green). Bar, 5 µm. (E) Quantification of the percentage of successful versus failed phagocytic uptake events of zymosan A particles in wild-type and Sptlc2$^{-/-}$ RAW264.7 cells. Data represent uptake events in >30 cells per condition. Bar, 5 µm.

internalized particles by immunostaining. Sites of F-actin polymerization were visualized by labeling cells with phalloidin Alexa Fluor 488. As shown in Figure S3.2E and F, Sptlc2$^{-/-}$ cells displayed a nearly 3-fold reduction in the ratio of internalized to cell surface-bound beads compared to wild-type cells. Together, these results indicate that sphingolipids are dispensable for the initial steps of phagocytosis, including pathogen recognition and the assembly of F-actin polymers at the contact site. Instead, it appears sphingolipids exert their critical role immediately downstream of these events, as Sptlc2$^{-/-}$ cells often fail to complete the sequential rearrangements of F-actin necessary for pathogen entry.

3.4.5. Sptlc2$^{-/-}$ cells fail to exclude CD45 from the pathogen contact site.

The engagement of PPRs with their ligands initiates receptor clustering at the phagocytic cup, followed by a lateral segregation of the inhibitory phosphatase CD45[259]. Because sphingolipids have been implicated as active participants in the organization of signaling complexes at the cell surface[284], we reasoned that sphingolipid levels at the plasma membrane may be critical for the aggregation of dectin-1 and/or exclusion of CD45 from that pathogen contact site. To experimentally address this idea, we transfected wild-type and Sptlc2$^{-/-}$ RAW264.7 cells with GFP-tagged dectin-1 and assessed the co-localization of the fluorescent receptor with CD45 following treatment with non-fluorescent zymosan A beads. As control, we also monitored the sub-cellular distribution of GFP-tagged dectin-1 in RAW264.7 cells upon infection with mCherry-expressing M. marinum. Dectin-1 readily accumulated at the particle contact site in M. marinum-exposed cells (Figure 3.4A; Figure S3.3A; Supplemental Movie 3 3.8.1 and Supplemental Movie 3 3.8.1). Besides supporting a role of dectin-1 in the phagocytic uptake of mycobacteria, these findings point to a significant overlap in the pathways that mediate host cell entry of zymosan A beads and mycobacteria. In both wild-type and Sptlc2$^{-/-}$ cells, dectin-1 aggregated at the zymosan A contact site within 2 min after bead exposure, indicating that sphingolipid biosynthesis is dispensable for ligand-induced receptor clustering. As expected, in wild-type cells, the inhibitory phosphatase CD45 was efficiently segregated from the dectin-1 clusters at the particle contact site (Figure 3.4B and C; Figure S3.3B)[259]. In contrast, CD45 failed to efficiently segregate from the dectin-1 clusters in zymosan A-treated Sptlc2$^{-/-}$ cells (Figure 3.4B and C).

To address whether a block in sphingolipid biosynthesis affects the overall surface levels of CD45 and dectin-1, wild-type and Sptlc2$^{-/-}$ RAW264.7 cells were stained with allophycocyanin (APC)-conjugated anti-CD45 and fluorescein isothiocyanate (FITC)-conjugated anti-dectin-1 antibodies and subjected to analytical flow cytometry. We found no differences in the overall fluorescent signals for both markers between wild-type and Sptlc2$^{-/-}$ cells (Figure S3.3C to F), indicating that the cell surface levels of endogenous dectin-1 and CD45 are unaffected by blocking sphingolipid biosynthesis. From this, we conclude that an intact sphingolipid biosynthetic pathway is required to enable a proper displacement of CD45 from the site of dectin-1 clustering, a step critical for the initiation of phagocytic synapse formation.

3.4.6. Activation of Rho GTPases Rac1 and Cdc42 is impaired in Sptlc2$^{-/-}$ cells.

Phagocytosis is strictly regulated through a signaling network that involves the recruitment of pathogen receptors and Rho GTPases to the particle contact site. Activated Rho GTPases

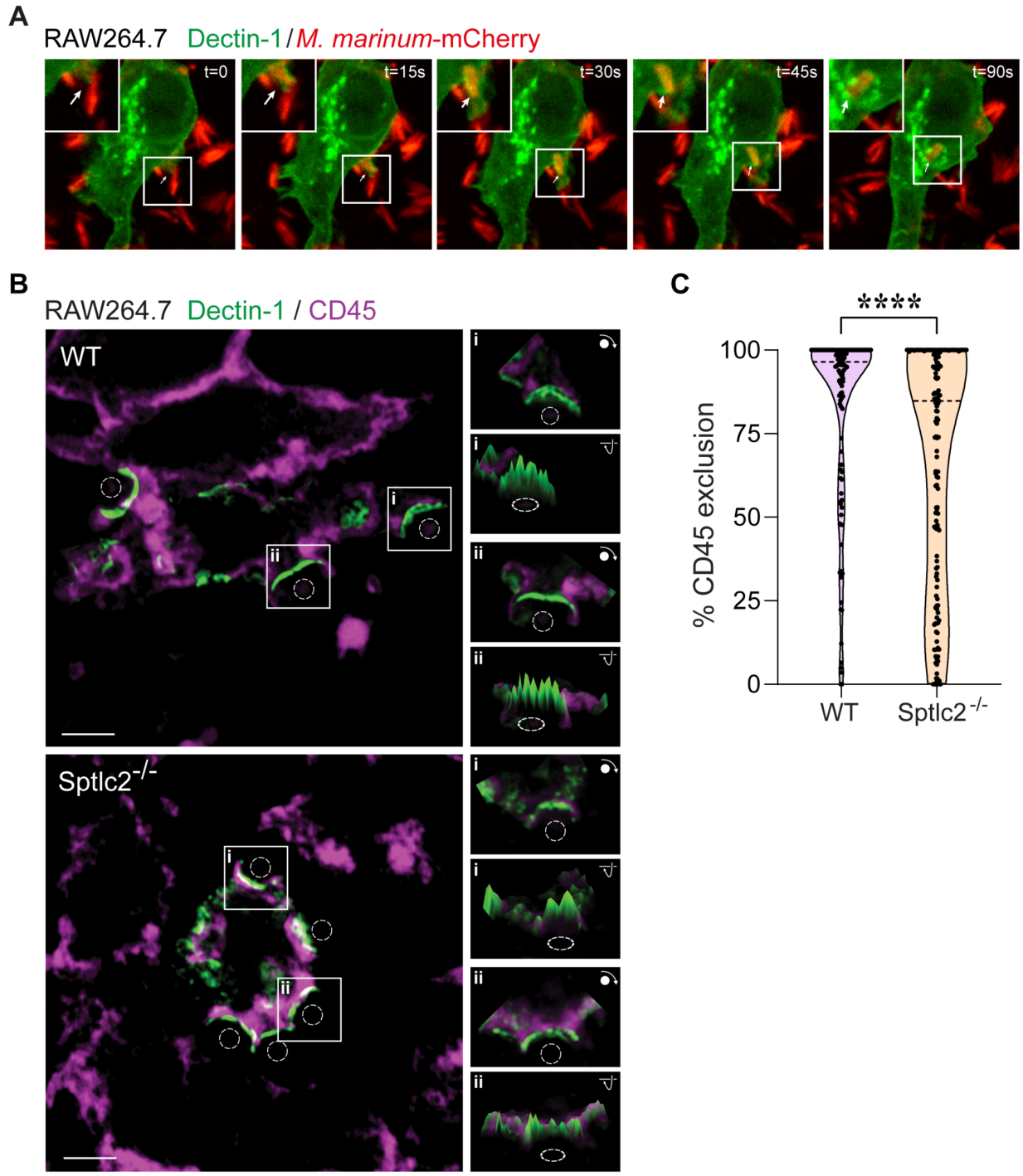


Figure 3.4. – **Segregation of CD45 from dectin-1 at the phagocytic cup is affected in Sptlc2$^{-/-}$ cells.** (A) Time-lapse confocal images of wild-type RAW264.7 cells transfected with GFP-tagged dectin-1 (green) and infected with mCherry-expressing *M. marinum* (red). Arrows indicate sites where mycobacteria trigger clustering of dectin-1. Bar, 5 µm. (B) Wild-type and Sptlc2$^{-/-}$ RAW264.7 cells transfected with GFP-tagged dectin-1 (green) were incubated with zymosan A particles (dashed circles) on ice, warmed to 37°C for 2 min to initiate phagocytosis, fixed, and then stained with antibodies against CD45 (purple). Representative slices of z-stacks are shown. Insets show fluorescence intensity profiles of CD45 and dectin-1-GFP signals in a single slice. Bar, 3 µm. (C) Violin plots showing the level of CD45 segregation from dectin-1-enriched phagocytic cups in wild-type and Sptlc2$^{-/-}$ RAW264.7 cells, defined as the percentage of dectin-1 volume containing no CD45 voxels. More than 100 individual cups were analyzed per cell line."****, P = 0.00006 by a two-tailed unpaired t test.

promote the conversion of phosphatidylinositol-4-phosphate (PI4P) to phosphatidylinositol-4,5-bis-phosphate [PI(4,5)P2] by stimulating phosphatidylinositol 5-kinase (PI5K). The local accumulation of PI(4,5)P2 is essential to initiate the polymerization of F-actin, a process that drives extension of the leading edges of the nascent phagosome around the particle[285]. However, to complete the engulfment and internalization of the particle, F-actin must disassemble at the base of the phagocytic cup. This is achieved through a local conversion of PI(4,5)P2 to phosphatidylinositol-3,4,5-tris-phosphate [PI(3,4,5)P3] by the phosphatidylinositol 3-kinase (PI3K) (Figure 3.5A)[257,285,286].

To determine whether blocking sphingolipid biosynthesis perturbs phagocytic signaling events downstream of pathogen receptor activation, we first focused on the activation and localization of the Rho GTPases Rac1 and Cdc42 in zymosan A-treated wild-type and Sptlc2$^{-/-}$ RAW264.7 cells. Visualization of activated Rho GTPases was enabled by transfecting cells with a fluorescent biosensor comprising yellow fluorescent protein (YFP) fused to the p21-binding domain of the p21-activated kinase PAK [PBD(PAK)-YFP][285,287]. At 24 h post-transfection, cells were incubated with zymosan A beads at an MOI of 10 and subjected to live-cell imaging. In wild-type cells, we observed a sharp increase in PBD(PAK)-YFP fluorescence at the particle contact site. Fluorescence levels peaked during particle engulfment, corresponding to the expected pattern of pathogen-induced Rac1/Cdc42 activation (Figure 3.5B and C; Supplemental Movie 5 3.8.1). In Sptlc2$^{-/-}$ cells, we also observed an increase in PBD(PAK)-YFP fluorescence upon particle recognition. However, the PBD(PAK)-YFP fluorescence intensity failed to reach the levels detected in zymosan A-treated wild-type cells and faded out prior to a successful particle internalization, suggesting that Sptlc2$^{-/-}$ cells are impaired in particle-induced activation of Rho GTPases (Figure 3.5B and C; Supplemental Movie 5 3.8.1).

3.4.7. Phosphoinositide turnover is impaired in Sptlc2$^{-/-}$ cells.

As PI(4,5)P2 and PI(3,4,5)P3 are key regulators of F-actin dynamics during phagocytosis (Figure 3.5A), we next monitored the spatial distribution of these phosphoinositides in zymosan A-treated wild-type and Sptlc2$^{-/-}$ RAW264.7 cells. To this end, cells were first transfected with a GFP fusion of the pleckstrin homology (PH) domain of the phospholipase Cδ [PH(PLCδ)-GFP], which serves as a fluorescent biosensor for PI(4,5)P2[257,288]. In zymosan A-treated wild-type cells, PH(PLCδ)-GFP was readily concentrated at the particle contact site and preferentially accumulated at the leading edges of the nascent phagosome during particle engulfment (Figure 3.5D and E; Supplemental Movie 6 3.8.1). In Sptlc2$^{-/-}$ cells, however, PH(PLCδ)-GFP was readily recruited to the contact site but remained associated with the base of the phagocytic cup, analogous to what we observed with the LifeAct-GFP probe (Figure 3.3D and E). This suggests that PI(4,5)P2 synthesis is initiated upon zymosan A binding but that PI(4,5)P2 turnover at the base of the phagocytic synapse is impaired in Sptlc2$^{-/-}$ cells (Figure 3.5D and E).

To check whether a block in sphingolipid biosynthesis affects the turnover of PI(4,5)P2 into PI(3,4,5)P3 in zymosan-A-treated cells, wild-type and Sptlc2$^{-/-}$ RAW264.7 cells were transfected with a GFP fusion of the PH domain of Akt (PH(AKT)-GFP), which serves as a fluorescent biosensor for PI(3,4,5)P3[257,288]. In wild-type cells, PH(AKT)-GFP was readily recruited to the particle contact site, and its membrane association increased sharply during particle engulfment (Figure 3.5F and G; Supplemental Movie 7 3.8.1). In contrast, Sptlc2$^{-/-}$ cells almost completely failed to mobilize PH(AKT)-GFP at the particle contact site (Figure 3.5F and G; Supplemental Movie 3.8.1). Together, these results indicate that blocking sphingolipid biosynthesis disrupts phosphoinositide metabolism

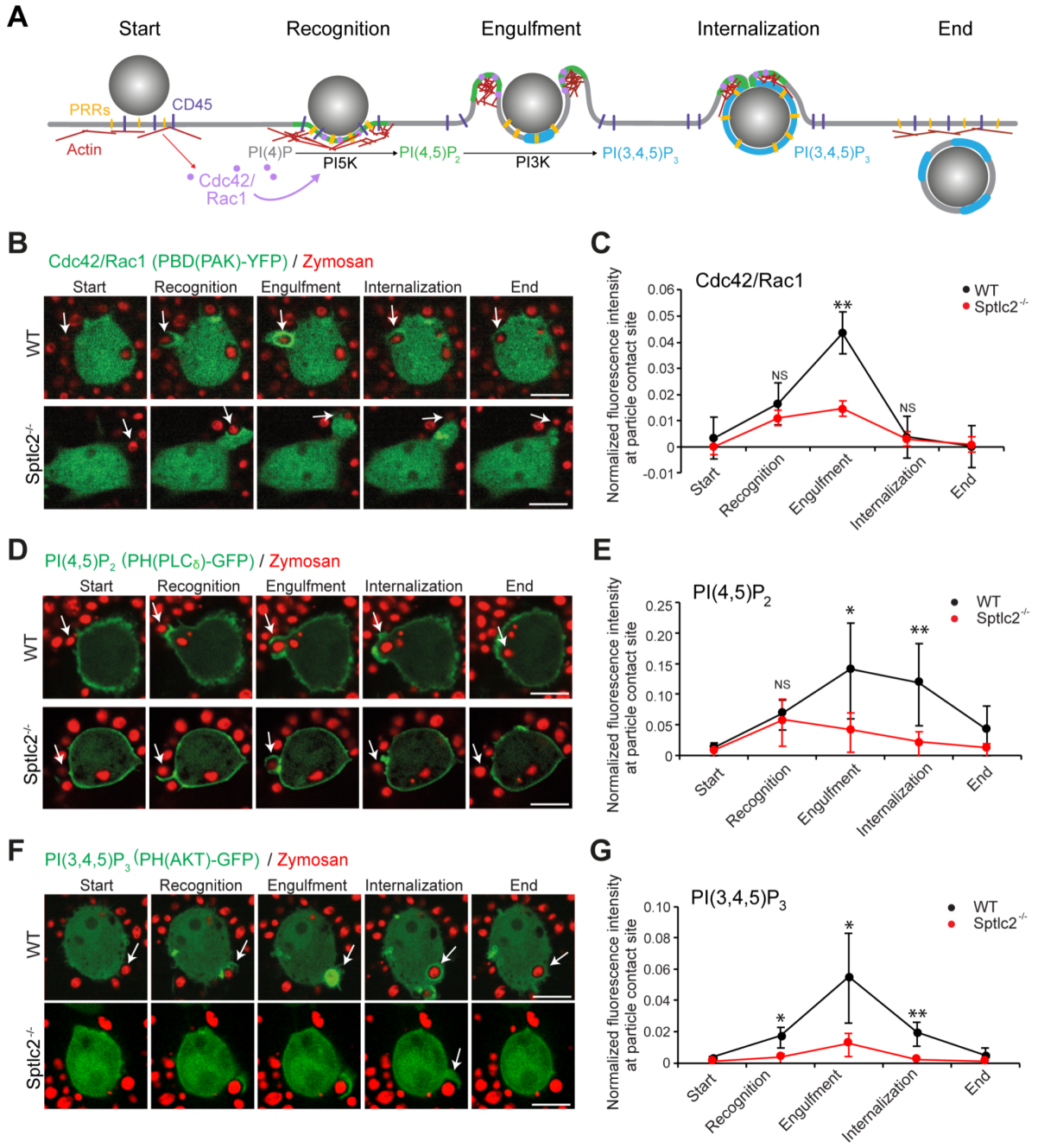


Figure 3.5. – **Sptlc2$^{-/-}$ cells display an impaired phosphoinositide turnover at the phagocytic cup.** (A) Schematic outline of molecular events underlying phagocytosis. Engagement of pattern recognition receptors (PRRs) with a pathogen initiates receptor clustering at the phagocytic cup, followed by a lateral segregation of the inhibitory CD45 phosphatase. This results in activation of the Rho GTPases Cdc42 and Rac1, which, in turn, stimulate PI5K activity to enable local production of PI(4,5)P2 and promote actin assembly. Next, PI3K orchestrates the turnover of PI(4,5)P2 to PI(3,4,5)P3, leading to actin disassembly at the base of the phagosome, a process required to complete the engulfment and internalization of the pathogen. (B) Time-lapse confocal images of wild-type and Sptlc2$^{-/-}$ RAW264.7 cells transfected with Cdc42 activity biosensor PAK(PBD)-GFP (green) and incubated with zymosan beads (red) at an MOI of 10. (C) Quantification of the PAK(PBD) fluorescence intensity in the course of phagocytic cup formation in cells treated as for panel B. (D) Time-lapse confocal images of wild-type and Sptlc2$^{-/-}$ RAW264.7 cells transfected with the PI(4,5)P2 biosensor PH(PLCδ)-GFP (green) and incubated with zymosan beads (red) as for panel B. (E) Quantification of the PH(PLCδ) fluorescence intensity in the course of phagocytic cup formation in cells treated as for panel D. (F) Time-lapse confocal images of wild-type and Sptlc2$^{-/-}$ RAW264.7 cells transfected with the PI(3,4,5)P3 biosensor PH(AKT)-GFP (green) and incubated with zymosan beads (red) as for panel B. Bar, 5 μm. (G) Quantification of the PH(AKT) fluorescence intensity in the course of phagocytic cup formation in cells treated as for panel F. Note that only a small fraction of the beads recognized by Sptlc2$^{-/-}$ mutant cells were internalized, in contrast to wild-type cells. Therefore, for Sptlc2$^{-/-}$ mutant cells, the normalized fluorescence intensity was determined at the particle contact site

at phagocytic synapses in zymosan A-treated macrophages, notably at the level of PI(4,5)P2-to-PI(3,4,5)P3 conversion, a step known to be critical for the internalization of pathogenic bacteria by professional phagocytes[289].

3.4.8. Production of sphingomyelin, not glycosphingolipids, is critical for efficient *Mtb* uptake.

Both SM and glycosphingolipids are highly enriched in the exoplasmic leaflet of the plasma membrane of mammalian cells. Therefore, we next addressed whether efficient phagocytic uptake of *Mtb* relies on the production of SM, glycosphingolipids, or both. Bulk production of SM is mediated by the enzyme sphingomyelin synthase 1 (SGMS1) in the trans-Golgi, whereas glycosphingolipid production is strictly dependent on the enzyme UDP-glucose ceramide glycosyltransferase (UGCG) in the cis-Golgi[182,290]. We used CRISPR (clustered regularly interspaced palindromic repeats)/Cas9 gene editing to ablate UGCG expression in THP-1 cells (Figure S3.3G), and the lab of S. V. Winter kindly provided us with SGMS1 knockout U937 cells[291]. Strikingly, SGMS1 knockout resulted in a major (□60%) reduction in the phagocytic uptake of mCherry-expressing *Mtb* by U937 cells (Figure 3.6A and B), similar to what we observed in myriocin- or FB1-treated U937 cells (Figure 3.2B and C; Figure S3.2A to D). In contrast, genetic ablation of UGCG had no impact on *Mtb* uptake by THP-1 cells (Figure 3.6C and D), even though phagocytosis of *Mtb* in THP-1 cells can be readily inhibited by myriocin and FB1 (Figure 3.2B and C; Figure S3.2C and D). Together, these data indicate that efficient uptake of *Mtb* by professional phagocytes is critically dependent on an intact SM biosynthetic pathway, whereas the production of glycosphingolipids is dispensable for this process.

3.5. Discussion

In this study, we report that the invasion of phagocytes by *Mtb* is critically dependent on an intact sphingolipid biosynthetic pathway. Blocking sphingolipid production does not impair clathrin-mediated endocytosis or macropinocytosis of herpes simplex virus, indicating that phagocytes remain susceptible to infection by pathogens that utilize other routes of cellular uptake. Strikingly, sphingolipid-deficient macrophages display normal pathogen-induced clustering of phagocytic receptors but fail to fully exclude the regulatory phosphatase CD45 from the phagocytic synapse. We also show that key steps in the downstream signaling cascade, notably Rho GTPase activation and phosphoinositide turnover, are significantly impaired in the mutant cells, leading to perturbations in actin dynamics and defective phagosome formation. Blocking production of SM, not glycosphingolipids, suffices to disrupt phagocytic uptake of *Mtb*. Collectively, our findings disclose a vital role of SM in an early step of *Mtb* invasion and establish a novel molecular framework for the underlying cellular process.

A major finding of this work is that macrophages defective in sphingolipid biosynthesis exhibit an impaired segregation of CD45 from pathogen-induced clusters of dectin-1 at the phagocytic cup. Dectin-1 belongs to a family of phagocytic cell surface receptors that participate in the internalization of pathogens, including *Mtb*[111,259,282] and *M. marinum* (this study). Upon pathogen engagement, these receptors cluster in the lateral plane of the membrane, bringing their cytosolic domains in close apposition[292]. The cytosolic domain of dectin-1 contains a hemi-immunoreceptor tyrosine-based activation motif (hemITAM), which becomes phosphorylated by Src and Syk family kinases

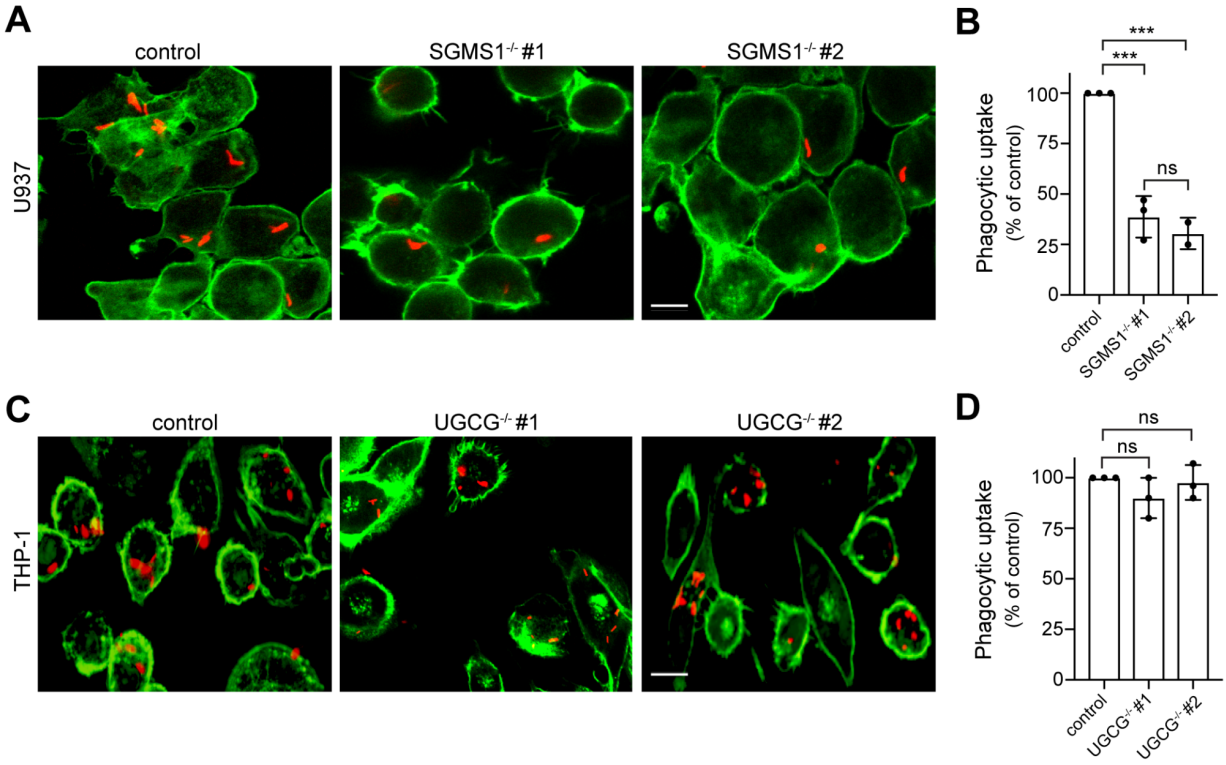


Figure 3.6. – **Production of sphingomyelin, not glycosphingolipids, is critical for efficient *Mtb* uptake.** (A) Wild-type and two independent SGMS1$^{-/-}$ knockout clones of U937 cells were infected with mCherry-*Mtb* (red) for 2 h, stained with phalloidin Alexa Fluor 488 (green), and then imaged by confocal fluorescence microscopy. (B) Quantification of *Mtb* uptake by cells treated as for panel A. (C) Wild-type and two independent UGCG$^{-/-}$ knockout clones of THP-1 cells were infected with mCherry-expressing *Mtb* (red) for 2 h, stained with phalloidin Alexa Fluor 488 (green), and then imaged by confocal fluorescence microscopy. Bar, 5 µm. (D) Quantification of *Mtb* uptake by cells treated as for panel C. U937 and THP-1 cells were activated with 50 nM PMA for 24 h before *Mtb* infection. Three independent experiments were performed, each in triplicate with at least 1,000 cells quantified per replicate. Data are means ± SD. ***, $P < 0.001$; ns, not significant (two-tailed unpaired t test).

upon receptor coalescence[259,293]. Importantly, segregation of the regulatory tyrosine phosphatase CD45 from the site of dectin-1 clustering is a crucial step in the amplification of a downstream phosphorylation cascade[259], which eventually culminates in the recruitment of phosphoinositide-modifying enzymes, including the phosphoinositide 3-kinase (PI3K)[257,294]. Thus, our finding that Sptlc2$^{-/-}$ macrophages fail to generate PI(3,4,5)P3 at the phagocytic cup might be due to an impaired phagocyte receptor signaling caused by a defective segregation of CD45. This is consistent with our immunoblot data, which show that sphingolipids are essential for phosphorylation of PI3K during phagocytosis. In particular, we found that blocking the de novo sphingolipid biosynthesis using myriocin in THP-1 cells resulted in a 3.5-fold reduction in phosphorylation of PI3K compared to that in control cells ($P < 0.01$; $n = 3$). PI3K activation and formation of PI(3,4,5)P3 at the pathogen engagement site are necessary for late stages of pseudopodium progression, the clearance of actin at the base of the phagocytic cup, and phagosome closure[257]. Indeed, time-lapse microscopy revealed that these processes are all significantly compromised in Sptlc2$^{-/-}$ macrophages. Collectively, our data suggest that blocking sphingolipid biosynthesis affects the phagocytic uptake of *Mtb* by precluding a proper activation of phagocyte receptors during pathogen engagement.

Another key observation is that production of SM rather than sphingolipid biosynthesis per se is critical for efficient phagocytic uptake of *Mtb*. SM is an abundant sphingolipid in the exoplasmic leaflet of the plasma membrane in mammalian cells. Owing to its saturated nature and hydrogen-bonding capacity, SM enables the formation of cholesterol-enriched microdomains[264]. In this capacity, SM may play a critical role in the lateral organization and activation of signaling complexes that promote *Mtb* invasion, consistent with prior reports indicating that cholesterol is essential for *Mtb* entry into macrophages[269]. However, an alternative scenario is that the phagocytic uptake of *Mtb* relies on the local generation of the SM-derived metabolite ceramide. Previous work revealed that hydrolysis of cell surface SM by acid SMase to liberate ceramide mediates the invasion of Gram-negative pathogens like *Neisseria gonorrhoeae* and *Pseudomonas aeruginosa* in mammalian cells[266,295,296]. Activation of acid SMase at the pathogen contact site appears to trigger local assembly of ceramide-enriched signaling platforms that initiate internalization[267]. While SMases and ceramides have also been implicated in mycobacterial infection[212,297,298], their role in the phagocytic uptake of *Mtb* remains to be established.

We previously reported that blocking sphingolipid biosynthesis in dendritic DC2.4 cells impairs phagocytosis of Candida albicans by preventing the assembly of F-actin at the particle contact site[205]. Moreover, the sphingolipid-deficient cells were unable to bind fungal particles and displayed a reduced number of dectin-1 receptors on their surface in comparison to controls. Here, we found that in sphingolipid-deficient RAW264.7 macrophages, which have normal dectin-1 levels, F-actin readily assembles at the particle contact site but fails to undergo subsequent remodeling to complete engulfment of the particle. Thus, sphingolipids in macrophages are required at a step in the phagocytic pathway downstream of particle recognition and receptor clustering. In dendritic cells, this requirement would be masked by a critical role of sphingolipids in maintaining an adequate number of dectin-1 receptors on their surface to enable actin polymerization at the particle recognition site. Why dectin-1 levels in macrophages are not affected by a loss of sphingolipids remains to be established. However, it is well known that the expression profiles of pattern recognition receptors vary considerably among different types of immune cells[299], and that macrophages expose a higher number of dectin-1 receptors on their surface than dendritic cells[300,301]. As these cell types likely also have different lipid compositions, it is conceivable that a block in sphingolipid biosynthesis differentially affects dectin-1 trafficking and/or turnover.

A 2-fold reduction in phagocytic uptake of *Mtb* caused by a block in sphingolipid biosynthesis re-

ported in here appears rather modest. However, it should be noted that both Sptlc2$^{-/-}$ mutant and myriocin-treated phagocytes still contain substantial amounts of SM, i.e., 30 to 40% of the amount found in control cells. As Sptlc2$^{-/-}$ mutant cells rely on serum-supplemented medium for growth (our unpublished observation), the residual amount of SM in these cells is likely derived from the serum. Consequently, our data may underestimate the actual functional relevance of SM in the phagocytic uptake of *Mtb*. While the therapeutic value of blocking sphingolipid production in the treatment of TB remains to be established, an ongoing clinical trial investigating the use of statins (a family of cholesterol-depleting drugs) as a synergistic co-therapeutic among a cocktail of frontline anti-tubercular agents has yielded encouraging results[295].

In sum, we show that *Mtb* relies on an intact SM biosynthetic pathway to efficiently invade professional phagocytes. While the latter process is critical for the clearance of pathogens, *Mtb* harnesses phagocytosis to gain entry into host immune cells and establish long-term survival. By offering fresh insights into the underlying mechanisms, our work provides a basis for the development of new strategies to fight this ancient pathogen.

3.6. Materials and Methods

3.6.1. Reagents

Myriocin and FB1 were purchased from Cayman Chemical Company. 3-l-[14C]serine was purchased from American Radioactivity. Phorbol 12-myristate 13-acetate (PMA) was purchased from BioLegend. Paraformaldehyde was purchased from Fisher Scientific. DyLight phalloidin 488 was purchased from Cell Signaling Technology, and Alexa Fluor 594- and 647-conjugated zymosan A (*Saccharomyces cerevisiae*) BioParticles were purchased from Thermo Fisher. Mouse monoclonal antibody against GAPDH (ab8245) was purchased from Abcam. Anti-rabbit IgG horseradish peroxidase (HRP)-linked antibody and anti-mouse IgG HRP-linked antibody were purchased from Cell Signaling. APC-conjugated rat monoclonal antibody against CD45 antibody (clone 30-F11) was purchased from BioLegend. Zymosan A BioParticles opsonization reagent was purchased from Invitrogen (no. Z2850). Cy3 AffiniPure donkey anti-rabbit IgG (heavy plus light chain [H+L]) was purchased from JIR (711-165-15). FITC-conjugated rat monoclonal antibody against dectin-1 (clone 2A11) was purchased from AbD Serotec. A Zombie Aqua fixable viability kit (no. 77143) was purchased from BioLegend.

3.6.2. Plasmids

The plasmids used for generation of lentivirus consists of the lentiviral vector (pCDH-sgRNA, pCW-Cas9 or pInducer20-LifeAct-mKate), the psPAX2 (packaging) and pMD2.G (envelope) plasmids. pCW-Cas9 plasmid was purchased from Addgene (no. 50661). For generation of pInducer20-LifeAct-mKate, DNA fragments encoding LifeAct-mKate (Addgene no. 54697) were created by PCR and inserted via KpnI and NotI sites into pENTR11 (Invitrogen). Using the Gateway cloning system (Thermo Fisher Scientific), the LifeAct-mKate fragment was transferred onto the lentiviral pInducer20 plasmid (Addgene no. 44012). pMXsIP-Dectin-1-GFP was kindly provided by the lab of Hidde Ploegh (Boston Children's Hospital, Boston, MA) (8). Active (GTP-bound) Rac1/Cdc42 was detected with PAK(PBD)-YFP, a plasmid encoding the PBD of PAK fused to YFP (40) obtained from

Addgene (no. 11407). PI(4,5)P2 was detected with PH(PLCδ)-GFP, a plasmid encoding the PH domain of PLCδ fused to GFP. PI(3,4,5)P3 levels were monitored by PH(AKT)-GFP, a plasmid encoding the PH domain of AKT fused to GFP[302]. These two fusion constructs were kindly provided by the lab of Hidde Ploegh (Boston Children's Hospital, Boston, MA).

3.6.3. Cell culture and small-molecule-inhibitor treatment

Human THP-1 monocytes (ATCC catalog no. TIB-22), human U937 monocytes (ATCC catalog no. CRL-1593.2), and mouse dendritic DC2.4 cells (Millipore catalog no. SCC142) were routinely cultured in RPMI medium supplemented with 10% FBS (Seradigm) and 1% penicillin-streptomycin (Pen/Strep) (Gibco). Mouse RAW264.7 macrophages (ATCC catalog no. TIB-71) were cultured in Dulbecco's modified Eagle medium (DMEM) supplemented with 10% fetal bovine serum (FBS) and 1% Pen/Strep. All cell lines were cultured at 37°C and 5% CO_2. Adherent cells (RAW264.7 and DC2.4), were trypsinized using 0.25% trypsin solution (Gibco) and counted using a hemocytometer and trypan blue solution (Gibco) as a counterstain. THP-1 and U937 cells were differentiated to macrophages in RPMI medium supplemented with 10% FBS and 50 ng/ml PMA. After 24 h, cells were washed and treated with 5 μM myriocin or 5 μM FB1 for 3 days in RPMI supplemented with 10% FBS and 1% Pen/Strep. RAW264.7 and DC2.4 cells were treated similarly with myriocin and FB1; however, 24 h before infection, cells were trypsinized, counted, and seeded at an appropriate density in 96-well plates or on coverslips. Biological replicates represent independent treatments with chemical inhibitors and infections on separate days.

3.6.4. Metabolic labeling and thin-layer chromatography

A total of 5×10^5 cells were seeded into a 6-well plate. Cells were labeled with 1 μCi/ml of 3-l-[14C]-serine for 4 h in Opti-MEM supplemented with the appropriate inhibitors. Cells were then washed twice with phosphate-buffered saline (PBS), and lipid extraction was done following the method of Bligh and Dyer[303].The methanol/chloroform-lipid extracts were dried with nitrogen gas. Dried lipids were redissolved in several drops of chloroform/methanol (1:2, vol/vol) and loaded on a TLC plate. Lipids were separated by developing the TLC plate first in acetone and then in a mixture of chloroform, methanol, and 25% ammonia solution (50:25:6, vol/vol/vol). Radio-labeled lipids were detected on a Storm 825 Phosphor-Imager (GE Healthcare).

3.6.5. Lipodome analysis

Liquid chromatography-tandem mass spectrometry (LC-MS/MS) analysis was performed as described previously (59). Lipids were extracted from lysed RAW246.7 cells according to 50 μg of protein by chloroform/methanol extraction. Before the extraction, a standard mix containing sphingosine (d17:1), ceramide (d18:1/17), glycosyl(β) (C12 Cer), and sphingomyelin (17:0) was used to spike each sample for normalization and quantification. The dried lipid films were dissolved in a mixture of mobile phase A (60:40, water/acetonitrile, including 10 mM ammonium formate and 0.1% formic acid) and mobile phase B (88:10:2, 2-propanol/acetonitrile/H2O, including 2 mM ammonium formate and 0.02% formic acid) with a ratio of 65:35. High-performance liquid chromatography (HPLC) analysis was performed using a C30 reverse-phase column (Thermo Acclaim C30; 2.1 by 250 mm; 3 μm; operated at 50°C; Thermo Fisher Scientific) connected to an HP 1100

series HPLC system (Agilent) and a QExactivePLUS Orbitrap mass spectrometer (Thermo Fisher Scientific) equipped with a heated electrospray ionization (HESI) probe. The elution was performed with a gradient of 45 min; during 0 to 3 min, elution started with 40% B and increased to 100% in a linear gradient over 23 min; 100% B was maintained for 3 min. Afterward, solvent B was decreased to 40% and maintained for another 15 min for column re-equilibration. The flow rate was set to 0.1 ml/min. MS spectra of lipids were acquired in full-scan, data-dependent MS2 mode. The maximum injection time for full scans was 100 ms, with a target value of 3,000,000 at a resolution of 70,000 at m/z 200 and a mass range of 200 to 2,000 m/z in both positive and negative mode. The 10 most intense ions from the survey scan were selected and fragmented with high-energy collisional dissociation (HCD) with a normalized collision energy of 30. Target values for MS/MS were set at 100,000, with a maximum injection time of 50 ms at a resolution of 17,500 at m/z 200. To avoid repetitive sequencing, the dynamic exclusion of sequenced lipids was set at 10 s. Peaks were analyzed using the Lipid Search algorithm (MKI, Tokyo, Japan). Peaks were defined through raw files and product ion and precursor ion accurate masses. Candidate molecular species were identified by a database (>1,000,000 entries) search of positive (+H+; +NH4+) ion adducts. Mass tolerance was set to 5 ppm for the precursor mass. Samples were aligned within a time window, and results were combined in a single report. From the intensities of lipid standards and lipid classes, absolute values for each lipid, in picomoles per milligram of protein, were calculated.

3.6.6. Generation of lentiviruses

Lentivirus production was performed as described previously[304]. Briefly, lentiviruses were produced by co-transfection of HEK293T cells with lentiviral transfer vectors containing the gene of interest (i.e., pCDH-sgRNA, pCW-Cas9, and pInducer20-LifeAct-mKate) and the packaging plasmids psPAX2 and pMD2.G. Transfection was performed with Lipofectamine 3000 (Thermo Fisher) according to the manufacturer's instructions. Cells were cultured in DMEM supplemented with 10% FBS, and the growth medium was replaced after 6 h. At 48 h after transfection, lentivirus-containing supernatants were harvested, centrifuged for 5 min at 1,250 rpm, and filtered through a 0.45-μm filter.

3.6.7. Generation of CRISPR/Cas9-mediated knockout cell lines

CRISPR/Cas9-mediated genome editing for genes involved in the sphingolipid pathway were performed as described previously[205]. Briefly, to generate the Sptlc2$^{-/-}$ knockout, RAW264.7 cells were infected with lentivirus (pCW-Cas9) encoding Cas9 cDNA and were cultured in medium containing 2 μg/ml of puromycin (Sigma-Aldrich). Potential target sequences for CRISPR interference were found with the rules outlined by Mali et al.[305]. The following two seed sequences (CRISPR target sequences) preceding PAM motifs found in the open reading frame of Sptlc2 gene were used: Sptlc2 #1, GAACGGCTGCGTCAAGAAC; Sptlc2 #2, AGCAGCACCGCCACCGTCG. The CRISPR target sequence for UGCG was GCTGTGGCTGATGCATTTCA. Potential off-target effects of the seed sequence were evaluated using the NCBI *Mus musculus* nucleotide BLAST. The CRISPR/Cas9-mediated Sptlc2-knockout RAW264.7 cell line and UGCG-knockout THP-1 cell line were generated as previously described[304]. Briefly, CRISPR gBlock was designed to be cloned into the NheI/BamHI site of pCDH-CMV(−) (SBI; CD515B-1) as follows: cacagtcagacagtgactcaGTGTCACAgctagcTTTCCCATGATTCCTT CATATTTGCATATACGATACAAGGCTGTTAGAGAGATAATTAGAATTAAT TTGACTGTAAACACAAAGATATTAGTACAAAATACGTGACGTAGAAAGTA ATAATTTCTTGGGTAGTTTGCAGTTTTAAAATTATGTTTTAAAATGGACT ATCATATGCTTACCGTAACTTGAAAGTATTTCGATTTCTTGGCTT-

TATAT ATCTTGTGGAAAGGACGAAACACCGnnnnnnnnnnnnnnnnnnnGTTTTA GAGCTAGAAATAG-CAAGTTAAAATAAGGCTAGTCCGTTATCAACTTGAAA AAGTGGCACCGAGTCGGTGCTTTTTTTg-gatccTGTGCACAgtcagtcac agtcagtctac (n, CRISPR target sequence; lowercase indicates extra nucleotides added to optimize synthesis or restriction enzyme sites). The gBlock was then digested using the restriction enzymes NheI and BamHI and ligated into the pCDH-CMV(−) vector, which had been linearized by digestion with the same restriction enzyme. The Cas9-inducible cells were infected with lentivirus carrying pCDH-CMV(−)-sgRNA and were cultured in medium containing 250 µg/ml of hygromycin B (Life Technology). To induce expression of Cas9, cells were treated with 1 µg/ml of doxycycline (Clontech) for 3 to 5 days. Clonal selection was performed by single-cell dilution on 96-well plates. The individual colonies were collected, and the expression of Sptlc2 was examined by immunoblotting using an anti-Sptlc2 antibody. U937 SGSM1$^{-/-}$ cells were kindly provided by Arturo Zychlinsky (Max Planck Institute of Biochemistry, Berlin, Germany), and the CRISPR/Cas9-mediated knockout cell lines were established as described by Virierra Winter et al.[291].

3.6.8. Culturing of *Mtb* and *M. marinum*

Culturing and infection of *Mtb* were conducted in a biosafety level 3 laboratory following general safety guidelines. *Mtb* strain H37R, constitutively expressing mCherry, was obtained from the Fortune lab (Ragon Institute, Cambridge, MA). *Mtb* was cultured with shaking at 150 rpm at 37°C in 7H9 broth medium supplemented with 50 µg/ml hygromycin B. Culturing and infection of *M. marinum* were conducted in a biosafety level 2 laboratory following general safety guidelines. *M. marinum* constitutively expressing mCherry was cultured with shaking at 150 rpm in 7H9 medium supplemented with 10% oleic acid-albumin-dextrose-catalase (OADC), 0.05% Tween 80, 0.2% glycerol, and 50 µg/ml hygromycin B at 32°C. To minimize clumping of the bacteria, Erlenmeyer flasks containing 5 mm glass beads were used. For infections, cultures with an optical density at 600 nm (OD600) of 0.8 to 1.0 were used.

3.6.9. *Mtb* and *M. marinum* infection

For infection of THP-1 and U937 cells, the cells were seeded in SensoPlate 96-well glass-bottom plates (Greiner Bio-One) at a density of 1.5×10^4 cells per well in RPMI supplemented with 10% FBS, 1% Pen/Strep and 50 ng/ml PMA at 37°C. One day after differentiation, cells were treated for 3 days with 5 µM myriocin, 5 µM FB1, or the vehicle. For infection of RAW264.7 and DC2.4 cells, the cells were cultured in RPMI supplemented with 10% FBS and 1% Pen/Strep and treated for 3 days before infection with 5 µM myriocin, 5 µM FB1, or the vehicle. At 24 h before infection, RAW264.7 and DC2.4 cells were used to seed SensoPlate 96-well glass-bottom plates (Greiner Bio-One) at a density of 2×10^4 cells per well. Before infection, the mycobacteria were first passaged through a 5-µm filter (SLSV025LS; Merck) and then passaged 10 times through a 25-gauge needle to avoid clumping. All cell lines and conditions were then infected with a multiplicity of infection (MOI) of 10 in RPMI supplemented with 10% FBS for 2 h at 37°C. Myr, FB1, and vehicle were kept during infection. Cells were washed with PBS and then fixed with 4% paraformaldehyde (PFA) overnight at 4°C.

3.6.10. Zymosan A uptake assay

For infection of RAW264.7 cells, 2.0×10^4 cells per well were seeded in SensoPlate 96-well glass-bottom plates (Greiner Bio-One). After 24 h, the cells were incubated with zymosan A beads at an MOI of 10 in RPMI supplemented with 10% FBS for 1 h at 37°C. Cells were washed with PBS and then fixed with 4% PFA overnight at 4°C.

3.6.11. Phagocytosis assay

The phagocytosis assay was performed as previously described[306]. Briefly, fixed cells were washed twice with PBS and incubated for 15 min in permeabilization buffer (0.1% Triton X-100 and 1% bovine serum albumin [BSA]). Cells were stained with phalloidin-Alexa Fluor 488 (Thermo Fisher) at a final concentration of 33 nM in permeabilization buffer for 60 min and washed once with PBS. After the phalloidin staining, cells were stained with DAPI for 10 min and washed 3 times with PBS. Cells were then imaged using a Keyence BZ-X700 microscope with a PlanFluor 20× objective. The parameters for imaging were kept the same for each sample. For image analysis, Keyence BZ-X Analyzer software was used. In brief, the outline of the cells was determined via the Alexa Fluor 488 signal (phalloidin staining), and the number and area of mCherry (*Mtb* and *M. marinum*) or Alexa Fluor 594 (zymosan A) signals in the Alexa Fluor 488 signal were detected by the program. In a second round, the number of cells was determined by counting the nuclei via DAPI staining. The number of bacteria or particles (mCherry or A594 signal) inside the cell was divided by the number of cells (DAPI signal) to identify the phagocytosis efficiency.

3.6.12. Herpes simplex virus 1 infection

HSV-1–mCherry reporter virus was kindly provided by the lab of David Johnson (Oregon Health and Science University, Portland, OR). Twenty-four hours prior to infection, 1×10^4 wild-type and Sptlc2 knockout RAW264.7 cells were seeded on glass coverslips in a 12-well plate. Cells were equally infected at an MOI of □1 and incubated for 12 h at 37°C and 5% CO_2. Coverslips were fixed for 20 min in 4% paraformaldehyde, stained with DAPI, and then imaged on a Keyence BZ-X700 microscope. Infection rates were calculated by dividing the mCherry-expressing cells by the total number of cells (DAPI signal).

3.6.13. Binding assay zymosan A particles

RAW264.7 cells were seeded in SensoPlate 96-well glass-bottom plates at 1.5×10^4 cells/well 24 h prior to the experiment. Before the experiment, unlabeled zymosan A particles were incubated with zymosan A opsonizing reagent (rabbit polyclonal IgG; Invitrogen) for 1 h at 37°C. The particles were washed 3 times with PBS and resuspended in RPMI supplemented with 10% FBS. Cell growth medium was replaced with medium containing opsonized zymosan A particles at an MOI of 10. The 96-well plates were centrifuged at 1,000 rpm for 30 s. Cells were incubated at 37°C for 10 min. Next, cells were placed on ice, washed twice with chilled PBS, and stained for 15 min at 4°C for external zymosan A particles with anti-rabbit-Cy3 (JIR). Afterwards, cells were fixed with 4% PFA for 15 min and stained with phalloidin Alexa Fluor 488 for 1 h. The ratio of internalized (blue)

beads to attached beads (red beads with clear phalloidin Alexa Fluor 488 signal) was quantified manually.

3.6.14. Real time imaging of phagocytosis

For transient transfection, RAW264.7 cells were seeded in SensoPlate 96-well glass-bottom plates at 1.5×10^4 cells/well 24 h prior to live imaging. Transfection was conducted with Lipofectamine 3000 according to manufacturer's instructions 16 h prior to imaging. Alternatively, RAW 264.7 cells containing a doxycycline-inducible LifeAct-mKate construct were seeded in SensoPlate 96-well glass-bottom plates at 1.5×10^4 cells/well 24 h prior to transfection, and the medium was supplemented with 1 µg/ml doxycycline. For imaging, the growth medium was aspirated and replaced with RPMI without phenol red, supplemented with 30 mM HEPES and containing mCherry-expressing *M. marinum* at an MOI of 25 or zymosan A BioParticles with Alexa Fluor 595 at an MOI of 10. The 96-well plates were centrifuged at 1,000 rpm for 30 s. The cells were imaged with an SDC microscope (Nikon), and 3 or 4 different spots per well were imaged at the same time for 60 min with capture intervals of 15 s. The parameters for imaging were kept the same for each sample.

3.6.15. Live imaging of dectin-1–GFP

RAW264.7 cells were seeded in SensoPlate 96-well glass-bottom plates at 1.5×10^4 cells/well 24 h prior to live imaging, and transfection was conducted with Lipofectamine 3000 according to the manufacturer's instructions 16 h prior to imaging. For imaging, the growth medium was aspirated and replaced with RPMI without phenol red, supplemented with 30 mM HEPES, and containing mCherry-expressing *M. marinum* at an MOI of 25. The 96-well plates were centrifuged at 1,000 rpm for 30 s. The cells were imaged with an SD microscope (Zeiss), and 3 or 4 different spots per well were imaged at the same time for 60 min with capture intervals of 15 s. The parameters for imaging were kept the same for each sample.

3.6.16. Live image analysis (quantification)

Of live cell images, individual images were selected for further analysis if they captured a cell bound to *M. marinum* or a zymosan A particle while maintaining a healthy morphology throughout the imaging time course. Imaging analysis was performed using FIJI software[301]. The parameters for image processing were kept constant when different data sets were compared. For Figure 3.3, all cells were included in the analysis that showed a clear recognition of the bacteria or particles, which was defined by an increase in F-actin signal around the bacterium or particle, and the number of successful versus failed internalizations was quantified. For Figure 3.5, all cells were included in the analysis that showed a clear recognition of the zymosan A particles, which was defined by an increase in the corresponding reporter signal at the particle contact site. For quantification of Figure 3.5, the area of the particle contact site was selected, cropped, and opened in a new window. The threshold for the particle contact site was set 1.5 times higher than the whole-cell threshold to exclusively detect an increase in fluorescence signal. The fluorescence intensity was measured at different time points by the analyze-measure function of FIJI. The values for the GFP threshold of the particle contact site area were divided by the values for the GFP threshold of the whole cell at the corresponding time points.

3.6.17. Dectin-1 and CD45 displacement assay

Raw 264.7 WT and Sptlc2$^{-/-}$ macrophages were seeded on glass coverslips in 24-well plates at a density of 50,000 cells per well and grown overnight. The next day, cells were transfected with dectin-1–GFP using Lipofectamine 3000 (Thermo Fisher) according to the manufacturer's instructions. At 24 h post-transfection, cells were washed three times with ice-cold PBS, chilled on ice for 5 min, and inoculated with a chilled suspension of zymosan A beads (250 μg/ml in serum-free DMEM, prepared with repeated vortexing). After brief centrifugation (3 min at 250 × g and 4°C), plates were incubated at 37°C for 3 min, washed three times with ice-cold PBS, and fixed for 15 min with room-temperature 4% PFA. Cells were permeabilized for 30 min with 0.2% saponin in PBS, incubated for 1 h in blocking buffer (5% normal goat serum, 0.01% saponin in PBS), and stained for 1 h with anti-CD45–APC (BioLegend) diluted 1:100 in blocking buffer. Coverslips were mounted on glass slides with ProLong Glass anti-fade mountant (Thermo Fisher). Super-resolution microscopy was performed on a Zeiss LSM 880 confocal microscope with the Airyscan module using a 63×, 1.4 numerical aperture (NA) oil immersion objective. Airyscan processing was performed with ZEN Black (Zeiss) using the software's preset parameters. Intensity profiles of dectin-1 and CD45 were created using the 2.5D visualization module. Measurement of CD45 exclusion from phagocytic cups was performed with Imaris 9.5 (Bitplane). All Airyscan images were converted to the .ims file format and subjected to background subtraction using the software's default settings. The Surfaces module was then used to build three-dimensional (3D) models of phagocytic cups using absolute intensity of dectin-1 signal and a volume cutoff of 1 μm3, followed by masking so that all signals outside the cups were set to zero. All images were fed through this Surfaces pipeline, and statistics files were downloaded in the Microsoft Excel format. Percent CD45 exclusion was calculated for each cup as [1 − (number of CD45 voxels/sum of CD45 and dectin-1 voxels)] × 100.

3.6.18. Immunoblot analysis

About 1×10^6 THP-1 cells were seeded in a 6-well plate and treated for 3 days with 5 μM myriocin or left untreated. Cells were then infected with *Mtb* (H37Rv) at an MOI of 10. At 10 min post-infection, cells were washed with PBS, lysed, separated by SDS-PAGE, and transferred to a membrane. Levels of PI3K phosphorylation were detected by immunoblot analysis using an anti-phospho-PI3K antibody (p85; clone 19H8; Cell Signaling Technology). Immunostaining with an anti-GAPDH antibody (clone D16H11; Cell Signaling Technology) served as a loading control. Results were from three independent biological replicates and normalized with GAPDH signal. Quantification of the bands was performed using FIJI, and a Student's t test was performed to show significance.

3.6.19. Flow cytometry

RAW264.7 wild-type and Sptlc2$^{-/-}$ cells were rinsed with PBS and lifted from the flask using treatment with trypsin. Fc receptor was blocked with CD16/32 antibody (1:100), and cells were stained with Zombie Aqua live/dead stain (1:200). Cells were then stained with either CD45-APC (1:200) or dectin-1–FITC (1:50) for 30 min. Finally, cells were fixed for 20 min in 4% paraformaldehyde and analyzed using an LSR-II flow cytometer. Cells independently stained with Zombie Aqua, CD45-APC, and dectin-1–FITC were used for compensation. Analysis was performed using FlowJo software.

3.6.20. Transferrin uptake analysis

Undifferentiated THP-1 cells were counted and plated in a SensoPlate 96-well glass-bottom plates (Greiner Bio-One) at a density of 2.5×10^4 in RPMI supplemented with 10% FCS, 1% PS, and 50 ng/ml PMA. Cells were allowed to differentiate at 37°C and 5% CO_2 for 3 days before being treated with 5 μM myriocin for another 3 days (or left untreated). These cells were then starved for 30 min in serum-free RPMI and treated with 100 nM Alexa Fluor 555-conjugated human transferrin (T35352; Thermo Fisher Scientific) resuspended in serum-supplemented RPMI. After a 30-min uptake, cells were washed once with PBS at pH 7.0 and once with PBS acidified to pH 5.0 (to release surface-bound transferrin) and fixed for 1 h at 4°C using 4% paraformaldehyde. Cells were stained with both DyLight 488-conjugated phalloidin (12935S; Cell Signaling Technology) and DAPI according to the manufacturer's specifications. Uptake comparison between untreated and myriocin treated cells was quantified using high-content imaging collected on a Keyence BZ-X700 microscope using a Super Fluor 40× oil immersion objective. Using Keyence BZ-X Analyzer software, cell interior was demarcated using the phalloidin signal, nuclear area was assessed using the 405 signal, and transferrin internalization was assessed using the 555 signal. Data are reported as the integrated 555 signal per cell, normalized by the 405-positive nuclear area, with three independent biological experiments and four technical replicates each. A competition assay was performed in the presence of additional non-fluorescent human transferrin (T8158-100MG; Sigma-Aldrich) and quantified with a CLARIOstar Plus fluorimeter (BMG Labtech). Fluorescence emission was collected using a spiral detection pattern averaging across 200 reads per well. Resultant data are reported as the raw fluorescence intensities, in arbitrary fluorescent units.

3.7. Acknowledgements

We thank Arturo Zychlinsky (Max Planck Institute of Biochemistry, Berlin, Germany), and David Johnson (Oregon Health and Science University, Portland, OR) for kindly providing reagents, cell lines, viruses, and plasmid constructs essential to the completion of this study. We also thank the members of the OHSU Advanced Light Microscopy Core and the OHSU Flow Cytometry Shared Resource for assistance and training in data collection and analysis; in particular, we thank Stefanie Kaech Petrie, Matthew Lewis, and Sara Christensen. Finally, we thank Madeleine Faucher, Marie Foss, and Jossef Osborn who kindly and patiently assisted in the editing and preparation of this work.

This work was supported by the Medical Research Foundation and National Institutes of Health (3R21AI124225-01A1 and 1R01AI141549-01A1) to F.G.T., and the Deutsche Forschungsgemeinschaft (projects SFB944-P14 and HO3539/1-1) to J.C.M.H.

We have no conflicts of interest to declare.

3.8. Supplementary materials

3.8.1. Supplementary videos

All supplemental movies are available online only! [Link to go here!]

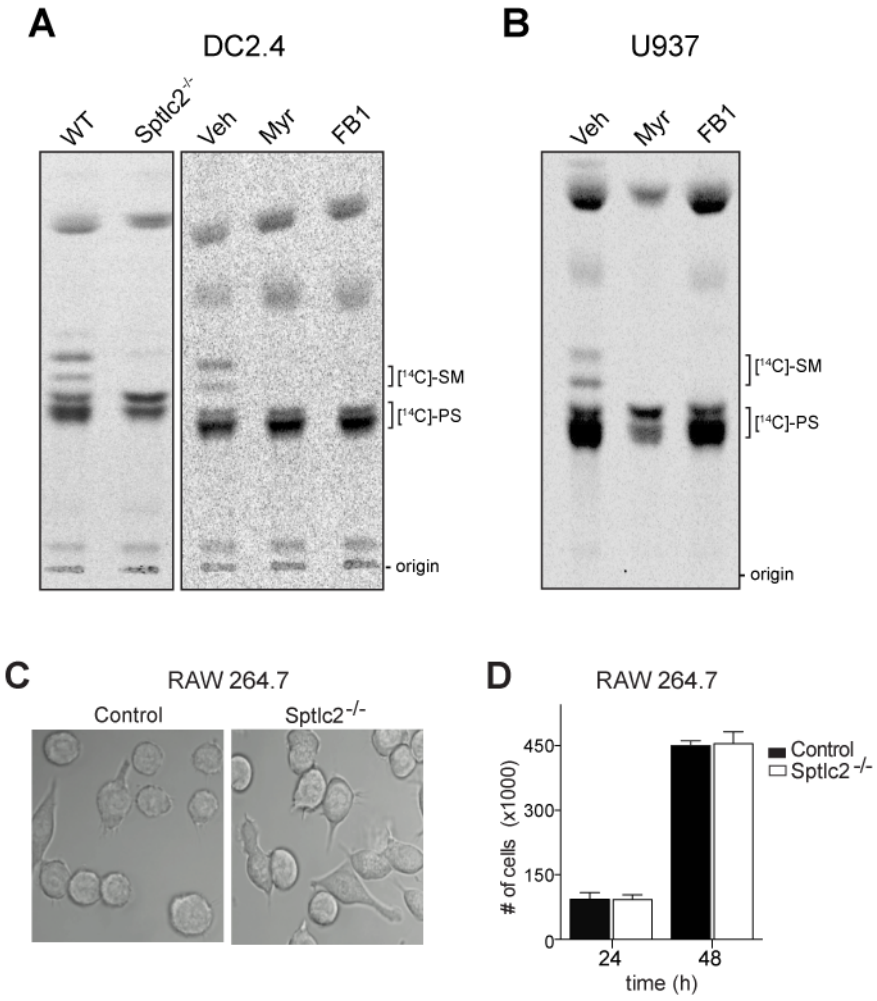


Figure S3.1 – Blocking de novo sphingolipid biosynthesis using genetics and chemical tools has no significant impact on cell growth. Sptlc2$^{-/-}$ and wild-type DC2.4 or U937 cells were treated with myriocin or fumonisin B1 for 3 days and then metabolically labelled with 3-l-[14C]serine for 4 h. Total lipids were extracted and analyzed by TLC and autoradiography. Data are representative of 3 independent experiments. Veh, vehicle-treated. (C) Phase-contrast microscopy images of wild-type and Sptlc2$^{-/-}$ RAW264.7 cells. (D) Numbers of wild-type and Sptlc2$^{-/-}$ RAW264.7 cells plated out at equal densities and grown for 24 or 48 h in serum-containing medium. Data are means ± SD (n = 3).

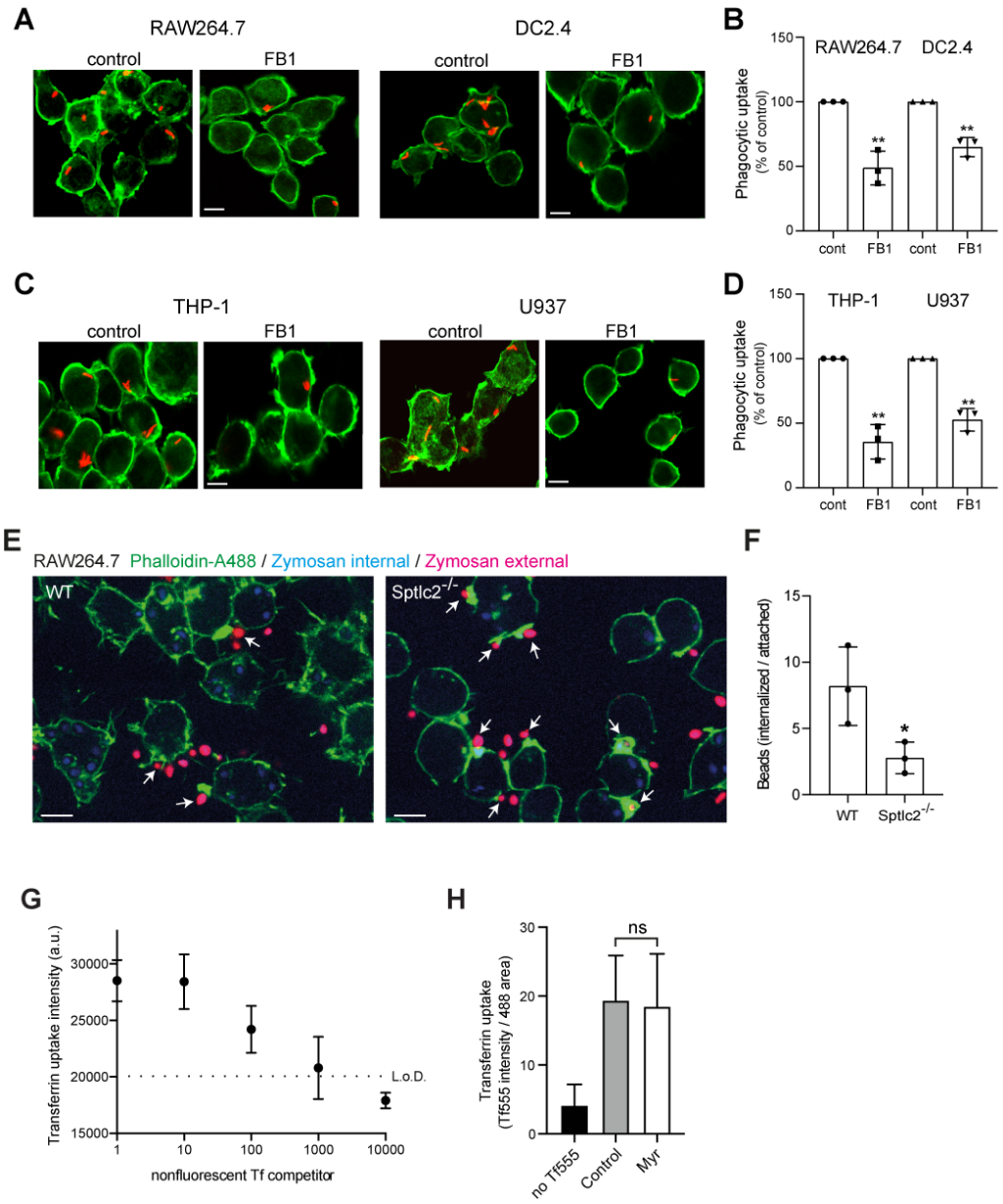


Figure S3.2 – Sphingolipid biosynthesis is required for efficient phagocytosis of *Mtb* but not for receptor-mediated uptake of transferrin. (A and C) RAW264.7, DC2.4, THP-1, and U937 cells were grown in the presence or absence of fumonisin B1 for 3 days, infected with mCherry-expressing *Mtb* for 2 h, washed, fixed, stained with phalloidin Alexa Fluor 488 and DAPI, and then imaged by fluorescence microscopy. (B and D) Quantification of *Mtb* uptake by cells treated as for panel A. (E and F) Sptlc2$^{-/-}$ cells bind but fail to internalize pathogen-mimicking beads; (E) Wild-type and Sptlc2$^{-/-}$ RAW264.7 cells were incubated with rabbit IgG-opsonized zymosan A particles for 5 min at 37°C. Next, cells were washed with chilled PBS and stained at 4°C with donkey anti-rabbit IgG-Cy3 in PBS supplemented with 1% BSA for 15 min to distinguish external beads (red) from internalized beads (blue). After chemical fixation, cells were stained for actin with phalloidin Alexa Fluor 488 (green) and analyzed by confocal fluorescence microscopy. (F) Quantification of the ratio of internal-

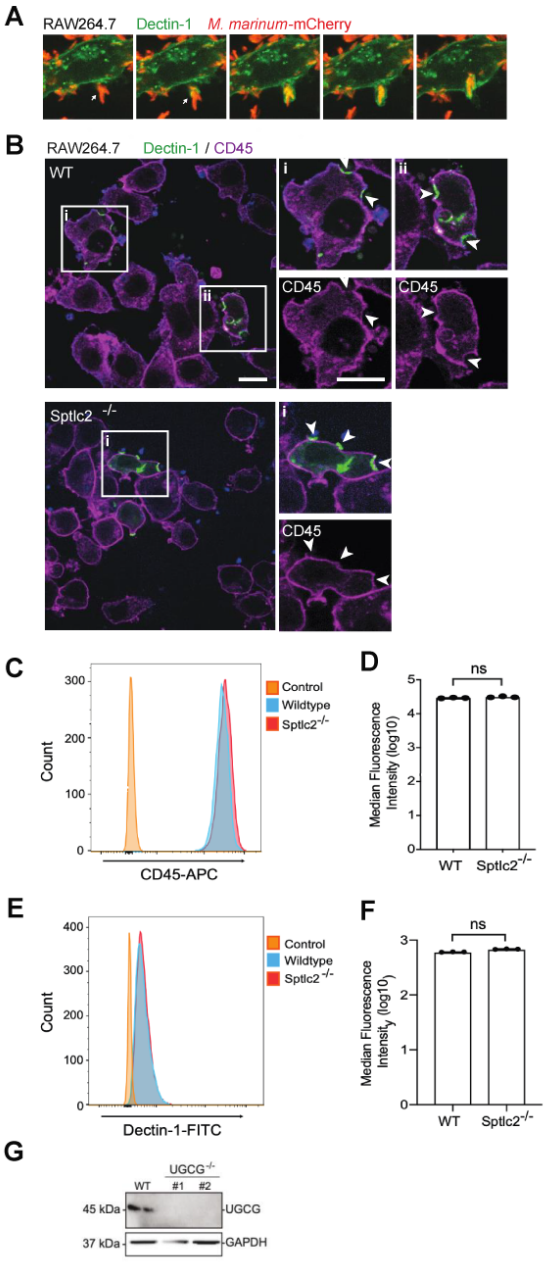


Figure S3.3 – (A) WT RAW264.7 cells transfected with GFP-tagged dectin-1 (green) were infected with mCherry-expressing *M. marinum* (red) as for Figure 3.4A. Bar, 5 µm. Data are means ± SD (n = 3). (B) No difference in sub-cellular localization of CD45 between WT and Sptlc2$^{-/-}$ cells. Wild-type and Sptlc2$^{-/-}$ RAW264.7 cells transfected with GFP-tagged dectin-1 (green) were incubated with zymosan A particles (blue) on ice, warmed to 37°C for 2 min to initiate phagocytosis, fixed, and then stained with antibodies against CD45 (purple). Boxed areas are magnified at right. Arrowheads mark sites of zymosan A binding. Bar, 5 µm. (C) WT and Sptlc2$^{-/-}$ RAW264.7 cells were stained with APC-conjugated anti-CD45 antibody, fixed, and subjected to flow cytometry analysis. (D) Quantitative analysis of median fluorescence intensity of cells treated as for panel C. (E) Wild-type and Sptlc2$^{-/-}$ RAW264.7 cells were stained with FITC-conjugated anti-dectin-1 antibody, fixed, and subjected to flow cytometry analysis. (F) Quantitative analysis of median fluorescence intensity of cells treated as for panel E

Chapter 4.

Sealing the Gaps

Sphingolipids are essential for repairing the endosomal damage caused by *Mycobacterium tuberculosis*

Authors: Gaelen Guzman[1], Alec Griffith[1], Mila Trank-Greene[1], Aidan Anastas[1] Hans C. Leier[1], Fikadu G. Tafesse[1,*]

[1]Department of Molecular Microbiology and Immunology, Oregon Health & Science University, Portland, Oregon, USA. [*]Corresponding author: tafesse@ohsu.edu

---

4.1. Abstract

Tuberculosis infection remains one of the leading causes of death worldwide, causing over 1.3 million deaths in 2022 alone. With the emergence of antibiotic-resistant strains of *Mycobacterium tuberculosis* (*Mtb*), there is a pressing need for novel and improved therapeutics. Here, we characterize the critical role of sphingolipids in restricting intracellular replication of *Mtb*. Sphingolipids are essential for rapidly responding to membrane damage and maintaining lysosomal integrity during Mtb infection. Additionally, sphingolipids enable the restriction of Mtb growth within host cells. Understanding the influence of host sphingolipids on Mtb infection may reveal novel routes for host-directed therapy. This research provides valuable insights into the pathogenesis of Mtb infection and could pave the way for developing new therapeutic strategies.

4.2. Introduction

Mycobacterium tuberculosis (*Mtb*) is an intracellular pathogen and remains a major global health threat, responsible for 1.3 million deaths in 2022 alone[1]. The increasing prevalence of antibiotic resistant strains threatens to dramatically alter the global tuberculosis landscape; accordingly, basic research into the underlying host-pathogen interactions between the *Mtb* bacillus and the human host has sought to uncover novel routes of host-directed antitubercular therapy. In this paradigm, manipulating the host environment may reduce permissivity to *Mtb* replication and serve as conjunctive to bactericidal treatment. In recent years, host lipid biology has become recognized for having an outsized role in influencing the growth and survival of *Mtb* within a human host cell[153,156,157]. A pivotal point in the progression of latent tuberculosis disease to active pathology is *Mtb*'s escape from the phagosome-derived *Mtb*-containing vacuole via membrane damage. Recent work has suggested that sphingolipid biology may be leveraged to increase a cell's resistance to membrane damage and to ininfluence the repairability of a damaged organelle.

Mtb is well-known for inducing endosomal and plasma membrane damage in host cells – both of which greatly aid the bacteria in replication and immune subversion[134,307–309]. The small proteins ESAT-6 and CFP-10 are the two most immunodominant *Mtb* antigens among of the most well-studied bacterial pore-forming proteins. Part of the WXG100 superfamily, ESAT-6 and CFP-10 form heterodimeric membrane-spanning pores[310]. Recent work by ourselves and others has shown that the membrane interaction and dimerization of ESAT-6 and CFP-10 are triggered by the partially acidic environment of the maturing endosome[311,312]. In conjunction with ESAT-6 and CFP-10, *Mtb* produces glycolipids, such as phthiocerol dimycocerosate (PDIM), which participate in membrane disruption[125,135,313]. Augenstreich et al. and others have shown that PDIM is shed from the bacterial cell wall and inserts into host membranes, significantly contributing to endosomal escape in a cholesterol-dependent manner[314]. Loss of these membrane-damaging pathogenicity factors results in a substantial attenuation of previously-pathogenic mycobacterial strains[315].

Endo/lysosomal membrane damage during infection is a significant risk to host cell survival. The low pH, high concentration of Ca^{2+}, and hydrolases (including proteases, lipases, and glycosidases) each pose lethal challenges to the cell; further, the dissolution of these antimicrobial factors prevents the destruction of pathogenic invaders[135]. Therefore, the cell employs several independent and redundant repair mechanisms that act in sequence to maintain endo/lysosomal integrity and homeostasis. The most well-studied of these mechanisms is the ESCRT pathway, which consists of several distinct heteromeric complexes[146]. In the ESCRT pathway, several sequestosome-like receptors, such as the Galectins, serve as cytosolic sensors of endo/lysosomal membrane damage, in which the exposure of the glycocalyx results in the deposition of these sensors at the site of damage and induces the recruitment of ESCRT machinery[145]. The ESCRT-III complex accumulates at the site of membrane damage and is directly responsible for membrane remodeling: the polymerized subunits of charged multivesicular body proteins (CHMPs 6, 4a, 4b, 4c, 3, 2b, 2c, and 1b) bind to the membrane and induce curvature and eventual scission of the damaged membrane region[146]. Several lipids play essential roles in the rapid repair of membrane damage. For example, Tan et al. and Radulovic et al. showed in 2022 that the coordination of lipid delivery to damaged membranes is necessary for membrane repair[143,316]. These studies each demonstrated that the phosphatidylinositol-4 kinase type 2α (PIK2A) is required for the rapid repair of membranes and promotes the formation of ER contact sites that enable the transfer of lipid content (primarily phosphatidylserine and cholesterol) to the damaged organelle[143,316]. Intriguingly, prior reports have suggested the existence of

an ESCRT-independent, sphingolipid-dependent membrane repair mechanism[199,200,317] – though the underlying mechanisms of this process are not yet fully clarified.

In the current study, we sought to understand host sphingolipids' role during an intracellular *Mycobacterium tuberculosis* infection. Given the known roles of lipids during the restoration of endo/lysosomal homeostasis after damage, we hypothesized that host sphingolipids may play an essential role in the cellular response to the membrane damage induced by *Mtb* during infection. We found that cells deficient in sphingolipid synthesis display more *Mtb*-induced membrane damage at earlier times. We further validate that sphingolipids both protect cells from lysosomal damage and enable membrane repair. We then show that sphingomyelin accumulates at the sites of membrane damage following damage induced by both LLOME and *Mtb*. Moreover, we finally show that the *de novo* synthesis of sphingolipids is essential in restricting the intracellular growth of *Mtb*. The sphingolipid pathway may represent a novel route of antitubercular therapy. Because these lipids appear to play an outsized role in restricting the intracellular growth of pathogenic *Mtb*, their synthesis may be leveraged in TB patients as an adjunctive to frontline antibiotics.

4.3. Results

4.3.1. Manipulating the sphingolipid metabolic pathway

Figure 4.1A depicts a simplified schematic of the sphingolipid biosynthetic cascade. Briefly, sphingolipid production begins with the sphingoid base in the ER through the condensation of serine and palmitoyl-CoA by the serine-palmitoyl transferase (SPT) enzyme. Still in the ER, the sphingoid base is converted to ceramide by a cohort of ceramide synthase enzymes (Cers1-6), which append secondary acyl chains of varying lengths. Ceramide represents a central nexus of sphingolipid metabolism; it is itself a potently active signaling molecule whose excess stimulates apoptosis[318–322]. In concert with its production, ceramide is rapidly transferred to the trans-Golgi via the Ceramide Transport Protein (CERT) and is primarily (>80%) converted to sphingomyelin (SM) by SM Synthase 1 (SMS1)[323]. SM is selectively trafficked towards the outer leaflet of the plasma membrane via sorting in the trans-Golgi network and export via the secretory pathway[188,324]. Other than the pool of sphingolipids undergoing active synthesis and trafficking, the most significant glut of intracellular sphingolipids is in the endosomal compartment, accumulated via the internalization and recycling of plasma membrane SM via endocytosis and phagocytosis, a process commonly referred to as the "salvage" pathway[88,317,325].

Small molecule inhibitors such as myriocin (Myr) and fumonisin B1 (FB1) enable the near-total blockade of sphingolipid production[178,205,271,326–329]. In our prior work, we showed that Myr treatment or genetic deletion of Sptlc2 (the catalytic subunit of the SPT complex) are both sufficient to block the *de novo* production of all higher sphingolipids by blocking the activity of SPT, the rate-limiting step in the sphingolipid pathway (Figure 4.1A)[179]. Similarly, treatment with the compound FB1 blocks the ceramide production by the ceramide synthases, blocking all higher sphingolipid synthesis[179,330]. We selected treatment concentrations of Myr and FB1 for this study based on their cytotoxicity, settling on concentrations that we and others have previously used (Figure 4.1C and Figure S4.1A and B)[179,205,297].

To validate the effectiveness of FB1, we exposed cells pre-treated with FB1 to fluorescent NBD-sphinganine to trace its conversion to ceramide or SM, as visualized via fluorescent thin-layer chro-

matography (TLC; Figure 4.1C and D). These data show that 3-day FB1 treatments are sufficient to block de novo sphingolipid synthesis, significantly reducing total sphingolipid content in these cells, including an 84% reduction of ceramide production, 89% reduction of SM production, and retention of the NBD-sphinganine input (192% more NBD-sphinganine than untreated control cells; Figure 4.1C and D). These findings agree with our previous work[179]. Our previous lipidomics analysis additionally showed that the total content of bulk lipids is unaffected and that total protein synthesis is unaffected following these treatments[179]. As a genetic means of inhibiting sphingolipid production, we utilized RAW 264.7 murine macrophages of wildtype, Sptlc2$^{-/-}$, and Sgms1/2$^{-/-}$ genetic backgrounds, as reported in our previous work[179,199]. We similarly validated the reduction in higher sphingolipid production in Sgms1/2$^{-/-}$ cells using a 1-hour treatment with NBD-ceramide and fluorescent TLC; we found an 83% reduction of conversion of NBD-ceramide into NBD-sphingomyelin (Figure S4.1D and F). As with FB1 treatment, Sgms1/2 double knockout cells retain a higher proportion of the NBD-ceramide input (Figure S4.1C and D). As above, the inhibiting effects of myriocin treatment and SPT knockout were validated in our previous reports[179,205].

Using these genetic models and small-molecule inhibitors, we sought to address sphingolipids' roles in the intracellular stage of an *Mtb* infection.

4.3.2. Host sphingolipids protect against *Mtb*-induced endosomal membrane damage.

Galectins 3, 5, and 8 are all recruited to the *Mtb*-containing endosome, and Galectins 5 and 8 both play essential roles in restricting *Mtb* growth in the cell. However, Galectin 3 (Gal3) was shown not to affect *Mtb* growth and represents a vital tool in visualizing membrane damage accumulation during *Mtb* infection. Here, we overexpressed a previously reported fluorescent fusion construct of Galectin 3 and mAzamiGreen (mAG-Gal3) in macrophages as a reporter of endosomal membrane damage[331].

Because we have previously reported that sphingolipids are required for *Mtb*'s entry into the host cell via phagocytosis, we performed infections in the absence of sphingolipid inhibition to allow for uniform *Mtb* infection with the fluorescent *Mtb* strain H37Rv-dsRed. After 4 hours of uptake time, non-internalized bacteria were removed via PBS wash, and cells were cultured in media with Myr, FB1, or vehicle control for 24 or 96 hours and visualized using confocal microscopy(Figure 4.1D).

We observe a significant accumulation of colocalized mAG-Gal3 punctate signal and H37Rv-dsRed (reflective of *Mtb*-induced endosomal membrane damage) at 24 hours post-treatment in Myr- and FB1-treated cells. In contrast, untreated control cells display a marked absence of Gal3 puncta (Figure 4.1D, upper and middle panels). Notably, treated-but-uninfected bystander cells display no change in Gal3 accumulation (Figure 4.1D, lower panels). In quantifying high-content images of these infections, we observe a significant increase in the rate of membrane damage at 24 hours post-infection (Figure 4.1D). Notably, by 96 hours of treatment, all infected cells display Gal3 puncta accumulation to a high and similar degree, regardless of treatment (Figure S4.2D and E).

These data show that *Mtb*-induced membrane damage is significantly mitigated by host sphingolipid production. However, these data do not indicate whether this is a result of increased sensitivity to membrane damage or whether membrane damage accumulates as a result of impaired membrane repair, a question explored below.

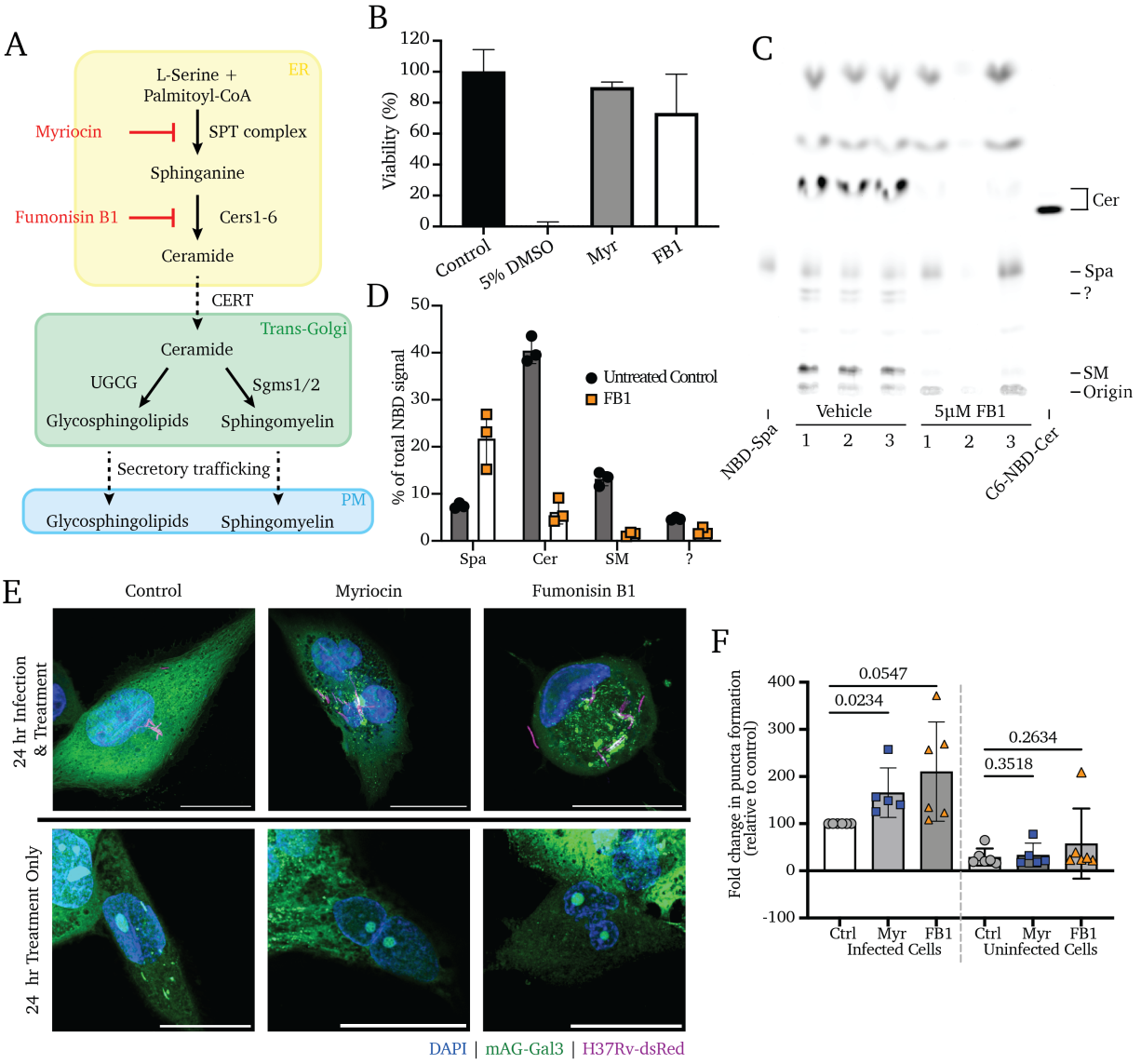


Figure 4.1. – **Sphingolipids limit *Mtb*-induced membrane damage.** (A) A simplified depiction of the sphingolipid biosynthetic pathway. The sites of action of the small molecule inhibitors Myr and FB1 are highlighted. (B) Resazurin viability assays show the cytotoxicity of Myr and FB1 at 15 μM and 5 μM, respectively; untreated and 5% DMSO (vol/vol)-treated control cells serve as controls for 100% and 0% viability, respectively. (C) Fluorescent thin-layer chromatography depicts the metabolism of NBD-sphinganine in THP-1 cells pre-treated with DMSO vehicle control and 5 μM FB1. The loading position (origin), and bands of sphingolipid metabolic products are labeled, as well as one unidentified band. (D) Quantification of the thin-layer chromatography shown in (C). (E) Representative confocal microscopy of cells infected and treated as in A, imaged at 24 hours post-infection start. Upper panels: images of cells treated with the denoted inhibitors; white boxes denote the inset images shown in the middle panels; lower panel depicts uninfected bystander cells treated with the denoted inhibitors. (Scale bars = 25 μm; Channels: Blue = DAPI; Green = mAG-Gal3; Magenta = H37Rv-dsRed; see Methods Section 4.5.7 for microscopy details). (F) Bar plots depict the relative percent of infected cells with Galectin 3 puncta colocalized with *Mtb* and the percentages of uninfected cells with Galectin 3 puncta. All points are normalized to the average ratio of untreated control cell technical replicates and reported as fold change in Galectin 3 puncta formation. Statistical testing was achieved via unpaired t-test versus respective control cells; p-values are as denoted. (Abbreviations: SPT = serine palmitoyltransferase; Cers1-6 = ceramide synthases 1-6; CERT = ceramide transferase; UGCG = UDP-glucose ceramide glycosyltransferase; Sgms1/2 = sphingomyelin synthase 1/2; ER = endoplasmic reticulum; PM = plasma membrane).

4.3.3. Sphingolipids protect cells from endo/lysosomal damage before the ESCRT repair pathway activation.

To clarify whether sphingolipid-deficient cells are more sensitive to membrane damage or whether these cells fail to repair endo/lysosomal membrane damage, we performed a recovery assay in which cells were exposed to a lysosomotropic membrane-damaging agent, leucine-leucine methyl ester (LLOME) and given increasing recovery periods. LLOME is a dipeptide that accumulates in the lysosome and is cleaved by a resident lysosome-resident dipeptidyl peptidase, DPP1, to release a membranolytic product[332]. To visualize intact lysosomes, we stained cells with Lysotracker, an agent with acidity-activated fluorogenicity.

In untreated control cells, we see that 15-minute LLOME treatment induces a loss of lysotracker fluorescence (indicative of reduced lysosomal integrity) that rebounds within 60 minutes of recovery and settles at the initial baseline fluorescence by 120 minutes of recovery (Figure 4.2A and B, black points). In contrast, cells pre-treated with Myr or FB1 experience a significant loss of lysosomal acidity and fail to recover to pre-LLOME levels of lysotracker signal (Figure 4.2A and B, blue and orange points, respectively).

Notably, Myr and FB1 pre-treatments significantly decrease lysotracker signal with 0 minutes of recovery time; these results indicate that sphingolipid inhibition results in an enhanced sensitivity to endo/lysosomal membrane damage. Similarly, while we observe a rebound effect in the sphingolipid-producing control cells, no such rebound is apparent in the Myr and FB1 pre-treated cells; this indicates impaired recovery from lysosomal damage in addition to the enhanced sensitivity to damage.

We next sought to clarify whether the inhibition of sphingolipid production incurs a defect in ESCRT-III assembly at the sites of membrane damage using fluorescence microscopy. While Gal3/ESCRT accumulation on an organelle induces autophagy at long time points, in the short term this pathway primarily enables the repair of damaged membranes[146,333]. Intriguingly, Mittal et al. showed in 2018 that the secreted *Mtb* effectors EsxG and EsxH directly interfere with the activity of the ESCRT membrane damage response pathway, inhibiting the cell's capacity to mitigate phago/lysosomal membrane damage[155]. The work by Mittal et al. do not explore the role of lipids in this counterbalanced interplay between the pathogen and the host. Thus, we sought to better understand whether sphingolipids are involved in the ESCRT response in the absence of these *Mtb* mechanisms of ESCRT interference, we visualized the accumulation of one ESCRT-III protein, CHMP4b, as a proxy for ESCRT-III polymerization in sphingolipid-deficient cells (Figure 4.2C). We find that cells treated with vehicle control display the formation of CHMP4b puncta after 10 minutes of treatment with LLOME, and a peak of CHMP4b punctate signal at 30 minutes (Figure 4.2C, upper panels). Intriguingly, pretreatment with either Myr or FB1 results in a strikingly similar degree of puncta accumulation (Figure 4.2C, lower panels). We quantified the number of puncta formed per cell in vehicle- or Myr/FB1-treated cells and found that sphingolipid inhibition appears to play no significant role in the assembly of the ESCRT-III complex (Figure 4.2D).

These data suggest that sphingolipids are crucial for the cell resisting endo/lysosomal membrane damage and restoring lysosomal homeostasis following damage – but that these lipids are dispensable for the ESCRT-mediated cellular response to damage. These results serve to partially recapitulate the reported findings of Niekamp et al., 2022[199] – though much more work is required to uncover the nuanced roles that these lipids play in the minutes following membrane damage.

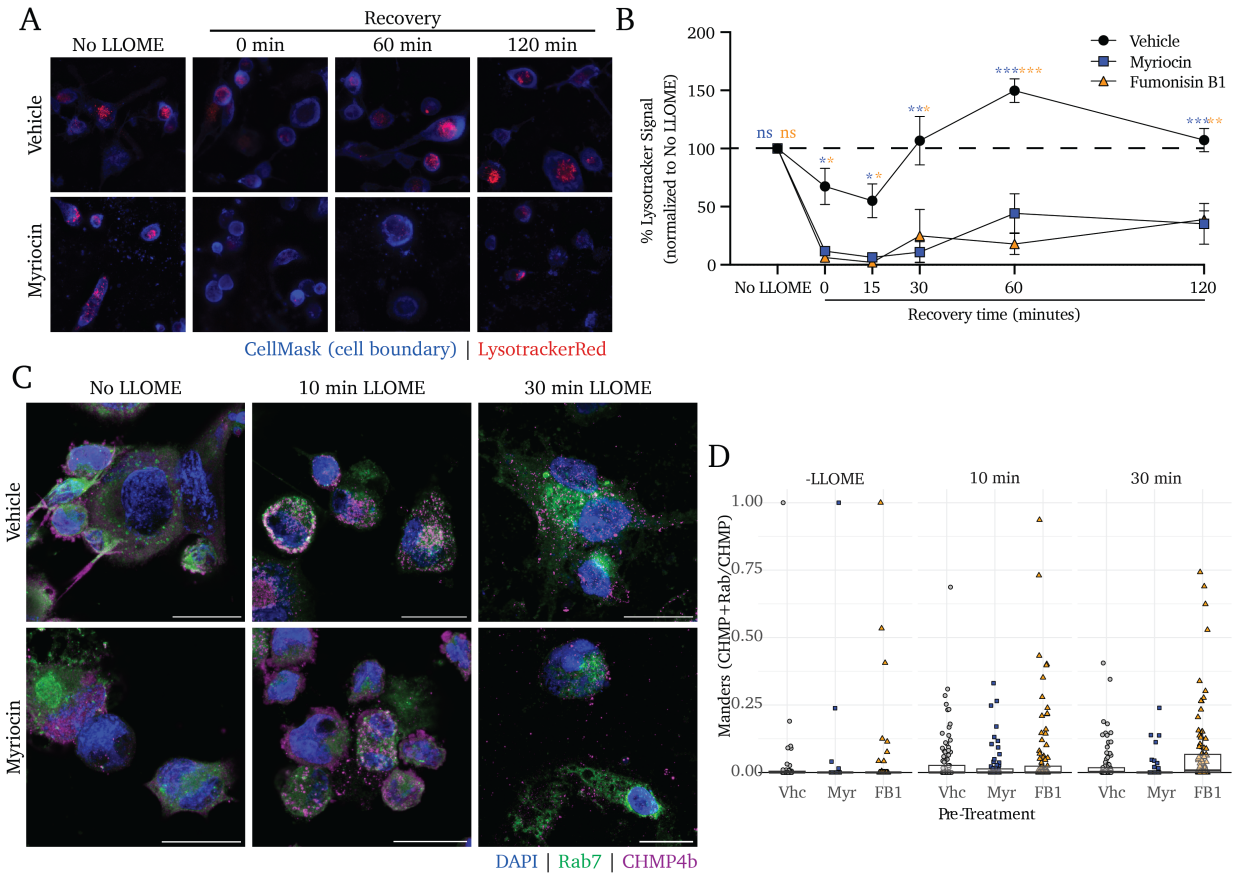


Figure 4.2. – Sphingolipids limit the accumulation of and enable the repair of endo/lysosomal membrane damage prior to ESCRT-III recruitment. (A) Representative images of untreated control and Myr-treated cells before LLOME treatment and following 0 minutes, 60 minutes, and 120 minutes of recovery. (Colors: Red = Lysotracker-Red, Blue = CellMaskDeepRed. Top panel: Untreated control cells; lower panel: Myr-treated cells. See Methods Section 4.5.8 for imaging details). (B) Quantification of images as in B. Each point denotes the average of 3 biological replicates, and error bars denote the standard error of the mean. (Statistical testing was achieved via multiple comparisons t-test versus untreated vehicle control; * = $p<0.05$, ** = $p<0.01$, *** = $p<0.005$, **** = $p<0.0001$. Abbreviations: LLOME = leucine-leucine dimethyl ester, a.f.u. = arbitrary fluorescence units). (C) Representative images of untreated control and Myr- or FB1-treated cells before and following 0, 10, and 30 minutes of LLOME treatment. (Scale bars = 25 µm. Colors: Blue = DAPI, Green = Rab7, Magenta = CHMP4b; See Methods Section 4.5.9 for microscopy details) (D) Quantification of the colocalization of ESCRT-III protein CHMP4b with Gal3. Coefficients of colocalization were gained via Pearson's correlation analysis (* = $p<0.05$, ** = $p<0.01$, *** = $p<0.001$.

4.3.4. Sphingomyelin accumulates at the sites of *Mtb*-induced membrane damage.

3 paragraphs

Though intuitive, the observation that lipid trafficking and metabolism are central to membrane repair has only been described in recent years. Tan et al. reported in 2022 that phosphatidylinosotide-4-phosphate kinase activty by PIK2A is essential to coordinate rapid membrane repair through the initiation of ER contact sites and transfer of phospholipids to the damaged organelle[316]. Also in 2022, Radulovic et al. showed that cholesterol delivery to damaged organelles is essential for membrane repair[143]. However, no prior reports have explored the delivery of sphingolipids to sites of membrane damage. We sought to clarify whether SM similarly accumulates at sites of organelle damage. The pore-forming toxin Lysenin was derived from the earthworm *Eisenia foetida* and has been widely used as a tool to visualize the cellular distribution of sphingomyelin in a cell when expressed as a modified, non-toxic fluorescent fusion protein, Lysenin-GFP[323,334,335]. While ectopic expression of this construct may be used as a cytosolic reporter of SM exposure, we employed it here as a staining reagent to visualize the intracellular distribution of SM after membrane damage in fixed cells.

To this end, we treated cells with LLOME for 15 minutes and visualized the localization of intracellular SM after fixation by staining the cells with purified Lysenin-GFP (Figure 4.3A). We find that there is a robust colocalization of BFP-Gal3 with Lysenin-GFP punctate signal, with an average Pearson's colocalization coefficient of 0.350 among nine images across three biological replicates (Figure 4.3B, right). In contrast, the untreated control cells display diffuse Lysenin-GFP and a wide spread of colocalization coefficients, averaging at 0.165 among ten images across three biological replicates (Figure 4.3B, bottom images). Analysis using an unpaired t-test reveals a statistically significant increase in Lysenin-GFP colocalization in cells pre-treated with LLOME (Figure 4.3B, right; $p<0.05$),

Given our findings above, we hypothesized that *Mtb* infection would induce accumulation of SM at the site of *Mtb* in infected cells. Thus, we infected cells with H37Rv-dsRed for 24, 48, 72, and 96 hours and stained them with Lysenin-GFP. We find that Lysenin-GFP colocalizes with *Mtb* in infected cells, increasing over time and reaching a peak at 96 hours post-infection (Figure 4.3C). We quantified the rate of colocalization between Lysenin-GFP and dsRed at each timepoint and found increasing rates of colocalization via Pearson's colocalization analysis (Figure 4.3D). Using a multiple-comparisons t-test, we found a statistically significant increase in colocalization starting at 72 hours post-infection ($p<0.05$), which dramatically increases by 96 hours ($p<0.001$). From these data, we conclude that cytosolic exposure of SM occurs concomitantly with the membrane damage that Mtb induces (as many sphingolipid-competent cells display membrane damage by 96 hours of infection, seen in Figure S4.2C and D). These findings suggest the activity of a sphingomyelin-dependent membrane repair process that plays a critical role in mitigating membrane damage during Mtb infection.

4.3.5. Sphingolipids restrict intracellular *Mtb* replication.

We finally sought to determine whether these findings are relevant to the success or severity of infection by asking the following question: does sphingolipid production influence the rate of intracellular replication for *Mtb*? To this end, we first utilized a live/dead fluorescent reporter strain

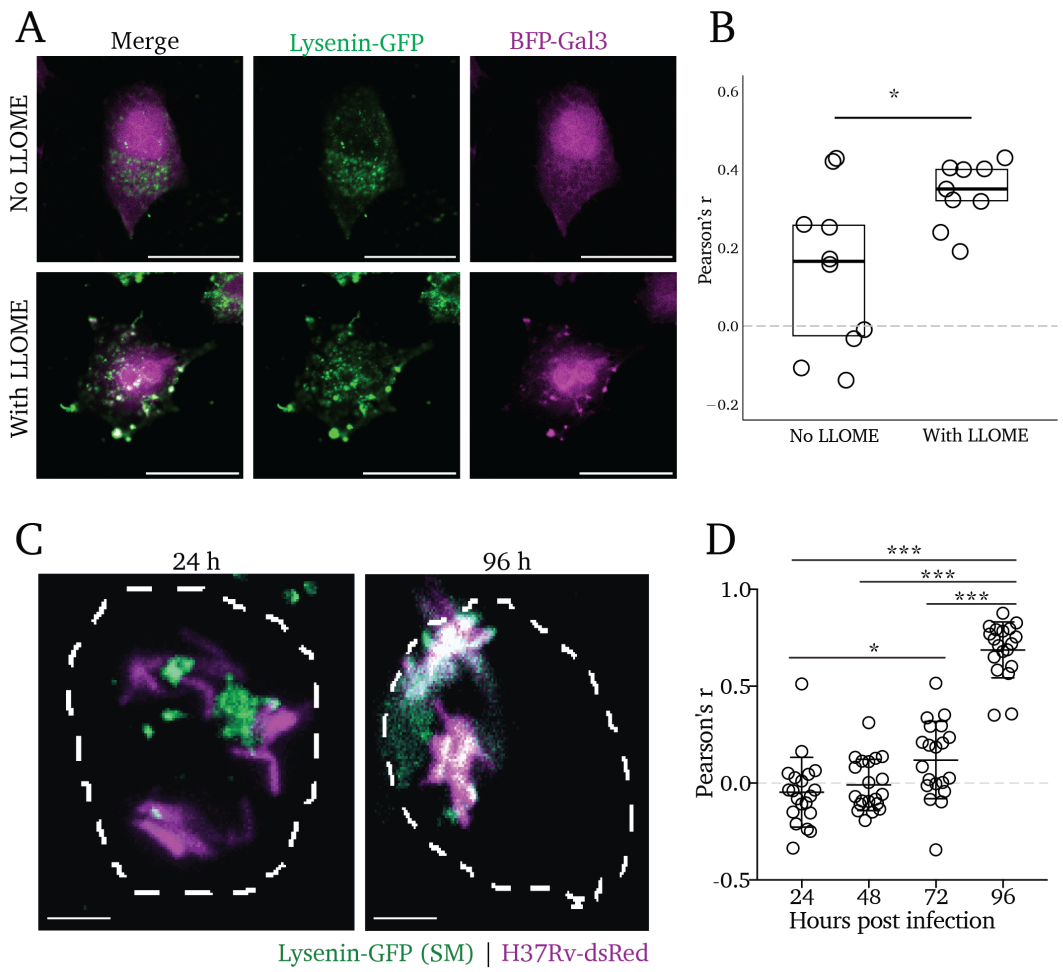


Figure 4.3. – **Sphingomyelin accumulates at the sites of *Mtb*-induced membrane damage.** (A) Representative confocal microscopy images of cells stably expressing BFP-Gal3 membrane damage reporter and treated with the membrane-damaging agent LLOME. Cells were stained after fixation with purified Lysenin-GFP (Scale bars = 25 µm. Colors: Green = BFP-Gal3, Magenta = Lysenin-GFP; see Methods Section 4.5.10 for details on microscopy). (B) Pearson's colocalization analysis of cells imaged as in A. (C) Representative confocal microscopy images of cells pre-treated with vehicle control or Myr and treated with the membrane-damaging agent LLOME, then stained for localization of the late-endosomal/lysosomal marker Rab7 and the ESCRT-III protein CHMP4b (Scale bars = 5 µm. Colors: Blue = DAPI, Green = Rab7, Magenta = CHMP4b; see Methods Section 4.5.10 for details on microscopy). (D) Pearson's colocalization analysis of cells imaged as in C. (* = $p<0.05$, ** = $p<0.01$, *** = $p<0.001$).

of *Mtb*, which constitutively expresses mCherry and expresses GFP upon induction with doxycycline (H37Rv-Live/Dead)[336,337]. THP-1 monocyte-derived macrophages were infected with H37Rv-Live/Dead for 4 hours without sphingolipid inhibition. At that point, extracellular bacteria were removed, sphingolipid inhibitors were added, and cells were incubated for 72 hours and induced with doxycycline for 24 hours (96 hours of total infection time). Cells were then visualized using confocal fluorescence microscopy (Figure 4.4A). By quantifying the ratio of red to green signal as a proxy for intracellular *Mtb* survival, we find that THP-1 cells treated with Myr or FB1 harbor a 1-3-fold increase in metabolically active mycobacteria (Figure 4.4B). We observed similar increases in *Mtb* growth when treating two donor-derived peripheral blood monocytes with Myr and FB1 (Figure 4.4C and D).

To validate and clarify these observations, we utilized a luminescent strain of *Mtb* (transformed with the pLux plasmid; H37Rv-pLux) to report the growth of the bacteria in host cells treated with sphingolipid biosynthesis inhibitors. One representative growth curve is shown, followed by the aggregated fold-growth of several biological replicates at 96 hours (Figure 4.4E and F). We observe a significant increase in overall mycobacterial replication in cells treated with sphingolipid biosynthesis inhibitors, supporting the hypothesis that sphingolipids are responsible for blocking *Mtb* replication, as opposed to mediating antimicrobial activity.

Together, these data suggest that *Mtb* metabolic activity is restricted in host cells with active sphingolipid biosynthetic pathways, signifying either an increase in replication rate or a decrease in antimicrobial activity by the host cell. The gold-standard methodology of quantifying all viable *Mtb* bacilli in the sphingolipid-depleted cells is quantifying colony-forming units extracted from infected cells. Using such an approach on cells infected using the same paradigm as above, we find that sphingolipid depletion increases the intracellular growth of *Mtb* strain H37Rv (Figure 4.4G).

The attenuated deletion mutant strain H37Rv-ΔRD1 lacks essential virulence factors, including the Type VII secretion system and the two immunodominant factors ESAT-6 and CFP-10[129,338–341]. When cells infected with H37Rv-ΔRD1 are treated with Myr and FB1, we find no change to the intracellular replication of the bacteria (Figure-Mtb-Replication H). Similarly, the mycobacteria vaccine *M. bovis* strain Bacillus Calmette-Guerin (*M. bovis* BCG) is highly attenuated, lacking many of the same virulence factors as the H37Rv-ΔRD1 strain (Figure 4.4I)[2,340,342].

Notably, we show that Myr and FB1 treatment are mildly toxic to mycobacteria strains H37Rv-pLux, H37Rv, and *M. bovis* BCG using luminescence and colony forming unit assays (Figure S4.4A-F). These data support a hypothesis that these compounds indirectly result in the increased replication of the mycobacteria by inhibiting the antimicrobial activity of the host cell.

4.4. Discussion

Here we present the first investigation into the role of sphingolipids in the cellular response to *Mtb*-induced membrane damage. We find that inhibiting sphingolipid production in *Mtb*-infected cells results in an accelerated accumlation of damage in the *Mtb*-containing vacuole. *In vitro* analysis showed that inhibiting sphingolipid production induces a simultaneous increase in the sensitivity to membrane damage and a reduction in the rate of restored lysosomal homeostasis after damage. Though still preliminary, we observe no major difference in the recruitment of the ESCRT-III complex to damaged organelles. And, while the mechanism is yet unclear, we observe a significant accumulation of SM at the site of *Mtb*-induced membrane damage. Finally, in observing the rate of

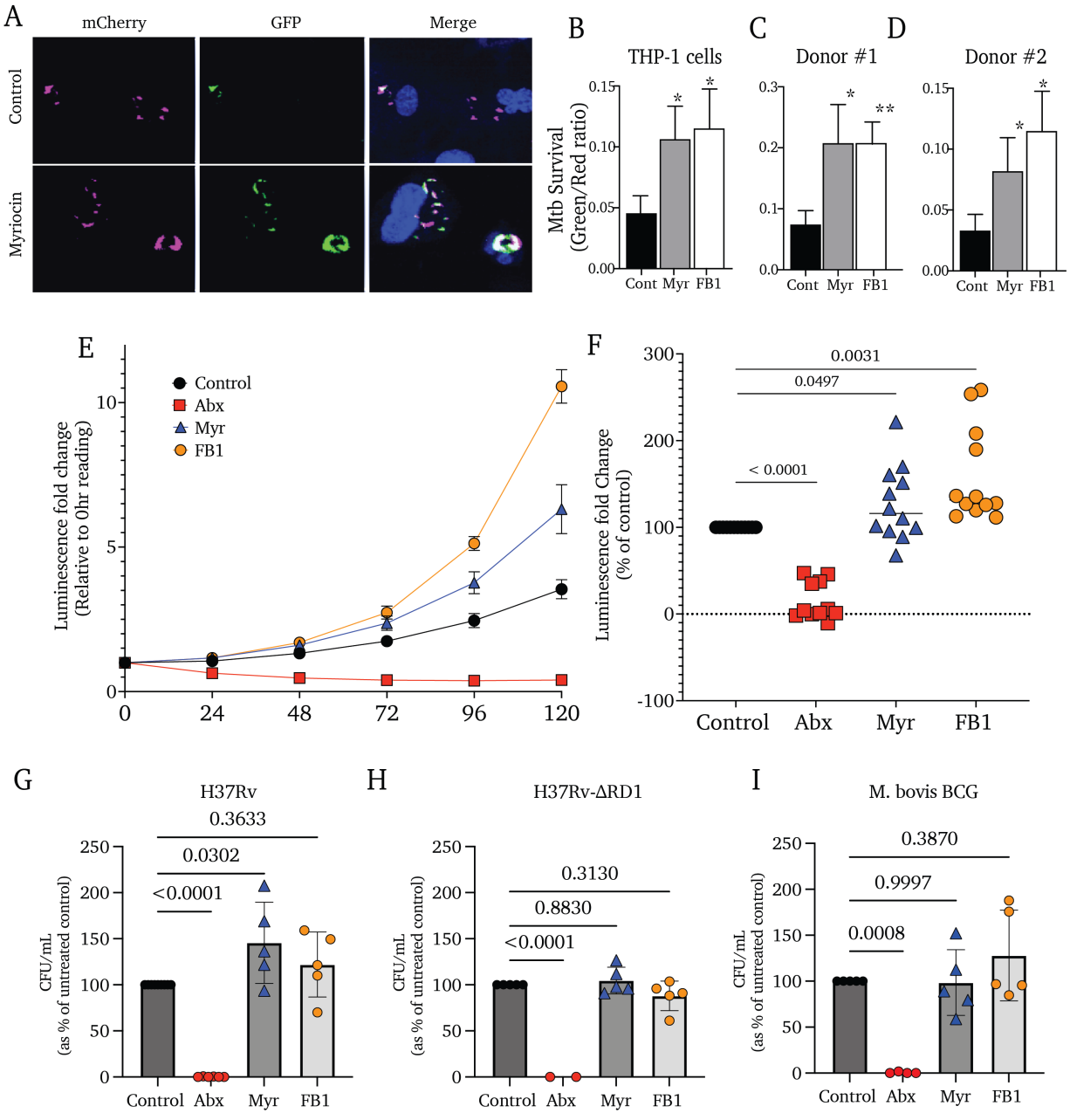


Figure 4.4. – **Host sphingolipid biosynthesis restricts intracellular *Mtb* growth** (A) Representative fluorescence microscopy images of THP-1 cells infected with the H37Rv Live/Dead reporter strain of *Mtb* (t = 96 hours post infection; see Methods Section 4.5.11 for microscopy details). (B) Quantification of *Mtb* survival in THP-1 macrophages treated with Myr or FB1. (C and D) Quantification of *Mtb* survival in two donor-derived peripheral blood macrophages treated with Myr or FB1 versus untreated controls. (E) Representative growth curve from a single biological replicate of THP-1 cells infected with the H37Rv-pLux luminescent reporter *Mtb* strain. (F) Luminescence fold change of H37Rv-pLux at 96 hours of treatment with Myr and FB1 (n= 12 biological replicates). Each point represents the percent growth of pLux after 96 hours post-infection compared to untreated control. (G, H, and I) Quantification of colony forming units of H37Rv (n = 5), H37Rv-ΔRD1 (n = 4), and Bacillus Calmette-Guerin (n = 4) collected from infected cells after 96 hours of treatment with Myr and FB1. (Abbreviations: Myr = myriocin, FB1 = fumonisin B1, NT = no treatment, Abx = antibiotics rifampicin and isoniazid. Statistical testing via unpaired t-test: * = p<0.05, ** = p<0.01, **** = p<0.0001)

bacterial growth during SL inhibition, we find that SLs are essential in restricting intracellular *Mtb* growth.

4.4.1. Lipids in early membrane repair

At early time points (~30 minutes post-damage induction), membrane repair complexes such as ESCRT-III mediate the direct repair of a perforated membrane[146]. This process is highly dependent on the coordinated delivery of membrane lipids to the damaged organelle. In 2022, Tan and Finkel showed that the phosphatidylinositol-4-phosphate kinase PIK2A is essential in coordinating the formation membrane contact sites between the ER and a damaged lysosome, and for the resulting transfer of phosphatidylserine and cholesterol to restore lysosomal homeostasis[316]. These results were verified and expounded upon by Radulovic et al. 2022[143]. Thus, it is known that the selective synthesis and delivery of lipids is essential for expeditious membrane repair.

In agreement with this, we observe that sphingomyelin accumulates at the sites of LLOME- and *Mtb*-induced membrane damage (Figure 4.3) throughout infection. These results do not clarify the source of this sphingomyelin: is our observed sphingomyelin produced locally or delivered pre-synthesized to the damaged membranes? The primary sphingomyelin synthase, SMS1, is a Golgi-resident membrane protein and is responsible for >80% of the total sphingomyelin production in the cell – inclusive of plasma membrane and endosomal sphingomyelin[343–345]; the secondary synthase, SMS2, primarily resides at the plasma membrane and produces no appreciable endosomal sphingomyelin[343,345].

The rapidity of our observed sphingomyelin accumulation at sites of LLOME-induced membrane damage (<15 minutes, Figure 4.3A) may suggest a mechanism for delivery of pre-synthesized sphingomyelin, though this remains an open question.

4.4.2. Sphingolipid production restricts *Mtb* replication

Of significant note, we find that blocking sphingolipid results in a significant increase in the intracellular growth and survival of *Mtb*, highlighting the importance of this lipid class in enabling antimicrobial activity (Figure 4.4).

At later time points, or in instances of extensive membrane damage, the ESCRT machinery serves as a coordinator of autophagy-mediated degradation of the damaged organelle[146,333]. Intriguingly, we see that the relative increase in membrane damage among sphingolipid-inhibited cells (versus untreated control cells) at 24 hours of sphingolipid inhibition is gone by 96 hours – at which point both sphingolipid-producing and sphingolipid-inhibited cells experience large and approximately equivalent degrees of *Mtb*-induced membrane damage (Figure S4.2). Numerous reports have found that *Mtb* secretes inhibitors of host autophagy, including the **e**nhancer of **i**ntracellular **s**urvival (Eis)[156], and several proline-glutamic acid (PE) or proline-proline-glutamic acid (PPE) proteins such as PE_-PGRS47[157] and PPE51[346]. We may thus hypothesize that *Mtb*-restriction of autophagy allows membrane damage to "catch up" in sphingolipid-replete cells at late time points. However, much work remains to characterize such an effect and whether sphingolipids also play a role in this process.

4.4.3. Conclusions

In this work, we show that sphingolipids are an essential component of the cell's restriction of *Mtb* growth. This appears to be the product of sphingolipids' role in enabling efficient membrane repair in response to pathogenic *Mtb* activity. Thus, leveraging the host sphingolipid metabolic network as a form of host-directed therapy may represent a novel route of antitubercular therapy.

4.5. Methods

4.5.1. Cell culturing and cell lines used

Wildtype THP-1 monocytes were sourced from American Type Culture Collection (ATCC TIB-202) and cultured in RPMI 1640 medium (Thermo Fisher Scientific, product #11875119) supplemented with 10% FBS (Seradigm), 1x Gibco Penicillin-Streptomycin (Thermo Fischer Scientific, product #15-140-163), and 1x Gibco Non-Essential Amino Acids (Thermo Fischer Scientific, product #11140050). Before experimental use, THP-1 cells were activated for 48 hours via treatment with 50nM phorbol 12-myristate 13-acetate (PMA; Sigma-Aldrich, product P8139-1MG). Donor peripheral blood monocytes were collected via blood draw and cultured in GM-CSF before plating on glass coverslips. All cell counting was done using a hemocytometer with trypan blue (Gibco) counterstain. Wildtype RAW 264.7 macrophages were sourced from the American Type Culture Collection (ATCC TIB-71). Sptlc2$^{-/-}$ RAW 264.7 macrophage line was cloned as reported in our prior report, Niekamp et al. 2021[179]. Sgms1/2$^{-/-}$ RAW 264.7 macrophages were cloned as reported in Niekamp et al. 2022[199] and kindly provided by Dr. Joost Holthuis of Osnabrück University. All RAW 264.7 lines were routinely cultured in were cultured in Dulbecco's modified Eagle medium (DMEM; Thermo Fisher Scientific, product #11965118) supplemented with 10% FBS (Seradigm), 1x Gibco Penicillin-Streptomycin (Thermo Fischer Scientific, product #15-140-163), and 1x Gibco Non-Essential Amino Acids (Thermo Fischer Scientific, product #11140050), trypsinized using 0.25% trypsin solution (Gibco) and counted using a hemocytometer and trypan blue solution (Gibco) as a counterstain.

All experiments' biological replicates represent cells plated, infected, and collected on separate days.

4.5.2. Plasmids and small molecule inhibitors

The mAG-Gal3 construct was initially produced in the laboratory of Dr. Niels Geijsen at KNAW-Hubrecht Institute in Utrecht, the Netherlands[331]; this plasmid was purchased from AddGene (Product #62734). The BFP-Galectin 3 plasmid was assembled using ligation of human Galectin 3 isolated from the mAG-Gal3 plasmid and EBFP2 from the plasmid EBFP2-N1 (AddGene product #182100). Restriction site extension PCR63 yielded the insertion of a NheI cut site to the C-terminus of EBFP2 from the EBFP2-N1 plasmid (primer: gatcttGCTAGCcttgtacagctcgtccatgcc; capital letters denote NheI cut site) and to the N-terminus of Galectin 3 from the mAG-Gal3 plasmid (primer: atcgatGCTAGCggaggaggaggatctgcagac; capital letters denote NheI cut site). Following ligation of BFP insert with Gal3 plasmid, individual clones were isolated and sequenced for verification of desired insertion.

Recombinant Lysenin-GFP protein was expressed in E. coli BL21 transformed with the pET28/His6-EGFP-NT-Lys plasmid. Bacteria was grown in LB supplemented with 10 mM MgSO4 and 0.02% Maltose. Bacterial pellets were lysed using sonication, and protein was purified from the supernatant using Ni-NTA resin.

Myriocin and FB1 stock solutions were made at 5 mM in DMSO. Working stocks were diluted in cell or bacterial culture media and added to cells at the denoted final concentrations. Antitubercular antibiotics rifampicin and isoniazid were used at 1 ng/mL and 0.4 ng/mL, respectively.

4.5.3. Cytotoxicity screening

Cytotoxicity of Myr and FB1 was assessed using resazurin, a compound converted into fluorescent resorufin via active oxidative metabolism[347]. A resazurin sodium (TCI Chemicals; product #R0203-1G) stock solution was prepared at 0.5 mg/mL in DMSO and added to cells at a final 0.15 mg/mL concentration. Cells were incubated at 37 °C for 4 hours. Fluorescence intensity was measured using a CLARIOstar (BMG Labtech) plate reader with the 560 nm excitation/590 nm emission setting.

4.5.4. Thin-layer chromatography

THP-1 and RAW 264.7 cells were cultured and treated with small molecule inhibitors for three days as above. Cells were additionally treated with either NBD-sphinganine (Avanti Polar Lipids, product #810205X-250ug), C6-NBD-ceramide (Avanti Polar Lipids, product #810209X-1mg), or radio-labeled serine for 1 hour at 37 °C in cell culture media. The cells were then washed 3x with PBS and scraped into 1 mL ice-cold PBS 2x. Lipids were extracted via the addition of 2:1 chloroform:methanol (vol:vol) and 30-second vigorous mixing. The biphasic solution was separated via 1-hour incubation at -20 °C and 10 min spin at 2,000 xg in a chilled centrifuge. The lower organic layer was carefully removed with a glass pipette and dried under the flow of nitrogen gas. Extracted lipids were resuspended in 10 µL chloroform and streaked onto the origin of a silica plate. Lipids were separated on the plate using a chromatography mobile phase consisting of 65:25:1 chloroform:methanol:ammonium hydroxide (vol:vol:vol). NBD-lipids were visualized using the 488 nm filter on a Sapphire FL (Azure Biosystems) biomolecular imager. Radio-labeled serine-containing lipids were visualized using a phosphor imaging plate. Quantification of lipid bands in each lane was achieved using the Fiji gel analysis tool.

4.5.5. Microscopy staining

All antibody-stained microscopy samples were treated as follows: 1-hour fixation in 4 % formaldehyde in PBS, 1-hour permeabilization/blocking in 0.1 % saponin and 5% normal goat serum in PBS, overnight primary stain with the denoted antibodies at the denoted dilutions in antibody staining buffer (0.1 % saponin and 5% bovine serum albumin in PBS), 3x washes with perm/block buffer, 2-hour secondary stain at room temperature with appropriate secondary antibody, 3x washes in perm/block buffer, 10-minute stain with 1x DAPI and 1x phalloidin where denoted. Coverslips were mounted to glass slides using ProLong Glass antifade mountant (Thermo Fisher, #P36980).

Antibodies: anti-EEA1 (Cell Signaling Technologies, Rabbit mAb Clone C45B10, product #3288); anti-Rab7 (Cell Signaling Technologies, Mouse mAb Clone E9O7E, product #95746); anti-LAMP1 antibody (Cell Signaling Technologies, rabbit mAb clone D2D11, product #9091S); anti-Galectin 3 (Thermo Fisher, Mouse mAb clone A3A12, product #MA1-940); anti-Rabbit secondary (Invitrogen, Goat mAb, product #A-11034 (Alexa-488) and #A-32722 (Alexa-647)); anti-Mouse secondary (Invitrogen, Goat mAb, product #A-11001 (Alexa-488) and #A-32728 (Alexa-647)). Where denoted, microscopy samples stained with Lysotracker Red DND-99 and Cellmask Deep Red were stained for 15 minutes at 1:10,000 and 1:20,000 dilutions in PBS, respectively, before fixation.

4.5.6. *Mtb* culturing and THP-1 infection

All *Mycobacterium tuberculosis* infections were performed in a dedicated biosafety level 3 facility according to approved safety guidelines.

Historical *Mtb* strain H37Rv and the attenuated RD1-deletion mutant strain H37Rv-ΔRD1 were gifts kindly given to us by Dr. David Lewinsohn at the Oregon Health & Science University and the Portland Veterans Affairs Medical Center; H37Rv-ΔRD1 was originally produced by the lab of Dr. Sherman[340]. The vaccine strain *Mycobacterium bovis* Bacillus Calmette-Guerin was sourced from the lab of Dr. Melanie Harriff at the Oregon Health & Science University and the Portland Veterans Affairs Medical Center. The luminescent H37Rv-pLux strain was a gift kindly provided to us by Dr. Bryan Branson at the Massachusetts Institute of Technology and was kept under antibiotic selection using Zeocin® (InvivoGen). The H37Rv-Live/Dead strain was provided from the lab of Dr. Sarah Fortune at the TH Chan School of Public Health, Harvard University, and was kept under antibiotic selection with Kanamycin[336]. The H37Rv-dsRed strain was kindly provided to us by the lab of Dr. Dave Lewinsohn at the Oregon Health & Science University and Portland Veterans Affairs Medical Center.

All *Mtb* strains were cultured at 37 °C in Difco™ Middlebrook 7H9 (Becton Dickinson, product #271310) broth medium supplemented with 10 % Difco™ Middlebrook oleic acid-albumin-dextrose-catalase enrichment (OADC; Beckton Dickinson, product #L12240), 0.2 % glycerol, and 0.05 % Tween-80 (Thermo Fisher Scientific, product #BP337-500), and carefully maintained between 600 nm optical density (OD_{600}) of 0.1 and 1.5 for up to 4 weeks before fresh frozen stocks were thawed. Infections were timed such that the OD_{600} fell between 0.5 and 1.0 at the time of collection. Before infection, cultures were collected and pelleted at 2000 xg for 5 minutes, washed 1x with PBS, and pelleted again. The bacterial pellet was resuspended in 1 mL antibiotic-free RPMI media (supplemented as described above otherwise), and a single-cell suspension was achieved by repeated passage through a blunt-tipped 18-gauge needle 25 x and filtration through a 5 μm filter (to remove any remaining clumps of bacteria). The OD_{600} of the single cell suspension was measured, and the concentration of bacteria was estimated from a modified McFarland standard of 1.0_{OD600} = 2.5 x 10^5 CFU/mL.

The bacterial suspension was diluted to prepare the denoted multiplicities of infection (MOI) in low volumes, depending on the plate surface area. For a 96-well plate, infections were performed in a volume of 50 μL; for a 24-well plate, infections were performed in 300 μL; for a 6-well plate, infections were performed in 1 mL. All infections were halted by the addition of 4% formaldehyde in PBS, in accordance with biosafety level 3 protocol.

4.5.7. *Mtb* membrane damage assay and quantification

We found that the mAG-Gal3 damage reporter was ideal for super-resolution microscopy, but that variation in fluorescence signal between cells impaired quantification of high-content imaging; the BFP-Gal3 fluorescent fusion protein was more uniformly expressed between individual cells and was used as the membrane damage reporter in all reported high-content imaging quantification. For both representative images and quantification, 1 x 10^5 THP-1 (BFP-Galectin 3-expressing, or mAG-Galectin 3-expressing, as denoted) cells were plated and activated for 48 hours with 50 nM PMA on 20 mm coverslips in a 24-well plate. Cells were infected at an MOI of 10 as above for four hours, and extracellular bacteria were removed after 4 hours of uptake. Cells were then incubated

with Myr or FB1 for 24-, 48-, and 96-hours post-infection start. Coverslips were then rinsed 2x with PBS and fixed for 1 hour in 4% formaldehyde. For representative images, cells were stained with DAPI and imaged on a Zeiss LSM 900 confocal microscope using AiryScan super-resolution and a 63x oil-immersion objective. Representative images are presented as maximum-intensity z-projections. For high-content images used in quantification, cells were stained with DAPI and Dylight^{TM} 488 Phalloidin (Cell Signaling Technology #12935S) and imaged using a 40x oil-immersion objective (NIKON CFI S FLUOR 40X OIL OBJECTIVE) on a Keyence BZ-X fluorescence microscope using multi-section image stitching (processed using the Keyence BZX Analyzer software).

Quantification was achieved by manual counting of at least 200 cells per image per biological replicate using FIJI. Cells were categorized cells by the presence or absence of BFP-Galectin 3 puncta colocalized with H37Rv-dsRed. Image filenames were blinded to the counter and de-blinded after quantification of the entirety of each biological replicate.

4.5.8. LLOME Membrane damage repair assay

1 x 10^5 THP-1 cells were plated in chamber slides (Ibidi) and activated for 48 hours in 50 nM PMA. Cells were treated with 1 mM LLOME for 15 minutes before being washed out and replaced with RPMI for the denoted recovery times. Cells were stained for 15min with Lysotracker Red DND-99 (1:20,000; Invitrogen, product #L7528) to visualize acidified lysosomes and CellMask Deep Red (1:20,000; Invitrogen, product #C10046) for counterstain. Total treatment or recovery time includes 15-minute stains (e.g., No Recovery samples were concurrently stained and treated with LLOME, and 120-minute Recovery samples were stained for 15 minutes at 105 minutes post-washout). For cells treated with Myr or FB1, recovery occurred in the presence of these inhibitors.

Imaging was performed immediately after staining on a Keyence BZ-X100 fluorescence microscope using a 40x oil-immersion objective (NIKON CFI S FLUOR 40X OIL OBJECTIVE). 3x3 or 5x5 tiled images were stitched using the Keyence Image Analysis software. Images were analyzed using the Cell Extraction tool in the Keyence Image Analysis software. Extraction conditions (i.e., thresholds for the CellMask and Lysotracker Red channels) were set using a “No LLOME” image and applied to each subsequent image automatically. The total cell area was defined using the CellMask signal, and we report the mean area of the Lysotracker signal above the threshold as a percentage of the total cell area for at least 200 cells per treatment condition and timepoint for each biological replicate. The mean lysotracker signal for cells of each treatment/genotype group was normalized to the mean percentage for each biological replicate to correct for differences in overall signal between replicates; at least three biological replicates were measured for each timepoint and cell type. Data visualization was achieved using the ggplot2 package in R; statistical testing was achieved via unpaired t-test against the untreated control (THP-1 cells) or wildtype control (RAW 264.7 cells) using GraphPad Prism.

4.5.9. ESCRT recruitment assay

1 x 10^5 THP-1 cells were activated and plated on 20 mm coverslips as above, and pretreated with either vehicle control (0.1 % DMSO) or Myr or FB1. Cells were then treated with the agent LLOME in order to induce lysosome-targeted damage. Cells were then stained for the late endosome/lysosome marker Rab7 and the ESCRT III complex member CHMP4b as described above in {#sec-MtbDamage-Methods-MicroscopyStaining}. Cells were then imaged using a Zeiss LSM 900 confocal microscope

using AiryScan super-resolution and a 63x oil-immersion objective. Quantification was achieved using the Manders colocalization test in FIJI.

4.5.10. Lysenin-GFP colocalization assays

For colocalization of Lysenin-GFP with BFP-Galectin 3 membrane damage reporter, cells were plated and activated as above on 20 mm glass coverslips. Cells were transfected with BFP-Galectin 3 plasmid for 48 hours using Lipofectamine 3000 transfection reagent (Thermo Fisher Scientific, #L3000075). Cells were treated with 100 uM LLOME in PBS for 30 minutes prior to fixation in 4% formaldehyde. Cells were permeabilized using 0.1% saponin and stained with purified Lysenin-GFP. Cells were imaged on a Nikon Spinning Disk confocal microscope (Nikon Yokogawa CSU-W1 Series Spinning Disk). Mander's correlation coefficients of Green□Red signal were quantified using FIJI. Statistical testing was achieved using an unpaired t-test.

For colocalization of Lysenin-GFP with *Mtb*, THP-1 cells were plated and activated as described above on 20 mm glass coverslips. Cells were infected with H37Rv-dsRed at an MOI of 10 as above for 24, 48, 72, and 96 hours before fixation. Cells were permeabilized using 0.1% Saponin and stained with purified Lysenin-GFP. Cells were imaged on a Zeiss LSM700 confocal microscope, and Pearson's correlation coefficients of Green□Red signal were quantified using FIJI. Statistical testing was achieved using an unpaired t-test performed in GraphPad Prism.

4.5.11. Live/Dead reporter-based mycobacterium growth assay

THP-1 cells were plated and activated as described above on 20 mm glass coverslips. Cells were infected at an MOI of 10 as above for 4 hours before the removal of extracellular bacteria via PBS wash. Myr and FB1 were added, and cells were incubated for 72 hours. At 72 hours post-infection, cell media was refreshed with doxycycline additive for another 24 hours. Coverslips were fixed and stained with DAPI before imaging using a NIKON Spinning Disk confocal microscope (Nikon Yokogawa CSU-W1 Series Spinning Disk). The ratio of live:dead bacteria was quantified by thresholding the green and red channels and quantifying the number of green-and-red pixels versus the number of red-only pixels. Depicted are the means of three independent biological replicates for THP-1 cells and PBMCs from two donors. Statistical testing was achieved via an unpaired t-test performed in GraphPad Prism.

4.5.12. Luminescence-based mycobacterium growth assay

THP-1 cells were plated and activated as described above in white-walled 96-well plates (ThermoFisher, product #165306). Cells were infected with H37Rv-pLux at an MOI of 5 in 50 µL for 4 hours at 37 °C, followed by 2x PBS washes and the addition of inhibitor in a final volume of 200 µL. Plates were sealed with an optically clear gas-permeable plate seal (Breathe-Easy, Sigma Aldrich, product #Z380059) to limit evaporation. The infected cells were incubated at 37 °C for 120 hours. On each 24-hour interval, the plates were equilibrated for 45 minutes in a pre-warmed luminescence plate reader (FLUOstar Omega, BMG Labtech) to limit condensation. Luminescence values were collected using the top optic and a well scan under the spiral average setting (diameter 5 mm). Final data are reported as the average fold-change in luminescence for technical replicates

after background subtraction and normalization (each well was normalized to its starting value). Statistical testing was achieved via an unpaired t-test.

For luminescence growth assays of H37Rv-pLux alone, bacteria were cultured in 7H9 liquid culture media supplemented with the denoted compounds and incubated in a 96-well plate inside a luminescence plate reader (FLUOstar Omega, BMG Labtech) for 120 hours. Luminescence data was collected every 15 minutes using the same acquisition settings as above.

4.5.13. CFU-based *mycobacterium* growth assay

THP-1 cells were activated for 48 hours with 50 nM PMA. Cells were infected as above at an MOI of 10 in 1 mL for 4 hours at 37 °C in the absence of sphingolipid inhibitors. After infection incubation, cells were washed 2x with PBS and fed with media containing vehicle control (DMSO at 0.3 % final vol:vol), 15 μM Myr, 5 μM FB1, or 1 ng/mL rifampicin and 0.4 ng/mL isoniazid. Infected cells were incubated with inhibitors for 96 hours before being gently washed 2x with PBS and lysed via incubation in PBS with 0.1 % Triton X-100 for 10 min at 37 °C and vigorous pipetting. Lysates were serially diluted to 1:20, 1:200, and 1:2000. 100 μL of diluted lysates were streaked on 7H10 agar plates and incubated at 37 °C for 3-5 weeks. At the end of this incubation period, streaked 7H10 agar plates were counted to determine CFU/mL.

For CFU assays on *mycobacteria* in culture (non-infection CFU assays, as in Figure S4.4 B, C, and D), incubation with the denoted inhibitors was performed in liquid 7H9 culturing media for 96 hours. Bacterial cultures were serially diluted to 1:100, 1:10,000, and 1:1,000,000 and streaked on 7H10 agar plates as above. After 3-5 weeks of incubation at 37 °C, streaked plates were counted to determine CFU/mL.

4.6. Contributions and Acknowledgements

GG designed the study, performed the majority of the work, and wrote the manuscript. AG performed LLOME-induced Lysenin-GFP accumulation experiments, ESCRT localization experiments, and assisted with writing and editing. MTG performed NBD-ceramide and NBD-Sphingosine TLCs, assisted with cell culturing, and edited the manuscript. Aidan Anastas purified Lysenin-GFP for LLOME-induced Lysenin-GFP localization experiments and edited the manuscript. HL performed Mtb-Lysenin-GFP colocalization experiments. FGT oversaw and directed the study, performed the radiographic TLC, and edited the manuscript.

We thank Dr. Joost Holthuis for providing cell lines and intellectual input. We thank Dr. Tim Bates for his help in cloning the BFP-Galectin 3 plasmid. We thank Dr. David Lewinsohn, Dr. Melanie Harriff, Dr. Bryan Bryson, and Dr. Sarah Fortune for providing Mtb strains used in this study. We thank Dr. Eric Barklis and Dr. Sascha Kuhn for their assistance in purifying Lysenin-GFP. We thank the OHSU Advanced Light Microscopy Core for significant assistance in image capture and analysis. We also thank Dr. Stephanie Kaech Petrie, Dr. Hannah Borstein, and Dr. Felice Kelly of the OHSU Advanced Light Microscopy Core facility for their image acquisition and analysis expertise. Finally, we thank Madeleine Faucher for her patience and assistance in preparing and editing this manuscript.

We have no conflicts of interest to declare.

4.7. Supplemental data

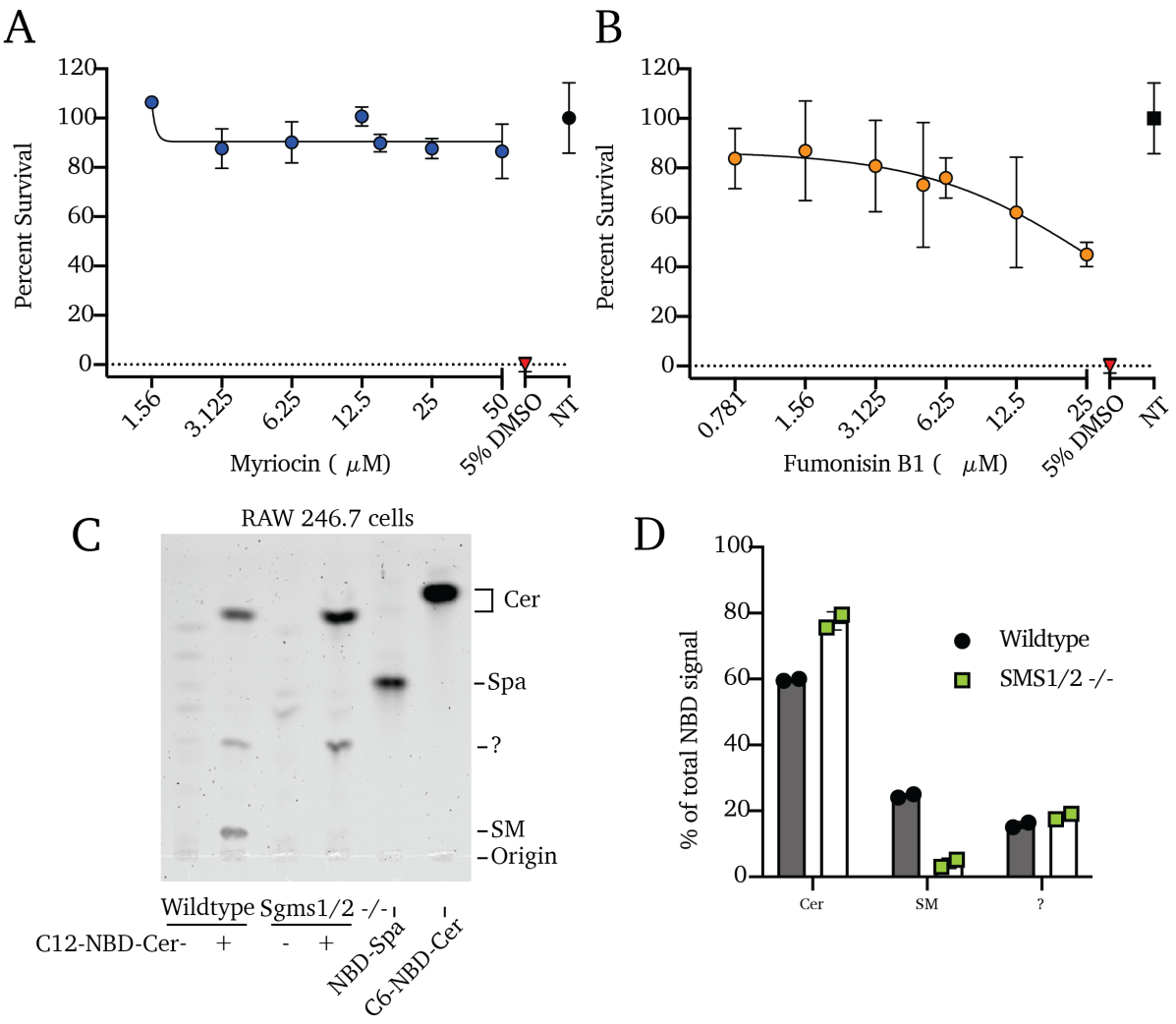


Figure S4.1 – **Cytotoxicity assay of Myr and FB1 treated cells** (A and B) THP-1 cells were treated with the denoted concentrations of Myr and FB1 for 72 hours. Cell viability is reported as percent survival in comparison to untreated control (defined as 100% viability, n = 18) and 5% DMSO negative control (defined as 0% viability, n = 6). All treated points are the product of 3 biological replicates. (C) Fluorescent thin-layer chromatography depicts the metabolism of C12-NBD-ceramide in either wildtype or Sgms1/2 double knockout RAW 246.7 cells. The loading position (origin), and bands of sphingolipid metabolic products are labeled, as well as one unidentified band. (D) Quantification of the thin-layer chromatography shown in (C).

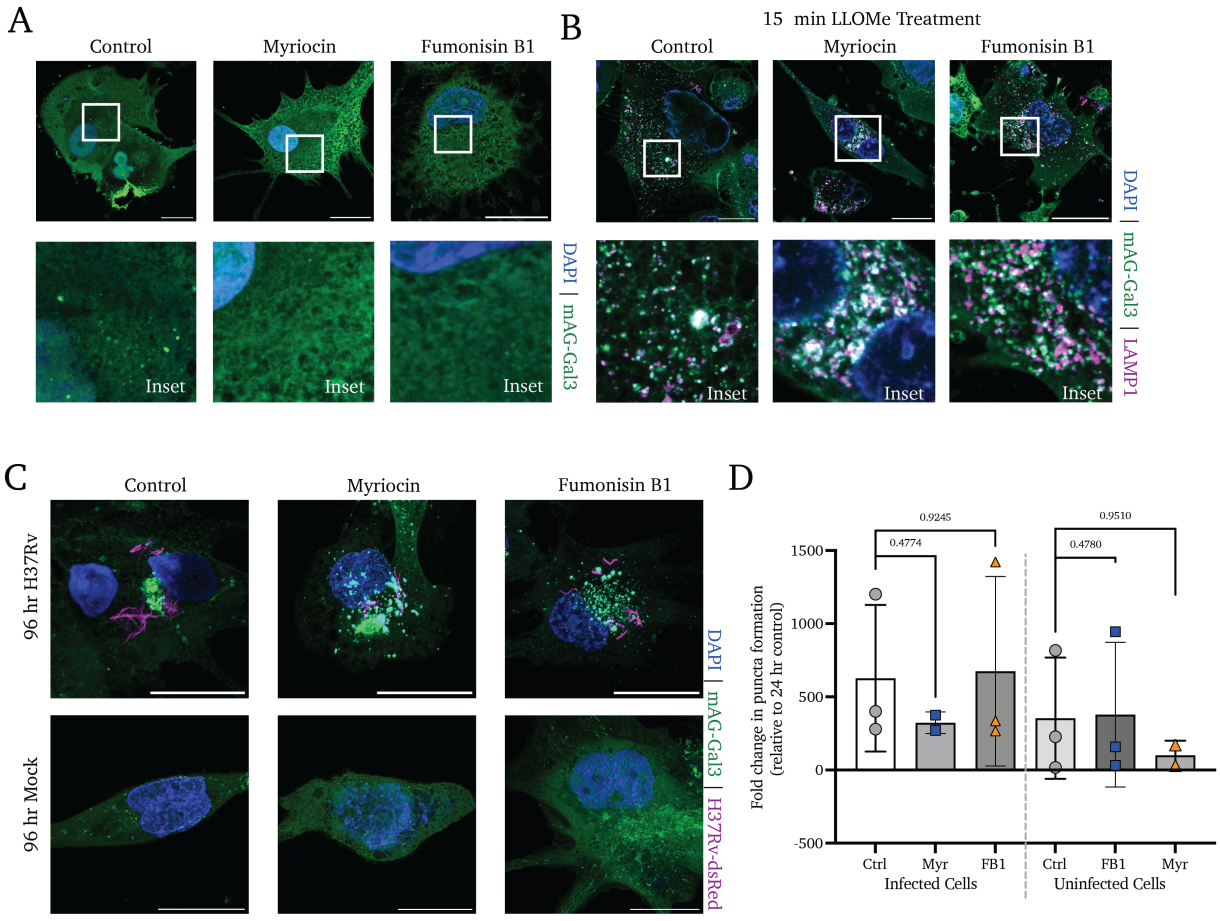


Figure S4.2 – Mtb-induced endosomal membrane damage at 96 hours post-infection. (A) Representative maximum-intensity projections of mAG-Gal3-expressing cells infected with H37Rv-dsRed and treated with vehicle control, Myr, or FB1. Cell stains are as denoted (see Methods Section 4.5.7 for microscopy details). (B) Representative images of mAG-Gal3-expressing cells pre-treated with Myr or FB1 and treated with LLOME for 15 minutes. Cell stains are as denoted (see Methods Section 4.5.7 for imaging details). (C) Representative images of THP-1 cells treated with DMSO vehicle control, Myr, or FB1 and infected with H37Rv-dsRed. Upper panels are infected cells; lower panels are uninfected cells treated for 96 hours (see Methods Section 4.5.7 for imaging details). (D) Quantification of the rates of puncta formation in Mtb-infected and uninfected cells at 96 hours of infection and treatment. (Statistical testing was achieved via unpaired t-test versus respective control images).

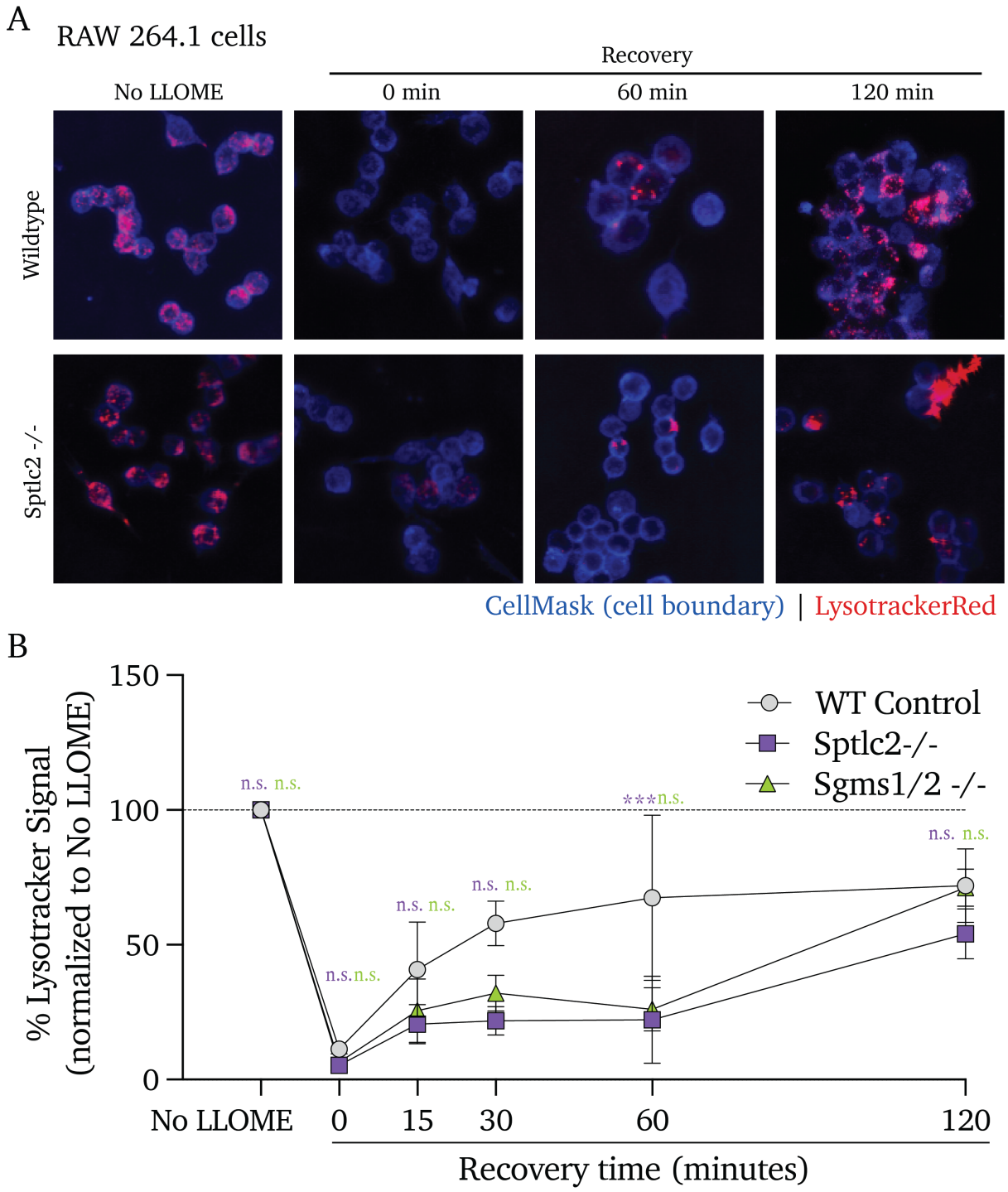
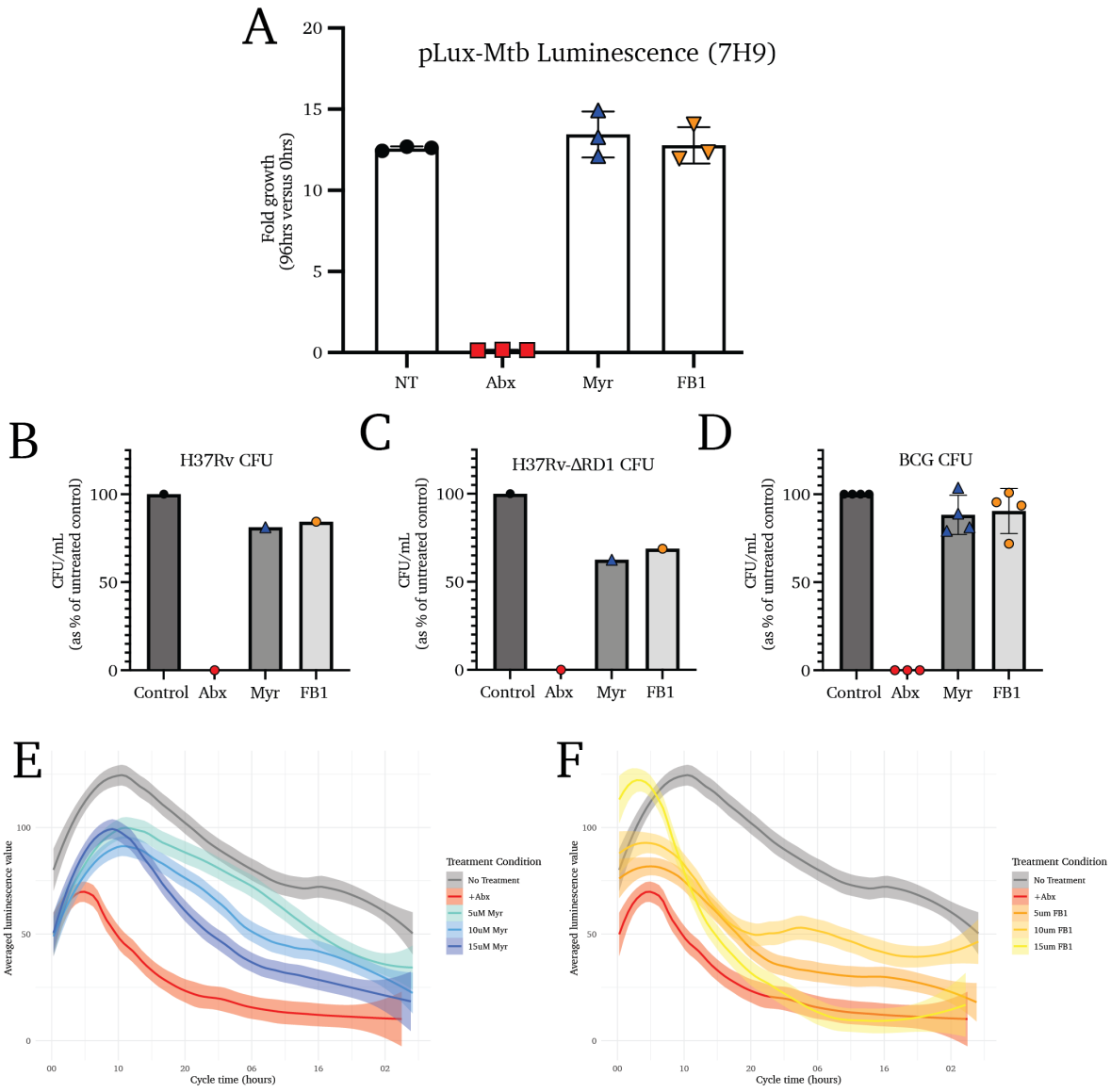


Figure S4.3 – Sphingolipid synthesis mediates rapid recovery from LLOME-induced damage. (A) Representative images of RAW 264.7 macrophages of wildtype, Sptlc2$^{-/-}$, or Sgms1/2$^{-/-}$ lineage were treated with LLOME and stained with Lysotracker to visualize the presence of acidified compartments at various times after LLOME removal (See Methods Section 4.5.8 for imaging details). (B) Quantification of images as in A. (Statistical testing via multiple comparisons t-test versus Vehicle control; error bars denote the standard error of the mean; * = $p<0.05$, ** = $p<0.01$, *** = $p<0.005$, *** = $p<0.0001$. Abbreviations: LLOME = leucine-leucine dimethyl ester, a.f.u. = arbitrary fluorescence units).



pLux-Mtb Luminescence (RPMI, no cells)

Figure S4.4 – ***Mtb* growth is inhibited by Myr and FB1 treatment** (A) Normalized pLux-*Mtb* luminescence signal after 96 hours growth in 7H9 bacterial media and treatment with 15 μM Myr, 5 μM FB1, or 1 μg/μL rifampicin and isoniazid, normalized to starting luminescence. Each point denotes a single biological replicate. (B, C, and D) Colony forming unit assay on *Mtb* strains H37Rv (B) or H37Rv-ΔRD1 (C) or *M. bovis* strain BCG (D) grown in 7H9 bacterial growth media and treated with 1 μg/μL rifampicin and isoniazid, 15 μM Myr, or 5 μM FB1. Each point denotes a single biological replicate. (E and F) Luminescence trace of pLux-*Mtb* grown in RPMI mammalian cell culture media (in the absence of cells) and 52 hours treatment with 1 μg/μL rifampicin and isoniazid, 15 μM Myr, or 5 μM FB1 (normalized to blank control, n = 3). Curves are smoothed with ggplot2::geom_smooth, method = 'loess', formula = 'x ~ y', span = 30 min

Chapter 5.

Living Off the Fat of the Cell

A lipidomics map of the *Mycobacterium tuberculosis*-infected cell

---

Authors: Gaelen Guzman[1], Scotland E. Farley[1], Michelle Garcia[1], Lisa Bramer[2], Jennifer Kyle[2], Fikadu G. Tafesse[1]

[1] Department of Molecular Microbiology and Immunology, Oregon Health & Science University, Portland, Oregon, USA. [2] Pacific Northwest National Laboratories, Integrative Omics Core, Richland, Washington, USA.

5.1. Abstract

For centuries, humans have been seeking reliable treatment for tuberculosis, but unfortunately, it still poses a significant threat to global health. Recent research has shown that host lipid biology may offer new opportunities for developing novel antitubercular therapy. Here, we identify unique signatures of Mycobacterium tuberculosis (Mtb) infection by comparing the global lipidome of cells infected with pathogenic and attenuated Mtb strains against the lipidomes of cells treated with isolated Mtb cell wall components. We find that pathogenic and attenuated infections and treatments with pathogen-associated molecular patterns induce significant upregulation of diacylglycerol production. However, only pathogenic infection increases the production of triacylglycerol and acylcarnitine, reflecting induced fatty acid β-oxidation, while inhibiting the synthesis of lysophospholipids and plasmalogens, which reflects concerted subversions of the macrophage antimicrobial program. This research shows great potential in identifying potential host-directed therapies.

5.2. Introduction

Mycobacterium tuberculosis (*Mtb*) is a pathogen with unique lipid needs from the host. To date, *Mtb* was responsible for over 1.3 million deaths in 2022 through active tuberculosis disease, and estimates suggest that up to 2 billion people harbor latent tuberculosis infection[1]. While frontline antibiotic therapy has a high success rate[1], the threat of antibiotic-resistant strains is the source of remarkable concern – driving renewed interest in developing host-directed therapy (HDT) to reduce the permissivity of the human host in conjunction with frontline antibacterial therapy. We and others have suggested that unexplored lipid biology may hide novel avenues for anti-TB HDT[348]. *Mtb* induces massive changes to the host lipid profile, and previous work has sought to reveal lipid-based biosignatures of TB infection[349]. However, no study has sought to systematically disentangle the antimicrobial host response from the Machiavellian manipulations that an *Mtb* infection induces in the host cell. Further, none has attempted to map the effects of *Mtb* infection to individual components of the *Mtb* cell wall.

Mtb is uniquely adapted to human hosts and thus has become a highly subtle pathogen: nearly an obligate intracellular bacterium, it needs to acquire all its nutrients and energy from the host cell in its protracted siege within the lung[53]. In infecting alveolar macrophages and other antimicrobial immune cells, *Mtb* seeks to subvert the host immune response by limiting antigen presentation to the adaptive immune system and suppressing inflammatory cytokine release. To this end, *Mtb* wields a molecular arsenal comprising many factors that allow it to redirect phagosomal maturation and thus avoid degradation in the lysosome. Curiously, this bacterium is well-suited to utilize host lipids as a significant carbon/energy source, having devoted over a third of its genome to lipid transport, metabolism, and catalysis[268,350,351]. The accumulation of foamy macrophages within the granuloma is a well described phenomenon preceding progression from latent to active TB disease. These cells are replete with lipid droplets and primed for fatty acid oxidation instead of glycolysis. Prior reports have shown that *Mtb* can utilize lipids from lipid droplet-replete host cells, reportedly through cholesterol metabolism[177], and that *Mtb* induces the recruitment of lipid droplets toward the *Mtb*-containing endosome. Intriguingly, conflicting reports describe both the pro-bacterial and pro-host effects that these foamy macrophage phenotypes have during the progression of an *Mtb* infection[108,352,353]. Notably, the alterations induced in a host cell by *Mtb* infection are the combined effects of *Mtb*'s pathogenic manipulations and the innate immune action of the cell. Throughout the infection, these influences will counterbalance each other to determine the winner in the tug-of-war between the host and the pathogen.

Layer et al.'s review on lipidomics techniques and advances discusses advances in lipidomics techniques and analysis tools. Among many challenges is an astounding diversity of solvent-extractable, apolar mycolic acids[354]. While numerous studies have utilized omics analyses to probe fundamental questions about the host-pathogen interactions during an *Mtb* infection, only one report has investigated the effects that infection has on the host lipidome[355]. Saquib et al. characterize profound ER changes, apoptosis inhibition, and induced cholesterol synthesis during pathogenic infection[355]. However, they do not attempt to map the *Mtb* components which induce such effects. Are they the product of active mycobacterial processes, or are these effects a component of the cellular response to infection?

In the present study, we aim to address these questions using untargeted lipidomics. We analyzed cells infected with pathogenic and attenuated strains of *Mtb* and compared their lipidomes with those of cells treated with five pathogenic *Mtb* components, including lipoarabinomannan, 1-tuberculosinyladenosine, phthiocerol dimycocerosate, phosphatidyl-*myo*-inositol dimannoside, and

sulfolipid-1. We find several such signatures. Among these, pathogenic infection induces the upregulation of triacylglycerol synthesis and acylcarnitine accumulation – likely indicators of upregulated fatty acid β-oxidation. We also find that pathogenic infection induces depletion of antimicrobial lysophospholipids and plasmalogens. Such findings are crucial steps in identifying routes of host-directed therapy.

5.3. Results

5.3.1. Global lipidomics reveals acute changes in the host lipidome during pathogenic Mycobacterium tuberculosis infection.

We performed untargeted lipidomics on human THP-1 monocyte-derived macrophages infected for either 24 hours or 96 hours with either the historical *Mycobacterium tuberculosis* strain H37Rv or with the attenuated deletion mutant strain H37Rv-ΔRD1 (ΔRD1) (Figure 5.1A). As control, we plated, incubated, and collected mock-infected cells to serve as a baseline control. We prepared all conditions in quintuplicate. Infection conditions were optimized to guarantee an infection rate of at least 70% for both time points for both infections (Figure S5.1). The total lipid content from the cells was extracted via the method of Bligh-Dyer, spiked with internal standards, and analyzed via liquid chromatography-electrospray ionization tandem mass spectrometry (LC-ESI-MS/MS) as previously described[356,357]. In total, 401 lipids were annotated and manually validated using LIQUID[244], including 261 phospholipids, 82 glycerolipids, 34 sphingolipids, 18 cardiolipins, five cholesteryl esters, and one long-chain acylcarnitine. The abundance of each lipid was normalized to the intensity of the spiked internal standards for each sample and was then averaged between replicates across each condition (Figure S5.2). Principal component analysis on all Mtb-infected samples shows a broad bifurcation between 24- and 96-hour samples as well as a modest separation of infected samples from mock samples (Figure 5.1B).

The relative enrichment of each lipid in each infection condition is reported here as a log2-transformed fold-change (Log2FC) versus the time-matched mock control (Figure 5.1C and Figure S5.3A). An upward shift on the bubble plots denotes relative enrichment during infection, whereas a downward shift denotes relative depletion. Log2FC enrichment values ranged from: -0.52 (for triacylglycerol TG(44:0)) to +5.34 (for phosphatidylinositol PI(16:0/19:0)) for the 24-hour infection and -0.87 (for lipid carnitine(16:0)) to +3.74 (for lipid PI(16:0/19/0)) for the 96-hour infection. Four lipid species are overwhelmingly dominant in this dataset: PE(17:0/18:0), PE(16:0/19:0), PI(16:0/19:0), and CL(68:2), each increasing by more than 4-fold (and up to 16-fold) over mock-infected cells.

We applied a one-way Analysis of Variance (ANOVA) with Benjamini-Hochberg correction for multiple comparisons to attribute statistical significance to each lipid species for each infection condition. Twenty-four lipids were assigned p-values < 0.05 at 24 hours post-infection, and ten lipids at 96 hours. More significant changes occur at 24hrs, reflecting a metabolic burst in response to exposure to a pathogen and a return to baseline for many lipids by 96hrs.

Because these samples contain a composite of human lipids and infecting mycobacterial lipids, we sought to determine which of the identified lipids may be derived from *Mtb*. We thus cross-referenced these results with the MycoMass database[354,358], an aggregated lipidomics database which characterizes the static *Mtb* lipidome across several *Mtb* strains, including H37Rv (curated by

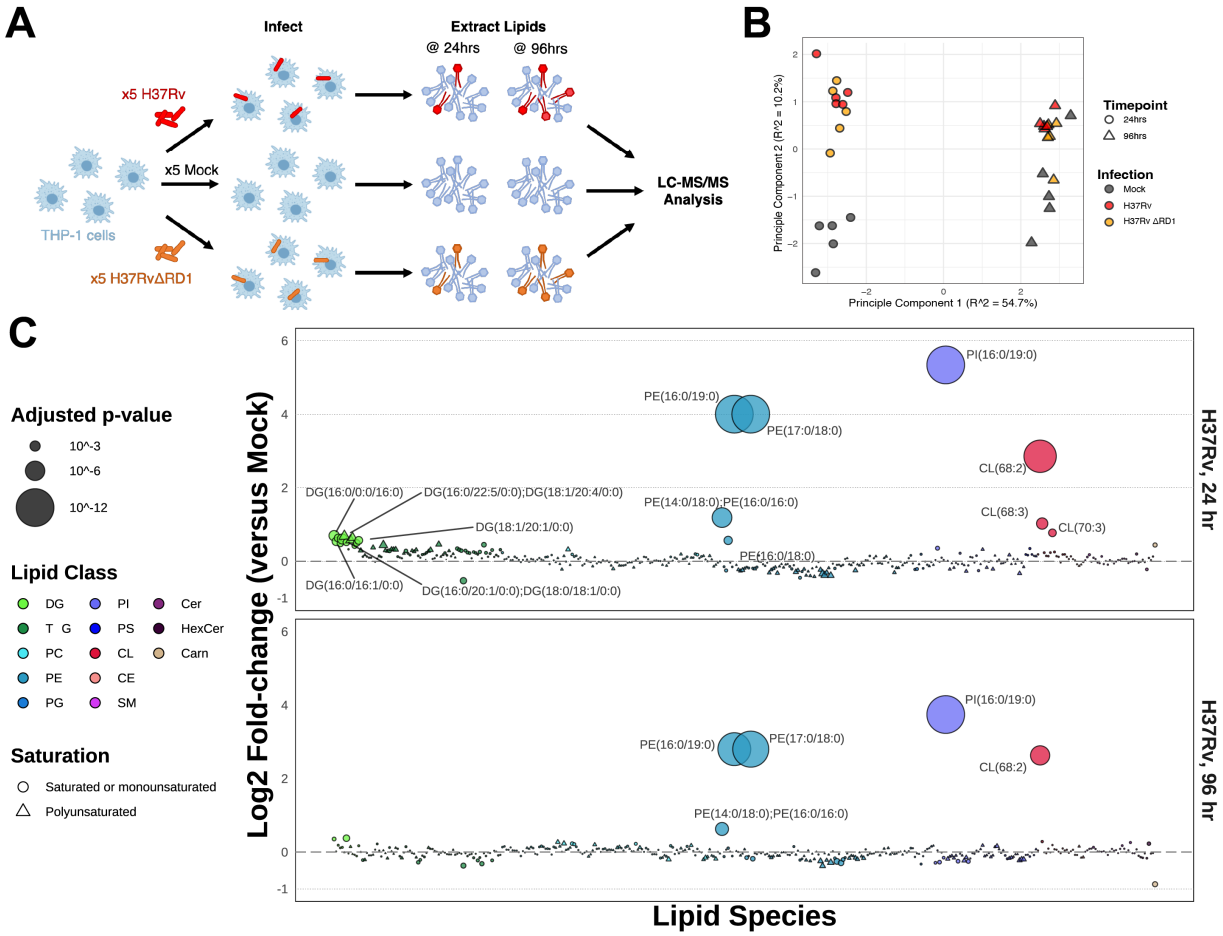


Figure 5.1. – **Lipidomics overview and H37Rv versus Mock results** (A) A schematic overview of the experimental design. Mock refers to uninfected cells cultured and incubated parallel to cells infected with *Mycobacterium tuberculosis* strains H37Rv and H37Rv-ΔRD1. Briefly, five replicates were prepared for mock-infected cells, cells infected with *Mtb* strain H37Rv, and cells infected with the attenuated deletion mutant *Mtb* strain H37Rv-ΔRD1 for 24 or 96 hours before sample collection and LC-MS/MS analysis. (B) Principal component analysis on the lipidomes of mock-, H37Rv-, and H37Rv-ΔRD1-infected cells at both 24 hours post-infection and 96 hours post-infection (each point represents a replicate of each infection and time point, n=5). (C) Bubble plots show each identified lipid species' relative enrichment (Log2FC = Log2 fold-change) versus mock control. Point size denotes the adjusted p-value resulting from a one-way ANOVA and multiple hypothesis correction; point color denotes the class of each lipid; point shape denotes whether each lipid is polyunsaturated (PUFA) or either monounsaturated or fully saturated.

the lab of Dr. Branch Moody at Brigham and Women's in Boston, MA). We aligned these datasets at the lipid species level (as opposed to the molecular lipid species, which describes the acyl chain composition of each lipid). We found that out of 401 lipids identified in these infection data, 88 overlap with this database. This includes some redundancy among hits that are indistinguishable at the lipid species level (e.g., the molecular lipid species PE(17:0/18:0) and PE(16:0/19:0) both match with PE(35:0) at the lipid species level, and it is unclear if one or both molecular lipid species are present in the MycoMass database). To aid in clarifying which lipids are most likely to be unique to *Mtb*, we plotted the ratios of infected versus uninfected data (Figure 5.2), partitioning data between human-only (absent from the MycoMass database) or potential *Mtb* lipids (present at the lipid species level in the MycoMass database).

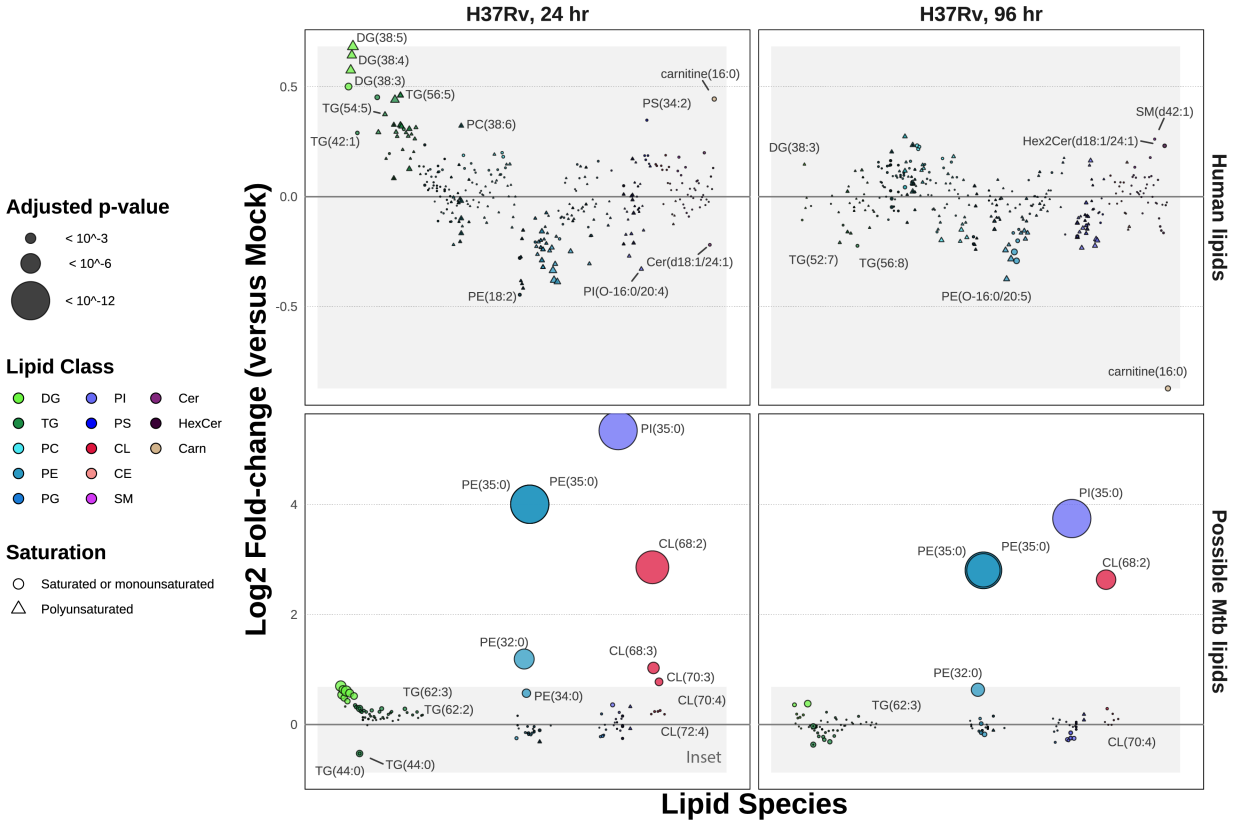


Figure 5.2. – **Infected cells upregulate polyunsaturated DG during H37Rv infection** The comparisons depicted in Figure 5.1 were partitioned between definitively human and possibly_Mtb_-derived via alignment with the MycoMass database. Left panels: 24-hour H37Rv infection (fold-change relative to mock); right panels: 96-hour H37Rv infection (fold change relative to mock); upper panels: Lipid species absent from the MycoMass database; lower panels: Lipids species present in the MycoMass database. The gray box denotes minimum and maximum values among "human only" lipids. (Abbreviations: DG = diacylglycerol, TG = triacylglycerol, PC = phosphatidylcholine, PE = phosphatidylethanolamine, PG = phosphatidylglycerol, PI = phosphatidylinositol, PS = phosphatidylserine, CL = cardiolipin, CE = cholesteryl ester, SM = sphingomyelin, Cer = ceramide, HexCer = hexosylceramide, Carn = acylcarnitine)

Notably, the three most enriched lipid species in H37Rv infection, PI(35:0), PE(35:0), and CE(68:2), are likely *Mtb* lipids. At the lipid species level of annotation, PI(35:0) is indistinguishable between its two possible constituents, PI(16:0/19:0) and PI(17:0/18:0). The same is true for PE(35:0). While C17:0 heptadecanoic acid is detectable (<1%) in human tissue and plasma[359,360], C19:0 is not observed in human samples[359]. Thus, the odd-chain acyl composition of these highly abundant

lipids may be the best designation for their being *Mtb* lipids.

In addition to its annotation in the MycoMass database, CL(68:2) was previously identified as a major *Mtb* lipid by Sartain et al. in their generation of the *Mtb* LipidDB in 2011[361]. Sarma et al. characterized a cardiolipin synthase in *Mycobacterium phlei* with high homology to that of *Mtb* and postulate that the synthesis of cardiolipins allows *Mtb* to better survive within macrophages[362]. Others, such as Fischer et al., describe that host cells present mycobacterial cardiolipins to NK T cells using the antigen presentation molecule CD1d[363].

Beyond the handful of massively enriched lipid species, it is difficult to determine the organismal source of the remaining 85 lipid species co-annotated in the MycoMass database. Further discountable are any "*Mtb*" lipids that are depleted during infection (A log2 fold-change < 0 between infection and mock samples) – this includes the majority of overlapping PE, PI, and PS species. When we apply a cutoff defined by the maximal fold-change among human (non-*Mtb*) lipids, only three additional lipid species appear enriched at 24 hours. Aside from these lipids, we postulate that the overall abundance of the remaining "*Mtb*" lipids in this dataset may be dominated by the host despite their co-annotation in the MycoMass database.

Considering the above, we note that most "human" diacylglycerides and triacylglycerides enriched at 24 hours post-infection contain polyunsaturated fatty acids. In contrast, the enriched "*Mtb*" DGs and TGs are composed of saturated or monounsaturated fatty acids. This observation supports the 2021 report by Laval et al., in which they show that *Mtb* infection stimulates PUFA DG production in the host that serves as carbon and energy for the invading *Mtb*[364].

We also observe wide-spread depletion of polyunsaturated phospholipids, including ester-linked lipids (e.g., PE(O-16:0/22:5) and PI(O-16:0/20:4)), lysolipids (e.g., PE(18:2/0:0)), and plasmalogens (e.g., PE(P-14:0/20:4)) at 24-hours post-infection. The well-described roles of lysolipids and plasmalogens as antimicrobial lipid factors do not escape our attention[365,366] – notably, in 2022 Jurkowitz et al. characterized a mycobacterial lysoplasmalogenase, MtbYhhN, that protects infecting *Mtb* against host-produced lysoplasmalogens[367]. We will discuss these lipids further below.

5.3.2. Comparing lipidomes during H37Rv and H37Rv-ΔRD1 reveals signatures of pathogenic *Mtb* infection

In addition to analyzing the effects of *Mtb* strain H37Rv infection, we prepared an analysis of cells infected with the attenuated deletion mutant *Mtb* strain H37Rv-ΔRD1. This mutant strain lacks the RD1 genomic locus, which contains the *Mtb* Type VII secretion system and many critical pathogenicity factors, including ESAT-6 and CFP-10. Lewis et al. reported in 2003 that the ΔRD1 strain mimics the vaccine strain of *M. bovis*, Bacille Calmette-Guerin[340]. As before, we infected cells for 24 and 96 hours before lipid extraction and mass spectrometric analysis. We find that H37Rv-ΔRD1 induces many changes to the host lipidome in comparison to mock-infected cells (Figure S5.3). We hoped to extract a signature for a pathogenic *Mtb* infection by mapping the differences between H37Rv and H37Rv-ΔRD1 infection. To this end, we compared the relative enrichment of lipids extracted during these infections (Figure 5.3). We faceted these data by timepoint and possible organismal source ("human" lipids versus "*Mtb*" lipids).

In viewing these comparisons, we observe several intriguing differences between these infections. At 24 hours post-infection, most DG species are equally abundant in both samples; this observation would suggest that the up-regulation of DG may be an effect of cell-intrinsic signaling initiated

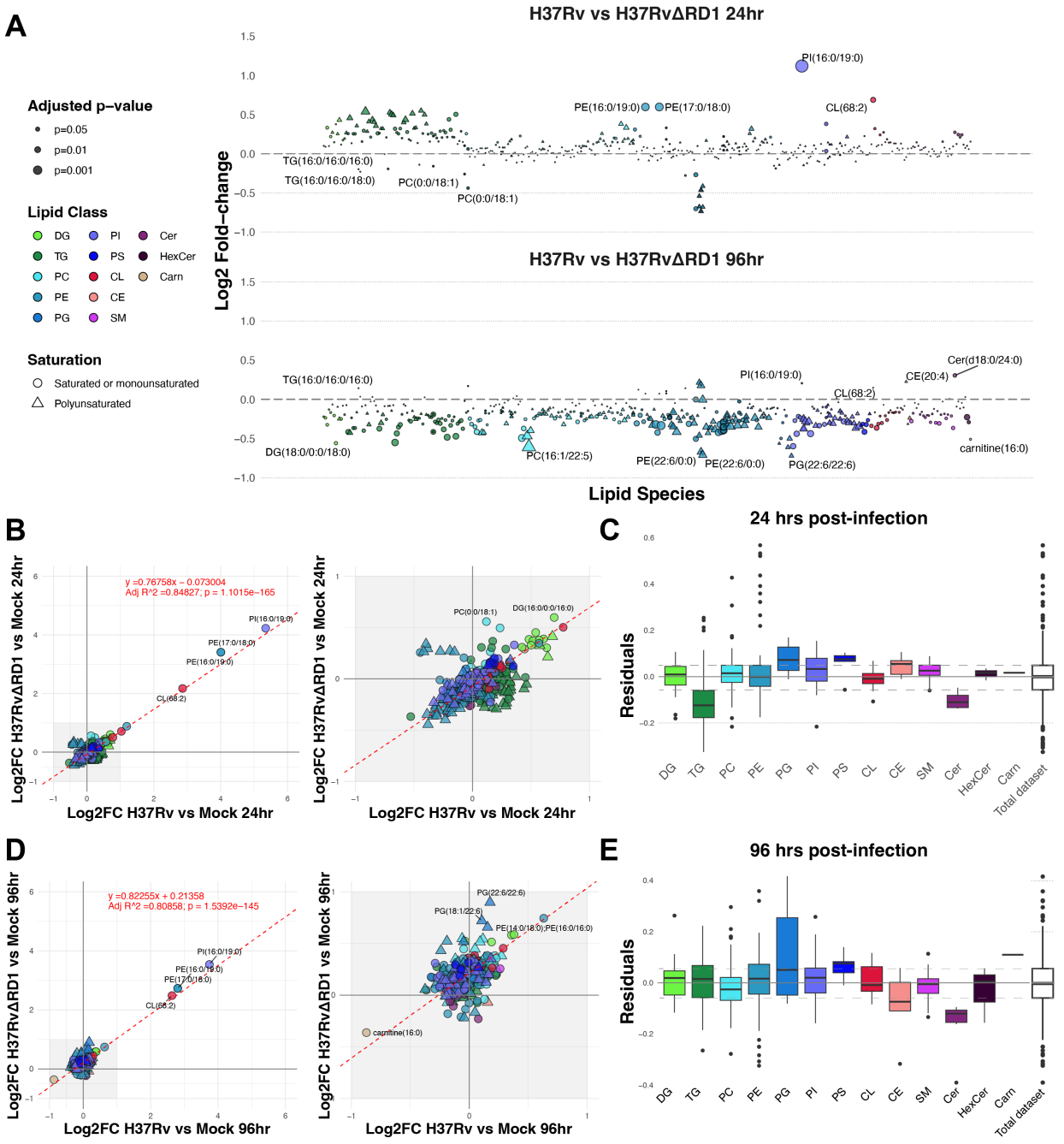


Figure 5.3. – **Pathogenic and attenuated *Mtb* strains induce distinct changes to the host lipidome** Bubbleplots show the relative enrichment of each lipid species between wildtype, pathogenic H37Rv and the attenuated deletion mutant H37Rv-ΔRD1. Plots are faceted by timepoint (vertical split) and possible organismal source (horizontal split). Point size denotes the adjusted p-value resulting from a one-way ANOVA and multiple hypothesis correction; point color denotes the class of each lipid; point shape denotes whether each lipid is polyunsaturated (triangles) or either monounsaturated or fully saturated (circles).

by mycobacterial uptake. At the same time, we observe significant enrichment of nearly all TG species toward H37Rv; this perhaps reflects lipid droplet formation in H37Rv infection, as prior reports show that the accumulation of lipid droplets is a notable difference between these two *Mtb* strains[167].

Similarly, while we observed that many lyso-PE species, such as PE(22:6/0:0), are significantly depleted during infection with H37Rv, the ΔRD1 deletion mutant induces an accumulation of these lipids. These data strongly suggest that pathogenicity factors in the RD1 locus enable the bacterium to inhibit or degrade host lysolipids. In contrast, H37Rv-ΔRD1 seems to induce minimal plasmalogen accumulation: species such as PC(P-16:0/20:3) are significantly enriched toward H37Rv infection.

At 96 hours of infection, we see significantly different patterns. The most apparent trend is that the overall distribution is skewed heavily toward ΔRD1 – perhaps indicative of cytotoxicity in the pathogenic infection or reduced total lipids extracted in H37Rv-infected samples, despite internal standard normalization. Among the lipids most enriched toward H37Rv-ΔRD1 at 96 hours are polyunsaturated PG species, such as PG(22:6/22:6). Intriguingly, PG(22:6/22:6) and several other enriched PG species may be the structural isomer bis(monoacylglycerol)phosphate, which is enriched in multivesicular endosomes and is involved in lysosomal degradation. Previous reports have connected BMPs as factors that control mycobacterial growth in infected cells[368]. The abundance of signature *Mtb* lipids such as PI(16:0/19:0) is equivalent at this time point; this may suggest similar total bacterial content in each sample despite differences in the total lipid content extracted from infected cells.

5.3.3. *Mtb* cell wall components map to selective *Mtb*-infection-induced lipidomic effects

Finally, we hoped to map the effects of antigenic *Mtb* cell wall components to the effects of *Mtb* infection on the cellular lipidome. To this end, treated cells with the following purified compounds isolated from the *Mtb* cell wall: lipoarabinomannan (LAM), 1-tuberculosinyladenosine (1-TbAd), phthiocerol dimycocerosate (PDIM), phosphatidyl-*myo*-inositol dimannoside (PIM-1,2), and sulfolipid-1 (SL-1) (Figure 5.4A). Finally, we treated cells with lipopolysaccharide as a control for TLR activation and resulting PAMP-induced cellular signaling. We used viability assays to select concentrations of each compound with minimal cytotoxicity (Figure S5.4). Total lipid content from these treated cells was extracted via Bligh-Dyer extraction[303], spiked with internal standards, and subjected to LC-MS/MS analysis. In these samples, we identify 377 unique molecular lipid species. Among these were 261 phospholipids, 69 glycerolipids, 29 sphingolipids, 17 cardiolipins, and one cholesterol ester. Principle component analysis shows the most significant separation was between the time points (Figure 5.4B, accounting for 54% of variability). We calculated the relative enrichment of each lipid in treated cells against cells treated with a solvent control (Vehicle), and we applied a one-way ANOVA to determine the statistical significance of each lipid (Figure 5.4B).

Among these data are clear checks of sanity. For example, Bedard et al. recently reported that treatment with 1-tuberculosinyladenosine induces lysosomal lipid storage, including lipids such as TG(52:2) and CE(18:1)[127]. Our findings recapitulate these results: we show that 24-hour 1-TbAd treatment induces significant up-regulation of many DG and TG species, PG, and the cholesteryl ester CE(18:1).

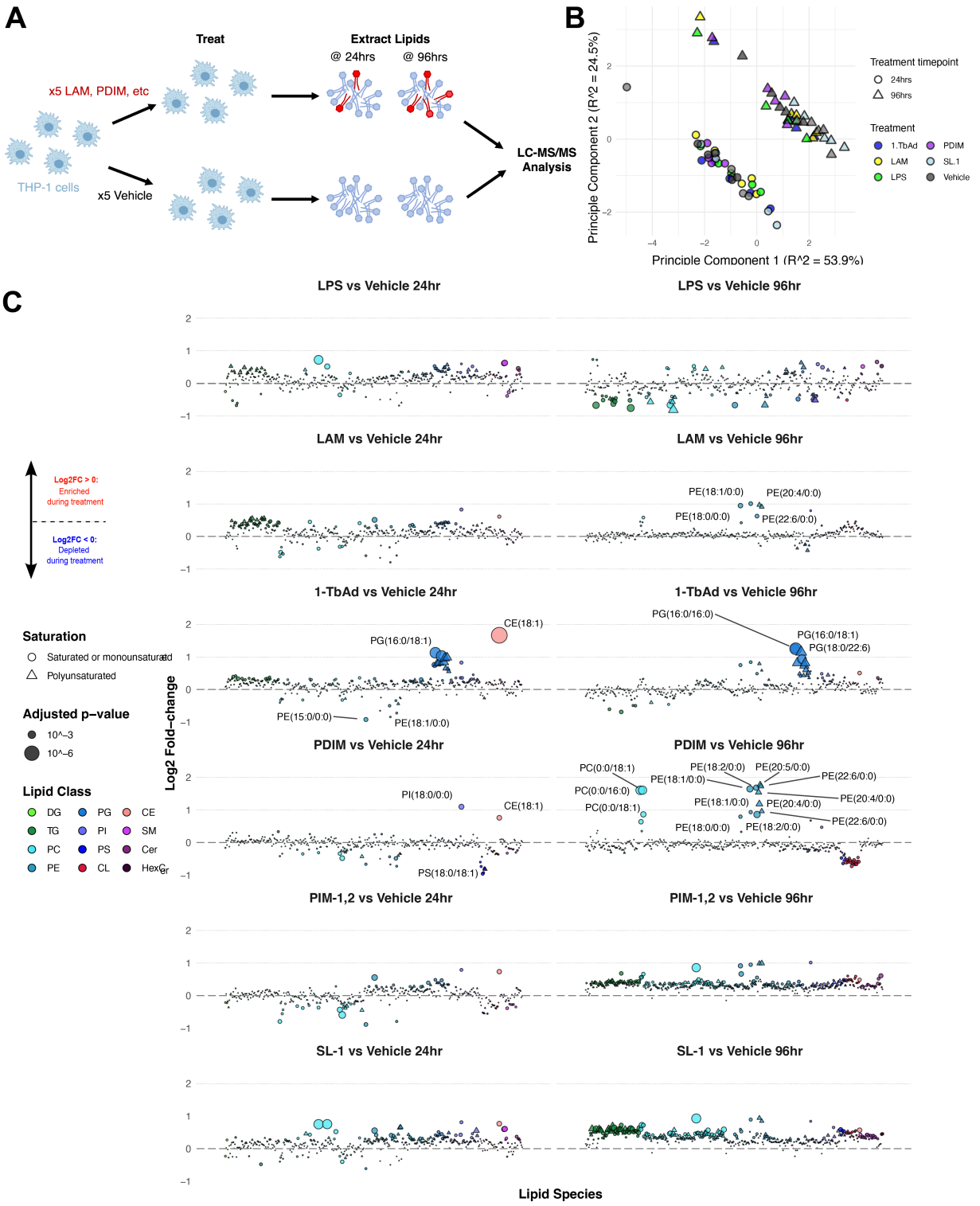


Figure 5.4. – **Overview of *Mtb* cell wall treatments lipidomics** (A) A schematic overview of *Mtb* wall treatment experimental design. (B) Principal component analysis on the lipidomes of treated and untreated cells collected at each time point. Each point represents a single treatment replicate; shape denotes the treatment condition; color denotes the collection time point. (C) Bubble plots represent the log2 fold-change of each lipid identified versus a vehicle-treated control collected simultaneously. Point color denotes the lipid class; point size denotes the Benjamini-Hochberg-adjusted p-value of a one-way ANOVA test; point shape denotes the polyunsaturation state of each lipid. (Abbreviations: LPS = lipopolysaccharide, LAM = lipoarabinomannan, 1-TbAd = 1-tuberculosinyladenosine, PDIM = phthiocerol dimycocerosate, PIM-1,2 = phosphatidyl-*myo*-inositol dimannoside, SL-1 = sulfolipid-1, Veh = vehicle).

In a brief aside, we cross-referenced the treatment dataset with the MycoMass database. We found that 94 lipids are co-annotated (75 share identity with lipid species in the infection results described above). The maximum log2 enrichment of any lipid in any treatment comparison versus vehicle control is +1.65, further obfuscating a clear delineation between lipids that were certainly host-derived from those that were certain *Mtb* lipids.

These results capture many changes among the 377 lipids identified in the treatment samples. To simplify these results and glean greater understanding from the infection results, we prepared a map between the effects of infection and treatment on sub-categories of each lipid class.

5.3.4. Treatments with *Mtb* cell wall components recapitulate some, but not all, effects of *Mtb* infection

In order to map the specific changes of the lipidome that individual *Mtb* components induce with the changes induced by *Mtb* infection, we aggregated these data to the lipid class level (e.g., DG and TG), partitioned between PUFA and non-PUFA for appropriate classes, and aligned the average log2 fold-change versus control for each class (Mock for infection results, Vehicle for treatment results; Figure 5.5).

In these data, we observe that at 24 hours post-treatment start, LPS, LAM, and 1-TbAd all induce a dramatic increase in PUFA diacylglycerol. Because this was a primary signature of 24-hour infection, we postulate that the increase in DG results from pathogen recognition receptor (PRR) signaling. Prior studies have found that *Mtb* activates several PRRs during infection, including TLR2, Mincle, and NOD2 receptors[369,370]. At first glance, the similarity in DG accumulation between LPS and both attenuated and pathogenic infection would suggest some degree of TLR/Myd88 activation. Prior reports have shown that TLR2 is potently activated by *Mtb* glycolipids including LAM, mannose-capped LAM (Man-LAM) and phosphatidyl-*myo*-inositol mannosides (both PIM-1,2 and PIM-6)[371] – as well as multiple lipoproteins (such as LprA, LprG, and LprH)[372]. However, Bedard et al. found no significant stimulation of PRRs following 1-TbAd treatment[127]. The biological significance of PUFA DG accumulation is yet to be determined.

Most compounds induce more significant effects at 24 hours than 96 hours. This trend is likely a result of compound deterioration or degradation. However, one exception to this trend is PDIM, which stimulates significant enrichment of lysophospholipids such as PC(0:0/18:1) and PE(18:2/0:0). Numerous prior reports show that PDIM directly disrupts TLR signaling[126,315,373] and directly induces lysosomal membrane damage[125]. Augenstriech et al. report that PDIM inserts in host membranes and dissolves the membrane bilayer by inducing inverted hexagonal phase formation[374]. To date, no reports have established a link between PDIM and lysophospholipids.

Intriguingly, we observe several treatment effects which lie in opposition to those in infection. Among these, PIM-1,2 and SL-1 appear to stimulate a mild depletion in PUFA DG, whereas H37Rv stimulates significant enrichment in this category. Similarly, the bulk of CL species are enriched during infection, but treatment with either PDIM or PIM-1,2 induces a depletion of CL. What do these orthogonal patterns suggest? Ongoing work seeks to address this question, among many sparked by these data.

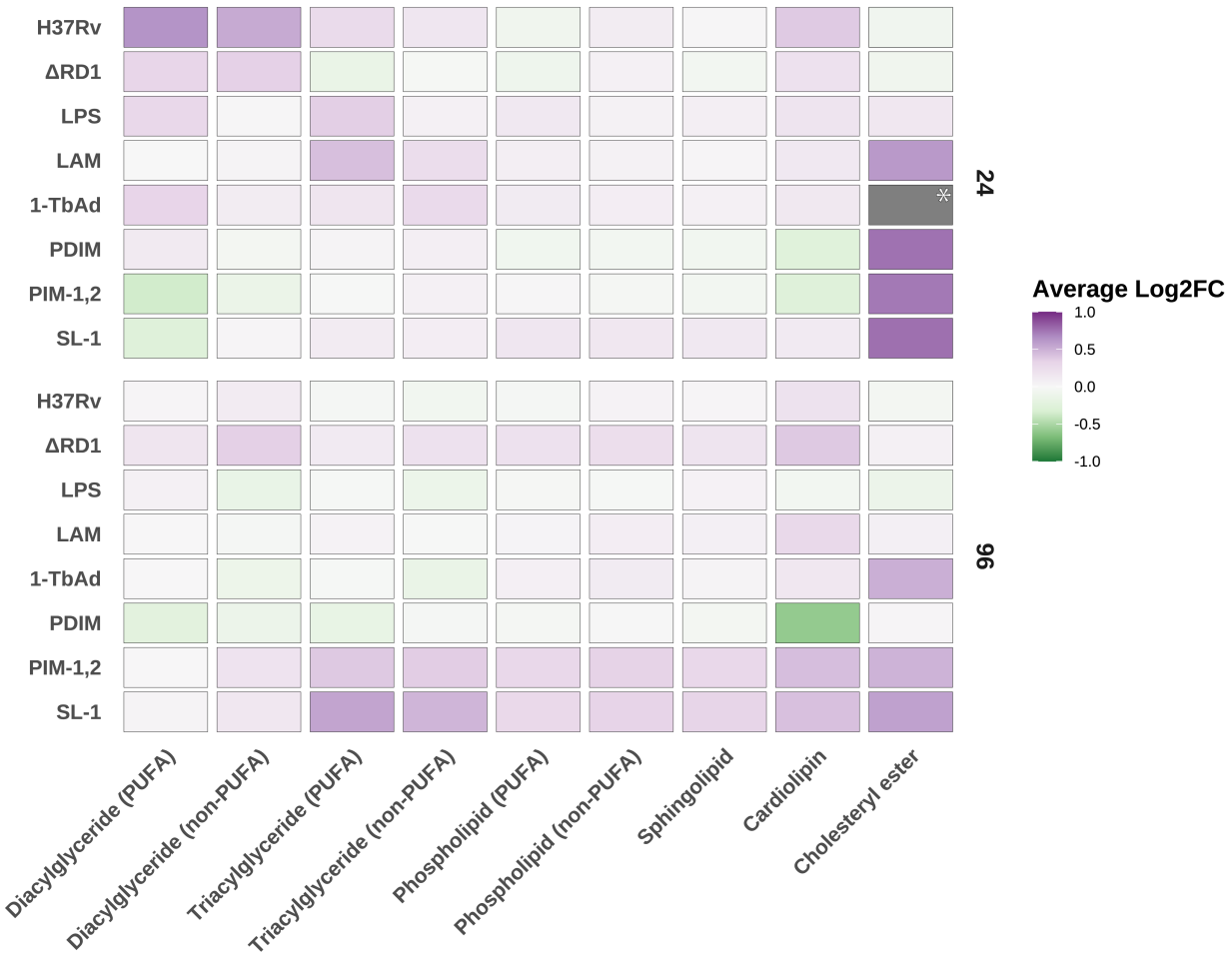


Figure 5.5. – **A map of lipidomic shifts resulting from *Mtb* infection and treatments** The average Log2 fold-change for each denoted lipid category and saturation state were calculated to depict the broad trends across these families resulting from infection and treatment. Those classes enriched relative to mock-infected or vehicle-treated cells are shaded in purple, while those classes relatively depleted during infection or treatment are shaded green (*1-TbAd induced up-regulation of CE to +1.66 LogFC at 24 hrs, well beyond the axis of the remainder of this map).

5.4. Discussion

In this study, we use untargeted lipidomics to investigate the effects that *Mtb* infection induces on the host lipidome. We are the first to use such a methodology to compare pathogenic and attenuated strains of *Mtb*, as we are the first to attempt to map these lipidomic changes to individual *Mtb* cell wall components. We identify several signatures of infection shared between pathogenic and attenuated infections and several signatures that may serve to distinguish these infections. Several such signatures may reveal concerted mycobacterial efforts to inhibit the host cell's antimicrobial activity and lysosomal function. We next showed that treatment with a cohort of compounds derived from the *Mtb* cell wall induces profound changes to the host lipidome, some of which align with broad trends during infection and some of which appear to oppose the effects of a live infection.

First, we identify a cohort of four phospholipids and cardiolipins that appear to be mycobacterial in origin. These include PE(16:0/19:0), PE(17:0/18:0), PI(16:0/19:0), and CL(68:2). Alongside these lipids are a large number of lipids for which the source organism is inconclusive. Cross-referencing with the MycoMass *Mtb* database is a somewhat crude method of partitioning the lipid composition of an infected cell. Though, the fact that we measure only four probable *Mtb* lipids with high confidence is unsurprising: the *Mtb* plasma membrane is a complex structure with a unique and complex lipid composition[165]. Many of the classic *Mtb* lipids require a specialized lipid extraction protocol to identify[361]. In this study, the bias towards host lipids in lipid extraction likely exacerbated the overarching disparity between the biomasses of the host and the infecting bacilli.

Despite the inconclusive organismal source of many identified lipids, we observe several signatures of infection with both pathogenic and attenuated strains of *Mtb*. We see a broad and significant enrichment of diacylglycerols at 24 hours of infection in both strains. We postulate that this increase is in part due to the activation of pathogen recognition receptors during infection, as the *Mtb* antigen lipoarabinomannan and the bacterial endotoxin lipopolysaccharide both induce a similar short-lived burst of DG production.

Intriguingly, we observe several signatures that distinguish pathogenic and attenuated *Mtb* infections. For example, the pathogenic strain H37Rv induces a significant and broad up-regulation in triacylglycerol production, whereas infection with the attenuated deletion strain H37Rv-ΔRD1 results in no concerted change to total TG content. This trend among TG between the strains may reflect the accumulation of lipid droplets. Costa et al. report this precise observation: they show that other attenuated strains, such as H37Ra and BCG, result in delayed expression of lipid droplet-associated genes[167]. Complementation of the RD1 locus confers the ability to induce lipid droplets to these attenuated strains[167].

Concurrent with this disparity in TG content, H37Rv induces a significant enrichment of acylcarnitine at 24 hours of infection – taken together, these results may suggest that the pathogenic strain is inducing an up-regulation in fatty acid and beta;-oxidation, utilizing TG as an energy source. Prior reports have described just such a mycobacterial program[170,171]. In this vein, Chandra et al. show that inhibiting fatty acid β-oxidation severely restricts the intracellular growth of *Mtb* and allows for enhanced clearance in mouse infection models[170]. Given these observations, we postulate that fatty acid β-oxidation inhibitors are prime candidates for future investigations.

Along with these differences, we also report that H37Rv infection induces a significant depletion of many lysophospholipids (e.g., PC(0:0/18:1) or PE(22:6/0)), ether-linked phospholipids (e.g., PI(O-16:0/20:4)), and plasmalogens (e.g., PE(P-14:0/20:4)). In contrast, the same cohorts of modified phospholipids are enriched in H37Rv-ΔRD1 infection, suggesting a concerted mycobacterial

pathogenicity program which limits the accumulation of these structures during infection. Gil-de-Gomez et al. show that the hydrolytic cleavage of an acyl chain from PE directly follows LPS stimulation, enabling enhanced eicosanoid production from arachidonic acid released from phospholipids and triacylglycerides by phospholipase A_2 cleavage[365]. Contrary to this report, however, we do not see enrichment of lyso-PE following treatment with LPS – though we do see numerous significant lyso-PI species upregulated following LPS stimulation. Our observation of plasmalogen depletion, however, aligns nicely with the findings of Jurkowitz et al., who show that a mycobacterial phospholipase A_2 enzyme named MtbYhhN degrades lysoplasmalogens. This enzyme protects mycobacteria from the toxic effects of these lipids[367]. Accordingly, these lipids may present another potential route of HDT.

In conclusion, this study identified several signatures unique to pathogenic *Mycobacterium tuberculosis* infection. We propose that these signatures underlie previously unrecognized avenues toward novel host-directed therapies. For a pathogen of such global significance, no stone may lie unturned.

5.5. Methods

5.5.1. Cell lines, *Mycobacterium tuberculosis* strains, and *Mycobacterium tuberculosis* cell wall components

THP-1 cells were sourced from American Type Culture Collection (ATCC TIB-202) and cultured in RPMI 1640 medium (Thermo Fischer Scientific #11875119) supplemented with 10 % FBS (Seradigm), 1x Gibco Penicillin-Streptomycin (Thermo Fischer Scientific #15-140-163), and 1x Gibco Non-Essential Amino Acids (Thermo Fischer Scientific #11140050). Before experimental use, THP-1 cells were activated for 48 hours via treatment with 50 nM phorbol 12-myristate 13-acetate (PMA; Sigma-Aldrich P8139-1MG). All cell counting was done using a hemocytometer with trypan blue (Gibco) counterstain. Biological replicates represent cells plated, infected, and collected on separate days.

All *Mycobacterium tuberculosis* culturing and infection were conducted in a biosafety level 3 facility following general safety guidelines. Historical *Mtb* strain H37Rv and the attenuated RD1-deletion mutant strain H37Rv-ΔRD1 were gifts kindly given to us by Dr. David Lewinsohn at the Oregon Health & Science University and Portland Veterans Affairs Medical Center; H37Rv-ΔRD was first produced by the lab of Dr. Sherman[340]. All *Mtb* strains were cultured at 37 °C in Difco™ Middlebrook 7H9 (Becton Dickinson #271310) broth medium supplemented with 10% Difco™ Middlebrook oleic acid-albumin-dextrose-catalase enrichment (OADC; Beckton Dickinson #L12240), and 0.1 % Tween-80 (Thermo Fisher Scientific #BP337-500), and carefully maintained between 600nm optical density (OD_{600}) of 0.1 and 1.5 to sustain expression of pathogenicity factors.

Mycobacterium tuberculosis cell wall components were acquired as described below.

5.5.2. *Mycobacterium tuberculosis* infection

THP-1 cells were plated and activated in quintuplicate as above on 6cm tissue culture dishes at a density of $1.6x10^6$ cells per dish and left to activate for 48 hours. On the day of infection, cultures of both H37Rv and H37Rv-ΔRD1 were pelleted and washed 1x with PBS at 2000 xg. Bacterial pellets were resuspended via repeated passage through an 18-gauge blunt-tipped needle and filtered through a 5 μm filter to prepare a single-cell suspension of bacteria in RPMI 1640. Bacterial concentration was estimated by taking an OD_{600}. Infectious solutions were prepared at a multiplicity of infection (MOI) of 3:1 (bacteria:cells) for the 24-hour samples and an MOI of 1:1 for the 96-hour samples; these MOIs were selected in optimization to guarantee a rate of infection >70% while minimizing host cell death at 96 hours (Figure S5.1). Cells were incubated at 37°C with 5% CO2 for 24 hours. At 24 hours post-infection, all host cell plates were washed 2x with PBS to remove non-internalized bacteria. At this point, 24-hour plates were collected as described below, while fresh media was added to 96-hour samples, and plates were left to incubate at 37 °C and 5 % CO_2. Lipid extracts were performed as described below.

5.5.3. *Mycobacterium tuberculosis* cell wall treatments

THP-1 cells were plated and activated in quintuplicate on 6cm tissue culture dishes at a density of 1.6×10^6 cells per dish. After 48 hours of activation, cell media was replaced with media containing

bacterial components at the below concentrations for either 24 or 96 hours until lipid extractions were performed as described below in Methods Section 5.5.5. The Chloroform:Methanol solvent solution was selected as the vehicle control because it had the highest relative cytotoxicity of the solvent solutions tested (Figure S5.4A). Treatment concentrations were selected based on the results of the resazurin viability assay described below in Methods Section 5.5.4 (Figure S5.4B).

The vehicle control (Veh) consisted of chloroform:methanol (2:1 vol:vol) at a final concentration of 0.1% of cell media. Lipopolysaccharide (LPS) was added to cells at a final concentration of 0.5 μg/mL in PBS. 1-tuberculosinyladenosine (1-TbAd) was added to cells at a final concentration of 1 μg/mL in methanol; this compound was kindly provided to us by Dr. Branch Moody of the Department of Immunology at Harvard, Cambridge, MA. Lipoarabinomannan (LAM) was added at a final concentration of 1 μg/mL in methanol:H_2O (2:1) (BEI Resources # NR-14848). Phthiocerol dimycocerosate (PDIM) was added at a final concentration of 1 μg/mL in chloroform:methanol (2:1) (BEI Resources # NR-20328). phosphatidyl-*myo*-inositol dimannoside (PIM-1,2) was added at 1 μg/mL in methanol (BEI resources # NR-14846). Sulfolipid-1 was added at a final concentration of 1 μg/mL in methanol (BEI Resources # NR-14845). These concentrations were selected for their limited cytopathic effect, assayed in Figure S5.4A & B.

5.5.4. Resazurin Viability Assay

THP-1 cells were plated and activated in clear-bottom 96-well plates at a density of 2 x 10^4 cells per well. After 48 hours of activation, cell media was replaced with media containing dilutions of each compound or solvent denoted in Methods Section 5.5.3 A and B at the denoted concentrations. Cells were then incubated at 37 °C for 96 hours in the presence of compounds and solvents. At the end of the 96-hour treatment, 10 μL of a 0.5 mg/mL stock solution of resazurin reagent in DMSO was added to each well and mixed thoroughly. Cells were incubated with resazurin for 3.5 hours at 37 °C before being read on a ClarioStar Plus fluorescence plate reader (BMG Laboratories). Cell viability was calculated from the ratio of OD_{570}:OD_{600}; the dynamic range was established using untreated control wells (defined as 100 % viability) and wells treated with 5 % DMSO (0.15 mg/mL; defined as 100 % lethal). We report viability as a percentage using the formula below:

$$PercentViability = \frac{(OD_{treatment} - OD_{DMSO})}{OD_{untreated} - OD_{DMSO}} * 100 \tag{5.1}$$

5.5.5. Lipid extraction & sample preparation

At the designated time point of infection or treatment, lipids were extracted through a modified Bligh-Dyer protocol[303]. Culture media was aspirated and cells were washed 2x with ice-cold PBS before being scraped into a 2:1 solution of ice-cold methanol:water and transferred to a glass vial containing ice-cold chloroform. Plates were scraped a second time with methanol:water, and cells were again transferred to chloroform to produce a final solution of 2:1:2 methanol:water:chloroform. Samples were vortexed for 30 seconds and left to separate into a biphasic solution for 1 hour at -20 °C. The lower phase of chloroform was carefully transferred to a new glass vial using a glass pipette. An equal volume of isotopic internal standards (Avanti Polar Lipids, EquiSplash™) was added to each sample and thoroughly mixed. Finally, samples were dried under the flow of N2 gas and stored at -80 °C.

5.5.6. Mass spectrometric analysis

Mass spectrometry analysis was performed as previously described[356,357,375,376]. LC-MS/MS instrumentation consisted of a Waters Acuity UPLC H class system interfaced with a Velos-ETD Orbitrap mass spectrometer. Samples were again dried in vacuo and resuspended in a 1:54 solution of chloroform:methanol (v:v) and injected onto a reverse-phase Waters CSH column and separated over a 34 min gradient (mobile phase A: acetonitrile/H2O (40:60, v:v); mobile phase B: acetonitrile/isopropanol (10:90, v:v) containing 10mM ammonium acetate) at a flow rate of 250 µL/min. Both positive- and negative-mode analyses were employed, using higher-energy collision dissociation and collision-induced dissociation to maximize lipidome coverage. The fragment ions used for lipid identifications were used as previously described[375]; in summary, these LC-MS/MS raw data files were analyzed using the LIQUID software[244] and all subsequent identifications were manually validated by examining the fragmentation spectra for diagnostic and fragment ions corresponding to the parent acyl chains. For quantification, a reference database was created using LIQUID[244] and then aligned to a reference database based on their identification, m/z, and retention times using MZmine 2[377]. Aligned features were then manually verified, and peak apex intensity values were exported for statistical analysis.

5.5.7. Data analysis and presentation

For *Mtb*-infected samples, 30 and 29 LC-MS runs were completed in negative and positive ionization mode, respectively. One 24-hour Mock sample was lost in preparation for positive ionization mode. Negative and positive ionization mode data had 179 and 240 unique lipids identified in at least one sample, respectively. There were two missing observations in the negative and none in the positive ionization data. Missing observations were coded as NA values. All abundances were log2 transformed.

For samples treated with *Mtb*-derived components, 70 and 70 LC-MS runs were completed in negative and positive ionization mode, respectively. Negative and positive ionization mode data had 184 and 210 unique lipids identified in at least one sample, respectively. There were nine missing observations in the negative and none in the positive ionization data. Missing observations were coded as NA values. All abundances were log2 transformed.

A robust Mahalanobis distance based on lipid abundance vectors (rMd-PAV) was calculated to identify potential sample outliers in the data[378]. This distance is calculated based on four metrics: average correlation with samples in the same condition, skewness of lipid abundance distribution, kurtosis of lipid abundance distribution, and median absolute deviation (MAD). A p-value corresponding to a test, where the null hypothesis is that the sample is not an outlier, can then be calculated based on the observed distance measure. No samples were identified as outliers in either ionization mode.

A total of 7 and 10 internal standards (ISs) were run in negative and positive ionization mode, respectively. Figure S5.2A & D show the log2 abundance values for each IS over all samples for the negative mode data and Figure S5.2B & E show the log2 abundance values for each IS over all samples for the positive mode data.

The coefficient of variation (CV) was calculated for each IS. For each sample, data was normalized by the median IS value of ISs, which were observed in every sample and had a CV of no more than 35 %. For the infection samples, of the 8 and 10 ISs, 6 and 6 were used in calculating normalization

factors for the negative and positive mode data, respectively. For the treatment samples, three (of seven) internal standards were used in calculating normalization factors for the negative mode data, and four (of ten) ISs were used for the positive mode data.

Figure S5.2C & F show the normalized log2 abundance profiles for each sample ordered and colored by time point and infection or treatment combination, respectively.

Sequential projection pursuit principal component analysis (PCA)[379] (Webb-Robertson et al. 2013), which does not require imputation of missing values, was run on the combined normalized ionization datasets. Figure 5.1B and Figure 5.4B show the first two component scores for sample colored by time point and condition, for infection and treatment samples, respectively. Timepoint is associated with the largest sources of variability in the data.

All data visualizations were completed using R.

5.6. Acknowledgements, & Contributions

5.6.1. Acknowledgements

We are grateful to Dr. David Lewinsohn at the Oregon Health & Science University and the United States Veterans Association in Portland, OR, for providing the Mtb strains H37Rv and H37Rv-ΔRD1. We also thank Dr. Branch Moody at the Harvard Department of Immunology in Cambridge, MA, for providing us with the 1-tuberculosinyladenosine used in this study.

5.6.2. Contributions

GG designed the study, performed *Mtb* infections and sample preparations of infection lipidomics samples for mass spectrometry analysis, prepared the data visualization and interpretation, and wrote the manuscript. SF optimized *Mtb* treatment concentrations, prepared treatment samples for mass spectrometry analysis, assisted in data interpretation, and edited the manuscript. MG assisted in optimizing *Mtb* treatment concentrations. JK & LB operated the mass spectrometer to collect the data, prepared the analysis pipeline, performed the statistical analysis, assisted in data interpretation, and edited the manuscript. FT designed and directed the study.

5.7. Supplementary figures

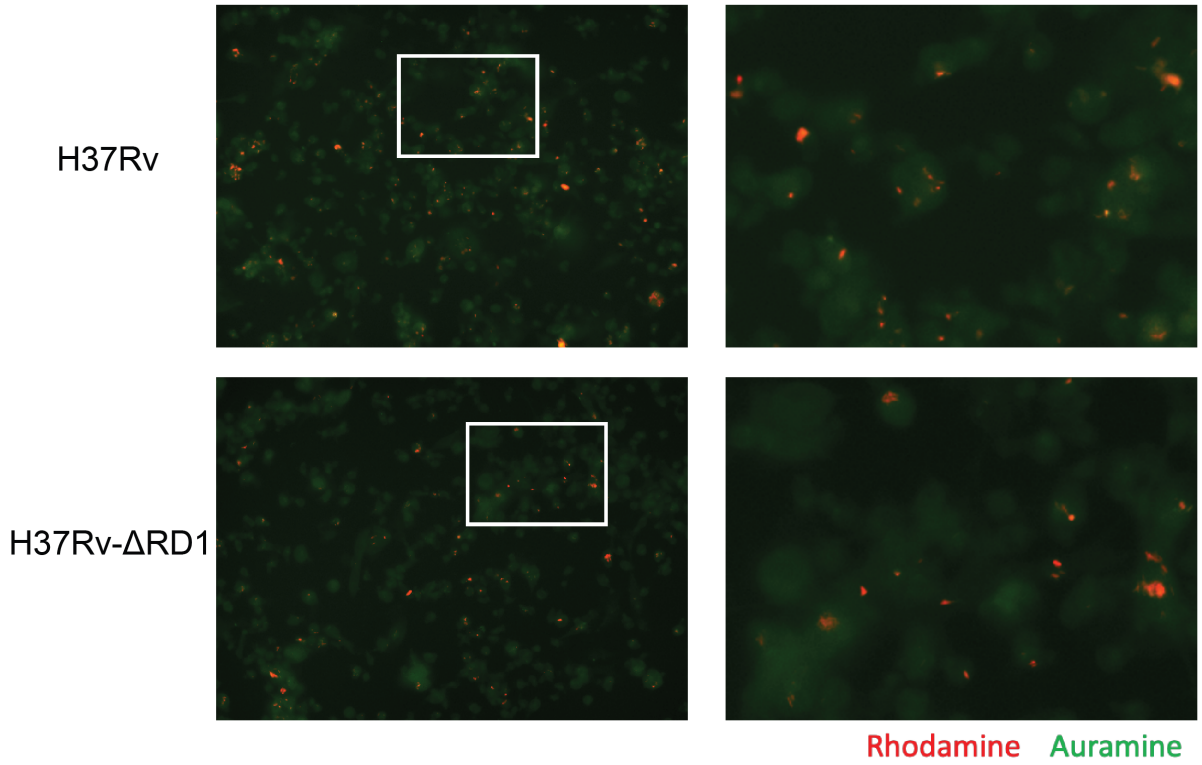


Figure S5.1 – **Biological sample quality control: MOI validation** THP-1 cells were activated for 48 hours in 10 cm dishes and then infected as described above in Methods Section 5.5.2 at an MOI of 1. Infection proceeded for 24 hours before plates were washed twice with PBS and media was refreshed. Plates were incubated at 37 °C for an additional 72 hours. At 96 hours post-infection, plates were washed twice with PBS and fixed for 1 hour in 4 % formaldehyde. Bacteria were stained using an Auramine and Rhodamine staining kit, destained in an acid alcohol solution, and imaged using a table-top Keyence BZ-X100 and a 20x air objective. Right images are zoomed insets of white boxes.

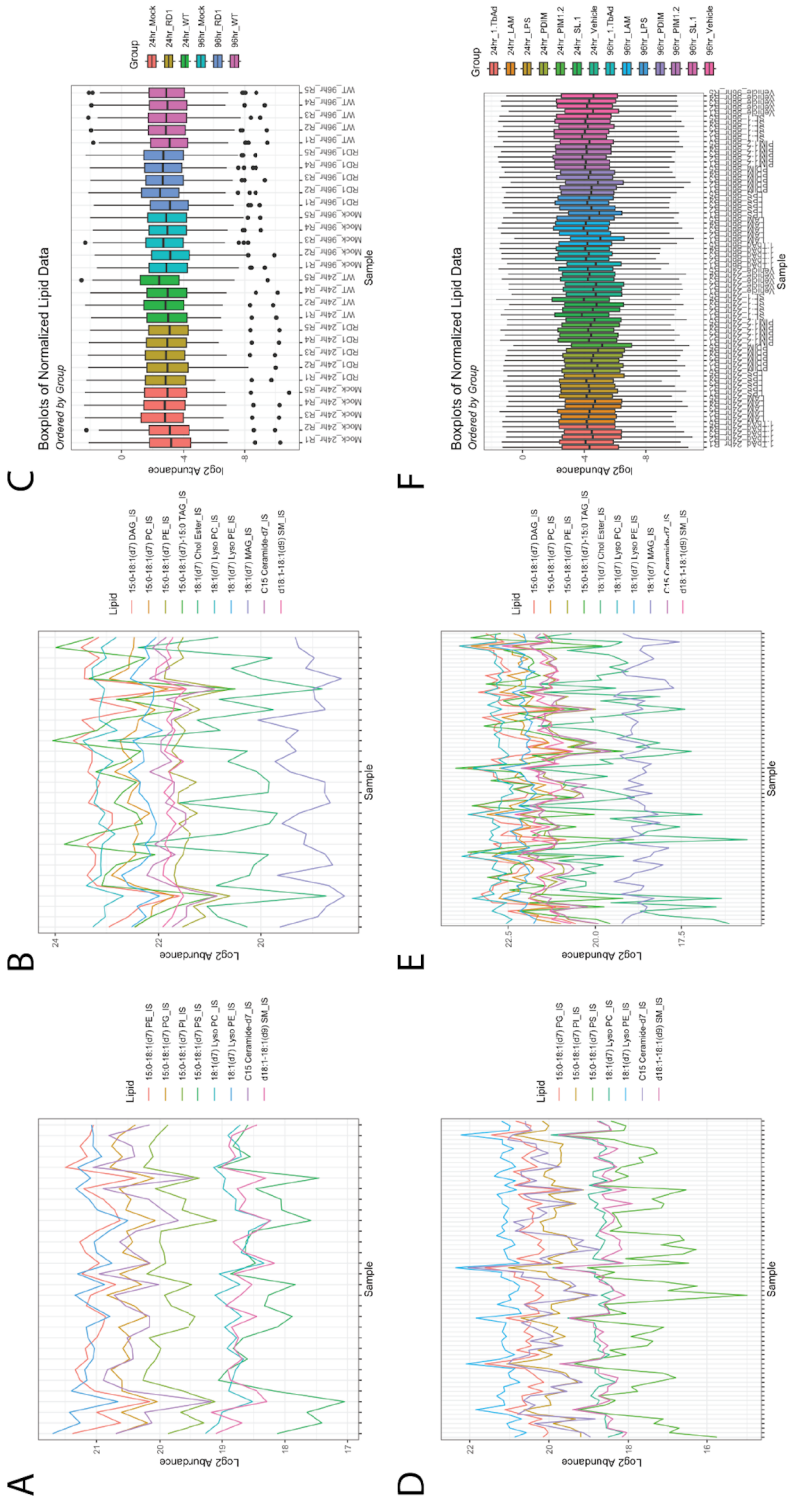


Figure S5.2 – Global lipidomics sample quality control and normalization (A & B) Internal standard intensities (Log2 transformed abundances) for the *Mtb*-infected samples in negative and positive ion modes, respectively. (C) Box plots depict the distribution of lipid intensities for all infected samples after normalization. Samples are ordered by group, as denoted by color. (D & E) Internal standard intensities (Log2 transformed abundances) for the *Mtb* component-treated samples in negative and positive ion modes, respectively. (F) Box plots depict the distribution of lipid intensities for all treated samples after normalization.

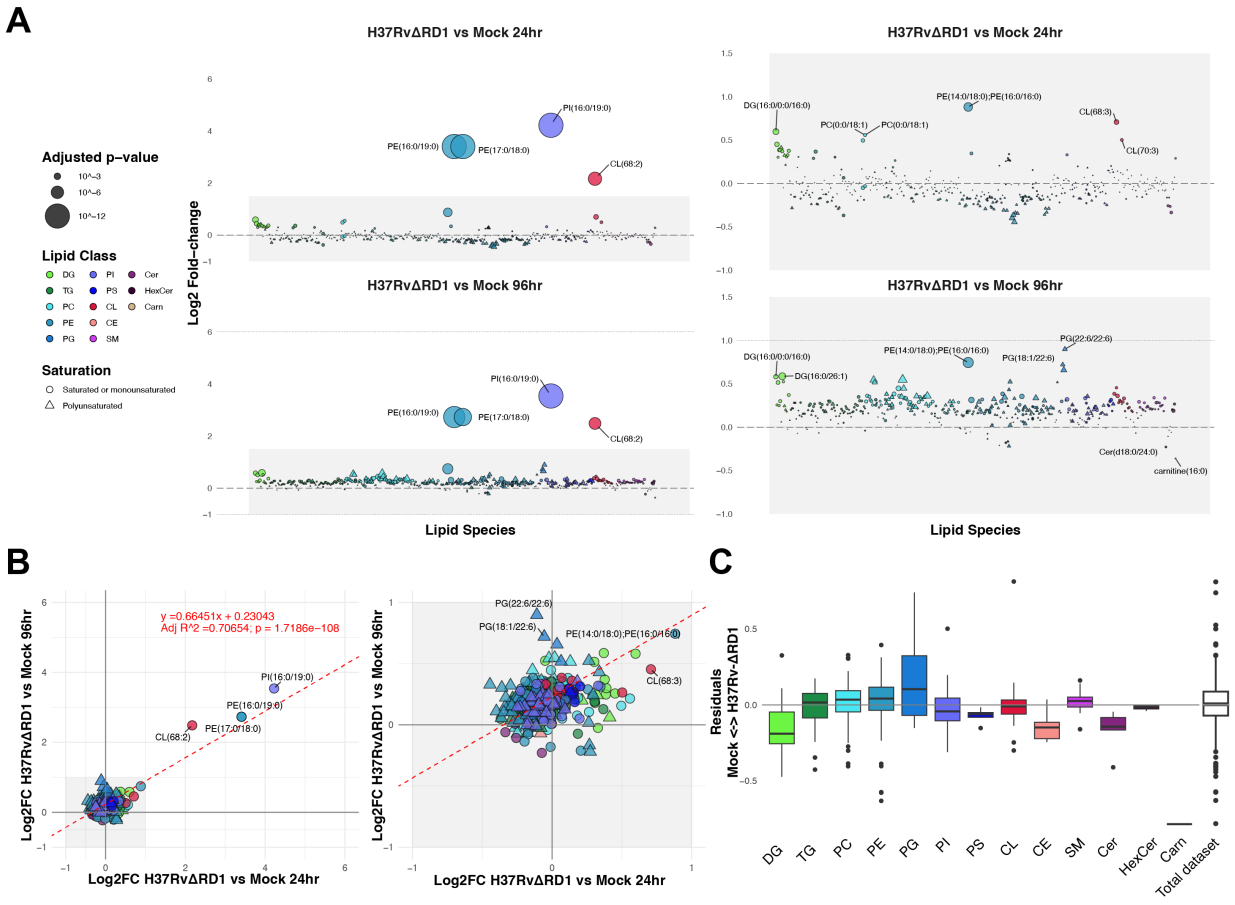


Figure S5.3 – Attenuated *Mtb* strain H37Rv-ΔRD1 induces broad lipidomic changes in host cells (A) Bubbleplots show the relative enrichment (Log2FC = Log2 fold-change) of each identified lipid species versus uninfected control. Point size denotes the adjusted p-value resulting from a one-way ANOVA and multiple hypothesis correction; point color denotes the class of each lipid; point shape denotes whether each lipid is polyunsaturated (PUFA) or either monounsaturated or fully saturated. The gray box denotes the inset region for the right panels. (B) Scatterplots show the relationship between each lipid's enrichment at 24 hours and 96 hours post H37Rv infection. The red dashed line shows the results of a linear regression analysis between the time points; the red text denotes the formula, adjusted R^2, and p-value associated with the linear regression analysis. The gray box denotes the inset region for the right panel. (C) A box and whisker plot shows the distribution of linear regression residuals within each lipid class. The white box-and-whisker to the right denotes the distribution of residuals of the entire dataset.

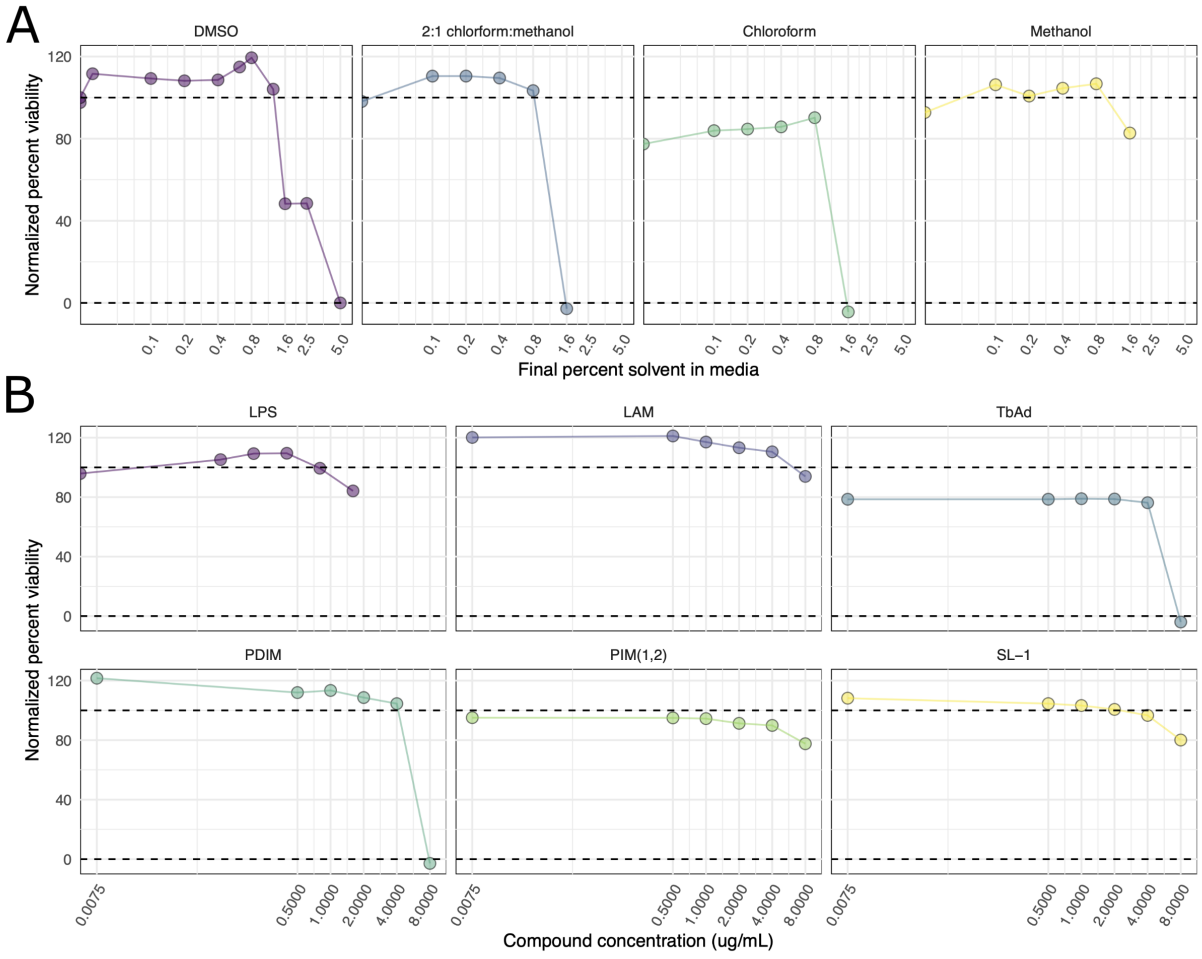


Figure S5.4 – Biological sample quality control: Cytotoxicity screening of *Mtb* compound treatments (A & B) THP-1 cells were activated for 48 hours and then treated for 96 hours with the denoted concentrations of solvent (A) or bacterial compounds (B). Viability is normalized according to the formula in Equation 5.1 and reported as a percentage of untreated cell viability. Points in B are arranged in increasing percent total solvent content. Each point represents the a single biological replicate.

Chapter 6.

An Affinity for Sphingolipids

Trifunctional lipid probes reveal protein-sphingolipid interactions during *Mycobacterium tuberculosis* infection

Authors Gaelen Guzman[1], Scotland E. Farley[1], Frank Stein[2], Per Haberkant[2], Carsten Schultz[3], Fikadu G. Tafesse[2,*]

[1] = Department of Molecular Microbiology and Immunology, Oregon Health & Science University, Portland, Oregon, USA. [2] = Proteomics Core, European Molecular Biology Laboratory, Heidelberg, Germany. [3] = Department of Biochemistry and Physiology, Oregon Health & Science University, Portland, OR, USA. [*] = corresponding author: tafesse@ohsu.edu.

6.1. Abstract

Understanding the molecular interactions underlying *Mtb*'s capacity for immune subversion and hijacking of the host cell can provide a unique insight into potential new routes of antitubercular therapy. Because *Mtb* is a pathogen with a unique sensitivity to the host lipid compartment, and because sphingolipids are a lipid family with emerging roles in regulating antimicrobial functions in macrophages, we sought to characterize the sphingolipid interactome of an *Mtb*-infected cell. To this end, we utilized trifunctionalized lipid analogs as affinity handles for enrichment proteomics. We found that *Mtb* infection induces a significant reprogramming of proteins that interact with sphingosine. These changes included a downregulation of interactions among proteins involved in secretory trafficking and lysosomal maturation and an upregulation of interactions with cytoskeletal proteins. We further identify a candidate *Mtb* protein that selectively interacts with trifunctional sphingosine. This analysis is the first of its kind and represents a crucial step in characterizing how sphingolipids mediate the cellular response to intracellular infection.

To accompany the main body of this report, we present an interactive format to explore the results of this study at the following: Trifunctional Proteomics Shiny App.

6.2. Introduction

As discussed in Chapter 2, *Mycobacterium tuberculosis* (*Mtb*) is a globally significant human pathogen. In the face of spreading antibiotic-resistant strains of *Mtb*, there is a growing need for novel host-directed therapy (HDT). Given their extensive roles in regulating mammalian cell survival and apoptosis, we and others have proposed sphingolipids as a strong candidate for anti-tubercular HDT (Chapter 3 and Chapter 4)[220,348]. Following this line of study, we sought to address whether the interactions between sphingolipids and proteins in the host cell are potential intervention points in host-directed therapy.

Lipid dynamics are a significant determinant of *Mtb* biology, as discussed in Barisch and Soldati's 2017 review[68]. We and others have shown that host lipids, such as diacyl- and triacylglycerides, and lipid storage structures, such as lipid droplets, are substantially upregulated in response to *Mtb* infection (Chapter 5)[68]. Previous authors have postulated that the sphingolipid pathway contains numerous potential targets for anti-*Mtb* HDT[220,348,380]. However, there are significant open questions regarding whether the interactions between sphingolipids and proteins in the host cell are potential intervention points in host-directed therapy. We use a trifunctionalized sphingosine analog to explore the interactions between sphingolipids and proteins during *Mtb* infection. We expect that the *Mtb*-host interface will be highly dependent on protein-lipid interactions – but, historically, few tools have existed which allow for identifying the protein interactors of a given lipid species.

The advent of trifunctionalized lipids has circumvented many of the long-standing challenges of lipid studies. These challenges have been discussed at length elsewhere[253]. However, they include 1. the small size and potent hydrophobicity of lipids, which preclude many chemical modifications and exogenous supplementation or add-back; 2. the rapid interconversion of lipid species along complex and convoluted metabolic pathways; and 3. the transience of interactions between lipids and proteins[250,253,255]. In particular, trifunctional sphingosine (tf-Sph) has enabled significant breakthroughs in studying the roles of bioactive sphingolipids in the cell. The native form of sphingosine is a transient and potent signaling lipid known to induce profound effects in the cell[[73];]. In 2015 and 2017, Höglinger showed that trifunctional sphingosine induces rapid calcium release from the lysosome and eventual lysophagy (targeted autophagy of the lysosome)[198,250]. Our recent report described a novel sphingolipid probe's synthesis and biological behavior: trifunctional sphinganine (tf-Spa)[255]. Tf-Spa Trifunctional lipids allow for nuanced investigation into the protein interaction partners of select sphingolipid species in various biological contexts.

In the present study, we utilize trifunctional sphingosine to explore selective interactions between proteins and sphingolipids in human THP-1 macrophages during infection with pathogenic and attenuated strains of *Mycobacterium tuberculosis*. To assess the specificity of identified interactions, we compare the interaction partners of tf-Sph with those of several other previously reported trifunctional probes. We find that, at baseline, sphingosine interacts with several lipid-modifying proteins such as phosphatidylinositol transfer protein beta (PITPNB) and lysosomal proteins such as Cathepsin D (CTSD) and lysosomal Pro-X carboxypeptidase (PRCP), among others. When applied to the *Mtb*-infected cell, we find that tf-Sph experiences a dramatically altered interactome – the many up- and down-regulated interactions reflect altered lysosomal activity, protein synthesis, and histone modifications, among others. We additionally identify modest enrichment of a single *Mtb* protein to tf-Sph, the uncharacterized Rv3466. We hope that revealing these alterations to the sphingosine-protein interactome will reveal novel avenues for manipulating the host-pathogen interface during *Mtb* infection.

6.3. Results

6.3.1. Trifunctional lipid probes offer unique utility in assessing functions, localization, and interaction partners of a given lipid species

The lipid biologist's toolbox was recently greatly expanded by adding trifunctional lipid analogs (trifunctional probes). These synthetic molecules maintain high structural similarities to their natural counterparts but have been modified with three chemical domains that allow for nuanced and tightly controlled dissection of a given lipid's cellular trafficking, metabolism, and interactions (Figure 6.1). We and others have previously reported on their synthesis and utility, including Farley et al.[255], Haberkant et al.[251,252,381], and Höglinger et al.[198,250]. While many such trifunctional probes are now available, we consigned our focus to four probes in this study: trifunctional-Sphingosine (tf-Sph), tf-Sphinganine (tf-Spa), trifunctional-8:3-Fatty acid (tf-8:3-FA), and trifunctional-1:10-Fatty acid (tf-1:10-FA), as previously described by Farley et al. in 2023[255].

Each of these probes is expected to elicit a distinct cellular response, traffic to a distinct cellular compartment, and interact with a distinct cohort of proteins. For example, the two fatty acid probes differ only in the position of the diazirine ring: tf-8:3-FA is expected to preferentially bind to proteins that penetrate deep into the membrane, such as transmembrane domain-containing proteins. In contrast, the tf-1:10-FA probe would be expected to enrich more transiently membrane-associated proteins because the diazirine crosslinking motif is nearer to the hydrophilic headgroup. We expect these fatty acid probes to be incorporated into a wide array of lipids, including phospholipids, glycerolipids, and sphingolipids via transacylation.

In contrast, the trifunctionalized sphingolipid probes are expected to be incorporated into the sphingolipid metabolic pathway primarily. These probes differ only in a single double carbon bond at the C4-C5 position: sphinganine (or dihydrosphingosine) is produced early in the sphingolipid synthesis pathway and is incorporated into dihydroceramide by the ceramide synthases before being desaturated by dihydroceramide Δ4-desaturase[182] and rarely accumulates in a typical cell. In contrast, sphingosine is a well-characterized signaling lipid produced primarily via the degradation of ceramide in response to signaling stimuli[182]. The production of sphingosine stimulates profound immediate effects in the cell[198] and can also be used in ceramide synthesis as a part of the sphingolipid salvage pathway[182]. We previously reported on the subcellular localization of both trifunctional sphinganine and sphingosine[255]. In this report, Farley found that both probes are trafficked through the endoplasmic reticulum and the Golgi, aligning with the well-described sphingolipid synthesis pathway[182,255]. In the same report, Farley et al. also showed that tf-Sph retains its biological fidelity: it induces lysosomal calcium release, as previously shown[198]. Notably, however, tf-Spa fails to induce calcium release. These results indicate that tf-Sph retains its activity as a signaling lipid, whereas tf-Spa is primarily a sphingolipid precursor. We thus expect that the products of tf-Spa metabolism will interact with many proteins and that tf-Sph will initially interact with proteins involved in lipid signaling before being trafficked to the ER[251,255].

To validate these trafficking patterns in THP-1 cells, we visualized the subcellular localization of tf-Spa in THP-1 cells at increasing times after photo-uncaging (Figure 6.2). We observe similar patterns in these cells as has been previously reported by Farley et al.: tf-Spa experiences a time-dependent enrichment to the Golgi apparatus. These images serve primarily as validation of the utility of trifunctional probes.

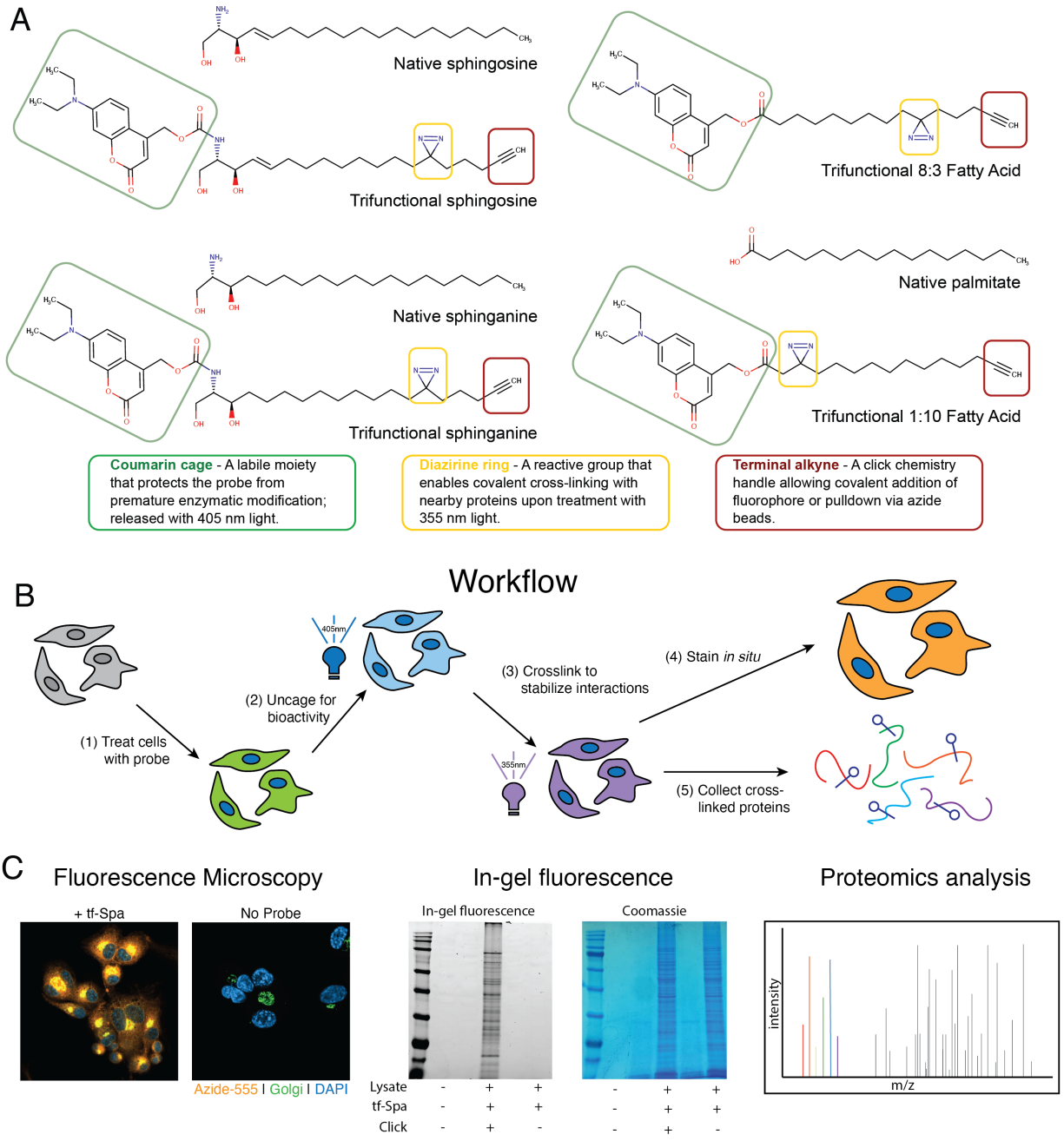


Figure 6.1. – **Lipid probe overview & workflows** (A) The chemical structure of native sphinganine, sphingosine, and free fatty acid, alongside their synthetic trifunctionalized analogs. The functional moieties are highlighted and described in the color-coordinated boxes. (B) A simplified overview of several trifunctional probe workflows. See Methods Section 6.7.3 for a detailed description of the workflow. Briefly, plated cells are treated with lipid probes for 30 minutes (1), uncaged via irradiation with blue-wavelength light (2), and then covalently crosslinked to nearby molecules via irradiation with UV-wavelength light (3). Next, the probe may be clicked to a fluorophore and stained with cellular markers for fluorescence microscopy (4) or lysed and protein collected for in-gel fluorescence or proteomics analysis (5). (C) Example uses of trifunctional probes: (left panel) fluorescence microscopy using tf-Spa; (middle panel) in-gel fluorescence using tf-Spa; (right panel) cartoon depiction of an MS2 scan of a peptide tagged with a tandem mass tag.

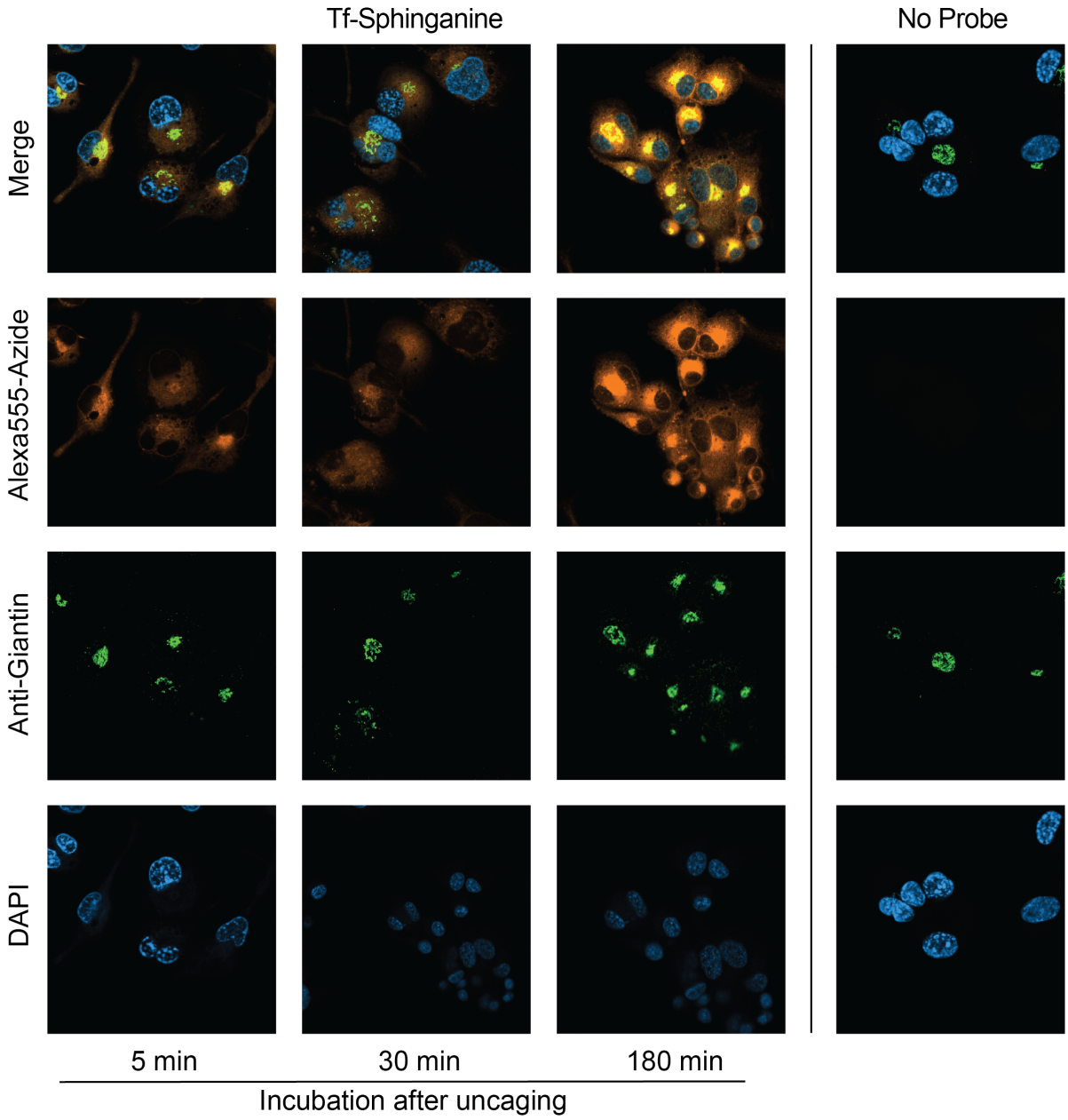


Figure 6.2. – **Fluorescence microscopy reveals intracellular trafficking of trifunctional sphinganine** THP-1 cells were treated with trifunctional sphinganine, uncaged via irradiation with blue light, and incubated for the denoted periods before UV-induced crosslinking and methanol fixation. Cells were stained with anti-Giantin antibody (to visualize the Golgi apparatus) and DAPI (to visualize the nucleus). Cells were imaged using a Zeiss LSM 900 confocal microscope using AiryScan super-resolution and a 63x oil-immersion objective. Prior to imaging, cells were stained with 1:500 mouse anti-Giantin primary antibody (abcam #ab37266) and 1:1000 goat anti-mouse Alexa488-conjugated secondary antibody (Invitrogen #A21042) (See Methods Section 4.5.5 for staining protocol).

6.3.2. Trifunctional probes reveal protein-lipid interactions of the THP-1 macrophage

To identify the proteins that selectively interact with sphingolipid precursors in activated THP-1 macrophages, we performed an initial proteomics analysis to determine the protein interaction partners of the four trifunctionalized lipid probes: tf-Sph, tf-Spa, tf-8:3-FA, and tf-1:10-FA. Previous studies have used these or similar probes in human cervical adenocarcinoma cells (HeLa) and human liver epithelial cells (Huh7)[198,250,255]. However, human monocyte-derived macrophages (THP-1) have not been subjected to such lipid interaction analysis. Given that macrophages have dramatically distinct roles from epithelial cells and adenocarcinoma cells, we expected to identify a unique cohort of lipid-interacting proteins in these cells – including, presumably, (immuno)proteasome subunits, lysosomal resident proteins, and proteins involved in free radical production. The probe treatment and affinity enrichment procedures are depicted in Figure 6.3A and described in detail in Methods Section 6.7.3. All treatment and sample preparation were performed as previously described[250,251,255]. As a negative control, we prepared samples treated with each probe and uncaged but not treated with UV (-UV) and thus lacked crosslinking-stabilized interactions during enrichment.

We performed quantitative proteomics analysis using the TMT-16 isotopic labeling platform and LC-MS/MS. PCA analysis showed a distinct separation between +UV and -UV samples for each probe (Figure S6.1 A). We used variance stabilization to normalize the raw signal intensity of each channel (Figure S6.1 B). We identified 869 unique proteins with at least two unique peptides in at least two replicates. To identify the fold-change in the enrichment of proteins via diazirine crosslinking, we took the +UV versus -UV ratio for each probe and log2 transformed (Log2 fold-change, Log2FC). These results are depicted in Figure 6.3B.

We applied Limma analysis[382] to attain statistical significance for each protein between the +UV and -UV conditions. We applied an arbitrary cutoff for significance: LogFC > 1 and p-value < 0.05. Using these significance thresholds, we found that UV-crosslinking induced the enrichment of six proteins to the tf-Sph probe, twenty proteins to the tf-Spa probe, eight proteins to the tf-8:3-FA probe, and six proteins to the tf-1:10-FA probe. The relative enrichment of each significant protein among each probe (+UV versus -UV) is depicted in Figure 6.4A. Some proteins, such as VDAC2 and PITPNB, are enriched to more than one probe; other proteins, such as ATP6V1A, are uniquely enriched to a single probe.

We manually clustered each of the 35 enriched proteins into the following groups: proteins containing transmembrane domains, proteins with reported membrane association, secreted proteins, and proteins localized to the mitochondria, nucleus, or ribosome. Many of these putative lipid-interacting proteins are transmembrane domain-containing or peripheral membrane proteins. Relatively few are cytosolic or secreted.

Our recent report investigated the sphingosine and sphinganine interacting proteins in Huh7 cells and characterized the similarities and differences between these two probes[255]. For both probes, we find significant overlap among significantly enriched hits. In the case of tf-Sphinganine, proteins such as NUC1 and NUCB2 (also named HEL-S-109), Cathepsin D (CTSD), ECH1, PITPNB, VDAC 1 and VDAC2 were enriched in both Huh7 and THP-1 cells. In contrast, we see several proteins that appear to be unique to THP-1 monocytes compared to previously reported interactors; these include Prosaposin (PSAP) and Neudesin (NENF).

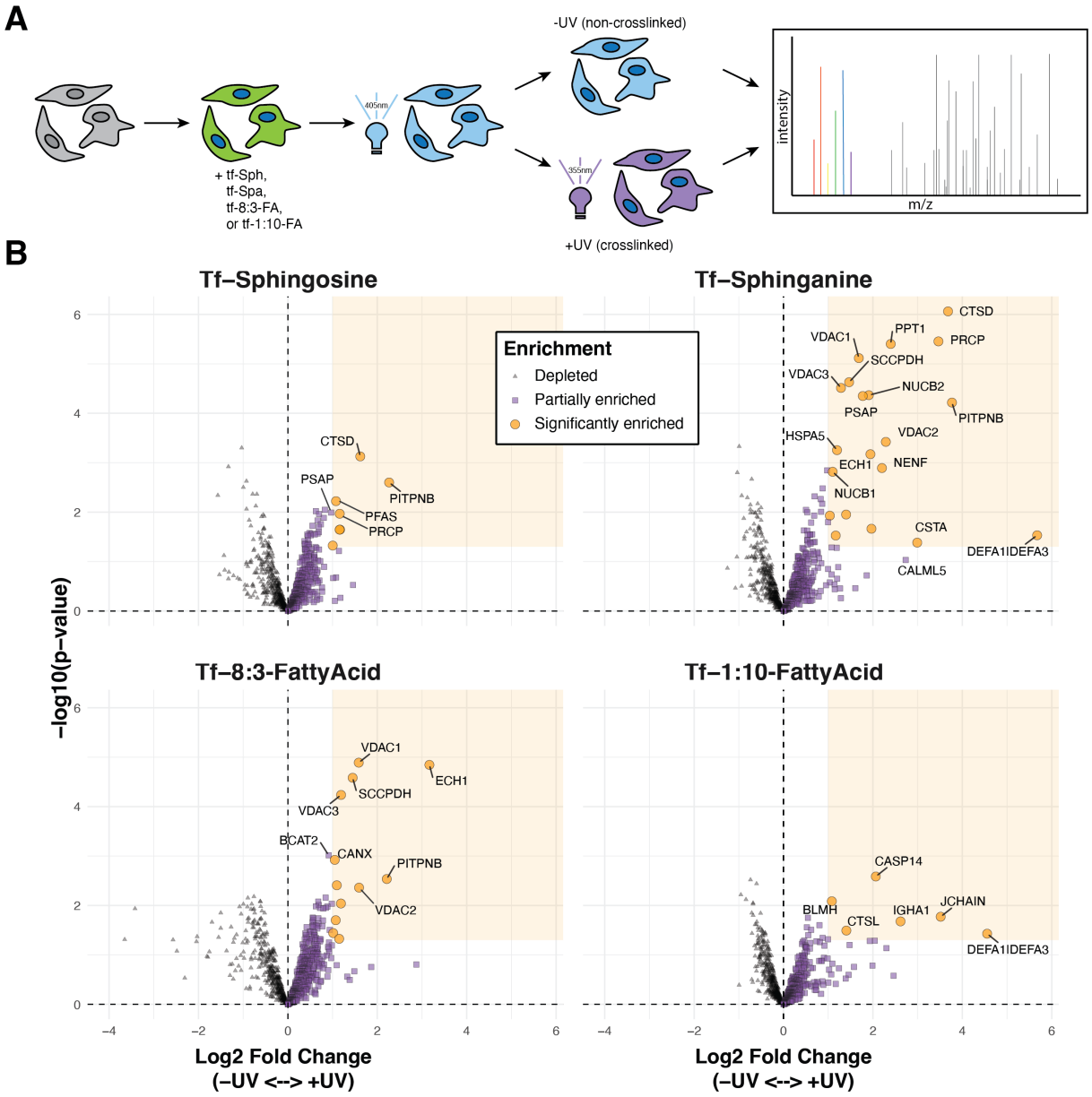


Figure 6.3. – **Affinity enrichment proteomics reveals the protein interactors of trifunctional lipid probes** (A) Schematic depiction of experimental design. Briefly, THP-1 cells were treated with the denoted probes described in Methods Section 6.7.3. Cells were lysed, and proteins were extracted; probe-protein conjugates were enriched using azide-coated beads and subjected to mass spectrometry analysis. (B) Volcano plots depict the relative enrichment of proteins to each probe compared to probe-matched no-crosslinking (-UV) control lysate. Enrichment is defined as follows: Depleted = Log2FC < 0, Partially enriched = Log2FC > 0 & p-value > 0.05, Significantly enriched = Log2FC > 1 & p-value < 0.05.

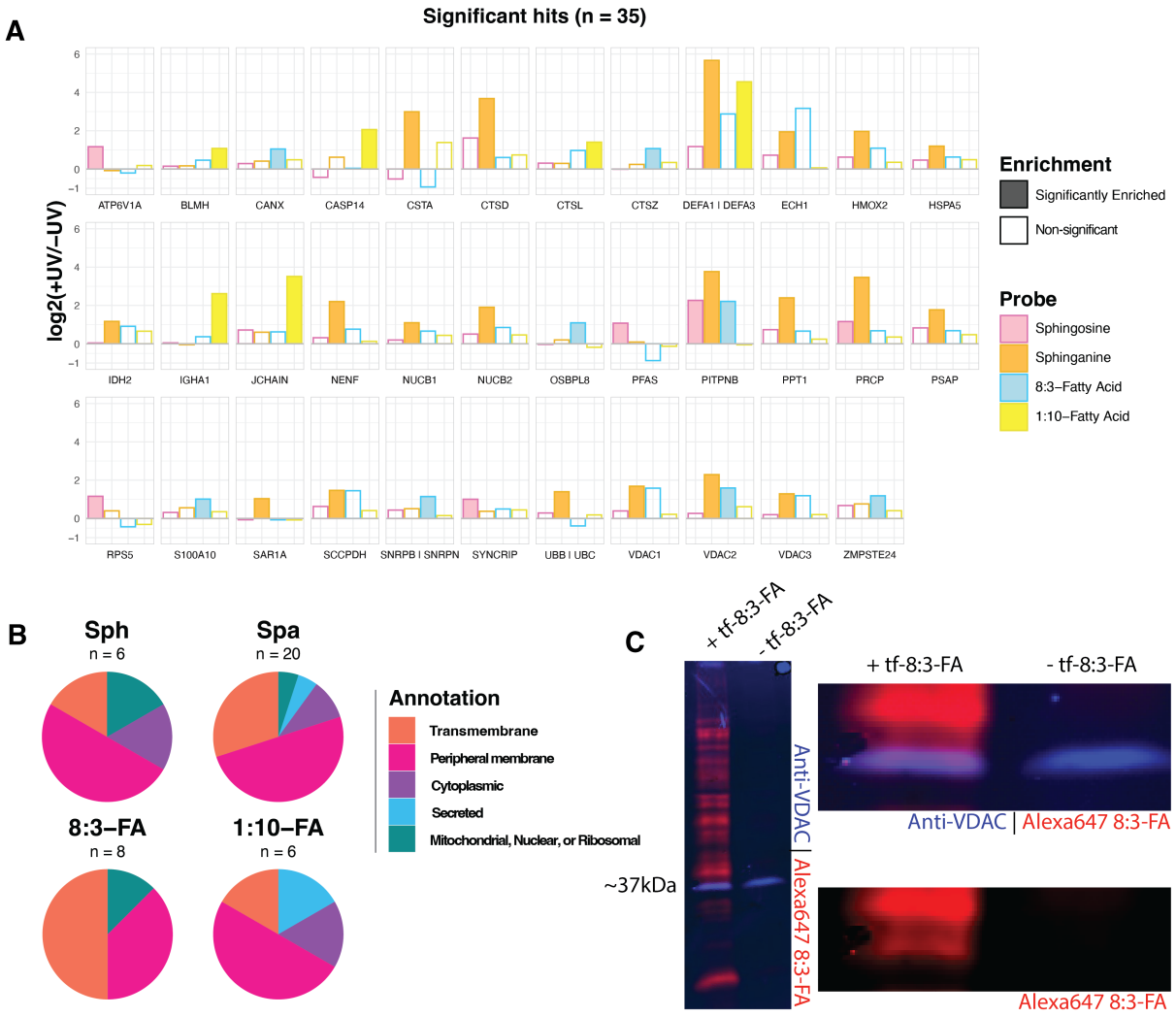


Figure 6.4. – **Proteins significantly enriched to lipid probes are known interactors of lipids** (A) Bar plots depict the Log2FC enrichment for each of the 26 significantly enriched proteins across all lipid probes (+UV versus -UV). Significance is denoted by fill coloring; probe is denoted by bar color. (B) Pie charts show the relative enrichment for transmembrane and membrane-associating proteins among the four lipid probes. (C) GO Term analysis of partially and significantly enriched proteins across each lipid probe. (D) Example on-blot fluorescence depicting simultaneous visualization of probe-crosslinked and antibody-stained VDAC proteins. (Red = Azide647-clicked probe; blue = anti-VDAC antibody).

Among these enriched hits are several interesting proteins with previously reported lipid interactions. Among these are the mitochondrial voltage-dependent anion channel isoforms VDAC1, VDAC2, and VDAC3. Previous studies have shown that VDAC2 contains a *bona fide* ceramide binding site and that interaction with ceramide is a potent trigger of apoptosis[319]. Further, Jahn et al. showed that VDAC1 and VDAC2 form a heterodimer which acts as a scramblase that transfers phospholipids synthesized in the ER into the inner mitochondrial membrane[383].

Notably, these enriched proteins include several Cathepsin aspartic peptidases. Cathepsins A and D are enriched to both tf-Sphingosine and tf-Sphinganine. Cathepsins L and Z are enriched to tf-8:3-FA and tf-1:10-FA, respectively. There are many reported interactions between Cathepsins and sphingolipids. For example, CTSB is activated by lysosomal ceramide generated via aSMase, a process involved in NK and T cell apoptosis[228]. Similarly, sphingolipids are known regulators of CTSD activity[226,227].

We also note the enrichment of Prosaposin to sphinganine and sphingosine. PSAP is a precursor polypeptide and is proteolytically cleaved into four small heat-stable glycoproteins: Saposins A, B, C, and D[384]. Each of these subunits is approximately 80 amino acids, with conserved glycosylation sites and identically placed cysteines[384,385]. Each Saposin appears to bind to a distinct cohort of higher sphingolipids. For example, Saposin A binds to glycosphingolipids, including glucocerebroside and galactocerebroside – and further, Saposin A stimulates acid β-glucosidase[384]. aSMase activity is regulated by the binding of Saposin[386]. Notably, Saposins have been shown to play critical roles in regulating lysosomal activity and immune function. Confusingly, there appears to be a cyclic regulation between Cathepsins and PSAP[387]. Cathepsins are the primary lysosomal peptidases responsible for cleaving PSAP into the mature Saposin subunits, and yet Saposins are widely reported for their capacity to stimulate CTSD activity[226,387]. What comes first? We find it intriguing that, in this proteomics analysis of the baseline interactions in THP-1 cells, we see "significant" enrichment of PSAP in sphinganine – however, PSAP was just below the Log2FC significance threshold.

These results reveal a diversity of lipid-interacting proteins in THP-1 monocyte-derived macrophages. Ongoing work seeks to validate and clarify these interactions' biological impacts within the cell. For the remainder of this study, we used these results to inform a subsequent proteomics analysis on THP-1 macrophages infected with pathogenic and attenuated strains of *Mycobacterium tuberculosis*.

6.3.3. Proteomics of trifunctional probes reveals protein-sphingolipid interactions during pathogenic *Mtb* infection

The main goal of this study was to analyze sphingosine interactions during *Mtb* infection. To achieve this, we infected cells with the pathogenic *Mtb* strain H37Rv for 24 and 96 hours, as depicted in Figure 6.5. Different multiplicities of infection were used for the two time points to maximize the infection rate at 24 hours and minimize cell cytotoxicity at 96 hoursFigure S6.3. At the desired time points, cells were treated with tf-Sphingosine as described in Section 6.7.3. We prepared a parallel experiment using the tf-8:3-Fatty acid probe as a control for non-specific lipid-binding proteins. After UV-induced crosslinking, cell lysates were collected, and a portion was used for in-gel fluorescence to validate sample quality (Figure S6.4 A). The remainder of each sample was clicked to azide-coated beads, and lipid-conjugated proteins were enriched. Samples were digested off the beads using trypsin and labeled with TMT-16 mass tags for LC-MS/MS proteomics analysis (one full TMT-16-plex for each probe). As above, data were normalized using variance stabilization

(Figure S6.4 C). PCA analysis shows a wide separation between infected and uninfected samples for both lipid probes (Figure S6.3 B).

In total, there were 1169 unique proteins identified in the tf-Sphingosine-treated samples and 1411 unique proteins identified in the tf-8:3-FA-treated samples. Of these, 1039 were identified in both experiments, and 502 were identified in only one. We calculated the log2 fold-change of each protein for each possible comparison within TMT-16-plexes(Figure S6.5). We again performed statistical testing using Limma analysis. However, for this experiment, we applied a more stringent threshold for significance: a log2 fold-change > 2, a false-discovery rate < 0.05, and a p-value < 0.01. The enrichment annotation of the baseline UV experiment was applied to the proteins identified in this infection experiment. As a notable exception, we included PSAP as a "Significant" protein in our UV annotation, as discussed below.

Table 6.1. – **Overview of statistically significant proteins** Hit = Log2FC > 1, p-value > 0.01, & FDR < 0.05.

Probe	Infection (versus mock)	Timepoint	# Hits enriched	# Hits depleted
tf-Sph	H37Rv	24 hrs	31	120
tf-Sph	H37Rv	96 hrs	35	109
tf-Sph	H37Rv-ΔRD1	24 hrs	19	78
tf-Sph	H37Rv-ΔRD1	96 hrs	35	101
tf-FA	H37Rv	24 hrs	30	140
tf-FA	H37Rv	96 hrs	23	86
tf-FA	H37Rv-ΔRD1	24 hrs	34	149
tf-FA	H37Rv-ΔRD1	96 hrs	25	118

In assessing these data, there are several initial observations to be made. First, we see many statistically "significant" differentially enriched proteins for infection versus mock comparisons (Table 6.1). There is a propensity for *decreased* interaction with trifunctional probes, as many more proteins are significantly depleted during infection.

We must emphasize that these results represent the relative abundance of each protein after affinity enrichment. While this measure is intended to reflect the rate of interaction between each protein and the trifunctional probe, it also encompasses changes in abundance that result from altered transcription, translation, trafficking, and degradation of each protein. To determine whether the transcriptional response to infection impacted these results, we cross-referenced our results with the 2023 findings of Jani et al., who investigated the transcriptomes of cells infected with H37Rv (Figure S6.6)[388]. Several proteins are concomitantly enriched between Jani et al.'s data and our own (e.g., the interferon-induced gene MX1). Notably, however, most significantly downregulated interactions among our findings were not significantly changed at the transcription level. Public data on the whole cell proteome of H37Rv infected cells are not publicly available, and we cannot comment on the overall protein abundance for our differentially enriched hits.

Focusing on 24-hour H37Rv infection, we observe several immunity-related genes among the protein interactions enriched during infection. These include MX1, IKBKB, and CTLA. We also observe several proteins related to motility and cytoskeletal trafficking, including Kinesin light chain 1 (KLC1), Tubulin, FLII, Microtubule-associated protein 4, Coronin-7, Myosin heavy chains 9 and 14 (MYH9 and MYH14), and Myosin light chain 12A (MYL12A). Intriguingly, we see a depletion of

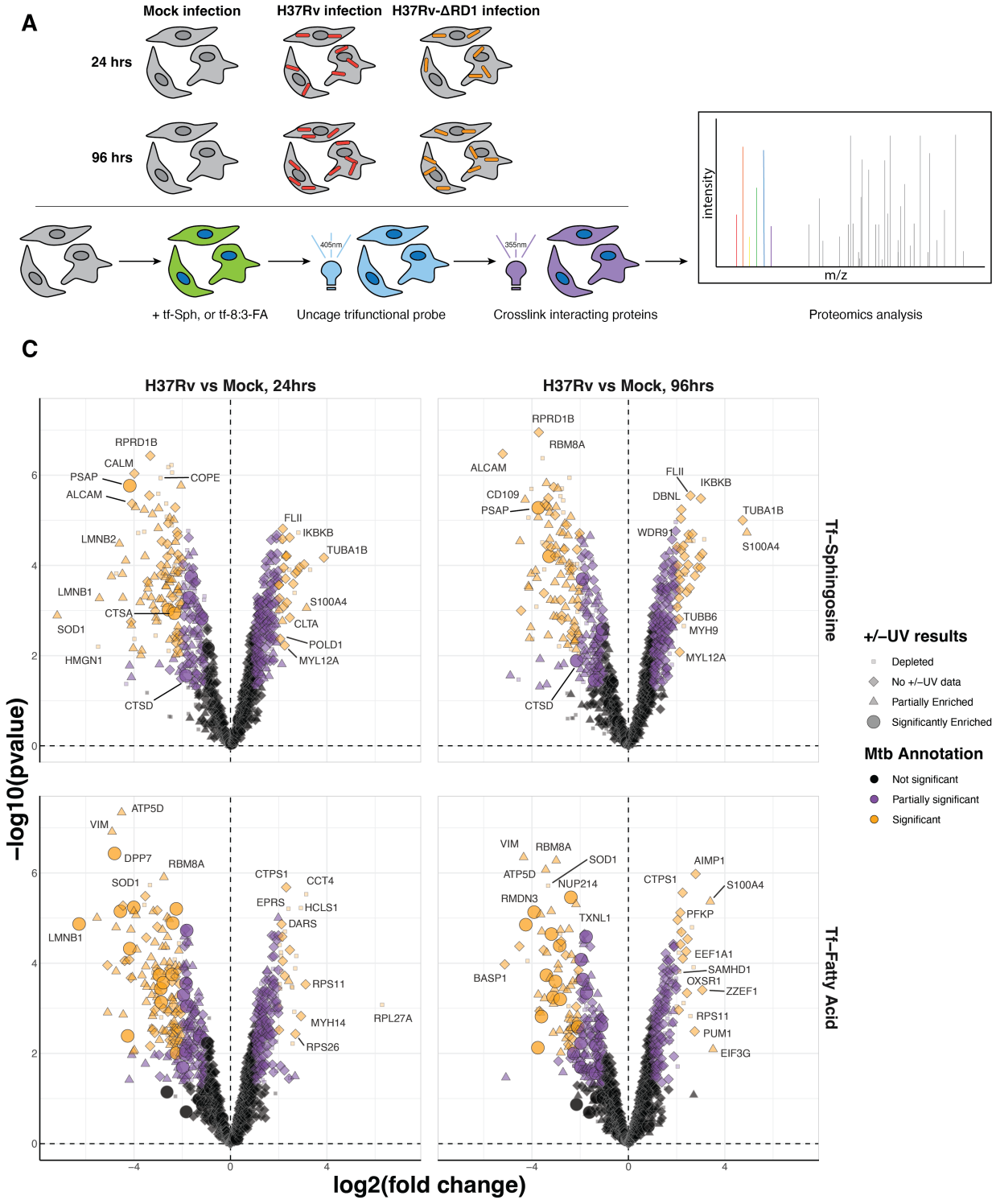


Figure 6.5. – ***Mtb* infection reprograms the sphingosine interactome** (A) A schematic overview of infection design and timeline. (B) Volcano plots depict the differential enrichment of proteins to the tf-Sphingosine and tf-8:3-Fatty Acid probes in H37Rv infection versus uninfected control. Statistical significance is as denoted (Partially significant, purple = Log2FC > 1 & p-value < 0.05; Significant, orange = Log2FC > 2, FDR < 0.05, & p-value < 0.01; No significance in black).

the activated leukocyte cell adhesion molecule (ALCAM), which is responsible for the extravasation of monocytes across the blood-brain barrier[389]. Some evidence suggests that BCG infection induces a transcriptional downregulation of ALCAM in PBMCs[390]. However, we do not observe this in our comparison to recent transcriptomics data reported by Jani et al.[388].

Among the downregulated interactions, we see a preponderance of proteins in the secretory/endosomal compartment. These include the Coatomer subunit epsilon (COPE), GOLGA2, Vescicle-associated membrane protein-associated protein A (VAPA), Rab11b, PSAP, Cathepsin A, Cathepsin B, and Cathepsin Z (and Cathepsin D, though it was only partially significant). We see many cytoskeletal proteins among the upregulated interactions, including Tubulin, FLII, Myosin-9 and Myosin-14, Microtubule-associated protein 4, and Coronin-7. We postulate that these results indicate dysregulation of endosomal trafficking.

At 24 hours post-infection, we observe differential enrichment of several proteins of high interest in the secretory/endosomal compartment. Among these are Cathepsins A, B, and Z (CTSA, CTSB, and CTSZ; and CTSD, though it was only partially significant), Prosaposin (PSAP), Coatomer subunit epsilon (COPE), Vescicle-associated membrane protein-associated protein A (VAPA), Rab11b. We also see several calcium-binding proteins among these downregulated interactions: Calumenin, Reticulocalbin-1, and Calmodulin-1 (CALM1).

As noted above, there are prior reports of Prosaposin being involved in *Mtb* restriction, including the 2020 report by Shepelkova that showed that Saposin D is essential in the restriction of *Mtb* growth[391]. An intriguing hit is PH4P, which is significantly depleted at 24 hours. There are many reported functions of the protein P4HB in the cell. Among these, it is a structural subunit of the microsomal triacylglycerol transfer protein (MTTP). MTTP complex loads triglycerides, cholesteryl esters, and phospholipids onto apolipoprotein B (apoB)[392]. This complex is essential for presenting lipid antigens to NK T cells via CD1d[393]. In 2014, De Libero and Mori discussed that lipid antigens are essential for the invariant Natural Killer T cell response during *Mtb* infection[394].

In comparing the enrichment of proteins to the tf-Sph and the tf-8:3-FA probe, we find a high degree of alignment among the co-identified protein at both time points (Figure S6.7). Linear regression analysis shows an adjusted R^2 value of 0.80 for the 24-hour comparisons versus mock infection, suggesting a robust correlation between the datasets. More analytical work will be needed to distinguish proteins that interact more robustly with tf-Sph than tf-8:3-FA.

6.4. Pathogenic versus attenuated *Mtb* infections induce highly similar changes to the tf-Sph interactome

A primary goal of this study was to compare the effect of pathogenic and attenuated *Mtb* infections on the sphingosine interactome. To this end, we prepared parallel samples of cells infected with the attenuated *Mtb* strain H37Rv-ΔRD1 (this strain was discussed extensively in Chapter 5). In comparing the protein interactors of tf-Sph and tf-8:3-FA in these ΔRD1-infected cells versus mock-infected cells, we see many of the same hits as were differentially enriched in the H37Rv versus mock comparison (Figure S6.8). This is particularly evident when the log2 fold-changes of H37Rv versus mock are plotted against those of H37Rv-ΔRD1 versus mock – linear regression shows that these datasets have an adjusted R^2 value of 0.87 (Figure S6.9 Upper panels).

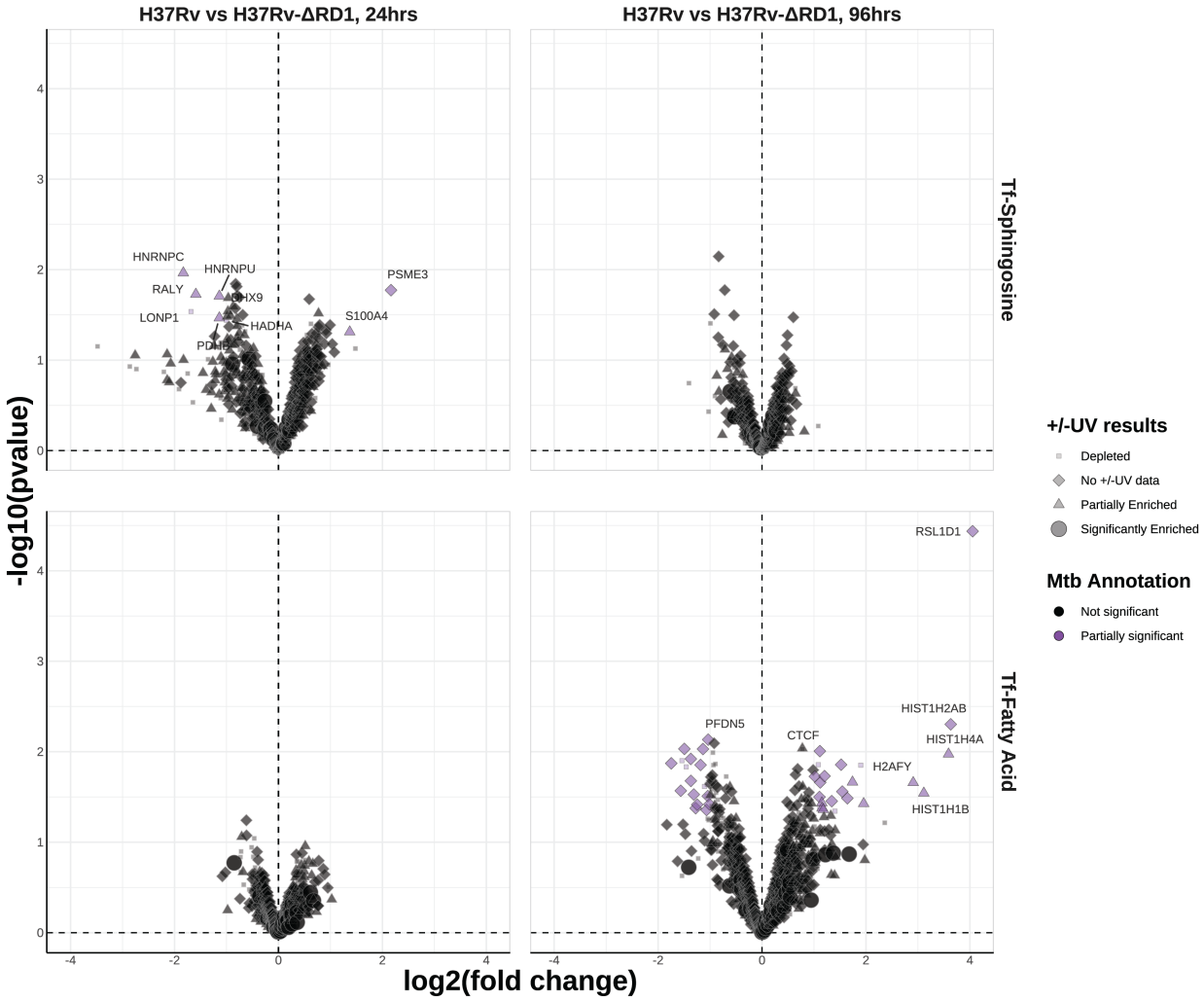


Figure 6.6. – Proteins enriched during H37Rv infection are highly similar to those enriched during H37Rv-ΔRD1 infection Volcano plots depict the enrichment of proteins in H37Rv infection in comparison to H37Rv-ΔRD1 infection for both tf-Sphingosine and tf-Fatty acid probe at 24- and 96-hours post-infection. Point size and shape denote the enrichment of each protein in the baseline proteomics experiment (+/-UV); point color denotes the statistical annotation among *Mtb* infection experimental results (as denoted).

Despite this, we continued our assessment of H37Rv versus H37Rv-ΔRD1 by plotting the log2 fold-change of proteins during each infection. Again, very few proteins are substantively different between pathogenic H37Rv infection and attenuated H37Rv-ΔRD1 infection (Figure 6.6). Among these few proteins of partial significance, we see PSME3 enriched toward H37Rv infection at 24 hours; this protein is a component of the immunoproteasome critical for antigen presentation and correlated with antigen presentation[395]. At 96 hours post-infection, we see a mild enrichment of several Type I Interferon-regulating genes, including poly(ADP-ribose) polymerase family member 9 (PARP9), 2'-5'-Oligoadenylate Synthetase 3 (OAS3), and MX Dynamin Like GTPases 1 and 2 (MX1 and MX2). Interestingly, PARP9 is involved in protection against *Mtb*[396], OAS3 restricts intracellular Mtb replication and enhances cytokine secretion[397], and MX1 and MX2 are well known interferon-stimulated genes transcriptionally upregulated during *Mtb* infection[388,398].

The only notable enriched gene for tf-8:3-FA was RSL1D1, enriched at 96 hours; this gene is known to suppress autophagy[399]. There is no reported connection to *Mycobacterium tuberculosis*.

6.5. *Mtb* protein Rv3466 is enriched by tf-Sphingosine during infection

The enrichment of mycobacterial proteins to either trifunctional sphingosine would be of profound significance – this would suggest direct evidence that mycobacteria utilize host sphingolipids during infection. The standard, though strict, criteria for confident protein identification above (at least two unique peptides identified in at least two replicates) yields no *Mtb* proteins. That we fail to identify *Mtb* proteins with high confidence may be expected in retrospect, given the disparity in total protein mass between an infected cell and an infecting bacillus. However, *Mtb* candidate peptides were identified aligning with the *Mtb* proteins accD2, Rv1910, and Rv3466 (Figure 6.7A). accD2 was only identified in the tf-8:3-FA TMT-16-plex, Rv3466 was only identified in the tf-Sph TMT-16-plex, and the same Rv1910c peptide was identified in both TMT-16-plexes. The relative enrichment of each protein toward H37Rv or H37Rv-ΔRD1 at both time points is depicted in Figure 6.7B. Among these three hits, only Rv3466 is enriched compared to mock infection for both strains at both time points.

The total knowledge regarding Rv3466 can be summarized in a few words: it is an uncharacterized protein with no functional annotation. Benq et al. report that Rv3466 lies in an MT-complex-specific genomic island – the genes that distinguish environmental mycobacteria from pathogenic *M. tuberculosis* complex members[400]. A 2019 genome-wide transposon mutagenesis study by Minato et al. showed that this protein is not essential for *in vitro* growth in MtbYM-rich medium[401]; its expression is significantly enriched following culture with the broad-spectrum antibiotic levofloxacin[402]; no protein domains are annotated in the sequence of Rv3466. Rv3466 is enriched to the lipid fraction in studies of the total *Mtb* proteome[403,404]. This gene is close genomic neighbors with rmlB and rmlC, two sugar-modifying enzymes involved in synthesizing peptidoglycan – suggesting a role for Rv3466 in peptidoglycan synthesis at the bacterial membrane. Rv3466 shares high sequence homology with another uncharacterized *Mtb* protein, Rv1588c.

Further mass spectrometry analysis will determine whether these or other *Mtb* protein interactors of sphingosine can be identified.

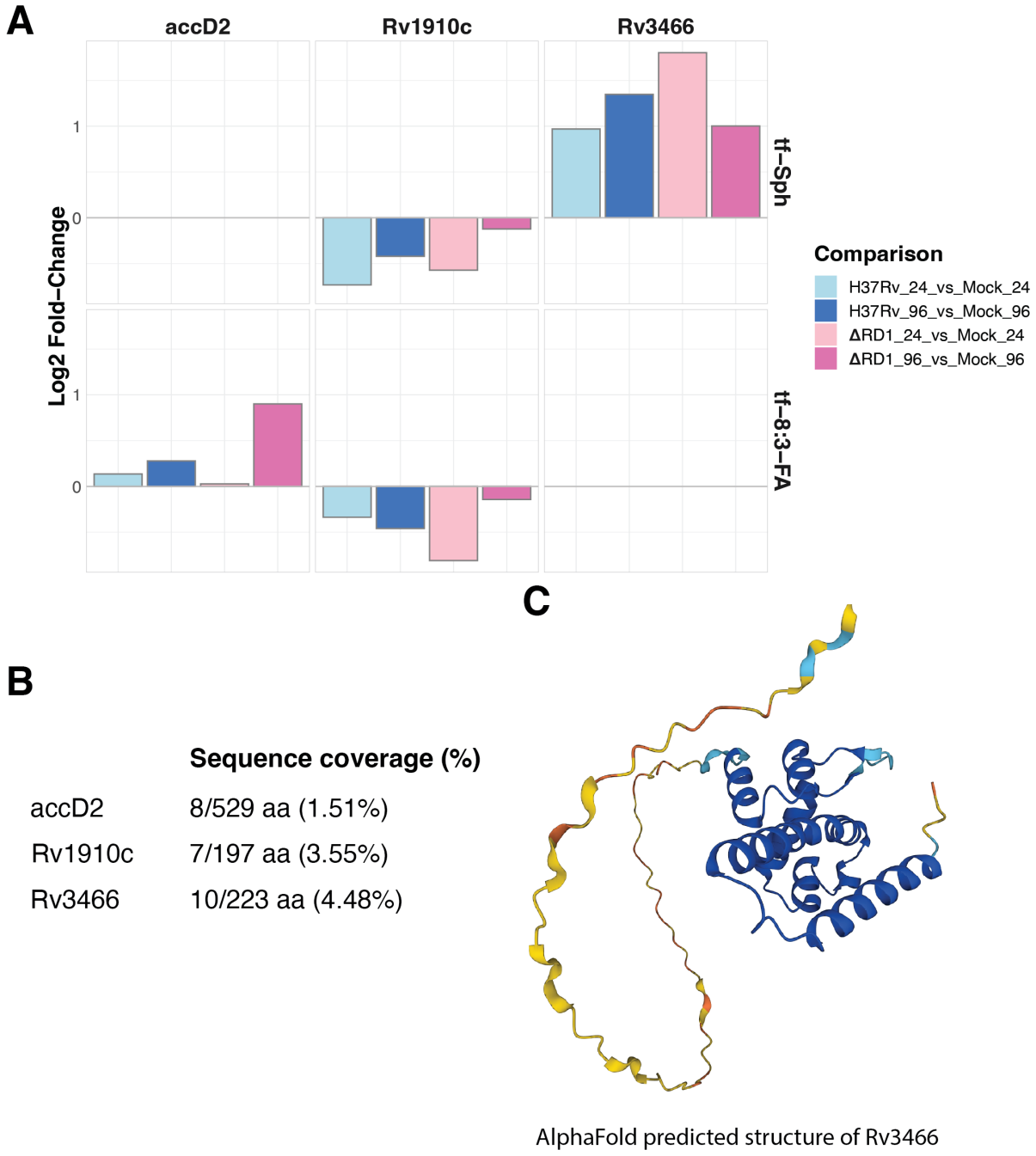


Figure 6.7. – **Potential *Mtb* protein identification: Rv3466** A summary of low-confidence identifications of three *Mtb* proteins accD2, RV1910c, and Rv3466. (A) Enrichment of each protein in infection versus mock comparisons. Blue bars are infections with pathogenic strain H37Rv; pink bars are infections with attenuated strain H37Rv-ΔRD1. (B) A depiction of the percentage of coverage for each protein. (C) Prediction of RV3466 structure using AlphaFold. Blue-coded sequence denotes high-confidence structure prediction; red- and yellow-coded sequence denotes low confidence prediction.

6.6. Discussion

In this study, we expand the application of trifunctionalized probes to assess the impact of intracellular bacterial infection on the sphingolipid interactome. We first identified the proteins that selectively interact with trifunctionalized sphinganine and sphingosine (as opposed to a pair of control trifunctionalized fatty acid probes). We identify a suite of differentially enriched protein interactors of trifunctional sphingosine upon infection with the pathogenic *Mtb* strain H37Rv. Most differentially enriched proteins do not align with published transcriptional signatures of *Mtb* infection, suggesting that these proteins' stability, localization, or function is altered during infection. We then compared the enriched interactions of cells infected with pathogenic and attenuated strains of *Mtb*. Finally, we hone in on a candidate *Mtb* protein enriched during infection (though its identification is below the confidence threshold).

Trifunctional probes are a precious resource for studying lipid biology. In this study, we primarily utilized these synthetic analogs of sphinganine and sphingosine as affinity handles to identify the protein interactors of these lipids in monocyte-derived macrophages. We note that a substantive majority of the enriched proteins either contain a transmembrane domain or are annotated as peripheral membrane proteins in the literature; very few are cytosolic or secreted. We identify several interactors reported in previous studies, such as Farley et al. 2024[255]. Such previously verified hits include ECH1, CTSD, VDACs 1 and 2, PITPNB, PRCP, and PSAP. We identify several intriguing, novel binding partners that appear to be unique to macrophages – these include NENF, CSTA, SCPDH, and HSPA5, among others. More work is needed to validate these interactions and to determine the biological effects of these interactions.

Before we can discuss the results of the *Mtb* infection interactomics experiments, we must make a technical note about +/-UV proteomics: we would have expected a dramatic disparity between the total protein input of +UV samples and -UV samples due to the stringency of sample wash. Notably, there are proteins substantially enriched to the -UV sample condition for tf-Sphingosine and tf-Sphinganine, though we expect little biological significance among these proteins. These proteins are likely the result of spurious interactions, spontaneous crosslinking, or artifacts of data normalization. Notably, the depth of coverage in the +/-UV results hinders its utility in filtering out candidates – there were over 300 proteins identified in the *Mtb* infection samples treated with tf-Sph and 542 proteins identified in the samples treated with tf-8:3-FA. It is unclear how to consider these proteins which have no annotation in the baseline interactome.

With the baseline interaction analysis in mind, we may now discuss the main results of this study. We hoped to determine whether *Mtb* infection induces changes in the protein-sphingolipid interactions of the cell. We found that a 24-hour infection with H37Rv induces significant differential enrichment of 151 proteins (31 were enriched during infection, and 120 were depleted). Our comparison to publicly available transcriptomics data shows that while some transcriptionally upregulated proteins are reflected by positive interaction enrichment, little change is reported for many of the most trustworthy hits. While this comparison does not preclude changes in the total abundance of proteins during *Mtb* infection, it serves to decouple our interaction analysis from the transcriptional response of the cell.

There are many potentially exciting hits for follow-up. There appear to be several pathways enriched in the up- and downregulated interactions. These include an upregulation of immunity related proteins (e.g., MX1, IKBKB, and CTLA), cytoskeleton and motility proteins (e.g., myosin heavy and light chains, kinesin light chain, tubulin, and Coronin-7). Among the downregulated pathways are

numerous secretory or vesicular trafficking proteins (e.g., COPE, GOLGA2, VAPA, and Rab11b). These results appear to suggest a significant dysregulation of cellular trafficking and endosomal protein composition. We also see a depletion of several calcium-binding proteins; this is intriguing because uncaging tf-sphingosine has been previously shown to induce the release of calcium from the lysosome[198] – are these infected cells unable to trigger sphingosine-mediated calcium signaling? Finally, we report the low-confidence identification of a candidate *Mtb* protein selectively enriched to tf-Sphingosine during infection: Rv3466. This protein is not expected to contain a transmembrane domain and has no known function. Follow-up experiments are needed to validate this hit and to explore the possibility of further yet-undiscovered *Mtb* proteins that selectively interact with host sphingolipids.

While much work remains on this project, this study is among the first to utilize trifunctionalized lipids in an affinity enrichment of *Mtb*-infected cells. These mark crucial first steps into establishing a toehold into the waters of sphingolipid-mediated host-pathogen interactions. These results may yield new insights into the molecular mechanisms underlying the pathogenicity of *Mycobacterium tuberculosis*.

6.7. Materials and Methods

6.7.1. THP-1 cell culturing and plating

Human THP-1 monocytes were sourced from American Type Culture Collection (ATCC catalog no. TIB-22) were maintained in culture using RPMI 1640 medium (Thermo Fischer Scientific #11875119) supplemented with 10% fetal bovine serum (Seradigm), 1x Gibco penicillin-streptomycin (Thermo Fischer Scientific #15-140-163), and 1x Gibco Non-Essential Amino Acids (Thermo Fischer Scientific #11140050). Cells were grown in suspension at 37 °C with 5% CO_2. Before experimental use, THP-1 monocytes were differentiated into macrophages via 48-hour treatment with 50 nM phorbol 12-myristate 13-acetate (PMA; Sigma-Aldrich P8139-1MG). All cell counting was achieved using a hemocytometer. For microscopy, cells were either plated in a 96-well plate at a density of 2.5 x 10^4 cells per well or on glass coverslips at 1.0 x 10^5 cells per well. For proteomics sample collection, cells were plated at a density of 4 x 10^6 cells per 10 cm dish.

6.7.2. Mycobacterium tuberculosis culturing and infection

Wildtype historical Mycobacterium tuberculosis strains H37Rv and H37Rv-ΔRD1 were gifts from the laboratory of Dr. David Lewinsohn at Oregon Health & Science University and Portland Veterans Association. Both Mtb strains were cultured in Difco™ Middlebrook 7H9 medium (Beckton Dickinson, Cat# 271310) supplemented with BBL™ Middlebrook OADC Enrichment (Beckton Dickinson, Cat# L12240) and 0.1% Tween-80. Bacterial cultures were carefully monitored to guarantee they did not overgrow (OD_{600} > 1.5) and were kept at a low passage before experimental use.

Before infection, THP-1 monocyte-derived macrophages were plated in 10 cm dishes at a density of 4 x 10^6 cells per dish and activated 48 hrs in 50 nM PMA. Mycobacterium tuberculosis (wildtype H37Rv and H37RvΔRD1) was cultured as above in 7H9 to mid-log phase and pelleted via 5 min spin at 2000 xg. Bacterial pellets were washed once with PBS and resuspended in RPMI. We prepared a single-cell suspension by passaging bacteria 25x through an 18-gauge blunt-tipped needle and

then through a 5 μm filter. Bacterial concentration was estimated as a proportion of the OD_{600} (assuming 2.5 x 10^8 CFU/mL at an OD_{600} of 1.0). For 24-hour infection samples, cells were infected overnight at an MOI of 3. For 96-hour infection samples, cells were infected overnight at an MOI of 1 and washed 2x with PBS before an additional 72-hour incubation. Infections were repeated in 3 biological replicates on independent days. We validated a minimum infection rate of ~70% by plating parallel coverslips of activated THP-1 cells, which we infected with both strains of Mtb and at both MOIs and inspected via fluorescence microscopy.

6.7.3. Trifunctionalized lipid treatments, uncaging, crosslinking

After a 48-hour activation with 50 nM PMA, THP-1 cells were treated with a trifunctional lipid probe at the below concentrations in Table 6.2. Cells were incubated with probes for 30 min at 37 °C to allow probe incorporation into cellular membranes. Lipid probes were then exposed to blue wavelength light (405 nm) for 5 min to release the coumarin cage and incubated for the times depicted below (Table 6.2). Probes were then diazirine crosslinked via 5-minute exposure to ultraviolet wavelength light (355 nm). For proteomics experiments, control cells were treated with trifunctional probes and uncaged but were left without UV-induced diazirine crosslinking (-UV conditions)

Table 6.2. – Trifunctional lipid probe treatments

Probe	Final treatment concentration	Incubation post-uncaging
Tf-8:3-Sphingosine	2 mM	15 min
Tf-8:3-Sphinganine	2 mM	15 min
Tf-8:3-Fatty Acid	50 mM	60 min
Tf-1:10-Fatty Acid	50 mM	60 min

6.7.4. Cell lysis and protein collection

After probe crosslinking, plates were washed 2x with ice-cold PBS, and cells were scraped into PBS using a cell scraper; for each sample, 2x 10 cm plates were combined during scraping for a total of 8 x 10^6 cells per sample. Cells were pelleted via 5 min spin at 500 xg and resuspended in a lysis buffer consisting of 8 M urea, 1x RIPA buffer (EMD Millipore, Cat# 20-188), and 1x HALT protease inhibitor cocktail (Thermo Fisher Scientific, Cat# 87786). Cell pellets were first broken up using repeated passage through an 18-gauge blunt-tipped needle, then passage through a lysis filter cartridge (from the Minute™ Plasma Membrane Protein Isolation and Cell Fractionation Kit, Invent Biotech, Cat# SM-005) to achieve a solution of lysed cellular proteins and intact nuclei. All lysis steps were performed on ice or in a pre-cooled centrifuge.

Finally, in accommodation of OHSU biosafety level 3 protocol, cell lysates from Mtb-infected samples (and corresponding mock-infected controls) were spun through a 0.5 μm centrifugal filter (Ultrafree-MC GV Centrifugal Filter, EMD Millipore, Cat# UFC30GV25) via 20-minute spin at 10,000 xg.

6.7.5. Fluorescence click reaction & In-gel/on-blot fluorescence

In-gel fluorescence was used as a quality control metric for infected samples. 5% of each sample was split off and conjugated with CalFluor647-azide via CuAAC. 50 µL of each sample was incubated with 100 µM tris(benzyltriazolylmethyl)amine (TBTA), 1 mM cupric sulfate ($CuSO_4$), 1 mM sodium ascorbate, and 20 µM CalFluor 647-azide (Click Chemistry Tools, Cat. #1372-1). Click reaction mixtures were incubated at room temperature for 60 minutes in the dark.

Following the click reaction, Laemmli sample buffer containing β-mercaptoethanol was added, and samples were heated to 42 °C for 30 minutes. Samples were spun at 10000 xg for 10 minutes. Each sample was loaded and was run on a 12.5% SDS-PAGE gel until the dye front had wholly run off the bottom of the gel – this removes much of the free, non-clicked 647-azide dye in each sample. After running, gels were left for at least 30 minutes in diH_2O to allow any remaining free dye to diffuse out of the gel. Gels were then imaged using the 647nm filter of a Sapphire™ FL biomolecular fluorescence imager (Azure Biosystems). Contrast and brightness were globally adjusted in FIJI.

For validation of hits using on-blot fluorescence, samples were fluorescently labeled and separated via SDS-PAGE as above, and gels were transferred to polyvinylidene difluoride blotting membranes via overnight wet transfer. Blots were blocked using 1% BSA and stained with denoted primary antibodies. Blots were then stained against the appropriate primary background with a secondary antibody conjugated to Alexa Fluor 555 fluorophore. Finally, blots were imaged as above on a Sapphire™ FL biomolecular fluorescence imager using the 555 nm and 647 nm filters. Contrast and brightness were globally adjusted in FIJI.

6.7.6. Affinity purification of probe-bound proteins

The remaining 95% of each sample was used as input for affinity purification via CuAAC to azide beads. First, Picolyl Azide Agarose resin (Click Chemistry Tools, Cat. #1408-2; 50% slurry) was transferred to new Eppendorf tubes and gently spun to pellet; storage solution supernatant was aspirated and beads were washed with diH_2O to remove any residual storage solution. CuAAC/click reaction was then initiated through the addition of 100 µM TBTA, 1 mM sodium ascorbate, 1 mM CuSO4, washed picolyl-azide agarose resin, and the remaining volume of probe-treated lysates. The final 1.25 mL reaction proceeded under vigorous shaking for 1 hour at room temperature.

6.7.6.1. Bead wash & digestion procedure

Bead/Click reaction mix transferred to a 2 mL gravity flow column (Pierce™ Centrifuge Columns 2 mL, Cat# 89896). Flow through was collected for each stage of the washing. Beads were washed a total of 25x with the buffers denoted below in Table 6.3.

Table 6.3. – **Details of bead washes in affinity enrichment**

	Composition	# of washes (volume per wash)
Wash Buffer #1	100 mM tris-HCl, 250 mM NaCl, 5 mM ethylenediaminetetraacetic acid (EDTA), 1% sodium dodecyl sulfate (SDS) (pH = 8.0)	5 (1 mL)
Wash Buffer #2	100 mM tris-HCl, 8 M urea (pH = 8.0)	10 (2 mL)
Wash Buffer #3	20 % acetonitrile, 80 % diH_2O (volume/volume)	10 (2 mL)

Beads were transferred to a new Eppendorf tube and pelleted. Bead-conjugated proteins were reduced via treatment with 1 mM dithiothreitol for 30 minutes at 42 °C. Beads were again pelleted and resuspended in an alkylating solution of 40 mM iodoacetamide for 30 minutes at room temperature (in the dark). Beads were then pelleted, and the alkylating solution was aspirated.

Finally, the beads were resuspended in 40 µL of a tryptic digestion solution consisting of 100 mM tris-HCl, 2 mM $CaCl_2$, and 10% acetonitrile. A total of 1 µg of trypsin (Promega Trypsin/Lys-C Mix, Mass Spec Grade, Cat. #V5071) was added to each sample for a 1:25 ratio of [LC-MS-grade trypsin/Lys C : substrate] (assuming 1mg/mL protein on beads). Beads were rocked vigorously at 37 °C overnight to digest bead-conjugated proteins.

6.7.6.2. Sample desalting

Following digestion from beads, the digestion solution was washed and desalted using a reverse phase C18 desalting spin column (BioPureSPN MIDI, PROTO 300 C18, Fisher Scientific Cat #NC1678004). At all stages of desalting, columns were spun at 110 xg for 1 minute. First, columns were conditioned with acetonitrile (ACN) and flushed with H_2O; columns were equilibrated with 2% ACN and blotted dry. The bead solution (including beads) was then transferred to the spin column and washed 2x with 2 % ACN to remove trace salts. The sample was released twice with an elution buffer of 80% ACN and 0.1 % trifluoroacetic acid. Finally, the eluted peptide solution was dried using a speedvac and stored at -80 °C.

6.7.7. Liquid chromatography and tandem mass spectrometry analysis (LC-MS/MS)

Mass spectrometric analyses were performed as previously described in Farley et al. 2024[255] and performed at the European Molecular Biology Laboratories Proteomics Core facility. Dried peptides were shipped to EMBL, labeled with isobaric mass tags using the TMT-16-plex system, and analyzed by LC-MS/MS on an Orbitrap Fusion Lumos mass spectrometer (Thermo Scientific).

Peptides were separated by reverse phase chromatography on an Ultimate 3000 nano RLSC system (Dionex) through a trapping cartridge (Precolumn C18 PepMap100, 5 mm, 300 µm i.d., 5 µm, 100 Å) and an analytical column (Acclaim PepMap 100, 75 x 50 cm C18, 3mm, 100 Å) connected to a nanospray-Flex ion source. The peptides were loaded onto the trap column at 30 µL/min using Solvent A (0.1% formic acid in H_2O) and eluted using a gradient from 2 to 80% Solvent B (0.1%

formic acid in acetonitrile) over 2 hr at 0.3 µL/min (all solvents were LC-MS grade). The Orbitrap Fusion Lumos was operated in positive ion mode with a spray voltage of 2.2 kV and a capillary temperature of 275 °C. Full scan MS spectra with a mass range of 375-1500 m/z were acquired in profile mode using a resolution of 120,000 with a maximum injection time of 50 ms, AGC operated in standard mode, and an RF lens setting of 30%. Fragmentation was triggered for 3 s cycle time for peptide-like features with a charge state of 2-7 on the MS scan (data-dependent acquisition).

Fragmentation was triggered for 3 second cycle time for peptide-like features with charge states of 2-7 on the MS scan (in data dependent acquisition). Precursors were isolated using the quadrupole with a window of 0.7 m/z and fragmented with a normalized collision energy of 34%. Fragment mass spectra were acquired in profile mode and with a resolution of 30,000. The maximum injection time was set to 94 ms and AGC target set to custom. The dynamic exclusion was set to 60 s[255].

6.7.8. Data analysis

Dr. Frank Stein prepared the data analysis pipeline at the European Molecular Biosciences Laboratories in Heidelberg, Germany and performed the analysis as previously reported in Farley et al., 2024[255]. The acquired MS data were analyzed using IsobarQuant[405] and Mascot V.24 (Matrix Science) using a reverse UniProt FASTA database including common contaminants; *Mtb* infection data were analyzed using a concatenated UniProt FASTA database including both human and *Mycobacterium tuberculosis* protein sequences. Only proteins with at least two unique peptides with lenght of at least 7 amino acids and a false-discovery rate below 0.01 were kept for protein-level analysis. The acquired spectra were scanned for the following peptide modifications: Carbamidomethyl (C, fixed), TMT-16-plex (K, fixed), Acetyl (N-term, variable), Oxidation (M, variable), TMT-16-plex (N-term, variable). The mass error tolerance for full-scan MS spectra was set to 10 ppm and for MS/MS spectra to 0.02 Da. A maximum of 2 missed cleavage sites was allowed. Batch effects were removed between replicates, a variance stabilization normalization was applied on the log2-transformed raw data[406], and changes in abundance of proteins in the experimental condition versus control condition were calculated using LIMMA analysis[382].

For the +/-UV experiment of baseline protein-lipid probe interactions, a protein was designated "significantly enriched" if it was enriched toward the +UV condition by at least a log2 fold-change of 1 and a p-value < 0.05. Proteins enriched toward the +UV condition but with p-value > 0.05 were designated "partially enriched". Due to the larger number of differentially enriched proteins in the *Mtb* infection affinity proteomics experiment, we used a modified designation of significance: proteins were deemed "significant" if they had a log2 fold-change enrichment of magnitude > 2 (both positive and negative), a p-value < 0.01 and a false-discovery rate < 0.05; proteins were deemed "partially significant" if the magnitude of their log2 fold-change enrichment was greater than 1 (in either the positive or negative direction) and a p-value < 0.05.

Data visualization was performed using R. Packages included: Bioconductor, ggplot2, dplyr, vsn, limma, MSnbase, gplots, fdrtool, biobroom, tidyverse, ggrepel.

Comparative transcriptomic data was found using the GEO database at the National Center for Biotechnology Information, initially reported by Jani et al. in 2023[388].

6.8. Contributions

GG designed the study, performed sample collection and analyzed results, prepared visualizations, prepared the figures, and wrote the manuscript. SF assisted in designing mass spectrometry experiments, designed and synthesized lipid probes, assisted in data visualization, and edited the manuscript. PH & FS assisted in designing mass spectrometry experiments, performed mass spectrometry and protein identification, and assisted in the interpretation of results. CS assisted in designing mass spectrometry experiments, oversaw the design and synthesis of lipid probes, provided reagents, and gave expert advice on study design. FT assisted in the study design and oversaw the study.

6.9. Supplemental Data

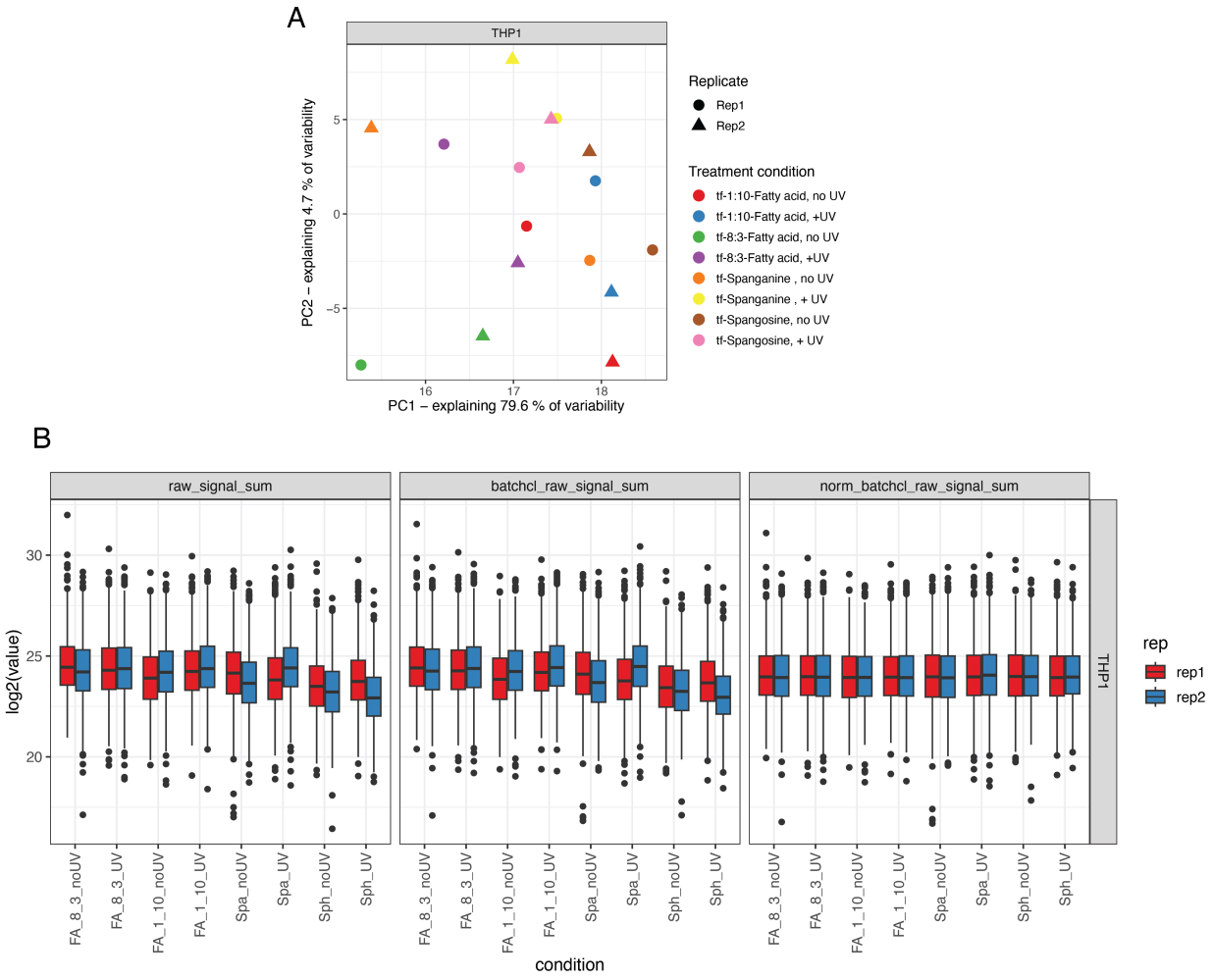


Figure S6.1 – Sample quality control for baseline probe interactomics experiment (A) Principle component analysis of protein abundance in each sample after batch effect removal and normalization. Shapes and colors denote conditions. (B) Box plots depict the normalization of MS data. Left panel: raw intensities of each sample for each condition; middle panel: batch-corrected intensities; right panel: median-normalized MS intensities. Color denotes replicate number.

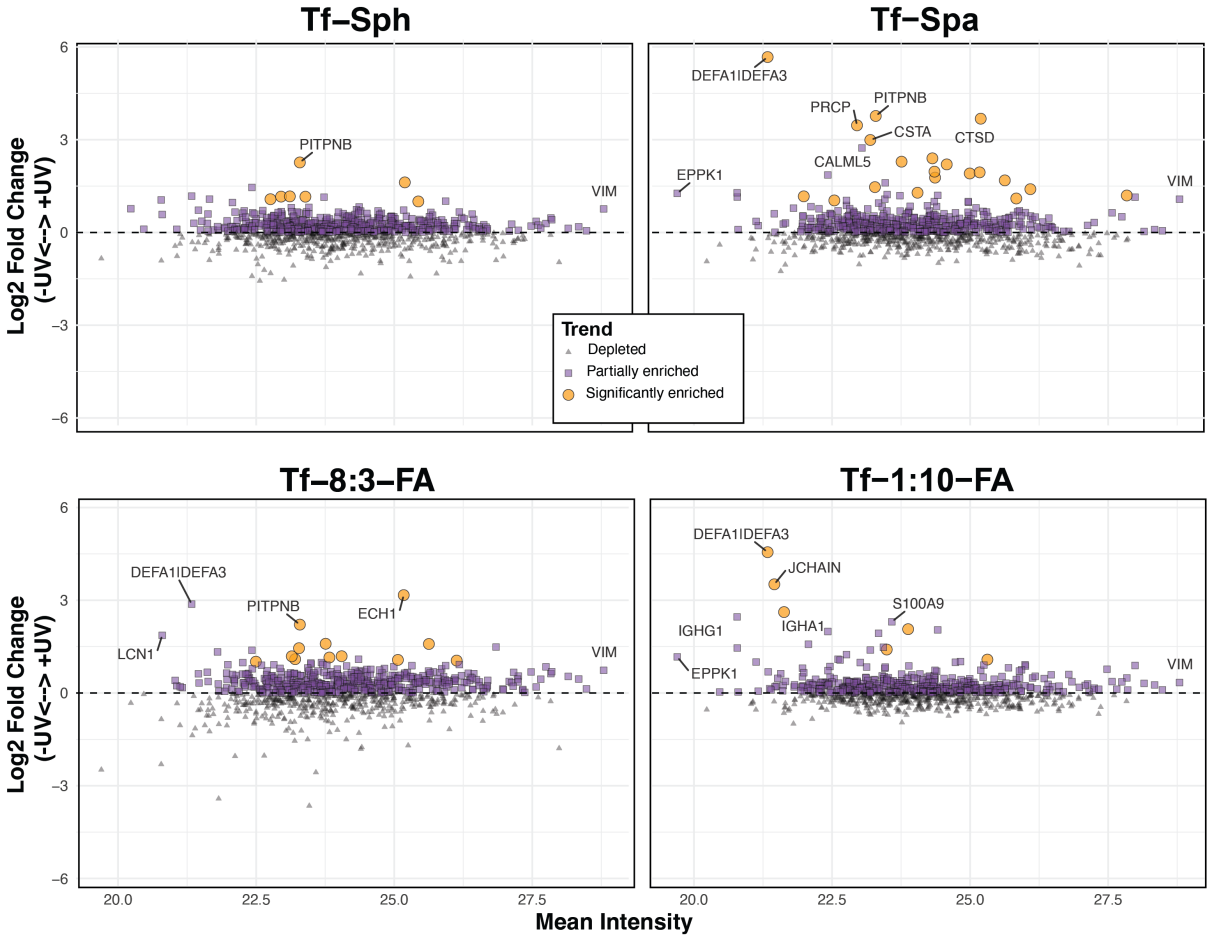


Figure S6.2 – **Baseline THP-1 probe proteomics, MA plots** MA plots depict the distribution of mean protein abundances between denoted conditions (x-axis) and the log2-transformed ratio of the denoted conditions (y-axis). Point size, shape, and color denote the enrichment annotation of each protein.

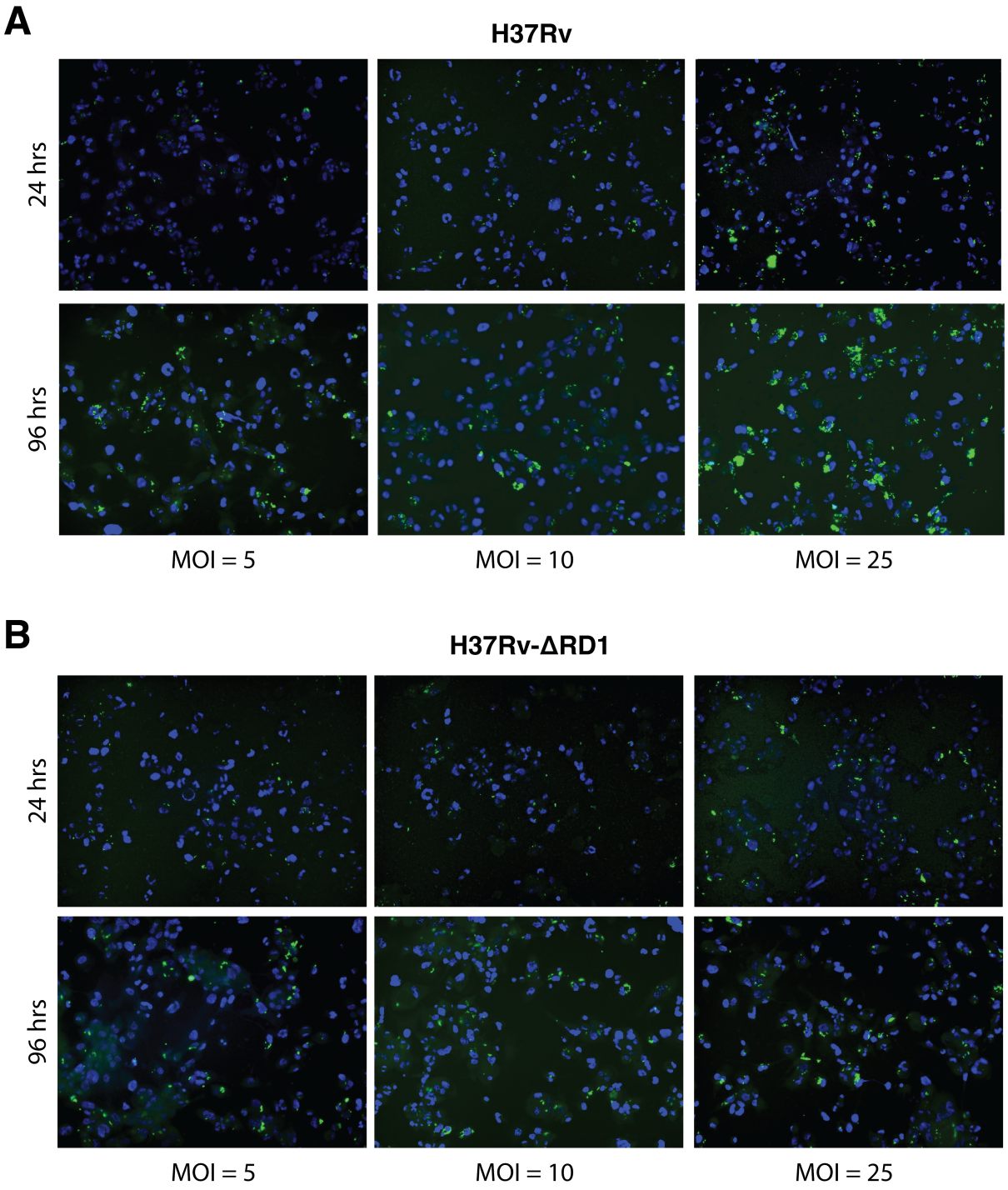


Figure S6.3 – **H37Rv and H37Rv-ΔRD1 MOI Optimization** THP-1 cells were infected with *Mtb* strains H37Rv (A) and H37Rv-ΔRD1 (B) at increasing multiplicities of infection (MOI) for 24 and 96 hours to determine optimal infection rates. At denoted time points, cells were fixed and stained with rhodamine (bacterial cell wall) and DAPI (nuclei) to determine how many cells were infected.

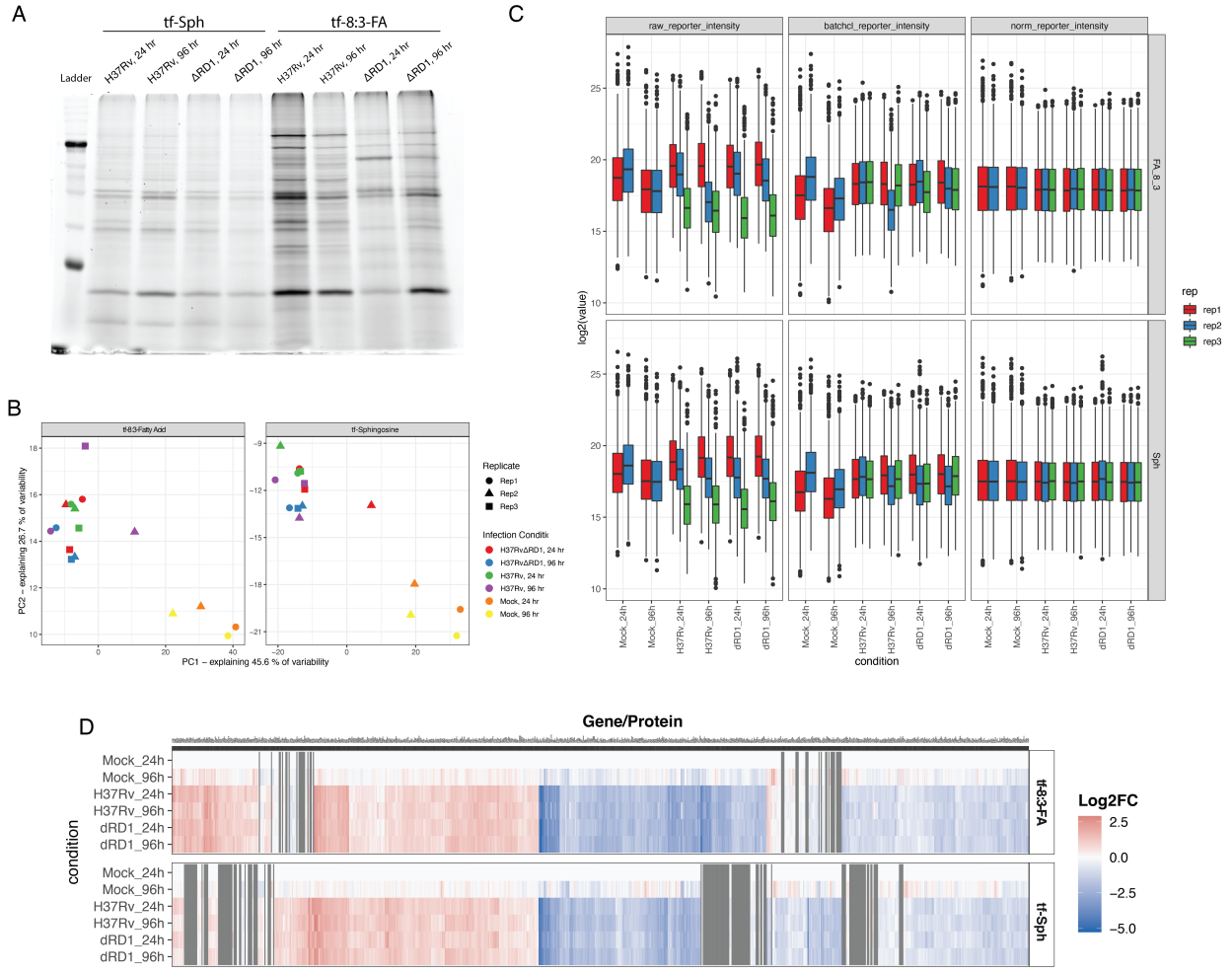


Figure S6.4 – **Sample quality control for Mtb infection interactomics experiment** (A) Representative in-gel fluorescence quality control of proteins isolated from *Mtb*-infected THP-1 cells treated with tf-Sphingosine or tf-8:3-Fatty acid. (B) Principle component analysis of protein abundance in each sample after batch effect removal and normalization. Shapes and colors denote infection conditions. (C) Box plots depict the normalization of MS data. Left panel: raw intensities of each sample for each condition; middle panel: batch-corrected intensities; right panel: median-normalized MS intensities. Color denotes replicate number.

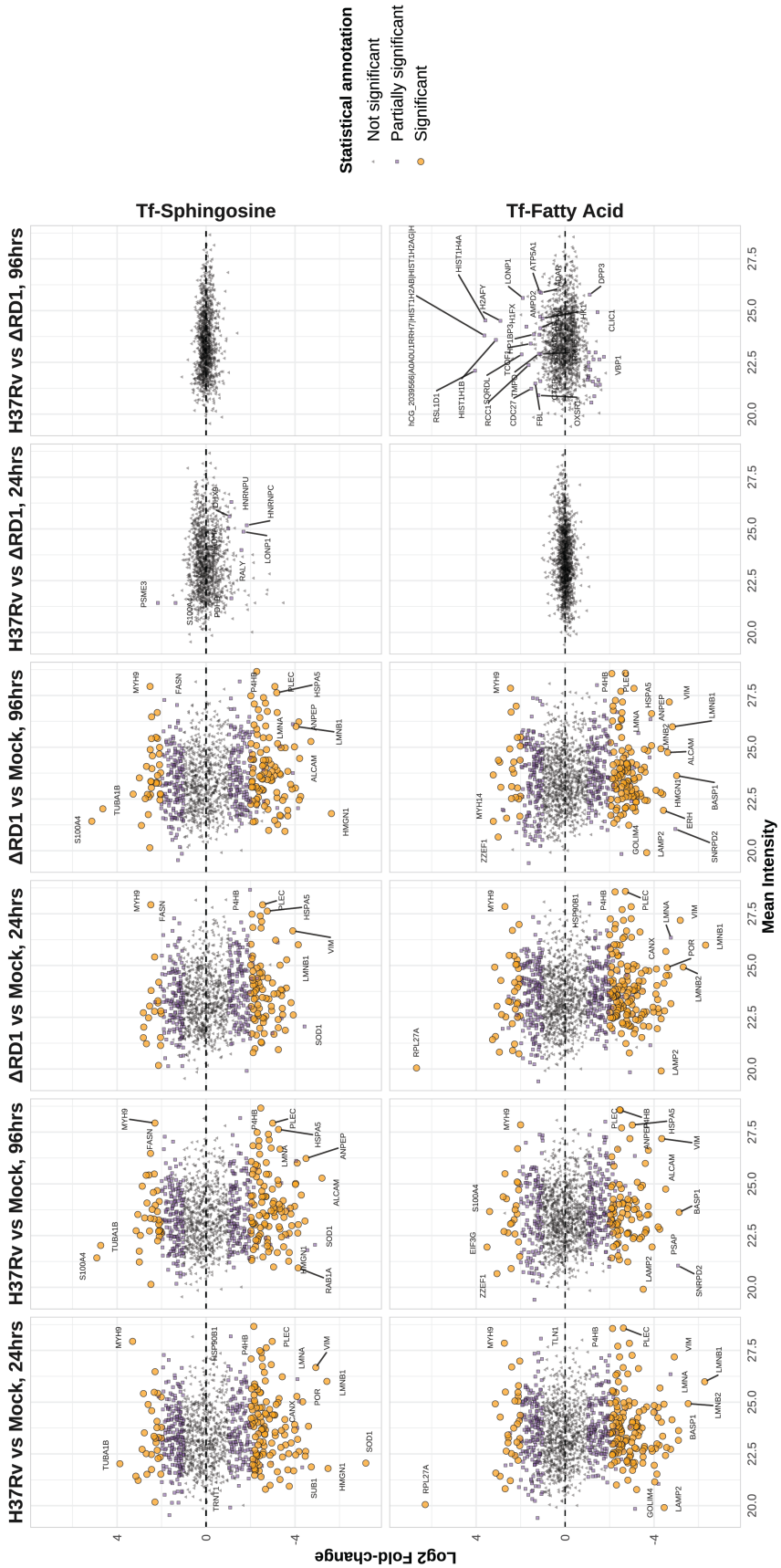


Figure S6.5 – *Mtb* infection proteomics data quality control, MA plots MA plots depict the distribution of average protein abundances between denoted conditions (x-axis) and the log2-transformed ratio of denoted conditions (y-axis). Point color denotes the statistical annotation of each protein (as denoted). Point size and shape denote enrichment toward tf-Sphingosine in baseline proteomics experiment (as denoted).

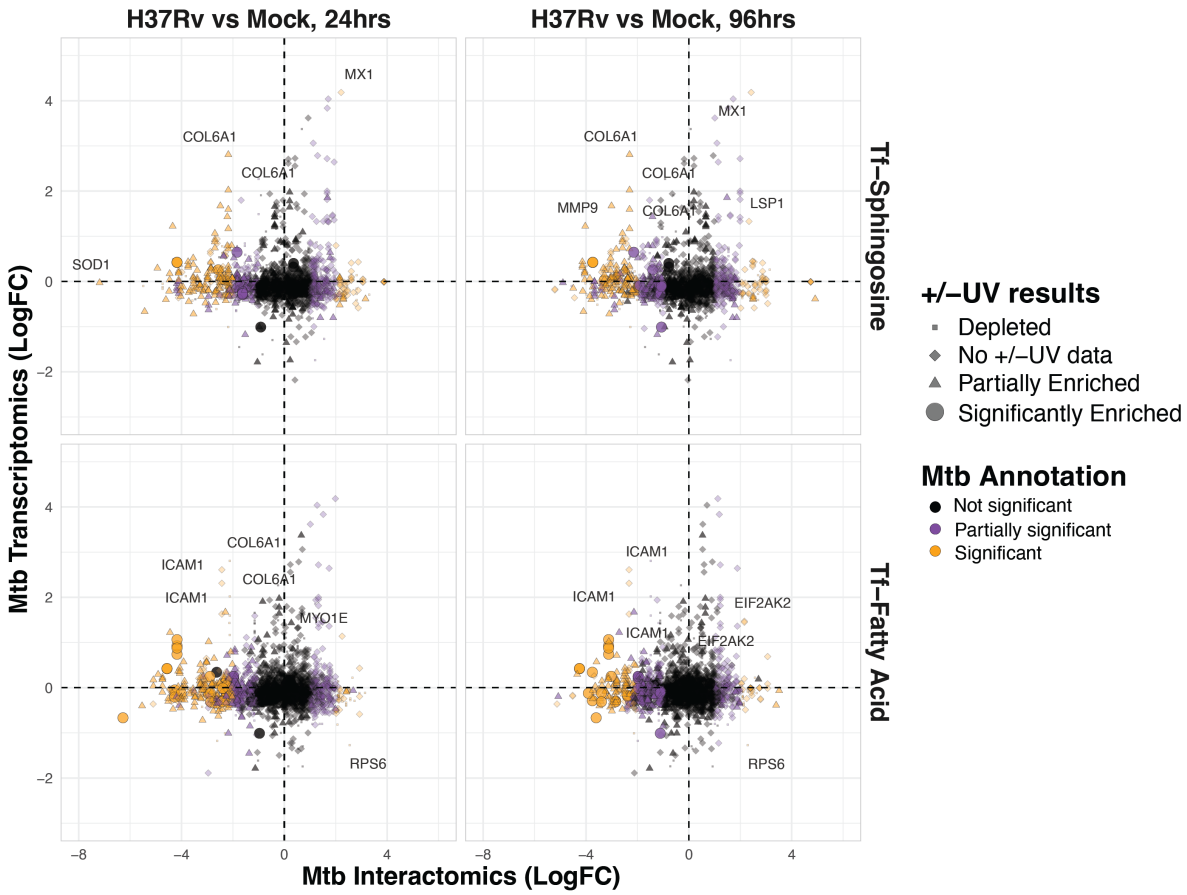


Figure S6.6 – Comparison against publicly-available transcriptomics data Transcriptomics data collected by Jani et al.[388] (publicly available at GEO accession GSE227851) were compared against log2-transformed ratios of H37Rv-versus-Mock infected cells treated with tf-Sphingosine to assess correlations between transcriptional regulation and interaction enrichment. Point size and shape denote the enrichment of each protein during the baseline proteomics experiment (+/-UV); point color denotes statistical annotation among *Mtb* infection data (as denoted).

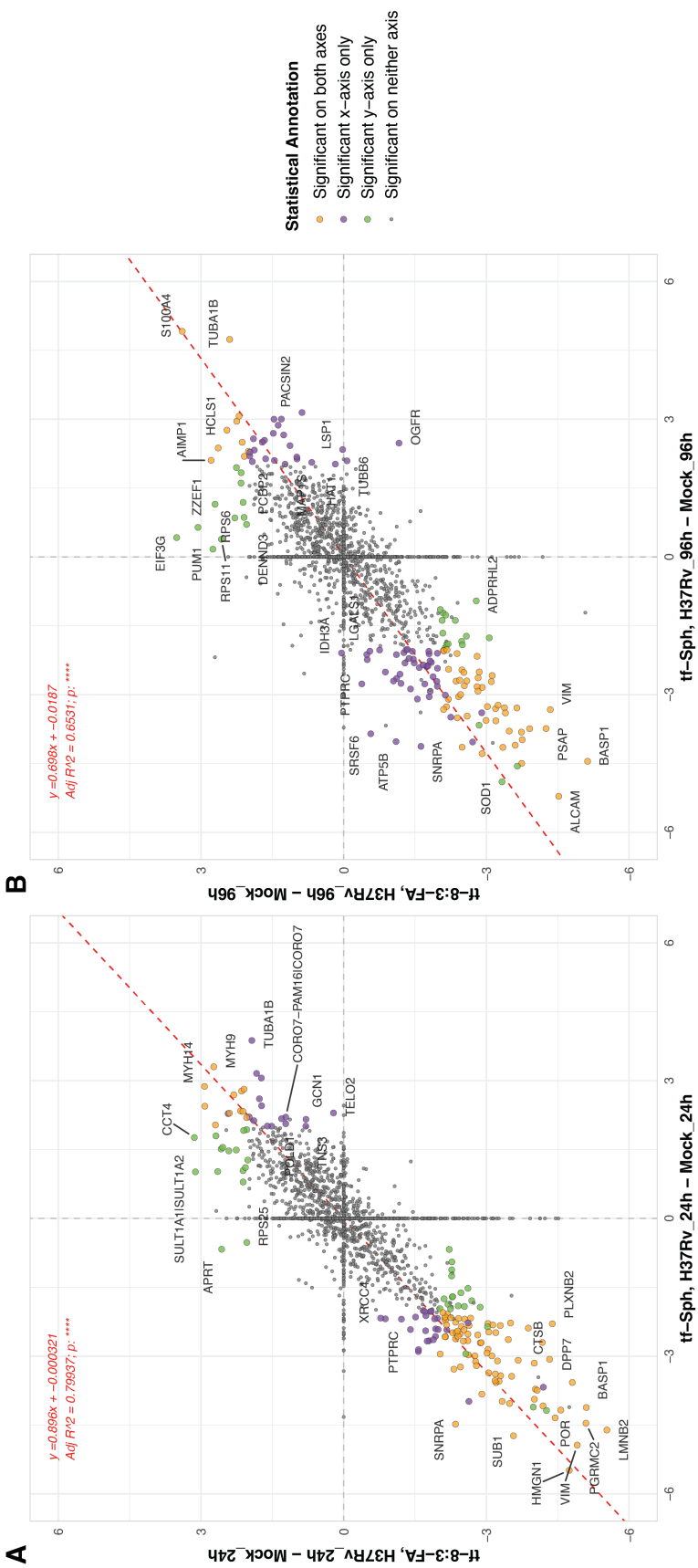


Figure S6.7 – Distinct protein enrichment to tf-Sph and tf-8:3-FA Dot plots depict the comparison between protein enrichment for tf-Sph (x-axes) and tf-8:3-FA (y-axes) for the H37Rv versus Mock ratios at 24 (left panel) and 96 hours (right panel). Point color denotes whether each protein was significantly enriched along the x-axis, the y-axis, or both axes. The red line denotes a linear regression analysis on proteins identified in both experiments; red text describes the formula and fit parameters of the line of best fit between the two comparisons.

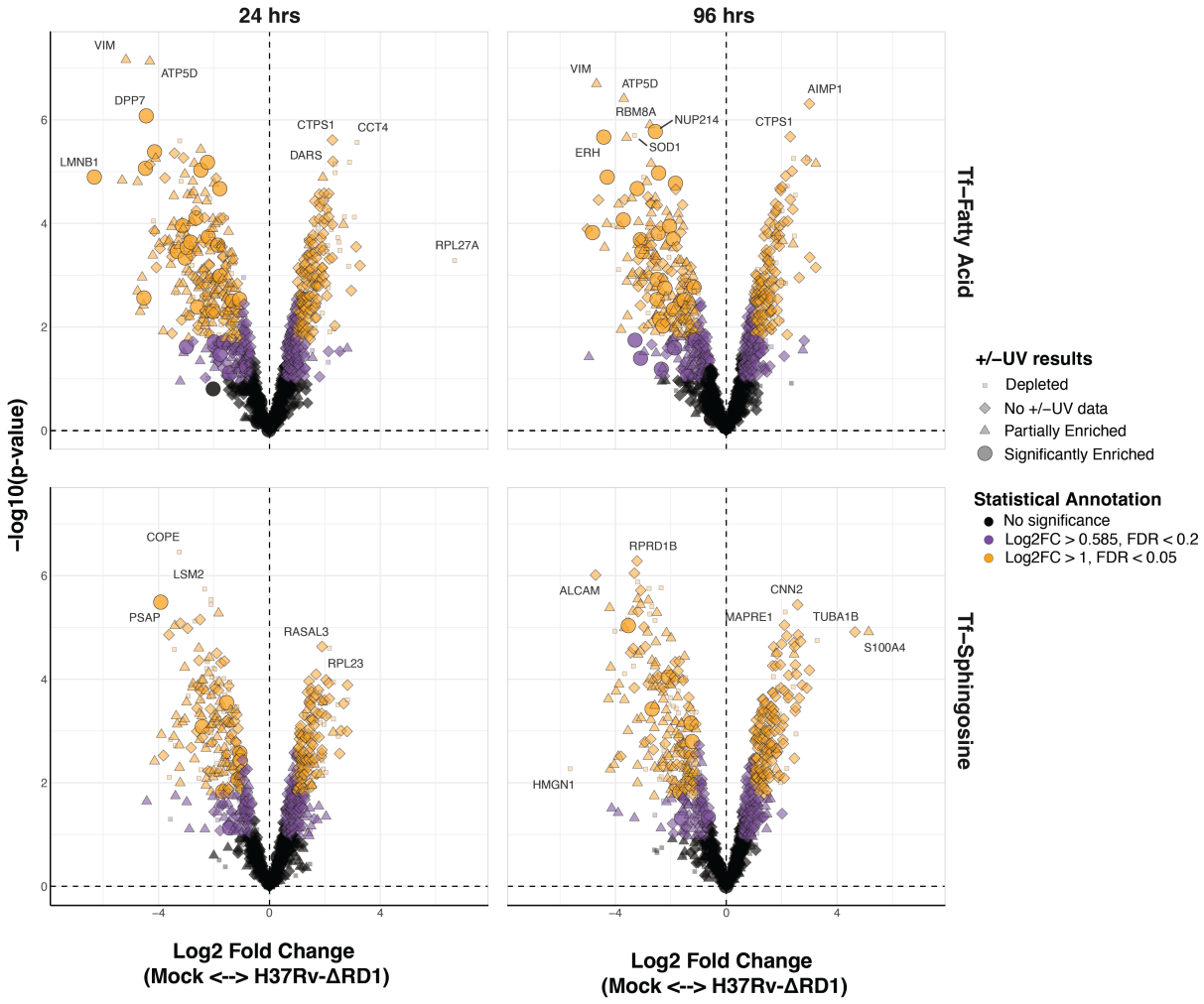


Figure S6.8 – **Lipid:protein interactions enriched during infection with H37Rv-ΔRD1** Volcano plots depict the enrichment of proteins toward tf-Sphingosine or tf-8:3-Fatty acid at 24- and 96-hours post-infection with *Mtb* strain H37Rv-ΔRD1 versus mock-infected control. Point size and shape denote the enrichment of each protein during the baseline proteomics experiment (+/-UV); point color denotes statistical annotation among *Mtb* infection experimental results (as denoted).

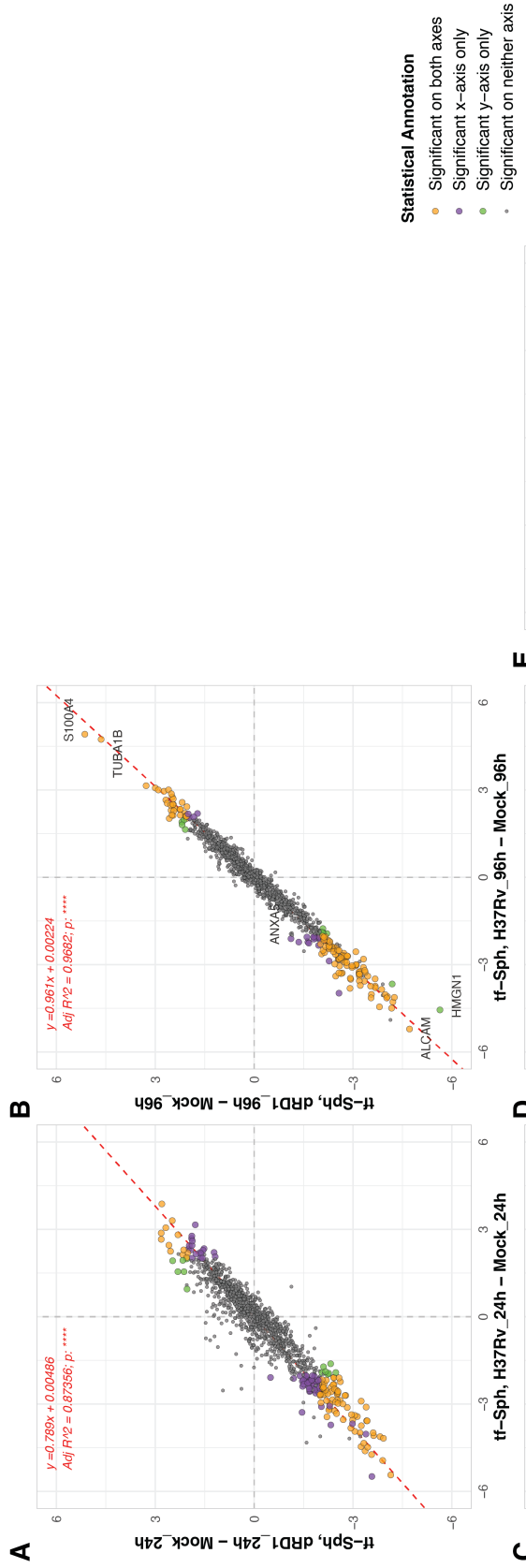


Figure S6.9 – Infection with H37Rv-ΔRD1 has minimal effects on the tf-Sph interactome Scatterplots depict the log2 fold-change of the denoted conditions against each other, enabling comparison of enriched proteins in control conditions. Point color and size denote the relative statistical annotation of each protein between the comparison conditions depicted on the x- and y-axes (hit = Log2FC > 1 & FDR < 0.05). The Red dashed line denotes the line of best fit between the axes (determined via linear regression); the red text describes the formula for a line of best fit and the R^2 value.

Part III.

Additional work

Section overview

The following four chapters are research, reviews, and methods publications which do not fit nicely within the main portion of this dissertation. Despite this, they represent significant work and deserve a place here – if only as an indication that I did a lot of work over the last 7 years.

Genetic tools to study sphingolipids in disease

In this review, we discuss the particulars of using genetic editing tools, such as CRISPR, to study lipid biology. Because lipids are products within complex metabolic networks, careful consideration must be applied when knocking out a lipid synthesizing enzyme.

The Squeaky Yeast Gets Greased

In this review, we discuss a few of the many ways that lipids are essential in destroying opportunistic fungal pathogens. We focus on the signaling lipids involved in phagocytosis and phagosome maturation.

Rapid visualization and quantification of phagocytosis in neutrophils

In this methods chapter, we describe a high-throughput technique for rapidly quantifying the phagocytic capacity of neutrophils in culture.

Systematic analysis of the sphingomyelin synthase family in *C. elegans*

In this research report, we report the identification and characterization of a novel family of sphingomyelin synthases in the nematode *Caenorhabditis elegans*. This work was initially started during Dr. Tafesse's PhD project, and is finally available online at BioRxiv.

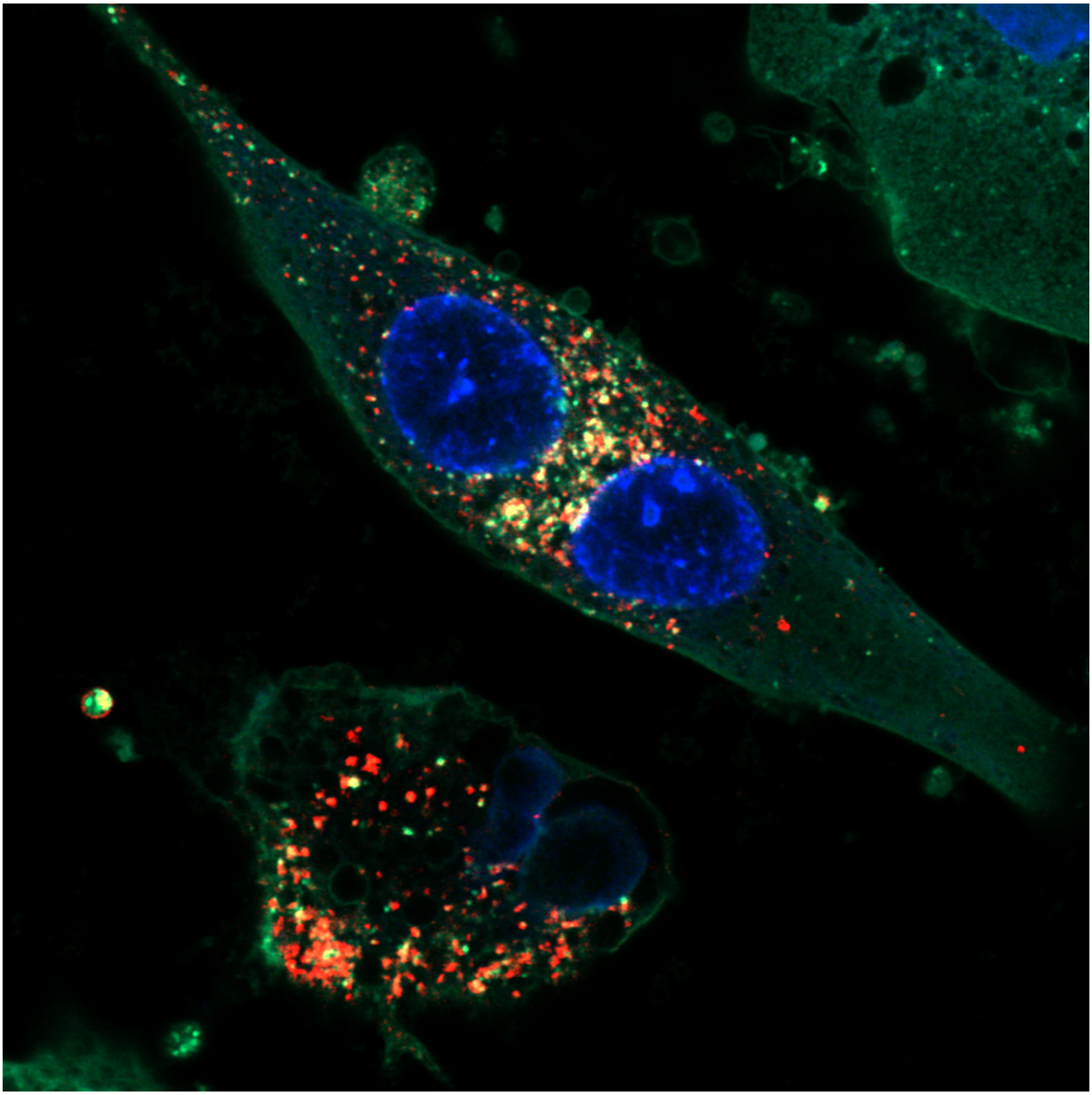


Figure 6.8. – **Macrophages subjected to widespread membrane damage.** THP-1 monocyte-derived macrophages expressing the membrane damage reporter mAG-Gal3 (Green) were treated with the lysosome damaging agent LLOME and fixed with 4% formaldehyde. After fixation, cells were stained for the lysosomal marker LAMP1 (Red), validating the selectivity of LLOME treatment and the utility of the mAG-Gal3 reporter. DAPI denotes nuclei (Blue).

Chapter 7.

Genetic tools to study sphingolipids in disease

This chapter has been adapted from our review published in Methods of Molecular Biology, the original version can be read here: https://doi.org/10.1007/978-1-0716-2895-9_1

Authors: Gaelen Guzman[1], Cameron Creek[1], Scotland E. Farley[1], Fikadu G. Tafesse[1,*]

[1] = Department of Molecular Microbiology and Immunology, Oregon Health & Science University, Portland, Oregon, USA. [2] = Molecular Cell Biology Division, Department of Biology and Chemistry, University of Osnabrück, Osnabrück, Germany. [*] = corresponding author: tafesse@ohsu.edu

7.1. Abstract

Sphingolipids are a critical family of membrane lipids with diverse functions in eukaryotic cells, and a growing body of literature supports that these lipids play essential roles during the lifecycles of viruses. While small molecule inhibitors of sphingolipid synthesis and metabolism are widely used, the advent of CRISPR-based genomic editing techniques allows for nuanced exploration into the manners in which sphingolipids influence various stages of viral infections. Here we describe some of these critical considerations needed in designing studies utilizing genomic editing techniques for manipulating the sphingolipid metabolic pathway, as well as the current body of literature regarding how viruses depend on the products of this pathway. Here, we highlight the ways in which sphingolipids affect viruses as these pathogens interact with and influence their host cell and describe some of the many open questions remaining in the field.

7.2. Introduction

Sphingolipids are a diverse family of membrane lipids that play critical roles in all eukaryotic cells, serving many functions ranging from maintaining membrane rigidity and curvature to directly serving as signaling molecules which regulate cell fate decisions. Until recently, the technical tools needed to assess the contributions of sphingolipids to viral infectivity and replication were limited. However, the emergence of chemical inhibitors and effective genomic editing techniques have allowed researchers to directly probe the effects that SLs have on virus lifecycles.

Viruses face multiple logistical challenges during their life cycle: host cell entry and/or cytosolic release of viral genome, genomic replication and protein expression, and protein sorting/viral particle assembly all require intimate interactions with host membranes and often involve dramatic reorganization of cellular compartments[272,356,407]. Crucially, it can be difficult to isolate the roles that a particular lipid plays because the metabolic pathways that maintain lipid homeostasis are complex and devilishly interconnected. In recent years, many groups have begun work on parsing the manners in which sphingolipids are critical components of various viruses' lifecycles. Recent reports show that various sphingolipids are essential for the host cell entry of viruses such as Ebolavirus and HIV-1[375,408], the survival or apoptosis of the host cell during viral infection[407,409], and the immune responses of the host organism[410]. In 2019, Yager and Konan proposed that the sphingolipid synthesis pathway may serve as a therapeutic target for treating enveloped human RNA viruses[411]. Similarly, our recent work suggests that genetically ablating the enzyme ceramide synthase 2 significantly suppresses HIV replication[375]. Here we primarily highlight the use of genomic ablation techniques to assess the roles that sphingolipids play during viral infection.

While a suite of chemical inhibitors is widely used to study sphingolipids, many have poorly characterized off-target effects and high cytotoxicity[327,412]. Utilizing a combination of small molecule inhibition in tandem with genetic ablation/reconstitution allows for conclusive study of specific sphingolipid species. In particular, CRISPR/Cas9-genome editing has emerged as a ubiquitous method for genetic ablation[413]; in recent years, the classical CRISPR/Cas9 paradigm has been improved to allow for multiplexed gene deletion while simultaneously reducing pleiotropic and off-target effects[414]. As technical descriptions of these methods abound, here we focus on describing several necessary considerations when editing genes that are involved in lipid metabolism pathways.

This chapter will first discuss the considerations necessary when altering sphingolipid metabolism. We will then describe the genetic elements composing the forward SL synthesis pathway, settling briefly on several of the major branches of mature/complex sphingolipids. Next, we will touch on the so-called salvage pathway, which enables the cell to recover complex sphingolipids from the extracellular environment and convert them into other sphingolipid species and even degrade them to free fatty acid. At each step throughout the pathway, we will discuss the current literature available on our understanding of how these genes influence viral biology and the swaths of still-open questions on the roles that sphingolipids play during viral infections.

7.3. Considerations When Ablating Lipid-Metabolizing Enzymes

This review is not an in-depth description of CRISPR/Cas9 or any particular genome-editing tool as these have been discussed at great length elsewhere[415,416], and recent works have described the technical limitations inherent to CRISPR-based genomic editing; further, novel techniques are

arising which enhance the selectivity and efficiency of multiplexed genetic ablation[414,417,418]. However, it is necessary to discuss the special considerations one must take when altering cellular lipid metabolism.

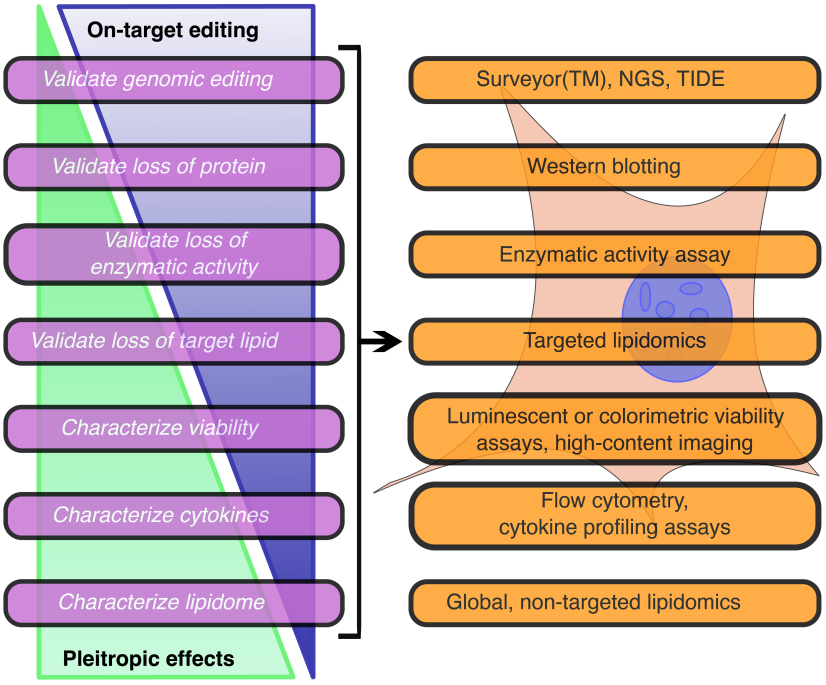


Figure 7.1. – **An overview of techniques for validating and characterizing genetically edited cells.** (Abbreviations: NGS = next generation sequencing, TIDE = tracking of indels by decomposition)

Because lipids are rapidly metabolized and interconverted, and their levels are tightly regulated throughout the cell, it can be difficult to disentangle the direct roles that a lipid plays from the extraneous effects that arise due to the loss of that lipid. This topic is discussed extensively by Harayama et al. in both 2018 and 2020[418,419]. In one notable example, sphingomyelin synthase knockout typically results in enhanced cell death and cytopathic effects[323,343]. This is likely not because sphingomyelin itself is a pro-survival molecule, but rather because it represents one of the most significant sinks that limits accumulation of ceramide, which is classically understood as a pro-apoptotic molecule[304,321,420,421]. Thus, while novel, engineered versions of Cas enzymes have emerged with increased on-target specificity[414], one must consider off-target effects beyond those related to spurious genomic editing.

Several techniques are available to validate that the desired genomic editing has occurred in the cell. Sentmanat et al. describe and compare four commonly used methodologies for evaluating site-specific nuclease activity[417]. We and others have utilized the Surveyor™ assay to detect targeted CRISPR genomic editing[422]. However, following validation of the desired genomic editing, it is necessary to validate the effects of the gene's ablation and characterize the resulting knockout cells. These validation and characterization steps include the following (Figure 7.1): (1) Western blotting to demonstrate whether the ablated gene product is translated and expressed; of course, this method is most tractable when Western-quality antibodies are commercially available for the target protein, and a Western signal does not necessarily connote protein functionality. (2) Measuring the enzymatic activity of the targeted protein. In some contexts, commercially available enzymatic

assays are available to show whether knockout cells retain capacity to synthesize or metabolize a particular lipid species, as used by Audi et al. to assess acid sphingomyelinase activity[423]; alternatively, one may assess enzymatic activity using radiographic metabolic labeling assays, as described by Ramstedt et al. in 1999[424]. (3) A researcher may also utilize targeted lipidomics to validate a reduction in the synthesis of a particular lipid species; for example, we and others have used internal standards to quantify the absolute abundances of certain lipid species in knockout cells[425,426]. Together, these strategies effectively demonstrate whether the genomic ablation results in the desired lipid synthesis deficiency.

Next, the researcher must consider the pleiotropic effects of their genomic editing—and must characterize the broader effects that the ablation has on cell survival and growth rate, differentiation state, and global lipidomic profile. Many luminescent and colorimetric cell viability assays are available, all of which can effectively demonstrate the levels of metabolic activity in different cellular conditions. One may also utilize high-content microscopy platforms to track and compare cellular growth rate and viability[427]. To further characterize the knockout cells, cytokine profiling may be used to assess whether the classical lineage expression markers are still present. Taciak et al. describe a methodology for assessing the phenotype of RAW 264.7 macrophages[428]. To explore broad changes to the lipidome of the genetically edited cells, one may utilize global, non-targeted lipidomics to quantify the relative abundance of many lipids in knockout versus wild-type cells[429]. As will be discussed below, ablating the synthesis of one lipid will block the production of all downstream metabolic products and can also result in an accumulation of the input components.

In some cases, it may be impossible to fully ablate a gene in a critical lipid synthesis pathway—either due to overly toxic effects or inhibited proliferation. In these circumstances, knockdown systems may be necessary to study the role of certain lipids. Several transient knockdown techniques are available, including RNAi[430,431], shRNA[432], and the new CRISPRi[433]. These techniques each have strengths and weaknesses, and many resources describe how to select the best tool to perform a knockdown and contrast these techniques[434,435]. Following knockdown, the researcher must utilize the above-described techniques to characterize the production of the sphingolipid in question.

7.4. The Early Sphingolipid Synthesis Cascade

De novo sphingolipid synthesis begins with several enzymatic reactions that occur in a rapid and coordinated fashion to produce the central nexus of sphingolipid biology: ceramide (Figure 7.2).

The first and rate-limiting step of sphingolipid synthesis is the production of the sphingoid backbone via the condensation of cytosolic serine and palmitoyl-CoA, mediated by the serine palmitoyltransferase complex (SPT). The heterodimeric SPT complex may be rendered fully nonfunctional by genetic ablation of either Sptlc1 or Sptlc2[182,270]. Intriguingly, reports suggest that other SPT subunits and SPT-associated proteins influence the downstream production of complex sphingolipids[436,437]. Because SPT mediates the de novo synthesis of all sphingolipids, we and others have utilized Sptlc2$-/-$ knockout cells to explore the manners in which this entire lipid class influences microbial pathogenesis and host–pathogen interactions[179,205]. However, only limited work has been done on the effects of SPT knockout/inhibition on the lifecycles of viruses. SPT inhibition suppresses replication of hepatitis C virus in a mouse model of infection[329]. Another study identified a novel SPT enzyme encoded within the genome of the Emiliania huxleyi virus, which specifically infects

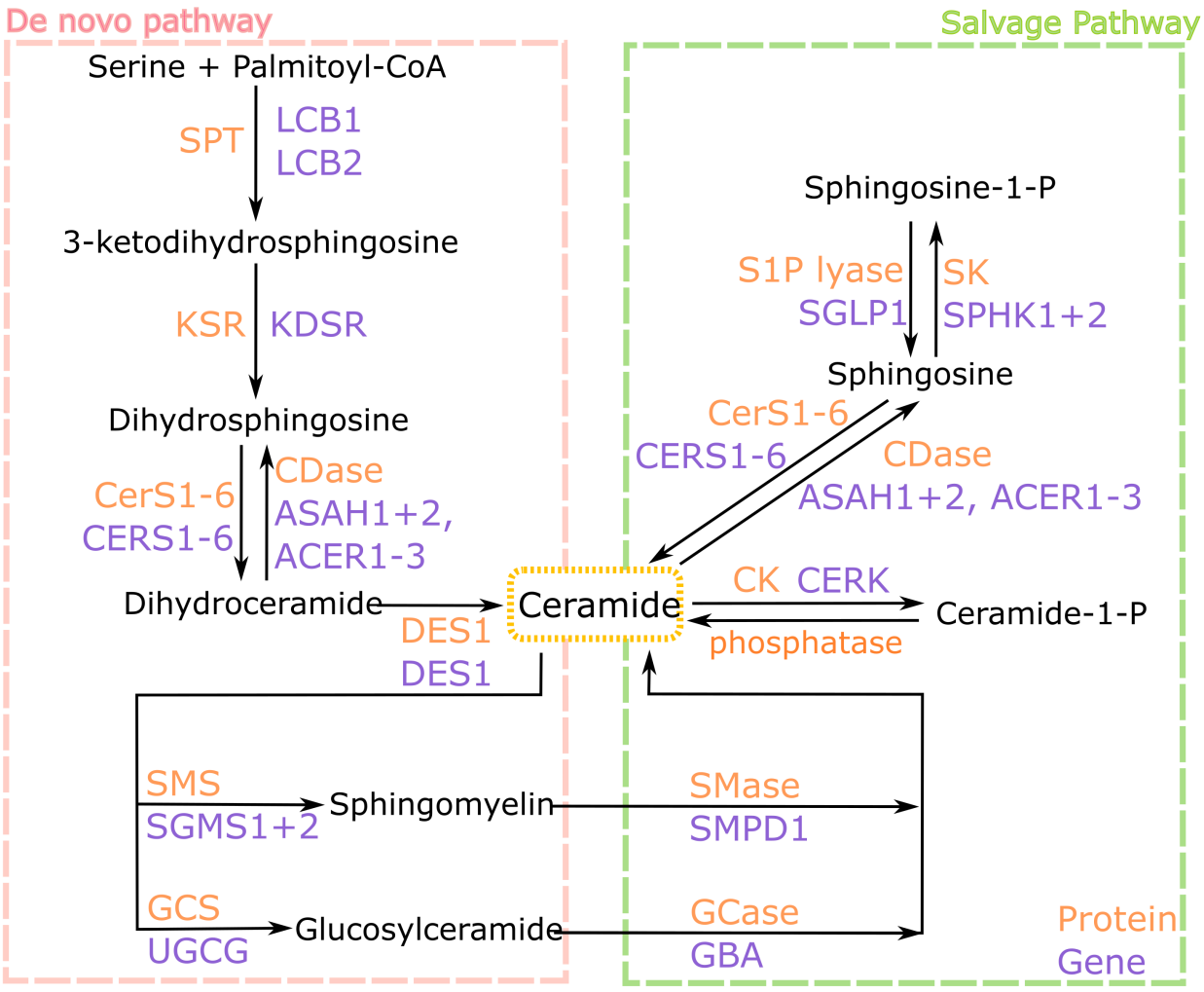


Figure 7.2. – **An overview of the sphingolipid metabolic network.** The pathway is split up into de novo and salvage pathways outlined in pink and green dashed boxes, respectively. Lipid metabolism reactions are depicted by arrows with the primary enzyme responsible for the reaction, shown in orange, and the corresponding gene, shown in purple. (Abbreviations: SPT = serine-palmitoyl transferase, LCB1+2 = long-chain base 1+2, KSR = 3-ketosphinganine reductase, KDSR = ketosphinganine reductase, CerS1-6 = ceramide synthases 1-6, CDase = ceramidase, ASAH1+2 = N-acylsphingosine amidohydrolase 1+2, ACER1-3 = alkaline ceramidase1-3, DES1 = dihydroceramide desaturase 1, SMS/SGMS 1+2 = sphingomyelin synthase 1+2, UGCG = ceramide glucosyltransferase, SMase = sphingomyelinase, SMPD1 = sphingomyelin phosphodiesterase 1, GCase = glucosyl ceramidase, GBA = glucosylceramidase beta, CK/CERK = ceramide kinase, S1P lyase = sphingosine-1-phosphate lyase, SGLP1 = sphingosine-1-phosphate lyase 1, SK = sphingosine kinase, SPHK1+2 = sphingosine kinase 1+2)

the marine coccolithophore E. huxleyi[438]. These studies reveal that there are many open questions regarding the manners in which viruses may depend on and manipulate SPT activity in their hosts.

The direct product of the SPT reaction is 3-ketodihydrosphingosine, an intermediate lipid kept at transient levels via rapid reduction into dihydrosphingosine by the ketodihydrosphingosine reductase (KSR) enzyme. Although this enzyme is critical to higher SL biosynthesis, few studies have been done on the effects that this enzyme has on viral biology. Mutations in KDHR are known to be causal to bovine spinal muscular atrophy and to drive steatosis and hepatic injury in zebrafish[439,440].

Following the production of dihydrosphingosine, a secondary acyl chain is added to the sphingoid backbone via reaction with one of the six mammalian ceramide synthase enzymes (CerS1–6)[441,442]. Each of these enzymes preferentially N-acylates dihydrosphingosine with a fatty acyl-CoA chain of differing length to result in distinct ceramide species with distinct biological effects[443]. CerS5 and CerS6 prefer to react palmitoyl-CoA to produce the so-called long-chain 16-carbon fatty acid chain ceramide (C16-Cer), whereas the CerS2 enzyme prefers to utilize 22- and 24-carbon fatty acyl-CoA substrates to produce "very long chain" C22- and C24-Cer[181,443–445]. Several reports have described how these distinct ceramide species can have profoundly differing cellular effects: C18-Cer induces ER stress and apoptosis[446], and C22- and C24-Cers cause mitochondrial dysfunction[322] — and both studies demonstrated that C16-Cer does not drive such cytopathic effects[322,446]. In the context of viral infections, there are few examinations into the role of particular CerS enzymes. We recently showed that CerS2 knockout dramatically decreases the infectivity of HIV-1 via inhibition of HIV-1 Env receptor binding and/or blocking membrane fusion[375]. Thus, there are many open questions remaining regarding how ceramide synthase enzymes influence viral lifecycles—especially given that the various chain length products of these enzymes have deeply context-dependent effects on cellular processes.

The dihydroceramide species directly produced by CerS enzymes are generally intermediate species that are rapidly desaturated to ceramide by Dihydroceramide Δ4-desaturase 1 (DES1). This enzyme inserts a single double-bond in dihydroceramide to produce the suite of ceramide species described above[182,447]. To these authors' knowledge, few, if any, studies have explored the effects of genetic DES1 deletion in the context of viral infection. However, Hayashi et al. recently showed that chemically inhibiting DES1 activity via N-(4-Hydroxyphenyl) retinamide treatment results in suppressed SARS-CoV2 membrane fusion[448]. This study (currently in preprint) postulates that the loss of DES1 results in an accumulation of unsaturated sphingolipids which drives a decrease in membrane fluidity, thus reducing spike-mediated membrane fusion and reducing SARS-CoV2 entry into host cells. Given this context, there remain open questions regarding the fluidity requirements that other viruses have during membrane fusion/invasion.

As the central nexus of sphingolipid metabolism, de novo ceramide production marks the conclusion of early sphingolipid biosynthesis. The levels of ceramide in the ER are tightly regulated, and it is rapidly transported out of the ER to be elaborated into a rich family of "higher" sphingolipids, which will be discussed below.

7.5. Terminal Branches of the Sphingolipid Synthesis Pathway

Ceramide and its precursors are typically kept at transient levels within the ER and throughout the cell; the vast majority of total sphingolipids typically accumulate as mature species such as sphingomyelin or glycosphingolipids[449]. Headgroup modifications distinguish these lipids from the

ceramide backbone and allow for complex biological function. There are some which primarily serve mechanical roles within the membrane—for example, sphingomyelin is known to tightly associate with cholesterol to form lipid rafts, which serve as rigid membrane platforms to enable cell-cell signaling interactions[450–453]. Another complex sphingolipid, ganglioside, appears to play several simultaneous roles during HIV-1 infection, where it may directly serve as a receptor for the HIV-1 glycoprotein gp120 and serve as a critical viral envelope component[454,455]. Below, we describe the synthesis of these and other common complex sphingolipids.

In the typical mammalian cell, the glut of sphingolipid composition is represented by sphingomyelin. This species is primarily produced via the enzyme sphingomyelin synthase 1 (SMS1) mediates the transfer of the phosphocholine headgroup from phosphatidylcholine to ceramide, releasing diacylglycerol (DAG) as a byproduct[182,456,457]. This occurs primarily in the *trans*-Golgi network and preferentially incorporates long chain C18-Cer[182,458]. Sphingomyelin is then transported to the plasma membrane by transport proteins such as P24 during secretory trafficking[188]. A small component of sphingomyelin content is produced via the same mechanism at the plasma membrane by SMS2 as a component of the so-called salvage pathway (described in more detail below). Loss of SMS activity results in dramatic reduction of both sphingomyelin and DAG, which simultaneously reduces cell proliferation and sensitivity to apoptotic cell death via orthogonal mechanisms[323,459]. We and others have utilized SMS1, SMS2, and SMS1/2 knockout systems as well as chemical SMS inhibition to study how sphingomyelin production affects host–pathogen interactions and pathogen lifecycles[179,328]. SMS1/SMS2 double knockout mice are shown to be susceptible to infection by Japanese encephalitis virus[460].

The remaining sphingolipid content of the cell is largely composed of a diverse family of glycosylated lipids produced by either UDP-glucose ceramide glycotransferase (UGCG) or ceramide galactosyltransferase (CGT), which produce glucosylceramide and galactosylceramide, respectively. This process primarily occurs in the cis-Golgi network and utilizes a higher proportion of very long chain ceramides such as C22- and C24-Cer[189,461–463]. Glucosylceramide is the precursor to several structurally diverse categories of glycosphingolipids which include the lacto-, globo-, and ganglioseries[464,465]. These glycosphingolipids have been shown to play significant roles as viral receptors: GM1 ganglioside is the primary receptor for SV40 virus[466], GD1a and GT1b gangliosides serve as the primary receptors for murine polyomavirus-like particles[466], and GM3 ganglioside is a HIV-1 gp120 fusion cofactor[454,467]. Galactosylceramide is the precursor to the sulfatides, cerebrosides, and other galactosylsphingolipids—which are primarily enriched in oligodendrocytes and necessary for maintaining myelin sheathes[182]. Few studies have investigated to the role of galactosylceramide in viral infections[468].

Given the breadth of these findings, complex sphingolipids such as sphingomyelin and gangliosides may play essential roles in many viral infections—and that much work remains to be done to uncover how these lipid structures influence host–pathogen interactions.

7.6. SL Degradation and Salvage

In addition to forward synthesis, or de novo synthesis, the sphingolipid metabolic pathway includes a complex series of degradative steps which allow cells to recover complex sphingolipids from the cellular periphery or the extracellular environment, cleave the glycosylated or phosphorylated headgroup to recover the ceramide backbone, and then shunt it back into the cell to fulfill immediate

sphingolipid requirements. In some contexts, however, the degradation of complex sphingolipids through ceramide into further derivative species such as sphingosine and sphingosine-1-phosphate directly induces potent signaling effects such cell proliferation and chemotactic recruitment of immune cell[420,468].

As the major sphingolipid species in the cell, sphingomyelin represents one of the largest pools for the salvage pathway to pull from. Several sphingomyelinase enzymes (SMases) mediate the cleavage of sphingomyelin's phosphocholine headgroup to release ceramide; the two primary isoforms localize to particular cellular compartments: neutral SMase (nSMase) preferentially localizes to the plasma membrane and is most active at neutral pH, whereas acid SMase (aSMase) localizes to the lysosomal compartment and is most active at low pH[469]. Because sphingomyelin is a cylindrical lipid and ceramide is more conical, the degradation of sphingomyelin results in localized negative membrane curvature—directly inducing membrane invagination and mechanistically contributing to phagocytosis and endocytosis[470]. This activity by SMases is critical for the membrane fission/fusion events that occur during the endosomal maturation process[133]. Indeed, as endosomal-lysosomal trafficking is essential for bacterial clearance, aSMase has been heavily investigated for its roles during bacterial infections by pathogens such as *Neisseria gonorrhoeae* and *Mycobacterium tuberculosis*[266,295,298]. Similarly, research suggests that these SMase enzymes play important roles during the entry stage of many viral infections, including Ebola virus, Japanese encephalitis virus, and HIV-1[408,471,472]. Thus, the production of ceramide via sphingomyelin degradation at the plasma membrane or the endosomal compartment likely plays multivariate roles in many yet-unstudied viral contexts.

Just as SMases degrade sphingomyelin, glucosylceramidases and galactosylceramidases mediate the degradation of glycosylated sphingolipids such as gangliosides and globosides. Several such enzymes localize to the lysosome and are involved in inheritable lysosomal storage disorders, including Gaucher's disease[473]. Glucosylceramidase is known to play roles in endocytosis and thereby is an important factor in the entry stages of enveloped viruses such as Ebola virus, influenza virus, and vesicular stomatitis virus[425].

Ceramide produced by SMase and glucosyl/galactosylceramidase activity has many potential direct effects, including negative membrane curvature and increased fluidity in highly localized membrane regions called ceramide-enriched platforms. There are several ways in which the ceramide produced in this process may be further modified, including phosphorylation into ceramide-1-phosphate by a Ca2-dependent ceramide kinase (CERK) in the trans-Golgi network[474]. The roles for ceramide-1-phosphate are still under investigation, but it appears to be involved in sensing ceramide levels and thereby may serve in regulating proliferation and migration of macrophages and monocytes, among other broad mitogenic effects[318,475–477]. Intriguingly, ceramide-1-phosphate phosphatase activity was observed in rat livers and brains, but no reports characterize or identify the enzyme directly responsible for this reaction[478].

In a better-understood reaction, the ceramide produced by complex sphingolipid degradation can be converted to sphingosine through the activity of ceramidases (CDases), which hydrolyze ceramide to release sphingosine and free fatty acid[182]. There are five CDase isoforms, categorized by pH optimum: alkaline CDases (ACER1, ACER2, and ACER3), acid CDase (ASAH1), and neutral CDase (ASAH2). The functions and regulatory mechanisms for these isoforms are diverse and have been extensively discussed elsewhere[479]. The sphingosine resulting from CDase-mediated ceramide degradation can drive potent cellular signals: sphingosine was shown to induce Ca2+ release from the lysosome, stimulate cell proliferation and survival, and abrogate the mitochondrial dysfunction associated with excess ceramide accumulation[73,304,479,480]. In the context of viral infections,

several studies show a role for CDase activity in modulating viral infectivity: Grafen et al. demonstrated in 2019 that inhibiting acid CDase effectively inhibited measles virus infection, and Lang et al. showed in 2020 that acid CDase within multivesicular bodies traps HSV-1 to reduce infection propagation[481,482]. One may expect that these enzymes play profound roles later in the infection process as well—viroid budding, convoluted membrane formation, and other phenotypes of viral infection may rely on the activity of one or more CDase.

Although sphingosine is itself a bioactive signaling molecule, it can be further modified into one of the strongest signaling sphingolipids in the cell: sphingosine-1-phosphate (S1P). Two sphingosine kinases (SK1 and SK2) mediate the phosphorylation of sphingosine into S1P, which interacts with proteins throughout the cell and in the extracellular space. A suite of G-protein-coupled S1P receptors (S1PRs) are differentially expressed on different cell types, which can induce chemotactic recruitment and extravasation of immune cells such as cytotoxic T cells and neutrophils[451]. S1P itself serves as an intracellular secondary messenger that induces cellular signaling via the platelet-derived growth factor receptor and the Fcγ receptor 1[412]. Given these roles as a mediator of inflammatory response, it may be no surprise that many researchers have looked toward the roles of SphKs during viral infection. SphK2 is shown to drive survival of cells latently infected with Kaposi's sarcoma-associated herpesvirus, revealing a potential therapeutic target for one of the most common AIDS-associated tumors worldwide[483]. Similarly, SK inhibition impeded measles virus infection[481]. Further work may show broader roles for SK1 and SK2 in other infections, and yet more work remains in the study of the role for S1PRs during viral infections.

The only known exit point of the sphingolipid metabolic pathway is through the activity of sphingosine-1-phosphate lyase (SGPL1 or SPL1), which cleaves S1P into a free ethanolamine-1-phosphate moiety and a membrane-bound C16-fatty aldehyde[182]. Gerl et al. extensively describe the utility of an SGPL1 knockout line in their 2016 study, highlighting that these cells enable nuanced analysis of sphingolipid-protein interactions in the cell. Intriguingly, studies have shown that the bacterium *Legionella pneumophila* injects an S1P Lyase (LpSpl) into its host cell as an effector protein via a type IV secretion system; this effector degrades S1P and appears to drive a blockade in autophagy to result in enhanced virulence[484]. Vijayan and colleagues used SPL1 overexpression and knockout to show that this lyase is critical for initiating IKKε activity and type I interferon responses during infection by influenza A virus[410].

With these enzymes, a cell can either reclaim the sphingoid base from complex sphingolipids from the extra- and intracellular environment and to fully degrade sphingolipids out of the metabolic network. Multiple stages of this salvage pathway produce potent signaling molecules that drive transcription, chemotaxis, and both intra- and intercellular immune responses. Thus, there are many open questions regarding how this pathway can influence the lifecycles of different viruses.

7.7. Discussion/Conclusion

Sphingolipids are a classically enigmatic family of membrane lipids, but a rapidly growing body of literature demonstrates repeatedly that these lipids play critical and nuanced roles throughout the cell. Recent years have come with a particular focus on how host sphingolipids influence the replication and propagation of infectious pathogens. Notably, the sphingolipid metabolic pathway may represent an effective therapeutic target for inhibiting viral infections; as has been discussed previously, blocking host factors may reduce the risk of mutagenic escape[485]. Indeed, we recently

showed that CerS2 is necessary for the entry/fusion stage of HIV-1 infection[375]. This observation is possibly supported by the prior observation that GM3 ganglioside is a receptor for the HIV-1 glycoprotein gp120, given that gangliosides are primarily synthesized from very long chain C22- and C24-Cer produced by CerS2[454]. In a similar vein, we previously showed that SM synthesis is essential for intracellular transport of influenza virus glycoproteins[328].

While numerous small molecule inhibitors are widely used to inhibit sphingolipid metabolism, they are complemented by genetic ablation techniques to allow for nuanced analysis of sphingolipid biology. However, the blockade of lipid pathways can also result in multifactorial off-target effects. For example, blocking sphingolipid production results in accumulation of their input ingredients (e.g., palmitoyl-CoA and phosphatidylcholine) and reduction of byproducts (e.g., DAG). Similarly, some lipid species drive highly nuanced regulation of local and general membrane fluidity (e.g., SM is a primary component of cholesterol-rich lipid rafts, and its loss can result in general increases in membrane fluidity). Further, one must consider various mechanisms of redundancy, including multiple synthesis genes (e.g., ceramide synthases 1–6) and the salvage pathway. Thus, to fully understand the particular role a lipid plays in any given context, a researcher must deeply consider these potential off-target effects and strive to characterize the knockout cells' growth rate, fluidity, lipid composition, and differentiation state.

Through careful study design, genomic editing techniques such as CRISPR/Cas9 can powerfully complement other methods of manipulating the sphingolipid axis of the host–pathogen interface. Given the rapid advancement of the field, we conclude that there are many yet-untested manners in which sphingolipids enable or restrict various aspects of viral infectious lifecycles. Few generalizations can be made about viruses because of the great variability in how they take advantage of the host systems to replicate and propagate—however, interactions with host lipid membranes are necessary at nearly every stage of every virus's lifecycle. Thus, exploring the manners in which host sphingolipids influence a virus offers profound insight into both host and viral biology.

7.8. Contributions

GG compiled the references and concepts discussed in this review and wrote the text; he prepared Figure 1 and gave editorial comments on the preparation of Figure 2. CC contributed to the compilation of concepts discussed in this review and text edits. SF provided text edits; he prepared figure Figure 2. FGT oversaw and guided the compilation of concepts and references discussed in this review and provided text edits.

Chapter 8.

The Squeaky Yeast Gets Greased

The Roles of Host Lipids in the Clearance of Pathogenic Fungi

Authors: Gaelen Guzman[1], Patrick Niekamp[2], Fikadu G. Tafesse[1,*]

[1] = Department of Molecular Microbiology and Immunology, Oregon Health & Science University, Portland, Oregon, USA. [2] = Molecular Cell Biology Division, Department of Biology and Chemistry, University of Osnabrück, Osnabrück, Germany. [*] = corresponding author: tafesse@ohsu.edu

This review was repurposed from its original publication in the Journal of Fungi, and can also be read here: https://doi.org/10.3390/jof6010019

8.1. Abstract

Fungal infections remain a global health threat with high morbidity and mortality. The human immune system must, therefore, perpetually defend against invasive fungal infections. Phagocytosis is critical for the clearance of fungal pathogens, as this cellular process allows select immune cells to internalize and destroy invading fungal cells. While much is known about the protein players that enable phagocytosis, the various roles that lipids play during this fundamental innate immune process are still being illuminated. In this review, we describe recent discoveries that shed new light on the mechanisms by which host lipids enable the phagocytic uptake and clearance of fungal pathogens.

8.2. Introduction

Humans must maintain a balletic coexistence with a variety of environmental fungi, such as *Candida albicans*, which are ubiquitous in the environment and common commensal members of the human microbiome but are primed for opportunistic pathogenicity. Alongside *Candida*, the genera *Aspergillus* and *Cryptococcus* continuously challenge the human immune system. Resultantly, a host of innate immune mechanisms act in concert to sense and combat fungal infections. Phagocytosis is a central mechanism in the clearance of pathogens in which designated innate immune cells use receptors to recognize pathogen-associated molecular patterns displayed on fungal cell walls. Once internalized, the pathogen is destroyed in a microbicidal vacuole called the phagolysosome. A large body of literature delineates the duality of the fungal lifestyle, as well as the interactions between fungal pathogens and the human immune system[486,487]. However, the roles of host lipids during the resolution of fungal infections remain poorly understood. Here, we summarize and discuss the state of the current knowledge about the interplay between the host lipids and fungi during infection. We specifically focus on recent findings that show that sphingolipid and phosphoinositide metabolism is critical in enabling the phagocytosis and the subsequent phagolysosomal degradation of fungal pathogens. This summary presents several manners in which lipids are known to play essential roles during phagocytosis.

8.3. The Offense

Three genera are responsible for the majority of fungal infections: *Candida*, *Aspergillus*, and *Cryptococcus*. Species of these genera are ubiquitous in the environment and are common constituents of the human microbiome. Primarily, they exhibit their opportunistic pathogenicity in immunocompromised individuals[487]. *Candida* species such as *C. albicans* maintain two morphologies, a yeast form associated with commensalism and a hyphal form associated with virulence. *Candida* species are most-commonly associated with vulvovaginal candidiasis but systemic infections are common in hospitalized patients, with candidemia ranked at the 10th most common bloodstream infection[486,488]. Among the *Aspergilli*, *A. fumigatus* is the most common species to cause infection. *A. fumigatus* is an airborne pathogen that has few pathological effects on immunocompetent hosts, but can rapidly progress to a fatal invasive pulmonary aspergillosis in individuals undergoing immunosuppressive therapies. *Cryptococci* are also highly prevalent in the environment, and species such as *C. neoformans* can initiate a pulmonary infection, which progresses to a lethal meningitis in immunocompromised hosts.

While antifungal therapies have been effective in the past, resistance is increasingly emerging. For extensive appraisal on the changing epidemiology of invasive fungal infections, we direct readers to the 2017 reviews by Enoch et al. and Benedict et al.[489,490].

8.4. The Defense

An invasive fungal infection begins with penetration of a barrier surface, such as the lung, intestinal, or vaginal epithelium, followed by systemic dissemination. Consequently, the innate immune defenses are layered to catch incipient infections first at these barrier sites and then at centralized

sites such as the liver and spleen. The primary cell types responsible for clearing a fungal infection are phagocytes such as macrophages, dendritic cells, and neutrophils.

Immune surveillance is conducted at epithelial surfaces by a defense network of resident macrophages and dendritic cells. These cells express an array of germline-encoded pattern recognition receptors (PRRs), which recognize a variety of pathogen-associated molecular patterns (PAMPs). Table 8.1 depicts the list of the main PRRs known to recognize fungus-specific PAMPs. Upon ligand engagement, these receptors are broadly responsible for initiating pro-inflammatory cytokine responses and phagocytic uptake of the invading fungus. Following inflammatory activation by macrophages and dendritic cells, neutrophils are rapidly recruited to the site of barrier breach. These cells are the so-called "first responders" of the innate immune system, and are significantly primed for antimicrobial activity.

Table 8.1. – Fungus-specific pattern recognition receptors and their cognate molecular patterns

PRR	PAMP	References
Mannose receptor	Mannan, mannoproteins	[491,492,493,494]
Dectin-1	β-1,3 glucan	[494,293,495,496,497]
Dectin-2	α-mannans	[487,497]
Mincle	α-mannose	[494,497,498,499]
DC-SIGN	Galactomannans	[500,497,501]
Galectin-3	β-1,2 mannosides	[494,502]
Complement receptor 3	C3b, β-glucans	[494,503]
Toll-like receptor 2	Chitin and other polysaccharides	[494,504,505]
Toll-like receptor 4	O-linked mannosyl residues	[506]

After the killing of the fungal cell, the phagocyte finds itself with a surfeit of uniquely fungal molecular components that may be used to train the adaptive immune repertoire to prime the host for defense against future infection. To this end, the phagocyte loads phagolysosomal detritus onto antigen-presentation complexes in order to direct clonal selection of antigen-specific T cells. The most well-known of these complexes are the class I and II major histocompatibility complexes (MHC-I and –II, respectively), which are loaded with peptides. However, a parallel series of antigen presentation complexes, the CD1 family, allows for the presentation of lipid structures in order to drive clonal selection of natural killer T cells (NKT)[507,508]. Kawakami et al. showed in 2001 that these NKT cells promote the development of an antigen-specific Th1 cell response and enhance resistance to *C. neoformans* reinfection[509]. Of particular note, Albacker et al. were the first to identify a fungal glycolipid which directly activates NKT cells via presentation on CD1; this lipid species was the glycosphingolipid asperamide B, isolated from *A. fumigatus*[510]. Thus, the presentation of fungal lipids to the adaptive immune compartment is an important component of host defense against future exposure to pathogenic fungi.

Seminal works by Bird et al. in 1970, Baine et al. in 1974, and Sawyer et al. in 1976 show that specialized macrophages in the liver, spleen, and lymph system are essential for clearing fungal pathogens from the bloodstream and interstitium in simulated systemic infections[511–513]. Thus, multiple layers of defense protect an immunocompetent host from fungal infections, both localized and systemic. Despite their distinct roles, macrophages, dendritic cells, and neutrophils all employ phagocytosis as a central mechanism for clearing fungal pathogens. As will be discussed below, lipids play essential roles in the uptake and clearance of pathogenic fungi.

8.5. Phagocytosis: The Weapon of Choice

Phagocytosis is a form of receptor-mediated endocytosis characterized by its dependency on actin cytoskeletal rearrangement, and its ability to mediate the internalization of particles larger than 0.5 μm in diameter[258]. Following internalization, the ingested particle or fungal cell encapsulated in the phagosome undergoes sequential maturation stages until it terminally fuses with the lysosome to form the phagolysosome, and is therein destroyed. The process of uptake involves highly orchestrated signaling interactions between GTPases, tyrosine and serine/threonine kinases, phospholipases, cytoskeletal components, and lipid species such as phosphoinositides[99,258]. While phagocytosis has been studied extensively over the last century, significant knowledge regarding the roles of lipids during this essential immunological process has been gleaned only recently. Intuitively, dramatic membrane reorganization must occur for the internalization of particles >0.5 μm in diameter, but techniques and tools which visualize these membrane dynamics are relatively recent advents for biologists[514].

Macrophages and dendritic cells constitutively sample and probe their environment using actin-driven protrusions. If a phagocytic receptor engages its cognate ligand on a particle, it tethers that particle to the cell and more receptors engage to form a signaling platform known as the "phagocytic synapse"[495]. This signaling platform closely resembles the specialized membrane microdomains known as lipid rafts. Proteomics studies of the phagosome revealed several proteins associated with isolated detergent-resistant membrane domains (one functional definition of a lipid raft), and the signaling capacity of the fungal receptor Dectin-1 was shown to be sensitive to treatment with the lipid raft-disrupting methyl-β-cyclodextrin[451,515,516]. As depicted in Figure 8.1A, both sphingomyelin and cholesterol are essential lipid components of lipid rafts, and are believed to be enriched to the phagocytic synapse. Of particular note, fluorescent sphingomyelin analogs reported by Kinoshita et al. in 2017 allow for the visualization of sphingomyelin in raft domains, and were used to demonstrate that sphingomyelin is recruited to the phagocytic synapse of IgG opsonized particles[453,517].

Similarly, we and others demonstrate that sphingolipid biosynthesis is essential for phagocytic uptake and clearance of *C. albicans* and other microbial pathogens[179,205,297,518]. In particular, we demonstrated evidence that sphingolipid biosynthesis is essential for formation of the phagocytic synapse upon contact with Zymosan A, a model particle for fungal cells composed of β-1,3-glucans. In sphingolipid-deficient cells, we observe that the phagocytic receptor Dectin-1 and the anti-phagocytic phosphatase CD45 remain colocalized at the contact site[179]. Thus, membrane order and composition at the phagosomal synapse have significant influences on the clearance of fungal pathogens.

Signaling lipids such as phosphatidylinositides are known to directly participate in the phagocytic signal cascade. Figure 1B depicts the interconversion of phosphatidylinositide species during phagocytosis. Briefly, phagocytic receptor aggregation at the phagocytic synapse induces a potent phosphorylation cascade which begins with the activation of tyrosine kinases, followed by the extension of actin-rich membrane protrusions, and culminates in actin disassembly and internalization of the particle[293,515,519]. One such tyrosine kinase, Syk, activates several enzymes that modify phosphatidylinositol-4,5-bisphosphate (PIP2), such as phosphatidylinositol-3 kinase (PI3K) which converts PIP2 to phosphatidylinositol-3,4,5-trisphosphate (PIP3), and phospholipase Cγ which produces diacylglycerol and soluble inositol(1,4,5)-trisphosphate (IP3)[520]. PIP3 serves as a membrane anchor and recruitment signal for proteins essential for phagocytic uptake[521]. For example, both the actin nucleation promoter Scar/WAVE and MyosinX contain so-called Plekstrin Homology (PH)

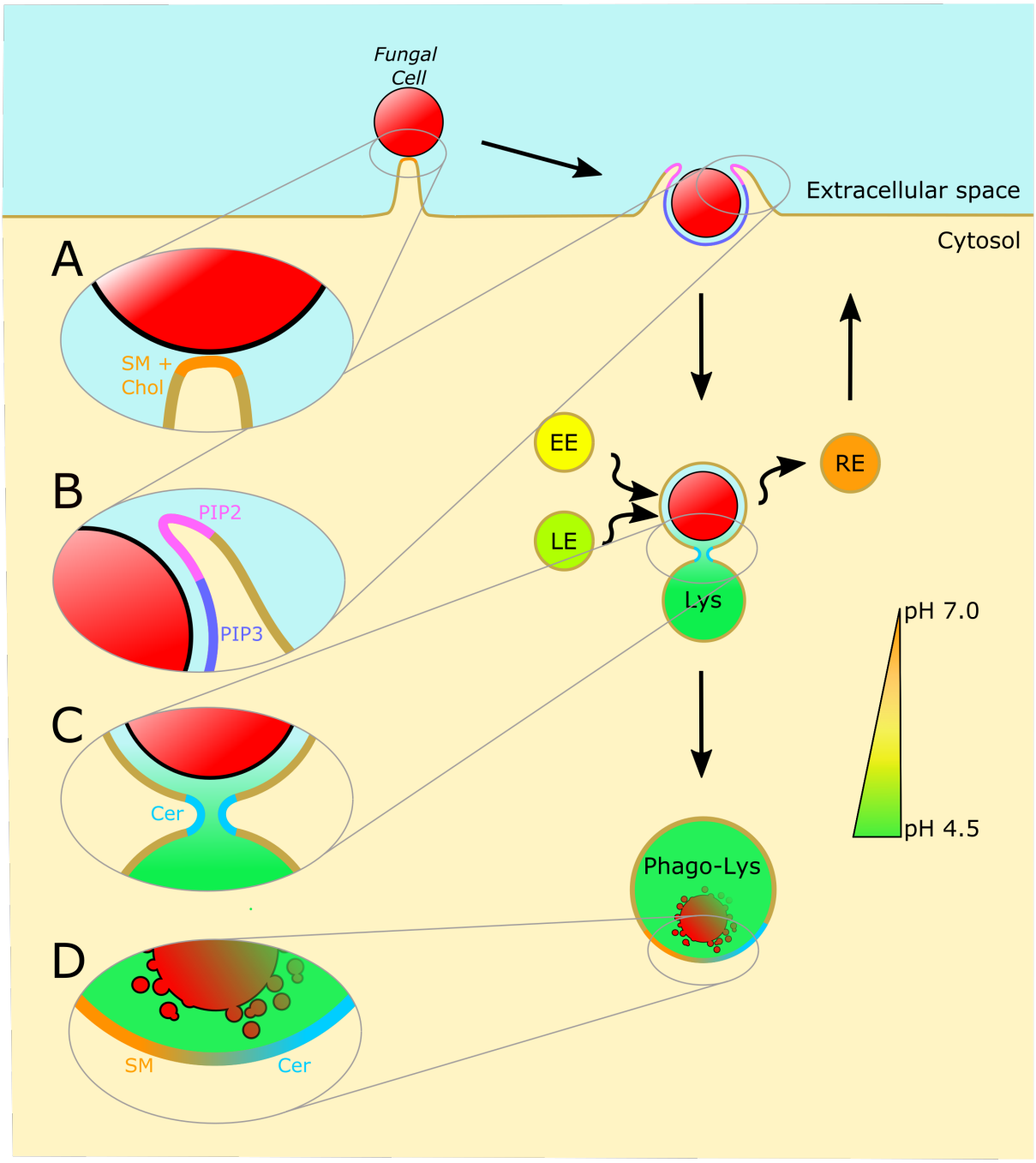


Figure 8.1. – **Host lipids are critical for the uptake and destruction of fungal pathogens.** A simplified depiction of several stages at which lipids are known to be essential for the clearance of fungi by phagocytic immune cells. (A) Upon the initial recognition of a fungal cell, pathogen recognition receptors cluster in a microdomain reminiscent of a lipid raft. This domain is enriched in sphingomyelin (SM) and cholesterol (Chol), and serves to form a signaling platform from which the phagocytic process is coordinated. (B) The turnover of phosphoinositide species is essential to the extension of pseudopodia around a particle. Emanating from the signaling platform at the center of the phagocytic synapse is a leading wave of PIP2, followed by a trailing wave of PIP3. High levels of PIP2 initiate filamentous actin polymerization and thereby initiate the actin-driven protrusion which extends the pseudopodia. The conversion of PIP2 to other lipid species such as PIP3 is essential for actin disassembly and recycling. (C) After internalization, lipids such as ceramide (Cer) are essential for the fusion and fission of the phagosome with the compartments of the endosomal pathway, such as the early endosome (EE), late endosome (LE), recycling endosome (RE), and lysosome (Lys). (D) After fusion with the lysosome, the degradation of sphingomyelin to ceramide is essential for the activation of lysosomal components such as cathepsins, which cooperate to destroy the fungal cell.

domains with high affinity for PIP3, meaning that the Syk-dependent activation of PI3K directly results in the recruitment of these cytoskeletal elements to the membrane[257]. Similarly, soluble IP3 serves as a secondary messenger that induces calcium flux from the endoplasmic reticulum. Evidence suggests that the resulting cytosolic burst of calcium is essential for the maturation of the phagosome and the lysosome, and PIP2 metabolism is thereby central to the antimicrobial activity of phagocytes[522,523].

Lipid metabolism also plays essential roles in modulating the fluidity and curvature of the plasma membrane at the phagocytic synapse. Early evidence by Hauck et al. shows that the activity of acid sphingomyelinase (ASM) is essential for uptake of the bacterial pathogen *Neisseria gonorrheae*[524]. A potential explanation for the role of sphingomyelin-derived ceramide during phagocytosis may lie in the well-known role ceramide has in inducing negative membrane curvature and vesicular budding[133,525]. Sphingomyelin has a characteristic cylindrical shape and preferentially maintains rigid, planar membrane structures such as raft-like domains, whereas ceramide's small headgroup induces invaginating membrane structures[133]. Similarly, the conversion of phosphatidylcholine to phosphatidic acid by phospholipase D during phagocytosis has been suggested to directly induce negative membrane curvature and thereby enhance the internalization of pathogens such as fungi[115,267]. Alternatively, it has been suggested that, at high localized concentrations, ceramide can assemble in hexagonal phase II structures in which the membrane bilayer is disrupted and becomes highly flexible. These two mechanisms may together explain the pro-fusion effect of ceramide production during phagosomal maturation[133].

8.6. The Phagolysosome: The Final Stage for Eliminating Fungal Pathogens

Phagocytic uptake alone is not sufficient for an innate immune cell to destroy an invasive fungal pathogen; this task is consigned to the lysosome. Following uptake, the fungus-containing phagosome is trafficked along the endocytic pathway, gradually becoming more acidic before fusing with the lysosome[99,116,526]. The resulting phagolysosome is a hostile environment that serves to degrade the phagosome contents to base molecular components. Few organisms are capable of surviving the extremely acidic pH, protease and nuclease activity, reactive oxygen and nitrogen species, pore-forming peptides, and metal ion depletion within the lysosome [55]. Significant evidence demonstrates that lipid metabolism plays essential roles throughout phagosomal maturation[133,296,527]. In particular, several lysosomal storage disorders are associated with high susceptibility to fungal infections.

The maturation of the phagosome requires a number of membrane fission and fusion events which are significantly dependent on the activity of lipid metabolizing enzymes. For example, extensive reviews describe the role of phosphoinositides as a coordinator of phagosome maturation[99,257,528,529]. The small GTPase Rab5 is quickly recruited to the newly-formed phagosome, and directly activates the class III phosphatidylinositol 3-kinase human vacuolar protein-sorting 34 (hvPS34). This kinase converts phosphatidylinositol to phosphatidylinositol-3-phosphate, which serves as a membrane anchor for proteins containing either PX (phagocytic oxidase) domains or FYVE (Fab1, YOTB, Vac 1, and EEA1) domains. One such FYVE-domain-containing protein is the early endosome antigen 1 (EEA1), which serves as a bridge to the early endosome by interacting with syntaxin 13, a member of the SNARE family of membrane fusors. Because phosphatidylinositol-3-phosphate production is essential for coordinating the interaction between EEA1 on the newly-formed phagosome and

syntaxin 13 on the early endosome, this phosphoinositide plays a direct role in the maturation of the phagosome[99,257,528,529]. Phosphoinositides are not the only lipid family required for proper phagosome maturation. As depicted in Figure 8.1C, the regulated conversion of sphingomyelin to ceramide by ASM within the maturing phagosome is essential for its propensity for fusion between the early and late endosomes and the lysosome[133].

Lipid metabolism continues to be essential for the neutralization of phagocytosed pathogens even after fusion with the lysosome. For example, it is well known that lysosomal ceramide interacts with and activates the aspartyl protease Cathepsin D[530]. The Ramakrishnan group has shown that lysosomal ceramide produced by ASM is required for the activation of Cathepsin D in a mycobacteria-induced necrosis circuit[234,275]. This role for the conversion of sphingomyelin to ceramide is depicted in Figure 8.1D. Lipidomic analysis of the composition of the maturing phagosome showed that the total levels of sphingomyelin decrease as the phagosome travels along the endocytic compartment, and there is sparingly little sphingomyelin by the time the phagosome merges with the lysosome[531]. Concordantly, patients with disorders associated with deficiencies of ASM function, such as Niemann Pick Disease of types A and B, are highly susceptible to recurrent infection by bacterial and fungal pathogens, as these patients are unable to efficiently eliminate pathogens after internalization[267,296].

In a related example, the genetic disorder cystic fibrosis culminates in an overabundance of ceramide in the lysosome due to improper regulation of ASM and acid ceramidase activities[296]. These individuals have an increased risk of chronic or recurrent infections by bacterial and fungal pathogens. It was shown that treatment with the ASM inhibitor amitriptyline normalized the balance of ceramide in the lysosome and prevented the chronic pulmonary inflammation and reversed susceptibility to P. aeruginosa in mouse models[527]. Thus, genetic disorders with opposing effects on ASM activity may result in the convergent phenotype of increased susceptibility to infection, highlighting the tight regulation on lipid metabolism required for proper clearance of infection.

8.7. Conclusions and Perspectives

Invasive fungal infections by *Candida*, *Aspergillus*, and *Cryptococcus* species are a developing public health concern. While these opportunistic pathogens largely act as benign environmental fungi or commensals in immunocompetent humans, they pose a significant risk to immunocompromised individuals. As modern medicine progresses, the prevalence of patients on immunosuppressive therapies such as organ transplant recipients and those with latent retroviral infections is increasing. As such, invasive fungal infections are poised to become a significant health crisis. The vignettes presented in this review are intended to highlight several of the well-known manners in which lipids are critical for the uptake and clearance of fungal pathogens. Recent years have shown that sphingolipids and phosphoinositides serve both as essential regulators of membrane fluidity and structure and potent signaling molecules.

Many open questions remain regarding the mechanisms by which pathogenic fungi may usurp host lipid metabolism pathways to effectively establish infection. Further studies are required to define the exact roles of myriad host lipid species in fungal pathogenesis and host immunity. Recent work has demonstrated that lipids found on the surface of the bacteria Mycobacterium tuberculosis may directly influence the fluidity of the host phagocyte's plasma membrane during uptake [64], but no work has yet been reported that would suggest that fungal lipids may play a similar direct role in

influencing host membrane architecture. Similarly, many non-fungal pathogens are known to influence host lipid metabolism networks[176,215,272], but little is known whether fungi similarly influence host lipid metabolism.

It is likely that many new findings will come to light in the coming years. With the burgeoning of the biologists' toolset, there is growing recognition that lipids are not merely the inert building blocks of membranes but rather active interaction partners and signaling molecules. A greater understanding of innate immunological mechanisms might provide insights into how immune cells utilize effector molecules such as lipids to selectively destroy invading fungi, which may, thus, reveal novel mechanisms for anti-fungal therapies.

8.8. Funding, Contributions, Acknowledgments, and Conflicts of Interest

8.8.1. Funding

This research was funded by the NIH grant R21AI124225 and R21AI133631 (F.G.T.); the NIH T32 Program in Enhanced Research Training (PERT; G.G.).

8.8.2. Contributions

GG compiled the concepts and references discussed in this review and wrote the review. PN provided assistance in structuring this review and text edits. FGT oversaw the preparation of this review and provided text edits.

8.8.3. Acknowledgements

Many thanks to the peers and partners who helped edit and refine this review—in particular, we would like to acknowledge Dr. Joost Holthuis and Madeleine Faucher.

8.8.4. Conflicts of Interest

The authors declare no conflict of interest. The funders had no role in the design of the study; in the collection, analyses, or interpretation of data; in the writing of the manuscript, or in the decision to publish the results.

Chapter 9.

Rapid visualization and quantification of phagocytosis in neutrophils

Authors: Gaelen Guzman[1], Fikadu G. Tafesse[1,*]

[1] = Department of Molecular Microbiology and Immunology, Oregon Health & Science University, Portland, Oregon, USA. [*] = corresponding author: tafesse@ohsu.edu

This methods article was published in Neutrophils: Methods and Protocols and can be found here: DOI: https://doi.org/10.1007/978-1-0716-0154-9_11

9.1. Abstract

Phagocytosis by phagocytes such as neutrophils is a crucial part of the host innate immune response against invading pathogens. Phagocytosis is a complex process that initiates with the binding of the particles on the cell surface of the phagocytes through the interaction of pattern recognition receptors with ligands on the surface of the pathogens. During this process, phagocytes undergo extensive membrane reorganization and cytoskeleton rearrangement at their cell surface. To gain better insight about the molecular mechanisms of this dynamic cellular process, visualization and quantification in a high-throughput manner is essential. Here, we describe a microscope-based method to visualize and quantify phagocytic uptake of pathogens (such as bacteria and fungi) and model particulates that are larger than 0.5 μm (such as Zymosan A and IgG-coated beads).

9.2. Key words

Neutrophils, phagocytosis, fluorescence microscopy, high-throughput, phenotypic analysis

9.3. Introduction

Neutrophils represent a first line of defense when the body encounters a pathogen. These cells are capable of rapid chemotaxis to sites of bodily damage – they are some of the fastest cells in the mammalian body, and are commonly referred to as "the first responders" upon the initiation of an inflammatory signal[532,533]. Once at an inflamed site, neutrophils are highly versatile in their anti-pathogenic response: they produce cytokines to induce a hostile environment for invading pathogens, they play roles in the activation and direction of the adaptive immune response, they modulate inflammation, and they directly act with potent microbicidal effect[532–536]. Understanding the mechanisms through which neutrophils respond to pathogenic invasion can give insight into how an infection is resolved – and understanding these mechanisms may allow for the implementation of therapeutic tools to enhance or direct the neutrophil response.

Of particular importance, neutrophils wield phagocytosis to destroy would-be pathogens, as well as effete cells and debris[537]. Phagocytosis is a form of receptor-mediated cellular uptake that allows a cell to ingest particles greater than 0.5 μm in size[258]. This cellular process has been well studied, but there remain open questions regarding the mechanisms and signaling events that drive the dramatic changes in membrane reorganization, cell morphology, cytoskeleton remodeling, and membrane lipid composition that must ensue for the complete ingestion of a pathogen or particulate. A host of techniques allow for the assessment of phagocytic capacity, but many are limited to gross overviews of internalization (e.g., antibiotic protection assays) or lack the speed necessary for high-throughput phenotypic screens.

Here, we present a methodology for rapidly visualizing and quantifying the phagocytic capacity of neutrophils using high-content imaging microscopy (Figure 9.1). As the HL-60 neutrophil-like cell line is a classical staple of neutrophil study[533,538,539], we focus on this line herein—however, these techniques are equally applicable to the study of primary neutrophils isolated from mouse or human peripheral blood . Similarly, any number of fluorophore-conjugated model particle or fluorescent reporter strain of pathogenic microbe may be used under this paradigm[205,306]. Through the use of fluorescent phagocytic particles and a cell membrane stain, one may rapidly acquire visual data sufficient to calculate the rate of phagocytic uptake of many hundreds or thousands of cells across experimental conditions. Combining a well-plate format and automated, high-content image acquisition, this technique allows for high-throughput phenotypic analysis following genetic or chemical screens.

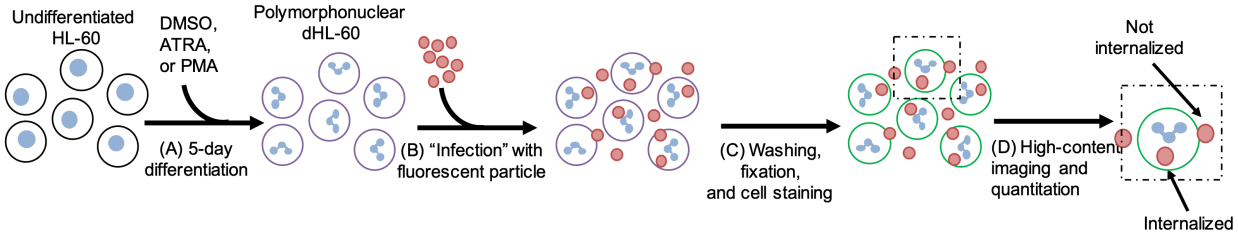


Figure 9.1. – An overview of the experimental workflow described in this methodology. (a) Induce polymorphonuclear differentiation of cultured HL-60 cells using 5-day treatment with one of the following: DMSO, ATRA, or PMA . Plate on polylysine-coated imaging surface. (b) Add fluorescent phagocytic particles to cells at a multiplicity of infection of approximately 1:10. (c) Wash unbound particles, fix using 4% paraformaldehyde, and stain using fluorescent cell boundary marker and nuclear stain. (d) Collect high-content images of "infected" cells using fluorescence microscopy . Uptake rate = (Number of InternalizedParticles)/(Number of NucleatedCells).

9.4. Materials

1. HL-60 peripheral blood promyeloblasts (ATCC) (Section 9.6.0.1).
2. Growth medium: RPMI 1640 supplemented with 10% fetal calf serum, nonessential amino acids, and optional antibiotics/antimycotics.
3. Phosphate-buffered saline (PBS).
4. Differentiation medium: Growth medium supplemented with 1.2% DMSO (v/v) (Section 9.6.0.1).
5. Imaging surface:
   (a) *Option 1:* Senso Microplate glass-bottom 96-well plate (Greiner Bio-One).
   (b) *Option 2:* Microscope coverslips(1.2 cm diameter) and standard 24-well plate.
6. 20× poly-L-lysine coating solution: 50 mg poly-L-lysine in 50 mL diH2O, filter through a 0.22 µm filter. Dilute in H2O for a 1× working stock.
7. Model phagocytic particle (Section 9.6.0.2):
   (a) *Option 1:* Zymosan A (S. cerevisiae) Bioparticles™ Alexa Fluor™ conjugate (Thermo Fisher Scientific; multiple fluorescence choices).
   (b) *Option 2:* Fluoro-Max™ Fluorescent Carboxylate-Modified Particles (Thermo Fisher Scientific).
   (c) *Option 3:* Mycobacterium tuberculosis H37Rv (ATCC 25618) expressing mCherry reporter (or another fluorescent reporter microbe).
8. 4% paraformaldehyde solution
9. Permeabilization/blocking buffer: 1% bovine serum albumin (w/v) and 0.1% Triton-X100 (v/v) in PBS.
10. Cell surface stain (Section 9.6.0.3): Phalloidin Alexa Fluor™ (e.g., Thermo Fisher Scientific; multiple fluorescence options) in permeabilization/blocking buffer at approximately 1:50 dilution (titration may be necessary).
11. Nuclear stain (Section 9.6.0.3): DAPI (4□,6-diamidino-2-phenylindole) in PBS at approximately 1µg/mL (titration may be necessary).

9.5. Methods

9.5.1. Differentiation of HL-60 Cells into Granulocytic Neutrophils

1. Grow HL-60 cells in growth media using standard tissue culture techniques. When cultured cells reach a density of approximately 1×10^6 cells/mL, replace growth media with an equal volume of differentiation media (Section 9.6.0.1).
2. Incubate cells at 37 °C and 5% CO2 for at least 5 days to obtain fully differentiated HL-60 (dHL-60) cells (Section 9.6.0.4).

9.5.2. Immobilization of dHL-60 Cells to Glass-Bottom Plate or Coverslip

1. Coat desired imaging surface (96-well plate, coverslips, etc.) according to steps below (Section 9.6.0.5)[540].
2. Add 1× polylysine solution to sterile multi-well plates or coverslips and incubate at 37 °C for 1 h.
3. Aspirate polylysine solution and leave to dry. Plates and coverslips may be kept at 4 °C.
4. From cultured dHL-60 cells, isolate an appropriate number of cells to your preferred imaging surfaces (Section 9.6.0.6, Section 9.6.0.7).
5. Resuspend cells in the minimum volume to cover surface of the well (approximately 50 µL for 96-well and 250 µL for 24-well plate), and add cells to the appropriate wells.
6. Centrifuge cells in plate for 5 min at 250 × g, and allow the cells to recover in differentiation media at 37 °C and 5% CO2 for at least 1 h (or overnight) to maximize immobilization.

9.5.3. Phagocytosis of Phagocytic Particles by dHL-60

1. Isolate an appropriate number of phagocytic particles for a multiplicity of infection (MOI) of approximately ten particles per cell.
2. Resuspend in growth medium or PBS at the minimum volume to cover the surface of the well (approximately 50 µL or 250 µL for 96- and 24-well respectively).
3. Particle solution may be sonicated for 5–10 min in a water bath or passed through a narrow-gauge syringe needle 10–20 times to reach a single-particle suspension.
4. Aspirate growth media from cells affixed to well-plate, wash gently with PBS, and add resuspended particle solution to the cells. Centrifuge plate for 1 min at 250 × g to sediment the particles to the bottom of the well.
5. Incubate cells and particles at 37 °C and 5% CO2 for 10 min (Section 9.6.0.8).
6. Gently wash cells twice with PBS to remove unbound particles.
7. Fix cells using ice-cold 4% paraformaldehyde solution for 30 min on ice. After fixation, remove formaldehyde solution and hydrate wells with PBS. Plate may be stored at 4 °C for up to a week after fixation, although it is recommended to proceed with staining as early as possible.

9.5.4. Fluorescent Cell Staining

1. If using phalloidin (Section 9.6.0.3): aspirate PBS, and treat cells for 15 min with permeabilization/blocking buffer.
2. Remove permeabilization/blocking buffer, add cell surface stain, and incubate for approximately 1 h at room temperature under cover from light (Section 9.6.0.9.
3. Remove cell surface stain solution and wash twice with PBS.

4. Stain nuclear DNA using nuclear staining solution for 10 min at room temperature under cover from light (Section 9.6.0.3).
5. Remove nuclear staining solution and wash twice with PBS. Leave cells in PBS under cover from light until imaging is completed.
6. If using a 96-well plate, imaging may be performed with no further preparation. If using glass coverslips, follow the steps below to mount the slips to microscopy slides.
7. On clean microscopy slide, pipette a single droplet (~15 μL) of anti-fade mounting medium and carefully place coverslip cell-side down on top of this droplet, taking care to minimize air bubbles.
8. It is recommended to use a lacquer to glue down the coverslips and prevent drying. Standard clear nail polish is a sufficient affixation agent.
9. Allow lacquer to fully dry before imaging .

9.5.5. Image Acquisition

1. Regardless of acquisition setup (Section 9.6.0.10), optimize parameters for excitation and exposure times for the respective fluorophores used in the experimental workflow.
2. We recommend image collection at 10× or 20× magnification to maximize the total number of cells captured per image. It is best to capture at least 500 cells across the majority of the well or coverslip per technical replicate per experimental condition.
3. For optimal quantification, images should be collected in a plane such that the nucleus, cell boundary, and any internalized beads are all clearly distinguishable across the relevant channels with minimal background and inter-channel fluorescence.

9.5.6. Image Analysis (Quantification)

1. To analyze images, identify the total number of cells captured per image and the number of fluorescent particles fully internalized (Section 9.6.0.11).
2. If using a manual counting method, count the number of nuclei cells and internalized beads per image.
3. If using an automated or semiautomated counting method, define threshold parameters for each fluorescent channel, and apply the same parameters for every experimental condition within a biological replicate.
4. Calculate rate of phagocytic uptake by aggregating the total number of internalized particles and dividing by the total number of isolated cells for every technical replicate across every experimental condition. Technical replicates may be aggregated to report a single uptake rate for every biological replicate.
5. Normalization between biological replicates may be necessary to compensate for inter-experimental variability.

6. Uptake rates may be reported as box- or dot-plots and differences between experimental condition may be assessed using a two-tailed, unpaired Student's T-test.
7. Alternatively, one may depict uptake rate using a histogram or violin-plot to represent the number of beads internalized per cell in order to visualize the distribution of uptake events across experimental conditions.
8. Differences between experimental conditions may be assessed using a discrete nonparametric test, such as the Chi-squared test or the Kolmogorov–Smirnov Test.

9.6. Footnotes

9.6.0.1. Footnote 1

HL-60 cells are derived from peripheral blood leukocytes isolated from a patient with acute promyelocytic leukemia, and can be differentiated into granulocytic neutrophil-like cells using 5-day treatments with DMSO, all trans-retinoic acid (ATRA), or phorbol 12-myristate 13-acetate (PMA)[533,538,541,542]. It is advisable to titrate concentrations of activating agent to identify the optimal differentiation conditions in one's own laboratory. Spontaneous, non-granulocytic differentiation can occur in the absence of activating reagents, and it is recommended to limit passage number to avoid spurious differentiation[538].

9.6.0.2. Footnote 2

One may select from a range of model phagocytic particles. This methodology requires only that the selected model particle is fluorophore-conjugated/labeled. Common models include: Zymosan A (which consists of a fungal glycan that acts as ligand to the pathogen recognition receptor Dectin-1), opsonized and non-opsonized silica beads (which act as ligands for FCγR and CR3, respectively), and live or heat-inactivated fluorescent reporter strains of bacteria such as *Salmonella enterica* Serovar Typhimurium or *Mycobacterium tuberculosis* (which are both decorated with ligands for a host of pathogen recognition receptors)[289,543].

9.6.0.3. Footnote 3

It is necessary to select cellular and nuclear stains with compatibility with the fluorescently labeled model phagocytic particle. We recommend phalloidin, a fungus-derived toxin that effectively stains filamentous actin. Phalloidin may be purchased as a fluorophore-conjugated cell boundary marker in multiple ranges of excitation/emission.

9.6.0.4. Footnote 4

Differentiated HL-60 cells will remain in suspension, and previous reports suggest that dHL-60 cells will die through apoptosis beginning on day 8 of treatment[541,542]. If performing genetic or chemical screens, it is recommended that transfection/transduction or treatment begin during the 5-day differentiation period such that cells are prepared for phagocytosis analysis by day 5.

9.6.0.5. Footnote 5

Poly-L-lysine coating may be used to affix dHL-60 cells to imaging glassware. Such coated products are available for purchase (See Materials 9.4), or may be prepared in-house as described previously[540].

9.6.0.6. Footnote 6

We recommend seeding approximately 2×10^4 cells when using a 96-well glass-bottom imaging plate, and approximately 5×10^4 cells when using 24 mm diameter coverslips in a standard 24-well plate.

9.6.0.7. Footnote 7

It is highly recommended to perform this uptake assay with multiple technical replicates, with differentiation and uptake assays performed on independent days for each biological replicate. Experimental conditions should be assayed in parallel for every biological replicate, as significant variation may occur between replicates.

9.6.0.8. Footnote 8

Exact uptake time may need to be optimized: 10 min may be too long if cells are highly activated, and one is characterizing a weak phenotype, or too short if the model phagocytic particle is taken up poorly. It is recommended to optimize this timing using a three- or four-point time course on wild-type cells.

9.6.0.9. Footnote 9

As with many staining protocols, it may be necessary to modulate both the concentration of staining reagent and the time to maximize signal and minimize background.

9.6.0.10. Footnote 10

Images for phagocytic analysis may be collected on a range of acquisition platforms—so long as the microscope has the excitation/detection capacities to capture the fluorophores used, it ought to be sufficient for this methodology. We recommend the KEYENCE BZ-X700 all-in-one fluorescence microscope (KEYENCE) due to its capacity for semiautomated image acquisition and multi-field image stitching.

9.6.0.11. Footnote 11

A number of image analysis software tools with compatible cell counting protocols are available, including CellProfiler (open access), FIJI (open access), Imaris (Oxford Instruments), and KEYENCE BZ-X Analyzer (KEYENCE). It is notable that a semiautomated cell counting tool is preferable to manual counting for enhanced throughput and reduced user bias.

9.7. Contributions

GG compiled the concepts and references reviewed and wrote this methods chapter. FGT provided text edits and oversaw the design of this methods chapter.

Chapter 10.

Systematic analysis of the sphingomyelin synthase family in *C. elegans*

Authors: Gaelen Guzman[1], Scotland E. Farley[1], Lisa Bramer[2], Jennifer Kyle[2], Sandra Hoeltzl[3], Joep van den Dikkenberg[3], Joost C.M. Holthuis[3], Fikadu G. Tafesse[1,*]

[1] = Department of Molecular Microbiology and Immunology, Oregon Health & Science University, Portland, Oregon, USA. [2] = Pacific Northwest National Laboratories, Integrative Omics Core, Richland, Washington, USA. [3] = Molecular Cell Biology Division, Department of Biology and Chemistry, University of Osnabrück, Osnabrück, Germany. [*] = corresponding author: tafesse@ohsu.edu

This chapter has been uploaded to bioRxiv and is pending review; it can be found here: https://doi.org/10.1101/2023.07.25.550547

10.1. Abstract

Sphingomyelin (SM) is a major component of mammalian cell membranes and particularly abundant in the myelin sheath that surrounds nerve fibers. Its production is catalyzed by SM synthases SMS1 and SMS2, which interconvert phosphatidylcholine and ceramide to diacylglycerol and SM in the Golgi and at the plasma membrane, respectively. As the lipids participating in this reaction fulfill both structural and signaling functions, SMS enzymes have considerable potential to influence diverse important cellular processes. The nematode *Caenorhabditis elegans* is an attractive model for studying both animal development and human disease. The organism contains five SMS homologues but none of these have been characterized in any detail. Here, we carried out the first systematic analysis of SMS family members in *C. elegans*. Using heterologous expression systems, genetic ablation, metabolic labeling and lipidome analyses, we show that *C. elegans* harbors at least three distinct SM synthases and one ceramide phosphoethanolamine (CPE) synthase. Moreover, *C. elegans* SMS family members have partially overlapping but also unique sub-cellular distributions and together occupy all principal compartments of the secretory pathway. Our findings shed light on crucial aspects of sphingolipid metabolism in a valuable animal model and opens avenues for exploring the role of SM and its metabolic intermediates in organismal development.

10.2. Introduction

Sphingolipids are a structurally diverse class of membrane lipids that co-emerged with sterols during the evolution of eukaryotes. They typically represent ~15% of cellular lipids and are highly enriched in the plasma membrane where they modulate key physical membrane properties, including fluidity, thickness, and curvature[544]. Their affinity for cholesterol and ability to self- associate into laterally segregated membrane microdomains that selectively concentrate or exclude membrane proteins to form dynamic platforms that modulate a range of key physiological processes, from phagocytosis and antigen recognition by T cells to synaptic transmission in neurons[547]. Other sphingolipid species serve as potent signaling molecules; for example, the recently characterized sphingolipid rheostat acts as a central regulator of cell fate: high levels of ceramide (Cer) initiate autophagy and cell death, whereas the conversion of Cer to sphingosine- 1-phosphate (S1P) promotes cell survival and is protective against starvation-induced apoptosis[548]. However, fundamental questions remain regarding the mechanisms which regulate and mediate the synthesis and metabolism of sphingolipids. The complexity of the sphingolipid metabolic cascade makes it difficult to study this lipid class in higher organism. Thus, understanding the mechanisms of sphingolipid regulation in model organisms such as *Caenorhabditis elegans* (*C. elegans*) may reveal new avenues for unravelling the individual roles that each lipid plays during organismal development and homeostasis.

While the sphingolipid composition varies by cell type, the lion's share of sphingolipids in mammalian cells accumulate as SM at the exofacial leaflet of the plasma membrane[549]. Alongside the major role of SM as a structural membrane lipid, the synthesis and degradation of SM serves as a central mechanism for regulating cellular Cer levels: small changes in the cellular levels of SM can dramatically affect the Cer content of a cell[296,550]. SM production is catalyzed by sphingomyelin synthases (SMS), which transfer the phosphocholine headgroup from phosphatidylcholine to Cer, producing diacylglycerol (DAG) as a side product. DAG is itself a known proliferative signaling molecule[551–553], and thus the production of SM simultaneously regulates Cer and DAG levels in opposing directions – suggesting that SM synthases can play a fundamental role in regulating cell fate towards survival. While numerous reports demonstrate parallel roles for Cer and SM in humans and *Caenorhabditis elegans* (*C. elegans*), to date there have been no analyses on the enzymes responsible for SM synthesis in this model organism[554–557].

We previously reported the identification of a conserved family of polytopic membrane proteins that display the classical characteristics of SMS enzymes in animals capable of SM production[456]. Strikingly, this study revealed multiple SMS genes in each of the organisms analyzed, suggesting a powerful selective pressure towards redundancy in SM synthesis. Human cells contain two isoforms of SM synthase, namely SMS1 in the Golgi complex and responsible for producing the bulk of cellular SM, and SMS2 at the plasma membrane and likely serving a principle role in signal transduction[343]. In addition, the human genome encodes a third, SMS- related enzyme (SMSr) that catalyses the production of the SM analog ceramide phosphoethanolamine (CPE) in the ER[264,421,456]. All three enzymes significantly contribute to the local regulation of ceramide levels and serve critical roles in cell growth and survival[343,421,558].

The identification of a multigenic SMS family opened important new avenues for studying sphingolipid function in animals. In this regard, *C. elegans* represent an attractive model system. The availability of a detailed description of this animal's morphology, development and physiology combined with the ease to manipulate gene function through mutation and RNAi makes this model ideal for dissecting the biological roles of SM synthases and related enzymes at the molecular level. In many cases where mammalian systems are too complicated to obtain clear information on the

molecular ordering of signaling pathways, *C. elegans* has been instructive. This is particularly true for the mechanisms controlling apoptosis and cell division, two integral and invariant components of *C. elegans* development[559,560]. The *C. elegans* genome encodes five SMS family members, but none of these have been characterized in any detail.

In this study, we carried out the first systematic analysis of SMS family members in *C. elegans*. Combining heterologous expression approaches with combinatorial knockout strategies, we established that several of these homologs function as bona fide SM and CPE synthases with unique sub-cellular distributions. Our findings lay the foundation for future in-depth investigations of the full regulatory potential of SM synthases and related enzymes in animal growth and development.

10.3. Results

10.3.1. Phylogenetic analysis and expression of SMS family members in *C. elegans*

The *C. elegans* genome encodes five SMS family members, which we named SMSα, SMSβ, SMSγ, SMSδ, and SMSr. These proteins contain six membrane spans, share a common LPP- like active site motif, and display at least 24% sequence identity with the human SM synthase SMS1. Phylogenetically, ceSMSα, ceSMSβ, ceSMSγ and ceSMSδ form clusters with homologues of other nematodes (i.e., *C. briggsae*, *C. remanei*, and *C. brenneri*) that separate from those containing vertebrate SMS1 and SMS2. In contrast, ceSMSr shows a higher degree of conservation and forms a cluster containing both vertebrate and invertebrate homologues (Figure 10.1A). To determine which of these SMS family members are actively expressed in *C. elegans*, we performed RT-PCR on total RNA isolated from a mixed-state population of the wildtype strain N2. This allowed the detection of transcripts for ceSMSα, ceSMSβ, ceSMSγ, and ceSMSr (Figure 1B). In contrast, we were unable to detect a transcript for ceSMSδ. The same was true when RT-PCR was performed with an independent SMSδ-specific primer set. This precluded cloning of the ceSMSδ cDNA. For the remainder of this study, we therefore focused on the characterization of ceSMSα, ceSMSβ, ceSMSγ, and ceSMSr.

10.3.2. *C. elegans* SMS family members display distinct sub-cellular distributions

Previous work revealed striking differences in sub-cellular distribution among members of the vertebrate SMS family, with SMS1 residing in the Golgi complex, SMS2 in the Golgi and at the plasma membrane, and SMSr in the ER[421,456]. Thus, one potential explanation for the expansion of SMS family members in *C. elegans* could be a further diversification of the cellular sites of SM production. To investigate this possibility, we expressed V5-tagged versions of ceSMSα, ceSMSβ, ceSMSγ and ceSMSr in human HeLa cells and analyzed their sub-cellular distributions by immunofluorescence microscopy. Intriguingly, ceSMSα, ceSMSβ and ceSMSγ each primarily localized to the plasma membrane (Figure 10.2A, C, and E). In addition, ceSMSα was also found in internal vesicles that were spread throughout the cytoplasm, did not contain the Golgi marker GM130, and likely correspond to compartments of the endosomal/lysosomal system (Figure 10.2A, B). Besides its association with the plasma membrane, a substantial portion of ceSMSβ co-localized with GM130, indicating that this protein partially resides in the Golgi (Figure 10.2D, insets). In contrast, ceSMSγ was found almost exclusively at the plasma membrane (Figure 10.2E, F). CeSMSr, like its human counterpart, resided in the ER, as evidenced by extensive co- localization with the ER marker calnexin (Figure 10.2G & H). From this we conclude that members of the *C. elegans* SMS family have partially overlapping

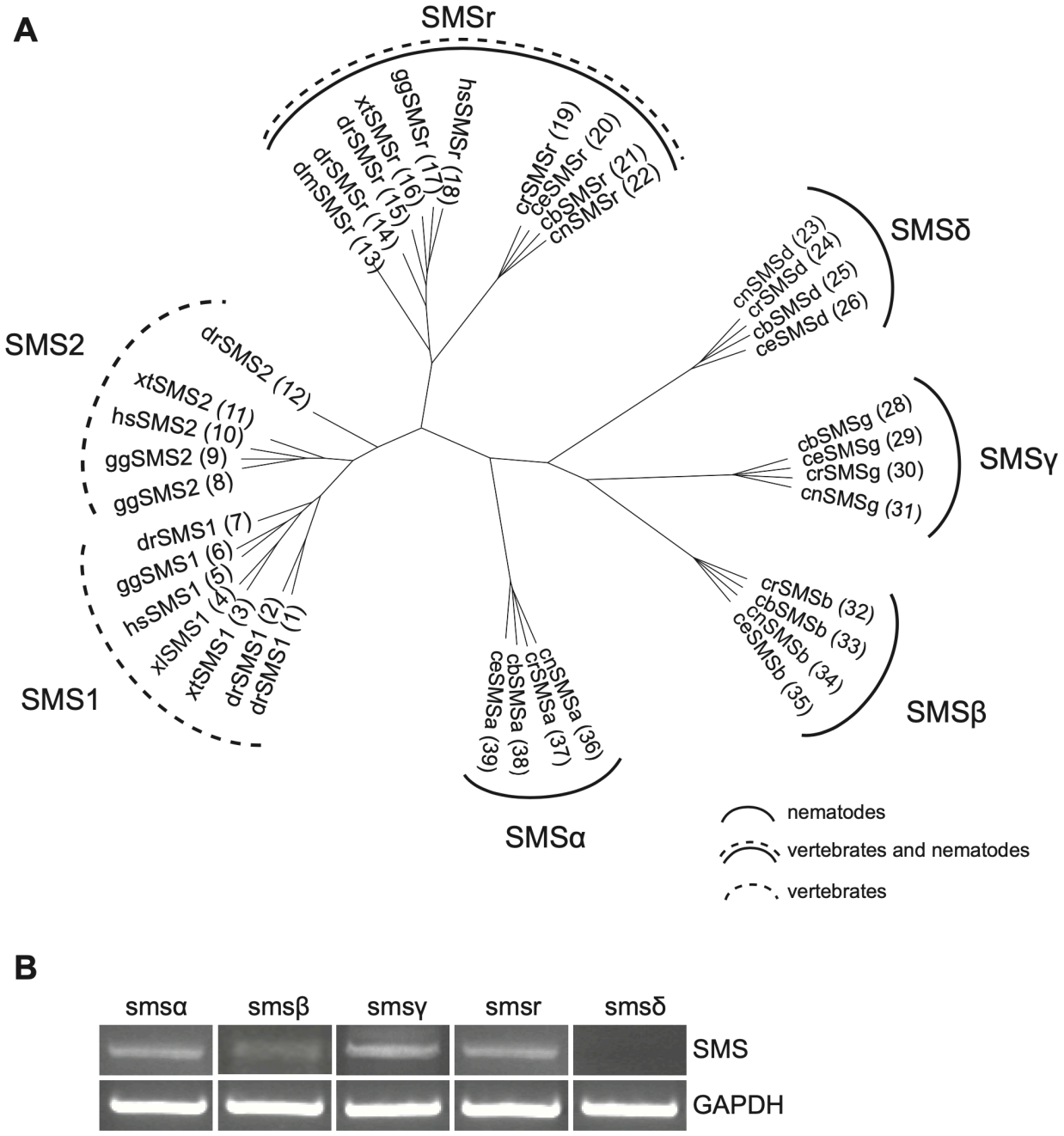


Figure 10.1. – **Phylogenetic analysis of SM synthase family and expression levels in *C. elegans*.** (A) Phylogenetic Tree of SM synthase proteins from Homo sapiens (hs), *Drosophila melanogaster* (dm), *Gallus gallus* (gg), *Xenopus tropicalis* (xt), *Xenopus laevis* (xl), *Danio rerio* (dr) and the nematodes *Caenorhabditis elegans* (ce), *Caenorhabditis briggsae* (cb), *Caenorhabditis remanei* (cr) and *Caenorhabditis brenneri* (cn). (B) Expression of SM synthase homologues in *C. elegans* using RT-PCR. Reverse transcription PCR of mRNAs of SMSα, SMSβ, SMSγ, SMSδ and SMSr using total RNA isolated from *C. elegans* N2 worms. To verify that same amounts of RNA were used for each reaction, the gapdh gene is shown.

but also unique sub-cellular distributions, together occupying all principal compartments of the secretory pathway (ER, Golgi, plasma membrane, and endosomes).

10.3.3. The *C. elegans* SMS family harbors both SM and CPE synthases

While human hsSMS1 and hsSMSr primarily serve as mono-functional SM and CPE synthases, respectively, hsSMS2 displays dual activity as SM and CPE synthase[421,456,561]. To analyze the enzymatic properties of the four *C. elegans* SMS homologues, V5-tagged ceSMSα, ceSMSβ, ceSMSγ and ceSMSr constructs were each expressed in budding yeast, an organism that produces ceramide phosphoinositol (CPI) but lacks endogenous SM and CPE synthase activity. Expression was verified by immunoblot analysis using an antibody against the V5 epitope (Figure 10.3A). ceSMS-expressing yeast cells were lysed and then incubated with fluorescent C6-NBD- ceramide (NBD-Cer). Thin layer chromatographic (TLC) analysis of the reaction mixture derived from ceSMSr-expressing cells showed the presence of an NBD-labeled product with a retention value distinct from that of C6-NBD-SM or C6-NBD-CPI but similar to that of C6-NBD-CPE (Figure 10.3B). This product was missing in reactions performed with control (empty vector, EV) cells but present in reactions carried out with cells expressing hsSMS2, hsSMSr or *D. melanogaster* drSMSr (Figure 10.3B and data not shown). These results indicate that *C. elegans* SMSr, like its human and Drosophila counterparts, functions as CPE synthase. TLC analysis of the reaction mixtures from cells expressing ceSMSα or ceSMSβ in each case revealed the presence of C6- NBD-SM (Figure 10.3C). Reaction mixtures from cells expressing SMSγ, on the other hand, were devoid of NBD-SM or NBD-CPE. However, all reaction mixtures, including those derived from mock-transfected yeast cells, contained C6-NBD-CPI, which is due to the presence of an endogenous CPI synthase. Together, these results indicate that SMSα and SMSβ function as SM synthases.

To verify the substrate specificities of *C. elegans* SMS family members and exclude the possibility that the lack of a detectable SM and/or CPE synthase activity of ceSMSγ is due to the use of yeast as a heterologous expression system, we next analyzed the ability of these proteins to support SM production in *Drosophila melanogaster* S2 cells. In comparison to budding yeast, *Drosophila* is evolutionarily closer related to *C. elegans* but also offers the advantage of having no endogenous SM synthase activity. We therefore expressed V5-tagged ceSMSα, ceSMSβ, ceSMSγ and ceSMSr in S2 cells and performed metabolic labeling with [14C]-choline to monitor the production of [14C]-labeled SM. S2 cells expressing hsSMS1 served as control. TLC analysis and autoradiography of labeled cell extracts showed that hsSMS1, ceSMSα and ceSMSβ each supported SM production (Figure 10.3D), consistent with the outcome of the experiments in yeast. In contrast, expression of ceSMSγ did not result in any detectable SM production in S2 cells.

Finally, we analyzed the enzymatic properties of *C. elegans* SMS family members in HeLa SMS1/2 double knockout cells that lack endogenous SM synthase activity. Toward this end, the SMS1/2$^{-/-}$ cells were transfected with V5-tagged ceSMSα, ceSMSβ, ceSMSγ and ceSMSr, metabolically labeled with [14C]-serine, and then subjected to TLC analysis and autoradiography. SMS1/2$^{-/-}$ cells transfected with hsSMS1 served as control. In line with metabolic labeling experiments in S2 cells, this confirmed that ceSMSα and ceSMSβ function as SM synthases (Figure 10.3E). In contrast, heterologous expression of either ceSMSγ or ceSMSr did not restore SM production in the SMS1/2$^{-/-}$ cells.

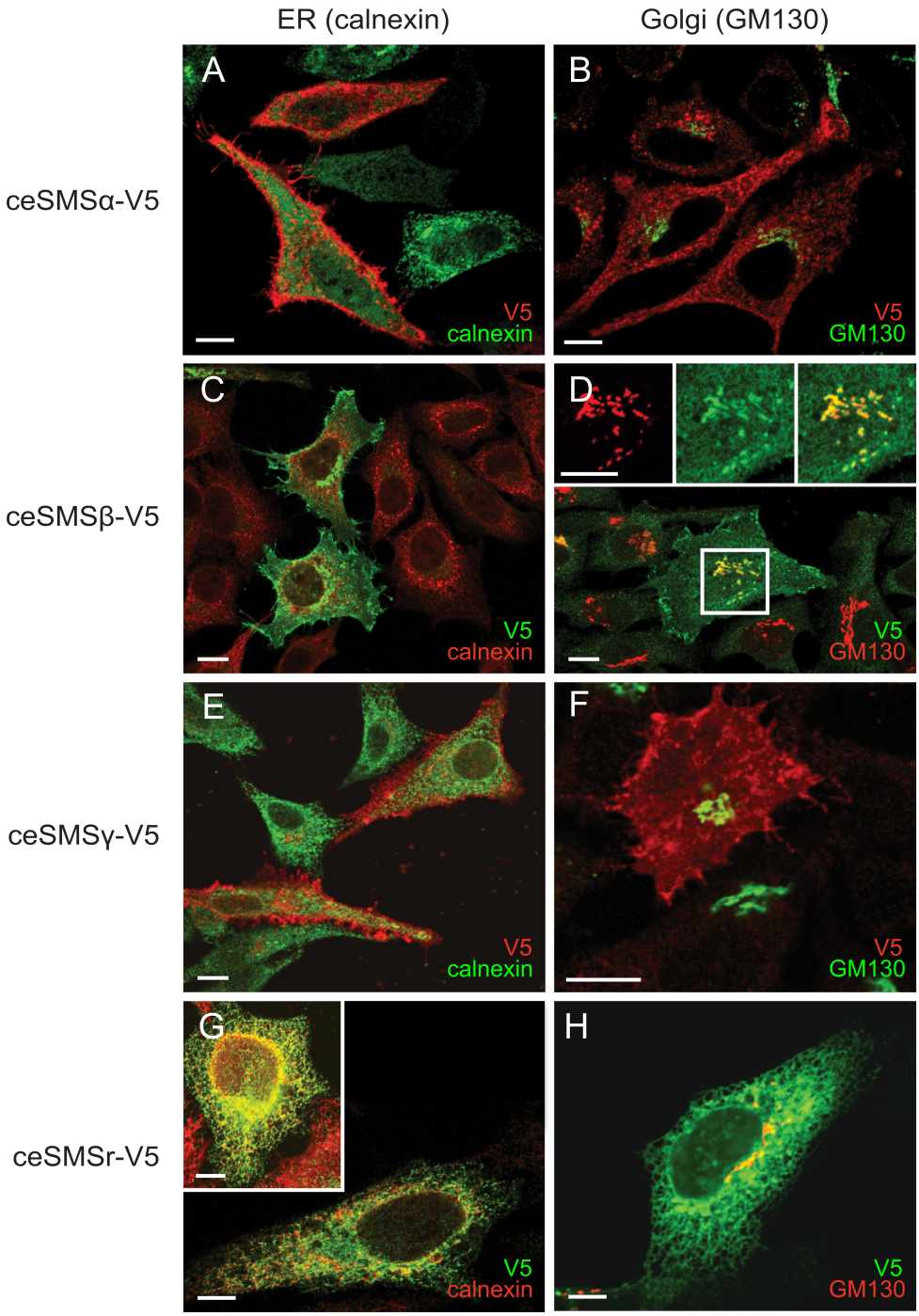


Figure 10.2. – **Sub-cellular localization of *C. elegans* SMS family members in HeLa cells.** Confocal immunofluorescence microscopy of HeLa cells transfected with V5-tagged *C. elegans* SMS family members and co-stained with antibodies against the V5 epitope and ER marker calnexin or Golgi marker GM130. Representative images are shown for HeLa cells transfected with ceSMSα-V5 (A, B), ceSMSβ-V5 (C, D), ceSMSγ-V5 (E, F), and ceSMSr-V5 (G, H). Bar, 10 μM. See Methods Section 10.5.9 for imaging details.

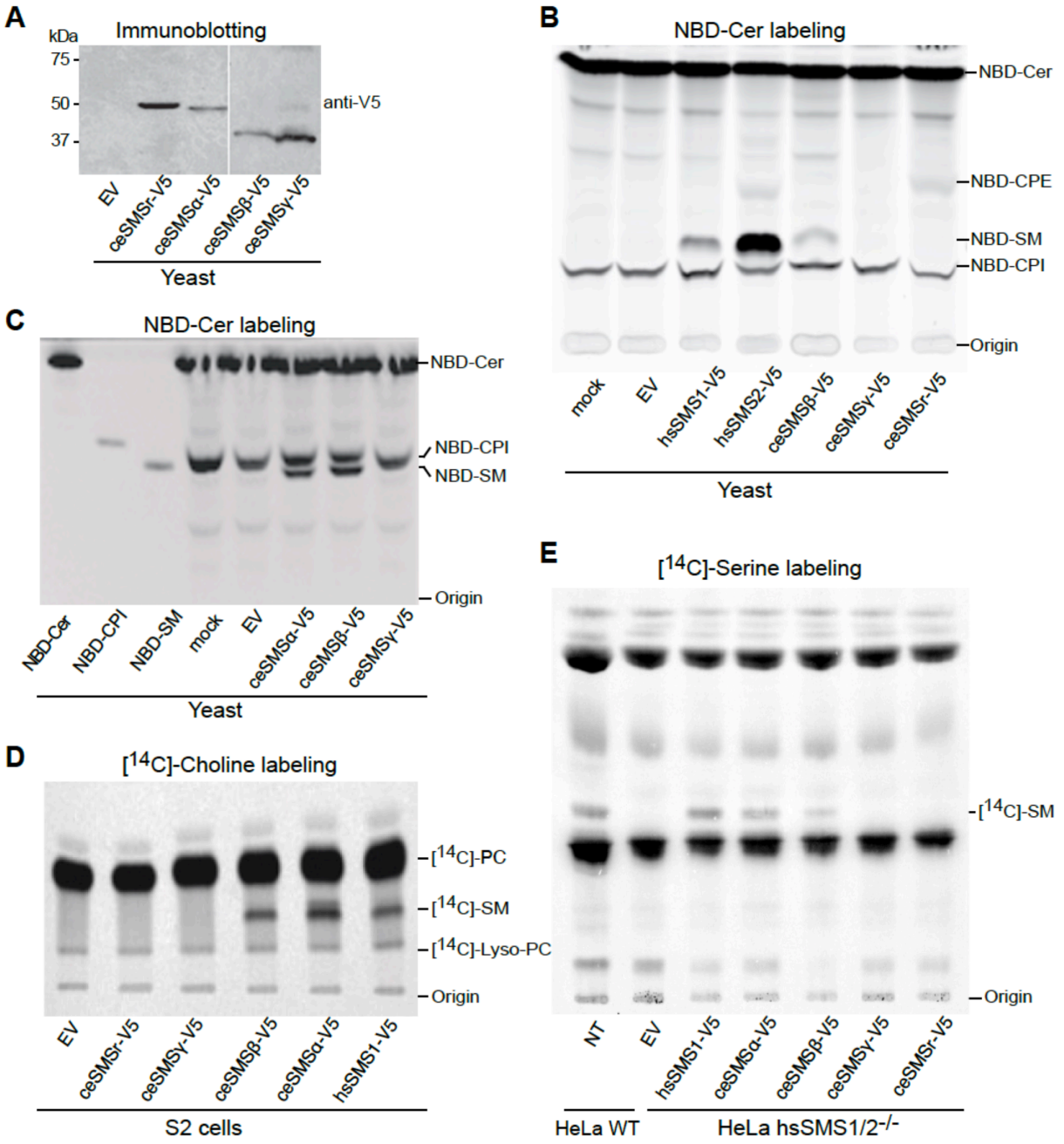


Figure 10.3. – **Heterologous expression of *C. elegans* SMS proteins reveal SM and CPE synthase activity.** (A) Expression of ceSMS-V5 proteins in yeast cells. Immunoblot of membrane protein extracts derived from yeast cells, transfected with empty vector (EV) or V5-tagged versions of *C. elegans* SMS proteins. Constructs were probed with mouse anti-V5 monoclonal antibody. (B) SM synthase and (C) CPE synthase activity in yeast cells (NBD-Cer labeling). Post- nuclear supernatants of yeast strains expressing human, drosophila and *C. elegans* SMS, or transformed with empty vector (EV) were incubated with NBD-Cer. NBD-labeled lipids were separated by TLC and detected by fluorescence scanning. (D) Drosophila S2 cells expressing the different SMS constructs were labeled with [14C]-Choline, after which total lipids were extracted and analyzed by radiographic TLC. (E) Radiographic TLC showing the metabolic conversion of [14C]-Serine in either wild-type or SMS1/SMS2 double-knockout HeLa cells transfected with hsSMS1 or *C. elegans* SMS genes. 'Origin' denotes the loading axis; expected retention values for NBD-Cer, NBD-CPE, NBD-CPI, NBD-SM, as well as [14C]-PC, [14C]-SM, and [14C]-lyso-PC, are indicated.

10.3.4. Lipid profiling of ceSMS-expressing HeLa SMS1/2$^{-/-}$ mutant cells

To interrogate the global impact of individual ceSMS family members on the cellular lipidome, we next performed quantitative lipidomics analysis on HeLa SMS1/2$^{-/-}$ cells transfected with V5- tagged ceSMSα, ceSMSβ, ceSMSγ and ceSMSr. SMS1/2$^{-/-}$ cells transfected with HA-tagged hsSMS1 served as control. Cellular lipids were extracted by the Bligh and Dyer method[303], spiked with deuterated internal standards, and analyzed with electrospray ionization tandem mass spectrometry (LC-ESI-MS/MS). The total signal of each sample was normalized using the internal standards(Figure S10.1A and B). Lipid extracts from untransfected SMS1/2$^{-/-}$ mutant cells were used to derive ratiometric comparisons against each ceSMS transfected condition and against wildtype HeLa cells.

In our analysis, we identified a total of 537 unique lipid species across all samples, spanning the major lipid classes, namely sphingolipids, phospholipids, glycerolipids, and sterols. The lipid profile of the untransfected SMS1/2$^{-/-}$ cells, as anticipated, exhibited a significant decrease in SM species compared to the wild type HeLa cells (Figure S10.2). Remarkably, upon transfection of SMS1/2$^{-/-}$ cells with hsSMS1, there was about 7-fold increase in total SM levels relative to the non-transfected control (Figure 10.4A, F).

Interestingly, when ceSMSα was overexpressed in SMS1/2-deficient cells, the lipid profile pattern closely resembled that of the SMS1/2$^{-/-}$ cells transfected with hsSMS1, and resulted in approximately 8-fold increase of total SM in comparison to the SMS1/2$^{-/-}$ cells (Figure 10.4B, G). In a similar manner, the overexpression of ceSMSβ in SMS1/2$^{-/-}$ cells resulted in lipid profiles comparable to those of ceSMSα and hsSMS1 expressing SMS1/2$^{-/-}$ cells, causing an increase of about 2.5-fold in total SM level (Figure 10.4C, H). In contrast, overexpressing either ceSMSβ or ceSMSr in SMS1/2$^{-/-}$ cells failed to yield any detectable SM species (Figure 10.4D, E, I, J). Furthermore, we observed minor alterations in the lipidomes of these SMS-transfected cells, such as slight increases in PC and PE, paired with mild but consistent reductions in TAG (Figure 10.4F-J).

To gain further insight into the acyl chain preferences of these SM synthases, we conducted a detailed analysis of the nature of the identified SM species. Similar patterns of enrichment were observed for hsSMS1, ceSMSα, and ceSMSβ: SM species, characterized by long-chain and very- long-chain fatty acids (C16:0 and C:20, C:22, and C24:0, respectively), appeared to be preferentially enriched (Figure 10.5A, B, C).

Collectively, these data indicate that ceSMSα and ceSMSβ are dedicated SM synthases while ceSMSγ and ceSMSr are devoid of any detectable SM synthase activity. As CPE species largely escaped detection in our lipidomics analysis, further work will be necessary to confirm the CPE synthase activity of ceSMSr detected in our in vitro enzyme assays (Figure 10.3B).

10.3.5. Characterization of *C. elegans* sms mutants

To analyze the impact of eliminating individual SMS family members in *C. elegans*, deletion mutants in the different ceSMS loci were obtained from the National Biosource Project (NBP) in Japan. Mutant strains with deletions in the open reading frames of ceSMSα (tm2660), ceSMSβ (tm2613), ceSMSδ (tm2615), and ceSMSr (tm2683) genes were obtained. The precise extent and location of the deletions in the sms mutants are depicted in Figure 10.6A and 6B. Mutations were mapped by single-worm PCR on genomic DNA using primers flanking the deletion areas (Figure 10.6C, upper

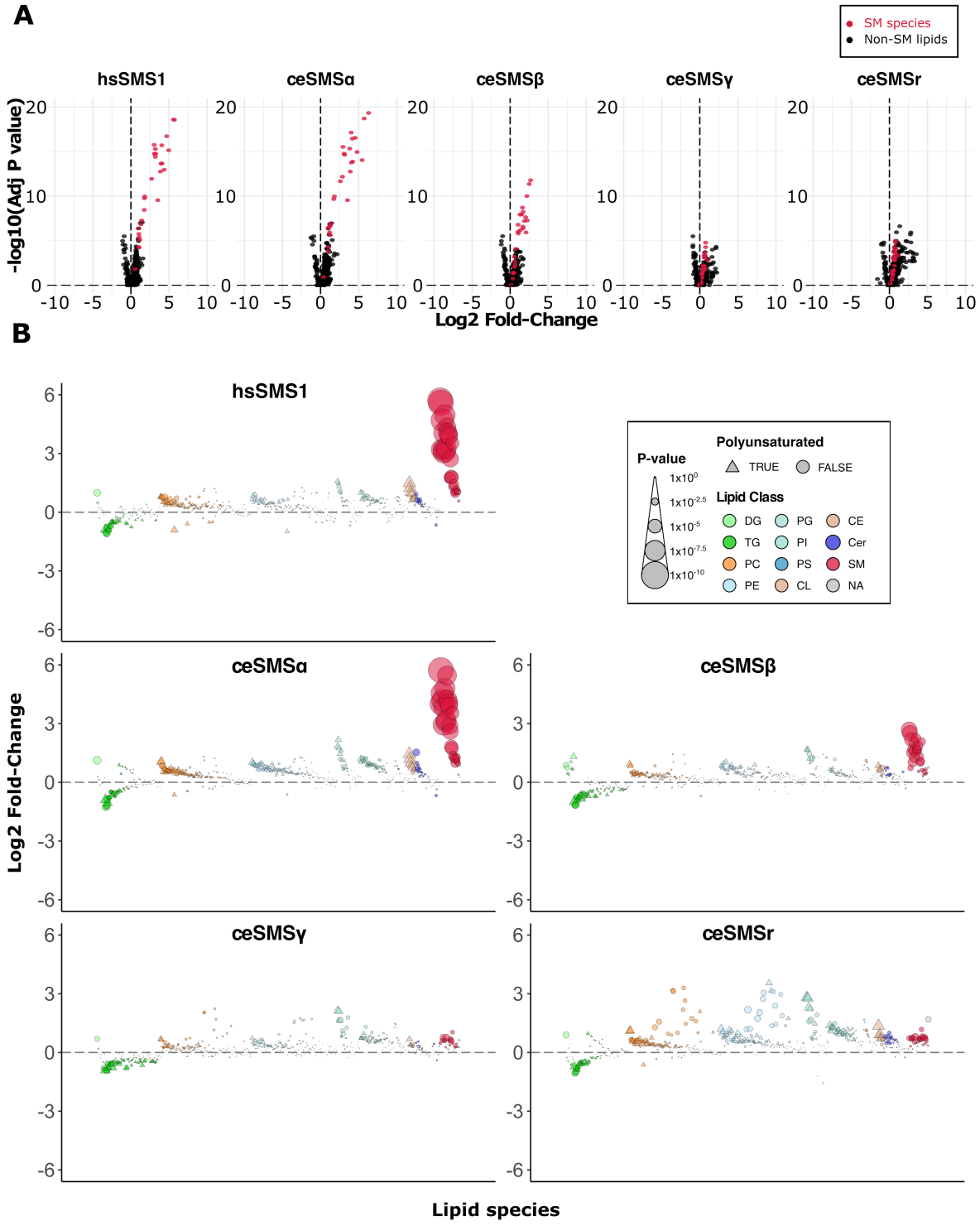


Figure 10.4. – ***C. elegans* SMS family members restore SM biosynthesis in SMS1/2-deficient HeLa cells.** (A) Volcano plots depicting the relative abundances and adjusted p-values of lipids quantified via lipidomic analysis, with ratiometric comparisons between transfected and untransfected SMS1/2$^{-/-}$ HeLa cells. Identified SM species are highlighted in red. (B) Bubble plots of log2 fold changes in abundance of lipid species in SMS1/2$^{-/-}$ HeLa cells transfected with SMS constructs relative to non-transfected controls. Data points are means from five biological replicates; each data point represents a lipid species. Only significantly changed ($P < 0.05$, one- way ANOVA, with Benjamini–Hochberg adjustment for multiple comparisons) lipids are shown. Individual lipid species are colored by the class of lipid that they belong to. DAG diacylglycerol; TAG triacylglycerol; PC phosphatidylcholine; PE phosphatidylethanolamine; PG phosphatidylglycerol; PI phosphatidylinositol; PS phosphatidylserine; CE cholesterol ester; CL cardiolipin; Cer ceramide; SM sphingomyelin.

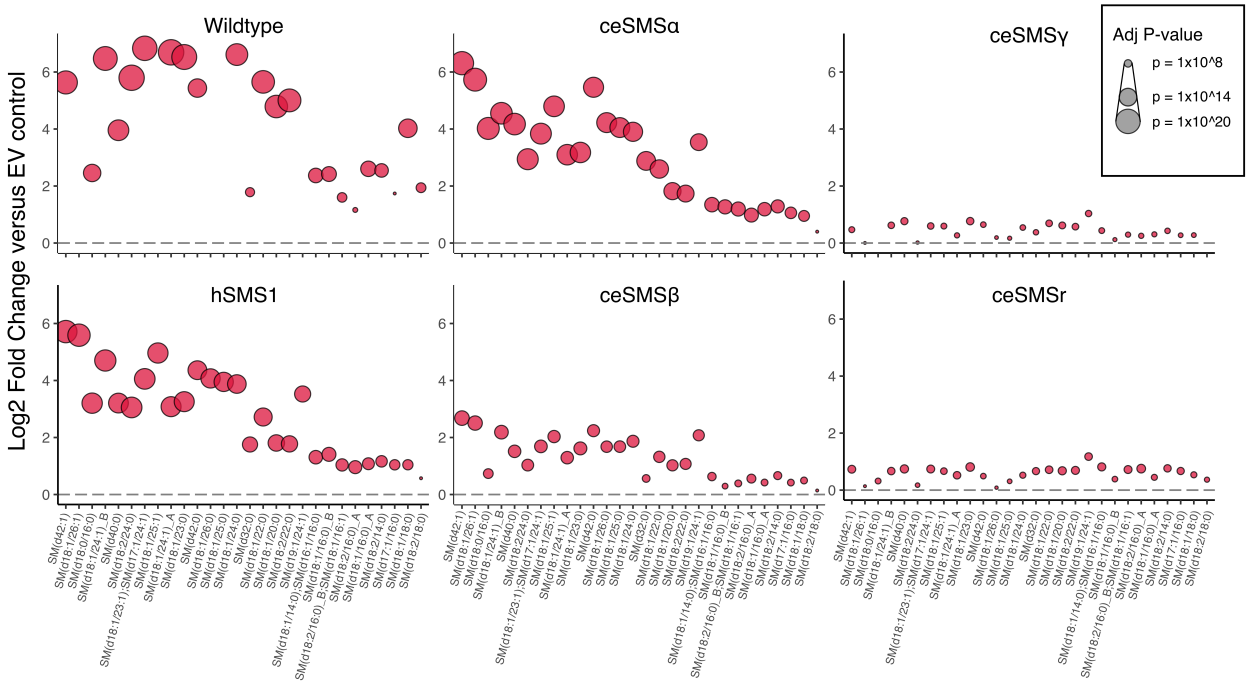


Figure 10.5. – **SM species produced by *C. elegans* SMS proteins.** Bubble plots of log2 fold changes in abundance of SM species in wildtype HeLa cells (A) and SMS1/2$^{-/-}$ cells transfected with hsSMS (B) or ceSMS constructs (C-F) relative to non-transfected controls. Data points are means from five biological replicates; each data point represents distinct SM species. Only significantly changed ($P < 0.05$, one-way ANOVA, with Benjamini–Hochberg adjustment for multiple comparisons) lipids are shown. SM species identity is denoted along the X-axis.

panel). To check wither the respective deletions in ceSMS genes would lead to a complete loss-of-function, the cDNAs corresponding to the mutated ceSMS genes were cloned by RT-PCR on total RNA isolated from the ceSMS mutant strains (Figure 10.6C, lower panel).

The tm2660 allele has a deletion of 588 bp that affects two exons in ceSMSα (Figure 10.6A). At the mRNA level, this results in a frameshift at the codon for Gly17 and introduces a premature stop codon after residue 37. The first available start methionine corresponds to Met 232 in wild-type ceSMSα. When used, this would give rise to a N-terminally truncated protein that lacks the first three membrane spans (Figure 10.6B). SMS family members normally have six membrane spanning regions, a feature conserved throughout the LPP superfamily[456]. Consequently, it is very unlikely that tm2660 encodes for an enzymatically active version of ceSMSα. A 176-bp deletion in the tm2613 allele leads to a gap in the protein-coding region of ceSMSβ from residue 234 to 292 (Figure 10.6A, B). This deletion covers membrane spans 5 and 6 as well as the conserved active site residues His339 and Asp 343. From this, we conclude that tm2613 corresponds to a total loss-of-function allele of ceSMSβ. A 507-bp deletion in tm2615 leads to removal of membrane spans 4 and 5 as well as active site residue His 255 in ceSMSδ. This indicates that tm2615 corresponds to a loss-of-function allele of ceSMSδ. Finally, a 210-bp deletion in tm2683 causes a gap in the protein-coding region of ceSMSr that covers the first two membrane spans. In view of the conserved membrane topology of SMS and LPP proteins, this most likely results in a complete loss of enzymatic activity. Unfortunately, no loss-of-function alleles could be obtained for ceSMSγ.

All four of ceSMS mutants were homozygous viable, and their overall growth and morphology were indistinguishable from that of wildtype. To eliminate background mutations, each mutant was crossed four times to the wildtype N2 strain. Next, we analyzed the impact of each mutation on SM synthase activity in *C. elegans* using both in vitro and in vivo assays.

10.3.6. *C. elegans* contains at least three distinct SM synthases

The foregoing heterologous expression studies in yeast and HeLa cells established that both ceSMSα and ceSMSβ function as SM synthases. To determine the contribution of each enzyme to SM biosynthesis in *C. elegans*, we incubated total worm lysates from corresponding deletion mutants tm2660 (Δsms-α) and tm2613 (ΔceSMSβ) with NBD-Cer and monitored the formation of NBD-SM via TLC. Lysates of the wild-type N2 strain served as control. This showed that disruption of ceSMSα or ceSMSβ in each case resulted in a moderate (20-30%) yet consistent decrease in SM synthase activity (Figure 10.7A). In contrast, deletion mutants tm2615 (ΔceSMSδ) and tm2683 (ΔceSMSr) showed no reduction in SM synthase activity. Together, these results indicate that both ceSMSα and ceSMSβ contribute to SM synthase activity in *C. elegans*.

To investigate whether ceSMSα and ceSMSβ represent the only SM synthases in *C. elegans*, we generated a ΔceSMSα ΔceSMSβ double-mutant by crossbreeding tm2660 and 2613. This double mutant exhibited normal growth, was viable, and did not show any noticeable behavioral phenotypes. Interestingly, the double mutant displayed a ~70% reduction in SM synthase activity compared to the N2 wildtype (Figure 10.7A, B). To investigate the contribution of ceSMSα and ceSMSβ to SM biosynthesis in vivo, the corresponding single and double mutants were metabolically labeled with [14C] choline for 4 hr at 20°C and the amount of [14C]-labeled SM synthesized was quantified by TLC and autoradiography. Loss of either ceSMSα or ceSMSβ caused only a minor drop (10-30%) in newly-synthesized SM levels, while worms lacking both ceSMSα and ceSMSβ showed a further drop in de novo SM synthesis – yet still retained 60% of the wildtype level (Figure 10.7C, D).

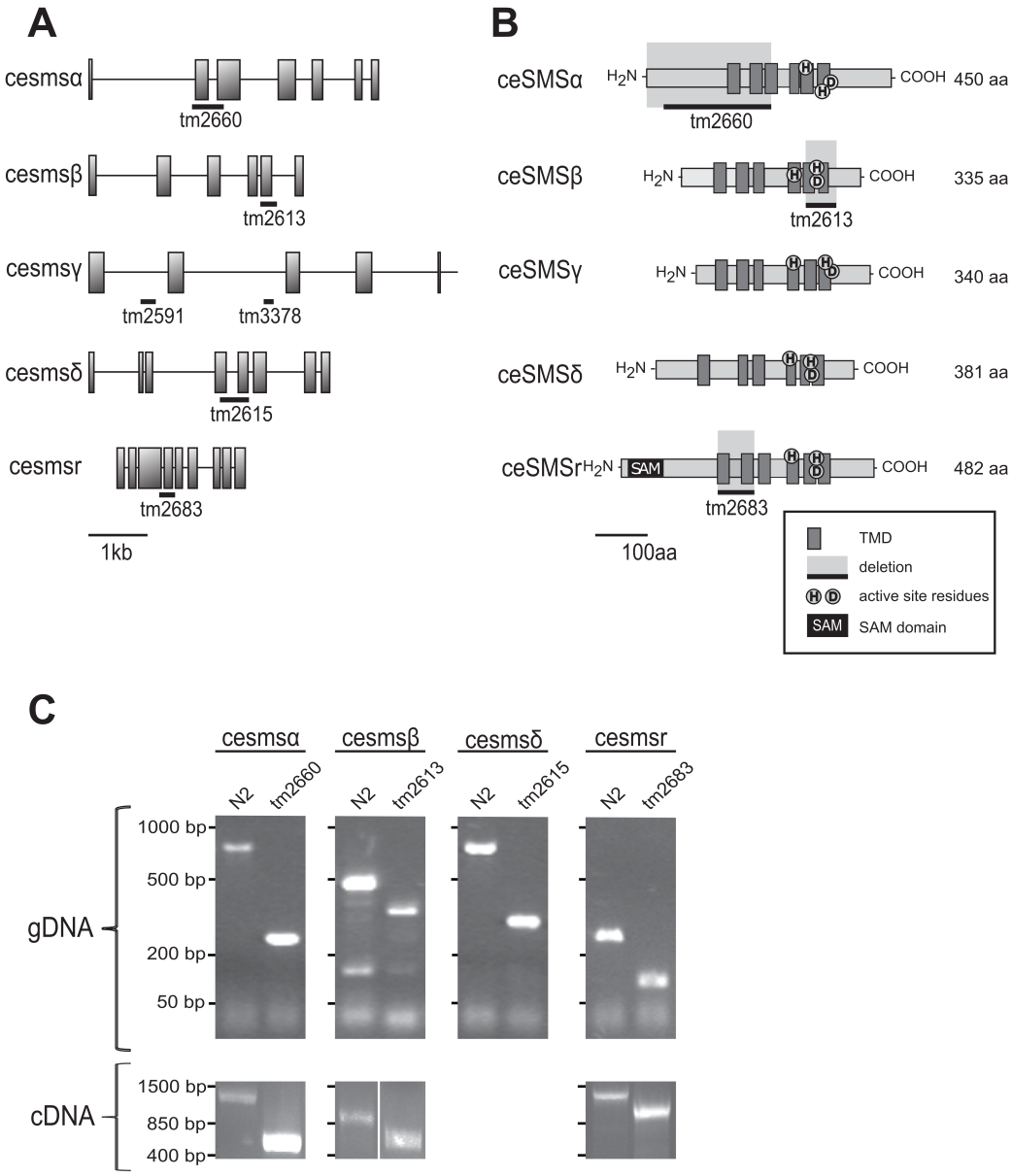


Figure 10.6. – **Characterization of SM synthases in *C. elegans*. (A) Genetic map of *C. elegans* sms genes.** The genomic structures of the sms-α, sms-β, sms-γ, sms-δ _and sms-r genes are shown. Gray boxes correspond to coding exons, introns are depicted as lines. The positions of mutations with respect to the gene are indicated below, namely tm2660, tm2613, tm2615 and tm2683. Mutation strains carrying deletions in the sms-γ gene, tm2591 and tm3378 have only recently become available, and are not included in this study. (B) Schematic structure of the *C. elegans* SMS proteins. The schemes show common domains as the transmembrane domains (solid boxes), the SAM domain (black box) and indicate the position of histidine (H) and aspartate (D) residues, forming the active site of the proteins. The positions of mutations are indicated, and the effect of the deletions on the proteins, are marked by the light gray box. In contrast to the other proteins, the position of the deletion in SMSδ _could not be confirmed by PCR on cDNA. (C) Mutant alleles and their mRNA transcripts were characterized by PCR. Locus-specific PCR tests on genomic DNA (gDNA) were used to track deletion alleles. On agarose gels, products from deletion alleles are visibly smaller than the wild type alleles. PCR tests on cDNA reveal a deletion of 588 bp for SMSα, a deletion of 176 bp for SMSβ and a deletion of 210 bp for SMSr. Primers used in this study are described in Material and Methods.

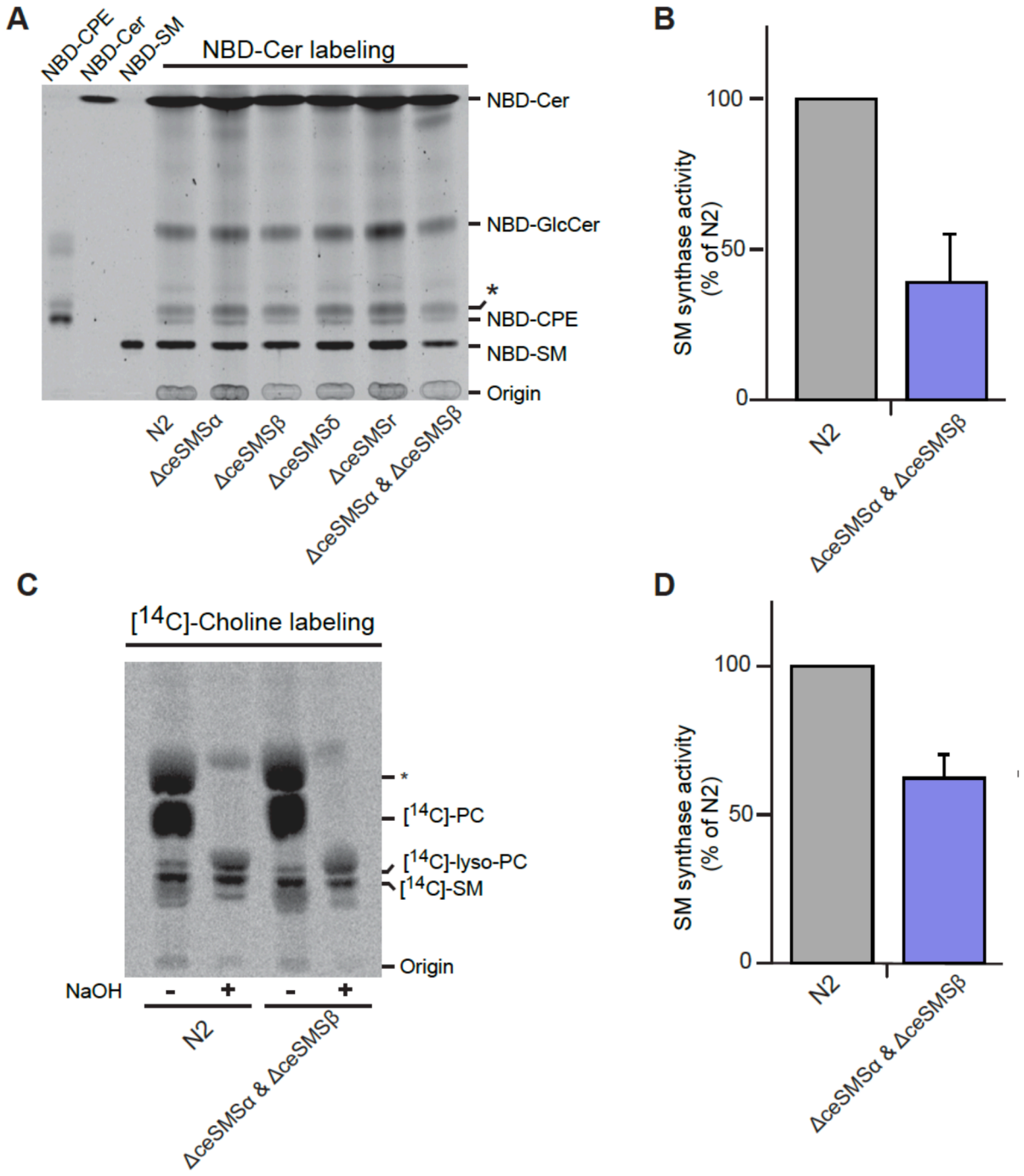


Figure 10.7. – **At least 3 different SM synthases contribute to SM synthesis in *C. elegans* worm.** (A) TLC analysis of reaction products formed, when worm lysates derived from N2 and single or double sms mutant strains were incubated with NBD-Cer for 1 h at 20°C. (B) SM synthase activity levels were determined based on quantitative analysis of NBD-SM reaction products formed in worm lysates incubated with NBD-Cer as in A and expressed relative to activity levels in wild type N2 worms. Data are means ± SD, n=5. (C) Wild type N2 worms and double mutant strains were labeled with [14C]-Choline for 5 h and subjected to lipid extraction, TLC analysis and autoradiography. Glycerolipids were deacylated by mild alkaline hydrolysis (NaOH). (D) Quantification of SM synthase activity levels of experiments done as in D. Unknown by-products are marked with an asterisk (*). Error bar: range, n=2.

Together, these results provide complementary evidence that ceSMSα and ceSMSβ both operate as SM synthases in *C. elegans*. They also indicate that, besides ceSMSα and ceSMSβ, *C. elegans* harbors at least one additional SM synthase that contributes to SM biosynthesis.

10.4. Discussion

In this study, we present the first systematic analysis of the SMS protein family in the nematode *C. elegans*. The use of heterologous expression systems and gene KO approaches enabled us to assign primary catalytic functions to three of the five SMS family members and map their intracellular sites of action, summarized in Table 10.1. We show that *C. elegans* ceSMSr catalyzes the production of CPE in the ER, hence analogous to SMSr homologues in mammals and Drosophila[421,561]. ceSMSα and ceSMSβ, on the other hand, primarily function as SM synthases at the plasma membrane. However, a substantial amount of SMSα resides in endosomes whereas SMSβ partially localized to the Golgi complex. Thus, SMSβ may well represent the *C. elegans* counterpart of SMS1 in mammals. ceSMSγ was found almost exclusively at the plasma membrane but we were unable to assign any enzymatic activity to this protein. The same was true for ceSMSδ, whose expression during the various stages of *C. elegans* development was below the limit of detection. Genetic ablation of both SMSα and SMSβ caused a substantial reduction in, but did not wipe out SM biosynthesis in the worm. This indicates that *C. elegans* contains at least one additional SM synthase, the identity of which remains to be established.

Table 10.1. – **Characteristics of *C. elegans* SMS family members** (Abbreviations: PM = plasma membrane, ER = endoplasmic reticulum, n.d. = no data)

	Predicted MW (kDa)	SM synthase activity	CPE synthase activity	Subcellular Localization
SMSα	50.9	+	-	Endosome, PM
SMSβ	38.7	+	-	Golgi, PM
SMSγ	38.1	-	-	PM
SMSδ	44.0	n.d.	n.d.	n.d.
SMSr	54.9	-	+	ER

We employed global lipidomics to evaluate how each of these *C. elegans* enzymes individually influences the lipid profiles, specifically the SM levels, of HeLa cells with SMS1/SMS2 deletion. In line with our expectations, the most notable and significant alterations in SMS1/2 double knockout cells overexpressing hsSMS1, ceSMSα, and ceSMSβ were observed in the SM species. However, overexpression of either ceSMSγ or ceSMSr in SMS1/2$^{-/-}$ cells did not result in detectable levels of SM. This strongly supports our central finding that ceSMSα and ceSMSβ are the primary SM synthases in *C. elegans*.

Previous work has shown that SMS and CPE synthases serve critical roles in cell growth and survival in mammals. For example, the SMS1-deficient mouse lymphoid cell line WR19L/Fas is growth inhibited when cultured under serum-free conditions – a phenotype that is rescued with ectopic SMS1 cDNA expression[558]. Similarly, our previous works showed that depletion of either hsSMS1 or hsSMS2 resulted in reduced growth in human HeLa cervical carcinoma cells and that hsSMSr

depletion triggers mitochondria-induced apoptosis in several human cell lines[343,421]. Intriguingly, siRNA knockdown of either hsSMS1 or hsSMS2 in THP-1-derived macrophages increased sensitivity to lipopolysaccharide-mediated apoptosis, suggesting that SM production plays a highly nuanced role in determining cell fate[323]. Given these previous findings, it is striking that disruption of SMSr or removal of both SMSα and SMSβ in *C. elegans* did not produce recognizable aberration in organismal growth, morphogenesis, or lifespan. It is possible that the corresponding mutants displayed only minor aberrations which escaped our attention, or that these mutants would become defective in growth given adequately stressful conditions. Notably, none of the mutants described in this study displayed complete deficiency in SM or CPE biosynthesis, thus it is feasible that the residual levels of SM and CPE synthase activities are sufficient to sustain growth and survival. Alternatively, the survival of the described ceSMS mutants may depend on the activation of pro-mitogenic and/or anti-apoptotic pathways. And finally, we cannot exclude the possibility that nematodes simply do not rely on SMS proteins for vital cell fate decisions in the same ways that mammals do. The creation of novel mutants lacking multiple SMS family members, combined with RNAi approaches, should allow one to address these different scenarios.

Remarkably, nematodes consistently contain more SMS homologues than all other currently known SM and/or CPE-producing organisms (e.g., mammals, insects, etc). While ceSMSα, ceSMSβ and ceSMSr synthesize SM or CPE, this may not necessarily be the case for ceSMSγ and ceSMSδ. A peculiar feature of *C. elegans* is the animal's ability to esterify its secreted N- glycoproteins and glycosphingolipids with phosphorylcholine[562]. This property is shared with filarial nematodes in which production of cholinephosphoryl-substituted oligosaccharides (CPOs) serves to avoid the host immune response and contributes to the chronic nature of diseases caused by these parasites[563]. Whether cholinephosphoryl-substituted glycoproteins and glycolipids also have intrinsic activities that contribute to nematode development or physiology is unclear. CPO synthesis is catalyzed by a PC:oligosaccharide cholinephosphoryl transferase[562]. Because this enzyme is absent in humans, it offers an ideal therapeutic modality for the treatment of filarial infections[563]. The identity of the CPO synthase is not known. Since CPO synthesis is mechanistically similar to SM and EPC synthesis, an attractive possibility is that ceSMSγ and/or ceSMSδ functions as a CPO synthase.

10.5. Materials and Methods

10.5.1. Chemicals and antibodies

NBD-Cer was obtained from Invitrogen (Leek, The Netherlands). NBD-SM, NBD-GlcCer, NBD-PC, POPE (1-palmitoyl-2-oleoyl-sn-glycerol-3-phosphoethanolamine), and POPC (1-palmitoyl-2-oleoyl-sn-glycerol-3-phosphocholine) were obtained from Avanti Polar Lipids, Inc (Alabaster, AL). NBD-CPE was generously provided by P. Devaux (Institut de Biologie Physico-chimique, Paris, France) and other cold lipids were from Matreya Inc. Methyl-[14C] choline chloride was obtained from MP Biomedicals (Santa Ana, CA). All other lipids and chemicals were obtained from Sigma- Aldrich (St Louis, MO). The following antibodies were used in this study: rabbit polyclonal anti- human calnexin (Santa Cruz, Santa Cruz, CA), rabbit anti-drosophila calnexin (Abcam Ltd., Cambridge, MA), mouse monoclonal anti-Golgi130 (BD Biomedicals, Alphen aan den Rijn, The Netherlands), mouse/rabbit polyclonal anti-V5 antibodies (Sigma), rabbit polyclonal anti-biotin (Rockland, Gilbertsville, PA) and mouse monoclonal anti-d120kd (EMD). As secondary antibodies we used: Alexa Fluor 488 conjugated goat anti-rabbit (Invitrogen), Alexa Fluor 568

conjugated goat anti-mouse (Invitrogen), HRP-conjugated goat anti-rabbit (Biorad, Veenendaal, The Netherlands) and HRP-conjugated goat anti-mouse (Perbio, Breda, The Netherlands).

10.5.2. Phylogenetic analysis of SM synthase family

The phylogenetic analysis of SM synthases in nematodes and vertebrates described in Figure 1 was done as described before (38). The proteins sequences were obtained from different sources. UniProt accession numbers, NCBI reference sequences, zebra fish ZFIN or wormbase protein IDs are as follow, organized by SMS family: SMS1: (1) ZDB-GENE-041114-201 (*D. rerio*); (2) Q5U3Z9 (*D. rerio*); (3) Q640R5 (*X. tropicalis*); (4) NP_001018461.1; (5) Q86VZ5 (*H. sapiens*); (6) Q7T3T4 (G. gallus); (7) A0JMNO (*D. rerio*). SMS2: (8) F1NLG9 (G. gallus); (9) XP_00123149.2 (G. gallus); (10) Q8NHU3 (*H. sapiens*) (11) Q5M7L7 (*X. tropicalis*); (12) Q6DEI3 (*D. rerio*). SMSr: (13) Q9VS60 (D. melanogaster); (14) A4QNV5 (*D. rerio*); (15) ZDB-GENE-080219-27 (*D. rerio*); (16) Q28CJ3 (*X. tropicalis*); (17) XP_426501.2 (G. gallus); (18) Q96LT4 (*H. sapiens*); (19) RP39824 (*C. remanei*); (20) Q20696 (*C. elegans*); (21) CBP26306 (*C. briggsae*); (22) CN16655 (*C. brenneri*). SMSδ: (23) CN19482 (*C. brenneri*); (24) RP33128 (*C. remanei*); (25) CBP15849 (*C. briggsae*); (26) Q9TYV2 (*C. elegans*). SMSγ: (28) CBP32601; (29) Q965Q4 (*C. elegans*); (30) RP06655 (*C. remanei*); (31) CN14615 (*C. brenneri*). SMSβ: (32) RP15984 (*C. remanei*); (33) CBP01983 (*C. briggsae*); (34) CN23351 (*C. brenneri*); (35) Q20735 (*C. elegans*). SMSα: (36) CN26856 (*C. brenneri*); (37) RP41176 (*C. remanei*); (38) CBP43882 (*C. briggsae*); (39) Q9U3D4 (*C. elegans*).

10.5.3. DNA constructs

hSMS1, ceSMSα, ceSMSβ, ceSMSγ and ceSMSr cDNAs were cloned into yeast expression vector pYES2.1/V5-His-TOPO and mammalian expression vector pcDNA3.1/V5-His-TOPO (Invitrogen) as described previously[456].For expression studies in Drosophila S2 cells, hsSMS1, ceSMSα, ceSMSβ, ceSMSγ and ceSMSr cDNAs were PCR amplified and ligated into the copper- inducible pMT/V5-His B vector (Invitrogen).

10.5.4. Yeast culture

Yeast strain 4Δ.Lass5 (MATa ade2-101ochre his3-Δ200 leu2-Δ1 lys2-801amber trp1-Δ63 ura3-52 lag1::TRP1 lac1::LEU2 ydc1::natMX ypc1::kanMX4 p413MET25:Lass5)[564] was transfected with human and *C. elegans* SMS cDNAs in pYES2.1/V5-His-TOPO and grown in selective synthetic medium containing 2% (wt/vol) galactose and 50 mg/l myo-inositol.

10.5.5. Cell culture and transfection

HeLa cells were grown in DMEM with 10% FCS (PAA laboratories GmbH, Pasching, Austria). Using Lipofectamine2000 and Lipofectamine3000 (Invitrogen), cells were transiently transfected with SMS-V5/pcDNA3.1 constructs. SMS1/SMS2 double-knockout HeLa cells were kindly provided by the lab of Joost Holthuis and were grown and transfected as wildtype cells. Drosophila S2 cells were grown in Schneider's insect medium with 10% FBS (Cambrex, Rockland, ME) at 27°C in a humidified atmosphere. Insect cells were transfected with SMS/pMT/V5-HisB constructs using Effectene

(Qiagen, Hilden, Germany) following the manufacturer's protocol. Expression of recombinant SMS protein was induced by addition of 1 mM CuSO4 for 3 h followed by a 2 h-chase.

10.5.6. Nematode culture

Worms were maintained on 10 cm nematode growth medium (NGM) agar plates carrying a lawn of E. coli OP50 or in liquid culture (S-medium[565]) supplemented with E. coli OP50. Culture plates and liquid cultures were maintained at 20°C. Worm strains used in these experiments were: N2 (wild type), ΔceSMSα (tm2660), ΔceSMSβ (tm2613), ΔceSMSr (tm2683) and ΔceSMSδ (tm2615). All strains were provided by the National Biosource Project in Japan (NBP). All mutant strains have been backcrossed 4 times to N2. Mutant alleles were followed by PCR on single worm lysates, detecting the presence of genomic deletions (588 bp in the case of tm2660, 176 bp in the case of tm2613, 507 bp in the case of tm2615 and 210 bp in the case of tm2683). Primers flanking the deletions alleles used are depicted in Table 10.2.

Table 10.2. – **Primers used for the characterization of *sms* deletion mutants**

Gene/mutant	Primer pairs 5'-3'
sms-α / tm2660	ttggctattcactccaccct / tcgaagtccccatggaatct
sms-β / tm2613	tctgcttacattgggcacat / tcattaacttggccagtgcag
sms-δ / tm2615	tctagggcgtcggttggct / tgtaatcgttgtggagcatac
sms-r / tm2683	cgacaagtcgagagacccg / cgggtctctcgacttgtcg

10.5.7. Creation of double mutant (ΔceSMSα ΔceSMSβ)

Backcrossed ΔceSMSα (tm2660) worms were heat shocked (30°C for 4 h) at L4 larval stage and 6 young resulting male offspring were transferred to a plate containing one single L4 ΔceSMSβ (tm2613) hermaphrodite. The progeny were singled out onto plates and maintained until maturity (identified by the presence of eggs). Following single worm lysis, a genomic polymerase chain reaction (PCR) was performed to screen and identify double knockout mutants. Homozygous double mutant strains were selected and assessed and confirmed over at least 2 generations.

10.5.8. RT-PCR

RNA of worms was isolated using NucleoSpin RNA II kit (Macherey-Nagel, Düren, Germany) according to manufacturer's protocol. The amount and quality were verified by gel electrophoresis and spectrophotometry. Single strand complementary DNA (cDNA) was generated from 1 µg RNA using dT-oligo primers and Superscript II reverse transcriptase (Invitrogen). PCR was performed using Phusion DNA polymerase (Finnzymes, Espoo, Finland) on 5 µl of cDNA using the cloning primers previously described in Huitema et al. (2004) except for sms-α[456] where the following primer pair was used 5'-gcggccgccttcgaaagcaggtcgtgcagctcc-3'/5'- ggtaccaagccatgaaaatgtcttggaatcatcaa-3'.

10.5.9. Immunofluorescence microscopy

Cells were fixed in 4% paraformaldehyde/PBS, processed for immunofluorescence as described previously for S2[566] and HeLa cells[421], and mounted in Vectashield medium containing DAPI (Vector Laboratories, Burlingame, CA). Images were captured at room temperature using an LSM 510 Meta confocal microscope (Carl Zeiss, Inc., Sliedrecht, The Netherlands). The fluorochromes used were DAPI, lex = 360 nm and lem= 460 nm; Alexa Fluor 488, lex = 488 nm and lem = 515 nm; Alexa Fluor 568, lex = 568 nm and lem = 585 nm. Images were captured using EZ-C1 software (Nikon Instruments Europe, Badhoevedorp, The Netherlands) and further processed using either Photoshop (version 7.0.1; Adobe) and FIJI (version 2.1.0/1.53c; ImageJ).

10.5.10. Western blotting

S2 and yeast cells were lysed in RIPA buffer (50mM Tris/HCl, 0.1% (wt/vol) SDS, 0.5% (vol/vol) NP40, 150 mM NaCl, 2 mM EDTA, pH 7.4), supplemented with Complete Protease Inhibitor Cocktail (PIC, Roche, Basle, Switzerland). Nuclear DNA was sheared by passing lysates through a 23G needle. Protein content of lysates was determined by the bicinchoninic acid method (Pierce, Breda, The Netherlands). Equal amounts of protein in 1x SDS sample buffer were separated by SDS-PAGE and subsequently transferred to a nitrocellulose membrane (Schleicher & Schuell, Dassel, Germany). Membranes were blocked in TBS (25 mM Tris/HCl, 137 mM NaCl, 2.7 mM KCl, pH 7.4) containing 0.05% (vol/vol) Tween 20 and 4% (wt/vol) dried skim milk (Fluka, Zwijndrecht, The Netherlands) and incubated overnight with primary antibody of interest. Membranes were washed three times in TBS containing 0.05% (vol/vol) Tween20 and incubated for 1 h with secondary antibody. Proteins were detected using HRP-conjugated secondary antibodies and enhanced chemiluminescence (Amersham, Roosendaal, The Netherlands).

10.5.11. In vitro enzyme assays

100 ODs of yeast cells was lysed by bead bashing in 10 ml ice-cold reaction buffer (0.3 M sucrose, 15 mM KCl, 5 mM NaCl, 1 mM EDTA, 20 mM Hepes-KOH, pH 7.0) containing freshly added protease inhibitors. 200 µl postnuclear supernatant (PNS; 700 g for 10 min at 4°C) were combined with 200 µl reaction buffer containing 0.002% Triton X-100, 40 nmol POPE and/or POPC, and 50 µM NBD-Cer (Avanti Polar Lipids, Inc.), and incubated at 37°C for 2 h. 2x105 worms were homogenized in an eppendorf tube with 40 strokes of a Teflon pestle in 300 µl ice-cold reaction buffer. 200 µl of worm lysate were combined with 200 µl reaction buffer containing 25 µM NBD-Cer (Avanti Polar Lipids, Inc.), and incubated at 20°C for 2 h. Reactions were stopped by adding 1 ml MeOH and 0.5 ml CHCl3, and lipids were extracted according to Bligh and Dyer[303]. The lower phase was evaporated under N2 and the reaction products analyzed by TLC, which was developed in CHCl3/acetone/MeOH/acetic acid/H2O (50/20/10/10/5 [vol/vol/vol/vol/vol]). Fluorescent lipids were visualized on an image analysis system (STORM 860; GE Healthcare) and quantified with Quantity One software (Bio-Rad Laboratories).

10.5.12. Metabolic labeling

S2 cells (2–5 x 106) grown in 0.5 ml complete Schneider's insect medium, SMS1/SMS2 double-knockout HeLa cells were grown in DMEM, and *C. elegans* worms (2x105) grown in liquid culture (S-medium) – all three of these models were subsequently radiographically labeled with 1 μCi [14C] choline for different time points as indicated. Lipids were extracted in CHCl3/MeOH/10 mM acetic acid (1/4.4/0.2 [vol/vol/vol]) and processed according to Bligh and Dyer[303]. Half of the extract was subjected to mild alkaline hydrolysis. Radiolabeled lipids were analyzed by TLC in CHCl3/MeOH/25% NH4OH (50/25/6 [vol/vol/vol] detected by exposure to imaging screens (BAS-MS; FujiFilm), scanned on a Personal Molecular Imager (Bio-Rad Laboratories), and quantified using Quantity One software.

10.5.13. Lipidomic analysis – sample preparation

SMS1/SMS2 double-knockout HeLa cells were seeded in 6cm dishes at a density of 2x106 cells per dish and transiently transfected in quadruplicate 24 hrs later with appropriate SMS constructs using Lipofectamine3000 (Invitrogen). At 48 hrs post-transfection, cells were washed twice in ice cold PBS and lipids were extracted using CHCl3:MeOH:H2O (2:1:1, v:v:v) according to Bligh and Dyer[303]. 10% of each sample was isolated and subjected to BCA analysis to quantify and normalize to protein content. Samples were each spiked with 8uL heavy standards (EquiSPLASH Mix; Avanti Polar Lipids), dried in vacuo, and stored at -80°C in a 2:1 solution of chloroform:methanol (v:v) until analysis.

10.5.14. Lipidomic analysis – LC-MS/MS analysis and lipid identification

LC-MS/MS analysis and lipid identification were performed as previously described[244,375]. LC-MS/MS instrumentation consisted of a Waters Acuity UPLC H class system interfaced with a Velos-ETD Orbitrap mass spectrometer. Samples were again dried in vacuo and resuspended in a 1:54 solution of chloroform:methanol (v:v) and injected onto a reverse-phase Waters CSH column and separated over a 34 min gradient (mobile phase A: acetonitrial/H2O (40:60, v:v); mobile phase B: acetonitrile/isopropanol (10:90, v:v) containing 10mM ammonium acetate) at a flow rate of 250 μL/min. Both positive- and negative-mode analyses were employed, using higher- energy collision dissociation and collision-induced dissociation to maximize lipidome coverage. The fragment ions used for lipid identifications were used as previously described[375]; in summary, these LC-MS/MS raw data files were analyzed using the LIQUID software[244] and all subsequent identifications were manually validated by examining the fragmentation spectra for diagnostic and fragment ions corresponding to the parent acyl chains. For quantification, a reference database was created using LIQUID[244] and then aligned to a reference database based on their identification, m/z, and retention times using MZmine 2[377]. Aligned features were then manually verified, and peak apex intensity values were exported for statistical analysis.

In total there were 3 (0.04%) and 272 (3.3%) missing observations in positive and negative mode, respectively; all missing observations were coded as NA values, and all observed abundances were log2 transformed. Lipid abundance profiles for each replicate were visualized via boxplot to identify any samples with substantial differences (Figure S10.2 B). We note that a single replicate of ceSMSβ transfection resulted in a lower overall abundance distribution in positive ionization mode. This

replicate was the lone replicate flagged as a potential outlier (p- value=0.0001) using a robust Mahalanobis distance algorithm (rMd-PAV) based on lipid abundance vectors[378]. This replicate was removed from both ionization modes of data, as only 21 of the 291 lipids were observed in negative mode for this replicate. A total of 9 and 8 heavy internal standards (IS) were spiked into the positive and negative ionization data, respectively. ISs with a coefficient of variation (CV) value less than 20% were used to derive normalization factors. 4 ISs (15:0-18:1(d7) DAG, 15:0-18:1(d7) PC, 18:1(d7) Lyso PE, C15 Ceramide-d7) and 3 ISs (15:0-18:1(d7) PC, 18:1(d7) Lyso PC, C15 Ceramide-d7) were used for the positive and negative data, respectively. The median value of ISs for each sample was calculated and used to normalize the data (Figure S10.2 C).

For each lipid, an analysis of variance (ANOVA) model was fit, using the R package pmartR[567], to the data and the following post-hoc pairwise differential expression tests were conducted: ceSMSα vs NT, ceSMSβ vs NT, ceSMSγ vs NT, ceSMSr vs NT, hSMS1 vs NT, and WT vs NT. A Holm multiple test correction[568] was used to adjust p-values for multiple comparisons; these adjusted p-values were then transformed to (-1)*Log10 adjusted p-values for visualization.

10.6. Acknowledgements

We thank Philippe Devaux and Andreas Conzelmann for gifts of reagents and cell lines and the National Biosource Project in Japan (NBP) for *C. elegans* strains. We also thank the members of the OHSU Advanced Light Microscopy core for their perennial guidance. J.C.M. Holthuis is supported by grants from the DFG (SFB 1557 – P9). F.G. Tafesse is supported by grants from the National Institutes of Health (NIAID R01 AI141549-02). Lipidomics analyses were performed in the Environmental Molecular Sciences Laboratory, a national scientific user facility sponsored by the Department of Energy (DOE) Office of Biological and Environmental Research located at PNNL. PNNL is a multiprogram national laboratory operated by Battelle for the DOE under Contract DE-AC05-76RLO 1830.

10.7. Contributions

GG wrote the text and performed the sample preparation and data visualization of the lipidomics analysis presented in Figures 4 and 5. SF provided text edits and guidance in lipidomics sample preparation. LB and JK oversaw the mass spectrometry data collection and analysis presented in Figures 4 and 5. SH and JvdD provided substantial experimental assistance. JCMH oversaw the initiation and structure of the study and provided text edits. FGT performed the majority of experimental work, oversaw the finalization of the study, and provided major text edits.

10.8. Supplemental materials

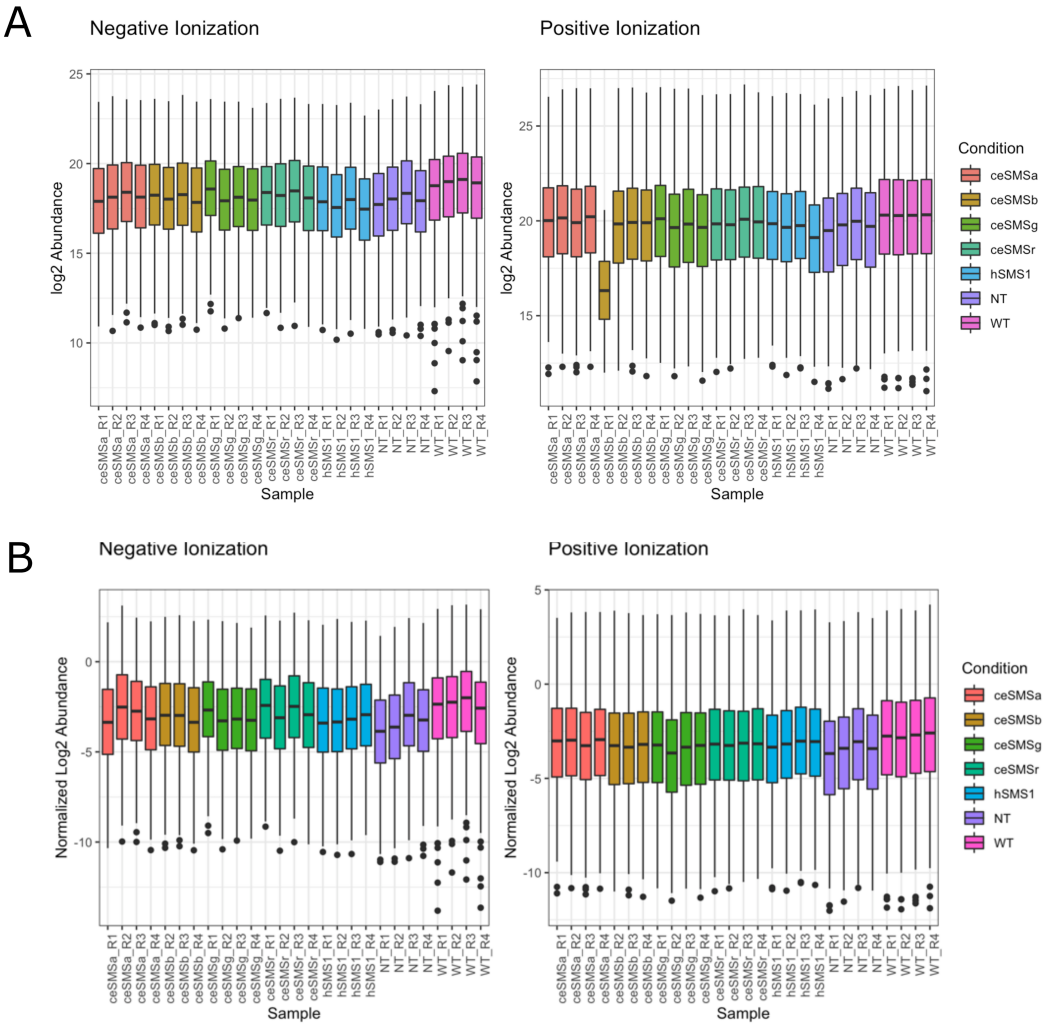


Figure S10.1 – Transfection lipidomics data quality control. (A & B) Boxplots depict distributions of total lipid abundances by replicate before and after normalization via internal standard, highlighting a single replicate of ceSMSβ with an overall lower distribution in positive ion mode.

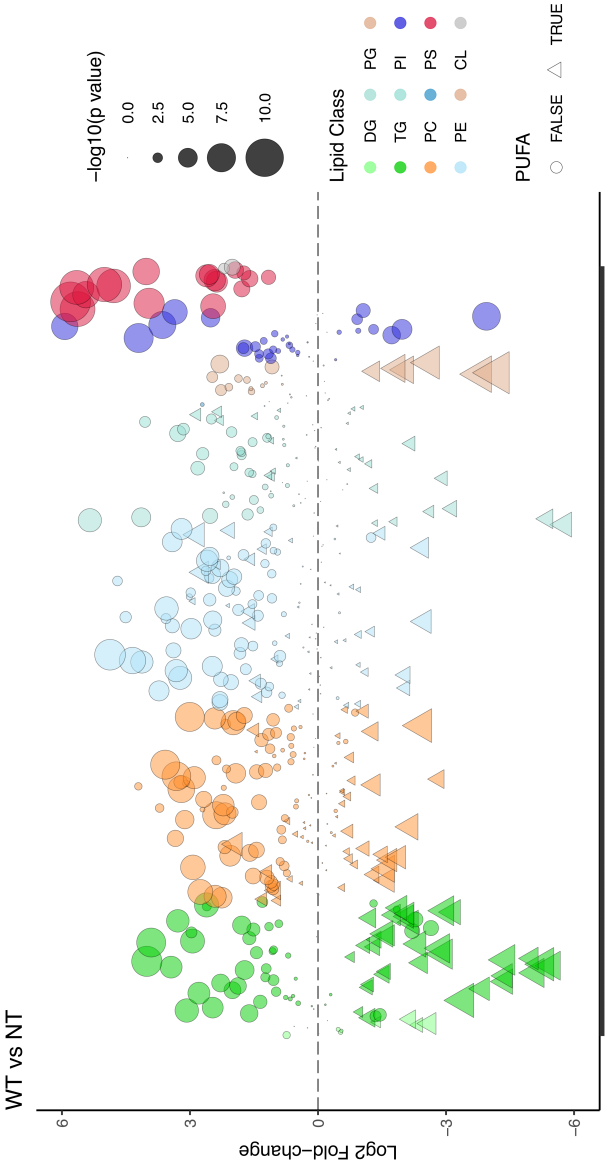


Figure S10.2 – Lipidomics comparison of wildtype and SMS1/2$^{-/-}$ HeLa cells. A bubble plot of log2 fold changes in abundance of lipid species in wildtype HeLa cells relative to SMS1/2$^{-/-}$ cells. Data points are means from five biological replicates. Each individual lipid species is assigned a unique color based on its lipid class. DAG, diacylglycerol; TAG, triacylglycerol; PC, phosphatidylcholine; PE, phosphatidylethanolamine; PG, phosphatidylglycerol; PI, phosphatidylinositol; PS, phosphatidylserine; CL, cardiolipin; Cer, ceramide; HexCer, hexosylceramide; SM, sphingomyelin; CE, cholesterol ester.

Part IV.

Final thoughts & future directions

Section overview

At long last, it is time to wrap this document up. In the following pages, I will briefly discuss the overarching themes that each of my main research projects touched on, and the future directions in which these projects will go.

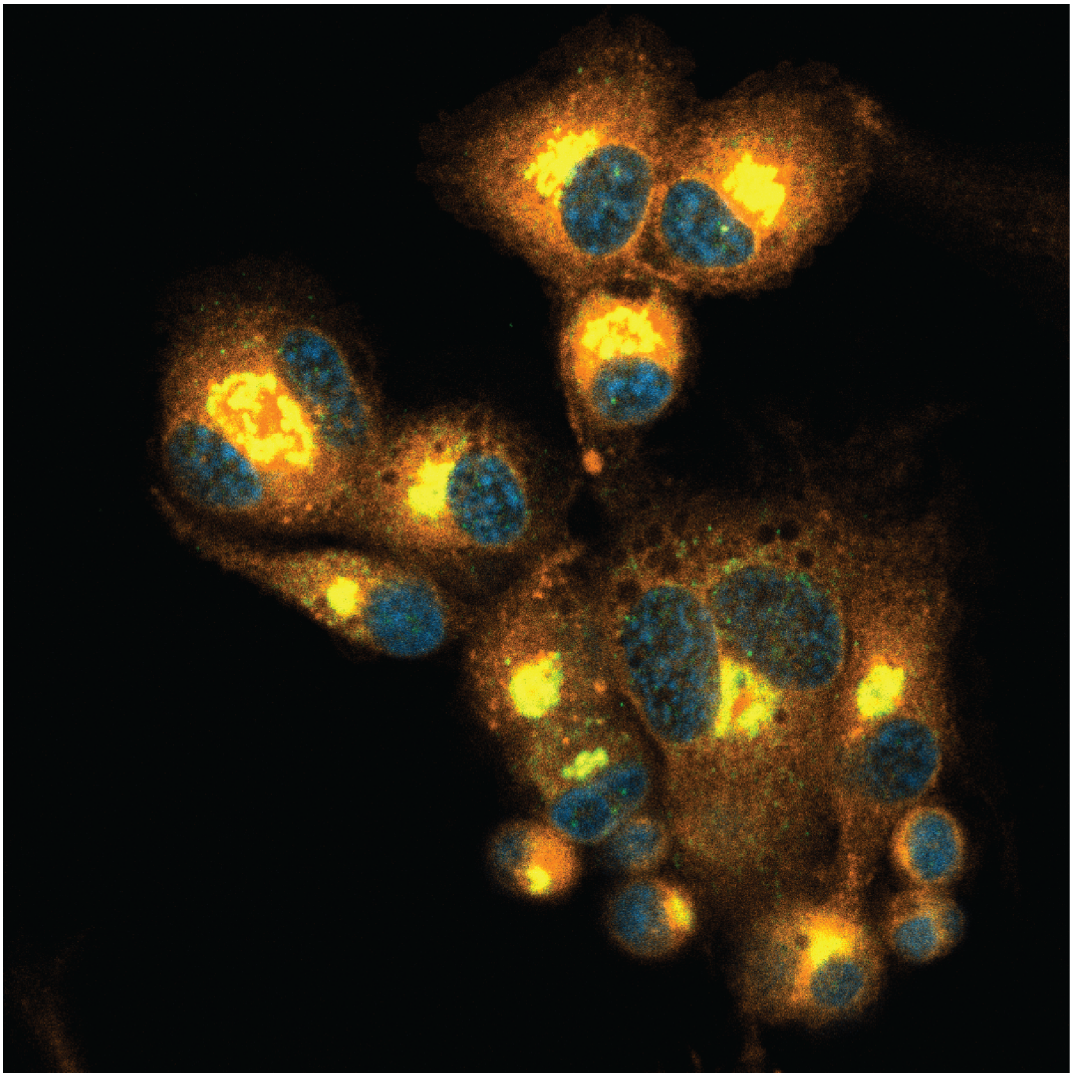


Figure 10.8. – **Trifunctional sphinganine traffics through the Golgi** THP-1 cells treated with tf-Sphinganine were uncaged and incubated for 60 minutes before fixation. Probe was clicked to Alexa-555 (yellow) and cell Golgi were stained against Giantin (green) and with DAPI (blue).

Chapter 11.

Discussion

I am now tasked with the ambitious project of summarizing the findings of this dissertation work. In our studies on the role of sphingolipids during *Mycobacterium tuberculosis* infection, we find evidence of a double-edged sword: sphingolipids enable *Mtb* to enter into host cells via phagocytosis, and yet they are a significant factor in restricting their growth within the infected cell. The total content of sphingolipids such as sphingomyelin and ceramide does not significantly change during pathogenic or attenuated *Mtb* infections. Still, we observe many intriguing changes among other lipid families. Finally, we find that the protein-sphingolipid interactions of a macrophage are dramatically altered during *Mtb* infection. Some of these differentially enriched interactions may be spurious results from lysosomal dysfunction and global changes to the proteome, but many are potentially biologically relevant observations.

11.1. Are sphingolipids a double-edged sword during *Mtb* infection?

As mentioned above, the results presented in Chapter 3 show that sphingolipids are *bad* for us during infection because they are required to initiate *Mtb* infection. In contrast, our findings in Chapter 4 show that sphingolipids are essential for restricting the intracellular growth of *Mtb*. So which effect is more important? The latter findings seem a more viable route toward antitubercular therapy – though an emerging story may complicate what this therapy may look like. Below, we will envisage several therapeutic options that our reports suggest and weigh the pros and cons of each.

One may imagine an antitubercular prophylactic therapy that blocks sphingolipid production to restrict the uptake of *Mtb* bacilli in the alveolar space. One must then ask, what happens to these bacilli if they are not internalized? This is not as clear as it may initially seem. Some have suggested that *Mtb* is an obligate intracellular pathogen[569]. However, this is undoubtedly untrue: more accurately, it is a facultative intracellular pathogen capable of replication without host factors. It is not immediately clear what these non-phagocytosed bacilli may do within the alveolar space, but previous authors have reviewed infection of non-phagocytic cells such as fibroblasts, pneumocytes, and mucosal epithelial cells[570,571]. The infection of these cells appears in part dependent on macropinocytosis, a process involving much of the same signaling and cytoskeletal architecture as phagocytosis[115,572]. It is not yet known whether sphingolipid inhibition would block macropinocytosis in addition to phagocytosis.

However, if one puts aside the question of what may happen if *Mtb* in the airway is not phagocytosed, other questions arise. What about the other environmental pathogens we encounter daily? What about dead or damaged cells in the alveolar space? What about effete material in the nervous

system? One may expect that inhibiting total phagocytosis throughout the body would result in dramatic immune suppression and disease[573,574].

In contrast, utilizing sphingolipids to restrict intracellular *Mtb* replication is much more appealing. Our results in Chapter 4 suggest that more sphingolipids would further limit bacterial growth. Here, too, there are questions about the effects of increasing sphingolipid content in cells. Sphingolipidosis (the harmful accumulation of sphingolipids) is associated with numerous diseases, including many lysosomal storage disorders[202,575]. Further, our results have yet to clarify which sphingolipid is primarily responsible for the antimycobacterial restriction we observe – does sphingomyelin play only a minor role in this process, outdone by a select glycosphingolipid species? Much work remains in addressing this question.

There is one final wrench to throw in these perspectives: an emerging body of work suggests that antimicrobial immune activity may drive the formation of persisters during bacterial infection and thereby induce antibiotic-resistant bacterial populations. Stapels et al. report that *Salmonella enterica* persisters undermine antibiotic therapy and immune response[576]. Persister bacteria are non-growing, antibiotic-tolerant bacterial cells that form upon sensing antimicrobial effectors – though ongoing work seeks to identify the specific drivers of persister formation in different bacterial families. Candidate signals include acidic pH, diauxic shift, and iron sequestration[577]. These authors describe a grey zone of antimicrobial activity, in which many or most bacteria are killed, but the infection is not wholly sterilized. These surviving bacteria, the persisters, have a *de facto* resistance to antibiotics through their absence of metabolic activity. They are also prime candidates for developing *bona fide* antibiotic resistance, as they survive sub-lethal doses of antibiotics. These conditions appear highly relevant to *Mtb* infection: a primary reason underlying the need for 6-9 months of antitubercular antibiotic therapy is the resistance of slow-growing persisters in the infection[578].

A logical, if frightening, question arises: Can we enhance the efficacy of frontline antibiotics by suppressing immune function? Several authors have already sought to address this question in *Staphylococcus aureus* infection. Beam et al. showed in 2022 that acute immunosuppression significantly reduced the numbers of antibiotic-tolerant bacteria in BMDM infection[579]. Sphingolipid synthesis inhibitors such as myriocin and fumonisin B1 are used in humans[580–583], though only rarely because there are many reported side effects, including hepatotoxicity, and immunosuppression[583,584]. In this context, the side effects of sphingolipid inhibition would be the desired effect.

So, is it preferable to give a TB patient immunosuppressive chemotherapy to shorten the length of their antibiotic therapy? Of course, this regimen would be risky. If the patient is infected with an antibiotic-resistant strain of *Mtb*, they may deteriorate rapidly and be exceedingly susceptible to other environmental pathogens such as *C. albicans* (as Tafesse et al. 2015 showed that sphingolipid inhibition significantly reduced survival in mice infected with *C. albicans*). Much more work must be done to answer these questions before such therapies can be implemented in humans, especially given the historical disparities in TB epidemiology and treatment.

11.2. A lipid map of the tug-of-war between *Mtb* and the macrophage

With Chapter 5, we venture beyond the sphingolipid family to investigate how *Mtb* infection alters the totality of the host lipidome. In this report, we decided to focus on three distinct phenotypes

of infection: the significant induction of diacylglycerol among pathogenic and attenuated *Mtb* infections and several pathogen-associated molecular patterns, the significant upregulation of triacylglycerol only in the pathogenic infection, and the significantly differential regulation of lysolipids and plasmalogens in pathogenic infection versus attenuated infection.

We find that diacylglycerol production is significantly upregulated in response to both pathogenic and attenuated *Mtb* infections, as well as in response to treatment with several PAMPs assayed in this study (namely, lipopolysaccharide, lipoarabinomannan, and 1-tuberculosinyladenosine). These findings may be described as a generalized antimicrobial program initiated via the sensing of mycobacteria. However, triacylglycerol production is only significantly stimulated due to pathogenic *Mtb* infection. This would support previous findings, including the 2023 report by Costa et al. regarding lipid droplet accumulation in H37Rv-infected cells[167]. Combined with the significant increase in acylcarnitine abundance, these data would suggest that fatty acid β-oxidation is upregulated in these infected cells, also in support of previous reports[170,171].

We also observe somewhat unique patterns among phospholipids in these results. These include the differential accumulation of lysophospholipids and plasmalogens between pathogenic and attenuated *Mtb* infections. In 2022, Jurkowitz et al. found that lysoplasmalogens have a direct antimycobacterial effect *in vitro*, and that a *Mtb* phospholipase A_2(MtbYhhN) in H37Rv degrades lysoplasmalogens[367]. The expression of this enzyme in *M. smegmatis* (a non-pathogenic environmental mycobacteria) confers resistance to lysoplasmalogen-induced bacterial death[367]. No prior reports have shown a disparity between lysophospholipid accumulation in H37Rv and H37Rv- ΔRD1 infections.

Before moving on, we must briefly return to sphingolipids. In these infection results, we see we see minor but consistent changes in the SL composition of *Mtb* infected cells - an increase in SM species and a decrease in Cer species, and intriguingly, the opposite for dihydrosphingomyelin and dihydroceramide. The accumulation of these dihydrosphingolipids is intriguing, though subtle. Dihydrosphingolipids are a category of sphingolipid that was long ignored as inactive and biologically irrelevant – a spurious sphingolipid precursor which was somehow missed by the ceramide Δ4-desaturase, DES1[585,586]. However, the upregulation of these lipids has been associated with several diseases involving dyslipidemia, particularly in diabetes[586]. Reports by Turpin et al. and Reali et al. verified that the accumulation of dihydroceramide promotes weight gain and insulin intolerance in mice and found that dihydroceramide is enriched in human adipose tissue in obese humans[587,588]. We omitted these findings in the main report for this chapter because the differential regulations of sphingolipids and dihydrosphingolipids were not statistically significant. However, we see a consistent pattern relating to the pathogenicity of the infecting bacteria: ΔRD1 infection results in depletion of dihydroceramide. This raises interesting questions about pathogenic *Mtb* infection inducing generalized dyslipidemia: Does this accumulation of dihydrosphingolipids during pathogenic infection coincide with upregulated fatty acid synthesis and lipid droplet formation?

11.3. Interacting with the Sphinx: does *Mtb* infection alter the sphingosine interactome?

In the report presented in Chapter 6, we seek to uncover the proteins that selectively interact with sphingosine during *Mtb* infection. To this end, we apply trifunctional sphingolipid analogs and perform affinity enrichment proteomics. An initial foray into using these probes in uninfected cells

revealed a narrow cohort of 35 proteins significantly enriched to at least one lipid probe. Intriguingly, twenty proteins were enriched to the sphingolipid precursor sphinganine, and only six proteins were enriched to the signaling sphingolipid sphingosine. Among these enriched proteins, half are reported membrane-associated or peripheral membrane proteins, and many include transmembrane domains. We additionally used two trifunctional fatty acid probes as a control, identifying generalized lipid-binding proteins among our sphingolipid-enriched hits.

Among our identified baseline interactors were several previously reported sphingolipid-interacting proteins, including VDAC1, VDAC2, VDAC3, CTSD, PSAP, and ECH1.

We used these interactomics results of activated THP-1 cells at baseline to inform a follow-up experiment in which cells infected with pathogenic and attenuated *Mtb* strains were analyzed for differential protein-sphingosine interactions. This analysis produced many differentially enriched proteins – some were upregulated during infection, but the majority were downregulated. By comparing these results to publicly available transcriptomics data, we find that most differentially enriched proteins do not coincide with differential transcriptional regulation – suggesting that these interaction results are the product of altered protein localization, degradation, or function within the infected cell.

Most of the proteins flagged as significantly or partially enriched in the baseline experiment are depleted during infection. Some of these hits may reflect biological function. For example, prior reports show that membrane-bound (inactive) Cathepsin D is activated upon interaction with ceramide in the lysosome and is released from the membrane into the lysosomal lumen[225–227]. Other interactions have a less clear connection to either sphingosine or *Mtb* infection.

HMGN1 is one such example. This protein is among the most down-regulated interactors at 24 hours of infection with pathogenic *Mtb*. While sphingosine is a known inhibitor of several calmodulin-binding proteins, such as HMGB1, no prior reports suggest sphingosine interaction with HMGN1. These proteins are both chromatin remodeling factors activated through their calmodulin binding site[589]. No previous reports suggest HMGN1 plays a role in *Mtb* infection, though the highly related HMGN2 is an antimicrobial peptide that has been shown to regulate mycobacterial survival in host cells[590,591].

There are also several intriguing proteins among the few differentially enriched hits between pathogenic H37Rv infection and attenuated H37Rv-ΔRD1 infection. The 20S proteasome subunit PSMA5 and the 20S proteasome subunit activator PSME3 are the third and first most enriched toward the pathogenic infection, respectively. No reports have tied these genes with *Mtb* infection. Why would proteasome subunits be enriched toward pathogenic infection and away from attenuated infection? Counter to these enrichments, the mitochondrial peptidase LONP1 is enriched toward attenuated infection. Do these findings indicate biologically relevant changes to the immunoproteasome? There were no proteins that were statistically significant in the comparison between H37Rv and H37Rv-ΔRD1, but there may still be interesting patterns in these results.

11.4. Thinking forward:

Where am I leaving this project? What directions will these stories go next? In the sections below, I summarize my thoughts on these four projects and detail the most apparent next steps for these works.

11.4.1. Chapter 1 – Does particle size affect the requirement for sphingolipids during phagocytosis?

In a brief side project, I found that sphingolipid depletion similarly reduced *Salmonella enterica* Typhimurium uptake by macrophages and dendritic cells (Figure 11.1 A-C). We decided not to pursue this as a project due to its overarching similarity to our previous publications in 2021[179] and 2015[205]. However, these data suggest an intriguing question that partially undercuts the findings of our prior publications: Do sphingolipids play a generalized role in phagocytosis?

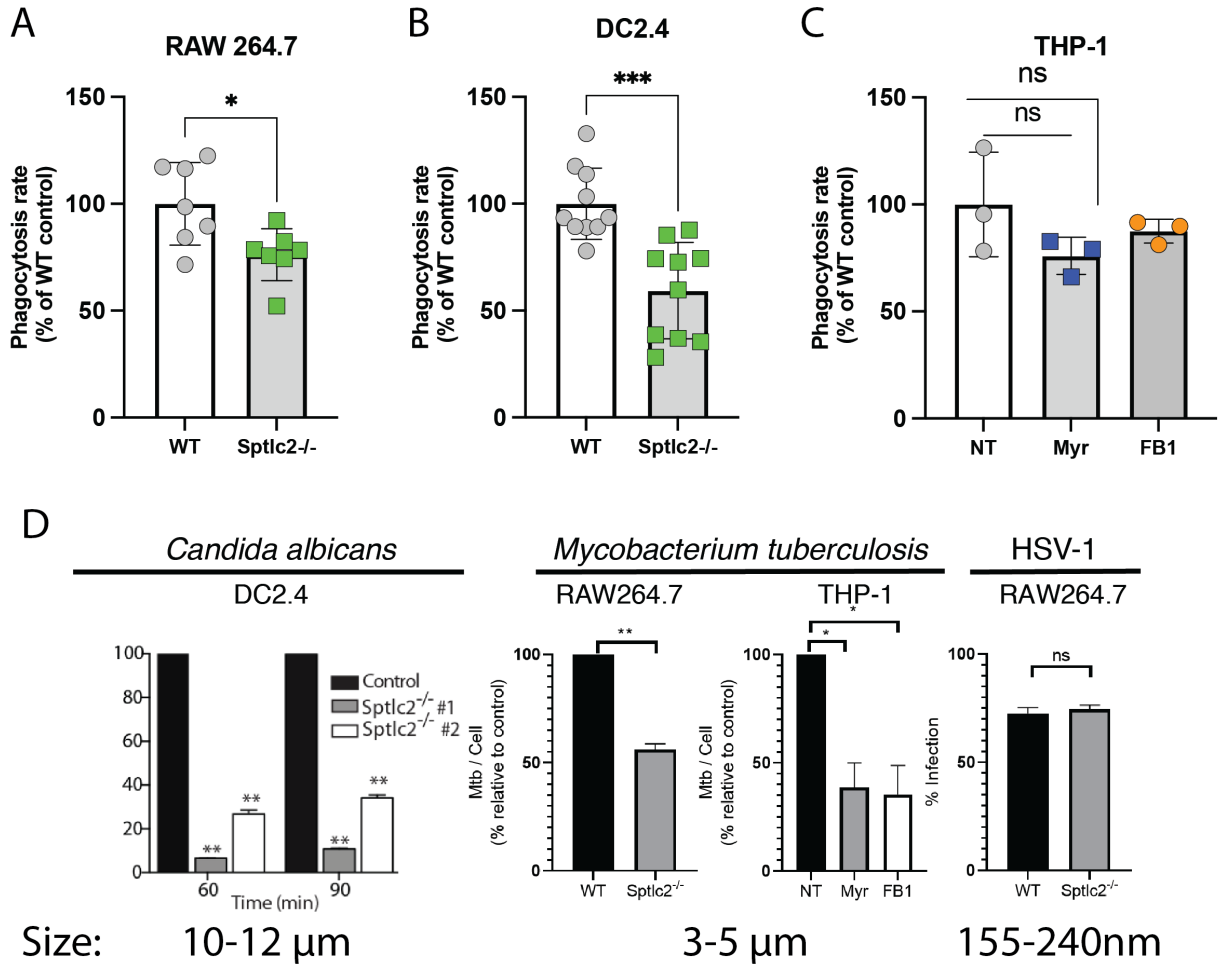


Figure 11.1. – **Sphingolipid inhibition reduces uptake of *S. enterica* along with several other pathogen-particles** (A-C) Unpublished data depicting the phagocytosis scores for *Salmonella enterica* uptake by RAW 264.7 cells (A), DC2.4 cells (B), and THP-1 cells (C) under the denoted means of sphingolipid depletion. Displayed are all technical replicates of 2 biological replicates (A), 3 biological replicates (B), and 1 biological replicate (C). (D) Published results from Tafesse et al. 2015[205] and Niekamp et al. 2021[179] depicting the phagocytosis scores for *Candida albicans*, *Mycobacterium tuberculosis*, and Herpes Simplex Virus-1 (HSV) following sphingolipid inhibition. Numbers below the plots are the range of reported sizes for each pathogen-particle.

I previously hypothesized that sphingolipids influence phagocytosis efficiency in proportion to the phagocytosed particle. In Figure 11.1 E, I depict our previously published results showing the magni-

tude of impact that sphingolipid depletion has on phagocytosis score. In the three projects along this vein of research, sphingolipids were absolutely essential for uptake of *Candida albicans*[205], required for *efficient* uptake of *Mtb*[179,297], and dispensable for receptor-mediated endocytosis[179]. The effect size (percent inhibition of phagocytosis rate) is nearly linearly proportional to the size of the particle in question. However, references greatly vary on the estimated sizes of each pathogen particle. Plotting each particle's (rough) size against the effect size of sphingolipid depletion on phagocytosis scores gives a nearly linear relationship between effect size and particle size (data not shown due to unreliability of reported particle size). Saharan et al. review our data and other similar reports to describe just such a postulate: that sphingolipids are intricately involved in phagocytosis[592].

Given these preliminary and somewhat subjective data, an interesting future project may look into the membrane dynamics of a sphingolipid depletion cell. If sphingolipids at the plasma membrane enable efficient uptake of large particles, there may be implications for pathologies resulting from deficient particle clearance. Silicosis comes to mind, in which phagocytes become "frustrated" and fail to fully internalize a particle – inadvertently releasing lysosomal contents into the extracellular space[593,594]. However, this project is neatly wrapped up with its publication in mBio and I find these questions less intriguing than those remaining from Chapter 2, discussed below.

11.4.2. Chapter 2 – Autophagy & a/nSMase: what happens to a chronically-damaged lysosome?

Following chronic, low-level lysosomal damage, the ESCRT membrane repair pathway recruits components of the autophagy pathway to culminate in lysophagy (the targeted autophagy of the lysosome)[147]. However, previous studies have shown that autophagy in *Mtb*-infected cells is inhibited[151,595]. Previous authors have also found that autophagy is essential in restricting *Mtb* infection[152]. The counterbalance of these effects is intriguing and suggests a complex interplay between host and *Mtb* factors. The role of sphingolipids in this process is currently undefined, though a ripe avenue for future research. This is a clear direction for future work.

Similarly, Chapter 4 does not explicitly address the role of sphingomyelin degradation in our observations. We intentionally excluded data regarding acid and neutral sphingomyelinase inhibition from this report because, in a word, they are confusing. Some of these results are depicted below in Figure 11.2.

The fact that we see a minor increase in pLux growth following neutral sphingomyelinase inhibition via GW4869 treatment (Figure 11.2, green points) aligns with the larger story involving neutral sphingomyelinase in an ESCRT-independent membrane repair process, as reported by Niekamp et al. (2022)[199]. These authors showed that lysosomal calcium is involved in this incomplete repair mechanism. As will be touched on below, we find a depletion of several calcium-interacting proteins in our sphingosine interaction proteomics data. There is likely an intriguing story to be fleshed out between these results. It must be noted that the underlying mechanism of the observations in Niekamp et al. 2022 have yet to be characterized, and there are many remaining open questions regarding how this supposedly-spontaneous repair process occurs.

Additionally, we observe significant restriction of pLux growth following inhibition with the acid sphingomyelinase inhibitors amitriptyline, though not following treatment with the highly related desipramine(Figure 11.2, light blue and purple points). It must be noted that the mechanisms of action for the nSMase inhibitor and the aSMase inhibitors are distinct. GW4869 is a lipid-competitive

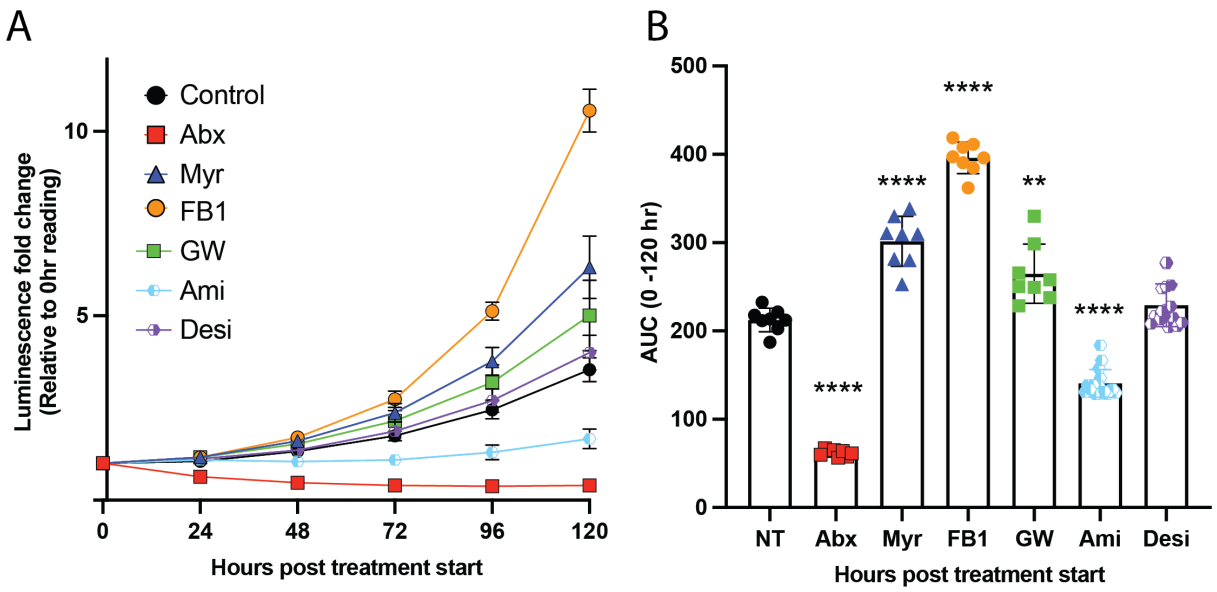


Figure 11.2. – Acid and neutral sphingomyelinase inhibitors induce opposing effects on *Mtb* intracellular growth (A) Representative growth curves from a single biological replicate (including the same data as presented in Chapter 4, Figure 4.4 E). Green squares depict technical replicates of cells treated with neutral sphingomyelinase inhibitor GW4869. Hexagons depict cells treated with acid sphingomyelinase inhibitors Amitriptyline (blue) and Desipramine (purple). (B) Areas under the curve were calculated as a measure of bacterial growth. Each point depicts a technical replicate from a single biological replicate. Statistics: Unpaired t-test; *: $p < 0.05$, **: $p < 0.01$, ***: $p < 0.001$, ****: $p < 0.0001$.

inhibitor of nSMase that selectively blocks enzymatic activity (though, interestingly, it does not compete with the substrate SM; it competes with phosphatidylserine)[596,597]. In contrast, amitriptyline and desipramine do not directly inhibit aSMase activity but rather induce the dissociation of aSMase from the lysosomal membrane and thereby drive its proteolytic degradation[598]. Amitriptyline and desipramine belong to a family of psychotropics widely used for their antidepressant effects[599]. These functional inhibitors of acid sphingomyelinase (FIASMAs) confer significant resistance to severe COVID-19 disease[599], *Staphylococcus aureus*-induced edema and sepsis[600], and *Escherichia coli*-induced apoptosis of dendritic cells during sepsis[601]. The data presented in Figure 11.2 are very preliminary, and we first need to verify the effects of amitriptyline treatment on *Mtb* replication. We also need to investigate the relative inhibitory capacity of these two related FIASMAs – we need to find the appropriate treatment concentrations of these compounds and adjust accordingly (it is highly probable that the difference apparent in these preliminary results is a simple product of different degrees of inhibitor activity).

Despite these caveats, these data would strongly support future work investigating aSMase as a potential target for antitubercular HDT. To my knowledge, there have been no observational reports investigating a link between FIASMA psychiatric use and TB incidence. A highly intriguing start may be an observational study comparing TB incidence rates of people taking these FIASMA antidepressants versus individuals not taking these drugs. An obvious challenge to this would be the fact that the underlying social determinants which enable access to clinical psychiatric treatment may be associated with inherently reduced TB incidence rates.

11.4.3. Chapter 3 – DG & TG? Lysolipids, Plasmalogens, & Lysoplasmalogens?

This project will need some follow-up before it is ready for publication. Ideally, we will select a vein of interest from the main findings delineated above and validate them directly. Each of the conclusions described may elicit an exciting project.

The role of diacylglycerol production has been observed before, but few reports have sought to characterize how DG signaling affects the intracellular stages of an *Mtb* infection. A previous project in the lab applied several small molecule inhibitors of DG synthesis to investigate the role of DG during phagocytosis of *Mtb* in a direct parallel to the report in Chapter 3. This project was discontinued, though perhaps too soon – we have yet to investigate the effect of these DG inhibitors on the intracellular replication of *Mtb*. The data reported here would suggest that DG plays a role in the antimicrobial response to mycobacterial infection, and a possible hypothesis would be that these DG inhibitors would release restriction on the bacteria in a similar fashion to sphingolipid inhibition.

Similarly, the role of TG synthesis in pathogenic infection is highly appealing: what factors distinguish the TG effects induced by pathogenic H37Rv strain? Is one of the pathogenicity factors in the RD1 region responsible for triggering lipid droplet accumulation, or is the *Mtb* Type VII secretion system required to translocate this mysterious lipid droplet-inducer into the cytosol? Will inhibition of TG synthesis restrict bacterial growth?

Finally, as mentioned above, the differential enrichment of lysolipids, plasmalogens, and dihydroceramide are each independently potential candidates for future research. How is the cell upregulating the production of these lipids? How is pathogenic *Mtb* attenuating the accumulation of these lipids?

Among these exciting observations and potential follow-up, we still await the results of an *in situ* spatial lipidomics analysis on *Mtb* infected cells. This analysis brought together the strengths of fluorescence microscopy and MALDI-TOF mass spectrometry and has been used to show profound asymmetries in the lipid composition of tissues[602]. These data would be massively helpful in determining if any upregulated TGs are localized to the *Mtb* or lipid droplets. Future experiments with lipid droplet staining tools such as Bodipy would coincide beautifully with our findings in the global lipidomics study.

11.4.4. Chapter 4 – Biological impact of interactions? *Mtb* sphingolipid interactome?

This project is far from publication as it stands. While the proteomics experiments yielded exciting results, a large body of follow-up work is needed to validate them and demonstrate their relevance to *Mtb* infection. In the shortest possible summary, there are three basic needs for these results to be published: validation, annotation, and characterization. There is also a fourth vein of intriguing work on protein-lipid interactions in cultured *Mtb*.

11.4.4.1. Validate the baseline interactions from the +/-UV experiment.

In the last two years, Dr. Scotland Farley and I have sought to optimize a reverse-pulldown protocol to enrich proteins crosslinked to trifunctional lipids by utilizing a bi-valent azide click handle,

which comprise both a fluorophore and a cleavable biotin. In this protocol, the cells will be initially treated much as they were in the proteomics experiments presented in Chapter 6, though instead of performing click reactions with azide-coated beads, we will click the lysates to the bivalent azide handle. We can thus use the same input lysate for two fluorescent Western blots: First, we can pull down using the biotin-conjugated trifunctional lipids to prepare blots much like those depicted in Figure 6.2, though these may be further stained for protein targets of interest (some of which are listed below). Secondly, the lysate may be used in a protein G pulldown using antibodies against targets of interest, and the fluorescently-labeled trifunctional lipids co-enriched to the target can be visualized on a Western blotting membrane. These efforts are still underway for the 35 significantly-enriched proteins identified in Figure 6.3 and Figure 6.4. Detection of fluorescence among each pulldown modality will serve as validation of our proteomics data.

Using this methodology, it is highly achievable to perform a reverse pulldown to orthogonally verify that a protein of interest interacts with the trifunctional lipid probe. As a starting point, we will apply this technique to the proteins identified as sphingosine and sphinganine binders in the absence of infection. For sphingosine, these hits include Cathepsin D (CTSD), Prosaposin (PSAP), phosphatidylinositol transfer protein beta (PITPNB), prolylcarboxypeptidase (PRCP), and phosphoribosylformylglycinamidine synthase (PFAS). For sphinganine-interacting proteins, we see all of the sphingosine significant hits and additional hits of interest, including the three voltage dependent anion channels (VDAC 1, 2, and 3), nucleobindins 1 and 2 (NUCB1 and NUCB2), and saccharopine dehydrogenase-like oxidoreductase (SCCPDH). Each of these proteins are involved in intriguing biological pathways – and several are involved in host response to pathogenic viral or bacterial infection – thus, each presents a possible story in which selective lipid interactions enable biological function.

A major challenge to these proposed pulldowns is the overall abundance of each target. In the event that no fluorescence can be detected for some hits, it may be necessary to use ectopic expression of tagged proteins as affinity targets (e.g. FLAG- or HA-tags). A remaining hurdle may be clarifying the specificity of interaction – utilizing treatment with a bolus of non-clickable lipid may serve to validate that a given interaction is selective.

11.4.4.2. Determine how *Mtb* infection changes the global proteome of the cell.

In order to understand whether our observed differential enrichment of interacting proteins is the product of true changes to the sphingosine interactome or the simple result of altered proteome content of the cell, we must measure the total proteome content of the *Mtb* infected cell. This would be performed at identical time points and with the same strains as used in the reported study. These results are essential for determining which hits are valid, biologically relevant interactions affected by *Mtb* infection and which hits are up- or down-regulated at the protein level. We have proposed preparing such global proteomics samples and cross-referencing our findings as I did with the publicly-available transcriptomics data presented in Figure S6.6. Other groups have performed such an analysis, but their data have yet to be made publicly available. Annotating our interaction data as the product of differential proteomic content is critical in determining which hits are biologically relevant.

With a stronger understanding of the global effects of *Mtb* infection on the host proteome, we can begin characterizing protein interactions which are dysregulated in a manner that is uncoupled from the total abundance of the protein – we are interested in understanding why the interaction

between sphingosine and a given target protein is differentially enriched or depleted during *Mtb* infection.

11.4.4.3. Uncover the biological relevance of protein-lipid interactions during *Mtb* infection.

Finally, we must determine if differentially-enriched interactions during Mtb infection influence the course of infection: up-/down-regulation of bacterial growth. We have proposed selecting 10-20 candidates and screening for their effect on infection via CRISPR knockout and high-throughput growth assays. However, notable challenges include the selection of high-confidence candidates for analysis (our data include broad changes which may simply reflect altered lysosomal function, immunoproteasome activity, and mitochondrial health), the feasibility of CRISPR knockout for these hits (sgRNA selection, validation, maintenance), and the feasibility of high-throughput analysis of intracellular growth (H37Rv-pLux is remarkably noisy, H37Rv-Live/Dead is not incredibly high throughput, colony-forming units are both noisy and incredibly low-throughput). Additionally, we may expect that *Mtb* pathogenicity factors drive the altered protein:lipid interactions – in which case, comparisons between pathogenic and attenuated *Mtb* strains would be essential.

The combined understandings of these three objectives will allow us to investigate the biological functions of our differentially-enriched hits. For example, we see a depletion of interaction between sphingosine and the COPI coat complex subunit ε, COPE, at 24 hours post-infection. Because the COPI coatomer protein complex is required for vesicular budding from the Golgi, we may hypothesize that the underlying lipid dynamics of this crucial cellular process are altered during infection. If the total abundance of this protein is unchanged, the question would become: where does COPE traffic during *Mtb* infection? Is vesicular trafficking globally affected by *Mtb*? Is this observation dependent on *Mtb* pathogenicity factors?

11.4.4.4. Identify protein-lipid interactions in purified *Mtb* cultures.

Though likely not a strict necessity for publishing the results I have prepared in Chapter 6, an additional and highly intriguing possible future direction is to use trifunctional probes to identify lipid-binding proteins within the *Mtb* proteome. However, identifying direct sphingolipid-binding proteins in the *Mtb* proteome would be highly impactful. An obvious continuation of this project will be to directly assay for *Mtb* proteins which selectively bind to tf-Sphingosine or tf-Sphinganine.

I wrote previously that *Mtb* encodes many lipid-metabolizing enzymes which enable the uptake, modification, and catabolism of many host lipids (Chapter 2). In this regard, it is somewhat disappointing that we did not confidently identify any such proteins in our interactomics analysis (Chapter 6). However, as I discussed in Chapter 6, it is somewhat unsurprising that we did not identify any *Mtb* proteins with high confidence; among many possible reasons, the lack of *Mtb* protein identification may have been due to the disparity between total host cellular mass and the expected mycobacterial mass within the prepared samples. Similarly, it may be expected that many of the lipid-binding proteins in both the host cell and the bacterium would be hydrophobic and predisposed to forming insoluble aggregates (even though we identified many membrane-spanning proteins among the host proteome, it is impossible to speculate how many interaction partners were lost in sample preparation due to insolubility).

I have performed some preliminary explorations into optimizing sample preparation and protein collection in cultured *Mtb* (Figure 11.3). These data show crosslinked protein enrichment in the tf-8:3-Fatty acid +UV sample. This is not surprising, given that it is widely known that *Mtb* utilizes fatty acid as an energy source and in its own lipid synthesis. Nonetheless, the identity of these proteins would be of great interest. This gel image does not show any apparent enrichment of tf-Sphingosine-interacting proteins. It must be noted, however, that this protocol is still being optimized, and there may yet be sphingosine-interacting proteins in the *Mtb* proteome. Future work on this project will certainly include the identification and characterization of proteins which selectively interact with sphingolipids, as these proteins would be of substantial interest as pathogenicity factors; as has been discussed previously in this document (Chapter 2), *Mtb* does not produce its own sphingolipids, and it may be expected that any protein which selectively interacts with this lipid class may be doing so as part of pathogenic action or as a source of carbon for replication or energy.

An interesting candidate may be Rv0888, tne *Mtb* enzyme known to direclty hydrolyze SM and confer the capacity to subsist on SM-enriched minimal media[212] – though the specificity for SM elicits several challenges given that trifunctional sphingomyelin has not yet been synthesized in the synthetic lipid analog boom. Nonetheless, the data shown in Figure 11.3 suggest that the described techniques ought to reveal sphingolipid-interacting proteins among the *Mtb* proteome.

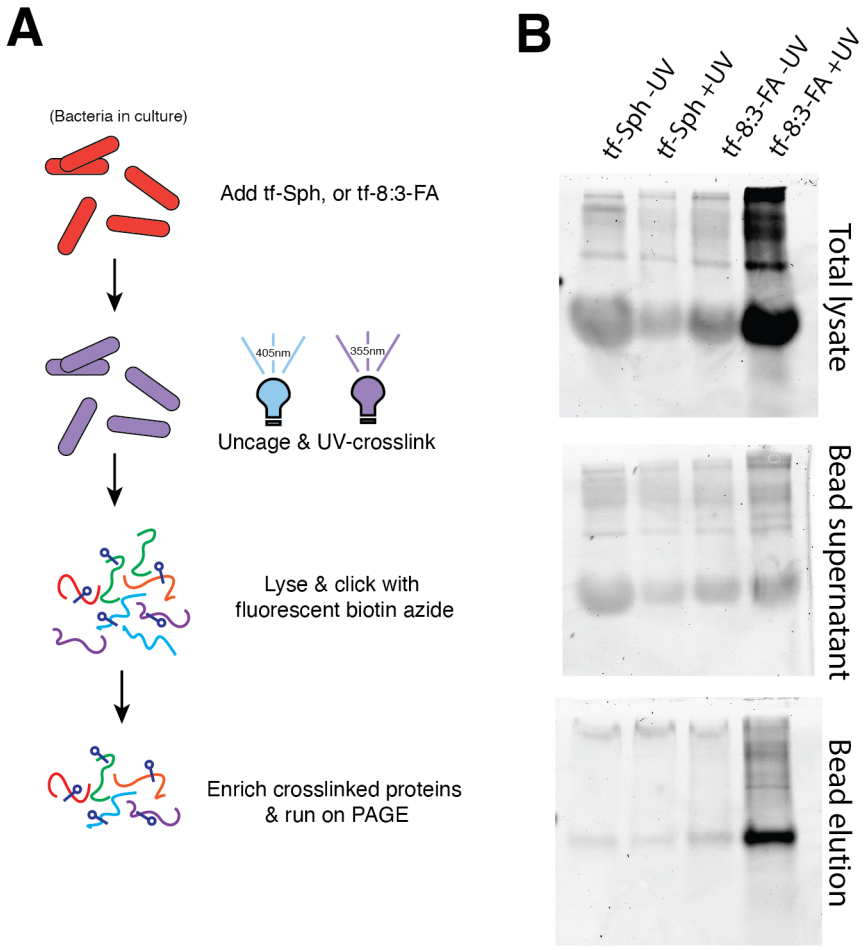


Figure 11.3. – **Preliminary enrichment of lipid-interacting proteins in *Mtb* culture** (A) A simple schematic of experimental procedure. Briefly, I treated cultured *Mtb* (strain H37Rv) with trifunctional sphingosine or 8:3-Fatty acid, uncaged, and crosslinked interactions. Control samples were left uncrosslinked. I then lysed the bacteria via chloroform:methanol wash, collected the protein fraction, and clicked crosslinked proteins with a bifunctional azide handle (containing both a fluorophore and a cleavable biotin tag). Using streptavidin beads, I enriched crosslinked proteins and cleaved the biotin tag using hydrazine. Finally, I ran unenriched lysate, bead supernatant, and bead elution on a polyacrylamide gel and visualized fluorescent proteins using a Sapphire fluorescent imager (Azure Bioscience). (B) In-gel fluorescence images of samples described above. Upper panel: raw lysate; middle panel: bead supernatant; lower panel: bead elution.

11.5. Concluding remarks

At long last, I must conclude this document. This is an odd feeling because its completion has less to do with the finality of my thoughts or a loss for words than it has to do with the sand having run out of my hourglass. This document has lived in my mind for the last six years, and there are infinite tweaks and rewrites that I could do. If any readers made it this far, thank you for your attention – I hope some of my thoughts on these topics have been interesting.

The PhD project presented herein sought to uncover and clarify the ways that host sphingolipids (and host lipids in general) influence and are influenced by *Mycobacterium tuberculosis* infection. We found many interconnecting manners in which *Mtb* is highly dependent on the nuanced balance of lipid metabolism in host cells – subtle changes to the host lipidome have outsize effects on *Mtb* entry, replication, and survival. Not everything in this document, by a far margin, has been published – I look forward to seeing where these data take us in the future! There is an irony to be found in practicing science: in answering one question, or even a hundred questions, one does not reduce the number of questions in the universe; instead, one finds that every question answered reveals an infinitude of new questions in a massive fractal spiraling down toward the great glowing coils of the universe.

The projects I've etched here have been a significant piece of my adult life. The last six years and six months have been a blur and an eternity. In that time, I have learned quite a lot about *Mycobacterium tuberculosis*. Despite hundreds of entries into the BSL-3, I have avoided learning what it feels like to have tuberculosis. I have also learned quite a lot about lipids in this time. However, I've mainly learned that there is too much to know about lipids for any one person to know everything about them. I have learned a lot about myself over this process. I have made lifelong friends and lived in a place I love. I can't begin to explain how grateful I feel to all the friends and family I have in my life, as none of this would have been possible without them. In some ways, writing a 300 page dissertation feels like screaming into the void – what use is a document that is traditionally never read once the degree is conferred? If even a single person reads any of this document (aside from my lovely committee, who read it by force), it will be a resounding validation of my effort over these years. If anyone is reading this, I hope you found some interesting something somewhere in this dissertation.

References

1. Organization, W.H. Global Tuberculosis Report 2023 (World Health Organization).

2. Daniel, T.M. (2006). The history of tuberculosis. Respiratory Medicine *100*, 1862–1870. 10.1016/j.rmed.2006.08.006.

3. Buzic, I., and Giuffra, V. (2020). The paleopathological evidence on the origins of human tuberculosis: A review. J Prev Med Hyg *61*, E3–E8. 10.15167/2421-4248/jpmh2020.61.1s1.1379.

4. Donoghue, H.D., Lee, O.Y.-C., Minnikin, D.E., Besra, G.S., Taylor, J.H., and Spigelman, M. (2010). Tuberculosis in Dr Granville's mummy: A molecular re-examination of the earliest known Egyptian mummy to be scientifically examined and given a medical diagnosis. Proc Biol Sci *277*, 51–56. 10.1098/rspb.2009.1484.

5. Karamanou, M., and Androutsos, G. (2012). The masterful description of pulmonary tuberculosis by Soranus of Ephesus (c. 98-138 A.D.). Am J Respir Crit Care Med *186*, 571. 10.1164/ajrccm.186.6.571.

6. Aurelianus, C., Drabkin, I.E., and Ephesus, S. of (1950). On acute diseases and On chronic diseases (Chicago: University of Chicago Press).

7. Newland, C. (2017). The Prettiest Way to Die. https://lithub.com/the-prettiest-way-to-die/.

8. Meier, A. (2018). How Tuberculosis Symptoms Became Ideals of Beauty in the 19th Century. https://hyperallergic.com/415421/consumptive-chic-a-history-of-beaty-fashion-disease/.

9. Day, C. (2017). Consumptive chic: A history of beauty, fashion, and disease (Bloomsbury Academic, an imprint of Bloomsbury Publishing Plc).

10. Mccarthy, O.R. (2001). The Key to the Sanatoria. J R Soc Med *94*, 413–417. 10.1177/014107680109400813.

11. Hajar, R. (2021). Medicine from galen to the present: A short history. Heart Views *22*, 307. 10.4103/heartviews.heartviews_125_21.

12. Mattern, S. (2011). Galen and his patients. The Lancet *378*, 478–479. 10.1016/S0140-6736(11)61240-3.

13. Riva, M.A. (2014). From milk to rifampicin and back again: History of failures and successes in the treatment for tuberculosis. J Antibiot *67*, 661–665. 10.1038/ja.2014.108.

14. Warren, P. (2006). The Evolution of the Sanatorium: The First Half-Century, 1854–1904. Canadian Bulletin of Medical History *23*, 457–476. 10.3138/cbmh.23.2.457.

15. Daniel, T.M. (2011). Hermann Brehmer and the origins of tuberculosis sanatoria. Int J Tuberc Lung Dis *15*, 161–162, i.

16. Kinghorn, H.M. (1922). Brehmer and dettweiler. American Review of Tuberculosis *5*, 950–972. 10.1164/art.1922.5.12.950.

17. Oregon Health & Science University (2014). University State Tuberculosis Hospital, 1953 (Oregon Health & Science University) 10.6083/M4Z31X94.

18. Silber, D.J. (2021). The Feel-Good Recliner That Cures What Ails You. Smithsonian Magazine.

19. Epstien, R.H. (2003). A Magic Mountain of Fresh Air, Sexual Frolicking and, Oh, Yes, Recovery. New York Times: Section F, 5.

20. Bäni, W. (2016). DAVOS – FROM HIGH-ALTITUDE SANATORIUM TO WORLD-RENOWNED HOLIDAY DESTINATION AND ECONOMIC CAPITAL. ASPETAR Sports Medicine Journal *Volume 5*.

21. Gale, S.L. (2022). The history of sanatoriums and surveillance. https://wellcomecollection.org/articles/Y3UIvxAAAGXXTsFx.

22. Murray, J.F., Schraufnagel, D.E., and Hopewell, P.C. (2015). Treatment of Tuberculosis. A Historical Perspective. Annals ATS *12*, 1749–1759. 10.1513/AnnalsATS.201509-632PS.

23. Parfitt, C.D. (1926). The Treatment of Laryngeal Tuberculosis in Sanatoria. Can Med Assoc J *16*, 1206–1210.

24. S. J. P. (1920). Pulmonary Tuberculosis: Mortality after Sanatorium Treatment. Journal of the Institute of Actuaries (1886-1994) *52*, 106–109.

25. Marten, B. (1720). A new theory of consumptions: More especially of a phthisis, or consumption of the lungs. ... By benjamin marten, M.D. (R. Knaplock).

26. Doetsch, R.N. (1978). Benjamin Marten and his "New Theory of Consumptions". Microbiol Rev *42*, 521–528. 10.1128/mr.42.3.521-528.1978.

27. Koch, R., Brock, T.D., and Fred, E.B. (1882). The Etiology of Tuberculosis. Reviews of Infectious Diseases *4*, 1270–1274.

28. Cross, A.N.R. (1919). The next to go. Fight tuberculosis! Red Cross Christmas seal campaign.

29. Iseman, M.D. (2002). Tuberculosis therapy: Past, present and future. European Respiratory Journal *20*, 87S–94s. 10.1183/09031936.02.00309102.

30. Carr, W., Kurbatova, E., Starks, A., Goswami, N., Allen, L., and Winston, C. (2022). Interim Guidance: 4-Month Rifapentine-Moxifloxacin Regimen for the Treatment of Drug-Susceptible Pulmonary Tuberculosis — United States, 2022. MMWR Morb. Mortal. Wkly. Rep. *71*, 285–289. 10.15585/mmwr.mm7108a1.

31. Nahid, P., Dorman, S.E., Alipanah, N., Barry, P.M., Brozek, J.L., Cattamanchi, A., Chaisson, L.H., Chaisson, R.E., Daley, C.L., Grzemska, M., et al. (2016). Executive Summary: Official American Thoracic Society/Centers for Disease Control and Prevention/Infectious Diseases Society of America Clinical Practice Guidelines: Treatment of Drug-Susceptible Tuberculosis. Clinical Infectious Diseases *63*, 853–867. 10.1093/cid/ciw566.

32. Droznin, M., Johnson, A., and Johnson, A.M. (2017). Multidrug resistant tuberculosis in prisons located in former Soviet countries: A systematic review. PLoS One *12*, e0174373. 10.1371/journal.pone.0174373.

33. Drobniewski, F., Balabanova, Y., Ruddy, M., Weldon, L., Jeltkova, K., Brown, T., Malomanova, N., Elizarova, E., Melentyey, A., Mutovkin, E., et al. (2002). Rifampin- and multidrug-resistant tuberculosis in Russian civilians and prison inmates: Dominance of the beijing strain family. Emerg Infect Dis *8*, 1320–1326. 10.3201/eid0811.020507.

34. Rusakova, L., Sterlikov, S., and Ponomarev, S. (2018). Extensively drug-resistant tuberculosis in the penitentiary facilities of the Russian Federation. In Tuberculosis (European Respiratory Society), p. PA3683. 10.1183/13993003.congress-2018.PA3683.

35. Brynildsrud, O.B., Pepperell, C.S., Suffys, P., Grandjean, L., Monteserin, J., Debech, N., Bohlin, J., Alfsnes, K., Pettersson, J.O.-H., Kirkeleite, I., et al. (2018). Global expansion of *Mycobacterium Tuberculosis* lineage 4 shaped by colonial migration and local adaptation. Sci. Adv. *4*, eaat5869. 10.1126/sciadv.aat5869.

36. Smith, A., Herington, E., and Loshak, H. (2021). Tuberculosis Stigma and Racism, Colonialism, and Migration: A Rapid Qualitative Review (Canadian Agency for Drugs and Technologies in Health).

37. Bennett, K. (2016). Telling the story of hundreds of Inuit, sick with TB, who were shipped to Hamilton. Canadian Broadcasting Company News.

38. Sponagle, J. (2016). National Inuit leader calls for apology from federal gov't over lost TB patients. Canadian Broadcasting Company News.

39. LaFreniere, M., Hussain, H., He, N., and McGuire, M. (2019). Tuberculosis in Canada: 2017. CCDR *45*, 68–74. 10.14745/ccdr.v45i23a04.

40. Uppal, A., Nsengiyumva, N.P., Signor, C., Jean-Louis, F., Rochette, M., Snowball, H., Etok, S., Annanack, D., Ikey, J., Khan, F.A., et al. (2021). Active screening for tuberculosis in high-incidence Inuit communities in Canada: A cost-effectiveness analysis. CMAJ *193*, E1652–E1659. 10.1503/cmaj.210447.

41. Indigenous Services Canada (2018). Actions Towards Eliminating Tuberculosis Across Inuit Nunangat. https://www.canada.ca/en/indigenous-services-canada/news/2018/12/actions-towards-eliminating-tuberculosis-across-inuit-nunangat.html.

42. Abdollahi, E., Keynan, Y., Foucault, P., Brophy, J., Sheffield, H., and Moghadas, S.M. (2022). Evaluation of TB elimination strategies in Canadian Inuit populations: Nunavut as a case study. Infectious Disease Modelling *7*, 698–708. 10.1016/j.idm.2022.07.005.

43. Connolly, C.A., and Gibson, M.E. (2011). The "White Plague" and Color: Children, Race, and Tuberculosis in Virginia 1900–1935. Journal of Pediatric Nursing *26*, 230–238. 10.1016/j.pedn.2010.01.011.

44. Schildknecht, K.R., Pratt, R.H., Feng, P.-J.I., Price, S.F., and Self, J.L. (2023). Tuberculosis — United States, 2022. MMWR Morb. Mortal. Wkly. Rep. *72*, 297–303. 10.15585/mmwr.mm7212a1.

45. Schildknecht, K.R., Pratt, R.H., Feng, P.-J.I., Price, S.F., and Self, J.L. (2023). Tuberculosis — United States, 2022. MMWR Morb. Mortal. Wkly. Rep. *72*, 297–303. 10.15585/mmwr.mm7212a1.

46. Carwile, M.E., Hochberg, N.S., and Sinha, P. (2022). Undernutrition is feeding the tuberculosis pandemic: A perspective. Journal of Clinical Tuberculosis and Other Mycobacterial Diseases *27*, 100311. 10.1016/j.jctube.2022.100311.

47. Ockenga, J., Fuhse, K., Chatterjee, S., Malykh, R., Rippin, H., Pirlich, M., Yedilbayev, A., Wickramasinghe, K., and Barazzoni, R. (2023). Tuberculosis and malnutrition: The European perspective. Clinical Nutrition *42*, 486–492. 10.1016/j.clnu.2023.01.016.

48. Lönnroth, K., Castro, K.G., Chakaya, J.M., Chauhan, L.S., Floyd, K., Glaziou, P., and Raviglione, M.C. (2010). Tuberculosis control and elimination 2010–50: Cure, care, and social development. The Lancet *375*, 1814–1829. 10.1016/S0140-6736(10)60483-7.

49. Imtiaz, S., Shield, K.D., Roerecke, M., Samokhvalov, A.V., Lönnroth, K., and Rehm, J. (2017). Alcohol consumption as a risk factor for tuberculosis: Meta-analyses and burden of disease. Eur Respir J *50*, 1700216. 10.1183/13993003.00216-2017.

50. Hayashi, S., and Chandramohan, D. (2018). Risk of active tuberculosis among people with diabetes mellitus: Systematic review and meta□analysis. Tropical Med Int Health *23*, 1058–1070. 10.1111/tmi.13133.

51. Emery, J.C., Richards, A.S., Dale, K.D., McQuaid, C.F., White, R.G., Denholm, J.T., and Houben, R.M.G.J. (2021). Self-clearance of Mycobacterium tuberculosis infection: Implications for lifetime risk and population at-risk of tuberculosis disease. Proceedings of the Royal Society B: Biological Sciences *288*. 10.1098/rspb.2020.1635.

52. Gideon, H.P., Hughes, T.K., Tzouanas, C.N., Wadsworth, M.H., Tu, A.A., Gierahn, T.M., Peters, J.M., Hopkins, F.F., Wei, J.-R., Kummerlowe, C., et al. (2022). Multimodal profiling of lung granulomas in macaques reveals cellular correlates of tuberculosis control. Immunity *55*, 827–846.e10. 10.1016/j.immuni.2022.04.004.

53. Queval, C.J., Brosch, R., and Simeone, R. (2017). The Macrophage: A Disputed Fortress in the Battle against Mycobacterium tuberculosis. Frontiers in Microbiology *8*. 10.3389/fmicb.2017.02284.

54. Burke, D.S. (1993). Of postulates and peccadilloes: Robert Koch and vaccine (tuberculin) therapy for tuberculosis. Vaccine *11*, 795–804. 10.1016/0264-410X(93)90354-Z.

55. Kaufmann, S.H.E. (2021). Vaccine Development Against Tuberculosis Over the Last 140 Years: Failure as Part of Success. Front. Microbiol. *12*, 750124. 10.3389/fmicb.2021.750124.

56. Okafor, C.N., Rewane, A., and Momodu, I.I. (2023). Bacillus Calmette Guerin. In StatPearls (StatPearls Publishing).

57. Zhuang, L., Ye, Z., Li, L., Yang, L., and Gong, W. (2023). Next-Generation TB Vaccines: Progress, Challenges, and Prospects. Vaccines *11*, 1304. 10.3390/vaccines11081304.

58. Strong, E.J., and Lee, S. (2021). Targeting Autophagy as a Strategy for Developing New Vaccines and Host-Directed Therapeutics Against Mycobacteria. Front. Microbiol. *11*, 614313. 10.3389/fmicb.2020.614313.

59. Shim, D., Kim, H., and Shin, S.J. (2020). Mycobacterium tuberculosis Infection-Driven Foamy Macrophages and Their Implications in Tuberculosis Control as Targets for Host-Directed Therapy. Front. Immunol. *11*, 910. 10.3389/fimmu.2020.00910.

60. Abreu, R., Giri, P., and Quinn, F. (2020). Host-Pathogen Interaction as a Novel Target for Host-Directed Therapies in Tuberculosis. Frontiers in Immunology *11*, 1–14. 10.3389/fimmu.2020.01553.

61. Korb, V., Chuturgoon, A., and Moodley, D. (2016). Mycobacterium tuberculosis: Manipulator of Protective Immunity. IJMS *17*, 131. 10.3390/ijms17030131.

62. Garcia-Vilanova, A., Chan, J., and Torrelles, J.B. (2019). Underestimated Manipulative Roles of Mycobacterium tuberculosis Cell Envelope Glycolipids During Infection. Front. Immunol. *10*, 2909. 10.3389/fimmu.2019.02909.

63. Casares, D., Escribá, P.V., and Rosselló, C.A. (2019). Membrane Lipid Composition: Effect on Membrane and Organelle Structure, Function and Compartmentalization and Therapeutic Avenues. IJMS *20*, 2167. 10.3390/ijms20092167.

64. van Meer, G., and De Kroon, A.I.P.M. (2011). Lipid map of the mammalian cell. Journal of Cell Science *124*, 5–8. 10.1242/jcs.071233.

65. Schlame, M. (2019). Mitochondrial cristae as insulated transformers of metabolic energy. The EMBO Journal *38*, e103472. 10.15252/embj.2019103472.

66. Poulaki, A., and Giannouli, S. (2022). Mitochondrial Lipids: From Membrane Organization to Apoptotic Facilitation. IJMS *23*, 3738. 10.3390/ijms23073738.

67. Michaud, J.M., Thompson, L.R., Kaul, D., Espinoza, J.L., Richter, R.A., Xu, Z.Z., Lee, C., Pham, K.M., Beall, C.M., Malfatti, F., et al. (2018). Taxon-specific aerosolization of bacteria and viruses in an experimental ocean-atmosphere mesocosm. Nat Commun *9*, 2017. 10.1038/s41467-018-04409-z.

68. Barisch, C., and Soldati, T. (2017). Breaking fat! How mycobacteria and other intracellular pathogens manipulate host lipid droplets. Biochimie *141*, 54–61. 10.1016/j.biochi.2017.06.001.

69. Roque, N.R., Lage, S.L., Navarro, R., Fazolini, N., Maya-Monteiro, C.M., Rietdorf, J., Melo, R.C.N., D'Avila, H., and Bozza, P.T. (2020). Rab7 controls lipid droplet-phagosome association during mycobacterial infection. Biochimica et Biophysica Acta (BBA) - Molecular and Cell Biology of Lipids *1865*, 158703. 10.1016/j.bbalip.2020.158703.

70. Dutta, N.K., Bruiners, N., Zimmerman, M.D., Tan, S., Dartois, V., Gennaro, M.L., and Karakousis, P.C. (2020). Adjunctive Host-Directed Therapy With Statins Improves Tuberculosis-Related Outcomes in Mice. The Journal of Infectious Diseases *221*, 1079–1087. 10.1093/infdis/jiz517.

71. Olson, D.K., Fröhlich, F., Farese, R.V., and Walther, T.C. (2016). Taming the sphinx: Mechanisms of cellular sphingolipid homeostasis. Biochimica et Biophysica Acta (BBA) - Molecular and Cell Biology of Lipids *1861*, 784–792. 10.1016/j.bbalip.2015.12.021.

72. Badimon, J.J., and Santos-Gallego, C.G. (2015). HDL Dysfunction. Journal of the American College of Cardiology *66*, 1486–1488. 10.1016/j.jacc.2015.08.008.

73. Weigert, A., Olesch, C., and Brüne, B. (2019). Sphingosine-1-Phosphate and Macrophage Biology—How the Sphinx Tames the Big Eater. Frontiers in Immunology *10*, 1–19. 10.3389/fimmu.2019.01706.

74. Guzman, G., Niekamp, P., and Tafesse, F.G. (2020). The Squeaky Yeast Gets Greased: The Roles of Host Lipids in the Clearance of Pathogenic Fungi. Journal of Fungi *6*, 19. 10.3390/jof6010019.

75. JMS Pearce (2022). JLW Thudichum: Neglected “Father of neurochemistry”. Hektoen International.

76. Thudichum, J.L.W. (1884). A treatise on the chemical constitution of the brain (Bailliere, Tindall and Cox London).

77. Breathnach, C.S. (2001). Johann Ludwig Wilhelm Thudichum 1829-1901, bane of the Protagonisers. Hist Psychiatry *12*, 283–296. 10.1177/0957154X0101204702.

78. Carman, G.M., and Taylor, A. (2016). Solving the Riddle of the Role of Sphingolipids in Cell Signaling. Journal of Biological Chemistry *291*, 11460–11461. 10.1074/jbc.O116.000003.

79. Sun, Y., Xu, Y., Che, X., and Wu, G. (2022). Development of a Novel Sphingolipid Signaling Pathway-Related Risk Assessment Model to Predict Prognosis in Kidney Renal Clear Cell Carcinoma. Front. Cell Dev. Biol. *10*, 881490. 10.3389/fcell.2022.881490.

80. Lachkar, F., Ferré, P., Foufelle, F., and Papaioannou, A. (2021). Dihydroceramides: Their emerging physiological roles and functions in cancer and metabolic diseases. American Journal of Physiology-Endocrinology and Metabolism *320*, E122–E130. 10.1152/ajpendo.00330.2020.

81. Quinville, B.M., Deschenes, N.M., Ryckman, A.E., and Walia, J.S. (2021). A Comprehensive Review: Sphingolipid Metabolism and Implications of Disruption in Sphingolipid Homeostasis. IJMS *22*, 5793. 10.3390/ijms22115793.

82. Lee, M., Lee, S.Y., and Bae, Y.-S. (2023). Functional roles of sphingolipids in immunity and their implication in disease. Exp Mol Med *55*, 1110–1130. 10.1038/s12276-023-01018-9.

83. Wu, J., Ma, S., Sandhoff, R., Ming, Y., Hotz-Wagenblatt, A., Timmerman, V., Bonello-Palot, N., Schlotter-Weigel, B., Auer-Grumbach, M., Seeman, P., et al. (2019). Loss of Neurological Disease HSAN-I-Associated Gene SPTLC2 Impairs CD8+ T Cell Responses to Infection by Inhibiting T Cell Metabolic Fitness. Immunity *50*, 1218–1231.e5. 10.1016/j.immuni.2019.03.005.

84. Qi, T., Li, L., and Weidong, T. (2021). The Role of Sphingolipid Metabolism in Bone Remodeling. Front. Cell Dev. Biol. *9*, 752540. 10.3389/fcell.2021.752540.

85. Elmore, S. (2007). Apoptosis: A Review of Programmed Cell Death. Toxicol Pathol *35*, 495–516. 10.1080/01926230701320337.

86. Kolesnick, R., and Hannun, Y.A. (1999). Ceramide and apoptosis. Trends in Biochemical Sciences *24*, 224–225. 10.1016/S0968-0004(99)01408-5.

87. Liu, Y.-Y., Hill, R.A., and Li, Y.-T. (2013). Ceramide Glycosylation Catalyzed by Glucosylceramide Synthase and Cancer Drug Resistance. In Advances in Cancer Research (Elsevier), pp. 59–89. 10.1016/B978-0-12-394274-6.00003-0.

88. Tang, H., Huang, X., and Pang, S. (2022). Regulation of the lysosome by sphingolipids: Potential role in aging. Journal of Biological Chemistry *298*. 10.1016/j.jbc.2022.102118.

89. Santos, T.C.B., Dingjan, T., and Futerman, A.H. (2022). The sphingolipid anteome: Implications for evolution of the sphingolipid metabolic pathway. FEBS Letters *596*, 2345–2363. 10.1002/1873-3468.14457.

90. Cooper, G.M. (2000). The cell: A molecular approach 2. ed. (ASM Press [u.a.]).

91. Hiesinger, H., Head, J.W., Wolf, U., Jaumann, R., and Neukum, G. (2003). Ages and stratigraphy of mare basalts in Oceanus Procellarum, Mare Nubium, Mare Cognitum, and Mare Insularum. J. Geophys. Res. *108*, 2002JE001985. 10.1029/2002JE001985.

92. Lantink, M.L., Davies, J.H.F.L., Ovtcharova, M., and Hilgen, F.J. (2022). Milankovitch cycles in banded iron formations constrain the Earth–Moon system 2.46 billion years ago. Proc. Natl. Acad. Sci. U.S.A. *119*, e2117146119. 10.1073/pnas.2117146119.

93. Wisdom, J., Dbouk, R., Militzer, B., Hubbard, W.B., Nimmo, F., Downey, B.G., and French, R.G. (2022). Loss of a satellite could explain Saturn's obliquity and young rings. Science *377*, 1285–1289. 10.1126/science.abn1234.

94. Olejarz, J., Iwasa, Y., Knoll, A.H., and Nowak, M.A. (2021). The Great Oxygenation Event as a consequence of ecological dynamics modulated by planetary change. Nat Commun *12*, 3985. 10.1038/s41467-021-23286-7.

95. Tobin, D.M. (2015). Host-Directed Therapies for Tuberculosis: Figure 1. Cold Spring Harb Perspect Med *5*, a021196. 10.1101/cshperspect.a021196.

96. Zhao, J., Jin, L., Wu, D., Xie, J., Li, J., Fu, X., Cong, Z., Fu, P., Zhang, Y., Luo, X., et al. (2022). Global airborne bacterial community—interactions with Earth's microbiomes and anthropogenic activities. Proc. Natl. Acad. Sci. U.S.A. *119*, e2204465119. 10.1073/pnas.2204465119.

97. Nocera, A.L., Mueller, S.K., Stephan, J.R., Hing, L., Seifert, P., Han, X., Lin, D.T., Amiji, M.M., Libermann, T., and Bleier, B.S. (2019). Exosome swarms eliminate airway pathogens and provide passive epithelial immunoprotection through nitric oxide. Journal of Allergy and Clinical Immunology *143*, 1525–1535.e1. 10.1016/j.jaci.2018.08.046.

98. Flynn, J.L., and Chan, J. (2022). Immune cell interactions in tuberculosis. Cell *185*, 4682–4702. 10.1016/j.cell.2022.10.025.

99. Rosales, C., and Uribe-Querol, E. (2017). Phagocytosis: A Fundamental Process in Immunity. BioMed Research International *2017*. 10.1155/2017/9042851.

100. Pfrommer, E., Dreier, C., Gabriel, G., Dallenga, T., Reimer, R., Schepanski, K., Scherließ, R., Schaible, U.E., and Gutsmann, T. (2020). Enhanced tenacity of mycobacterial aerosols from necrotic neutrophils. Sci Rep *10*, 9159. 10.1038/s41598-020-65781-9.

101. O'grady, F., and Riley, R. (1963). Experimental airborne tuberculosis. Adv. Tuberc. Res *12*, 150–190.

102. Riley, R.L., Mills, C.C., Nyka, W., Weinstock, N., Storey, P.B., Sultan, L.U., Riley, M.C., and Wells, W.F. (1995). AERIAL DISSEMINATION OP PULMONARY TUBERCULOSIS: A TWO-YEAR STUDY OF CONTAGION IN A TUBERCULOSIS WARD1. American Journal of Epidemiology *142*, 3–14. 10.1093/oxfordjournals.aje.a117542.

103. Martin, C.J., Cadena, A.M., Leung, V.W., Lin, P.L., Maiello, P., Hicks, N., Chase, M.R., Flynn, J.L., and Fortune, S.M. (2017). Digitally Barcoding *Mycobacterium Tuberculosis* Reveals *In Vivo* Infection Dynamics in the Macaque Model of Tuberculosis. mBio *8*, e00312–17. 10.1128/mBio.00312-17.

104. Lin, P.L., Ford, C.B., Coleman, M.T., Myers, A.J., Gawande, R., Ioerger, T., Sacchettini, J., Fortune, S.M., and Flynn, J.L. (2014). Sterilization of granulomas is common in active and latent tuberculosis despite within-host variability in bacterial killing. Nat Med *20*, 75–79. 10.1038/nm.3412.

105. Ehlers, S., and Schaible, U.E. (2013). The Granuloma in Tuberculosis: Dynamics of a Host–Pathogen Collusion. Front. Immun. *3*. 10.3389/fimmu.2012.00411.

106. Keller, C., Hoffmann, R., Lang, R., Brandau, S., Hermann, C., and Ehlers, S. (2006). Genetically Determined Susceptibility to Tuberculosis in Mice Causally Involves Accelerated and Enhanced Recruitment of Granulocytes. Infect Immun *74*, 4295–4309. 10.1128/IAI.00057-06.

107. Cardona, P.-J. (2009). A Dynamic Reinfection Hypothesis of Latent Tuberculosis Infection. Infection *37*, 80–86. 10.1007/s15010-008-8087-y.

108. Kim, M., Wainwright, H.C., Locketz, M., Bekker, L., Walther, G.B., Dittrich, C., Visser, A., Wang, W., Hsu, F., Wiehart, U., et al. (2010). Caseation of human tuberculosis granulomas correlates with elevated host lipid metabolism. EMBO Molecular Medicine *2*, 258–274. 10.1002/emmm.201000079.

109. Hunter, R.L., Jagannath, C., and Actor, J.K. (2007). Pathology of postprimary tuberculosis in humans and mice: Contradiction of long-held beliefs. Tuberculosis *87*, 267–278. 10.1016/j.tube.2006.11.003.

110. Van Kooyk, Y., and Geijtenbeek, T.B.H. (2003). DC-SIGN: Escape mechanism for pathogens. Nature Reviews Immunology *3*, 697–709. 10.1038/nri1182.

111. Hossain, Md.M., and Norazmi, M.-N. (2013). Pattern Recognition Receptors and Cytokines in Mycobacterium tuberculosis Infection—The Double-Edged Sword? BioMed Research International *2013*, 1–18. 10.1155/2013/179174.

112. Kleinnijenhuis, J., Oosting, M., Joosten, L.A.B., Netea, M.G., and Van Crevel, R. (2011). Innate Immune Recognition of *Mycobacterium Tuberculosis*. Clinical and Developmental Immunology *2011*, 1–12. 10.1155/2011/405310.

113. Arish, M., and Naz, F. (2022). Macrophage plasticity as a therapeutic target in tuberculosis. Eur J Immunol *52*, 696–704. 10.1002/eji.202149624.

114. Purdy, G.E. (2011). Taking Out TB–Lysosomal Trafficking and Mycobactericidal Ubiquitin-Derived Peptides. Front. Microbio. *2*. 10.3389/fmicb.2011.00007.

115. Flannagan, R.S., Jaumouillé, V., and Grinstein, S. (2012). The Cell Biology of Phagocytosis. Annual Review of Pathology: Mechanisms of Disease *7*, 61–98. 10.1146/annurev-pathol-011811-132445.

116. Harrison, R.E., Bucci, C., Vieira, O.V., Schroer, T.A., and Grinstein, S. (2003). Phagosomes Fuse with Late Endosomes and/or Lysosomes by Extension of Membrane Protrusions along Microtubules: Role of Rab7 and RILP. Molecular and Cellular Biology *23*, 6494 LP–6506. 10.1128/MCB.23.18.6494-6506.2003.

117. Chernomordik, L.V., and Kozlov, M.M. (2003). Protein-Lipid Interplay in Fusion and Fission of Biological Membranes. Annual Review of Biochemistry *72*, 175–207. 10.1146/annurev.biochem.72.121801.161504.

118. Tan, S., Sukumar, N., Abramovitch, R.B., Parish, T., and Russell, D.G. (2013). Mycobacterium tuberculosis Responds to Chloride and pH as Synergistic Cues to the Immune Status of its Host Cell. PLoS Pathogens *9*. 10.1371/journal.ppat.1003282.

119. Carranza, C., and Chavez-Galan, L. (2019). Several Routes to the Same Destination: Inhibition of Phagosome-Lysosome Fusion by Mycobacterium tuberculosis. The American Journal of the Medical Sciences *357*, 184–194. 10.1016/j.amjms.2018.12.003.

120. Poirier, V., and Av-Gay, Y. (2012). Mycobacterium tuberculosis modulators of the macrophage's cellular events. Microbes and Infection *14*, 1211–1219. 10.1016/j.micinf.2012.07.001.

121. Upadhyay, S., Mittal, E., and Philips, J.A. (2018). Tuberculosis and the art of macrophage manipulation. Pathogens and Disease *76*. 10.1093/femspd/fty037.

122. Jaber, N., and Zong, W. (2013). Class III PI3K Vps34: Essential roles in autophagy, endocytosis, and heart and liver function. Annals of the New York Academy of Sciences *1280*, 48–51. 10.1111/nyas.12026.

123. Schnettger, L., Rodgers, A., Repnik, U., Lai, R.P., Pei, G., Verdoes, M., Wilkinson, R.J., Young, D.B., and Gutierrez, M.G. (2017). A Rab20-Dependent Membrane Trafficking Pathway Controls M. Tuberculosis Replication by Regulating Phagosome Spaciousness and Integrity. Cell Host and Microbe *21*, 619–628.e5. 10.1016/j.chom.2017.04.004.

124. Mendum, T.A., Wu, H., Kierzek, A.M., and Stewart, G.R. (2015). Lipid metabolism and Type VII secretion systems dominate the genome scale virulence profile of Mycobacterium tuberculosis in human dendritic cells. BMC Genomics *16*, 372. 10.1186/s12864-015-1569-2.

125. Quigley, J., Hughitt, V.K., Velikovsky, C.A., Mariuzza, R.A., El-Sayed, N.M., and Briken, V. (2017). The Cell Wall Lipid PDIM Contributes to Phagosomal Escape and Host Cell Exit of *Mycobacterium Tuberculosis*. mBio *8*, e00148–17. 10.1128/mBio.00148-17.

126. Osman, M.M., Pagán, A.J., Shanahan, J.K., and Ramakrishnan, L. (2020). Mycobacterium marinum phthiocerol dimycocerosates enhance macrophage phagosomal permeabilization and membrane damage. PLoS ONE *15*, e0233252. 10.1371/journal.pone.0233252.

127. Bedard, M., Van Der Niet, S., Bernard, E.M., Babunovic, G., Cheng, T.-Y., Aylan, B., Grootemaat, A.E., Raman, S., Botella, L., Ishikawa, E., et al. (2023). A terpene nucleoside from M. Tuberculosis induces lysosomal lipid storage in foamy macrophages. Journal of Clinical Investigation *133*, e161944. 10.1172/JCI161944.

128. Peng, X., and Sun, J. (2016). Mechanism of ESAT-6 membrane interaction and its roles in pathogenesis of Mycobacterium tuberculosis. Toxicon *116*, 29–34. 10.1016/j.toxicon.2015.10.003.

129. Simeone, R., Bobard, A., Lippmann, J., Bitter, W., Majlessi, L., Brosch, R., and Enninga, J. (2012). Phagosomal Rupture by Mycobacterium tuberculosis Results in Toxicity and Host Cell Death. PLoS Pathogens *8*, e1002507. 10.1371/journal.ppat.1002507.

130. Buter, J., Cheng, T.-Y., Ghanem, M., Grootemaat, A.E., Raman, S., Feng, X., Plantijn, A.R., Ennis, T., Wang, J., Cotton, R.N., et al. (2019). Mycobacterium tuberculosis releases an antacid that remodels phagosomes. Nat Chem Biol *15*, 889–899. 10.1038/s41589-019-0336-0.

131. Bedard, M., van der Niet, S., Bernard, E.M., Babunovic, G., Cheng, T.-Y., Aylan, B., Grootemaat, A.E., Raman, S., Botella, L., Ishikawa, E., et al. (2023). A terpene nucleoside from M. Tuberculosis induces lysosomal lipid storage in foamy macrophages. Journal of Clinical Investigation *133*. 10.1172/jci161944.

132. Russell, D.G. (2016). The ins and outs of the Mycobacterium tuberculosis-containing vacuole. Cellular Microbiology *18*, 1065–1069. 10.1111/cmi.12623.

133. Utermöhlen, O., Herz, J., Schramm, M., and Krönke, M. (2008). Fusogenicity of membranes: The impact of acid sphingomyelinase on innate immune responses. Immunobiology *213*, 307–314. 10.1016/j.imbio.2007.10.016.

134. Houben, D., Demangel, C., Van Ingen, J., Perez, J., Baldeón, L., Abdallah, A.M., Caleechurn, L., Bottai, D., Van Zon, M., De Punder, K., et al. (2012). ESX□1□mediated translocation to the cytosol controls virulence of mycobacteria. Cellular Microbiology *14*, 1287–1298. 10.1111/j.1462-5822.2012.01799.x.

135. Barisch, C., Holthuis, J.C.M., and Cosentino, K. (2023). Membrane damage and repair: A thin line between life and death. Biological Chemistry *404*, 467–490. 10.1515/hsz-2022-0321.

136. Sachdeva, K., and Sundaramurthy, V. (2020). The Interplay of Host Lysosomes and Intracellular Pathogens. Front. Cell. Infect. Microbiol. *10*, 595502. 10.3389/fcimb.2020.595502.

137. Santucci, P. (2021). Intracellular pathogens, membrane damage and cytosolic access. Cellular Microbiology *23*. 10.1111/cmi.13296.

138. Simeone, R., Bottai, D., Frigui, W., Majlessi, L., and Brosch, R. (2015). ESX/type VII secretion systems of mycobacteria: Insights into evolution, pathogenicity and protection. Tuberculosis *95*, S150–S154. 10.1016/j.tube.2015.02.019.

139. Osman, M.M., Shanahan, J.K., Chu, F., Takaki, K.K., Pinckert, M.L., Pagán, A.J., Brosch, R., Conrad, W.H., and Ramakrishnan, L. (2022). The C terminus of the mycobacterium ESX-1 secretion system substrate ESAT-6 is required for phagosomal membrane damage and virulence. Proc. Natl. Acad. Sci. U.S.A. *119*, e2122161119. 10.1073/pnas.2122161119.

140. Smith, J., Manoranjan, J., Pan, M., Bohsali, A., Xu, J., Liu, J., McDonald, K.L., Szyk, A., LaRonde-LeBlanc, N., and Gao, L.-Y. (2008). Evidence for Pore Formation in Host Cell Membranes by ESX-1-Secreted ESAT-6 and Its Role in *Mycobacterium Marinum* Escape from the Vacuole. Infect Immun *76*, 5478–5487. 10.1128/IAI.00614-08.

141. De Jonge, M.I., Pehau-Arnaudet, G., Fretz, M.M., Romain, F., Bottai, D., Brodin, P., Honoré, N., Marchal, G., Jiskoot, W., England, P., et al. (2007). ESAT-6 from *Mycobacterium Tuberculosis* Dissociates from Its Putative Chaperone CFP-10 under Acidic Conditions and Exhibits Membrane-Lysing Activity. J Bacteriol *189*, 6028–6034. 10.1128/JB.00469-07.

142. Hsu, T., Hingley-Wilson, S.M., Chen, B., Chen, M., Dai, A.Z., Morin, P.M., Marks, C.B., Padiyar, J., Goulding, C., Gingery, M., et al. (2003). The primary mechanism of attenuation of bacillus Calmette–Guérin is a loss of secreted lytic function required for invasion of lung interstitial tissue. Proc. Natl. Acad. Sci. U.S.A. *100*, 12420–12425. 10.1073/pnas.1635213100.

143. Radulovic, M., Wenzel, E.M., Gilani, S., Holland, L.K., Lystad, A.H., Phuyal, S., Olkkonen, V.M., Brech, A., Jäättelä, M., Maeda, K., et al. (2022). Cholesterol transfer via endoplasmic reticulum contacts mediates lysosome damage repair. The EMBO Journal *41*, e112677. 10.15252/embj.2022112677.

144. Papadopoulos, C., and Meyer, H. (2017). Detection and Clearance of Damaged Lysosomes by the Endo-Lysosomal Damage Response and Lysophagy. Current Biology *27*, R1330–R1341. 10.1016/j.cub.2017.11.012.

145. Deretic, V. (2012). Autophagy as an innate immunity paradigm: Expanding the scope and repertoire of pattern recognition receptors. Current Opinion in Immunology *24*, 21–31. 10.1016/j.coi.2011.10.006.

146. Henne, W.M., Buchkovich, N.J., and Emr, S.D. (2011). The ESCRT Pathway. Developmental Cell *21*, 77–91. 10.1016/j.devcel.2011.05.015.

147. Maejima, I., Takahashi, A., Omori, H., Kimura, T., Takabatake, Y., Saitoh, T., Yamamoto, A., Hamasaki, M., Noda, T., Isaka, Y., et al. (2013). Autophagy sequesters damaged lysosomes to control lysosomal biogenesis and kidney injury. EMBO J *32*, 2336–2347. 10.1038/emboj.2013.171.

148. Khandia, R., Dadar, M., Munjal, A., Dhama, K., Karthik, K., Tiwari, R., Yatoo, Mohd.I., Iqbal, H.M.N., Singh, K.P., Joshi, S.K., et al. (2019). A Comprehensive Review of Autophagy and Its Various Roles in Infectious, Non-Infectious, and Lifestyle Diseases: Current Knowledge and Prospects for Disease Prevention, Novel Drug Design, and Therapy. Cells *8*, 674. 10.3390/cells8070674.

149. Schütter, M., Giavalisco, P., Brodesser, S., and Graef, M. (2020). Local Fatty Acid Channeling into Phospholipid Synthesis Drives Phagophore Expansion during Autophagy. Cell *180*, 135–149.e14. 10.1016/j.cell.2019.12.005.

150. Golovkine, G.R., Roberts, A.W., Morrison, H.M., Rivera-Lugo, R., McCall, R.M., Nilsson, H., Garelis, N.E., Repasy, T., Cronce, M., Budzik, J., et al. (2023). Autophagy restricts Mycobacterium tuberculosis during acute infection in mice. Nat Microbiol *8*, 819–832. 10.1038/s41564-023-01354-6.

151. Siregar, T.A.P., Prombutara, P., Kanjanasirirat, P., Kunkaew, N., Tubsuwan, A., Boonmee, A., Palaga, T., Khumpanied, T., Borwornpinyo, S., Chaiprasert, A., et al. (2022). The autophagy-resistant *Mycobacterium Tuberculosis* Beijing strain upregulates KatG to evade starvation-induced autophagic restriction. Pathogens and Disease *80*, ftac004. 10.1093/femspd/ftac004.

152. Typas, D. (2023). Autophagy counteracts Mycobacterium tuberculosis infection at early stages. Nat Struct Mol Biol *30*, 720–720. 10.1038/s41594-023-01024-5.

153. Saini, N.K., Baena, A., Ng, T.W., Venkataswamy, M.M., Kennedy, S.C., Kunnath-Velayudhan, S., Carreño, L.J., Xu, J., Chan, J., Larsen, M.H., et al. (2016). Suppression of autophagy and antigen presentation by Mycobacterium tuberculosis PE_PGRS47. Nat Microbiol *1*, 16133. 10.1038/nmicrobiol.2016.133.

154. Divangahi, M., Chen, M., Gan, H., Desjardins, D., Hickman, T.T., Lee, D.M., Fortune, S., Behar, S.M., and Remold, H.G. (2009). Mycobacterium tuberculosis evades macrophage defenses by inhibiting plasma membrane repair. Nat Immunol *10*, 899–906. 10.1038/ni.1758.

155. Mittal, E., Skowyra, M.L., Uwase, G., Tinaztepe, E., Mehra, A., Köster, S., Hanson, P.I., and Philips, J.A. (2018). Mycobacterium tuberculosis Type VII Secretion System Effectors Differentially Impact the ESCRT Endomembrane Damage Response. mBio *9*, e01765–18. 10.1128/mBio.01765-18.

156. Duan, L., Yi, M., Chen, J., Li, S., and Chen, W. (2016). Mycobacterium tuberculosis EIS gene inhibits macrophage autophagy through up-regulation of IL-10 by increasing the acetylation of histone H3. Biochemical and Biophysical Research Communications *473*, 1229–1234. 10.1016/j.bbrc.2016.04.045.

157. Strong, E.J., Jurcic Smith, K.L., Saini, N.K., Ng, T.W., Porcelli, S.A., and Lee, S. (2020). Identification of Autophagy-Inhibiting Factors of Mycobacterium tuberculosis by High-Throughput Loss-of-Function Screening. Infect Immun *88*, e00269–20. 10.1128/IAI.00269-20.

158. Olzmann, J.A., and Carvalho, P. (2019). Dynamics and functions of lipid droplets. Nat Rev Mol Cell Biol *20*, 137–155. 10.1038/s41580-018-0085-z.

159. Mattos, K.A., Lara, F.A., Oliveira, V.G.C., Rodrigues, L.S., D'Avila, H., Melo, R.C.N., Manso, P.P.A., Sarno, E.N., Bozza, P.T., and Pessolani, M.C.V. (2011). Modulation of lipid droplets by Mycobacterium leprae in Schwann cells: A putative mechanism for host lipid acquisition and bacterial survival in phagosomes: M. Leprae-driven lipid droplets in Schwann cells. Cellular Microbiology *13*, 259–273. 10.1111/j.1462-5822.2010.01533.x.

160. Othieno, C., Hirsch, C.S., Hamilton, B.D., Wilkinson, K., Ellner, J.J., and Toossi, Z. (1999). Interaction of *Mycobacterium Tuberculosis* -Induced Transforming Growth Factor B1 and Interleukin-10. Infect Immun *67*, 5730–5735. 10.1128/IAI.67.11.5730-5735.1999.

161. Fortes, A., Pereira, K., Antas, P.R.Z., Franken, C.L.M.C., Dalcolmo, M., Ribeiro-Carvalho, M.M., Cunha, K.S., Geluk, A., Kritski, A., Kolk, A., et al. (2005). Detection of *in Vitro* interferon-γ and serum tumour necrosis factor-α in multidrug-resistant tuberculosis patients. Clinical and Experimental Immunology *141*, 541–548. 10.1111/j.1365-2249.2005.02872.x.

162. Berns, S.A., Isakova, J.A., and Pekhtereva, P. (2022). The Therapeutic potential of interferon-gamma in tuberculosis. ADMET DMPK. 10.5599/admet.1078.

163. Young, C., Walzl, G., and Du Plessis, N. (2020). Therapeutic host-directed strategies to improve outcome in tuberculosis. Mucosal Immunology *13*, 190–204. 10.1038/s41385-019-0226-5.

164. Gao, X.-F., Yang, Z.-W., and Li, J. (2011). Adjunctive therapy with interferon-gamma for the treatment of pulmonary tuberculosis: A systematic review. International Journal of Infectious Diseases *15*, e594–e600. 10.1016/j.ijid.2011.05.002.

165. Ghazaei, C. (2018). Mycobacterium tuberculosis and lipids: Insights into molecular mechanisms from persistence to virulence. J Res Med Sci *23*, 63. 10.4103/jrms.JRMS_904_17.

166. Guerrini, V., and Gennaro, M.L. (2019). Foam Cells: One Size Doesn't Fit All. Trends in Immunology *40*, 1163–1179. 10.1016/j.it.2019.10.002.

167. Costa, M.F.D.S., Pereira□Dutra, F., Deboosere, N., Jouny, S., Song, O., Iack, G., Souza, A.L., Roma, E.H., Delorme, V., Bozza, P.T., et al. (2023). *Mycobacterium tuberculosis* induces delayed lipid droplet accumulation in dendritic cells depending on bacterial viability and virulence. Molecular Microbiology *119*, 224–236. 10.1111/mmi.15023.

168. Owens, R.M., Hsu, F.F., VanderVen, B.C., Purdy, G.E., Hesteande, E., Giannakas, P., Sacchettini, J.C., McKinney, J.D., Hill, P.J., Belisle, J.T., et al. (2006). M. Tuberculosis Rv2252 encodes a diacylglycerol kinase involved in the biosynthesis of phosphatidylinositol mannosides (PIMs). Mol Microbiol *60*, 1152–1163. 10.1111/j.1365-2958.2006.05174.x.

169. Jain, M., Petzold, C.J., Schelle, M.W., Leavell, M.D., Mougous, J.D., Bertozzi, C.R., Leary, J.A., and Cox, J.S. (2007). Lipidomics reveals control of *Mycobacterium Tuberculosis* virulence lipids via metabolic coupling. Proceedings of the National Academy of Sciences *104*, 5133–5138. 10.1073/pnas.0610634104.

170. Chandra, P., He, L., Zimmerman, M., Yang, G., Köster, S., Ouimet, M., Wang, H., Moore, K.J., Dartois, V., Schilling, J.D., et al. (2020). Inhibition of Fatty Acid Oxidation Promotes Macrophage Control of Mycobacterium tuberculosis. mBio *11*, e01139–20. 10.1128/mBio.01139-20.

171. Yang, H., Wang, F., Guo, X., Liu, F., Liu, Z., Wu, X., Zhao, M., Ma, M., Liu, H., Qin, L., et al. (2021). Interception of host fatty acid metabolism by mycobacteria under hypoxia to suppress anti-TB immunity. Cell Discov *7*, 90. 10.1038/s41421-021-00301-1.

172. Segal, W., and Bloch, H. (1956). BIOCHEMICAL DIFFERENTIATION OF *MYCOBACTERIUM TUBERCULOSIS* GROWN *IN VIVO* AND *IN VITRO*. J Bacteriol *72*, 132–141. 10.1128/jb.72.2.132-141.1956.

173. McKinney, J.D., Zu Bentrup, K.H., Muñoz-Elías, E.J., Miczak, A., Chen, B., Chan, W.-T., Swenson, D., Sacchettini, J.C., Jacobs, W.R., and Russell, D.G. (2000). Persistence of Mycobacterium tuberculosis in macrophages and mice requires the glyoxylate shunt enzyme isocitrate lyase. Nature *406*, 735–738. 10.1038/35021074.

174. Schnappinger, D., Ehrt, S., Voskuil, M.I., Liu, Y., Mangan, J.A., Monahan, I.M., Dolganov, G., Efron, B., Butcher, P.D., Nathan, C., et al. (2003). Transcriptional Adaptation of *Mycobacterium Tuberculosis* within Macrophages. The Journal of Experimental Medicine *198*, 693–704. 10.1084/jem.20030846.

175. Timm, J., Post, F.A., Bekker, L.-G., Walther, G.B., Wainwright, H.C., Manganelli, R., Chan, W.-T., Tsenova, L., Gold, B., Smith, I., et al. (2003). Differential expression of iron-, carbon-, and oxygen-responsive mycobacterial genes in the lungs of chronically infected mice and tuberculosis patients. Proc. Natl. Acad. Sci. U.S.A. *100*, 14321–14326. 10.1073/pnas.2436197100.

176. Wilburn, K.M., Fieweger, R.A., and VanderVen, B.C. (2018). Cholesterol and fatty acids grease the wheels of Mycobacterium tuberculosis pathogenesis. Pathogens and Disease *76*, 1–14. 10.1093/femspd/fty021.

177. Lee, W., VanderVen, B.C., Fahey, R.J., and Russell, D.G. (2013). Intracellular Mycobacterium tuberculosis Exploits Host-derived Fatty Acids to Limit Metabolic Stress. Journal of Biological Chemistry *288*, 6788–6800. 10.1074/jbc.M112.445056.

178. Guzman, G., Creek, C., Farley, S., and Tafesse, F.G. (2023). Genetic Tools for Studying the Roles of Sphingolipids in Viral Infections. In Methods in Molecular Biology (Humana Press Inc.), pp. 1–16. 10.1007/978-1-0716-2895-9_1.

179. Niekamp, P., Guzman, G., Leier, H.C., Rashidfarrokhi, A., Richina, V., Pott, F., Barisch, C., Holthuis, J.C.M.M., and Tafesse, F.G. (2021). Sphingomyelin Biosynthesis Is Essential for Phagocytic Signaling during Mycobacterium tuberculosis Host Cell Entry. mBio *12*, 1–19. 10.1128/mBio.03141-20.

180. Hannun, Y.A., and Obeid, L.M. (2018). Sphingolipids and their metabolism in physiology and disease. Nat Rev Mol Cell Biol *19*, 175–191. 10.1038/nrm.2017.107.

181. Wattenberg, B.W. (2018). The long and the short of ceramides. Journal of Biological Chemistry *293*, 9922–9923. 10.1074/jbc.H118.003522.

182. Gault, C.R., Obeid, L.M., and Hannun, Y.A. (2010). An Overview of Sphingolipid Metabolism: From Synthesis to Breakdown. In Adv Exp Med Biol, pp. 1–23. 10.1007/978-1-4419-6741-1_1.

183. Ho, Q.W.C., Zheng, X., and Ali, Y. (2022). Ceramide Acyl Chain Length and Its Relevance to Intracellular Lipid Regulation. IJMS *23*, 9697. 10.3390/ijms23179697.

184. Newton, J., Lima, S., Maceyka, M., and Spiegel, S. (2015). Revisiting the sphingolipid rheostat: Evolving concepts in cancer therapy. Experimental Cell Research *333*, 195–200. 10.1016/j.yexcr.2015.02.025.

185. Villani, M., Subathra, M., Im, Y.-B., Choi, Y., Signorelli, P., Del Poeta, M., and Luberto, C. (2008). Sphingomyelin synthases regulate production of diacylglycerol at the Golgi. Biochemical Journal *414*, 31–41. 10.1042/BJ20071240.

186. Cerbón, J., and Del Carmen López-Sánchez, R. (2003). Diacylglycerol generated during sphingomyelin synthesis is involved in protein kinase C activation and cell proliferation in Madin-Darby canine kidney cells. Biochemical Journal *373*, 917–924. 10.1042/bj20021732.

187. Koivusalo, M., Jansen, M., Somerharju, P., and Ikonen, E. (2007). Endocytic Trafficking of Sphingomyelin Depends on Its Acyl Chain Length. MBoC *18*, 5113–5123. 10.1091/mbc.e07-04-0330.

188. Contreras, F.X., Ernst, A.M., Haberkant, P., Björkholm, P., Lindahl, E., Gönen, B., Tischer, C., Elofsson, A., Von Heijne, G., Thiele, C., et al. (2012). Molecular recognition of a single sphingolipid species by a protein's transmembrane domain. Nature *481*, 525–529. 10.1038/nature10742.

189. D'Angelo, G., Polishchuk, E., Tullio, G.D., Santoro, M., Campli, A.D., Godi, A., West, G., Bielawski, J., Chuang, C.-C., van der Spoel, A.C., et al. (2007). Glycosphingolipid synthesis requires FAPP2 transfer of glucosylceramide. Nature *449*, 62–67. 10.1038/nature06097.

190. Boath, A., Graf, C., Lidome, E., Ullrich, T., Nussbaumer, P., and Bornancin, F. (2008). Regulation and Traffic of Ceramide 1-Phosphate Produced by Ceramide Kinase. Journal of Biological Chemistry *283*, 8517–8526. 10.1074/jbc.M707107200.

191. Quinn, P., and Allan, D. (1992). Two separate pools of sphingomyelin in BHK cells. Biochimica et Biophysica Acta (BBA) - Lipids and Lipid Metabolism *1124*, 95–100. 10.1016/0005-2760(92)90131-E.

192. Freysz, L., and Mandel, P. (1980). Turnover of Molecular Species of Sphingomyelin in Microsomes and Myelin of Rat Brain. Journal of Neurochemistry *34*, 305–308. 10.1111/j.1471-4159.1980.tb06597.x.

193. Freysz, L., Lastennet, A., and Mandel, P. (1976). METABOLISM OF BRAIN SPHINGOMYELINS: HALF□LIVES OF SPHINGOSINE, FATTY ACIDS AND PHOSPHATE FROM TWO TYPES OF RAT BRAIN SPHINGOMYELIN. Journal of Neurochemistry *27*, 355–359. 10.1111/j.1471-4159.1976.tb12253.x.

194. Książek, M., Chacińska, M., Chabowski, A., and Baranowski, M. (2015). Sources, metabolism, and regulation of circulating sphingosine-1-phosphate. Journal of Lipid Research *56*, 1271–1281. 10.1194/jlr.R059543.

195. Garris, C.S., Blaho, V.A., Hla, T., and Han, M.H. (2014). Sphingosine□1□phosphate receptor 1 signalling in T cells: Trafficking and beyond. Immunology *142*, 347–353. 10.1111/imm.12272.

196. Menuz, V., Howell, K.S., Gentina, S., Epstein, S., Riezman, I., Fornallaz-Mulhauser, M., Hengartner, M.O., Gomez, M., Riezman, H., and Martinou, J.-C. (2009). Protection of *C. Elegans* from Anoxia by HYL-2 Ceramide Synthase. Science *324*, 381–384. 10.1126/science.1168532.

197. Noureddine, L., Azzam, R., Nemer, G., Bielawski, J., Nasser, M., Bitar, F., and Dbaibo, G.S. (2008). Modulation of total ceramide and constituent ceramide species in the acutely and chronically hypoxic mouse heart at different ages. Prostaglandins & Other Lipid Mediators *86*, 49–55. 10.1016/j.prostaglandins.2008.02.003.

198. Höglinger, D., Haberkant, P., Aguilera-Romero, A., Riezman, H., Porter, F.D., Platt, F.M., Galione, A., and Schultz, C. (2015). Intracellular sphingosine releases calcium from lysosomes. eLife *4*. 10.7554/eLife.10616.

199. Niekamp, P., Scharte, F., Sokoya, T., Vittadello, L., Kim, Y., Deng, Y., Südhoff, E., Hilderink, A., Imlau, M., Clarke, C.J., et al. (2022). Ca2+-activated sphingomyelin scrambling and turnover mediate ESCRT-independent lysosomal repair. Nature Communications *13*. 10.1038/s41467-022-29481-4.

200. Ramírez-Montiel, F., Mendoza-Macías, C., Andrade-Guillén, S., Rangel-Serrano, Á., Páramo-Pérez, I., Rivera-Cuéllar, P.E., España-Sánchez, B.L., Luna-Bárcenas, G., Anaya-Velázquez, F., Franco, B., et al. (2019). Plasma membrane damage repair is mediated by an acid sphingomyelinase in Entamoeba histolytica. PLoS Pathog *15*, e1008016. 10.1371/journal.ppat.1008016.

201. Hla, T., and Dannenberg, A.J. (2012). Sphingolipid Signaling in Metabolic Disorders. Cell Metabolism *16*, 420–434. 10.1016/j.cmet.2012.06.017.

202. Sun, A. (2018). Lysosomal storage disease overview. Ann. Transl. Med *6*, 476.–476. 10.21037/atm.2018.11.39.

203. Do, J., McKinney, C., Sharma, P., and Sidransky, E. (2019). Glucocerebrosidase and its relevance to Parkinson disease. Mol Neurodegeneration *14*, 36. 10.1186/s13024-019-0336-2.

204. Beutler, E. (2004). Enzyme Replacement in Gaucher Disease. PLoS Med *1*, e21. 10.1371/journal.pmed.0010021.

205. Tafesse, F.G., Rashidfarrokhi, A., Schmidt, F.I., Freinkman, E., Dougan, S., Dougan, M., Esteban, A., Maruyama, T., Strijbis, K., and Ploegh, H.L. (2015). Disruption of Sphingolipid Biosynthesis Blocks Phagocytosis of Candida albicans. PLoS pathogens *11*, e1005188. 10.1371/journal.ppat.1005188.

206. Olsen, I., and Jantzen, E. (2001). Sphingolipids in Bacteria and Fungi. Anaerobe *7*, 103–112. 10.1006/anae.2001.0376.

207. Brown, E.M., Ke, X., Hitchcock, D., Jeanfavre, S., Avila-Pacheco, J., Nakata, T., Arthur, T.D., Fornelos, N., Heim, C., Franzosa, E.A., et al. (2019). Bacteroides-Derived Sphingolipids Are Critical for Maintaining Intestinal Homeostasis and Symbiosis. Cell Host & Microbe *25*, 668–680.e7. 10.1016/j.chom.2019.04.002.

208. Wang, J., Chen, Y.-L., Li, Y.-K., Chen, D.-K., He, J.-F., and Yao, N. (2021). Functions of Sphingolipids in Pathogenesis During Host–Pathogen Interactions. Front. Microbiol. *12*, 701041. 10.3389/fmicb.2021.701041.

209. Bai, X., Ya, R., Tang, X., and Cai, M. (2023). Role and interaction of bacterial sphingolipids in human health. Front. Microbiol. *14*, 1289819. 10.3389/fmicb.2023.1289819.

210. Oh, S.F., Praveena, T., Song, H., Yoo, J.-S., Jung, D.-J., Erturk-Hasdemir, D., Hwang, Y.S., Lee, C.C., Le Nours, J., Kim, H., et al. (2022). Publisher Correction: Host immunomodulatory lipids created by symbionts from dietary amino acids. Nature *601*, E32–E32. 10.1038/s41586-021-04276-7.

211. Griffin, J.E., Gawronski, J.D., DeJesus, M.A., Ioerger, T.R., Akerley, B.J., and Sassetti, C.M. (2011). High-Resolution Phenotypic Profiling Defines Genes Essential for Mycobacterial Growth and Cholesterol Catabolism. PLoS Pathog *7*, e1002251. 10.1371/journal.ppat.1002251.

212. Speer, A., Sun, J., Danilchanka, O., Meikle, V., Rowland, J.L., Walter, K., Buck, B.R., Pavlenok, M., Hölscher, C., Ehrt, S., et al. (2015). Surface hydrolysis of sphingomyelin by the outer membrane protein Rv0888 supports replication of M ycobacterium tuberculosis in macrophages. Molecular Microbiology *97*, 881–897. 10.1111/mmi.13073.

213. Lee, W., VanderVen, B.C., Fahey, R.J., and Russell, D.G. (2013). Intracellular Mycobacterium tuberculosis Exploits Host-derived Fatty Acids to Limit Metabolic Stress. Journal of Biological Chemistry *288*, 6788–6800. 10.1074/jbc.M112.445056.

214. Daniel, J., Deb, C., Dubey, V.S., Sirakova, T.D., Abomoelak, B., Morbidoni, H.R., and Kolattukudy, P.E. (2004). Induction of a Novel Class of Diacylglycerol Acyltransferases and Triacylglycerol Accumulation in *Mycobacterium Tuberculosis* as It Goes into a Dormancy-Like State in Culture. J Bacteriol *186*, 5017–5030. 10.1128/JB.186.15.5017-5030.2004.

215. Daniel, J., Maamar, H., Deb, C., Sirakova, T.D., and Kolattukudy, P.E. (2011). Mycobacterium tuberculosis Uses Host Triacylglycerol to Accumulate Lipid Droplets and Acquires a Dormancy-Like Phenotype in Lipid-Loaded Macrophages. PLoS Pathogens *7*, e1002093. 10.1371/journal.ppat.1002093.

216. Srinivas, M., Rajakumari, S., Narayana, Y., Joshi, B., Katoch, V.M., Rajasekharan, R., and Balaji, K.N. (2008). Functional characterization of the phospholipase C activity of Rv3487c and its localization on the cell wall of Mycobacterium tuberculosis. J Biosci *33*, 221–230. 10.1007/s12038-008-0039-2.

217. Dang, G., Cui, Y., Wang, L., Li, T., Cui, Z., Song, N., Chen, L., Pang, H., and Liu, S. (2018). Extracellular Sphingomyelinase Rv0888 of Mycobacterium tuberculosis Contributes to Pathological Lung Injury of Mycobacterium smegmatis in Mice via Inducing Formation of Neutrophil Extracellular Traps. Front. Immunol. *9*, 677. 10.3389/fimmu.2018.00677.

218. Nadella, V., Sharma, L., Kumar, P., Gupta, P., Gupta, U.D., Tripathi, S., Pothani, S., Qadri, S.S.Y.H., and Prakash, H. (2020). Sphingosine-1-Phosphate (S-1P) Promotes Differentiation of Naive Macrophages and Enhances Protective Immunity Against Mycobacterium tuberculosis. Front. Immunol. *10*, 3085. 10.3389/fimmu.2019.03085.

219. Heo, J.-Y., and Im, D.-S. (2019). Pro-Inflammatory Role of $S1P_3$ in Macrophages. Biomolecules & Therapeutics *27*, 373–380. 10.4062/biomolther.2018.215.

220. Mohammed, S.A., Saini, R.V., Jha, A.K., Hadda, V., Singh, A.K., and Prakash, H. (2022). Sphingolipids, mycobacteria and host: Unraveling the tug of war. Front. Immunol. *13*, 1003384. 10.3389/fimmu.2022.1003384.

221. Maguire, T.J.A., Yung, S., Ortiz-Zapater, E., Kayode, O.S., Till, S., Corrigan, C., Siew, L.Q.C., Knock, G.A., and Woszczek, G. (2023). Sphingosine-1-phosphate induces airway smooth muscle hyperresponsiveness and proliferation. Journal of Allergy and Clinical Immunology *152*, 1131–1140.e6. 10.1016/j.jaci.2023.05.028.

222. McGovern, M.M., Avetisyan, R., Sanson, B.-J., and Lidove, O. (2017). Disease manifestations and burden of illness in patients with acid sphingomyelinase deficiency (ASMD). Orphanet J Rare Dis *12*, 41. 10.1186/s13023-017-0572-x.

223. Wu, Y., Li, C., Peng, H., Swaidan, A., Riehle, A., Pollmeier, B., Zhang, Y., Gulbins, E., and Grassmé, H. (2020). Acid Sphingomyelinase Contributes to the Control of Mycobacterial Infection via a Signaling Cascade Leading from Reactive Oxygen Species to Cathepsin D. Cells *9*, 2406. 10.3390/cells9112406.

224. Vázquez, C.L., Rodgers, A., Herbst, S., Coade, S., Gronow, A., Guzman, C.A., Wilson, M.S., Kanzaki, M., Nykjaer, A., and Gutierrez, M.G. (2016). The proneurotrophin receptor sortilin is required for Mycobacterium tuberculosis control by macrophages. Sci Rep *6*, 29332. 10.1038/srep29332.

225. Diment, S., Leech, M.S., and Stahl, P.D. (1988). Cathepsin D is membrane-associated in macrophage endosomes. J Biol Chem *263*, 6901–6907.

226. Heinrich, M., Wickel, M., Schneider-Brachert, W., Sandberg, C., Gahr, J., Schwandner, R., Weber, T., Brunner, J., Krönke, M., and Schütze, S. (2000). Cathepsin D targeted by acid sphingomyelinase-derived ceramide. EMBO J *19*, 315–315. 10.1038/sj.emboj.7592140.

227. Žebrakovská, I., Máša, M., Srp, J., Horn, M., Vávrová, K., and Mareš, M. (2011). Complex modulation of peptidolytic activity of cathepsin D by sphingolipids. Biochimica et Biophysica Acta (BBA) - Molecular and Cell Biology of Lipids *1811*, 1097–1104. 10.1016/j.bbalip.2011.09.005.

228. Taniguchi, M., Ogiso, H., Takeuchi, T., Kitatani, K., Umehara, H., and Okazaki, T. (2015). Lysosomal ceramide generated by acid sphingomyelinase triggers cytosolic cathepsin B-mediated degradation of X-linked inhibitor of apoptosis protein in natural killer/T lymphoma cell apoptosis. Cell Death Dis *6*, e1717–e1717. 10.1038/cddis.2015.82.

229. Bharath, L.P., Ruan, T., Li, Y., Ravindran, A., Wan, X., Nhan, J.K., Walker, M.L., Deeter, L., Goodrich, R., Johnson, E., et al. (2015). Ceramide-Initiated Protein Phosphatase 2A Activation Contributes to Arterial Dysfunction In Vivo. Diabetes *64*, 3914–3926. 10.2337/db15-0244.

230. Zhang, Y., Li, X., Carpinteiro, A., Goettel, J.A., Soddemann, M., and Gulbins, E. (2011). Kinase suppressor of Ras-1 protects against pulmonary Pseudomonas aeruginosa infections. Nat Med *17*, 341–346. 10.1038/nm.2296.

231. Li, C., Guo, S., Pang, W., and Zhao, Z. (2020). Crosstalk Between Acid Sphingomyelinase and Inflammasome Signaling and Their Emerging Roles in Tissue Injury and Fibrosis. Front. Cell Dev. Biol. *7*, 378. 10.3389/fcell.2019.00378.

232. Gulbins, E., Walter, S., Becker, K.A., Halmer, R., Liu, Y., Reichel, M., Edwards, M.J., Müller, C.P., Fassbender, K., and Kornhuber, J. (2015). A central role for the acid sphingomyelinase/ceramide system in neurogenesis and major depression. Journal of Neurochemistry *134*, 183–192. 10.1111/jnc.13145.

233. Jin, J., Hou, Q., Mullen, T.D., Zeidan, Y.H., Bielawski, J., Kraveka, J.M., Bielawska, A., Obeid, L.M., Hannun, Y.A., and Hsu, Y.T. (2008). Ceramide generated by sphingomyelin hydrolysis and the salvage pathway is involved in hypoxia/reoxygenation-induced bax redistribution to mitochondria in NT-2 cells. Journal of Biological Chemistry *283*, 26509–26517. 10.1074/jbc.M801597200.

234. Roca, F.J., Whitworth, L.J., Redmond, S., Jones, A.A., and Ramakrishnan, L. (2019). TNF Induces Pathogenic Programmed Macrophage Necrosis in Tuberculosis through a Mitochondrial-Lysosomal-Endoplasmic Reticulum Circuit. Cell *178*, 1344–1361.e11. 10.1016/j.cell.2019.08.004.

235. Butler, R.E., Brodin, P., Jang, J., Jang, M.-S., Robertson, B.D., Gicquel, B., and Stewart, G.R. (2012). The Balance of Apoptotic and Necrotic Cell Death in Mycobacterium tuberculosis Infected Macrophages Is Not Dependent on Bacterial Virulence. PLoS ONE *7*, e47573. 10.1371/journal.pone.0047573.

236. Park, J.S., Tamayo, M.H., Gonzalez-Juarrero, M., Orme, I.M., and Ordway, D.J. (2005). Virulent clinical isolates of *Mycobacterium Tuberculosis* grow rapidly and induce cellular necrosis but minimal apoptosis in murine macrophages. Journal of Leukocyte Biology *79*, 80–86. 10.1189/jlb.0505250.

237. Derrick, S.C., and Morris, S.L. (2007). The ESAT6 protein of Mycobacterium tuberculosis induces apoptosis of macrophages by activating caspase expression. Cell Microbiol *9*, 1547–1555. 10.1111/j.1462-5822.2007.00892.x.

238. Santucci, M.B., Amicosante, M., Cicconi, R., Montesano, C., Casarini, M., Giosuè, S., Bisetti, A., Colizzi, V., and Fraziano, M. (2000). *Mycobacterium tuberculosis* –Induced Apoptosis in Monocytes/Macrophages: Early Membrane Modifications and Intracellular Mycobacterial Viability. J INFECT DIS *181*, 1506–1509. 10.1086/315371.

239. Chavoshian, O., Biari, N., Badiee, A., Khamesipour, A., Abbasi, A., Saberi, Z., Jalali, S.A., and Jaafari, M.R. (2013). Sphingomyelin Liposomes Containing Soluble Leishmania major antigens Induced Strong Th2 Immune Response in BALB/c Mice. Iran J Basic Med Sci *16*, 965–972.

240. Kasagi, N., Doi, I., Nakabayashi, J., Saito, K., Tadakuma, A., Muraki, N., Hori, R., Kimura, T., Okada, K., Yamada, N., et al. (2023). Optimization of dihydrosphingomyelin/cholesterol mol ratio in topotecan-loaded liposomes to enhance drug retention and plasma half-life by understanding physicochemical and thermodynamic properties of the lipid membrane. Journal of Molecular Structure *1283*, 135333. 10.1016/j.molstruc.2023.135333.

241. Shabbits, J.A., and Mayer, L.D. (2003). Intracellular delivery of ceramide lipids via liposomes enhances apoptosis in vitro. Biochimica et Biophysica Acta (BBA) - Biomembranes *1612*, 98–106. 10.1016/S0005-2736(03)00108-1.

242. Li, Z., Hailemariam, T.K., Zhou, H., Li, Y., Duckworth, D.C., Peake, D.A., Zhang, Y., Kuo, M.-S., Cao, G., and Jiang, X.-C. (2007). Inhibition of sphingomyelin synthase (SMS) affects intracellular sphingomyelin accumulation and plasma membrane lipid organization. Biochimica et Biophysica Acta (BBA) - Molecular and Cell Biology of Lipids *1771*, 1186–1194. 10.1016/j.bbalip.2007.05.007.

243. Jiang, X.-C., Li, Z., and Yazdanyar, A. (2014). Sphingolipids and HDL Metabolism. In The HDL Handbook (Elsevier), pp. 133–158. 10.1016/B978-0-12-407867-3.00006-8.

244. Kyle, J.E., Crowell, K.L., Casey, C.P., Fujimoto, G.M., Kim, S., Dautel, S.E., Smith, R.D., Payne, S.H., and Metz, T.O. (2017). LIQUID: An-open source software for identifying lipids in LC-MS/MS-based lipidomics data. Bioinformatics *33*, 1744–1746. 10.1093/bioinformatics/btx046.

245. Greene, M., Hernandez-Corbacho, M.J., Ostermeyer-Fay, A.G., Hannun, Y.A., and Canals, D. (2023). A simple, highly sensitive, and facile method to quantify ceramide at the plasma membrane. Journal of Lipid Research *64*, 100322. 10.1016/j.jlr.2022.100322.

246. Yamaji, A., Sekizawa, Y., Emoto, K., Sakuraba, H., Inoue, K., Kobayashi, H., and Umeda, M. (1998). Lysenin, a Novel Sphingomyelin-specific Binding Protein. Journal of Biological Chemistry *273*, 5300–5306. 10.1074/jbc.273.9.5300.

247. Bakrač, B., Kladnik, A., Maček, P., McHaffie, G., Werner, A., Lakey, J.H., and Anderluh, G. (2010). A Toxin-based Probe Reveals Cytoplasmic Exposure of Golgi Sphingomyelin. Journal of Biological Chemistry *285*, 22186–22195. 10.1074/jbc.M110.105122.

248. Krishnamurthy, K., Dasgupta, S., and Bieberich, E. (2007). Development and characterization of a novel anti-ceramide antibody. Journal of Lipid Research *48*, 968–975. 10.1194/jlr.D600043-JLR200.

249. Rotolo, J., Stancevic, B., Zhang, J., Hua, G., Fuller, J., Yin, X., Haimovitz-Friedman, A., Kim, K., Qian, M., Cardó-Vila, M., et al. (2012). Anti-ceramide antibody prevents the radiation gastrointestinal syndrome in mice. J. Clin. Invest. *122*, 1786–1790. 10.1172/JCI59920.

250. Höglinger, D., Nadler, A., Haberkant, P., Kirkpatrick, J., Schifferer, M., Stein, F., Hauke, S., Porter, F.D., and Schultz, C. (2017). Trifunctional lipid probes for comprehensive studies of single lipid species in living cells. Proceedings of the National Academy of Sciences *114*, 1566–1571. 10.1073/pnas.1611096114.

251. Haberkant, P., Stein, F., Höglinger, D., Gerl, M.J., Brügger, B., Van Veldhoven, P.P., Krijgsveld, J., Gavin, A.-C.C., and Schultz, C. (2016). Bifunctional Sphingosine for Cell-Based Analysis of Protein-Sphingolipid Interactions. ACS Chemical Biology *11*, 222–230. 10.1021/acschembio.5b00810.

252. Haberkant, P., and Holthuis, J.C.M. (2014). Fat & fabulous: Bifunctional lipids in the spotlight. Biochimica et Biophysica Acta - Molecular and Cell Biology of Lipids *1841*, 1022–1030. 10.1016/j.bbalip.2014.01.003.

253. Schultz, C. (2023). Chemical Tools for Lipid Cell Biology. Acc. Chem. Res. *56*, 1168–1177. 10.1021/acs.accounts.2c00851.

254. Schultz, C., Farley, S.E., and Tafesse, F.G. (2022). "Flash & Click": Multifunctionalized Lipid Derivatives as Tools To Study Viral Infections. J. Am. Chem. Soc. *144*, 13987–13995. 10.1021/jacs.2c02705.

255. Farley, S., Stein, F., Haberkant, P., Tafesse, F.G., and Schultz, C. (2024). Trifunctional Sphinganine: A New Tool to Dissect Sphingolipid Function. ACS Chem. Biol. 10.1021/acschembio.3c00554.

256. World Health Organization (2018). Global tuberculosis report 2018 (World Health Organization).

257. Levin, R., Grinstein, S., and Schlam, D. (2015). Phosphoinositides in phagocytosis and macropinocytosis. Biochimica et Biophysica Acta (BBA) - Molecular and Cell Biology of Lipids *1851*, 805–823. 10.1016/j.bbalip.2014.09.005.

258. Stuart, L.M., and Ezekowitz, R.A.B. (2005). Phagocytosis: Elegant complexity. Immunity *22*, 539–550. 10.1016/j.immuni.2005.05.002.

259. Goodridge, H.S., Reyes, C.N., Becker, C. a, Katsumoto, T.R., Ma, J., Wolf, A.J., Bose, N., Chan, A.S.H., Magee, A.S., Danielson, M.E., et al. (2011). Activation of the innate immune receptor Dectin-1 upon formation of a "phagocytic synapse." Nature *472*, 471–475. 10.1038/nature10071.

260. Tailleux, L., Schwartz, O., Herrmann, J.-L., Pivert, E., Jackson, M., Amara, A., Legres, L., Dreher, D., Nicod, L.P., Gluckman, J.C., et al. (2003). DC-SIGN Is the Major *Mycobacterium Tuberculosis* Receptor on Human Dendritic Cells. The Journal of Experimental Medicine *197*, 121–127. 10.1084/jem.20021468.

261. Yadav, M., and Schorey, J.S. (2006). The β-glucan receptor dectin-1 functions together with TLR2 to mediate macrophage activation by mycobacteria. Blood *108*, 3168–3175. 10.1182/blood-2006-05-024406.

262. Killick, K.E., Ní Cheallaigh, C., O'Farrelly, C., Hokamp, K., MacHugh, D.E., and Harris, J. (2013). Receptor-mediated recognition of mycobacterial pathogens: Cellular recognition of mycobacteria. Cell Microbiol *15*, 1484–1495. 10.1111/cmi.12161.

263. Lingwood, C.A., Manis, A., Mahfoud, R., Khan, F., Binnington, B., and Mylvaganam, M. (2010). New aspects of the regulation of glycosphingolipid receptor function. Chemistry and Physics of Lipids *163*, 27–35. 10.1016/j.chemphyslip.2009.09.001.

264. Slotte, J.P. (2013). Biological functions of sphingomyelins. Progress in Lipid Research *52*, 424–437. 10.1016/j.plipres.2013.05.001.

265. Heung, L.J., Luberto, C., and Del Poeta, M. (2006). Role of sphingolipids in microbial pathogenesis. Infection and Immunity *74*, 28–39. 10.1128/IAI.74.1.28-39.2006.

266. Grassmé, H., Gulbins, E., Brenner, B., Ferlinz, K., Sandhoff, K., Harzer, K., Lang, F., and Meyer, T.F. (1997). Acidic sphingomyelinase mediates entry of N. Gonorrhoeae into nonphagocytic cells. Cell *91*, 605–615.

267. Grassmé, H., Jendrossek, V., Riehle, A., von Kürthy, G., Berger, J., Schwarz, H., Weller, M., Kolesnick, R., and Gulbins, E. (2003). Host defense against Pseudomonas aeruginosa requires ceramide-rich membrane rafts. Nature Medicine *9*, 322–330. 10.1038/nm823.

268. Lovewell, R.R., Sassetti, C.M., and VanderVen, B.C. (2016). Chewing the fat: Lipid metabolism and homeostasis during M. Tuberculosis infection. Current Opinion in Microbiology *29*, 30–36. 10.1016/j.mib.2015.10.002.

269. Gatfield, J., and Pieters, J. (2000). Essential role for cholesterol in entry of mycobacteria into macrophages. Science (New York, N.Y.) *288*, 1647–1650. 10.1126/science.288.5471.1647.

270. Hanada, K. (2003). Serine palmitoyltransferase, a key enzyme of sphingolipid metabolism. Biochimica et biophysica acta *1632*, 16–30.

271. Wang, E., Norred, W.P., Bacon, C.W., Riley, R.T., and Merrill, A.H. (1991). Inhibition of sphingolipid biosynthesis by fumonisins. Implications for diseases associated with Fusarium moniliforme. J Biol Chem *266*, 14486–14490.

272. Leier, H.C., Messer, W.B., and Tafesse, F.G. (2018). Lipids and pathogenic flaviviruses : An intimate union. 1–7. 10.1371/journal.ppat.1006952.

273. Meivar-Levy, I., Sabanay, H., Bershadsky, A.D., and Futerman, A.H. (1997). The Role of Sphingolipids in the Maintenance of Fibroblast Morphology. Journal of Biological Chemistry *272*, 1558–1564. 10.1074/jbc.272.3.1558.

274. Ramakrishnan, L., and Falkow, S. (1994). Mycobacterium marinum persists in cultured mammalian cells in a temperature-restricted fashion. Infect Immun *62*, 3222–3229. 10.1128/iai.62.8.3222-3229.1994.

275. Roca, F.J., and Ramakrishnan, L. (2013). TNF dually mediates resistance and susceptibility to mycobacteria via mitochondrial reactive oxygen species. Cell *153*, 521–534. 10.1016/j.cell.2013.03.022.

276. Clement, C., Tiwari, V., Scanlan, P.M., Valyi-Nagy, T., Yue, B.Y.J.T., and Shukla, D. (2006). A novel role for phagocytosis-like uptake in herpes simplex virus entry. Journal of Cell Biology *174*, 1009–1021. 10.1083/jcb.200509155.

277. Tiwari, V., and Shukla, D. (2012). Nonprofessional Phagocytosis Can Facilitate Herpesvirus Entry into Ocular Cells. Clinical and Developmental Immunology *2012*, 1–8. 10.1155/2012/651691.

278. He, Q., Sun, X., Chu, C., Jiang, Q., Zhu, H., He, Y., Yue, T., Wang, R., Lei, P., and Shen, G. (2015). Endocytosis of a Functionally Enhanced GFP-Tagged Transferrin Receptor in CHO Cells. PLOS ONE *10*, e0122452. 10.1371/journal.pone.0122452.

279. Srinivasan, S., Wang, F., Glavas, S., Ott, A., Hofmann, F., Aktories, K., Kalman, D., and Bourne, H.R. (2003). Rac and Cdc42 play distinct roles in regulating PI(3,4,5)P3 and polarity during neutrophil chemotaxis. Journal of Cell Biology *160*, 375–385. 10.1083/jcb.200208179.

280. Mansour, M.K., Tam, J.M., Khan, N.S., Seward, M., Davids, P.J., Puranam, S., Sokolovska, A., Sykes, D.B., Dagher, Z., Becker, C., et al. (2013). Dectin-1 Activation Controls Maturation of β-1,3-Glucan-containing Phagosomes. Journal of Biological Chemistry *288*, 16043–16054. 10.1074/jbc.M113.473223.

281. Underhill, D.M. (2003). Macrophage recognition of zymosan particles. Journal of Endotoxin Research *9*, 176–180. 10.1179/096805103125001586.

282. Rothfuchs, A.G., Bafica, A., Feng, C.G., Egen, J.G., Williams, D.L., Brown, G.D., and Sher, A. (2007). Dectin-1 Interaction with Mycobacterium tuberculosis Leads to Enhanced IL-12p40 Production by Splenic Dendritic Cells. The Journal of Immunology *179*, 3463–3471. 10.4049/jimmunol.179.6.3463.

283. Wagener, M., Hoving, J.C., Ndlovu, H., and Marakalala, M.J. (2018). Dectin-1-Syk-CARD9 Signaling Pathway in TB Immunity. Frontiers in Immunology *9*. 10.3389/fimmu.2018.00225.

284. Simons, K., and Toomre, D. (2000). Lipid rafts and signal transduction. Nature Reviews Molecular Cell Biology *1*, 31–39. 10.1038/35036052.

285. Schlam, D., Bagshaw, R.D., Freeman, S.A., Collins, R.F., Pawson, T., Fairn, G.D., and Grinstein, S. (2015). Phosphoinositide 3-kinase enables phagocytosis of large particles by terminating actin assembly through Rac/Cdc42 GTPase-activating proteins. Nature Communications *6*, 8623. 10.1038/ncomms9623.

286. Ledvina, H.E., Kelly, K.A., Eshraghi, A., Plemel, R.L., Peterson, S.B., Lee, B., Steele, S., Adler, M., Kawula, T.H., Merz, A.J., et al. (2018). A Phosphatidylinositol 3-Kinase Effector Alters Phagosomal Maturation to Promote Intracellular Growth of Francisella. Cell Host & Microbe *24*, 285–295.e8. 10.1016/j.chom.2018.07.003.

287. Hoppe, A.D., and Swanson, J.A. (2004). Cdc42, Rac1, and Rac2 Display Distinct Patterns of Activation during Phagocytosis. Molecular Biology of the Cell *15*, 3509–3519. 10.1091/mbc.e03-11-0847.

288. Marshall, J.G., Booth, J.W., Stambolic, V., Mak, T., Balla, T., Schreiber, A.D., Meyer, T., and Grinstein, S. (2001). Restricted Accumulation of Phosphatidylinositol 3-Kinase Products in a Plasmalemmal Subdomain during Fcγ Receptor-Mediated Phagocytosis. Journal of Cell Biology *153*, 1369–1380. 10.1083/jcb.153.7.1369.

289. Agramonte-Hevia, J. (2002). Gram-negative bacteria and phagocytic cell interaction mediated by complement receptor 3. FEMS Immunology and Medical Microbiology *34*, 255–266. 10.1016/S0928-8244(02)00408-X.

290. Wegner, M.S., Gruber, L., Mattjus, P., Geisslinger, G., and Grösch, S. (2018). The UDP-glucose ceramide glycosyltransferase (UGCG) and the link to multidrug resistance protein 1 (MDR1). BMC Cancer *18*, 1–10. 10.1186/s12885-018-4084-4.

291. Virreira Winter, S., Zychlinsky, A., and Bardoel, B.W. (2016). Genome-wide CRISPR screen reveals novel host factors required for Staphylococcus aureus α-hemolysin-mediated toxicity. Scientific Reports *6*, 24242. 10.1038/srep24242.

292. Jaumouillé, V., and Grinstein, S. (2011). Receptor mobility, the cytoskeleton, and particle binding during phagocytosis. Current Opinion in Cell Biology *23*, 22–29. 10.1016/j.ceb.2010.10.006.

293. Kerrigan, A.M., and Brown, G.D. (2010). Syk-coupled C-type lectin receptors that mediate cellular activation via single tyrosine based activation motifs. Immunological Reviews *234*, 335–352. 10.1111/j.0105-2896.2009.00882.x.

294. Zhu, J.W., Brdicka, T., Katsumoto, T.R., Lin, J., and Weiss, A. (2008). Structurally Distinct Phosphatases CD45 and CD148 Both Regulate B Cell and Macrophage Immunoreceptor Signaling. Immunity *28*, 183–196. 10.1016/j.immuni.2007.11.024.

295. Li, C., Wang, A., Wu, Y., Gulbins, E., Grassmé, H., and Zhao, Z. (2019). Acid Sphingomyelinase-Ceramide System in Bacterial Infections. Cellular physiology and biochemistry : international journal of experimental cellular physiology, biochemistry, and pharmacology *52*, 280–301. 10.33594/000000021.

296. Smith, E.L., and Schuchman, E.H. (2008). The unexpected role of acid sphingomyelinase in cell death and the pathophysiology of common diseases. The FASEB Journal *22*, 3419–3431. 10.1096/fj.08-108043.

297. Viswanathan, G., Jafurulla, M., Kumar, G.A., Raghunand, T.R., and Chattopadhyay, A. (2018). Macrophage sphingolipids are essential for the entry of mycobacteria. Chemistry and Physics of Lipids *213*, 25–31. 10.1016/j.chemphyslip.2018.03.004.

298. Wu, Y., Gulbins, E., and Grassmé, H. (2018). The function of sphingomyelinases in mycobacterial infections. Biological Chemistry *399*, 1125–1133. 10.1515/hsz-2018-0179.

299. Erkelens, M.N., Goverse, G., Konijn, T., Molenaar, R., Beijer, M.R., Van Den Bossche, J., De Goede, K.E., Verberk, S.G.S., De Jonge, W.J., Den Haan, J.M.M., et al. (2020). Intestinal Macrophages Balance Inflammatory Expression Profiles via Vitamin A and Dectin-1-Mediated Signaling. Front. Immunol. *11*, 551. 10.3389/fimmu.2020.00551.

300. Taylor, P.R., Brown, G.D., Reid, D.M., Willment, J.A., Martinez-Pomares, L., Gordon, S., and Wong, S.Y.C. (2002). The beta-glucan receptor, dectin-1, is predominantly expressed on the surface of cells of the monocyte/macrophage and neutrophil lineages. J Immunol *169*, 3876–3882. 10.4049/jimmunol.169.7.3876.

301. Garfoot, A.L., Dearing, K.L., VanSchoiack, A.D., Wysocki, V.H., and Rappleye, C.A. (2017). Eng1 and Exg8 Are the Major β-Glucanases Secreted by the Fungal Pathogen Histoplasma capsulatum. J Biol Chem *292*, 4801–4810. 10.1074/jbc.M116.762104.

302. Feng, S., Laketa, V., Stein, F., Rutkowska, A., MacNamara, A., Depner, S., Klingmüller, U., Saez-Rodriguez, J., and Schultz, C. (2014). A Rapidly Reversible Chemical Dimerizer System to Study Lipid Signaling in Living Cells. Angewandte Chemie International Edition *53*, 6720–6723. 10.1002/anie.201402294.

303. Bligh, E.G., and Dyer, W.J. (1959). A RAPID METHOD OF TOTAL LIPID EXTRACTION AND PURIFICATION. Canadian Journal of Biochemistry and Physiology *37*, 911–917. 10.1139/o59-099.

304. Tafesse, F.G., Guimaraes, C.P., Maruyama, T., Carette, J.E., Lory, S., Brummelkamp, T.R., and Ploegh, H.L. (2014). GPR107, a G-protein-coupled Receptor Essential for Intoxication by Pseudomonas aeruginosa Exotoxin A, Localizes to the Golgi and Is Cleaved by Furin. Journal of Biological Chemistry *289*, 24005–24018. 10.1074/jbc.M114.589275.

305. Mali, P., Yang, L., Esvelt, K.M., Aach, J., Guell, M., DiCarlo, J.E., Norville, J.E., and Church, G.M. (2013). RNA-guided human genome engineering via Cas9. Science (New York, N.Y.) *339*, 823–826. 10.1126/science.1232033.

306. Rashidfarrokhi, A., Richina, V., and Tafesse, F.G. (2017). Visualizing the Early Stages of Phagocytosis. Journal of Visualized Experiments. 10.3791/54646.

307. Van Der Wel, N., Hava, D., Houben, D., Fluitsma, D., Van Zon, M., Pierson, J., Brenner, M., and Peters, P.J. (2007). M. Tuberculosis and M. Leprae Translocate from the Phagolysosome to the Cytosol in Myeloid Cells. Cell *129*, 1287–1298. 10.1016/j.cell.2007.05.059.

308. Simeone, R., Bobard, A., Lippmann, J., Bitter, W., Majlessi, L., Brosch, R., and Enninga, J. (2012). Phagosomal Rupture by Mycobacterium tuberculosis Results in Toxicity and Host Cell Death. PLoS Pathog *8*, e1002507. 10.1371/journal.ppat.1002507.

309. Simeone, R., Sayes, F., Song, O., Gröschel, M.I., Brodin, P., Brosch, R., and Majlessi, L. (2015). Cytosolic Access of Mycobacterium tuberculosis: Critical Impact of Phagosomal Acidification Control and Demonstration of Occurrence In Vivo. PLOS Pathogens *11*, e1004650. 10.1371/journal.ppat.1004650.

310. Poulsen, C., Panjikar, S., Holton, S.J., Wilmanns, M., and Song, Y.-H. (2014). WXG100 Protein Superfamily Consists of Three Subfamilies and Exhibits an α-Helical C-Terminal Conserved Residue Pattern. PLoS ONE *9*, e89313. 10.1371/journal.pone.0089313.

311. De Leon, J., Jiang, G., Ma, Y., Rubin, E., Fortune, S., and Sun, J. (2012). Mycobacterium tuberculosis ESAT-6 Exhibits a Unique Membrane-interacting Activity That Is Not Found in Its Ortholog from Non-pathogenic Mycobacterium smegmatis. Journal of Biological Chemistry *287*, 44184–44191. 10.1074/jbc.M112.420869.

312. Bates, T.A., Trank-Greene, M., Nguyenla, X., Anastas, A., Merutka, I.R., Dixon, S.D., Shumate, A., Groncki, A.R., Parson, M.A., Barklis, E., et al. (2023). ESAT-6 undergoes self-association at phagosomal pH and an ESAT-6 specific nanobody restricts M. Tuberculosis growth in macrophages (Biochemistry) 10.1101/2023.08.16.553641.

313. Lerner, T.R., Queval, C.J., Fearns, A., Repnik, U., Griffiths, G., and Gutierrez, M.G. (2018). Phthiocerol dimycocerosates promote access to the cytosol and intracellular burden of Mycobacterium tuberculosis in lymphatic endothelial cells. BMC Biol *16*, 1. 10.1186/s12915-017-0471-6.

314. Augenstreich, J., Arbues, A., Simeone, R., Haanappel, E., Wegener, A., Sayes, F., Le Chevalier, F., Chalut, C., Malaga, W., Guilhot, C., et al. (2017). ESX-1 and phthiocerol dimycocerosates of *Mycobacterium Tuberculosis* act in concert to cause phagosomal rupture and host cell apoptosis. Cellular Microbiology *19*, e12726. 10.1111/cmi.12726.

315. Cambier, C., Banik, S.M., Buonomo, J.A., and Bertozzi, C.R. (2020). Spreading of a mycobacterial cell-surface lipid into host epithelial membranes promotes infectivity. eLife *9*, e60648. 10.7554/eLife.60648.

316. Tan, J.X., and Finkel, T. (2022). A phosphoinositide signalling pathway mediates rapid lysosomal repair. Nature *609*, 815–821. 10.1038/s41586-022-05164-4.

317. Draeger, A., and Babiychuk, E.B. (2013). Ceramide in Plasma Membrane Repair. In Sphingolipids in Disease, E. Gulbins and I. Petrache, eds. (Springer Vienna), pp. 341–353. 10.1007/978-3-7091-1511-4_17.

318. Arana, L., Gangoiti, P., Ouro, A., Trueba, M., and Gómez-Muñoz, A. (2010). Ceramide and ceramide 1-phosphate in health and disease. Lipids in Health and Disease *9*, 1–12. 10.1186/1476-511X-9-15.

319. Dadsena, S., Bockelmann, S., Mina, J.G.M., Hassan, D.G., Korneev, S., Razzera, G., Jahn, H., Niekamp, P., Müller, D., Schneider, M., et al. (2019). Ceramides bind VDAC2 to trigger mitochondrial apoptosis. Nature Communications *10*, 1832. 10.1038/s41467-019-09654-4.

320. Gómez-Muñoz, A. (2006). Ceramide 1-phosphate/ceramide, a switch between life and death. Biochimica et Biophysica Acta - Biomembranes *1758*, 2049–2056. 10.1016/j.bbamem.2006.05.011.

321. Kolesnick, R.N., and Krönke, M. (1998). REGULATION OF CERAMIDE PRODUCTION AND APOPTOSIS. Annual Review of Physiology *60*, 643–665. 10.1146/annurev.physiol.60.1.643.

322. Law, B.A., Liao, X., Moore, K.S., Southard, A., Roddy, P., Ji, R., Szulc, Z., Bielawska, A., Schulze, P.C., and Cowart, L.A. (2018). Lipotoxic very-long-chain ceramides cause mitochondrial dysfunction, oxidative stress, and cell death in cardiomyocytes. FASEB Journal *32*, 1403–1416. 10.1096/fj.201700300R.

323. Ding, T., Li, Z., Hailemariam, T., Mukherjee, S., Maxfield, F.R., Wu, M.-P., and Jiang, X.-C. (2008). SMS overexpression and knockdown: Impact on cellular sphingomyelin and diacylglycerol metabolism, and cell apoptosis. Journal of Lipid Research *49*, 376–385. 10.1194/jlr.M700401-JLR200.

324. Milhas, D., Clarke, C.J., and Hannun, Y.A. (2010). Sphingomyelin metabolism at the plasma membrane: Implications for bioactive sphingolipids. FEBS Letters *584*, 1887–1894. 10.1016/j.febslet.2009.10.058.

325. Lefrancois, S., May, T., Knight, C., Bourbeau, D., and Morales, C.R. (2002). The lysosomal transport of prosaposin requires the conditional interaction of its highly conserved D domain with sphingomyelin. Journal of Biological Chemistry *277*, 17188–17199. 10.1074/jbc.M200343200.

326. Li, Z., Park, T.S., Li, Y., Pan, X., Iqbal, J., Lu, D., Tang, W., Yu, L., Goldberg, I.J., Hussain, M.M., et al. (2009). Serine palmitoyltransferase (SPT) deficient mice absorb less cholesterol. Biochimica et Biophysica Acta - Molecular and Cell Biology of Lipids *1791*, 297–306. 10.1016/j.bbalip.2009.01.010.

327. Riley, R.T., and Merrill, A.H. (2019). Ceramide synthase inhibition by fumonisins: A perfect storm of perturbed sphingolipid metabolism, signaling, and disease. Journal of Lipid Research *60*, 1183–1189. 10.1194/jlr.S093815.

328. Tafesse, F.G., Sanyal, S., Ashour, J., Guimaraes, C.P., Hermansson, M., Somerharju, P., and Ploegh, H.L. (2013). Intact sphingomyelin biosynthetic pathway is essential for intracellular transport of influenza virus glycoproteins. Proceedings of the National Academy of Sciences *110*, 6406–6411. 10.1073/pnas.1219909110.

329. Umehara, T., Sudoh, M., Yasui, F., Matsuda, C., Hayashi, Y., Chayama, K., and Kohara, M. (2006). Serine palmitoyltransferase inhibitor suppresses HCV replication in a mouse model. Biochemical and Biophysical Research Communications *346*, 67–73. 10.1016/j.bbrc.2006.05.085.

330. Zeng, H.-Y., Li, C.-Y., and Yao, N. (2020). Fumonisin B1: A Tool for Exploring the Multiple Functions of Sphingolipids in Plants. Front. Plant Sci. *11*, 600458. 10.3389/fpls.2020.600458.

331. D'Astolfo, D.S., Pagliero, R.J., Pras, A., Karthaus, W.R., Clevers, H., Prasad, V., Lebbink, R.J., Rehmann, H., and Geijsen, N. (2015). Efficient Intracellular Delivery of Native Proteins. Cell *161*, 674–690. 10.1016/j.cell.2015.03.028.

332. Kobayashi, Y., Takasaki, A., Kurosaka, K., Sakurai, Y., Iwamura, M., and Watanabe, N. (2000). Cell-Type Specificity of l-Leucyl l-Leucine Methyl Ester. Biochemical and Biophysical Research Communications *272*, 687–690. 10.1006/bbrc.2000.2836.

333. Liu, J., Kang, R., and Tang, D. (2021). ESCRT-III-mediated membrane repair in cell death and tumor resistance. Cancer Gene Ther *28*, 1–4. 10.1038/s41417-020-0200-0.

334. Ellison, C.J., Kukulski, W., Boyle, K.B., Munro, S., and Randow, F. (2020). Transbilayer Movement of Sphingomyelin Precedes Catastrophic Breakage of Enterobacteria-Containing Vacuoles. Current Biology *30*, 2974–2983.e6. 10.1016/j.cub.2020.05.083.

335. Yamaji, A., Sekizawa, Y., Emoto, K., Sakuraba, H., Inoue, K., Kobayashi, H., and Umeda, M. (1998). Lysenin, a novel sphingomyelin-specific binding protein. The Journal of biological chemistry *273*, 5300–5306.

336. Bryson, B.D., Rosebrock, T.R., Tafesse, F.G., Itoh, C.Y., Nibasumba, A., Babunovic, G.H., Corleis, B., Martin, C., Keegan, C., Andrade, P., et al. (2019). Heterogeneous GM-CSF signaling in macrophages is associated with control of Mycobacterium tuberculosis. Nat Commun *10*, 2329. 10.1038/s41467-019-10065-8.

337. Kalsum, S., Otrocka, M., Andersson, B., Welin, A., Schön, T., Jenmalm-Jensen, A., Lundbäck, T., and Lerm, M. (2022). A high content screening assay for discovery of antimycobacterial compounds based on primary human macrophages infected with virulent Mycobacterium tuberculosis. Tuberculosis *135*, 102222. 10.1016/j.tube.2022.102222.

338. Daugelat, S., Kowall, J., Mattow, J., Bumann, D., Winter, R., Hurwitz, R., and Kaufmann, S.H.E. (2003). The RD1 proteins of Mycobacterium tuberculosis: Expression in Mycobacterium smegmatis and biochemical characterization. Microbes and Infection *5*, 1082–1095. 10.1016/S1286-4579(03)00205-3.

339. Etna, M.P., Giacomini, E., Pardini, M., Severa, M., Bottai, D., Cruciani, M., Rizzo, F., Calogero, R., Brosch, R., and Coccia, E.M. (2015). Impact of Mycobacterium tuberculosis RD1-locus on human primary dendritic cell immune functions. Scientific Reports *5*. 10.1038/srep17078.

340. Lewis, K.N., Liao, R., Guinn, K.M., Hickey, M.J., Smith, S., Behr, M.A., and Sherman, D.R. (2003). Deletion of RD1 from *Mycobacterium Tuberculosis* Mimics Bacille Calmette□Guérin Attenuation. J INFECT DIS *187*, 117–123. 10.1086/345862.

341. Yang, R., Xi, C., Sita, D.R., Sakai, S., Tsuchiya, K., Hara, H., Shen, Y., Qu, H., Fang, R., Mitsuyama, M., et al. (2014). The RD1 locus in the Mycobacterium tuberculosis genome contributes to the maturation and secretion of IL-1α from infected macrophages through the elevation of cytoplasmic calcium levels and calpain activation. Pathogens and Disease *70*, 51–60. 10.1111/2049-632X.12075.

342. Gutierrez, M.G., Master, S.S., Singh, S.B., Taylor, G.A., Colombo, M.I., and Deretic, V. (2004). Autophagy Is a Defense Mechanism Inhibiting BCG and Mycobacterium tuberculosis Survival in Infected Macrophages. Cell *119*, 753–766. 10.1016/j.cell.2004.11.038.

343. Tafesse, F.G., Huitema, K., Hermansson, M., van der Poel, S., van den Dikkenberg, J., Uphoff, A., Somerharju, P., and Holthuis, J.C.M.M. (2007). Both Sphingomyelin Synthases SMS1 and SMS2 Are Required for Sphingomyelin Homeostasis and Growth in Human HeLa Cells. Journal of Biological Chemistry *282*, 17537–17547. 10.1074/jbc.M702423200.

344. Yeang, C., Ding, T., Chirico, W.J., and Jiang, X.-C. (2011). Subcellular Targeting Domains of Sphingomyelin Synthase 1 and 2. Nutr Metab (Lond) *8*, 89. 10.1186/1743-7075-8-89.

345. Yachi, R., Uchida, Y., Balakrishna, B.H., Anderluh, G., Kobayashi, T., Taguchi, T., and Arai, H. (2012). Subcellular localization of sphingomyelin revealed by two toxin□based probes in mammalian cells. Genes to Cells *17*, 720–727. 10.1111/j.1365-2443.2012.01621.x.

346. Strong, E.J., Wang, J., Ng, T.W., Porcelli, S.A., and Lee, S. (2022). Mycobacterium tuberculosis PPE51 Inhibits Autophagy by Suppressing Toll-Like Receptor 2-Dependent Signaling. mBio *13*, e02974–21. 10.1128/mbio.02974-21.

347. Kumar, P., Nagarajan, A., and Uchil, P.D. (2018). Analysis of Cell Viability by the alamarBlue Assay. Cold Spring Harbor Protocols *2018*, pdb.prot095489. 10.1101/pdb.prot095489.

348. Sharma, L., and Prakash, H. (2017). Sphingolipids are dual specific drug targets for the management of pulmonary infections: Perspective. Frontiers in Immunology *8*. 10.3389/fimmu.2017.00378.

349. Long, N.P., Anh, N.K., Yen, N.T.H., Phat, N.K., Park, S., Thu, V.T.A., Cho, Y.-S., Shin, J.-G., Oh, J.Y., and Kim, D.H. (2022). Comprehensive lipid and lipid-related gene investigations of host immune responses to characterize metabolism-centric biomarkers for pulmonary tuberculosis. Sci Rep *12*, 13395. 10.1038/s41598-022-17521-4.

350. Aguilar-Ayala, D.A., Palomino, J.C., Vandamme, P., Martin, A., and Gonzalez-y-Merchand, J.A. (2017). "Genetic regulation of Mycobacterium tuberculosis in a lipid-rich environment." Infection, Genetics and Evolution *55*, 392–402. 10.1016/j.meegid.2016.10.015.

351. Aguilar-Ayala, D.A., Tilleman, L., Van Nieuwerburgh, F., Deforce, D., Palomino, J.C., Vandamme, P., Gonzalez-Y-Merchand, J.A., and Martin, A. (2017). The transcriptome of Mycobacterium tuberculosis in a lipid-rich dormancy model through RNAseq analysis. Sci Rep *7*, 17665. 10.1038/s41598-017-17751-x.

352. Agarwal, P., Gordon, S., and Martinez, F.O. (2021). Foam Cell Macrophages in Tuberculosis. Front. Immunol. *12*, 775326. 10.3389/fimmu.2021.775326.

353. Knight, M., Braverman, J., Asfaha, K., Gronert, K., and Stanley, S. (2018). Lipid droplet formation in Mycobacterium tuberculosis infected macrophages requires IFN-γ/HIF-1α signaling and supports host defense. PLoS Pathogens *14*, 1–26. 10.1371/journal.ppat.1006874.

354. Layre, E., Al-Mubarak, R., Belisle, J.T., and Branch Moody, D. (2014). Mycobacterial Lipidomics. Microbiol Spectr *2*, 2.3.03. 10.1128/microbiolspec.MGM2-0033-2013.

355. Saquib, N.M., Jamwal, S., Midha, M.K., Verma, H.N., and Manivel, V. (2015). Quantitative Proteomics and Lipidomics Analysis of Endoplasmic Reticulum of Macrophage Infected with *Mycobacterium Tuberculosis*. International Journal of Proteomics *2015*, 1–13. 10.1155/2015/270438.

356. Leier, H.C., Weinstein, J.B., Kyle, J.E., Lee, J.Y., Bramer, L.M., Stratton, K.G., Kempthorne, D., Navratil, A.R., Tafesse, E.G., Hornemann, T., et al. (2020). A global lipid map defines a network essential for Zika virus replication. Nature Communications *11*, 1–15. 10.1038/s41467-020-17433-9.

357. Farley, S.E., Kyle, J.E., Leier, H.C., Bramer, L.M., Weinstein, J.B., Bates, T.A., Lee, J.-Y., Metz, T.O., Schultz, C., and Tafesse, F.G. (2022). A global lipid map reveals host dependency factors conserved across SARS-CoV-2 variants. Nat Commun *13*, 3487. 10.1038/s41467-022-31097-7.

358. Layre, E., Sweet, L., Hong, S., Madigan, C.A., Desjardins, D., Young, D.C., Cheng, T.-Y., Annand, J.W., Kim, K., Shamputa, I.C., et al. (2011). A Comparative Lipidomics Platform for Chemotaxonomic Analysis of Mycobacterium tuberculosis. Chemistry & Biology *18*, 1537–1549. 10.1016/j.chembiol.2011.10.013.

359. Jenkins, B., West, J., and Koulman, A. (2015). A Review of Odd-Chain Fatty Acid Metabolism and the Role of Pentadecanoic Acid (C15:0) and Heptadecanoic Acid (C17:0) in Health and Disease. Molecules *20*, 2425–2444. 10.3390/molecules20022425.

360. Mori, K., Naganuma, T., and Kihara, A. (2023). Role of 2-hydroxy acyl-CoA lyase HACL2 in odd-chain fatty acid production via α-oxidation in vivo. MBoC *34*, ar85. 10.1091/mbc.E23-02-0042.

361. Sartain, M.J., Dick, D.L., Rithner, C.D., Crick, D.C., and Belisle, J.T. (2011). Lipidomic analyses of Mycobacterium tuberculosis based on accurate mass measurements and the novel "Mtb LipidDB." Journal of Lipid Research *52*, 861–872. 10.1194/jlr.M010363.

362. Department of Biotechnology, Sri Venkateswara Institute of Medical Sciences, Tirupati 517507, Sarma, P., Srikanth, L., Venkatesh, K., Murthy, P.S., and Sarma, P.U. (2013). Isolation, purification and characterization of Cardiolipin synthase from Mycobacterium phlei {PRIVATE}. Bioinformation *9*, 690–695. 10.6026/97320630009690.

363. Fischer, K., Chatterjee, D., Torrelles, J., Brennan, P.J., Kaufmann, S.H.E., and Schaible, U.E. (2001). Mycobacterial Lysocardiolipin Is Exported from Phagosomes upon Cleavage of Cardiolipin by a Macrophage-Derived Lysosomal Phospholipase A2. The Journal of Immunology *167*, 2187–2192. 10.4049/jimmunol.167.4.2187.

364. Laval, T., Pedró-Cos, L., Malaga, W., Guenin-Macé, L., Pawlik, A., Mayau, V., Yahia-Cherbal, H., Delos, O., Frigui, W., Bertrand-Michel, J., et al. (2021). De novo synthesized polyunsaturated fatty acids operate as both host immunomodulators and nutrients for Mycobacterium tuberculosis. Elife *10*, e71946. 10.7554/eLife.71946.

365. Gil-de-Gómez, L., Astudillo, A.M., Lebrero, P., Balboa, M.A., and Balsinde, J. (2017). Essential Role for Ethanolamine Plasmalogen Hydrolysis in Bacterial Lipopolysaccharide Priming of Macrophages for Enhanced Arachidonic Acid Release. Front. Immunol. *8*, 1251. 10.3389/fimmu.2017.01251.

366. Weltzien, H.U. (1979). Cytolytic and membrane-perturbing properties of lysophosphatidylcholine. Biochimica et Biophysica Acta (BBA) - Reviews on Biomembranes *559*, 259–287. 10.1016/0304-4157(79)90004-2.

367. Jurkowitz, M.S., Azad, A.K., Monsma, P.C., Keiser, T.L., Kanyo, J., Lam, T.T., Bell, C.E., and Schlesinger, L.S. (2022). Mycobacterium tuberculosis encodes a YhhN family membrane protein with lysoplasmalogenase activity that protects against toxic host lysolipids. Journal of Biological Chemistry *298*, 101849. 10.1016/j.jbc.2022.101849.

368. Sachdeva, K., Goel, M., Sudhakar, M., Mehta, M., Raju, R., Raman, K., Singh, A., and Sundaramurthy, V. (2020). Mycobacterium tuberculosis (Mtb) lipid mediated lysosomal rewiring in infected macrophages modulates intracellular Mtb trafficking and survival. Journal of Biological Chemistry *295*, 9192–9210. 10.1074/jbc.RA120.012809.

369. Geisel, R.E., Sakamoto, K., Russell, D.G., and Rhoades, E.R. (2005). In Vivo Activity of Released Cell Wall Lipids of *Mycobacterium Bovis* Bacillus Calmette-Guérin Is Due Principally to Trehalose Mycolates. The Journal of Immunology *174*, 5007–5015. 10.4049/jimmunol.174.8.5007.

370. Ishikawa, E., Ishikawa, T., Morita, Y.S., Toyonaga, K., Yamada, H., Takeuchi, O., Kinoshita, T., Akira, S., Yoshikai, Y., and Yamasaki, S. (2009). Direct recognition of the mycobacterial glycolipid, trehalose dimycolate, by C-type lectin Mincle. Journal of Experimental Medicine *206*, 2879–2888. 10.1084/jem.20091750.

371. El-Zayat, S.R., Sibaii, H., and Mannaa, F.A. (2019). Toll-like receptors activation, signaling, and targeting: An overview. Bull Natl Res Cent *43*, 187. 10.1186/s42269-019-0227-2.

372. Jo, E.-K., Yang, C.-S., Choi, C.H., and Harding, C.V. (2007). Intracellular signalling cascades regulating innate immune responses to Mycobacteria: Branching out from Toll-like receptors. Cell Microbiol *9*, 1087–1098. 10.1111/j.1462-5822.2007.00914.x.

373. Kugelberg, E. (2014). Mycobacteria hide from TLRs. Nat Rev Immunol *14*, 62–63. 10.1038/nri3604.

374. Augenstreich, J., Haanappel, E., Ferré, G., Czaplicki, G., Jolibois, F., Destainville, N., Guilhot, C., Milon, A., Astarie-Dequeker, C., and Chavent, M. (2019). The conical shape of DIM lipids promotes *Mycobacterium Tuberculosis* infection of macrophages. Proc. Natl. Acad. Sci. U.S.A. *116*, 25649–25658. 10.1073/pnas.1910368116.

375. Barklis, E., Alfadhli, A., Kyle, J.E., Bramer, L.M., Bloodsworth, K.J., Barklis, R.L., Leier, H.C., Petty, R.M., Zelnik, I.D., Metz, T.O., et al. (2021). Ceramide synthase 2 deletion decreases the infectivity of HIV-1. Journal of Biological Chemistry *296*, 100340. 10.1016/J.JBC.2021.100340.

376. Guzman, G.G., Farley, S., Kyle, J.E., Bramer, L.M., Hoeltzl, S., Van Den Dikkenberg, J., Holthuis, J.C.M., and Tafesse, F.G. (2023). Systematic analysis of the sphingomyelin synthase family in *C. Elegans* (Molecular Biology) 10.1101/2023.07.25.550547.

377. Pluskal, T., Castillo, S., Villar-Briones, A., and Orešič, M. (2010). MZmine 2: Modular framework for processing, visualizing, and analyzing mass spectrometry-based molecular profile data. BMC Bioinformatics *11*. 10.1186/1471-2105-11-395.

378. Matzke, M.M., Waters, K.M., Metz, T.O., Jacobs, J.M., Sims, A.C., Baric, R.S., Pounds, J.G., and Webb-Robertson, B.-J.M. (2011). Improved quality control processing of peptide-centric LC-MS proteomics data. Bioinformatics (Oxford, England) *27*, 2866–2872. 10.1093/bioinformatics/btr479.

379. Webb-Robertson, B.J.M., McCue, L.A., Waters, K.M., Matzke, M.M., Jacobs, J.M., Metz, T.O., Varnum, S.M., and Pounds, J.G. (2010). Combined statistical analyses of peptide intensities and peptide occurrences improves identification of significant peptides from MS-based proteomics data. Journal of Proteome Research *9*, 5748–5756. 10.1021/pr1005247.

380. Malik, Z.A., Thompson, C.R., Hashimi, S., Porter, B., Iyer, S.S., and Kusner, D.J. (2003). Cutting Edge: Mycobacterium tuberculosis Blocks Ca2+ Signaling and Phagosome Maturation in Human Macrophages Via Specific Inhibition of Sphingosine Kinase. The Journal of Immunology *170*, 2811–2815. 10.4049/jimmunol.170.6.2811.

381. Haberkant, P., Schmitt, O., Contreras, F.-X., Thiele, C., Hanada, K., Sprong, H., Reinhard, C., Wieland, F.T., and Brügger, B. (2008). Protein-sphingolipid interactions within cellular membranes. Journal of Lipid Research *49*, 251–262. 10.1194/jlr.D700023-JLR200.

382. Ritchie, M.E., Phipson, B., Wu, D., Hu, Y., Law, C.W., Shi, W., and Smyth, G.K. (2015). Limma powers differential expression analyses for RNA-sequencing and microarray studies. Nucleic Acids Research *43*, e47–e47. 10.1093/nar/gkv007.

383. Jahn, H., Bartoš, L., Dearden, G.I., Dittman, J.S., Holthuis, J.C.M., Vácha, R., and Menon, A.K. (2023). Phospholipids are imported into mitochondria by VDAC, a dimeric beta barrel scramblase. Nat Commun *14*, 8115. 10.1038/s41467-023-43570-y.

384. Kishimoto, Y., Hiraiwa, M., and O'Brien, J.S. (1992). Saposins: Structure, function, distribution, and molecular genetics. Journal of lipid research *33*, 1255–1267.

385. Morimoto, S., Martin, B.M., Yamamoto, Y., Kretz, K.A., O'Brien, J.S., and Kishimoto, Y. (1989). Saposin A: Second cerebrosidase activator protein. Proc. Natl. Acad. Sci. U.S.A. *86*, 3389–3393. 10.1073/pnas.86.9.3389.

386. Xiong, Z.J., Huang, J., Poda, G., Pomès, R., and Privé, G.G. (2016). Structure of Human Acid Sphingomyelinase Reveals the Role of the Saposin Domain in Activating Substrate Hydrolysis. Journal of Molecular Biology *428*, 3026–3042. 10.1016/j.jmb.2016.06.012.

387. Kim, M.J., Jeong, H., and Krainc, D. (2022). Lysosomal ceramides regulate cathepsin B-mediated processing of saposin C and glucocerebrosidase activity. Human Molecular Genetics *31*, 2424–2437. 10.1093/hmg/ddac047.

388. Jani, C., Solomon, S.L., Peters, J.M., Pringle, S.C., Hinman, A.E., Boucau, J., Bryson, B.D., and Barczak, A.K. (2023). TLR2 is non-redundant in the population and subpopulation responses to *Mycobacterium Tuberculosis* in macrophages and *in Vivo*. mSystems, e00052–23. 10.1128/msystems.00052-23.

389. Lyck, R., Lécuyer, M.-A., Abadier, M., Wyss, C.B., Matti, C., Rosito, M., Enzmann, G., Zeis, T., Michel, L., García Martín, A.B., et al. (2017). ALCAM (CD166) is involved in extravasation of monocytes rather than T cells across the blood–brain barrier. J Cereb Blood Flow Metab *37*, 2894–2909. 10.1177/0271678X16678639.

390. Fletcher, H.A., Keyser, A., Bowmaker, M., Sayles, P.C., Kaplan, G., Hussey, G., Hill, A.V., and Hanekom, W.A. (2009). Transcriptional profiling of mycobacterial antigen-induced responses in infants vaccinated with BCG at birth. BMC Med Genomics *2*, 10. 10.1186/1755-8794-2-10.

391. Shepelkova, G.S., Evstifeev, V.V., Ergeshov, A.E., and Yeremeev, V.V. (2020). Saposin D acting on macrophage bacteriostatic function in experimental tuberculosis infection. Russian Journal of Infection and Immunity *11*, 473–480. 10.15789/2220-7619-TEO-1386.

392. Hussain, M.M., Shi, J., and Dreizen, P. (2003). Microsomal triglyceride transfer protein and its role in apoB-lipoprotein assembly. Journal of Lipid Research *44*, 22–32. 10.1194/jlr.R200014-JLR200.

393. Dougan, S.K., Salas, A., Rava, P., Agyemang, A., Kaser, A., Morrison, J., Khurana, A., Kronenberg, M., Johnson, C., Exley, M., et al. (2005). Microsomal triglyceride transfer protein lipidation and control of CD1d on antigen-presenting cells. The Journal of Experimental Medicine *202*, 529–539. 10.1084/jem.20050183.

394. De Libero, G., and Mori, L. (2014). The T-Cell Response to Lipid Antigens of Mycobacterium tuberculosis. Front. Immunol. *5*. 10.3389/fimmu.2014.00219.

395. Yang, X., Yan, J., Xue, Y., Sun, Q., Zhang, Y., Guo, R., Wang, C., Li, X., Liang, Q., Wu, H., et al. (2023). Single-cell profiling reveals distinct immune response landscapes in tuberculous pleural effusion and non-TPE. Front. Immunol. *14*, 1191357. 10.3389/fimmu.2023.1191357.

396. Thirunavukkarasu, S., Ahmed, M., Rosa, B.A., Boothby, M., Cho, S.H., Rangel-Moreno, J., Mbandi, S.K., Schreiber, V., Gupta, A., Zuniga, J., et al. (2023). Poly(ADP-ribose) polymerase 9 mediates early protection against Mycobacterium tuberculosis infection by regulating type I IFN production. Journal of Clinical Investigation *133*, e158630. 10.1172/JCI158630.

397. Leisching, G., Cole, V., Ali, A.T., and Baker, B. (2019). OAS1, OAS2 and OAS3 restrict intracellular M. Tb replication and enhance cytokine secretion. International Journal of Infectious Diseases *80*, S77–S84. 10.1016/j.ijid.2019.02.029.

398. Yi, F., Hu, J., Zhu, X., Wang, Y., Yu, Q., Deng, J., Huang, X., Ma, Y., and Xie, Y. (2021). Transcriptional Profiling of Human Peripheral Blood Mononuclear Cells Stimulated by Mycobacterium tuberculosis PPE57 Identifies Characteristic Genes Associated With Type I Interferon Signaling. Front. Cell. Infect. Microbiol. *11*, 716809. 10.3389/fcimb.2021.716809.

399. Liu, X., Chen, J., Long, X., Lan, J., Liu, X., Zhou, M., Zhang, S., and Zhou, J. (2022). RSL1D1 promotes the progression of colorectal cancer through RAN-mediated autophagy suppression. Cell Death Dis *13*, 43. 10.1038/s41419-021-04492-z.

400. Becq, J., Gutierrez, M.C., Rosas-Magallanes, V., Rauzier, J., Gicquel, B., Neyrolles, O., and Deschavanne, P. (2007). Contribution of Horizontally Acquired Genomic Islands to the Evolution of the Tubercle Bacilli. Molecular Biology and Evolution *24*, 1861–1871. 10.1093/molbev/msm111.

401. Minato, Y., Gohl, D.M., Thiede, J.M., Chacón, J.M., Harcombe, W.R., Maruyama, F., and Baughn, A.D. (2019). Genomewide Assessment of Mycobacterium tuberculosis Conditionally Essential Metabolic Pathways. mSystems *4*, e00070–19. 10.1128/mSystems.00070-19.

402. Boshoff, H.I.M., Myers, T.G., Copp, B.R., McNeil, M.R., Wilson, M.A., and Barry, C.E. (2004). The Transcriptional Responses of Mycobacterium tuberculosis to Inhibitors of Metabolism. Journal of Biological Chemistry *279*, 40174–40184. 10.1074/jbc.M406796200.

403. Galagan, J.E., Minch, K., Peterson, M., Lyubetskaya, A., Azizi, E., Sweet, L., Gomes, A., Rustad, T., Dolganov, G., Glotova, I., et al. (2013). The Mycobacterium tuberculosis regulatory network and hypoxia. Nature *499*, 178–183. 10.1038/nature12337.

404. Lew, J.M., Kapopoulou, A., Jones, L.M., and Cole, S.T. (2011). TubercuList – 10 years after. Tuberculosis *91*, 1–7. 10.1016/j.tube.2010.09.008.

405. Mateus, A., Määttä, T.A., and Savitski, M.M. (2016). Thermal proteome profiling: Unbiased assessment of protein state through heat-induced stability changes. Proteome Sci *15*, 13. 10.1186/s12953-017-0122-4.

406. Huber, W., Von Heydebreck, A., Sültmann, H., Poustka, A., and Vingron, M. (2002). Variance stabilization applied to microarray data calibration and to the quantification of differential expression. Bioinformatics *18*, S96–S104. 10.1093/bioinformatics/18.suppl_1.S96.

407. Schneider-Schaulies, J., and Schneider-Schaulies, S. (2015). Sphingolipids in viral infection. Biological Chemistry *396*, 585–595. 10.1515/hsz-2014-0273.

408. Miller, M.E., Adhikary, S., Kolokoltsov, A.A., and Davey, R.A. (2012). Ebolavirus Requires Acid Sphingomyelinase Activity and Plasma Membrane Sphingomyelin for Infection. Journal of Virology *86*, 7473–7483. 10.1128/JVI.00136-12.

409. Dai, L., Trillo-Tinoco, J., Bai, A., Chen, Y., Bielawski, J., Valle, L.D., Smith, C.D., Ochoa, A.C., Qin, Z., and Parsons, C. (2015). Ceramides promote apoptosis for virus-infected lymphoma cells through induction of ceramide synthases and viral lytic gene expression. Oncotarget *6*, 24246–24260. 10.18632/oncotarget.4759.

410. Vijayan, M., Xia, C., Song, Y.E., Ngo, H., Studstill, C.J., Drews, K., Fox, T.E., Johnson, M.C., Hiscott, J., Kester, M., et al. (2017). Sphingosine 1-Phosphate Lyase Enhances the Activation of IKKε To Promote Type I IFN–Mediated Innate Immune Responses to Influenza A Virus Infection. The Journal of Immunology *199*, 677–687. 10.4049/jimmunol.1601959.

411. Yager, E.J., and Konan, K.V. (2019). Sphingolipids as potential therapeutic targets against enveloped human RNA viruses. Viruses *11*, 1–14. 10.3390/v11100912.

412. Cao, M., Ji, C., Zhou, Y., Huang, W., Ni, W., Tong, X., and Wei, J.F. (2018). Sphingosine kinase inhibitors: A patent review. International Journal of Molecular Medicine *41*, 2450–2460. 10.3892/ijmm.2018.3505.

413. Hsu, P.D., Lander, E.S., and Zhang, F. (2014). Development and Applications of CRISPR-Cas9 for Genome Engineering. Cell *157*, 1262–1278. 10.1016/j.cell.2014.05.010.

414. Yang, Y., Xu, J., Ge, S., and Lai, L. (2021). CRISPR/Cas: Advances, Limitations, and Applications for Precision Cancer Research. Frontiers in Medicine *8*, 1–11. 10.3389/fmed.2021.649896.

415. Ran, F.A., Hsu, P.D., Wright, J., Agarwala, V., Scott, D.A., and Zhang, F. (2013). Genome engineering using the CRISPR-Cas9 system. Nature Protocols *8*, 2281–2308. 10.1038/nprot.2013.143.

416. Cui, X., Balcerzak, M., Schernthaner, J., Babic, V., Datla, R., Brauer, E.K., Labbé, N., Subramaniam, R., and Ouellet, T. (2019). An optimised CRISPR/Cas9 protocol to create targeted mutations in homoeologous genes and an efficient genotyping protocol to identify edited events in wheat. Plant Methods *15*, 1–12. 10.1186/s13007-019-0500-2.

417. Sentmanat, M.F., Peters, S.T., Florian, C.P., Connelly, J.P., and Pruett-Miller, S.M. (2018). A Survey of Validation Strategies for CRISPR-Cas9 Editing. Scientific Reports *8*, 1–8. 10.1038/s41598-018-19441-8.

418. Harayama, T., Hashidate-Yoshida, T., Aguilera-Romero, A., Hamano, F., Morimoto, R., Shimizu, T., and Riezman, H. (2020). Establishment of a highly efficient gene disruption strategy to analyze and manipulate lipid co-regulatory networks. bioRxiv. 10.1101/2020.11.24.395632.

419. Harayama, T., and Riezman, H. (2018). Understanding the diversity of membrane lipid composition. Nature Reviews Molecular Cell Biology *19*, 281–296. 10.1038/nrm.2017.138.

420. Taha, T.A., Mullen, T.D., and Obeid, L.M. (2006). A house divided: Ceramide, sphingosine, and sphingosine-1-phosphate in programmed cell death. Biochimica et Biophysica Acta - Biomembranes *1758*, 2027–2036. 10.1016/j.bbamem.2006.10.018.

421. Vacaru, A.M., Tafesse, F.G., Ternes, P., Kondylis, V., Hermansson, M., Brouwers, J.F.H.M., Somerharju, P., Rabouille, C., and Holthuis, J.C.M. (2009). Sphingomyelin synthase-related protein SMSr controls ceramide homeostasis in the ER. Journal of Cell Biology *185*, 1013–1027. 10.1083/jcb.200903152.

422. Qiu, P., Shandilya, H., D'Alessio, J.M., O'Connor, K., Durocher, J., and Gerard, G.F. (2004). Mutation detection using Surveyor™ nuclease. BioTechniques *36*, 702–707. 10.2144/04364PF01.

423. Audi, A., Soudani, N., Dbaibo, G., and Zaraket, H. (2020). Depletion of Host and Viral Sphingomyelin Impairs Influenza Virus Infection. Frontiers in Microbiology *11*, 1–13. 10.3389/fmicb.2020.00612.

424. Ramstedt, B., Leppimäki, P., Axberg, M., and Slotte, J.P. (1999). Analysis of natural and synthetic sphingomyelins using high-performance thin-layer chromatography. European Journal of Biochemistry *266*, 997–1002. 10.1046/j.1432-1327.1999.00938.x.

425. Drews, K., Calgi, M.P., Harrison, W.C., Drews, C.M., Costa-Pinheiro, P., Shaw, J.J.P., Jobe, K.A., Han, J.D., Fox, T.E., White, J.M., et al. (2020). Glucosylceramide synthase maintains influenza virus entry and infection. PLOS ONE *15*, e0228735. 10.1371/journal.pone.0228735.

426. Shaner, R.L., Allegood, J.C., Park, H., Wang, E., Kelly, S., Haynes, C.A., Sullards, M.C., and Merrill, A.H. (2009). Quantitative analysis of sphingolipids for lipidomics using triple quadrupole and quadrupole linear ion trap mass spectrometers. Journal of Lipid Research *50*, 1692–1707. 10.1194/jlr.D800051-JLR200.

427. Garvey, C.M., Spiller, E., Lindsay, D., Chiang, C.-T., Choi, N.C., Agus, D.B., Mallick, P., Foo, J., and Mumenthaler, S.M. (2016). A high-content image-based method for quantitatively studying context-dependent cell population dynamics OPEN. 10.1038/srep29752.

428. Taciak, B., Białasek, M., Braniewska, A., Sas, Z., Sawicka, P., Kiraga, Ł., Rygiel, T., Król, M., and Król, M. (2018). Evaluation of phenotypic and functional stability of RAW 264.7 cell line through serial passages. PLOS ONE *13*, e0198943. 10.1371/journal.pone.0198943.

429. Pathak, D., Mehendale, N., Singh, S., Mallik, R., and Kamat, S.S. (2018). Lipidomics Suggests a New Role for Ceramide Synthase in Phagocytosis. ACS Chemical Biology *13*, 2280–2287. 10.1021/acschembio.8b00438.

430. Buckingham, S.D. (2004). RNA interference: From model organisms towards therapy for neural and neuromuscular disorders. Human Molecular Genetics *13*, R275–R288. 10.1093/hmg/ddh224.

431. Mocellin, S., and Provenzano, M. (2004). RNA interference: Learning gene knock-down from cell physiology. Journal of Translational Medicine *2*, 39. 10.1186/1479-5876-2-39.

432. Taxman, D.J., Moore, C.B., Guthrie, E.H., and Huang, M.T.-H. (2010). Short Hairpin RNA (shRNA): Design, Delivery, and Assessment of Gene Knockdown. In Methods in molecular biology (Clifton, N.J.), pp. 139–156. 10.1007/978-1-60761-657-3_10.

433. Qi, L.S., Larson, M.H., Gilbert, L.A., Doudna, J.A., Weissman, J.S., Arkin, A.P., and Lim, W.A. (2013). Repurposing CRISPR as an RNA-Guided Platform for Sequence-Specific Control of Gene Expression. Cell *152*, 1173–1183. 10.1016/j.cell.2013.02.022.

434. Boettcher, M., and McManus, M.T. (2015). Choosing the Right Tool for the Job: RNAi, TALEN, or CRISPR. Molecular Cell *58*, 575–585. 10.1016/j.molcel.2015.04.028.

435. Thorne, L. (2019). The Best Functional Genomic Screening Method: CRISPR or RNAi? https://www.biocompare.com/Editorial-Articles/360194-The-Best-Functional-Genomic-Screening-Method-CRISPR-or-RNAi/.

436. Breslow, D.K., Collins, S.R., Bodenmiller, B., Aebersold, R., Simons, K., Shevchenko, A., Ejsing, C.S., and Weissman, J.S. (2010). Orm family proteins mediate sphingolipid homeostasis. Nature *463*, 1048–1053. 10.1038/nature08787.

437. Lone, M.A., Hülsmeier, A.J., Saied, E.M., Karsai, G., Arenz, C., von Eckardstein, A., and Hornemann, T. (2020). Subunit composition of the mammalian serine-palmitoyltransferase defines the spectrum of straight and methyl-branched long-chain bases. Proceedings of the National Academy of Sciences of the United States of America *117*, 15591–15598. 10.1073/pnas.2002391117.

438. Ziv, C., Malitsky, S., Othman, A., Ben-Dor, S., Wei, Y., Zheng, S., Aharoni, A., Hornemann, T., Vardi, A., and Karl, D.M. (2016). Viral serine palmitoyltransferase induces metabolic switch in sphingolipid biosynthesis and is required for infection of a marine alga. Proceedings of the National Academy of Sciences of the United States of America *113*, E1907–E1916. 10.1073/pnas.1523168113.

439. Krebs, S., Medugorac, I., Röther, S., Strässer, K., and Förster, M. (2007). A missense mutation in the 3-ketodihydrosphingosine reductase FVT1 as candidate causal mutation for bovine spinal muscular atrophy. Proceedings of the National Academy of Sciences of the United States of America *104*, 6746–6751. 10.1073/pnas.0607721104.

440. Park, K.H., Ye, Z. wei, Zhang, J., Hammad, S.M., Townsend, D.M., Rockey, D.C., and Kim, S.H. (2019). 3-Ketodihydrosphingosine Reductase Mutation Induces Steatosis and Hepatic Injury in Zebrafish. Scientific Reports *9*, 1–13. 10.1038/s41598-018-37946-0.

441. Levy, M., and Futerman, A.H. (2010). Mammalian ceramide synthases. IUBMB Life *62*, NA–NA. 10.1002/iub.319.

442. Stiban, J., Tidhar, R., and Futerman, A.H. (2010). Ceramide synthases: Roles in cell physiology and signaling. Advances in experimental medicine and biology *688*, 60–71. 10.1007/978-1-4419-6741-1_4.

443. Laviad, E.L., Albee, L., Pankova-Kholmyansky, I., Epstein, S., Park, H., Merrill, A.H., and Futerman, A.H. (2008). Characterization of ceramide synthase 2: Tissue distribution, substrate specificity, and inhibition by sphingosine 1-phosphate. Journal of Biological Chemistry *283*, 5677–5684. 10.1074/jbc.M707386200.

444. Venkataraman, K., Riebeling, C., Bodennec, J., Riezman, H., Allegood, J.C., Sullards, M.C., Merrill, A.H., and Futerman, A.H. (2002). Upstream of Growth and Differentiation Factor 1 (Uog1), a Mammalian Homolog of the Yeast Longevity Assurance Gene 1 (LAG1), RegulatesN-Stearoyl-sphinganine (C18-(Dihydro)ceramide) Synthesis in a Fumonisin B1-independent Manner in Mammalian Cells. Journal of Biological Chemistry *277*, 35642–35649. 10.1074/jbc.M205211200.

445. Guillas, I., Jiang, J.C., Vionnet, C., Roubaty, C., Uldry, D., Chuard, R., Wang, J., Jazwinski, S.M., and Conzelmann, A. (2003). Human Homologues of LAG1 Reconstitute Acyl-CoA-dependent Ceramide Synthesis in Yeast. Journal of Biological Chemistry *278*, 37083–37091. 10.1074/jbc.M307554200.

446. Senkal, C.E., Ponnusamy, S., Manevich, Y., Meyers-Needham, M., Saddoughi, S.A., Mukhopadyay, A., Dent, P., Bielawski, J., and Ogretmen, B. (2011). Alteration of ceramide synthase 6/C 16-ceramide induces activating transcription factor 6-mediated Endoplasmic Reticulum (ER) stress and apoptosis via perturbation of cellular Ca 2+ and ER/golgi membrane network. Journal of Biological Chemistry *286*, 42446–42458. 10.1074/jbc.M111.287383.

447. Ternes, P., Franke, S., Zähringer, U., Sperling, P., and Heinz, E. (2002). Identification and Characterization of a Sphingolipid Δ4-Desaturase Family. Journal of Biological Chemistry *277*, 25512–25518. 10.1074/jbc.M202947200.

448. Hayashi, Y., Tsuchiya, K., Yamamoto, M., Nemoto-Sasaki, Y., Tanigawa, K., Hama, K., Tanikawa, T., Gohda, J., Maeda, K., Inoue, J., et al. (2021). N-(4-Hydroxyphenyl)retinamide suppresses SARS-CoV-2 spike protein-mediated cell-cell fusion and viral infection in vitro. Research Square. 10.21203/rs.3.rs-148750/v4.

449. Breslow, D.K., and Weissman, J.S. (2010). Membranes in Balance: Mechanisms of Sphingolipid Homeostasis. Molecular Cell *40*, 267–279. 10.1016/j.molcel.2010.10.005.

450. García-Arribas, A.B., Alonso, A., and Goñi, F.M. (2016). Cholesterol interactions with ceramide and sphingomyelin. Chemistry and Physics of Lipids *199*, 26–34. 10.1016/j.chemphyslip.2016.04.002.

451. Xu, S., Huo, J., Gunawan, M., Su, I.-H., and Lam, K.-P. (2009). Activated Dectin-1 Localizes to Lipid Raft Microdomains for Signaling and Activation of Phagocytosis and Cytokine Production in Dendritic Cells. Journal of Biological Chemistry *284*, 22005–22011. 10.1074/jbc.M109.009076.

452. Dong, L., Watanabe, K., Itoh, M., Huan, C.-R., Tong, X.-P., Nakamura, T., Miki, M., Iwao, H., Nakajima, A., Sakai, T., et al. (2012). CD4+ T-cell dysfunctions through the impaired lipid rafts ameliorate concanavalin A-induced hepatitis in sphingomyelin synthase 1-knockout mice. International Immunology *24*, 327–337. 10.1093/intimm/dxs008.

453. Kinoshita, M., Suzuki, K.G.N., Murata, M., and Matsumori, N. (2018). Evidence of lipid rafts based on the partition and dynamic behavior of sphingomyelins. Chemistry and Physics of Lipids *215*, 84–95. 10.1016/j.chemphyslip.2018.07.002.

454. Hammache, D., Yahi, N., Piéroni, G., Ariasi, F., Tamalet, C., and Fantini, J. (1998). Sequential Interaction of CD4 and HIV-1 Gp120 with a Reconstituted Membrane Patch of Ganglioside GM3: Implications for the Role of Glycolipids as Potential HIV-1 Fusion Cofactors. Biochemical and Biophysical Research Communications *246*, 117–122. 10.1006/bbrc.1998.8531.

455. Izquierdo-Useros, N., Lorizate, M., Puertas, M.C., Rodriguez-Plata, M.T., Zangger, N., Erikson, E., Pino, M., Erkizia, I., Glass, B., Clotet, B., et al. (2012). Siglec-1 Is a Novel Dendritic Cell Receptor That Mediates HIV-1 Trans-Infection Through Recognition of Viral Membrane Gangliosides. PLoS Biology *10*. 10.1371/journal.pbio.1001448.

456. Huitema, K., van den Dikkenberg, J., Brouwers, J.F.H.M., and Holthuis, J.C.M. (2004). Identification of a family of animal sphingomyelin synthases. The EMBO Journal *23*, 33–44. 10.1038/sj.emboj.7600034.

457. Tafesse, F.G., Ternes, P., and Holthuis, J.C.M. (2006). The multigenic sphingomyelin synthase family. Journal of Biological Chemistry *281*, 29421–29425. 10.1074/jbc.R600021200.

458. Pinto, S.N., Laviad, E.L., Stiban, J., Kelly, S.L., Merrill, A.H., Prieto, M., Futerman, A.H., and Silva, L.C. (2014). Changes in membrane biophysical properties induced by sphingomyelinase depend on the sphingolipid N -acyl chain. Journal of Lipid Research *55*, 53–61. 10.1194/jlr.M042002.

459. Cerbón, J., and del Carmen López-Sánchez, R. (2003). Diacylglycerol generated during sphingomyelin synthesis is involved in protein kinase C activation and cell proliferation in Madin-Darby canine kidney cells. The Biochemical journal *373*, 917–924. 10.1042/BJ20021732.

460. Taniguchi, M., Tasaki, T., Ninomiya, H., Ueda, Y., Kuremoto, K.I., Mitsutake, S., Igarashi, Y., Okazaki, T., and Takegami, T. (2016). Sphingomyelin generated by sphingomyelin synthase 1 is involved in attachment and infection with Japanese encephalitis virus. Scientific Reports *6*, 1–11. 10.1038/srep37829.

461. Backman, A.P.E., Halin, J., Nurmi, H., Möuts, A., Kjellberg, M.A., and Mattjus, P. (2018). Glucosylceramide acyl chain length is sensed by the glycolipid transfer protein. PLOS ONE *13*, e0209230. 10.1371/journal.pone.0209230.

462. Grösch, S., Schiffmann, S., and Geisslinger, G. (2012). Chain length-specific properties of ceramides. Progress in Lipid Research *51*, 50–62. 10.1016/j.plipres.2011.11.001.

463. Halter, D., Neumann, S., van Dijk, S.M., Wolthoorn, J., de Mazière, A.M., Vieira, O.V., Mattjus, P., Klumperman, J., van Meer, G., and Sprong, H. (2007). Pre- and post-Golgi translocation of glucosylceramide in glycosphingolipid synthesis. Journal of Cell Biology *179*, 101–115. 10.1083/jcb.200704091.

464. Ichikawa, S., and Hirabayashi, Y. (1998). Glucosylceramide synthase and glycosphingolipid synthesis. Trends in Cell Biology *8*, 198–202. 10.1016/S0962-8924(98)01249-5.

465. Liu, Y.-Y., Hill, R.A., and Li, Y.-T. (2013). Ceramide Glycosylation Catalyzed by Glucosylceramide Synthase and Cancer Drug Resistance. In Bone, pp. 59–89. 10.1016/B978-0-12-394274-6.00003-0.

466. Burckhardt, C.J., and Greber, U.F. (2009). Virus Movements on the Plasma Membrane Support Infection and Transmission between Cells. PLoS Pathogens *5*, e1000621. 10.1371/journal.ppat.1000621.

467. Puri, A., Rawat, S.S., Lin, H.-M.J., Finnegan, C.M., Mikovits, J., Ruscetti, F.W., and Blumenthal, R. (2004). An inhibitor of glycosphingolipid metabolism blocks HIV-1 infection of primary T-cells. AIDS *18*, 849–858. 10.1097/00002030-200404090-00002.

468. Aoki, M., Aoki, H., Ramanathan, R., Hait, N.C., and Takabe, K. (2016). Sphingosine-1-Phosphate Signaling in Immune Cells and Inflammation: Roles and Therapeutic Potential. Mediators of Inflammation *2016*, 1–11. 10.1155/2016/8606878.

469. Marchesini, N., and Hannun, Y.A. (2004). Acid and neutral sphingomyelinases: Roles and mechanisms of regulation. Biochemistry and Cell Biology *82*, 27–44. 10.1139/o03-091.

470. Magenau, A., Benzing, C., Proschogo, N., Don, A.S., Hejazi, L., Karunakaran, D., Jessup, W., and Gaus, K. (2011). Phagocytosis of IgG-Coated Polystyrene Beads by Macrophages Induces and Requires High Membrane Order. Traffic *12*, 1730–1743. 10.1111/j.1600-0854.2011.01272.x.

471. Tani, H., Shiokawa, M., Kaname, Y., Kambara, H., Mori, Y., Abe, T., Moriishi, K., and Matsuura, Y. (2010). Involvement of Ceramide in the Propagation of Japanese Encephalitis Virus. Journal of Virology *84*, 2798–2807. 10.1128/JVI.02499-09.

472. Finnegan, C.M., Rawat, S.S., Puri, A., Wang, J.M., Ruscetti, F.W., and Blumenthal, R. (2004). Ceramide, a target for antiretroviral therapy. Proceedings of the National Academy of Sciences *101*, 15452–15457. 10.1073/pnas.0402874101.

473. Boot, R.G., Verhoek, M., Donker-Koopman, W., Strijland, A., van Marle, J., Overkleeft, H.S., Wennekes, T., and F G Aerts, J.M. (2006). Identification of the Non-lysosomal Glucosylceramidase as-Glucosidase 2 * plays a role in cellular glucosylceramide metabolism. Journal of Biological Chemistry *282*, 1305–1312. 10.1074/jbc.M610544200.

474. Bajjalieh, S.M., Martin, T.F.J., and Floor, E. (1989). Synaptic Vesicle Ceramide Kinase. Journal of Biological Chemistry *264*, 14354–14360. 10.1016/S0021-9258(18)71685-2.

475. Hoeferlin, L.A., Wijesinghe, D.S., and Chalfant, C.E. (2013). The Role of Ceramide-1-Phosphate in Biological Functions. In Sphingolipids: Basic Science and Drug Development, E. Gulbins and I. Petrache, eds. (Springer Vienna), pp. 153–166. 10.1007/978-3-7091-1368-4_8.

476. Tuson, M., Marfany, G., and Gonzàlez-Duarte, R. (2004). Mutation of CERKL, a Novel Human Ceramide Kinase Gene, Causes Autosomal Recessive Retinitis Pigmentosa (RP26). The American Journal of Human Genetics *74*, 128–138. 10.1086/381055.

477. Gangoiti, P., Granado, M.H., Wang, S.W., Kong, J.Y., Steinbrecher, U.P., and Gómez-Muñoz, A. (2008). Ceramide 1-phosphate stimulates macrophage proliferation through activation of the PI3-kinase/PKB, JNK and ERK1/2 pathways. Cellular Signalling *20*, 726–736. 10.1016/j.cellsig.2007.12.008.

478. Boudker, O., and Futerman, A.H. (1993). Detection and characterization of ceramide-1-phosphate phosphatase activity in rat liver plasma membrane. Journal of Biological Chemistry *268*, 22150–22155. 10.1016/S0021-9258(20)80660-7.

479. Saied, E.M., and Arenz, C. (2016). Inhibitors of Ceramidases. Chemistry and Physics of Lipids *197*, 60–68. 10.1016/j.chemphyslip.2015.07.009.

480. Snider, A.J., Alexa Orr Gandy, K., and Obeid, L.M. (2010). Sphingosine kinase: Role in regulation of bioactive sphingolipid mediators in inflammation. Biochimie *92*, 707–715. 10.1016/j.biochi.2010.02.008.

481. Grafen, A., Schumacher, F., Chithelen, J., Kleuser, B., Beyersdorf, N., and Schneider-Schaulies, J. (2019). Use of Acid Ceramidase and Sphingosine Kinase Inhibitors as Antiviral Compounds Against Measles Virus Infection of Lymphocytes in vitro. Frontiers in Cell and Developmental Biology *7*. 10.3389/fcell.2019.00218.

482. Lang, J., Bohn, P., Bhat, H., Jastrow, H., Walkenfort, B., Cansiz, F., Fink, J., Bauer, M., Olszewski, D., Ramos-Nascimento, A., et al. (2020). Acid ceramidase of macrophages traps herpes simplex virus in multivesicular bodies and protects from severe disease. Nature Communications *11*, 1338. 10.1038/s41467-020-15072-8.

483. Dai, L., Plaisance-Bonstaff, K., Voelkel-Johnson, C., Smith, C.D., Ogretmen, B., Qin, Z., and Parsons, C. (2014). Sphingosine Kinase-2 Maintains Viral Latency and Survival for KSHV-Infected Endothelial Cells. PLoS ONE *9*, e102314. 10.1371/journal.pone.0102314.

484. Rolando, M., Escoll, P., Nora, T., Botti, J., Boitez, V., Bedia, C., Daniels, C., Abraham, G., Stogios, P.J., Skarina, T., et al. (2016). Legionella pneumophila S1P-lyase targets host sphingolipid metabolism and restrains autophagy. Proceedings of the National Academy of Sciences *113*, 1901–1906. 10.1073/pnas.1522067113.

485. Warfield, K.L., Schaaf, K.R., DeWald, L.E., Spurgers, K.B., Wang, W., Stavale, E., Mendenhall, M., Shilts, M.H., Stockwell, T.B., Barnard, D.L., et al. (2019). Lack of selective resistance of influenza A virus in presence of host-targeted antiviral, UV-4B. Scientific Reports *9*, 7484. 10.1038/s41598-019-43030-y.

486. Cauchie, M., Desmet, S., and Lagrou, K. (2017). Candida and its dual lifestyle as a commensal and a pathogen. Research in Microbiology *168*, 802–810. 10.1016/j.resmic.2017.02.005.

487. Iliev, I.D., and Leonardi, I. (2017). Fungal dysbiosis: Immunity and interactions at mucosal barriers. Nature Reviews Immunology *17*, 635–646. 10.1038/nri.2017.55.

488. Mayer, F.L., Wilson, D., and Hube, B. (2013). Candida albicans pathogenicity mechanisms. Virulence *4*, 119–128. 10.4161/viru.22913.

489. Enoch, D.A., Yang, H., Aliyu, S.H., and Micallef, C. (2017). The Changing Epidemiology of Invasive Fungal Infections. In, pp. 17–65. 10.1007/978-1-4939-6515-1_2.

490. Benedict, K., Richardson, M., Vallabhaneni, S., Jackson, B.R., and Chiller, T. (2017). Emerging issues, challenges, and changing epidemiology of fungal disease outbreaks. The Lancet Infectious Diseases *17*, e403–e411. 10.1016/S1473-3099(17)30443-7.

491. Pustylnikov, S., Sagar, D., Jain, P., and Khan, Z.K. (2014). Targeting the C-type lectins-mediated host-pathogen interactions with dextran. Journal of pharmacy & pharmaceutical sciences : a publication of the Canadian Society for Pharmaceutical Sciences, Societe canadienne des sciences pharmaceutiques *17*, 371–392.

492. Wang, R., and Chandawarkar, R.Y. (2010). Phagocytosis of fungal agents and yeast via macrophage cell surface scavenger receptors. Journal of Surgical Research *164*. 10.1016/j.jss.2010.08.039.

493. Guo, M., Härtlova, A., Dill, B.D., Prescott, A.R., Gierliński, M., and Trost, M. (2015). High-resolution quantitative proteome analysis reveals substantial differences between phagosomes of RAW 264.7 and bone marrow derived macrophages. PROTEOMICS *15*, 3169–3174. 10.1002/pmic.201400431.

494. Richardson, J.P., and Moyes, D.L. (2015). Adaptive immune responses to Candida albicans infection. Virulence *6*, 327–337. 10.1080/21505594.2015.1004977.

495. Goodridge, H.S., Wolf, A.J., and Underhill, D.M. (2009). Β-glucan recognition by the innate immune system. Immunological Reviews *230*, 38–50. 10.1111/j.1600-065X.2009.00793.x.

496. Li, X., Utomo, A., Cullere, X., Choi, M.M., Milner, D.A., Venkatesh, D., Yun, S.H., and Mayadas, T.N. (2011). The β-glucan receptor dectin-1 activates the integrin Mac-1 in neutrophils via vav protein signaling to promote Candida albicans clearance. Cell Host and Microbe *10*, 603–615. 10.1016/j.chom.2011.10.009.

497. Goyal, S., Castrillón-Betancur, J.C., Klaile, E., and Slevogt, H. (2018). The Interaction of Human Pathogenic Fungi With C-Type Lectin Receptors. Frontiers in Immunology *9*. 10.3389/fimmu.2018.01261.

498. Wells, C.A., Salvage-Jones, J.A., Li, X., Hitchens, K., Butcher, S., Murray, R.Z., Beckhouse, A.G., Lo, Y.-L.-S., Manzanero, S., Cobbold, C., et al. (2008). The Macrophage-Inducible C-Type Lectin, Mincle, Is an Essential Component of the Innate Immune Response to Candida albicans. The Journal of Immunology *180*, 7404–7413. 10.4049/jimmunol.180.11.7404.

499. Yamasaki, S., Matsumoto, M., Takeuchi, O., Matsuzawa, T., Ishikawa, E., Sakuma, M., Tateno, H., Uno, J., Hirabayashi, J., Mikami, Y., et al. (2009). C-type lectin Mincle is an activating receptor for pathogenic fungus, Malassezia. Proceedings of the National Academy of Sciences of the United States of America *106*, 1897–1902. 10.1073/pnas.0805177106.

500. Richards, D.M., and Endres, R.G. (2017). How cells engulf: A review of theoretical approaches to phagocytosis. Reports on Progress in Physics *80*, 126601. 10.1088/1361-6633/aa8730.

501. Serrano-Gómez, D., Antonio Leal, J., and Corbí, A.L. (2005). DC-SIGN mediates the binding of Aspergillus fumigatus and keratinophylic fungi by human dendritic cells. Immunobiology *210*, 175–183. 10.1016/j.imbio.2005.05.011.

502. Jouault, T., El Abed-El Behi, M., Martínez-Esparza, M., Breuilh, L., Trinel, P.-A., Chamaillard, M., Trottein, F., and Poulain, D. (2006). Specific Recognition of Candida albicans by Macrophages Requires Galectin-3 to Discriminate Saccharomyces cerevisiae and Needs Association with TLR2 for Signaling. The Journal of Immunology *177*, 4679–4687. 10.4049/jimmunol.177.7.4679.

503. Brown, G.D., Taylor, P.R., Reid, D.M., Willment, J.A., Williams, D.L., Martinez-Pomares, L., Wong, S.Y.C., and Gordon, S. (2002). Dectin-1 Is A Major β-Glucan Receptor On Macrophages. The Journal of Experimental Medicine *196*, 407–412. 10.1084/jem.20020470.

504. Gantner, B.N., Simmons, R.M., Canavera, S.J., Akira, S., and Underhill, D.M. (2003). Collaborative induction of inflammatory responses by dectin-1 and toll-like receptor 2. Journal of Experimental Medicine *197*, 1107–1117. 10.1084/jem.20021787.

505. Hawn, T.R., and Underhill, D.M. (2005). Toll-like Receptors in Innate Immunity. In Measuring Immunity (Elsevier), pp. 80–90. 10.1016/B978-012455900-4/50268-3.

506. Inoue, M., and Shinohara, M.L. (2014). Clustering of Pattern Recognition Receptors for Fungal Detection. PLoS Pathogens *10*, 2–4. 10.1371/journal.ppat.1003873.

507. Sköld, M., and Behar, S.M. (2003). Role of CD1d-Restricted NKT Cells in Microbial Immunity. Infection and Immunity *71*, 5447–5455. 10.1128/IAI.71.10.5447-5455.2003.

508. Pereira, C.S., and Macedo, M.F. (2016). CD1-restricted T cells at the crossroad of innate and adaptive immunity. Journal of Immunology Research *2016*. 10.1155/2016/2876275.

509. Kawakami, K., Kinjo, Y., Yara, S., Koguchi, Y., Uezu, K., Nakayama, T., Taniguchi, M., and Saito, A. (2001). Activation of Vα14+ natural killer T cells by α-galactosylceramide results in development of Th1 response and local host resistance in mice infected with Cryptococcus neoformans. Infection and Immunity *69*, 213–220. 10.1128/IAI.69.1.213-220.2001.

510. Albacker, L.A., Chaudhary, V., Chang, Y.-J., Kim, H.Y., Chuang, Y.-T., Pichavant, M., DeKruyff, R.H., Savage, P.B., and Umetsu, D.T. (2013). Invariant natural killer T cells recognize a fungal glycosphingolipid that can induce airway hyperreactivity. Nat Med *19*, 1297–1304. 10.1038/nm.3321.

511. Bird, D.C., and Sheagren, J.N. (1970). Evaluation of Reticuloendothelial System Phagocytic Activity During Systemic Candida albicans Infection in Mice. Experimental Biology and Medicine *133*, 34–37. 10.3181/00379727-133-34401.

512. Baine, W.B., Koenig, M.G., and Goodman, J.S. (1974). Clearance of Candida albicans from the bloodstream of rabbits. Infection and Immunity *10*, 1420–1425.

513. Sawyer, R.T., Moon, R.J., and Beneke, E.S. (1976). Hepatic clearance of Candida albicans in rats. Infection and Immunity *14*, 1348–1355.

514. Zhao, H., and Lappalainen, P. (2012). A simple guide to biochemical approaches for analyzing protein–lipid interactions. Molecular Biology of the Cell *23*, 2823–2830. 10.1091/mbc.e11-07-0645.

515. Yoshizaki, F., Nakayama, H., Iwahara, C., Takamori, K., Ogawa, H., and Iwabuchi, K. (2008). Role of glycosphingolipid-enriched microdomains in innate immunity: Microdomain-dependent phagocytic cell functions. Biochimica et Biophysica Acta - General Subjects *1780*, 383–392. 10.1016/j.bbagen.2007.11.004.

516. Iwabuchi, K., and Nagaoka, I. (2002). Lactosylceramide-enriched glycosphingolipid signaling domain mediates superoxide generation from human neutrophils. Blood *100*, 1454–1464. 10.1182/blood.v100.4.1454.h81602001454_1454_1464.

517. Kinoshita, M., Suzuki, K.G.N., Matsumori, N., Takada, M., Ano, H., Morigaki, K., Abe, M., Makino, A., Kobayashi, T., Hirosawa, K.M., et al. (2017). Raft-based sphingomyelin interactions revealed by new fluorescent sphingomyelin analogs. Journal of Cell Biology *216*, 1183–1204. 10.1083/jcb.201607086.

518. Bryan, A.M., Del Poeta, M., and Luberto, C. (2015). Sphingolipids as Regulators of the Phagocytic Response to Fungal Infections. Mediators of Inflammation *2015*. 10.1155/2015/640540.

519. Brown, G.D. (2006). Dectin-1: A signalling non-TLR pattern-recognition receptor. Nature Reviews Immunology *6*, 33–43. 10.1038/nri1745.

520. Hemmings, B.A., and Restuccia, D.F. (2012). PI3K-PKB/Akt Pathway. Cold Spring Harbor Perspectives in Biology *4*, a011189–a011189. 10.1101/cshperspect.a011189.

521. Razzinit, G., Brancaccio, A., Lemmon, M.A., Guarnieri, S., and Falasca, M. (2000). The role of the pleckstrin homology domain in membrane targeting and activation of phospholipase Cβ1. Journal of Biological Chemistry *275*, 14873–14881. 10.1074/jbc.275.20.14873.

522. Melendez, A.J. (2008). Calcium Signaling during Phagocytosis. In Molecular Mechanisms of Phagocytosis (Landes Bioscience), pp. 117–132. 10.1007/978-0-387-28669-3_9.

523. Wilsson, åsa, Lundqvist, H., Gustafsson, M., and Stendahl, O. (1996). Killing of phagocytosed Staphylococcus aureus by human neutrophils requires intracellular free calcium. Journal of Leukocyte Biology *59*, 902–907. 10.1002/jlb.59.6.902.

524. Hauck, C.R., Grassmé, H., Bock, J., Jendrossek, V., Ferlinz, K., Meyer, T.F., and Gulbins, E. (2000). Acid sphingomyelinase is involved in CEACAM receptor-mediated phagocytosis of Neisseria gonorrhoeae. FEBS Letters *478*, 260–266. 10.1016/S0014-5793(00)01851-2.

525. Trajkovic, K. (2008). Ceramide triggers budding of exosome vesicles into multivesicular endosomes (Science (1244)). Science *320*, 179. 10.1126/science.320.5873.179.

526. Jordens, I., Fernandez-Borja, M., Marsman, M., Dusseljee, S., Janssen, L., Calafat, J., Janssen, H., Wubbolts, R., and Neefjes, J. (2001). The Rab7 effector protein RILP controls lysosomal transport by inducing the recruitment of dynein-dynactin motors. Current Biology *11*, 1680–1685. 10.1016/S0960-9822(01)00531-0.

527. Teichgräber, V., Ulrich, M., Endlich, N., Riethmüller, J., Wilker, B., De Oliveira–Munding, C.C., van Heeckeren, A.M., Barr, M.L., von Kürthy, G., Schmid, K.W., et al. (2008). Ceramide accumulation mediates inflammation, cell death and infection susceptibility in cystic fibrosis. Nature Medicine *14*, 382–391. 10.1038/nm1748.

528. Teng, O., En Ang, C.K., and Guan, X.L. (2017). Macrophage-bacteria interactions-A lipid-centric relationship. Frontiers in Immunology *8*. 10.3389/fimmu.2017.01836.

529. Kinchen, J.M., and Ravichandran, K.S. (2008). Phagosome maturation: Going through the acid test. Nat Rev Mol Cell Biol *9*, 781–795. 10.1038/nrm2515.

530. Heinrich, M., Wickel, M., Schneider-Brachert, W., Sandberg, C., Gahr, J., Schwandner, R., Weber, T., Brunner, J., Krönke, M., and Schütze, S. (1999). Cathepsin D targeted by acid sphingomyelinase-derived ceramide. EMBO Journal *18*, 5252–5263. 10.1093/emboj/18.19.5252.

531. Schroeder, F. (1982). Phagosomal membrane lipids of LM fibroblasts. The Journal of Membrane Biology *68*, 141–150. 10.1007/BF01872260.

532. Aulakh, G.K. (2018). Neutrophils in the lung: "The first responders." Cell and Tissue Research *371*, 577–588. 10.1007/s00441-017-2748-z.

533. Hauert, A.B., Martinelli, S., Marone, C., and Niggli, V. (2002). Differentiated HL-60 cells are a valid model system for the analysis of human neutrophil migration and chemotaxis. The International Journal of Biochemistry & Cell Biology *34*, 838–854. 10.1016/S1357-2725(02)00010-9.

534. Cassatella, M.A. (2017). Human mature neutrophils as atypical APC. Blood *129*, 1895–1896. 10.1182/blood-2017-02-767574.

535. Lee, W.L., Harrison, R.E., and Grinstein, S. (2003). Phagocytosis by neutrophils. Microbes and Infection *5*, 1299–1306. 10.1016/j.micinf.2003.09.014.

536. Koup, R.A., Liang, F., Loré, K., Vono, M., Lin, A., and Norrby-Teglund, A. (2017). Neutrophils acquire the capacity for antigen presentation to memory CD4 + T cells in vitro and ex vivo. Blood *129*, 1991–2001. 10.1182/blood-2016-10-744441.

537. Herant, M. (2006). Mechanics of neutrophil phagocytosis: Experiments and quantitative models. Journal of Cell Science *119*, 1903–1913. 10.1242/jcs.02876.

538. Fleck, R.A., Romero-Steiner, S., and Nahm, M.H. (2005). Use of HL-60 Cell Line To Measure Opsonic Capacity of Pneumococcal Antibodies. Clinical and Vaccine Immunology *12*, 19–27. 10.1128/CDLI.12.1.19-27.2005.

539. Collins, S.J. (1987). The HL-60 promyelocytic leukemia cell line: Proliferation, differentiation, and cellular oncogene expression. Blood *70*, 1233–1244.

540. Polylysine-coated tissue culture surfaces (2012). https://www.protocolsonline.com/recipes/stock-solutions/polylysine-coated-tissue-culture-surfaces/.

541. Martin, S.J., Bradley, J.G., and Cotter, T.G. (1990). HL-60 cells induced to differentiate towards neutrophils subsequently die via apoptosis. Clinical and experimental immunology *79*, 448–453. 10.1111/j.1365-2249.1990.tb08110.x.

542. Millius, A., and Weiner, O.D. (2010). Manipulation of Neutrophil-Like HL-60 Cells for the Study of Directed Cell Migration. In Histochemical Journal, pp. 147–158. 10.1007/978-1-60761-404-3_9.

543. Futosi, K., Fodor, S., and Mócsai, A. (2013). Reprint of Neutrophil cell surface receptors and their intracellular signal transduction pathways. International Immunopharmacology *17*, 1185–1197. 10.1016/j.intimp.2013.11.010.

544. Sokoya, T., Parolek, J., Foged, M.M., Danylchuk, D.I., Bozan, M., Sarkar, B., Hilderink, A., Philippi, M., Botto, L.D., Terhal, P.A., et al. (2022). Pathogenic variants of sphingomyelin synthase SMS2 disrupt lipid landscapes in the secretory pathway. eLife *11*, e79278. 10.7554/eLife.79278.

545. Wang, M., and Hajishengallis, G. (2008). Lipid raft-dependent uptake, signalling and intracellular fate of Porphyromonas gingivalis in mouse macrophages. Cellular Microbiology *10*, 2029–2042. 10.1111/j.1462-5822.2008.01185.x.

546. Sebastião, A.M., Colino-Oliveira, M., Assaife-Lopes, N., Dias, R.B., and Ribeiro, J.A. (2013). Lipid rafts, synaptic transmission and plasticity: Impact in age-related neurodegenerative diseases. Neuropharmacology *64*, 97–107. 10.1016/j.neuropharm.2012.06.053.

547. Jay, A.G., and Hamilton, J.A. (2017). Disorder Amidst Membrane Order: Standardizing Laurdan Generalized Polarization and Membrane Fluidity Terms. Journal of Fluorescence *27*, 243–249. 10.1007/s10895-016-1951-8.

548. Taniguchi, M., Kitatani, K., Kondo, T., Hashimoto-Nishimura, M., Asano, S., Hayashi, A., Mitsutake, S., Igarashi, Y., Umehara, H., Takeya, H., et al. (2012). Regulation of Autophagy and Its Associated Cell Death by "Sphingolipid Rheostat." Journal of Biological Chemistry *287*, 39898–39910. 10.1074/jbc.M112.416552.

549. Subbaiah, P.V., and Sargis, R.M. (2001). Sphingomyelin: A natural modulator of membrane homeostasis and inflammation. Medical Hypotheses *57*, 135–138. 10.1054/mehy.2001.1336.

550. Perrotta, C., and Clementi, E. (2010). Biological Roles of Acid and Neutral Sphingomyelinases and Their Regulation by Nitric Oxide. Physiology *25*, 64–71. 10.1152/physiol.00048.2009.

551. Hampton, R., and Morand, O. (1989). Sphingomyelin synthase and PKC activation. Science *246*, 1050–1050. 10.1126/science.2555921.

552. Hannun, Y., and Bell, R. (1989). Functions of sphingolipids and sphingolipid breakdown products in cellular regulation. Science *243*, 500–507. 10.1126/science.2643164.

553. Yang, C., and Kazanietz, M.G. (2003). Divergence and complexities in DAG signaling: Looking beyond PKC. Trends in Pharmacological Sciences *24*, 602–608. 10.1016/j.tips.2003.09.003.

554. Cutler, R.G., Thompson, K.W., Camandola, S., Mack, K.T., and Mattson, M.P. (2014). Sphingolipid metabolism regulates development and lifespan in Caenorhabditis elegans. Mechanisms of Ageing and Development *143–144*, 9–18. 10.1016/j.mad.2014.11.002.

555. Cheng, X., Jiang, X., Tam, K.Y., Li, G., Zheng, J., and Zhang, H. (2019). Sphingolipidomic Analysis of C. Elegans reveals Development- and Environment-dependent Metabolic Features. International Journal of Biological Sciences *15*, 2897–2910. 10.7150/ijbs.30499.

556. Cui, M., Wang, Y., Cavaleri, J., Kelson, T., Teng, Y., and Han, M. (2017). Starvation-induced stress response is critically impacted by ceramide levels in Caenorhabditis elegans. Genetics *205*, 775–785. 10.1534/genetics.116.194282.

557. Mosbech, M.-B., Kruse, R., Harvald, E.B., Olsen, A.S.B., Gallego, S.F., Hannibal-Bach, H.K., Ejsing, C.S., and Færgeman, N.J. (2013). Functional Loss of Two Ceramide Synthases Elicits Autophagy-Dependent Lifespan Extension in C. elegans. PLoS ONE *8*, e70087. 10.1371/journal.pone.0070087.

558. Yamaoka, S., Miyaji, M., Kitano, T., Umehara, H., and Okazaki, T. (2004). Expression Cloning of a Human cDNA Restoring Sphingomyelin Synthesis and Cell Growth in Sphingomyelin Synthase-defective Lymphoid Cells. Journal of Biological Chemistry *279*, 18688–18693. 10.1074/jbc.M401205200.

559. Metzstein, M.M., Stanfield, G.M., and Horvitz, H.R. (1998). Genetics of programmed cell death in C. Elegans: Past, present and future. Trends in Genetics *14*, 410–416. 10.1016/S0168-9525(98)01573-X.

560. Koreth, J., and van den Heuvel, S. (2005). Cell-cycle control in Caenorhabditis elegans: How the worm moves from G1 to S. Oncogene *24*, 2756–2764. 10.1038/sj.onc.1208607.

561. Ternes, P., Brouwers, J.F.H.M., van den Dikkenberg, J., and Holthuis, J.C.M. (2009). Sphingomyelin synthase SMS2 displays dual activity as ceramide phosphoethanolamine synthase. Journal of Lipid Research *50*, 2270–2277. 10.1194/jlr.M900230-JLR200.

562. Cipollo, J.F., Awad, A., Costello, C.E., Robbins, P.W., and Hirschberg, C.B. (2004). Biosynthesis in vitro of Caenorhabditis elegans phosphorylcholine oligosaccharides. Proceedings of the National Academy of Sciences *101*, 3404–3408. 10.1073/pnas.0400384101.

563. HOUSTON, K.M., and HARNETT, W. (2004). Structure and synthesis of nematode phosphorylcholine-containing glycoconjugates. Parasitology *129*, 655–661. 10.1017/S0031182004006171.

564. Cerantola, V., Vionnet, C., Aebischer, O.F., Jenny, T., Knudsen, J., and Conzelmann, A. (2007). Yeast sphingolipids do not need to contain very long chain fatty acids. Biochemical Journal *401*, 205–216. 10.1042/BJ20061128.

565. Kenyon, C. (1988). The Nematode *Caenorhabditis Elegans*. Science *240*, 1448–1453. 10.1126/science.3287621.

566. Kondylis, V., and Rabouille, C. (2003). A novel role for Dp115 in the organization of tER sites in Drosophila. Journal of Cell Biology *162*, 185–198. 10.1083/jcb.200301136.

567. Stratton, K.G., Webb-Robertson, B.J.M., McCue, L.A., Stanfill, B., Claborne, D., Godinez, I., Johansen, T., Thompson, A.M., Burnum-Johnson, K.E., Waters, K.M., et al. (2019). PmartR: Quality Control and Statistics for Mass Spectrometry-Based Biological Data. Journal of Proteome Research *18*, 1418–1425. 10.1021/acs.jproteome.8b00760.

568. Holm, S. (1979). A Simple Sequentially Rejective Multiple Test Procedure. Scandinavian Journal of Statistics *6*, 65–70.

569. Agarwal, S., Ghosh, S., Sharma, S., Kaur, K., and Verma, I. (2018). Mycobacterium tuberculosis H37Rv expresses differential proteome during intracellular survival within alveolar epithelial cells compared with macrophages. Pathogens and Disease *76*. 10.1093/femspd/fty058.

570. Garćıa-Pérez, B.E., Mondragón-Flores, R., and Luna-Herrera, J. (2003). Internalization of Mycobacterium tuberculosis by macropinocytosis in non-phagocytic cells. Microbial Pathogenesis *35*, 49–55. 10.1016/S0882-4010(03)00089-5.

571. Scordo, J.M., Knoell, D.L., and Torrelles, J.B. (2016). Alveolar Epithelial Cells in ***Mycobacterium Tuberculosis*** Infection: Active Players or Innocent Bystanders? J Innate Immun *8*, 3–14. 10.1159/000439275.

572. Lim, J.P., and Gleeson, P.A. (2011). Macropinocytosis: An endocytic pathway for internalising large gulps. Immunology and Cell Biology *89*, 836–843. 10.1038/icb.2011.20.

573. Nagre, N., Cong, X., Pearson, A.C., and Zhao, X. (2019). Alveolar Macrophage Phagocytosis and Bacteria Clearance in Mice. JoVE, 59088. 10.3791/59088.

574. Podleśny-Drabiniok, A., Marcora, E., and Goate, A.M. (2020). Microglial Phagocytosis: A Disease-Associated Process Emerging from Alzheimer's Disease Genetics. Trends in Neurosciences *43*, 965–979. 10.1016/j.tins.2020.10.002.

575. Brady, R.O. (1998). Therapy for the Sphingolipidoses. Arch Neurol *55*, 1055. 10.1001/archneur.55.8.1055.

576. Stapels, D.A.C., Hill, P.W.S., Westermann, A.J., Fisher, R.A., Thurston, T.L., Saliba, A.-E., Blommestein, I., Vogel, J., and Helaine, S. (2018). *Salmonella* persisters undermine host immune defenses during antibiotic treatment. Science *362*, 1156–1160. 10.1126/science.aat7148.

577. Fisher, R.A., Gollan, B., and Helaine, S. (2017). Persistent bacterial infections and persister cells. Nat Rev Microbiol *15*, 453–464. 10.1038/nrmicro.2017.42.

578. Lee, J.J., Lee, S.-K., Song, N., Nathan, T.O., Swarts, B.M., Eum, S.-Y., Ehrt, S., Cho, S.-N., and Eoh, H. (2019). Transient drug-tolerance and permanent drug-resistance rely on the trehalose-catalytic shift in Mycobacterium tuberculosis. Nat Commun *10*, 2928. 10.1038/s41467-019-10975-7.

579. Beam, J.E., Maiocchi, S., Cartaya, A., Rowe, S.E., Bahnson, E.S.M., and Conlon, B.P. (2022). The Use of Acute Immunosuppressive Therapy to Improve Antibiotic Efficacy against Intracellular Staphylococcus aureus. Microbiol Spectr *10*, e00858–22. 10.1128/spectrum.00858-22.

580. Homans, C., Yalcin, E.B., Tong, M., Gallucci, G., Bautista, D., Moriel, N., and Monte, S.D.L. (2022). Therapeutic Effects of Myriocin in Experimental Alcohol-Related Neurobehavioral Dysfunction and Frontal Lobe White Matter Biochemical Pathology. JBBS *12*, 23–42. 10.4236/jbbs.2022.122003.

581. Bonezzi, F., Piccoli, M., Dei Cas, M., Paroni, R., Mingione, A., Monasky, M.M., Caretti, A., Riganti, C., Ghidoni, R., Pappone, C., et al. (2019). Sphingolipid Synthesis Inhibition by Myriocin Administration Enhances Lipid Consumption and Ameliorates Lipid Response to Myocardial Ischemia Reperfusion Injury. Front. Physiol. *10*, 986. 10.3389/fphys.2019.00986.

582. Ji, R., Akashi, H., Drosatos, K., Liao, X., Jiang, H., Kennel, P.J., Brunjes, D.L., Castillero, E., Zhang, X., Deng, L.Y., et al. (2017). Increased de novo ceramide synthesis and accumulation in failing myocardium. JCI Insight *2*, e96203. 10.1172/jci.insight.96203.

583. Mak, T.W., and Saunders, M.E. (2006). Transplantation. In The Immune Response (Elsevier), pp. 873–921. 10.1016/B978-012088451-3.50029-6.

584. Salaun, E., Lefeuvre-Orfila, L., Cavey, T., Martin, B., Turlin, B., Ropert, M., Loreal, O., and Derbré, F. (2016). Myriocin prevents muscle ceramide accumulation but not muscle fiber atrophy during short-term mechanical unloading. Journal of Applied Physiology *120*, 178–187. 10.1152/japplphysiol.00720.2015.

585. Magaye, Ruth.R., Savira, F., Hua, Y., Kelly, D.J., Reid, C., Flynn, B., Liew, D., and Wang, B.H. (2019). The role of dihydrosphingolipids in disease. Cell. Mol. Life Sci. *76*, 1107–1134. 10.1007/s00018-018-2984-8.

586. Babiy, B., Ramos-Molina, B., Ocaña, L., Sacristán, S., Burgos-Santamaría, D., Martínez-Botas, J., Busto, R., Perna, C., Frutos, M.D., Albillos, A., et al. (2023). Dihydrosphingolipids are associated with steatosis and increased fibrosis damage in non-alcoholic fatty liver disease. Biochimica et Biophysica Acta (BBA) - Molecular and Cell Biology of Lipids *1868*, 159318. 10.1016/j.bbalip.2023.159318.

587. Turpin, S.M., Nicholls, H.T., Willmes, D.M., Mourier, A., Brodesser, S., Wunderlich, C.M., Mauer, J., Xu, E., Hammerschmidt, P., Brönneke, H.S., et al. (2014). Obesity-Induced CerS6-Dependent C16:0 Ceramide Production Promotes Weight Gain and Glucose Intolerance. Cell Metabolism *20*, 678–686. 10.1016/j.cmet.2014.08.002.

588. Reali, F., Morine, M.J., Kahramanoğulları, O., Raichur, S., Schneider, H.-C., Crowther, D., and Priami, C. (2017). Mechanistic interplay between ceramide and insulin resistance. Sci Rep *7*, 41231. 10.1038/srep41231.

589. Kaur, G., Delluc-Clavieres, A., Poon, I.K.H., Forwood, J.K., Glover, D.J., and Jans, D.A. (2010). Calmodulin-dependent nuclear import of HMG-box family nuclear factors: Importance of the role of SRY in sex reversal. Biochemical Journal *430*, 39–48. 10.1042/BJ20091758.

590. Ghanavi, J., Farnia, P., Farnia, P., and Velayati, A. (2021). The role of interferon-gamma and interferon-gamma receptor in tuberculosis and nontuberculous mycobacterial infections. Int J Mycobacteriol *10*, 349. 10.4103/ijmy.ijmy_186_21.

591. Wang, X., Chen, S., Ren, H., Chen, J., Li, J., Wang, Y., Hua, Y., Wang, X., and Huang, N. (2019). HMGN2 regulates non□tuberculous mycobacteria survival via modulation of M1 macrophage polarization. J Cellular Molecular Medi *23*, 7985–7998. 10.1111/jcmm.14599.

592. Saharan, O., Mehendale, N., and Kamat, S.S. (2022). Phagocytosis: A (Sphingo)Lipid Story. Current Research in Chemical Biology *2*, 100030. 10.1016/j.crchbi.2022.100030.

593. Gilberti, R.M., Joshi, G.N., and Knecht, D.A. (2008). The Phagocytosis of Crystalline Silica Particles by Macrophages. American Journal of Respiratory Cell and Molecular Biology *39*, 619–627. 10.1165/rcmb.2008-0046OC.

594. Mularski, A., Marie-Anaïs, F., Mazzolini, J., and Niedergang, F. (2018). Observing Frustrated Phagocytosis and Phagosome Formation and Closure Using Total Internal Reflection Fluorescence Microscopy (TIRFM). In Macrophages, G. Rousselet, ed. (Springer New York), pp. 165–175. 10.1007/978-1-4939-7837-3_16.

595. Deretic, V. (2014). Autophagy in Tuberculosis. Cold Spring Harbor Perspectives in Medicine *4*, a018481–a018481. 10.1101/cshperspect.a018481.

596. Luberto, C., Hassler, D.F., Signorelli, P., Okamoto, Y., Sawai, H., Boros, E., Hazen-Martin, D.J., Obeid, L.M., Hannun, Y.A., and Smith, G.K. (2002). Inhibition of Tumor Necrosis Factor-induced Cell Death in MCF7 by a Novel Inhibitor of Neutral Sphingomyelinase. Journal of Biological Chemistry *277*, 41128–41139. 10.1074/jbc.M206747200.

597. Airola, M.V., Shanbhogue, P., Shamseddine, A.A., Guja, K.E., Senkal, C.E., Maini, R., Bartke, N., Wu, B.X., Obeid, L.M., Garcia-Diaz, M., et al. (2017). Structure of human nSMase2 reveals an interdomain allosteric activation mechanism for ceramide generation. Proc. Natl. Acad. Sci. U.S.A. *114*. 10.1073/pnas.1705134114.

598. Beckmann, N., Sharma, D., Gulbins, E., Becker, K.A., and Edelmann, B. (2014). Inhibition of acid sphingomyelinase by tricyclic antidepressants and analogons. Front. Physiol. *5*. 10.3389/fphys.2014.00331.

599. Hoertel, N., Sánchez-Rico, M., Gulbins, E., Kornhuber, J., Carpinteiro, A., Abellán, M., De La Muela, P., Vernet, R., Beeker, N., Neuraz, A., et al. (2022). Association between FIASMA psychotropic medications and reduced risk of intubation or death in individuals with psychiatric disorders hospitalized for severe COVID-19: An observational multicenter study. Transl Psychiatry *12*, 90. 10.1038/s41398-022-01804-5.

600. Peng, H., Li, C., Kadow, S., Henry, B.D., Steinmann, J., Becker, K.A., Riehle, A., Beckmann, N., Wilker, B., Li, P.-L., et al. (2015). Acid sphingomyelinase inhibition protects mice from lung edema and lethal Staphylococcus aureus sepsis. J Mol Med *93*, 675–689. 10.1007/s00109-014-1246-y.

601. Falcone, S., Perrotta, C., De Palma, C., Pisconti, A., Sciorati, C., Capobianco, A., Rovere-Querini, P., Manfredi, A.A., and Clementi, E. (2004). Activation of Acid Sphingomyelinase and Its Inhibition by the Nitric Oxide/Cyclic Guanosine 3□,5□-Monophosphate Pathway: Key Events in *Escherichia Coli*- Elicited Apoptosis of Dendritic Cells. The Journal of Immunology *173*, 4452–4463. 10.4049/jimmunol.173.7.4452.

602. Kaya, I., Nilsson, A., Luptáková, D., He, Y., Vallianatou, T., Bjärterot, P., Svenningsson, P., Bezard, E., and Andrén, P.E. (2023). Spatial lipidomics reveals brain region-specific changes of sulfatides in an experimental MPTP Parkinson's disease primate model. npj Parkinsons Dis. *9*, 118. 10.1038/s41531-023-00558-1.

About

Gaelen Guzman earned his PhD in Microbiology from the OHSU School of Medicine, in the Department of Molecular Microbiology and Immunology.

He has prepared this document as partial fulfillment of the degree requirements for Doctor of Philosophy. He defended this dissertation on Friday, February 16th, 2024.

Philosophy

The projects presented in this dissertation each sought to understand how host lipids affect (or are affected by) the progression of a *Mycobacterium tuberculosis* (*Mtb*) infection. Chapters 3, 4, and 6 of this document apply an array of biochemical techniques to unravel the manners in which host sphingolipids mediate the cellular response to infection. Chapters 5 and 6 utilize unbiased 'omics' technologies (lipidomics and proteomics, respectively) to investigate the broad effects that an *Mtb* infection has on the cellular lipid landscape.

In Gaelen's post-graduation career, he seeks to the same philosophies to contribute to the understanding and treatment of human disease: How do protein:protein or protein:lipid interactions mediate pathological effects? Can we leverage lipid metabolism to treat diseases?

The current version of this site incorporates the suggested edits supplied by Gaelen's dissertation advisory committee. It includes substantial edits to Chapters 2, 4, and 11 – as well as minor edits to many of the other sections of this document.

If the reader has any questions or comments about the contents of this document, they should feel free to message Gaelen at the following: gaelenguzman@gmail.com

To see more of Gaelen's publication history, please visit his ORCID:

ORCID: 0000-0002-7696-6034